University of Missouri, St. Louis
IRL @ UMSL

Dissertations | UMSL Graduate Works

11-8-2010

The Molecular Transport and Intercalation of Guest Molecules into Hydrogen–Bonded Metal-Organic Frameworks (HMOFs)

Greg Anthony Hogan
University of Missouri-St. Louis, gahvx8@mail.umsl.edu

Follow this and additional works at: https://irl.umsl.edu/dissertation

Part of the Chemistry Commons

Recommended Citation
Hogan, Greg Anthony, "The Molecular Transport and Intercalation of Guest Molecules into Hydrogen–Bonded Metal-Organic Frameworks (HMOFs)" (2010). *Dissertations*. 459.
https://irl.umsl.edu/dissertation/459

This Dissertation is brought to you for free and open access by the UMSL Graduate Works at IRL @ UMSL. It has been accepted for inclusion in Dissertations by an authorized administrator of IRL @ UMSL. For more information, please contact marvinh@umsl.edu.

The Molecular Transport and Intercalation of Guest Molecules into Hydrogen–Bonded Metal-Organic Frameworks (HMOFs)

By

Greg Anthony Hogan

B.S., Chemistry, University of Louisiana-Lafayette

A DISSERTATION

Submitted to the Graduate School of the

UNIVERSITY OF MISSOURI- ST. LOUIS

In partial Fulfillment of the Requirements for the Degree

DOCTOR OF PHILOSOPHY

In

CHEMISTRY

With an emphasis in Inorganic Chemistry

Advisory Committee
Dr. Alicia M. Beatty
Chairperson

Dr. George Gokel
Dr. Stephen Holmes
Dr. James Chickos

© Copyright 2010
By
Greg A. Hogan

Abstract

The Molecular Transport and Intercalation of Guest Molecules into Hydrogen-Bonded Metal-Organic Frameworks (HMOFs)

(August 2010)

Greg A. Hogan, B.S. University of Louisiana-Lafayette

Chair of Committee: Dr. Alicia M. Beatty

The process of molecular transport and intercalation has been widely studied for many years, resulting in the discovery of molecular frameworks that are capable of hosting guest molecules or ions. Layered and porous metal-organic frameworks (MOFs) have been found to have applications in the field of catalysis, storage, separations, and ion-exchange. More recently, molecular components with peripheral hydrogen-bonding moieties have been used to affect the synthesis of hydrogen-bonded metal-organic frameworks (HMOFs) as an alternative to MOFs, which are interconnected via coordinate-covalent bonds. While MOFs are perhaps stronger materials, HMOFs have the advantage of being easily modifiable and more flexible. Because HMOFs have not been extensively studied for their ability to host molecules, and because their ability to withstand guest loss and guest exchange is essentially unknown, here we report the synthesis and molecular transport properties of both close-packed and porous HMOFs.

Layered materials can mimic the behavior of naturally occurring clays, where guest molecules are absorbed and the layer will expand to accommodate the entering guest molecule. We have created a clay mimic composed of a metal pyridine-dicarboxylates and ammonium counterions (a layered HMOF), which is suitable for studying the ability of such materials to

absorb guest molecules. We can control the distance of the interlayer region, as well as the chemical nature (hydrophobic or hydrophilic) by varying the organic amine. The metal complex contains axial water ligands that are replaceable, and such ligand exchange has precedence in coordination polymer (MOF) systems, and has been termed “coordinative intercalation”. Using the synthesized layered material we examined the process of intercalation, having chosen a variety of guest molecules ranging from alkyl to aryl molecules, each of which have substituents varying in size, shape and electronics. The first set of guest molecules are non-coordinating and are theoretically capable of entering the layer and anchoring freely through the use of non-covalent interactions. The second set of guest molecules contain a pyridine moiety that can exchange with the coordinated water ligand through coordinative-intercalation. The products have been characterized by TGA, DSC, UV-Vis, and powder XRD.

Further work was dedicated to examining porous materials, which were created using organic diamines, rather than simple primary amines, as starting materials. The resulting diammonium cations act as pillars, forming open channels. The predefined channel dimensions allow the insertion of specific sized guest molecules. The walls of the channel are close-packed, so that in theory guest molecules can travel in one direction through the solid. Using the synthesized pillared structure we investigated guest inclusion and selectivity through the process of co-crystallization. The stability of the pillared structure in the absence of guests is also reported, as well as the potential for the empty pillared structure to withstand guest re-insertion and removal.

DEDICATION

This dissertation is dedicated to my loving wife, Crissy, without her devotion and persistence all of this would not be possible.

ACKNOWLEDGEMENTS

I would first like to thank my research advisor Dr. Alicia M. Beatty who has guided and molded me through the years, in efforts to obtain my Ph.D. There were brief moments where I thought the possibility of finishing my Ph.D. would not feasible. I thank her for being patient and believing in me and my potential as a chemist. I would like to thank the Department of Chemistry at the University of Missouri – St. Louis for allowing me to continue the pursuit of my Ph.D. without any extra hassles, especially since I transferred schools. I would like to thank the members of my dissertation committee, Dr. Gokel, Dr. Holmes, and Dr. Chickos, without you the completion my Ph.D. would not be possible. I thank you for your valued experience and expertise, which was bestowed upon me from our multiple conversions during the past two years. Also I would like to thank Dr. Nigam Rath for his dedication and patience when solving my crystal structures, especially modeling the highly disordered guest molecules. Next, I would like to thank Dr. Rudolph Winter and Mr. Joe Kramer for their knowledge and expertise in running the GC/MS. I would also like to thank Mr. Frank May for running and acquiring my initial powder x-ray patterns.

Secondly, I will like to thank my previous committee members when I attended Mississippi State University, Dr. David Wipf, Dr. Steven Gwaltney, Dr. Bill Henry, and Dr. Andrjea Sygula. I appreciate your time and opinions during my studies at Mississippi State University.

Finally, I would to thank all of people who have assisted me in my research who worked with in the lab from our post doctoral researchers to other graduate students to the undergraduate students that I have mentored over the years.

Table of Contents

Page

Abstract ..... **iii**
Dedication ..... **v**
Acknowledgements ..... **vi**
Table of Contents ..... **viii**
List of Figures ..... **xii**
List of Tables ..... **xvii**

Chapter 1: Introduction 1

1.1 Overview of Research Goals 2
1.2 General Introduction to Supramolecular Chemistry 2
1.3 Crystal Engineering 3
1.3.1 Engineering of Organic Solids 5
1.3.2 Engineering of Inorganic Solids 9
1.4 Host/Guest Materials 13
1.4.1 Organic Host-Guest Solids 14
1.4.2 Inorganic Host/Guest Solids 17
1.5 Intercalation Chemistry 20
1.5.1 Classical Examples of Intercalation 21
1.5.2 Intercalation into 2-D Coordination Polymers 22
1.5.3 Intercalation into Hydrogen Bonded Frameworks 23
1.6 Molecular Transport 25
1.7 Conclusion 26
1.8 References 28

Chapter 2: Instrumental Methods **35**

2.1 Introduction 36
2.2 X-Ray Diffraction 36
2.2.1 Methods of Generating X-Rays 37
2.2.2 Laue Equations 39
2.2.3 Braggs's Law 40
2.2.4 Reciprocal Lattice 41
2.2.5 Single Crystal X-Ray Diffraction (SCRXD) 41
2.2.6 Powder X-Ray Diffraction (PXRD) 42
2.3 Thermal Analysis 43
2.3.1 Thermogravimetric Analysis (TGA) 43
2.3.2 Differential Scanning Calorimetry (DSC) 46
2.4 References 48

Chapter 3: Intercalation of Lewis Bases and Non-coordinating Guest Molecules into an Inorganic-Organic Hybrid Material 49

3.1 Background 50
3.2 Goals and Purpose of Research.....50
3.3 Methods.....51
3.4 Experimental 52
3.4.1 Materials and Instruments.....52
3.4.2 Synthesis of Closed Packed HMOF.....53
3.4.3 Intercalation of Non-Coordinating Molecules 55
3.4.4 Coordinative Intercalation of Small Molecules 57
3.4.5 Characterizations.....58
3.5 Intercalation of Non-Coordinating Small Molecules.....59
3.5.1 Results from TGA of Non-Coordinating Molecules 60
3.5.2 Results from DSC of Non-Coordinating Molecules 61
3.5.3 Results from Powder XRD of Non-Coordinating Molecules 62
3.6 Intercalation of Pyridine-based Molecules 64
3.6.1 Results from TGA Analysis of Pyridine Molecules 65
3.6.2 Results from DSC of Pyridine Molecules.....69
3.6.3 Results from Powder XRD of Pyridine Molecules.....70
3.7 Discussion 73
3.8 Conclusion 75
3.9 References.....77

Chapter 4: Construction and Guest Inclusion into Pillared HMOFs 79

4.1 Background 80
4.2 Purpose of Research.....80
4.3 Experimental 81
4.3.1 Materials 81
4.3.2 Experimental Procedures 82
4.4 Guest Molecules used for Co-Crystallization 83
4.4.1 Guests that Showed Inclusion.....84
4.4.2 Guests that did not Show Inclusion 88
4.5 Procedures for Characterized Crystals.....98
4.5.1 Synthesis of [o-tolidinium] $Zn(PDCA)_2(H_2O)_2\cdot$ guest molecule 99
4.6 Characterization of Crystal Structures 99
4.7 Discussion of Crystal Structures Containing Guest Molecules 103
4.7.1 Structure of [o-tolidinium] $Zn(PDCA)_2(H_2O)_2\cdot$ acetone 104
4.7.2 Structure of [o-tolidinium] $Zn(PDCA)_2(H_2O)_2\cdot$ nitrobenzene.....107
4.7.3 Structure of [o-tolidinium] $Zn(PDCA)_2(H_2O)_2\cdot$

p-xylene.....110
4.7.4 Structure of [o-tolidinium] $Zn(PDCA)_2(H_2O)_2 \cdot$ 1-hexanol.....112
4.7.5 Structure of [o-tolidinium] $Zn(PDCA)_2(H_2O)_2 \cdot$ 1-pentanol.....115
4.7.6 Structure of [o-tolidinium] $Zn(PDCA)_2(H_2O)_2 \cdot$ *p*-difluorobenzene.....118
4.8 Stability Studies of the Hydrogen Bonded Framework.....121
4.9 Conclusions.....124
4.10 References.....126

Chapter 5: Small Molecule Transport and Intercalation in Pillared HMOFs.....128

5.1 Background.....129
5.2 Purpose of Research.....129
5.3 Experimental.....130
5.3.1 Materials.....130
5.3.2 Experimental Procedure.....130
5.4 Non-Coordinating Molecules.....131
5.4.1 Aromatic Guest Molecules.....131
5.4.1.1 TGA Results.....134
5.4.1.2 DSC Results.....134
5.4.1.3 Powder XRD Results.....135
5.4.2 Alkyl-based Guest Molecules.....136
5.4.2.1 TGA Results.....139
5.4.2.2 DSC Results.....139
5.4.2.3 Powder XRD Results.....139
5.4.3 Discussion of Non-Coordinating Molecules.....140
5.5 Coordinating Guest Molecules.....142
5.5.1 TGA Results.....144
5.5.2 DSC Results.....145
5.5.3 Powder XRD Results.....145
5.5.4 Discussion of Coordinating Guest Molecules.....146
5.6 Conclusion.....147
5.7 References.....149

Chapter 6: Competition Studies of Mono- and Disubstituted Benzenes into Pillared HMOFs.....150

6.1 Background.....151
6.2 Purpose and Goals of Research.....151
6.3 Determination of Selectivity.....152
6.4 Experimental.....153

6.4.1 Materials and Instruments 153
6.4.2 Experimental Procedures 154
6.4.3 Characterizations.....155
6.5 Results from Competition Reactions 156
6.5.1 Results from Monosubstituted Benzene Studies.....156
6.5.2 Results from Disubstituted Benzene Studies 162
6.6 Discussion of Selectivity.....171
6.7 Conclusion 175
6.8 References.....176

Chapter 7: Conclusions 177

7.1 Concluding Remarks.....178

Appendix A: Crystal Structure Information and Tables.....182

Appendix B: Thermal Analysis Data for Chapter 3 214

Appendix C: TGA Data for Chapter 4 251

Appendix D: Thermal Analysis Data for Chapter 5.....264

Appendix E: Powder X-ray Patterns and Indexing.....352

List of Figures

Page

1.1 Homomeric synthons (a) carboxylic acid-carboxylic acid, (b) amide-amide and (c) pyridone-pyridone; heteromeric synthons (d) carboxylic acid-amide, (e) carboxylic acid-pyridone and (f) amide-pyridone 4

1.2 Crystal structure of isophthalic acid forming a zigzag assembly 6

1.3 Crystal structure of terephthalic acid forming a 1-D chain assembly.....6

1.4 2-D honeycomb network of trimesic acid.....7

1.5 Crystal structure of [Benzylammonium][3,5-pyrazole dicarboxylate] 8

1.6 A building block for Wuest's 3-D hydrogen-bonded network 9

1.7 An example of a 1-D hydrogen-bonded metal containing chain 10

1.8 1-D zigzag hydrogen-bonded network.....11

1.9 Crystal structure of a 2-D hydrogen-bonded grid network containing a Pt(II) metal center 12

1.10 Crystal structure of a 3-D hydrogen-bonded network containing a Cu(I) metal center 13

1.11 Examples of host molecules (a) crown ether, (b) cryptand, and (c) spherands.....14

1.12 A crystal structure of a guanidium disulfonate with an included *p*-xylene guest molecule (shown as a space-filled model).....15

1.13 A pillared framework exhibiting m-xylene selectivity 17

1.14 Crystal structure of a metal complex with included DMF molecules ...18

1.15 A crystal structure of Shimizu's metal containing hydrogen-bonded framework with an included aniline molecule (space filled).....19

1.16 A crystal structure of $[Pt(isonicotinamide)_4][Cl]_2 \cdot 4(isonicotinamide)$. Isonicotinamide guest are shown as space-filled models 20

1.17 A general cartoon showing the intercalation of the green hexagon into a layered material.....21

1.18 A an example of a coordination polymer that is used in an intercalation study 23

1.19 Hydrogen-bonded layered framework with a guest ion residing between the layers 25

1.20 A porous MOF used for gas adsorption 26

2.1 A Schematic of the production of an X-ray 37

2.2 A general schematic of an X-ray tube.....39

2.3 Derivation of Bragg's law for diffraction 41

2.4 An example of a general unit cell with cell parameters.....42

2.5 Theoretical data collected from a TGA. Where H = Host, G = Guest, H·2G refers to a host with two guest molecules 45

2.6A Generalized DSC output and its different process, (a) glass transition, (b) an exothermic peak, and (c) an endothermic peak 47

3.1 Crystal structure of Zn(pyridine-2,4-dicarboxylic acid)$_2$(H_2O)$_2$ 52

3.2 A close-packed layered structure containing benzylammonium groups between the metal-containing layers.....55

3.3 Compilation of TGA spectra associated with intercalation of non-coordinating guest molecules into Ni(4-mBA) layered solid 61

3.4 Compilation of DSC spectra associated with the intercalation of non-coordinating guest molecules into Ni(4-mBA) layered solid 62

3.5 Compilation of powder XRD patterns from the intercalation of non-coordinating molecules into Ni(4-mBA) layered solid. Where (a) Ni(4-mBA), (b) ethyl acetate, (c) pentanol, (d) hexanol, (e) toluene, (f) *p*-xylene, (g) anisole, (h) hydroquinone.....64

3.6 IR comparisons between Ni(4-mBA) starting material (blue) and the pyridine intercalated sample (red) 68

3.7 Compilation of TGA spectra associated with intercalation of pyridine-based molecules into Ni(4-mBA) layered solid.....69

3.8 Compilation of DSC spectra associated with intercalation of pyridine-based molecules into Ni(4-mBA) layered solid.....70

3.9 Compilation of powder XRD pattern from the intercalation of pyridine-based molecules into Ni(4-mBA) layered material. Where (a) Ni(4-mBA), (b) pyridine, (c) 2-picoline, (d) 4-picoline, (e) 4-ethylpyridine, (f) 4-cyanopyridine, (g) 4,4′-bipyridine, (h) 4-*t*-butylpyridine, (i) 4-N,N'dimethylaniline, and (j) 4-chloropyridine. 73

4.1 The synthetic approach for creating a pillared framework 83

4.2 Open channels showing the voided area: (a) view down the a axis and (b) rotated 90° 84

4.3 The hydrogen bonded layer (showing the ammonium – carboxylate Hydrogen bonding) 103

4.4 Packing diagram of the pillar containing acetone.....106

4.5 Packing diagram of the pillar containing nitrobenzene 108

4.6 Packing diagram of the pillar containing p-xylene 111

4.7 Packing diagram of the pillar containing hexanol 114

4.8 Packing diagram of the pillar containing pentanol 117

4.9 Packing diagram of the pillar containing p-difluorobenzene.....120

4.10 Stability of the hydrogen-bonded framework study showing the repeated inclusion of ethyl acetate (Bottom pattern is the crystallized solid and the repeated attempts to include ethyl acetate, 1-7 trials) 123

4.11 Combined PXRD patterns after the guest was removed (bottom pattern is the sonicated trial 1 and above are subsequent trials). 124

5.1 PXRD patterns from aromatic guests: (a) benzene, (b) toluene, (c) anisole, (d) cumene, (e) *p*-diethylbenzene, (f) *p*-difluorobenzene, and (g) *p*-dichlorobenzene, and (h) theoretical pattern from single crystal XRD containing an acetone guest molecule.....136

5.2 PXRD patterns from the alkyl-based guest molecules: (a) pentane, (b) decane, (c) hexanol, (d) nonanol, (e) ethyl acetate, and (f) cyclohexane, (g) theoretical powder pattern from single crystal XRD containing an acetone guest molecule 140

5.3 PXRD patterns from pyridine-based guest molecules: (a) pyridine, (b) 2-picoline, (c) 4-picoline, (d) 4-ethylpyridine, (e) 4-cyanopyridine, (f) 4-*t*-butylpyridine, and (g) theoretical powder pattern from single crystal XRD containing an acetone guest molecule.....146

6.1 Various options in determining selectivity: (a) moderate selectivity, (b) high selectivity, (c) concentration dependent and (d) no selectivity 153

6.2 Selectivity plot of toluene vs. nitrobenzene study 157

6.3 Selectivity plot of toluene vs. anisole study.....158

6.4 Selectivity plot of toluene vs. hexanol study 159

6.5 Selectivity plot from toluene vs. iodobenzene study 160

6.6 Selectivity plot from toluene vs. ethyl acetate study 161

6.7 Selectivity plot of nitrobenzene vs. iodobenzene study.....162

6.8 Combined selectivity plots from *p*-xylene vs. *p*-difluorobenzene study.....163

6.9 Combined selectivity plots from *p*-xylene vs. *p*-diethylbenzene study.....164

6.10 Combined selectivity plot from *p*-diethylbenzene vs. *p*-difluorobenzene study.....165

6.11 Combined selectivity plot from *m*-xylene vs. *m*-difluorobenzene study.....166

6.12 Combined selectivity plot from *m*-xylene vs. *m*-diethylbenzene study.....167

6.13 Combined selectivity plot from *m*-diethylbenzene vs. *m*-difluorobenzene study.....168

6.14 Combined selectivity plot from *o*-xylene vs. *o*-difluorobenzene study.....169

6.15 Combined selectivity plot from *o*-xylene vs. *o*-diethylbenzene study.....170

6.16 Combined selectivity plot from *o*-difluorobenzene vs. *o*-diethylbenzene study.....171

6.17 Guest ranking from competition studies 174

List of Tables

Page

3.1 Non-polar molecules for intercalation studies 56

3.2 The pyridine-based guest molecules 57

3.3 TGA results showing the weight loss for each intercalation sample 60

3.4 Powder XRD data for the *100*, *010* and *001* parameters and a Δ d-spacing value 63

3.5 Different pyridine possibilities and experimental TGA results (SM = starting material, G = guest, and W = water ligand) 66

3.6 Powder XRD data for the *100*, *010* and *001* parameters and a Δ d-spacing value 71

4.1 Guest molecules that co-crystallized with the pillared framework 85

4.2 Guest molecules that did not co-crystallize with the pillared framework (# indicates melting point) 89

4.3 Crystallization information 99

4.4 Weight losses (expected and actual) for each crystal structure 104

5.1 Non-coordinating aromatic guest molecules, molecular weight, TGA results, and conclusion on intercalation (by PXRD) 131

5.2 Alkyl-based guest molecules, molecular weight, TGA results, and conclusion on intercalation (by PXRD) 137

5.3 A list possible coordinating guest molecules, molecular weight, TGA results, conclusion on intercalation (by PXRD). 143

6.1 General amounts of each guest molecule used in a competition reaction 155

Chapter 1

Introduction

1.1 Overview of Research Goals

The design of crystalline materials has been an ongoing theme in the area of supramolecular chemistry, where non-covalent interactions bring a variety of molecules and complexes together, leading to new materials. This idea of using non-covalent interactions to crystallize solids is the central theme of crystal engineering, which is sub-field of supramolecular chemistry. Crystal engineering can be viewed simplistically as building a crystalline structure, where molecules are bricks, and the mortar that holds the bricks together are attractive intermolecular interactions. The major goals are developing reliable and reproducible syntheses of materials with specific and tunable properties, and using these materials for e.g. chemical separations,[1-3] non-linear optical,[4,5] magnetic,[6,7] or catalytic properties.[8-10] In particular, the research presented here will focus on synthesizing host frameworks capable of including, intercalating, and exchanging guest molecules, following the methods for intermolecular design and synthesis that have been developed by supramolecular chemists and crystal engineers.

1.2 General Introduction to Supramolecular Chemistry

Supramolecular chemistry means, literally, "chemistry beyond the molecule." The term was coined by Jean Marie Lehn[11] to describe chemistry that involves interactions between molecules, rather than chemistry involving covalent bonds. The area of supramolecular chemistry is one of the most vigorous and fast-growing fields of chemical endeavor. The research focuses on the use of non-covalent interaction to create supermolecules or develop extended array of molecules. The non-covalent

interactions used are typically ion-ion (100-350 kJ/mol), ion-dipole (50-200 kJ/mol), dipole-dipole (5-50 kJ/mol), hydrogen bonding (4-120 kJ/mol), cation-π (5-80 kJ/mol), π-π (0-50 kJ/mol), and van der Waals forces (<5 kJ/mol).[11-13] Supermolecules can be thought of as an aggregate of molecules that are held together by these non-covalent interactions. Extended arrays and networks of molecules that form crystalline solids are the focus of crystal engineers.

1.3 Crystal Engineering

Crystal engineering involves the prediction, design and synthesis of novel synthetic crystalline solids, using knowledge of intermolecular interactions and supramolecular synthons. This term was coined by Gerhard Schmidt[14] when looking at how a specific orientation of neighboring molecules led to the solid state photodimerization of trans-cinnamic acid. Supramolecular synthons,[15-19] as defined by Desiraju[18-20] are reoccurring intermolecular motifs within a solid state structure. Because the work presented herein focuses on the use of hydrogen-bonding to yield crystalline materials, some common hydrogen-bonding synthons are shown in Figure 1.1. These include homomeric dimers (e.g. carboxylic acid dimers, amide-amide, etc.) and heteromeric interactions such as (acid-amide, pyridone-carboxylic acid, etc.)

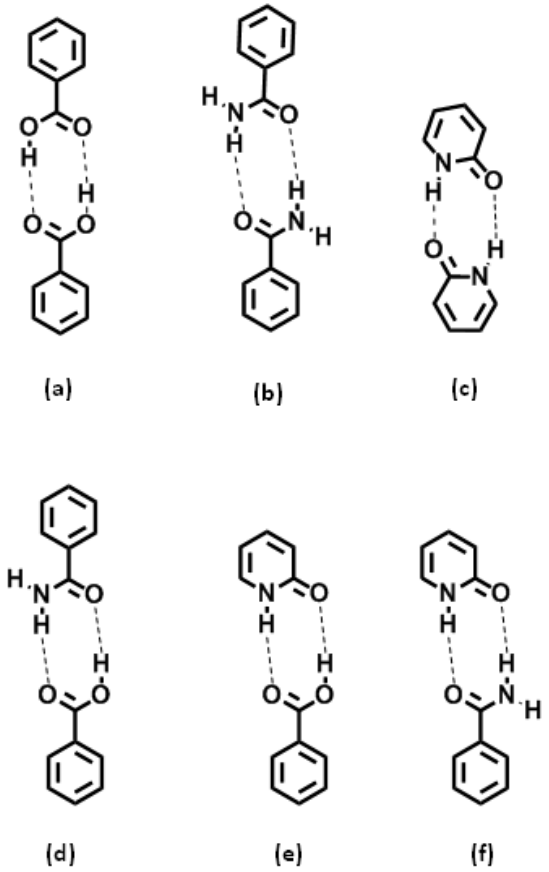

Figure 1.1 Homomeric synthons (a) carboxylic acid-carboxylic acid, (b) amide-amide and (c) pyridone-pyridone; heteromeric synthons (d) carboxylic acid-amide, (e) carboxylic acid-pyridone and (f) amide-pyridone.

As seen in Figure 1.1, hydrogen bonding occurs between hydrogen atoms that are covalently bonded to an electronegative atom such as oxygen or nitrogen (the hydrogen-bond donor) and another electronegative atom, which acts as the acceptor. The rules for hydrogen-bonding were devised by Margaret Etter in 1990, and are known as Etter's Rules. These rules are as follows: [21]

1. "All good proton donors and acceptors are used in hydrogen bonding."

2. “Six-membered-ring intramolecular hydrogen bonds form in preference to intermolecular hydrogen bonds.”
3. “The best proton donors and acceptors remaining after intramolecular hydrogen bond formation form intermolecular hydrogen bonds to one another.”

The rules, in combination with knowledge about hydrogen-bonding synthons, can be used to predict the structural outcome of bringing together molecules in the solid state. Although other intermolecular forces are known and are commonly used, the work presented here is based on hydrogen-bonding. Therefore, the development of hydrogen-bonding solids is described below.

1.3.1 Engineering of Organic Solids

Organic molecules can be used to generate solids having discrete (0-D) or extended (1-D, 2-D or 3-D) motifs. The formation of these different motifs depends on the size and shape of these molecules involved, as well as on the spatial orientation of the hydrogen bonding substituents. When looking at discrete (0-D) organic solids, a simplistic example is benzoic acid. As seen in Figure 1.1, benzoic acid forms a hydrogen-bonded dimer in the solid-state. The dimer is a 0-D assembly – in other words, the hydrogen bonding does not lead to an infinite network.

In order to engineer 1-D hydrogen bonding networks in organic solids, synthons should be linear, with hydrogen bonding substituents arranged at 120° - 180° for zig-zag or linear motifs, respectively. An example of a zig-zag motif is found with the structure of isophthalic acid. Because the carboxylic acid groups are

oriented at 120° angles with respect to each other, the solid-state structure of isophthalic acid exhibits a zig-zag structure, as shown in Figure 1.2.

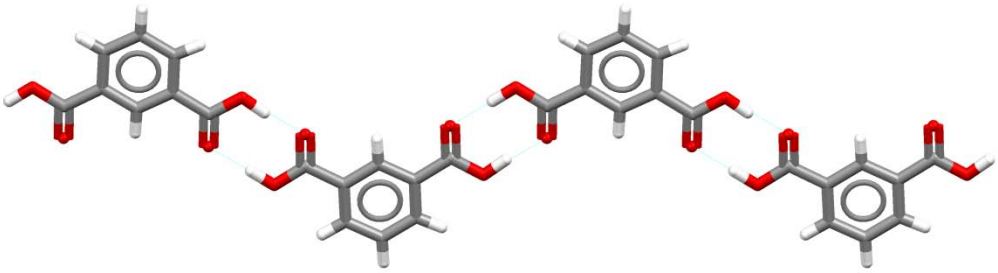

Figure 1.2 Crystal structure of isophthalic acid forming a zigzag assembly.[22]

Terephthalic acid, on the other hand, makes a straight chain assembly, because in this molecule the carboxylic acid groups are oriented linearly, as shown in Figure 1.3.

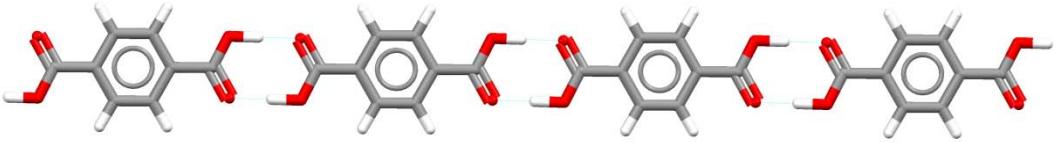

Figure 1.3 Crystal structure of terephthalic acid forming a 1-D chain assembly.[23]

The creation of a 2-D organic assembly requires molecular components that contain multiple complementary functional groups that are oriented so as to form hydrogen bonds in two dimensions. For example, trimesic acid, (1, 3, 5-benzene tricarboxylic acid) generates a 2-D honeycomb network in the solid state via carboxylic acid, Figure 1.4.[24]

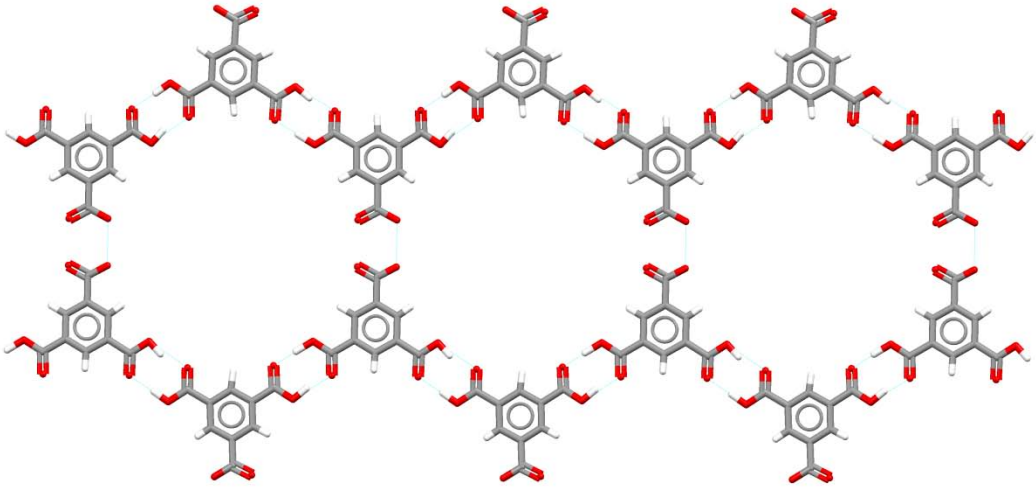

Figure 1.4 2-D honeycomb network of trimesic acid.[24]

Mixtures of two different molecules or ions can also be used in crystal design. An example of a 2-D assembly that is composed of organic ions has been presented by Beatty and co-workers,[25,26] where a lamellar structure results from mixing 3, 5-pyrazole dicarboxylic acid with a variety of primary amines. The lamellar structure is generated by charge-assisted ammonium-carboxylate hydrogen bonds, which are very strong hydrogen bonds due to an additional electrostatic effect. This is a close-packed system where the ionic layers are separated by a hydrophobic interlayer, Figure 1.5.

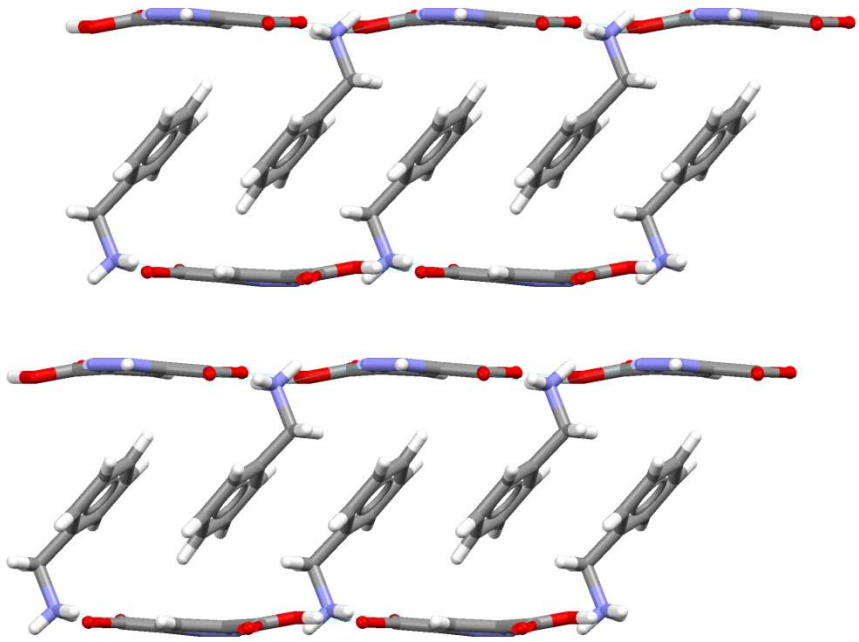

Figure 1.5 Crystal structure of [Benzylammonium][3,5-pyrazole dicarboxylate].[25]

In order to engineer a 3-D hydrogen bonded organic network, the organic components used must contain a 3-D arrangement of multiple hydrogen bond functionalities. One example of a 3-D network was created by Wuest and co-workers,[27-29] where they developed a silicon-based tetrahedral molecule that contains four pyridone moieties. The molecules are connected via homomeric pyridone – pyridone hydrogen bonds to form a diamondoid 3-D network, Figure 1.6.[28]

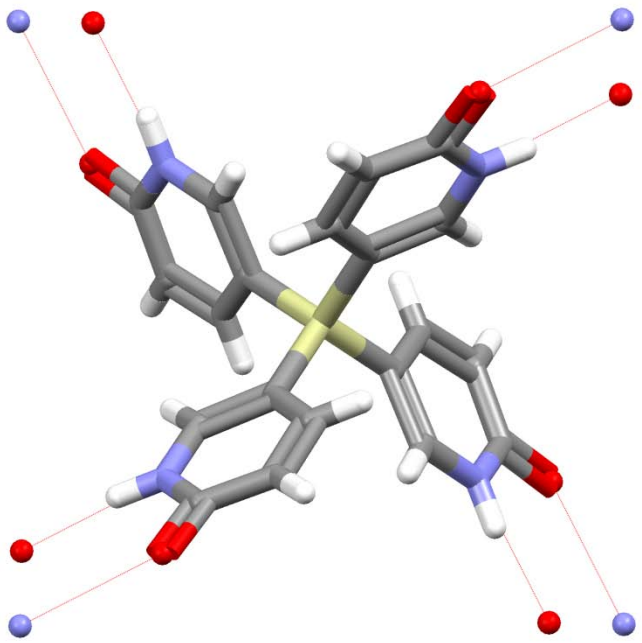

Figure 1.6 A building block for Wuest's 3-D hydrogen-bonded network.[29]

It is important to note that the organic hydrogen bonded frameworks can be stable to guest loss. Some of Wuest's hydrogen bonded organic frameworks are stable to guest loss and exchange[27-30].

1.3.2 Engineering of Inorganic Solids

Inorganic assemblies can also be functionalized to yield discrete (0-D) and extended 1-D, 2-D, 3-D motifs. There are two main types of interactions that yield extended assemblies: coordinate-covalent and hydrogen bonds. Because many coordination geometries are available, the architecture can be influenced using ions that give linear, trigonal, tetrahedral or octahedral geometries. The use of strictly coordinate-covalent bonding leads to a class of materials called coordination

polymers,[31] which are discussed in greater detail in section 1.4.2. The following discussion focuses on extended hydrogen bonded assemblies (1-D – 3-D) of coordination compounds.

The development of 1-D inorganic hydrogen-bonded networks is controlled by the use of peripheral hydrogen bonding moieties and by geometric control of the metal ion. They can be created by using linear Ag(I), square planar Pd(II), or octahedral Fe(II) complexes, where the hydrogen bonding ligands are in a trans-configuration. A good example of a linear assembly that contains Ag(I) is the $[Ag(isonicotinamide)_2]^+$ complex, where homomeric hydrogen bonding occurs between the isonicotinamide substituents.[32] In this structure, the hydrogen bonds and the ligands form a near-linear assembly, Figure 1.7.

Figure 1.7 An example of a 1-D hydrogen-bonded metal containing chain[32]

Other 1-D assemblies that can be created through hydrogen-bonding are zigzag, chains, ladders, and ribbons. These assemblies can be created by varying the position of the hydrogen-bonding functional group, similar to the orientation in the organic structures discussed in section 1.3.1. For example, while isonicotinamide ligands lead to straight linear chains (Figure 1.7), nicotinic acid ligands yield zig-zag chains, Figure 1.8.[33] In this structure, the metal center is 4-coordinate, but two of the ligands

are not capable of forming strong hydrogen bonds, thus allowing only a 1-D arrangement.

Figure 1.8 1-D zigzag hydrogen-bonded network.[33]

Creating grid-like or lamellar 2-D networks through hydrogen-bonding can result from square planar,[34] octahedral,[35,36] or even linear metal complexes.[37] Some of the common metal ions that are used in the formation of 2-D networks are Pt(II), Pd(II), Ni(II), and Co(II). For example, a 2-D grid structure forms when Pt(II) metal ions are combined with isonictinic/nicotinate ligands,[34] Figure 1.9.

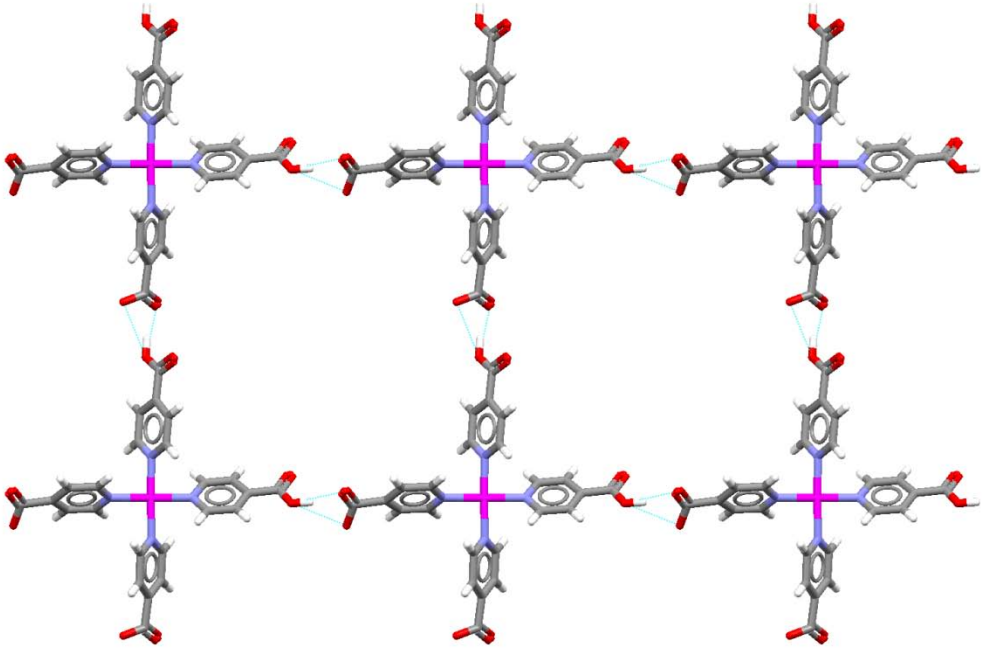

Figure 1.9 Crystal structure of a 2-D hydrogen-bonded grid network containing a Pt(II) metal center.

One of the first known examples of a 3-D hydrogen bonded coordination network was generated by Munakata and co-workers,[38,39] where the framework was based on $[Cu(3\text{-cyano-6-methyl-2-pyridinone})_4]^+$. This molecule is structurally similar to the tetrahedral organic molecules used by Wuest (Section 1.3.1). If the counter-ion used in the synthesis is hexafluorophosphate or triflate, head-to-head pyridone - pyridone hydrogen bonds create a diamondiod 3-D network, Figure 1.10. Some of these networks also create space that is filled with solvent or other guest molecules.[40,41]

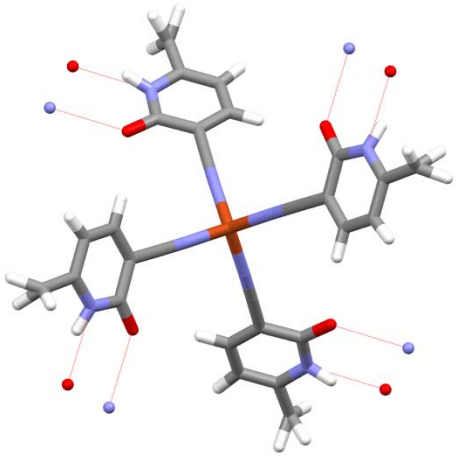

Figure 1.10 Crystal structure of a 3-D hydrogen bonding building block containing a Cu(I) metal center.

1.4 Host/Guest Materials

Using a Crystal Engineering approach, it is also possible to design materials for host-guest applications. Host/guest chemistry can be viewed as the study of large 'host' molecules or networks that are capable of enclosing smaller 'guest' molecules via non-covalent interactions. Some of the common host molecules are classics in supramolecular chemistry, and include crown ethers,[42] cryptands,[43] and spherands.[44] These molecules have electron-donating atoms pointed toward the center of the molecule, which bind to metal cations, and can be modified to selectivity bind cations. Examples of these classic host molecules are shown in Figure 1.11.

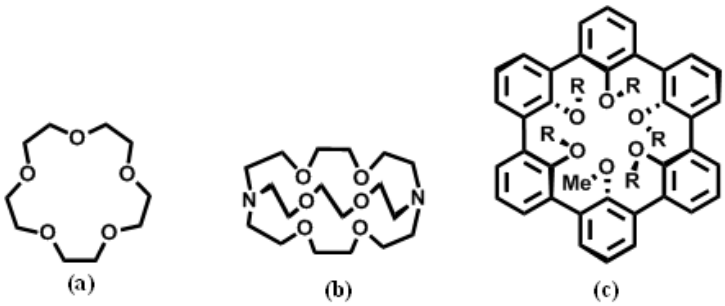

Figure 1.11 Examples of host molecules (a) crown ether, (b) cryptand, and (c) spherands.

Host frameworks typically contain 2-D or 3-D networks. For example, 2-D host frameworks can absorb guest molecules in the interlayer region, with guest molecules varying from water to solvent to ions, depending on the nature of the layer and the interlayer region (e.g. hydrophobic/hydrophilic). On the other hand, 3-D networks such as zeolites have cavities in which the guest molecules reside. Synthetic 2-D and 3-D host/guest solids are discussed in the following sections.

1.4.1 Organic Host-Guest Solids

Organic molecules can be tailored to produce "organoporous" networks, connected through hydrogen-bonding. Using molecular design and organic synthetic methodology, the rational manipulation of void size, shape, and chemical environment can be achieved. This can lead to a library of "organoporous" materials that contain different void dimensions and chemical properties. For example Ward and co-workers[45-54] have created reproducible and robust hydrogen-bonded

frameworks using guanidium organosulfonates that form predictable layered frameworks. The layer comprises guanidium cations and sulfonate anions that are connected via complementary charge-assisted hydrogen bonds. The nature of the interlayer region varies depending on the organic group of the organosulfonate. When disulfonates are used, a porous framework is generated, yielding a pillared structure. One example is a guanidium disulfonate that has included *p*-xylene guest molecules from solution, Figure 1.12.

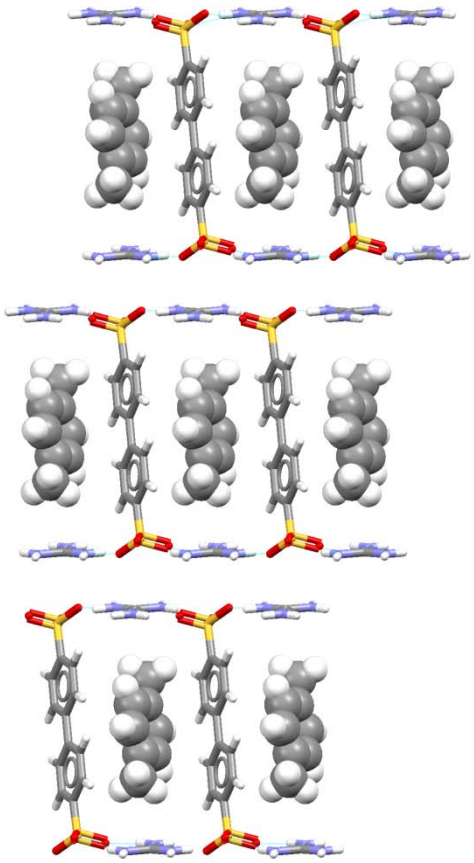

Figure 1.12 A crystal structure of a guanidium disulfonate with an included *p*-xylene guest molecule (shown as a space-filled model).

The method of inclusion by crystallization has been used successfully to separate isomers of small molecules in solution. For example, Nassimbeni and Toda[55] chose 1, 1, 2, 2-tetraphenylethane-1, 2-diol as a host and were successful in separating picoline, methylquinoline, and lutidine isomers. To do this, the diol host and the competing guest molecules were dissolved in a solution and allowed to crystallize. The crystals were then treated with gentle heat to remove to the guest molecules from the crystalline material and then analyzed through GC/MS. Similar experiments are discussed in Chapter 6.4. Other studies have led to the successful separation of aminobenzonitrile isomers, and cresol, phenylenediamines, and benzenediol isomers.[56,55]

The Ward group[46,57] has also looked into the determination of selectivity for certain guest molecules using their **GS** hosts. For example, a guanidinium p-toluenesulfonate framework was used in the separation of xylene isomers. The competition studies were performed through co-crystallization of the host and guest, and the analysis of the competition reactions were performed through the use of GC/MS. The framework was found to be selective for m-xylene, Figure 1.13.

While the hydrogen bonding used to connect these complexes results in lower thermal stability, it offers one clear advantage, because the guest molecule can be retrieved by disassembly of the organic host under mild conditions, usually by dissolution in an appropriate solvent.

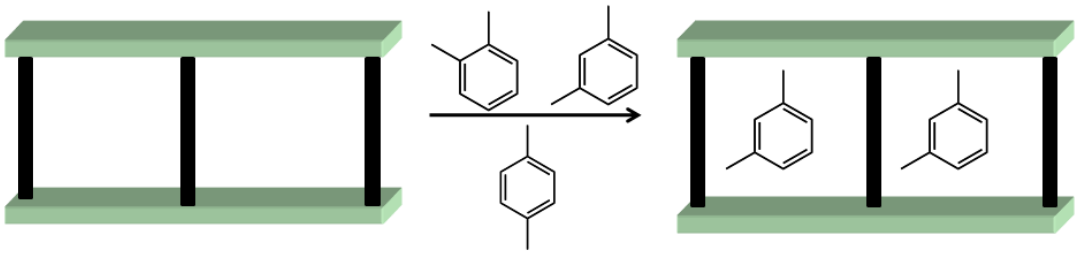

Figure 1.13 A pillared framework exhibiting m-xylene selectivity.

1.4.2 Inorganic Host/Guest Solids

While organic hydrogen bonded frameworks have been studied extensively, less work has been done on the design and synthesis of hydrogen bonded metal organic frameworks (HMOFs). Extensive research has been conducted on networks containing only coordinate-covalent bonds, which are known as coordination polymer networks. Coordination polymer-based frameworks have shown a tendency to include a variety of guest molecules from gases (N_2, CO_2, CH_4 and Ar)[58-60] to slightly larger molecules that ranges from solvents to benzene-based molecules.[61,62] These metal-organic frameworks can absorb guest molecules, and guests can also be included via co-crystallization, where the host complex crystallizes around the guest molecule. For example, Kitagawa,[63-65] used dicarboxylates, in combination with metal ions, to create a 2-D coordination polymer that co-crystallized with DMF solvent molecules, Figure 1.14.

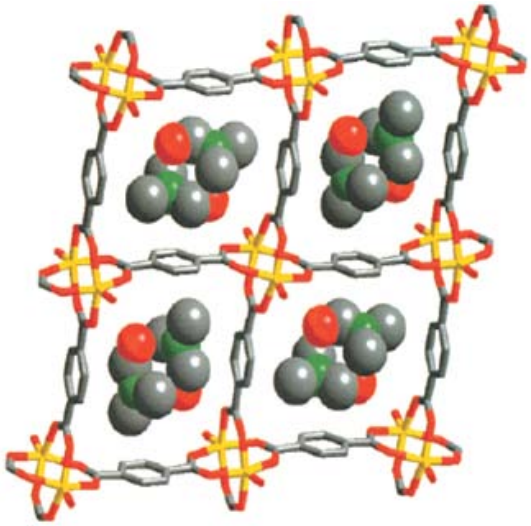

Figure 1.14 Crystal structure of a metal complex with included DMF molecules.

Coordination polymers can have high thermal stability, owing to the coordinate covalent bonding that holds the framework together, and therefore the removal and insertion of the guest molecules can occur without disruption of the framework.[31,64,66]

HMOFs, because they are connected via hydrogen bonds,[67] can be seen as the inorganic counterpart of the organic hydrogen-bonded networks. As discussed previously (section 1.3.2), coordination chemistry has a lot to offer in the area of developing hydrogen-bonded networks because of the variety of coordination geometries that are provided by metal ions in a variety of oxidation states. These same strategies can be used to create porous or channeled host-guest frameworks.

Akin to Ward's organic guanidinium-sulfonate frameworks, Shimizu and co-workers[68-74] have developed some metal hexaamine cations combined with disulfonate anions that form hydrogen-bonded networks and include guest molecules. The layer is composed of a complex metal cation $[Co(NH_3)_6]^{3+}$ connected via hydrogen bonds to sulfonate anions, Figure 1.15.

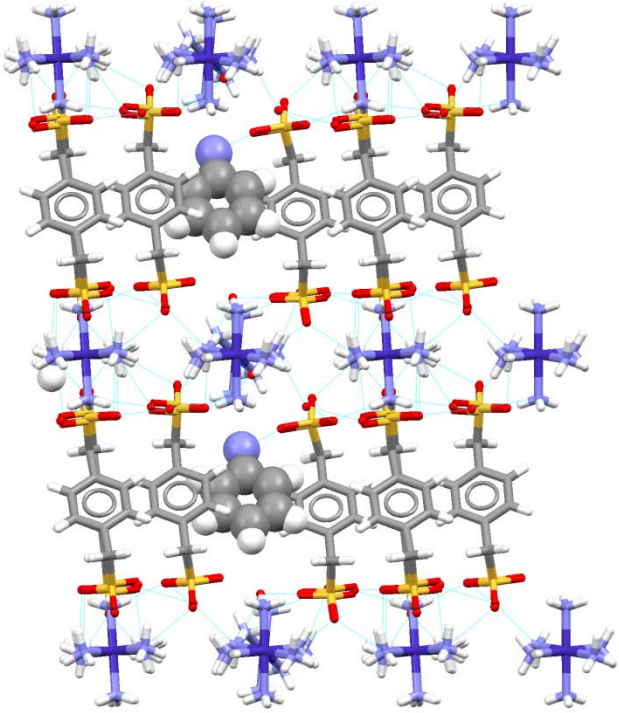

Figure 1.15 A crystal structure of Shimizu's metal containing hydrogen-bonded framework with an included aniline molecule (space filled).

The organic group of the sulfonate is aryl, and the structure houses aniline guest molecules. The aniline guest molecule exhibits some hydrogen-bonding to the disulfonate anion, and the extra cooperative interaction anchors the guest in the framework.

Another example of inorganic hydrogen-bonded assemblies as hosts was reported by Aakeroy and Beatty,[75,76] where $[Ni(4\text{-isonicotinamide})_4][Cl]_2$ forms a grid-like 3-D structure using a combination of amide-amide and amide-chloride hydrogen bonds. Isonicotinamide guest molecules are located in the void spaces, Figure 1.16. Again, hydrogen bonds between the host and guest molecules anchor the

guests in the framework. However, some host-guest systems contain mobile and/or exchangeable guests, as discussed in Section 1.5.

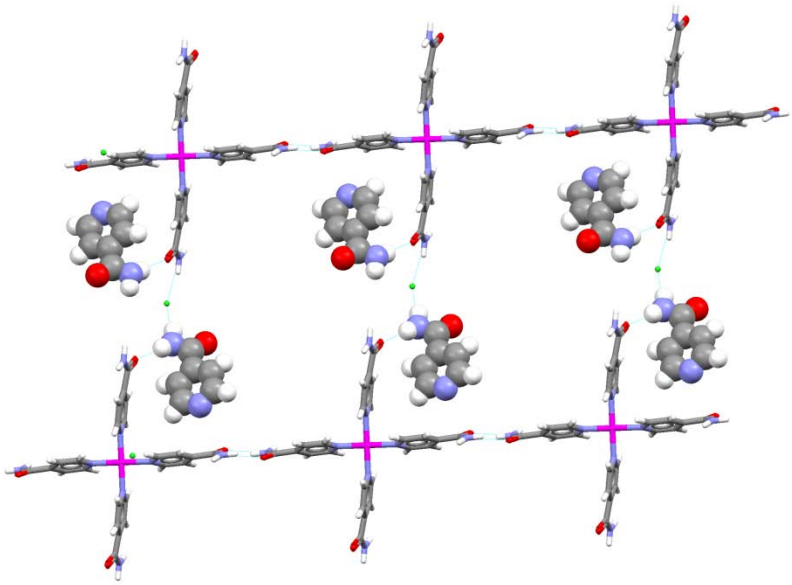

Figure 1.16 A crystal structure of $[Pt(isonicotinamide)_4][Cl]_2 \cdot 4(isonicotinamide)$. Isonicotinamide guest are shown as space-filled models.

1.5 Intercalation Chemistry

Intercalation is the insertion of guest molecules into a layered solid (while the solid remains intact), and has been observed in studies of graphite,[77] naturally occurring clays,[78] and other layered solids.[79,80] A general scheme of intercalation can be found in Figure 1.17. Intercalation is often confused with molecular encapsulation, inclusion, and co-crystallization because all result in host/guest compounds.

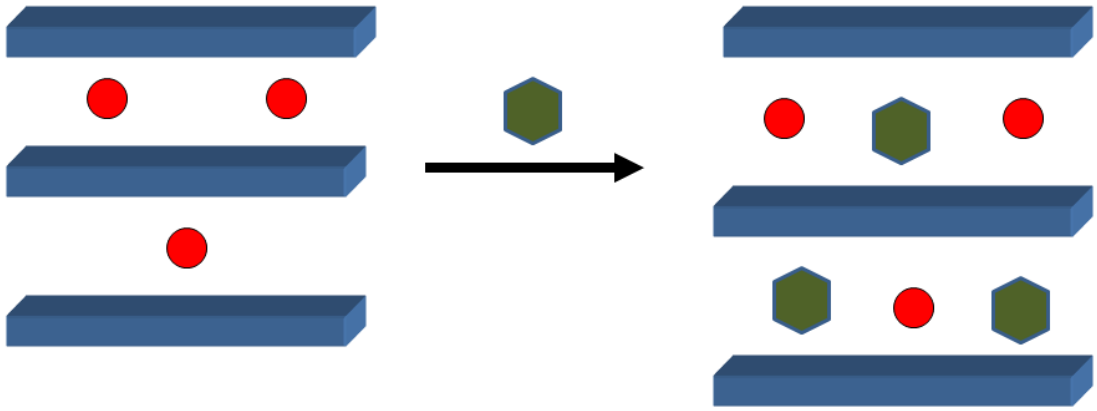

Figure 1.17 A general cartoon showing the intercalation of the green hexagon into a layered material.

While intercalation entails the transport of molecules and ions in an existing host framework, molecular encapsulation and inclusion compounds occur through co-crystallization. That is, the guests are incorporated during the crystallization process; the host and guest crystallize from solution simultaneously.

1.5.1 Classical Examples of Intercalation

Layered aluminosilicates, or clays, have been widely studied for their ability to intercalate ions and neutral molecules, such as water or other solvents.[81] For example, a recent review article[82] describes the use of natural and modified kaolinite and montmorillonite to adsorb heavy metals from aqueous solutions. These clays were soaked in aqueous solutions of As(III), Cd(II), Cr(III), Co(II), Cu(II), Fe(II), Pb(II), Mn(II), Ni(II), and Zn(II), and the heavy metal ions were adsorbed between the aluminosilicate layers.

Some research has been done on materials that mimic the aluminosilicate layered structure found in natural clays. For example, manganese oxide layered

materials have been shown to intercalate large metal complex cations[83] such as $[Co(H_2O)_6]^{3+}$, $[Co(NH_3)_5Cl]^{3+}$, and $[Co(NH_3)_6]^{3+}$. In other studies of intercalation of amines into layered materials has been examined. For example, potassium calcium niobium oxide ($KCa_2Nb_3O_{10}$) was used, and this metal oxide framework was exposed to an excess amount of octylamine in heptane.[84] An acid-base reaction occurred, and the potassium counter ion was replaced by an octylammonium cation.

1.5.2 Intercalation into 2-D Coordination Polymers

There have been some of examples of intercalation into lamellar coordination polymer frameworks. Clearfield,[85,86] Kitagawa,[65,87,88] and Fujita[61,62,89] have been involved in such work. These studies generally entail the inclusion of small molecules and gases such as NH_3, alkyl amines, CO_2, CH_4, DMF, DMSO, and benzene. Since the layers in clays are made up of metal-oxide bonds, other researchers have made synthetic clays by creating metal-oxide bonds using phosphonates,[85,86,90-92] phosphates,[93-95] mixed phosphonates,[85,96] chalcogenides,[97,98] and other metal-based coordination polymers.[87,99,100] These layered materials have been known to intercalate small molecules such as ammonia,[86] alkyl amines,[91] and polyether amines.[101] The nature (hydrophobic, hydrophilic) of the interlayer can be altered by using suitable chemical components in the synthesis. The solids can "swell" (the interlayer distance can expand) to accommodate a wide variety of guests, either neutral guest molecules or charged species.[78]

The Clearfield group performed a studies of intercalation that involved the use of ammonia and short alkyl amines[86] into layered zirconium phenylphosphonates, as

seen in Figure 1.18. The metal ion is coordinated to two water ligands, so the solid was subjected to heat and vacuum in to remove these ligands and create a coordinatively unsaturated metal ion. Afterwards, gases of ammonia or alkyl amines were added to the solid. The goal was to have the nitrogen-based molecule coordinate to the metal center, which was shown to be successful in the examples of ammonia and short alkyl amines (# of carbon's < 6). Intercalation of guests that coordinate to the metal center is called "coordinative intercalation" by Clearfield.[102]

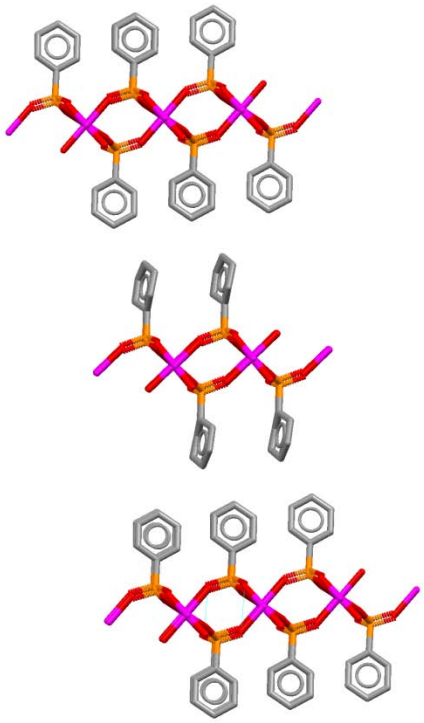

Figure 1.18 A an example of a coordination polymer that is used in an intercalation study.

1.5.3 Intercalation into Hydrogen-Bonded Frameworks

Hydrogen bonded frameworks have also been studied, and groups have claimed to observe intercalation, [69-71,103,104] but often it seems more likely that the frameworks are dissolved and recrystallized around the new guest. For example, Kitagawa studied a hydrogen-bonded framework generated from an iron – chloroanilate complex,[105,106] where the hydrogen-bonded layer extends from peripheral oxygen groups to coordinated water ligands. The "guest" is the pyridinium counterion, which balances the overall charge. This "guest" can be exchanged by other ions by placing the solid material in an ethanol/acetonitrile solution containing other "guest" ions, such as 4, 4'-bipyridinium and ferrocenium. These new counterions did replace the original pyridinium counterions; however, because the cation is an integral part of the structure and because the solution is quite polar, it seems more likely dissolution and recrystallization than intercalation. An example of the iron-chloroanilate framework with decamethyl ferrocenium counter ion is shown in Figure 1.19.

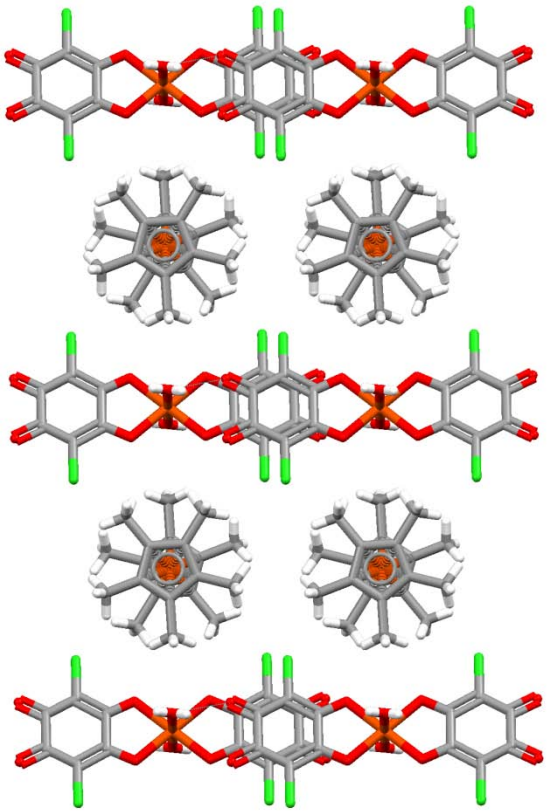

Figure 1.19 Hydrogen-bonded layered framework with a guest ion residing between the layers.[105]

1.6 Molecular Transport

While host/guest chemistry is important, molecular transport is also an important consideration. Transport of ions and molecules through membranes is important biologically, and concerted motion of guest molecules within a crystalline solid can also lead to interesting properties. For example, the Hollingsworth[107,108] group noticed an unanticipated large guest motion in a hydrogen bonded urea host. Urea crystallizes in the presence of guest molecules to form a 3-D hydrogen bonded

“honeycomb” network, where the guest molecules reside in the channels of the honeycomb. When the guest is a halide-substituted cyanohexane [$X(CH_2)_6CN$, where X = Cl or Br], the guest molecules moves 5.5Å when mechanical stress is applied to the crystal. Once the stress was removed from the crystalline solid, the guest showed a reversible return to its original domain. Guest molecules can also be added or removed from a synthetic host framework. For example, the cubic porous MOFs synthesized by Yaghi shows gas adsorption and loss,[109] Figure 1.20.

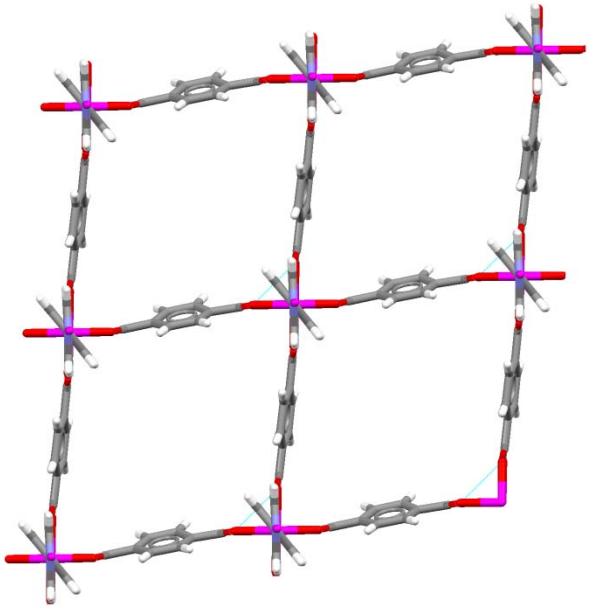

Figure 1.20 A Porous MOF used for gas adsorption.

1.7 Conclusion

The research discussed in the following chapters concerns the synthesis of close-packed and porous HMOFs, using a combination of coordination complexes (metal dicarboxylic acids) and organic counterions (from amine and diamine starting

materials) crystallized from solution. These crystalline solids have been used to pursue our interest in determining the following:

1. Can we use crystal engineering principles to reliably, reproducibly, and predictably construct layered hydrogen bonded metal organic frameworks (HMOFs)?
2. Historically, hydrogen bonded materials have been considered too weak to be useful. Can we construct HMOFs that are thermally stable and capable of host/guest selectivity, intercalation, and guest exchange?

The answers to these questions can be found in the following chapters.

1.8 References

(1) Jacobs, A.; Nassimbeni, L. R.; Nohako, K. L.; Su, H.; Taljaard, J. H. *Cryst. Growth & Des.* **2008**, *8*, 1301-1305.

(2) Bourne, S. A.; Corin, K. C.; Nassimbeni, L. R. *Supramol. Chem.* **2006**, *18*, 587-592.

(3) Nassimbeni, L. R. *Acc. Chem. Res.* **2003**, *36*, 631-637.

(4) Muthuraman, M.; Masse, R.; Nicoud, J.-F.; Desiraju, G. R. *Chem. Mater.* **2001**, *13*, 1473-1479.

(5) Evans, O. R.; Lin, W. *Acc. Chem. Res.* **2002**, *35*, 511-522.

(6) Stumpf, H. O.; Quahab, L.; Pei, Y.; Grandjean, D.; Kahn, O. *Science* **1993**, *261*, 447.

(7) Kahn, O. *Acc. Chem. Res.* **2000**, *33*, 647-657.

(8) Pluth, M. D.; Bergman, R. G.; Raymond, K. N. *J. Am. Chem. Soc.* **2008**, *130*, 11423-11429.

(9) Kang, J.; Rebek, J., Jr. *Nature* **1997**, *385*, 50-52.

(10) Endo, K.; Koike, T.; Sawaki, T.; Hayashida, O.; Masuda, H.; Aoyama, Y. *J. Am. Chem. Soc.* **1997**, *119*, 4117-4122.

(11) Lehn, J.-M. *Supramolecular Chemistry: Concepts and Perspectives*; 1 ed.; VCH: Weinheim, Germany, 1995.

(12) Steed, J. W.; Atwood, J. L. *Supramolecular Chemistry*; 1 ed.; John Wiley & Sons, Ltd: Chichester, UK, 2000.

(13) Steed, J. W.; Turner, D. R.; Wallace, K. J. *Core Concepts in Supramolecular Chemistry and Nanochemistry*; 1 ed.; John Wiley & Sons: West Sussex, 2007.

(14) Schmidt, G. M. J. *Pure Appl. Chem.* **1971**, *27*, 647-678.

(15) Desiraju, G. R. *Angew. Chem., Int. Ed.* **2007**, *46*, 8342-8356.

(16) Desiraju, G. R. *Journal of the Indian Chemical Society* **2003**, *80*, 151-155.

(17) Braga, D.; Desiraju, G. R.; Miller, J. S.; Orpen, A. G.; Price, S. L. *CrystEngComm* **2002**, *4*, 500-509.

(18) Desiraju, G. R. *Stimul. Concepts Chem.* **2000**, 293-306.

(19) Desiraju, G. R. *Angew. Chem., Int. Ed. Engl.* **1995**, *34*, 2311-2327.

(20) Desiraju, G. R. *Crystal Engineering: The Design of Organic Solids*; Elsevier: New York, 1989.

(21) Etter, M. C. *Acc. Chem. Res.* **1990**, *23*, 120-126.

(22) Derissen, J. L. *Acta Crystallogr. Sect. B* **1974**, *30*, 2764.

(23) Bailey, M.; Brown, C. J. *Acta Crystallogr.* **1967**, *22*, 387.

(24) Duchamp, D. J.; Marsh, R. E. *Acta Crystallogr.* **1969**, *B25*, 5-19.

(25) Beatty, A. M.; Granger, K. E.; Simpson, A. E. *Chem.--Eur. J.* **2002**, *8*, 3254-3259.

(26) Beatty, A. M.; Schneider, C. M.; Simpson, A. E.; Zaher, J. L. *CrystEngComm* **2002**, *4*, 282-287.

(27) Wuest, J. D. *Chem. Comm.* **2005**, 5830-5837.

(28) Perron, M.-E.; Monchamp, F.; Duval, H.; Boils-Boissier, D.; Wuest, J. D. *Pure Appl. Chem.* **2004**, *76*, 1345-1351.

(29) Saied, O.; Maris, T.; Wuest, J. D. *J. Am. Chem. Soc.* **2003**, *125*, 14956-14957.

(30) Brunet, P.; Simard, M.; Wuest, J. D. *J. Am. Chem. Soc.* **1997**, *119*, 2737-2738.

(31) Robson, R. *Dalton Trans.* **2008**, 5113-5131.

(32) Aakeroy, C. B.; Beatty, A. M. *Crystal Engineering* **1998**, *1*, 39.

(33) Qin, Z.; Jennings, M. C.; Puddephatt, R. J.; Muir, K. W. *Inorg. Chem.* **2002**, *41*, 5174.

(34) Aakeroy, C. B.; Beatty, A. M.; Leinen, D. S. *J. Am. Chem. Soc.* **1998**, *120*, 7383.

(35) Braga, D.; Grepioni, F. *Acc. Chem. Res.* **2000**, *33*, 601-608.

(36) Braga, D. *Dalton* **2000**, 3705-3713.

(37) Aakeroy, C.; Beatty, A. M. *Ausralian Journal of Chemistry* **2001**, *54*, 409-421.

(38) Munakata, M.; Wu, L. P.; Kuroda-Sawa, T. *Bull. Chem. Soc. Jpn.* **1997**, *70*, 1727.

(39) Munakata, M.; Wu, L. P.; Yamamoto, M.; Kuroda-Sawa, T.; Maekawa, M. *J. Am. Chem. Soc.* **1996**, *118*, 3117-3124.

(40) Zeng, M.-H.; Feng, X.-L.; Zhang, W.-X.; Chen, X.-M. *Dalton Trans.* **2006**, 5294-5303.

(41) Zheng, Y.-Q.; Kong, Z.-P. *J. Chem. Crystallogr.* **2002**, *32*, 119-125.

(42) Pedersen, C. J. *J. Am. Chem. Soc.* **1967**, *89*, 7017-7036.

(43) Dietrich, B.; Lehn, J.-M.; Sauvage, J.-P. *Tetrahedron Lett.* **1969**, 2885.

(44) Gokel, G. W. *Comprehensive Supramolecular Chemistry*; Pergamon: Oxford, 1996; Vol. 1.

(45) Tranchemontagne, D. J.; Mendoza-Cortes, J. L.; O'Keeffe, M.; Yaghi, O. M. *Chem. Soc. Rev.* **2009**, *38*, 1257-1283.

(46) Pivovar, A. M.; Holman, K. T.; Ward, M. D. *Chem. Mater.* **2001**, *13*, 3018-3031.

(47) Holman, K. T.; Pivovar, A. M.; Swift, J. A.; Ward, M. D. *Acc. Chem. Res.* **2001**, *34*, 107-118.

(48) Swift, J. A.; Ward, M. D. *Chem. Mater.* **2000**, *12*, 1501-1504.

(49) Holman, K. T.; Ward, M. D. *Stimul. Concepts Chem.* **2000**, *221*, 221-234.

(50) Russell, V. A.; Ward, M. D. *J. Mater. Chem.* **1997**, *7*, 1123-1133.

(51) Russell, V. A.; Evans, C. C.; Li, W.; Ward, M. D. *Science* **1997**, *276*, 575-579.

(52) Ward, M. D.; Russell, V. A. *NATO ASI Ser., Ser. C* **1997**, *499*, 397-407.

(53) Russell, V. A.; Etter, M. C.; Ward, M. D. *Chem. Mater.* **1994**, *6*, 1206-17.

(54) Russell, V. A.; Etter, M. C.; Ward, M. D. *J. Am. Chem. Soc.* **1994**, *116*, 1941-52.

(55) Toda, F. *Advances in Supramolecular Chemistry* **1992**, *2*, 141-191.

(56) Caira, M. R.; Horne, A.; Nassimbeni, L. R.; Toda, F. *J. Chem. Soc., Perkin Trans. 2* **1997**, 1717-1720.

(57) Kim, J.; Lee, S.-O.; Yi, J.; Kim, W.-S.; Ward, M. D. *Separation and Purification Technology* **2008**, *62*, 517-522.

(58) Rowsell, J. L. C.; Yaghi, O. M. *Microporous and Mesoporous Materials* **2004**, *73*, 3-14.

(59) Eddaoudi, M.; Moler, D. B.; Li, H.; Chen, B.; Reineke, T. M.; O'Keeffe, M.; Yaghi, O. M. *Acc. Chem. Res.* **2001**, *34*, 319-330.

(60) Yaghi, O. M.; Li, H.; Davis, C.; Richardson, D.; Groy, T. L. *Acc. Chem. Res.* **1998**, *31*, 474-484.

(61) Biradha, K.; Fujita, M. In *Crystal Design: Structure and Function*; Desiraju, G. R., Ed.; John Wiley & sons: 2003, p 211-239.

(62) Biradha, K.; Fujita, M. *Journal of Inclusion Phenomena and Macrocyclic Chemistry* **2001**, *49*, 201-208.

(63) Maji, T. K.; Kitagawa, S. *Pure Appl. Chem.* **2007**, *79*, 2155-2177.

(64) Kitagawa, S.; Kitaura, R.; Noro, S.-i. *Angew. Chem. Int. Ed.* **2004**, *43*, 2334-2375.

(65) Kondo, M.; Okubo, T.; Asami, A.; Noro, S.-i.; Yoshitomi, T.; Kitagawa, S.; Ishii, T.; Matsuzaka, H.; Seki, K. *Angew. Chem. Int. Ed.* **1999**, *38*, 140-143.

(66) Kitagawa, S.; Matsuda, R. *Coord. Chem. Rev.* **2007**, *251*, 2490-2509.

(67) Beatty, A. M. *Coord. Chem. Rev.* **2003**, *246*, 131-143.

(68) Dalrymple, S. A.; Shimizu, G. K. H. *J. Am. Chem. Soc.* **2007**, *129*, 12114-12116.

(69) Dalrymple, S. A.; Shimizu, G. K. H. *Chem. Comm.* **2006**, 956-958.

(70) Reddy, D. S.; Duncan, S.; Shimizu, G. K. H. *Angew. Chem., Int. Ed.* **2003**, *42*, 1360-1364.

(71) Dalrymple, S. A.; Parvez, M.; Shimizu, G. K. H. *Chem. Comm.* **2001**, 2672-2673.

(72) Cote, A. P.; Shimizu, G. K. H. *Chem. Comm.* **2001**, 251-252.

(73) Shimizu, G. K. H.; Vaidhyanathan, R.; Taylor, J. M. *Chem. Soc. Rev.* **2009**, *38*, 1430-1449.

(74) Liang, J.; Shimizu, G. K. H. *Inorg. Chem.* **2007**, *46*, 10449-10451.

(75) Beatty, A. M. *CrystEngComm* **2001**, *51*, 1-13.

(76) Aakeroy, C. B.; Beatty, A. M.; Leinen, D. S. *Angew. Chem., Int. Ed.* **1999**, *38*, 1815-1819.

(77) Alberti, G.; Costantino, U. *Compr. Supramol. Chem.* **1996**, *7*, 1-23.

(78) Hensen, E. J. M.; Smit, B. *Journal of Physical Chemistry. B* **2002**, *106*, 12664-12667.

(79) Pinnavaia, T. J. *Science* **1983**, *220*, 365-71.

(80) Clearfield, A. In *Advanced catalysts and nonostructures materials: modern synthetic methods*; Moser, W. R., Ed.; Academic Press, Inc.: San Diego, California, 1996, p 345-435.

(81) Solin, S. A. *Annu. Rev. Mater. Sci.* **1997**, *27*, 89-115.

(82) Bhattacharyya, K. G.; Gupta, S. S. *Advances in Colloid and Interface Science* **2008**, *140*, 114-131.

(83) Liu, Z.-H.; Yang, X.; Ooi, K. *J. Colloid and Interface Sci.* **2003**, *265*, 115-120.

(84) Jacobson, A. J.; Johnson, J. W.; Lewandowski, J. T. *Inorg. Chem.* **1985**, *24*, 3727-3729.

(85) Scott, K. J.; Zhang, Y.; Wang, R.-C.; Clearfield, A. *Chem. Mater.* **1995**, *7*, 1095-1102.

(86) Frink, K. J.; Wang, R. C.; Colon, J. L.; Clearfield, A. *Inorg. Chem.* **1991**, *30*, 1438-41.

(87) Uemura, K.; Kitagawa, S.; Kondo, M.; Fukui, K.; Kitaura, R.; Chang, H.-C.; Mizutani, T. *Chem.--Eur. J.* **2002**, *8*, 3586-3600.

(88) Noro, S.-i.; Kitagawa, S.; Kondo, M.; Seki, K. *Angew. Chem. Int. Ed.* **2000**, *39*, 2082-2084.

(89) Kumazawa, K.; Biradha, K.; Kusukawa, T.; Okano, T.; Fujita, M. *Angew. Chem. Int. Ed.* **2003**, *42*, 3909-3913.

(90) Martin, K. J.; Squattrito, P. J.; Clearfield, A. *Inorg. Chim. Acta* **1989**, *155*, 7-9.

(91) Zhang, Y.; Scott, K. J.; Clearfield, A. *J. Mater. Chem.* **1995**, *5*, 315-18.

(92) Zhang, B.; Poojary, D. M.; Clearfield, A. *Chem. Mater.* **1996**, *8*, 1333-1340.

(93) Clearfield, A.; Tindwa, R. M. *J. Inorg. Nucl. Chem.* **1979**, *41*, 871-8.

(94) Clearfield, A.; Costantino, U. *Compr. Supramol. Chem.* **1996**, *7*, 107-149.

(95) Sun, L.; Boo, W. J.; Browning, R. L.; Sue, H.-J.; Clearfield, A. *Chem. Mater.* **2005**, *17*, 5606-5609.

(96) Shvareva, T. Y.; Skanthakumar, S.; Soderholm, L.; Clearfield, A.; Albrecht-Schmitt, T. E. *Chem. Mater.* **2007**, *19*, 132-134.

(97) Johnson, J. W. *Intercalation Chem.* **1982**, 267-83.

(98) Rouxel, J. *Compr. Supramol. Chem.* **1996**, *7*, 77-105.

(99) Kawata, S.; Kitogawa, S.; Kumagai, H.; Kudo, C.; Kamesaki, H.; Ishiyama, T.; Suzuki, R.; Kondo, M.; Katada, M. *Inorg. Chem.* **1996**, *35*, 4449-4461.

(100) Groeneman, R. H.; Atwood, J. L. *Supramol. Chem.* **2001**, *12*, 353-356.

(101) Bestaoui, N.; Spurr, N. A.; Clearfield, A. *J. Mater. Chem.* **2006**, *16*, 759-764.

(102) Poojary, D. M.; Clearfield, A. *J. Am. Chem. Soc.* **1995**, *117*, 11278-84.

(103) Hamilton, B. H.; Kelly, K. A.; Wagler, T. A.; Espe, M. P.; Ziegler, C. J. *Inorg. Chem.* **2004**, *43*, 50-56.

(104) Zaworotko, M. J. *Chem. Comm.* **2001**, 1-9.

(105) Nagayoshi, K.; Kabir, M. K.; Tobita, H.; Honda, K.; Kawahara, M.; Katada, M.; Adachi, K.; Nishikawa, H.; Ikemoto, I.; Kumagai, H.; Hosokoshi, Y.; Inoue, K.; Kitagawa, S.; Kawata, S. *J. Am. Chem. Soc.* **2003**, *125*, 221-232.

(106) Kabir, M. K.; Miyazaki, N.; Kawata, S.; Adachi, K.; Kumagai, H.; Inoue, K.; Kitagawa, S.; Iijima, K.; Katada, M. *Coord. Chem. Rev.* **2000**, *198*, 157-169.

(107) Hollingsworth, M. D. *Science* **2002**, *295*, 2410-2413.

(108) Hollingsworth, M. D.; Peterson, M. L.; Pate, K. L.; Dinkelmeyer, B. D.; Brown, M. E. *J. Am. Chem. Soc.* **2002**, *124*, 2094-2095.

(109) Rosi, N. L.; Eckert, J.; Eddaoudi, M.; Vodak, D. T.; Kim, J.; O'Keeffe, M.; Yaghi, O. M. *Science* **2003**, *300*, 1127-1130.

Chapter 2

Instrumental Methods

2.1 Introduction

Many different techniques were used to characterize the samples in the proceeding chapters, varying from X-ray diffraction to thermal analysis to standard spectroscopic and chromatographic techniques. The X-ray diffraction methods consisted of single crystal X-ray diffraction (SCXRD) and powder x-ray diffraction (PXRD). Single crystal X-ray diffraction was solely used on crystals grown for Chapter 4 and powder X-ray diffraction were used on samples in Chapters 3, 4, and 5. The thermal analysis methods consisted of thermogravimetric analysis (TGA) and differential scanning calorimetry (DSC). Thermogravimetric analysis (TGA) was used on all samples in Chapters 3, 4, 5, and 6. Differential scanning calorimetry (DSC) was used on samples in Chapters 3, 4, and 5. Infra-red spectroscopy (IR spectroscopy) and was used on some samples from Chapter 3. The chromatographic method was gas chromatography coupled with mass spectrometry (GC/MS), and was used on samples from Chapter 6.

2.2 X-ray Diffraction

One of the most important methods of characterization is the use of single crystal x-ray diffraction in order to determine the crystal structure, and this was used extensively where applicable. The determination of a crystal structure is a multi-step process that starts with growing crystals and ends with the structure solution. The downfall with single crystal X-ray diffraction is that it is difficult to grow crystals and maintain a certain quality of the crystals. Therefore, powder X-ray diffraction was used to identify the material and to determine if intercalation/inclusion occurred.

2.2.1 Method of Generating X-Rays

X-rays are electromagnetic radiation waves of approximately 1Å.[1] Standard X-ray diffraction methods produce monochromatic X-rays when electrons are accelerated toward the target metal, usually molybdenum for single crystal and copper for powder diffraction. For example, enough energy is provided to remove a copper 1s (K shell) electron. The vacant 1s orbital is then filled either by a 2p or 3p outer electron and the excess energy that is released from this transition is emitted in the form of an X-ray.[2] A generalized schematic of this process is shown in Figure 2.1.

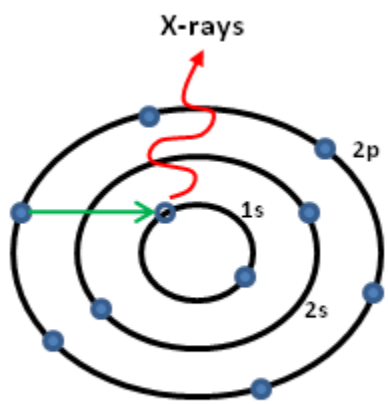

Figure 2.1 A Schematic of the production of an X-ray.

X-rays are produced because the energy transitions contain fixed values. Using copper as the target metal, the Kα wavelength is 1.5418 Å corresponding to the 2p to 1s transition and the Kβ wavelength is 1.3922 Å corresponds to the 3p to 1s

transition.[2] The Kα transition is more intense than the Kβ because the Kα peak is a doublet containing $K\alpha_1$ and $K\alpha_2$. The wavelength of the target metal is dependent on the Z, shielding effect, of the metal. The greater the Z value the higher the energy, which means lower wavelength since wavelength and energy are inversely proportional.[2]

A common source of X-ray for laboratory use is an x-ray tube. This X-ray tube contains a tungsten filament that is enclosed in an evacuated tube, a target material, and a beryllium window. A high voltage is applied to the cathode (contains the tungsten filament) emitting an electron and when high energy electrons decelerate in materials, X-rays are emitted.[3] The voltage that is applied to the cathode is typically 50Kv. The target source, either molybdenum or copper, will emit an X-ray, which travels through the beryllium window and is focused through an X-ray optical device.[2] Because high energy is required to release an electron, the X-ray tube needs to be cooled to prevent further damage to the filament or target material. The X-rays are emitted in every direction, therefore limiting the amount of useful X-rays. A general schematic of an X-ray tube is shown in Figure 2.2.[3]

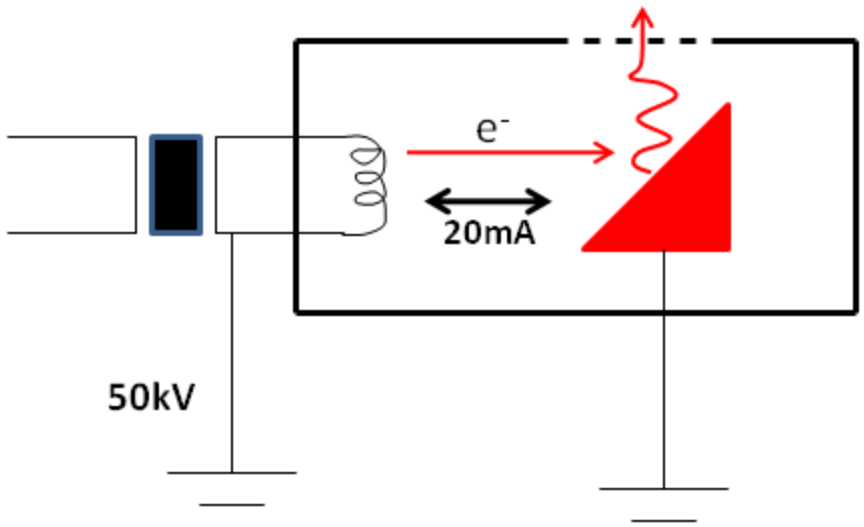

Figure 2.2 A General Schematic of an X-ray tube.[4]

2.2.2 Laue Equations

Max Theodore von Laue derived the mathematical relationship between incident radiation and the direction in which it is diffracted through three equations and each equation (now known as the Laue equations) corresponds to diffraction conditions in one particular direction.[2] These equations must be satisfied in order for diffraction to occur.

$$a \sin\Theta_a = h\,\lambda$$

$$b \sin\Theta_b = k\,\lambda$$

$$c \sin\Theta_c = l\,\lambda$$

The lattice parameters are defined as a, b, and c while Θ_a, Θ_b, and Θ_c are the angles of diffraction. The wavelength of the radiation is presented by λ and *h*, *k*, and *l* are the Miller indices of the corresponding reflections.[2] The Laue equations provide a

mathematical method to describe the diffraction of radiation. An alternative theory to diffraction based on Bragg's Law has derived a simpler equation and is discussed in the following section.

2.2.3 Bragg's Law

The father and son combination of William Lawrence and William Henry Bragg developed another theory of diffraction known as Bragg's Law.[2] The main principle of this theory is that crystals are projected as repeating planes that reflect the incoming x-rays. These incoming x-rays are reflected by the first plane at an equal incident angle while the remaining x-rays are transmitted through the first level.

When looking at the diagram of two incoming beams, 1 and 2, are scattered from adjacent planes within the crystal, A and B, where the corresponding diffracting beams, 1' and 2', are in phase and have constructive interference, as shown in Figure 2.3. The distance of xyz can be calculated using the Bragg angle, Θ, and the spacing between the parallel planes, known as the d-spacing, d.[3]

$$xy = yz = d \sin\Theta \qquad (1)$$

Since xy = yz in equation 1, the equation can be simplified to:

$$xyz = 2d \sin\Theta \qquad (2)$$

The distance of xyz must be equal to a positive integer of wavelengths to remain in phase, therefore:

$$xyz = n \lambda \qquad (3)$$

Combing equations 2 and 3 will yield Bragg's Law:

$$2d \sin\Theta = n \lambda \qquad (4)$$

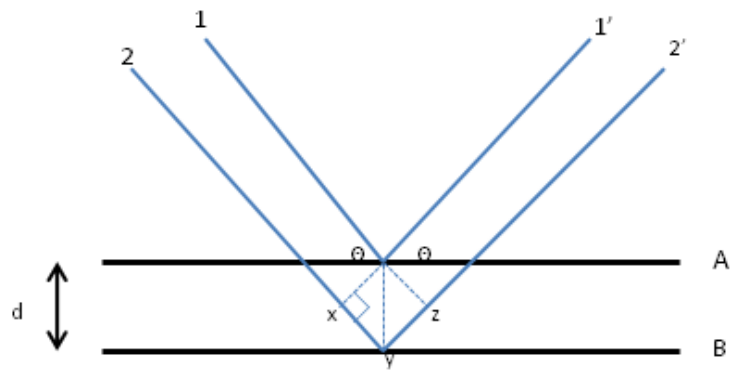

Figure 2.3 Derivation of Bragg's Law for diffraction.[2]

2.2.4 Reciprocal Lattice

The reciprocal lattice is in reciprocal space and is inversely related to the real lattice of the crystal.[2] Each point in the reciprocal lattice corresponds to a set of lattice planes (*hkl*) in the real space. The direction of the reciprocal lattice vector (d^*) is normal to the real space planes and the magnitude of the reciprocal lattice vector is equal to the reciprocal of the distance between real lattice planes (d).

2.2.5 Single Crystal X-Ray Diffraction (SCXRD)

Single crystal X-ray diffraction is employed when suitable crystals can be grown from solution. Knowing the structure is vital, when developing new materials, because the crystal structure allows viewing of packing schemes and all associated interactions with the molecule. SCXRD can used be used to generate a theoretical powder pattern, which can be used for comparative analysis. The determination of the structure from a single crystal is a multi-step process that includes unit cell

determination, data collection, indexing reflections, integration and absorption correction, space group determination, structure solution and crystal structure refinement.[3] In our case, the *ab* plane of the unit cell coincides with the metal dicarboxylic acid, which forms a lamellar region. Therefore, the *c* parameter defines the interlayer distance.

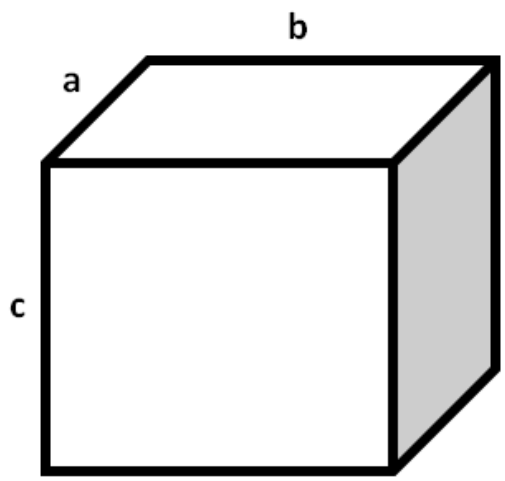

Figure 2.4 An example of a general unit cell with cell parameters.

2.2.6 Powder X-Ray Diffraction (PXRD)

Powder diffraction is a similar technique to single crystal where a sample is exposed to incoming x-rays and the diffraction pattern of the crystalline sample is collected by a detector. The output from powder XRD will show the degree 2Θ vs. intensity. The 2Θ can be converted to the d-spacing (interlayer distance) by using the before mentioned Bragg's equation.[5]

Powder X-ray diffraction is an important technique for many reasons; it can be used to quickly confirm the structure of a sample, determine if intercalation has occurred, and can also be used for actual structure determination using the Rietveld method.[6] The other important use of PXRD is to obtain a quick characterization of the material in question when there is a crystal structure present for that material. The crystal structure can generate a theoretical powder pattern and this generated powder pattern can be compared to the experimental powder pattern. If the peaks correlate to each other then the materials are the same. In our case, the observation of peak shifts is the main focus for using powder diffraction because we follow the shifting of the *001* peak, which is designated for the interlayer distance or the c parameter. The *100* and *010* index should not vary in our study because they make up the hydrogen-bonded ab plane, but the interlayer distance can change upon intercalation of guests.

2.3 Thermal Analysis

Here we will describe the two main techniques that are based on the use of heat to acquire information about our sample, thermogravimetric analysis and differential scanning calorimetry. The majority of our samples will be characterized through the use of these two techniques.

2.3.1 Thermogravimetric Analysis (TGA)

In a thermogravimetric analysis the mass of a sample is controlled in an inert atmosphere and the data is recorded continuously as a function of temperature or time. The data that was collected from the TGA is output as temperature versus

weight loss %, giving a thermogram or a thermal decomposition curve. Standard commercial instruments for thermogravimetry consists of: a sensitive microbalance, a furnace, a purge gas system for providing an inert atmosphere, and microcomputer/microprocessor for instrument control and data acquisition. In addition, a purge gas switching system is often used for applications that require the exchange of gases during an experiment. The microbalance of a TGA is capable of providing quantitative information about a sample from 1mg to 100mg. The sample holder is housed within the furnace; the rest of the balance must be thermally isolated from the furnace. The furnace of a TGA can be programmed to run from ambient temperature to 1500 °C. Often, heating and cooling rates of the furnace can be selected from around zero to as high as 200°C/min. Insulation and cooling of the exterior of the furnace is needed to avoid heat transfer to the balance. Nitrogen or argon is usually used to purge the furnace and prevent oxidation of the sample.

The information provided by thermogravimetric methods is often limited because a temperature variation must bring about a change in mass of the sample. Thus, thermogravimetric methods are largely limited to decomposition and oxidation reactions and to such physical processes as vaporization, sublimation, and desorption. An example of theoretical collected data from a TGA is shown in Figure 2.5, indicating the loss of mass at each step while the temperature increases.

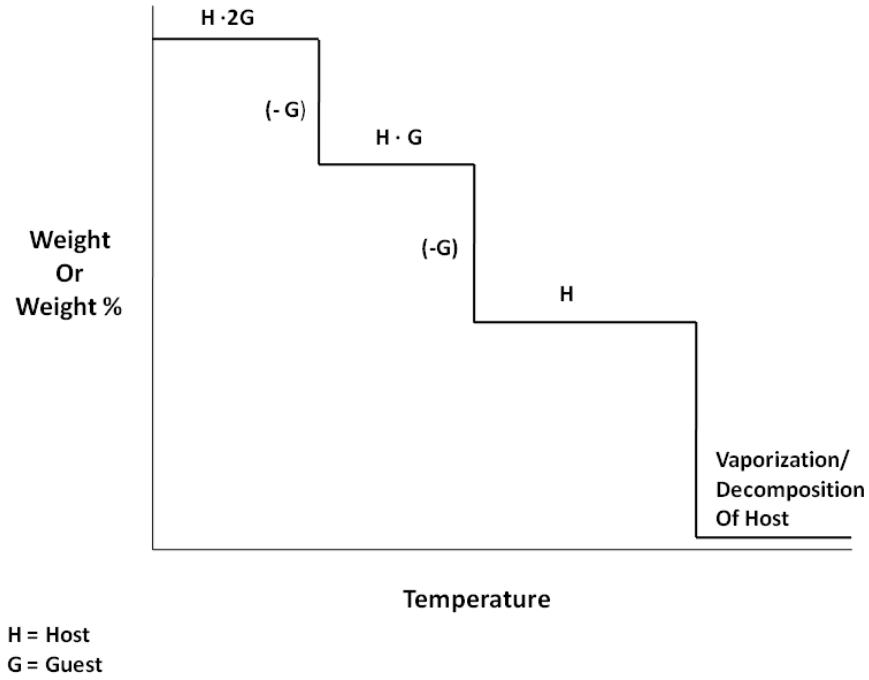

Figure 2.5 Theoretical data collected from a TGA. Where H = Host, G = Guest, H·2G refers to a host with two guest molecules.

Our standard procedure is to hold the sample isothermally for five minutes to ensure surface solvent is removed, followed by a scan from 40°C to 550°C at a rate of 10°C/min. A standard calculation is expressed in equation 2.4. Our analysis of the thermogram consists of calculating the change in weight as the temperature increases. We generate a TGA of the host material that will be used to compare if a guest molecules has been inserted into the host material. For each experiment, if a guest is present, the appearance of an extra weight loss is expected. Depending on the strength of the host/guest interaction the guest leaves at a characteristic temperature. The amount of weight loss depends on the % occupancy of the guest. If there is only

one guest per host unit, the total loss corresponds to the weight % of G in the H·G complex. Other fractions of H:G ratios can be determined using this method.

$$\Delta \text{ weight } \% = \frac{(\text{Starting weight} - \text{Final weight})}{\text{Starting weight}} \times 100\%$$

Equation 2.1 Equation for determining the weight loss.

2.3.2 Differential Scanning Calorimetry (DSC)

The use of differential scanning calorimetry (DSC) is another thermal analysis technique, used to measure the difference in heat flow between a sample and a reference as a function of temperature while the two are subjected to a controlled temperature program.

We used a power compensated DSC for the analysis. A power compensated DSC is distinguished by the heating of the sample and reference by separate heaters in a way to keep their temperatures are equal whether it's heating or cooling. The sample must be weighed and recorded prior to analysis and the sample limit it dependent on the sample pan. The sample pans can be comprised of many different materials depending on the desire temperature range. We used a standard aluminum pan, where the allowed temperature range is from ambient to 450 °C. The heating rate is the same as in TGA, from 1° to as high as 200°C/min. A purge gas flows through the sample holder to eliminate the possibility of oxidation.

The DSC can be used to measure enthalpimetric changes associated with a particular process. It is commonly used to measure specific heats, heats of fusion, and enthalpimetric changes associated with physical and chemical changes. DSC can be used to measure activation energies and rate constants for a particular transition. Finally, in the drug industry DSC is used to determine purity of some drugs. A general DSC thermogram is shown in Figure 2.6.

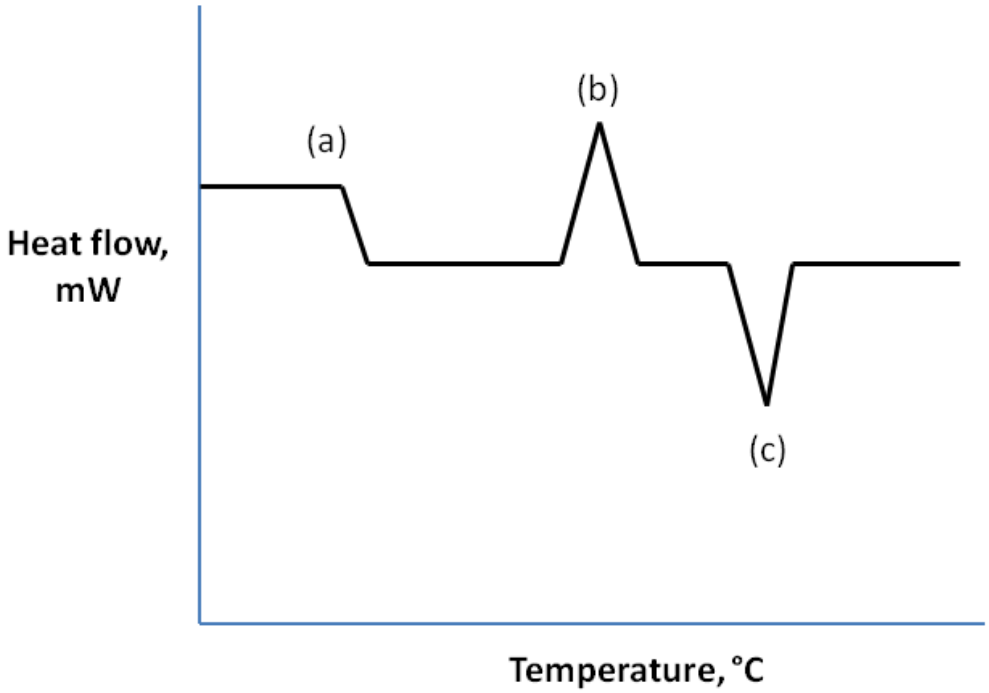

Figure 2.6A Generalized DSC output and its different process, (a) glass transition, (b) an exothermic peak, and (c) an endothermic peak.

2.4 References

(1) West, A. R. *Solid State Chemistry and its Applications*; John Wiley & Sons Ltd.: New York, 1990.

(2) Cullity, B. D.; Stock, S. R. *Elements of X-ray Diffraction*; Prentice Hall: Upper Saddle River, NJ, 2001.

(3) Giacovazzo, C.; Viterbo, D.; Artioli, G.; Ferraris, G. *Fundamentals of Crystallography*; 2 ed.; Oxford Univ. Press, 2002.

(4) Clegg, W.; Blake, A. J.; Gould, R. O.; Main, P. *Crystal Structure Analysis*; Oxford University Press: New York, 2006.

(5) Will, G. *Powder Diffraction: The rietveld method and the two-stage method to determine and refine crystal structures from powder diffraction data*; Springer-Verlag, 2006.

(6) Harris, K. D. M.; Tremayne, M. *Chem. Mater.* **1996**, *8*, 2554-2570.

Chapter 3

Intercalation of Lewis Bases and Non-Coordinating Small Molecules into an Inorganic-Organic Hybrid Material

3.1 Background

Metal organic frameworks have been investigated because of their potential applications in areas such as catalysis, storage, and separations.[1-9] Mainly these porous solids are made from coordination polymers, such as the metal phosphonates mention previously (Section 1.5.2), which are beneficial when looking into the phenomenon of intercalation. There are limitations to these solids in that the metrics of the layer are not changeable (substituents always the same distance apart) and the chemical nature of the layer can be changed only by changing the metal ion used in the assembly. Our work is centered on using hydrogen bonds instead of the traditional coordinate covalent bonding because the nature of hydrogen bonds indicates flexibility. The work shown herein incorporates metal organic framework that are connected through hydrogen bonds and the nature of the interlayer region can be adjusted by changing the organic substituents that reside in between the layers. The focus of our HMOF will be on intercalation and molecular transport to study if the hydrogen bonded layer can withstand guest insertion and removal.

3.2 Goals and Purpose of Research

Our goal is to utilize hydrogen bonding along with molecular components to synthesize a layered hydrogen bonded metal-organic framework. The hydrogen bonds permit flexibility within the framework thus allowing for the inclusion of guest molecules. The chemical nature of the layers can be easily altered by using various organic ligands and substituents.

Furthermore, there has been a growing realization that hydrogen bonded frameworks are very stable and can withstand the loss of guest molecule[10,11]. Therefore, we wish to test the limits of our hydrogen bonded metal organic frameworks. In this chapter, a close-packed system is described, where the hydrogen bonded layers are separated by a hydrophobic interlayer. Initially, it was necessary to find a reliable molecular combination to build the frameworks. Finally, these layered materials (which have membrane-like structures) were investigated to determine their stability upon the intercalation of small guest molecules.

3.3 Methods

To design hydrogen bonded frameworks, we investigated the strategies employed to synthesize analogous organic compounds. It was previously illustrated (Section 1.3.1) that a combination of carboxylic acids and amines yields reproducible layered structures. Thus we chose to combine a metal complex having peripheral carboxylic acid functionalities with organic amines. To achieve reactivity at the metal complexes' peripheral carboxylic acid moieties and not at the metal center itself, bidentate ligands were used for kinetic stability. Therefore, neutral metal complexes with peripheral carboxylic acid moieties were specifically chosen to replace the organic counterparts. An example of the metal-containing dicarboxylic acid is shown in Figure 3.1. A wide variety of organic amines were used as the second molecular component. In order to study intercalation of guests into these layers, the compounds were placed in anhydrous solutions containing non-polar guest molecules and sonicated. This treatment is similar to methods used for intercalation

into other materials.[12-15] Because there are replaceable, axial water ligands on the metal complex, the "coordinative intercalation" of small Lewis base molecules was also investigated.

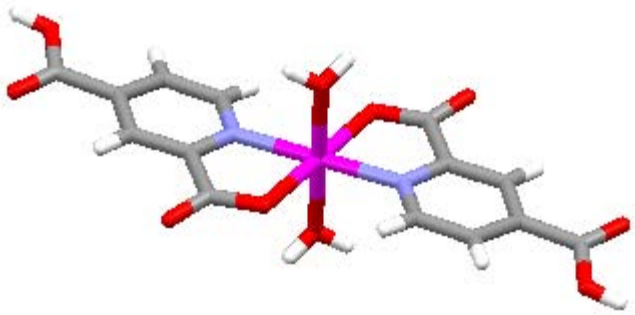

Figure 3.1 Crystal structure of Zn(pyridine-2,4-dicarboxylic acid)$_2$(H_2O)$_2$.

3.4 Experimental

3.4.1 Materials and Instruments

All chemicals and solvents were purchased from Sigma-Aldrich and used without further modification. The solvents used (methanol, ethyl acetate, hexanes and toluene) were anhydrous, ACS grade.

TGA spectra were collected on a Thermal Advantage TGA Q50 and TA Universal Analysis software was used to generate the spectra and assist in the analysis of the data. DSC spectra were collected on a Thermal Advantage DSC Q2000 equipped with an auto sampler and TA Universal Analysis software was used

to generate the spectra and assist in the analysis of the data. XRD patterns were collected on a Rigaku Ultima IV X-ray diffractometer containing a CuKα source (λ = 1.54051Å) and the powder patterns were viewed using MDI Jade 9 software. The sonicating bath used in these experiments was a Branson 5510.

3.4.2 Synthesis of Close Packed HMOF

The metal-containing dicarboxylic acid was synthesized by combining $NiSO_4 \cdot 6H_2O$ (0.1mol) dissolved in H_2O (50 mL) with a 500mL 50% methanol solution of 2,4-pyridine dicarboxylic acid (0.2 mol). The combined solutions were stirred for 2 hours. The solid was isolated by filtration and washed with excess water and allowed to air dry overnight in a vacuum hood.

In order to create the layered material, 0.1 mol of Ni(2,4-pyridine dicarboxylic acid)$_2$ $(H_2O)_2$ or Ni(HPDCA) was suspended in 2mL of methanol while 0.2ml of 4-methylbenzylamine was added to the mixing solution. Upon addition of the amine, the resulting cloudy blue suspension turned into a clear blue solution that was subsequently layered with acetone to afford X-ray quality single crystals. After slow evaporation of the solvent, a crystalline solid remained, [4-methylbenzylammonium]$_2$ [Ni(2,4-PDCA)$_2$(H_2O)$_2$] or simply Ni(4-mBA). The layer is defined by the a and b parameters (*100*, *010* Miller indices). The interlayer distance is defined by the c parameter (*001* Miller index).

The crystal structure of the layered material is shown in Figure 3.2. The crystal structure shows the presence of two ammonium counterions per metal dianion. The cations reside between the sheets, and overall motif is a single-layer arrangement.

The metal ions are located at crystallographic inversion centers in the middle of each layer such that there is an identical 2-D ammonium – carboxylate hydrogen-bonded network lining the top and bottom of each layer. The ammonium ion is attached where ammonium – carboxylate N – H^+ ---- O^- hydrogen bonds connect peripheral carboxylate moieties in 1-D, and further N – H^+ ---- O cross-linking occurs between the ammonium cations and the carboxylate attached to the metal center. The aqua ligands also connect via O – H ---- O^- hydrogen bonds to both types of carboxylate moieties. The asymmetric unit in each case comprises one ammonium cation, one 2,4-HPDCA ligand attached in a bidentate fashion to a metal ion resides at the inversion center of the unit cell, and one aqua ligand. The organic substituents are essentially closed-packed, and no guest molecules were found in the structure. The benzyl groups are interdigitated, but there is no evidence for significant attractive aryl – aryl interactions.

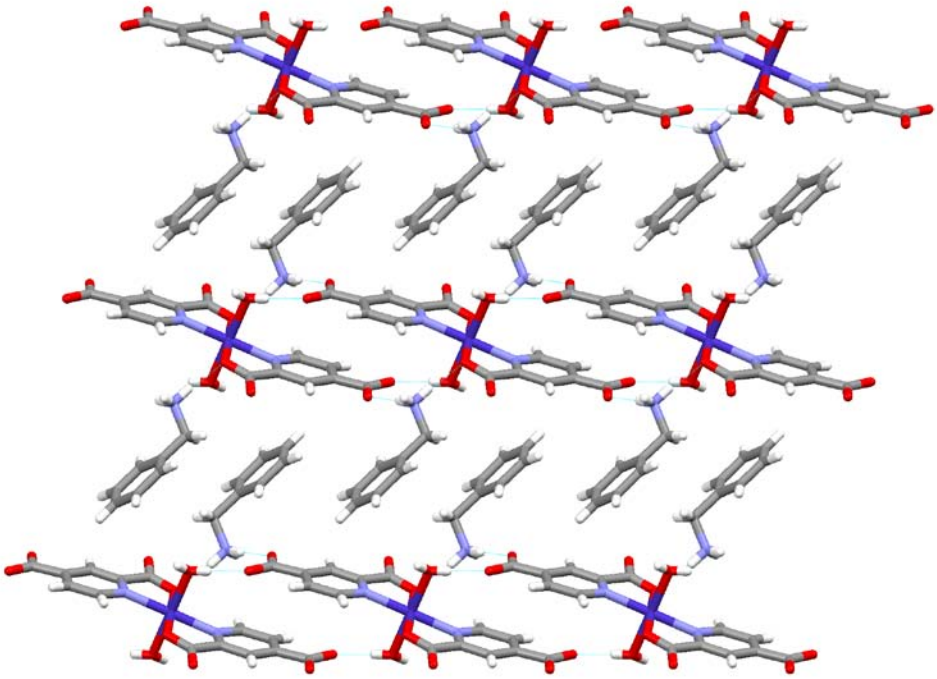

Figure 3.2 A close-packed layered structure containing benzylammonium groups between the metal-containing layers.

3.4.3 Intercalation of Non-Coordinating Molecules

0.15mmol of Ni(4-mBA) was placed in a 20mL scintillation vial with 10mL of anhydrous toluene or hexanes. Solvent can either be anhydrous hexanes or anhydrous toluene because they do not dissolve the host solid. 1mL of the guest species was then placed in the vial and the mixture was allowed to sonicate overnight. The mixture was then filtered and the solid was rinsed with excess hexanes to wash off any additional toluene (the guest species) that might be lingering on the surface. Finally, the solid was allowed to air dry. A similar synthetic approach was used to combine Ni(4-mBA) with solids such as hydroquinone (1.0 mmol) as the guest

species. All guest molecules used in this study (Table 3.1) follow the same experimental procedure as mentioned above.

Table 3.1 Non-polar molecules for intercalation studies.

Name of Guest Molecule	Guest Molecule	Molecular Weight (g/mol)	Boiling Point
ethyl acetate	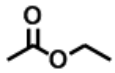	**88.11**	**76-77° C**
1-pentanol		**88.15**	**136-138° C**
1-hexanol		**102.17**	**156-157° C**
toluene	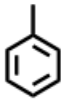	**92.14**	**110-111° C**
***p*-xylene**		**106.16**	**138° C**
anisole	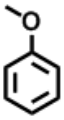	**108.14**	**154° C**
hydroquinone		**110.11**	**285° C**

nitrobenzene	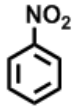	**123.11**	**210-211° C**

3.4.4 Coordinative Intercalation of Small Lewis Bases

The same intercalation procedure was followed from section 3.4.3 and the guest molecules used in this procedure are shown in Table 3.2.

Table 3.2 The pyridine-based guest molecules.

Name of Guest Molecule	Guest Molecule	Molecular Weight (g/mol)	Boiling Point (# denotes melting point)
pyridine		**79.10**	**115° C**
2-picoline		**93.13**	**128-129° C**
4-picoline	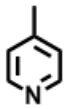	**93.13**	**145° C**
4-ethylpyridine	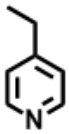	**107.15**	**168° C**

4-cyanopyridine	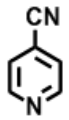	**104.11**	**76-79° C (#)**
4,4′-bipyridine		**156.18**	**305° C**
4-*t*-butylpyridine	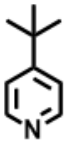	**135.21**	**196-197° C**
4-(dimethylamino) pyridine		**122.17**	**108-110° C (#)**
4-chloropyridine	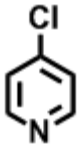	**113.54**	**210° C**

3.4.5 Characterizations

The solids were characterized by TGA, DSC, PXRD, and UV-Vis to determine if intercalation has occurred. A standard procedure to isolate the sample needed for characterization was as follows: the solid was collected from solution by standard gravimetric filtration techniques.

For TGA analysis, the sample was placed on the platinum TGA pan and scanned from 40 to 550° C with a heating rate of 10° C per minute. The sample was held for five minutes at 40° to allow the evaporation of any solvent remaining on the surface of the crystals. The temperature range that was used to calculate weight loss

was derived from the differential plot generated from the Universal Analysis software.

For DSC analysis, the powder was weighed out and sealed into a Tzero aluminum pan containing a lid and crimped for complete enclosure. The samples were held for five minutes at 40° C to ensure all solvent was removed from the surface of the powder and then scanned from 40-450C with a heating rate of 10C per minute.

For PXRD analysis, the powder was placed on a quartz sample holder, prior to data collection. Patterns were collected in 2Θ (2 - 30°) at 0.02° per step and a step size of 1.5 seconds per step. By overlaying the powder patter of the starting material with the treated material (not sure the proper term here), any difference associated with the 001 peak will indicate if intercalation was successful. Additionally, the d-spacing was determined for the 001 peak, also an indication of the separation of the layers following soaking treatment.

For UV-Vis analysis, each sample was mixed with Nujol, ground in a mortar and applied to KBr plates. Scans were conducted from 200nm to 800nm. A background scan consisting of Nujol only was acquired prior to any sample scan. Data analysis consisted of overlaying the scans of the starting material with each pyridine intercalated sample scan to observe any changes in peak position.

3.5 Intercalation of Non-Coordinating Small Molecules

A variety of guest molecules ranging from small alkyl-based molecules to slightly larger substituted benzene molecules were sonicated with the host solid. A

full list is given in Table 3.1. The guests are capable of non-covalent interactions ranging from van der Waals to π-π interactions to hydrogen bonding.

3.5.1 Results from TGA of Non-Coordinating Molecules

Each sample was analyzed by TGA, and all samples showed nearly identical weight losses, regardless of the molecular weight of the sample, Figure 3.3. These results indicate that intercalation of a guest molecule did not occur, as there been an increased weight loss if intercalation has occurred.

Table 3.3 TGA results showing the weight loss for each intercalation sample.

Guest Molecules	0 Guest molecules (% H_2O)	% Inclusion of 1 Guest Molecule	% Inclusion of 2 Guest Molecules	TGA Experimental Results (% Guest)
None	5.38%	0.00%	0.00%	0.00%
ethyl acetate	5.38%	11.26%	20.84%	1.5%
1-pentanol	5.38%	11.63%	21.00%	1.1%
1-hexanol	5.38%	13.24%	23.55%	0.00%
toluene	5.38%	12.19%	21.74%	0.00%
p-xylene	5.38%	13.79%	24.25%	0.9%
anisole	5.38%	14.01%	24.59%	1.7%

hydroquinone	**5.38%**	**14.23%**	**24.92%**	**0.00%**
nitrobenzene	**5.38%**	**15.65%**	**27.07%**	**0.00%**

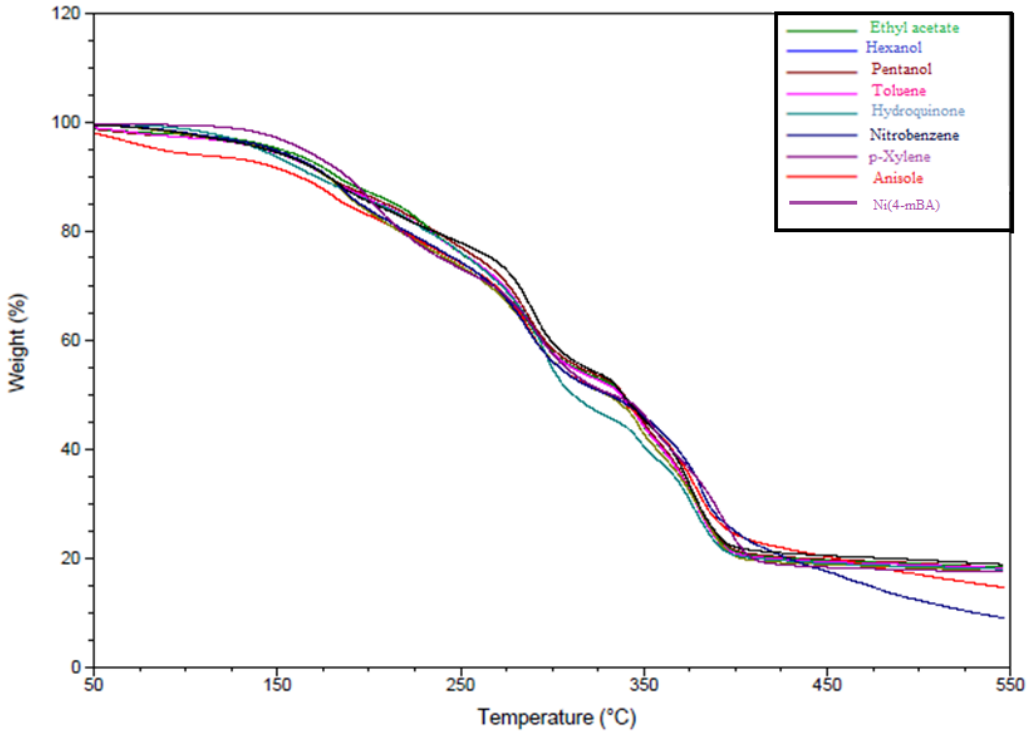

Figure 3.3 Compilation of TGA spectra associated with intercalation of non-coordinating guest molecules into Ni(4-mBA) layered solid.

3.5.2 Results from DSC of Non-Coordinating Molecules

The spectra acquired from the DSC indicated a similar pattern throughout each sample - three visible endotherms. The three DSC endotherms all match with

the temperature at which the corresponding weight losses occur in the TGA data. The combined data from the DSC analysis can be found in Figure 3.4. There is also no visual evidence such as color change to indicate that intercalation has occurred.

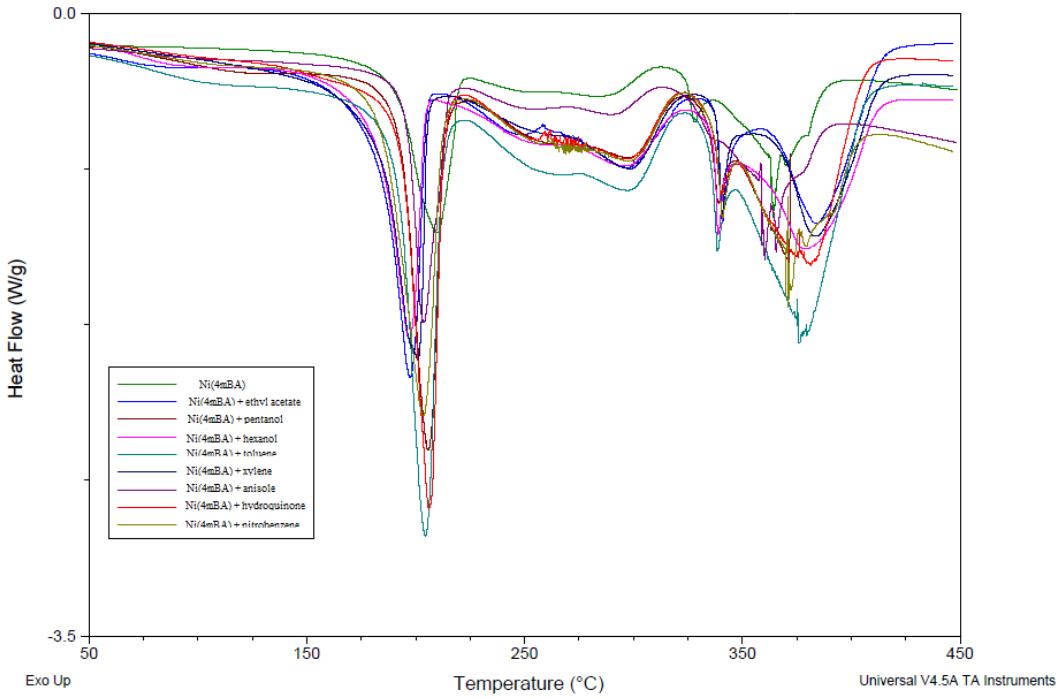

Figure 3.4 Compilation of DSC spectra associated with the intercalation of non-coordinating guest molecules into Ni(4-mBA) layered solid.

3.5.3 Results from Powder XRD of Non-Coordinating Molecules

Because the c parameter of the crystal structure corresponds to the interlayer distance, a shift in the *001* peak (to a lower 2Θ value) would indicate an expansion of layers and has the presence of guest molecules. However, powder XRD shows no change (Figure 3.5). The *100*, *010*, and the *001* peak position are given in Table 3.4.

Table 3.4 Powder XRD data for the *100*, *010* and *001* parameters and a Δ d-spacing value.

Guest Molecules	a parameter (*100*)	b parameter (*010*)	c parameter (*100*)	Δ d-spacing
None	**5.83Å**	**9.77Å**	**12.76Å**	**0.00Å**
ethyl acetate	**5.84Å**	**9.79Å**	**13.06Å**	**0.30Å**
pentanol	**5.84Å**	**9.79Å**	**12.98Å**	**0.22Å**
hexanol	**5.83Å**	**9.79Å**	**12.99Å**	**0.23Å**
toluene	**5.81Å**	**9.79Å**	**13.03Å**	**0.27Å**
***p*-xylene**	**5.83Å**	**9.81Å**	**13.03Å**	**0.27Å**
anisole	**5.84Å**	**9.81Å**	**13.03Å**	**0.27Å**
hydroquinone	**5.84Å**	**9.76Å**	**13.10Å**	**0.34Å**
nitrobenzene	**5.84Å**	**9.84Å**	**13.06Å**	**0.30Å**

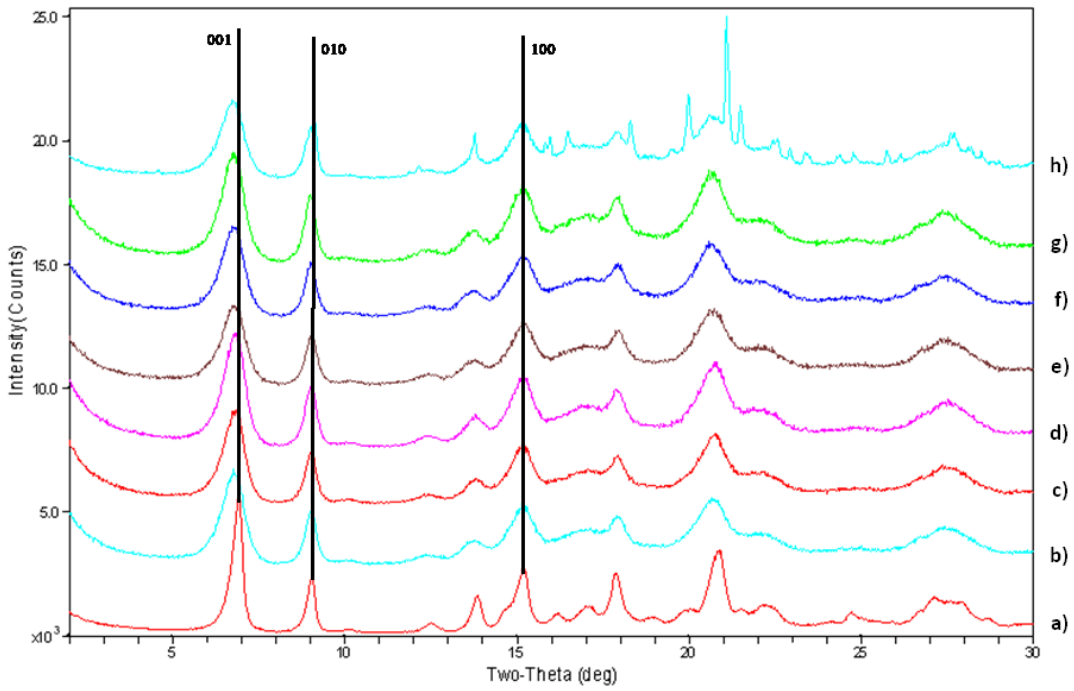

Figure 3.5 Compilation of powder XRD patterns from the intercalation of non-coordinating molecules into Ni (4-mBA) layered solid. Where (a) Ni(4-mBA), (b) ethyl acetate, (c) pentanol, (d) hexanol, (e) toluene, (f) *p*-xylene, (g) anisole, (h) hydroquinone.

3.6 Intercalation of Pyridine-based Molecules

To overcome the unsuccessful attempts to intercalate non-coordinating guest molecules we shifted our focus towards molecules that contain a higher propensity to coordinate to a metal center. Therefore, in this portion of the study, the objective was to introduce pyridine-based molecules to the metal containing layered material, Ni(4-mBA) and replace the coordinated axial H_2O ligands with the corresponding pyridine molecule. Solid-liquid intercalation via sonication was used to allow the layered component and the pyridine-based molecules to come together. The guest molecules

that were chosen contain a pyridyl moiety, such as: pyridine, 2-picoline, 4-picoline, 4-ethylpyridine, 4-cyanopyridine, 4, 4′-bipyridine, 4-*t*-butylpyridine, 4-(dimethylamino)pyridine, and 4-chloropyridine (Table 3.2).

3.6.1 Results from TGA Analysis of Pyridine Molecules

The TGA spectra from the pyridine-based molecule intercalation have shown promise in the ability to replace the coordinated water ligands with the pyridine molecules at the vacated coordination site through the use of sonication. A noticeable difference was observed when comparing the starting material to the pyridines because of a large weight loss that was observed in the 100° to 200° C range. Table 3.5 shows the different possibilities for each guest molecule and the experimental weight loss % that is associated with the loss of the pyridine guest molecules.

Table 3.5 Different pyridine possibilities and experimental TGA results (SM = starting material, G = guest, and W = water ligand).

Guest Molecule	SM	SM + G	SM + 2G	SM - W + G	SM - W + 2G	SM -2W + 2G	SM -2W + 3G	TGA weight loss
None	5.38%	0.00%	0.00%	0.00%	0.00%	0.00%	0.00%	11.60%
Pyridine	5.38%	10.56%	19.10%	10.83%	19.53%	19.99%	27.26%	18.01%
2-Picoline	5.38%	12.22%	21.75%	12.51%	22.22%	22.73%	30.61%	11.07%
4-Picoline	5.38%	12.22%	21.75%	12.51%	22.22%	22.73%	30.61%	31.24%
4-Ethylpyridine	5.38%	13.78%	24.23%	14.13%	24.73%	25.28%	33.67%	23.59%
4-Cyanopyridine	5.38%	13.45%	23.71%	13.78%	24.21%	24.74%	33.03%	5.75%
4,4'-Bipyridine	5.38%	23.31%	31.80%	19.34%	32.39%	33.03%	42.52%	10.53%
4-t-Butylpyridine	5.38%	16.79%	28.75%	17.19%	29.31%	29.92%	39.04%	6.93%
4-(Dimethylamino) pyridine	5.38%	15.42%	26.72%	15.79%	27.26%	27.84%	36.66%	16.14%
4-Chloropyridine	5.38%	14.45%	25.25%	14.84%	25.76%	26.39%	34.97%	3.38%

Samples treated with pyridine, 4-picoline, 4-ethylpyridine and 4-(dimethylamino) pyridine shows a significant increase in weight loss, compared to the starting material alone. The guests can coordinate to the metal center (water is lost) or reside in the frameworks, or both. Scenarios in which water is lost (either 1 or 2) and guests are added (either 1, 2 or 3) are possible, so the corresponding weight loss for each case is given in Table 3.5. The starting material by itself should lose 5.3% of

its weight (loss of 2 waters) but 11.6% weight loss is observed (this is reproducible). Therefore, it is clear that the exact composition of any guest-containing material will be impossible to determine with great certainty. However, it is clear that the guests mentioned above [pyridine, 4-picoline, 4-ethylpyridine and 4-(dimethylamino)pyridine] have been incorporated in some capacity.

In the case of pyridine and 4-ethylpyridine intercalation, the data would appear to be associated closely with a loss of two guest molecules within the layered framework. To determine if the water ligands had been replaced completely, infrared spectroscopy (IR) of the samples was determined. The IR data was inconclusive because all of the spectra were similar to the starting material's spectrum. The similarity in the spectra is due to an overabundance of similar stretching frequencies in the area where water (O-H) stretches would occur (3500-3000 cm^{-1}). Figure 3.6 shows a combination of IR spectra involving the intercalation of pyridine and the starting material. The weight loss percentage in the TGA spectra is in good agreement with this hypothesis when compared to the other three choices. The solid material's appearance has changed over the course of sonication, the starting material was a light blue material and the final product has a light purple color.

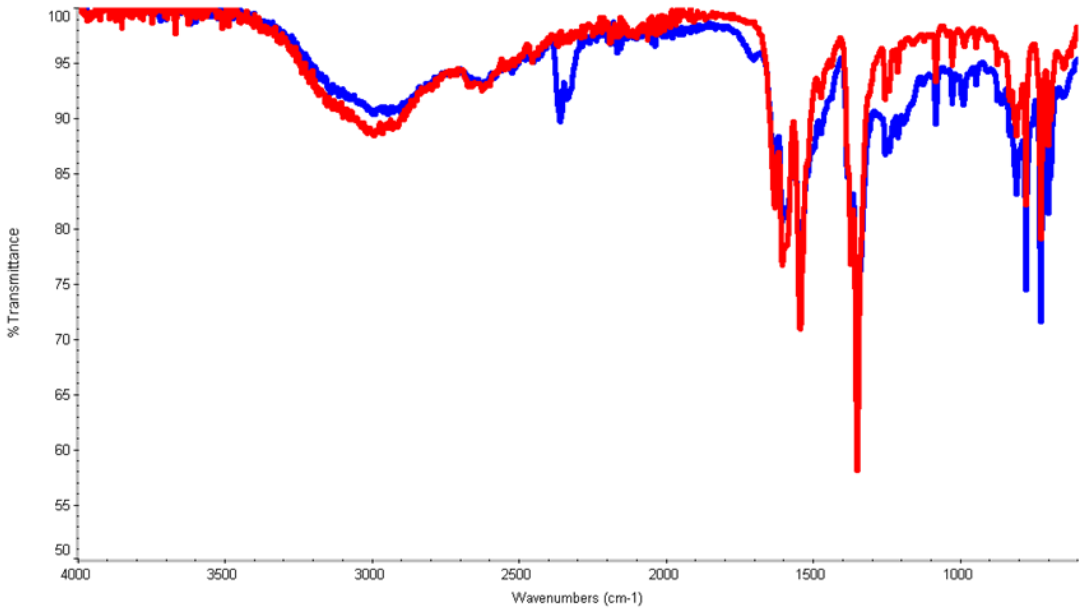

Figure 3.6 IR comparisons between Ni (4-mBA) starting material (blue) and the pyridine intercalated sample (red).

Based on the TGA data, the 4-picoline intercalation has appeared to result in the replacement of both water ligands as well as including one free 4-picoline molecule. After the sonication process, the exterior of the solid sample changed colors from a light blue color to a light purple color.

In the two cases involving 2-picoline and 4-cyanopyridine, the weight loss percentage is approximately the same as the starting material – it appears that TGA spectrum confirm a loss of the two water ligands and not a loss of pyridine-based molecules. These samples also did not show any visual evidence of a color change after sonication.

The 4-(dimethylamino)pyridine sample appeared to have one water ligand replaced with a pyridine-based molecule according to the TGA weight loss calculations. The theoretical calculations are in good agreement with the actual

experimental results for this conclusion. The exterior of these solid samples appeared to have a slight color change from a light blue color to a faint light purple color after the sonication process. Again, the color change was very faint and therefore a conclusive result regarding the color change could not be determined. Figure 3.7 shows a compilation of the TGA spectra associated with the intercalation of pyridine-based molecules into the Ni (4-mBA) layered solid.

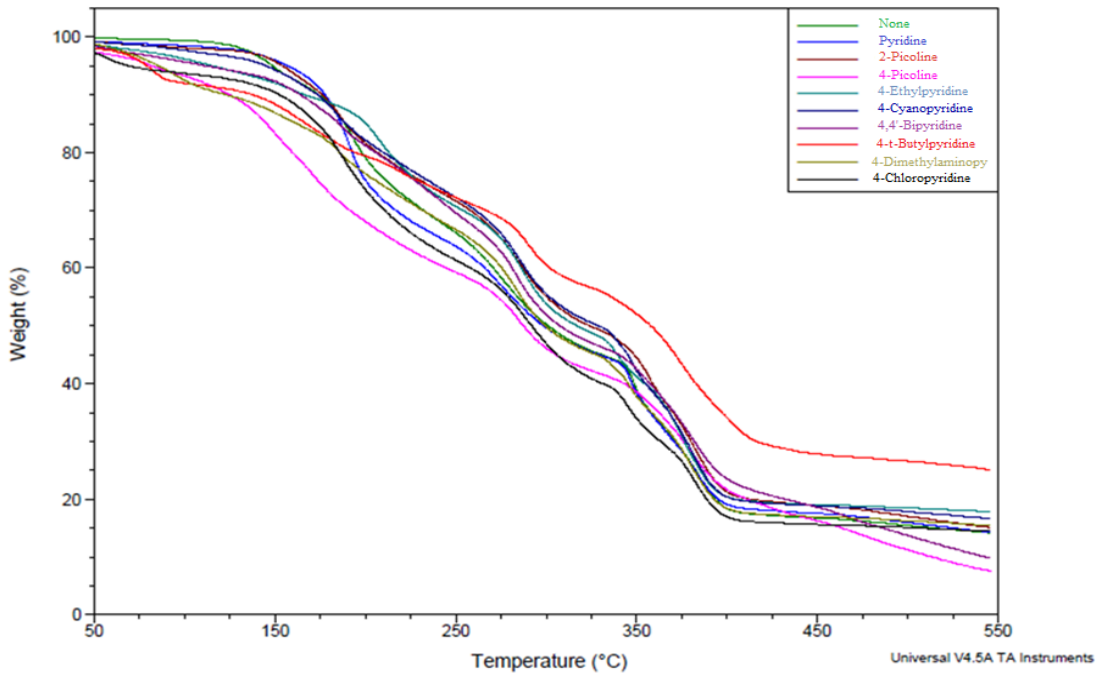

Figure 3.7 Compilation of TGA spectra associated with intercalation of pyridine-based molecules into Ni (4-mBA) layered solid.

3.6.2 Results from DSC of Pyridine Molecules

The data acquired from the DSC indicated a similar pattern; for each sample there are three visible endotherms. Three samples show a distinct difference in the

location of the first endotherm, which corresponds to the pyridine, 4-picoline, and 4-ethylpyridine intercalated samples. The 4-(dimethylamino) pyridine sample shows a broadening of the first endotherm indicating the presence of an additional guest molecule. These DSC traces are in agreement with TGA evidence of a guest molecule. The rest of the samples are similar to the starting materials, in agreement with TGA evidence that no intercalation occurs. A compilation of the DSC spectra can be found in Figure 3.8.

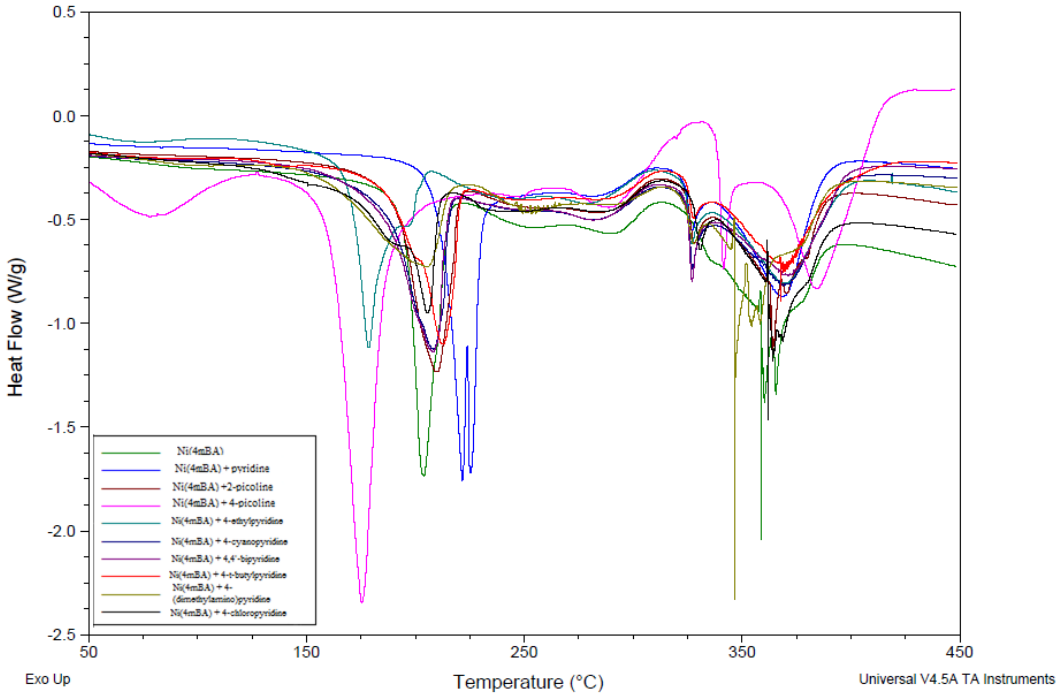

Figure 3.8 Compilation of DSC spectra associated with intercalation of pyridine-based molecules into Ni (4-mBA) layered solid.

3.6.3 Results from Powder XRD of Pyridine Molecules

Powder XRD patterns show an indication that intercalation is occurring in some samples because of the change in the *001* peak, which shifts to lower 2Θ values, indicating a larger distance between the layers. An increase in the interlayer distance is expected if guest molecules are inserted between the layers. Two samples showed a larger expansion of the layers: 4-picoline and 4-ethylpyridine. The numerical values for each of these peaks can be found in Table 3.6. Other samples showed slight shifts or broadening, but are not significant enough to confirm that intercalation has occurred.

Table 3.6 Powder XRD data for the *100*, *010* and *001* parameters and a Δ d-spacing value.

Intercalated Guest	a parameter (*100*)	b parameter (*010*)	c parameter (*001*)	Δ d-spacing
None	5.83Å	9.77Å	12.76Å	0.00Å
pyridine	5.88Å	9.86Å	12.98Å	0.22Å
2-picoline	5.84Å	9.85Å	12.81Å	0.05Å
4-picoline	5.82Å	9.47Å	17.11Å	4.35Å
4-ethylpyridine	5.80Å	9.67Å	15.50Å	2.74Å
4-cyanopyridine	5.83Å	9.83Å	13.03Å	0.27Å
4,4′-bipyridine	5.84Å	9.84Å	13.00Å	0.24Å
4-*t*-butylpyridine	5.83Å	9.80Å	12.89Å	0.13Å

4-(dimethyl amino)pyridine	**5.83Å**	**9.79Å**	**13.14Å**	**0.38Å**
4-chloropyridine	**5.81Å**	**9.79Å**	**12.85Å**	**0.09Å**

Figure 3.9 shows a compilation of powder patterns referring to the intercalation of pyridine-based guest molecules into the Ni (4-mBA) layered solid. The framework appears to be maintained through the intercalation process because the *100* and the *010* parameters are in agreement for each sample. In this case, the data confirms that the hydrogen-bonded layer withstands intercalation without significant interruption.

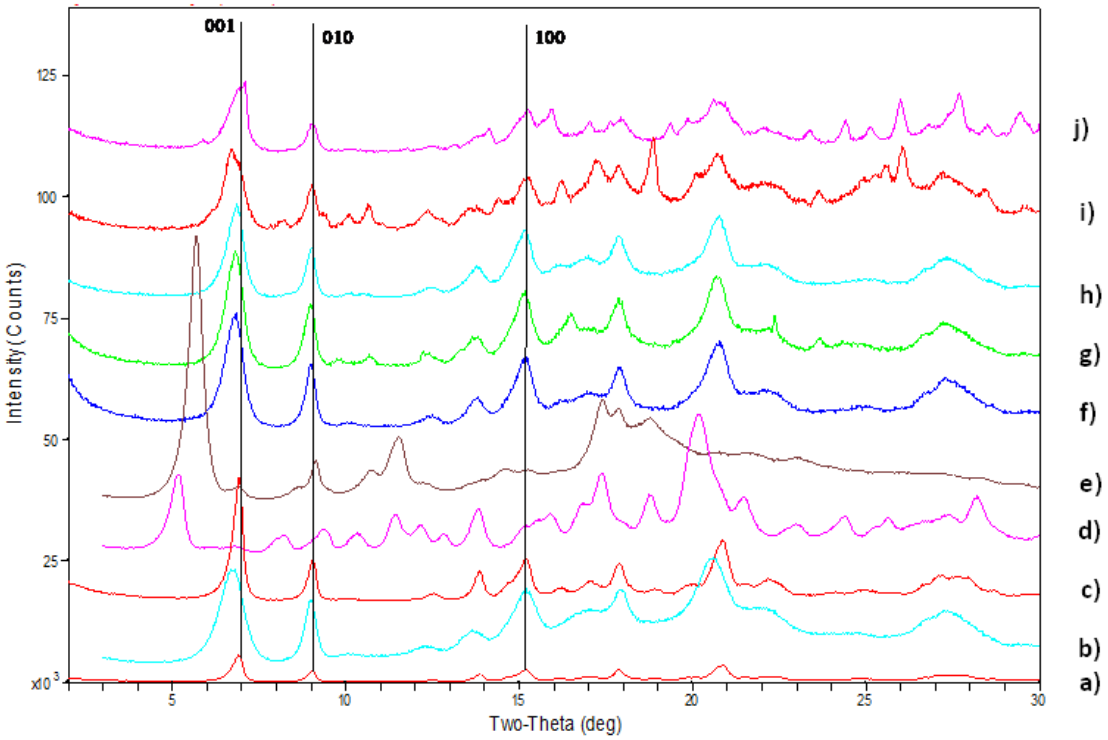

Figure 3.9 Compilation of powder XRD pattern from the intercalation of pyridine-based molecules into Ni (4-mBA) layered material. Where (a) Ni(4-mBA), (b) pyridine, (c) 2-picoline, (d) 4-picoline, (e) 4-ethylpyridine, (f) 4-cyanopyridine, (g) 4,4′-bipyridine, (h) 4-*t*-butylpyridine, (i) 4-N,N′-dimethylaniline, and (j) 4-chloropyridine.

3.7 Discussion

For the attempts to intercalate non-coordinating guest molecules, no spectroscopic or gravimetric evidence indicated that intercalation had occurred. If intercalation occurred, the TGA would have shown a weight loss that corresponds to extra guest molecules, as was shown in Table 3.3. Likewise, if intercalation occurred then the powder XRD might show an increase in the d-spacing which corresponds to an increase in the distance between the layers, but as can be seen in Table 3.4, no changes occurred. Two factors may have prevented intercalation of the non-

coordinating guests: the size of the molecule and the strength of the interaction between the guest and the host layer. Even small molecules with alcohol functionality do not provide a hydrogen-bonding anchor to the hydrophilic layer.

For the attempts to intercalate coordinating guest molecules, there is some spectroscopic and gravimetric evidence that intercalation occurs with certain guest molecules. One guest molecule that intercalated was 4-picoline. The TGA showed a very large weight loss that was in agreement with the inclusion of three guest molecules. The powder XRD showed a dramatic increase in the interlayer distance that is also in agreement with the conclusion that the layer "swelled" to allow the extra guest molecules to reside between the layers.

Samples intercalated with 4-ethylpyridine also showed a large weight loss by TGA, which is in agreement with the inclusion of two guest molecules. The powder XRD exhibited a shift to lower 2Θ in the example of 4-ethypyridine, which is in agreement with the idea of the layer expansion. On the other hand, while pyridine showed TGA evidence of inclusion, the PXRD showed very little evidence of expansion. The pyridine molecules might not be large enough to show a significant change in the interlayer distance.

Of the remaining pyridine-based guests, only 4-(dimethylamino) pyridine intercalated, with an approximately 1:1 Guest: Host ratio. The TGA showed an increased weight loss that would agree with the presence of an extra guest molecule. However, the powder XRD exhibited a very small increase in layer expansion.

Guest molecules such as 2-picoline and 4-cyanopyridine did not show signs of intercalation. The main reason could be due to sterics and electronic properties. The

2-picoline contains some steric hindrance and the 4-cyanopyridine contains a highly electron withdrawing group on the ring.

3.8 Conclusion

We have successfully created a close packed layered host comprised of hydrogen bonds and a hydrophobic interlayer. We have also investigated the ability of this layered host to intercalate two different types of small molecules: non-coordinating and coordinating.

Non-polar non-coordinating molecules did not intercalate the layered host. Even guest molecules that have stronger hydrogen bonding functionalities were not observed to anchor themselves within the host material. Non-pyridine guest molecules, aryl or alkyl, were not observed to intercalate at all. The molecules presented in this chapter were not an exhausted listed but a representation of the molecules attempted for intercalation. The exhausted listed can be found in the reference section.[16]

Coordinative intercalation appears to have occurred to a great extent in three samples, as confirmed by both TGA and powder XRD data, and by the observation of a color change. These three guest molecules are pyridine, 4-ethylpyridine and 4-picoline, where the guest molecules included in 1: 2 or 1: 3 H: G ratios. 4-(dimethylamino) pyridine was also incorporated at a 1:1 H: G ratio. It is likely that the strong Lewis bases functionalities anchor these guests into the solid. In order to include guest molecules without coordinative covalent bonding, our focus shifts to

developing porous hydrogen bonded pillared frameworks, where the guest molecules will reside between pillars.

3.9 References

(1) Ma, L.; Carter, A.; Lin, W. *Chem. Soc. Rev.* **2009**, *38*, 1248-1256.

(2) Maji, T. K.; Kitagawa, S. *Pure Appl. Chem.* **2007**, *79*, 2155-2177.

(3) Finn, R. C.; Burkholder, E.; Zubieta, J. *Perspect. Supramol. Chem.* **2003**, *7*, 241-274.

(4) Seo, J. S.; Whang, D.; Lee, H.; Jun, S. I.; Oh, J.; Jeon, Y. J.; Kim, K. *Nature* **2000**, *404*, 982-986.

(5) Endo, K.; Koike, T.; Sawaki, T.; Hayashida, O.; Masuda, H.; Aoyama, Y. *J. Am. Chem. Soc.* **1997**, *119*, 4117-4122.

(6) Wilson, R. E.; Skanthakumar, S.; Knope, K. E.; Cahill, C. L.; Soderholm, L. *Inorg. Chem.* **2008**, *47*, 9321-9326.

(7) Murray, L. J.; Dinca, M.; Long, J. R. *Chem. Soc. Rev.* **2009**, *38*, 1294-1314.

(8) Han, S. S.; Furukawa, H.; Yaghi, O. M.; Goddard III, W. A. *J. Am. Chem. Soc.* **2008**, *130*, 11580-11581.

(9) Rosi, N. L.; Eckert, J.; Eddaoudi, M.; Vodak, D. T.; Kim, J.; O'Keeffe, M.; Yaghi, O. M. *Science* **2003**, *300*, 1127-1130.

(10) Perron, M.-E.; Monchamp, F.; Duval, H.; Boils-Boissier, D.; Wuest, J. D. *Pure Appl. Chem.* **2004**, *76*, 1345-1351.

(11) Saied, O.; Maris, T.; Wuest, J. D. *J. Am. Chem. Soc.* **2003**, *125*, 14956-14957.

(12) Mallouk, T. E.; Gavin, J. A. *Acc. Chem. Res.* **1998**, *31*, 209-217.

(13) Solin, S. A. *Annu. Rev. Mater. Sci.* **1997**, *27*, 89-115.

(14) Poojary, D. M.; Clearfield, A. *J. Am. Chem. Soc.* **1995**, *117*, 11278-84.

(15) Zhang, Y.; Scott, K. J.; Clearfield, A. *J. Mater. Chem.* **1995**, *5*, 315-18.

(16) 1-butanol,1,3-propanediol,1,4-butanediol,1,5-pentanediol,1,6-hexanediol,1,8-octanediol,1,10-decanediol , 2,4-pentanedione, acetamide, 1,4-dioxane, pyrrolidine, benzene, naphthalene, antracene, biphenyl, diphenylmethane, fluorobenzene, chlorobenzene, phenol, pyrocatechol, resorcinol, hydroquinone, 2-aminophenol, 3-aminophenol, 4-aminophenol, o-cresol, m-cresol, p-cresol, 2-cyanophenol, 4-cyanophenol, 2-chlorophenol, 3-chlorophenol, 4-chlorophenol, 2-bromophenol, 3-bromophenol, 4-bromophenol, 2-phenylphenol, 1-naphthol, 2-naphthol, 1,5-dihydroxynaphthalene, 1,6-dihydroxynaphthalene, 1,7-dihydroxynaphthalene, 2,3-dihydroxynaphthalene, 2,6-dihydroxynaphthalene, 2,7-dihydroxynaphthalene, p-dicyanobenzene, m-dicyanobenzene, o-dicyanobenzene, 4-nitro-o-xylene, 5-iodo-m-xylene, 4-nitrobenzaldehyde, 4-nitrobenzoic acid, nicotinic acid, nicotinamide, isonicotinic acid, isonicotinamide, 2-methylnicotinic acid, 2-chloronicotinic acid, 6-methylnicotinic acid, 6-chloronicotinic acid, 2-methyl-6-chloronicotinic acid, 5-bromonicotinic acid, 2-chloronicotinamide, 6-chloronicotinamide, p-xylylenediamine, m-xylylenediamine, hexafluorobenzene, 4,4′-dimethylbiphenyl, benzophenone, 4-bromo-4′-methoxybiphenyl, 4-bromo-[1,1′-biphenyl]-4-ol, acetone, ethyl acetate, 1-pentanol, 1-hexanol, 1-octanol, toluene, p-xylene, m-xylene, o-xylene, p-diethylbenzene, m-diethylbenzene, o-diethylbenzene, nitrobenzene, p-dinitrobenzene, p-difluorobenzene, m-difluorobenzene, o-difluorobenzene, nitrotoluene, bromobenzene, anisole, iodobenzene, 4,4′-biphenol, hexafluorobenzene, ethylbenzene, 2-phenylphenol, o-difluorobenzene, m-difluorobenzene, 1,4-dichlorobenzene, cumene, anisole, n,n-dimethylaniline, pentane, hexane, heptane, octane, nonane, decane, cyclohexane.

.

Chapter 4

Construction and Guest Inclusion into a Pillared HMOF

4.1 Background

The design and supramolecular synthesis of porous solids have been widely studied by the organic and inorganic communities because these materials have the potential for use in the area such as size-selective separation,[1-3] gas adsorption,[4-7] and heterogeneous catalysis.[8-10] The organic analogs of the inorganic/organic hybrid "clay mimics" have been widely studied by a variety of groups[11-14] including our own.[15,16] Using the same approach to create the organic "clay mimics," the inorganic/organic hybrids frameworks can be modified in a similar fashion.[17] The ability to control the nature of the interlayer region can determine which molecules will reside within these clay mimics. When compared to MOFs, which often form interpenetrated networks that decrease the ability to include larger molecules, layered hydrogen bonded frameworks have the potential to include larger guest molecules because their networks do not interpenetrate like traditional MOFs. These clay mimics can be studied to determine if they have the ability to absorb gases or small solvents.

4.2 Purpose of Research

The general purpose of this research is to logically develop, synthesize, and characterize a hydrogen-bonded pillared framework that would have the ability to include a variety of guest molecules into the framework's pores. We can logically develop an idea based on known hydrogen-bonding principles and some previous work that was completed in our lab. Previously, we were able to synthesize

inorganic/organic layered framework that are connected through charge-assisted hydrogen-bonding. The hydrogen-bonded framework allows the framework to "flex" upon guest insertion and guest removal without disruption of the layered framework. Our approach to the design and synthesis of hydrogen-bonded metal organic frameworks (HMOFs) is to again use molecular components as the building units for pillared structures. We have already demonstrated that metal/organic dicarboxylic acids (i.e. a coordination complex with peripheral carboxylic moieties) combined with organic primary amines yield layered solids upon crystallization. To create a pillared framework we will use different molecular components. We reasoned that replacing the primary amine with a primary diamine should yield a guest containing pillared framework. The guest molecules included in this study vary from alkyl to aryl, from short chain to long chain, and from electron donating groups to electron withdrawing groups in order to fully determine a range of guest molecules that can be inserted into a host complex. In this study, we have chosen to explore co-crystallization methods in order to insert guest molecules into the host framework. The development of an experimental procedure was challenging because all of the components needed to be in solution simultaneously in order to promote co-crystallization of the guest molecules.

4.3 Experimental

4.3.1 Materials and Instrumentation

All chemicals and solvents were purchased from Sigma-Aldrich and used without further modification. The solvents used, methanol and N, N-dimethylformamide, were ACS grade, and the deionized (DI) water was obtained from a Millipore MilliQ Plus purifier. The metal dicarboxylic acid was synthesized based on the synthetic method given in 3.4.2 but in this case a Zn(II) ion was used. The synthesis was performed using $ZnSO_4 \cdot 6\ H_2O$ in the synthesis instead of $NiSO_4 \cdot 6\ H_2O$. The organic diamine used in this study was either 3,3'-dimethylbenzidine or *o*-tolidine. The guest molecules that were used in the above synthesis can be found in Table 4.1 and 4.2.

All isolated materials were analyzed by thermogravimetric analysis (TGA), differential scanning calorimetry (DSC), powder x-ray diffraction (PXRD), and by single crystal X-ray diffraction when possible.

4.3.2 Experimental Procedure

The synthetic procedure for generating the pillared hydrogen-bonded metal-organic frameworks proceeded by combining molecular components and then allowing the material to crystallize. The molecular components used in this synthesis are the metal dicarboxylic acid (Zn(pyridine 2,4-dicarboxylic acid)$_2$(H_2O)$_2$) and the organic diamine (3,3'-methylbenzidine), which creates the three-dimensional HMOF as observed in Figure 4.1. The synthetic ratio of dicarboxylic acid to diamine that will be followed throughout all synthetic procedures in this chapter is 1:1. Detailed

synthetic procedures for the sample yielding good single-crystal X-ray structures are given in Section 4.5.

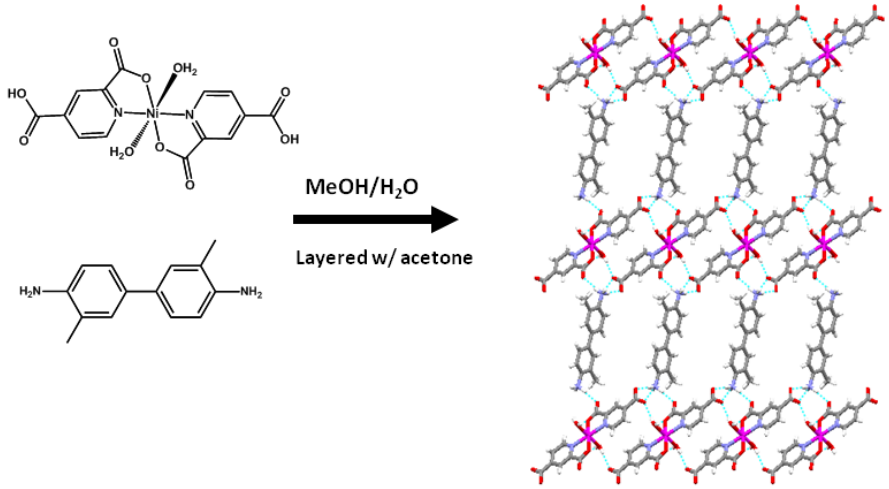

Figure 4.1 The synthetic approach for creating a pillared framework.

4.4 Guest Molecules used for Co-crystallization

A variety of guest molecules were used during attempts to co-crystallize the pillared framework, but not all were incorporated into the accessible pore spaces of the host. Figure 4.3 illustrates where the guest molecules (black) would reside within the pillared framework. For samples that did not yield good quality single crystals, a

combination of TGA analysis (extra weight loss) and powder XRD (position of the lowest 2Θ peak) were used to confirm the presence of guest molecules.

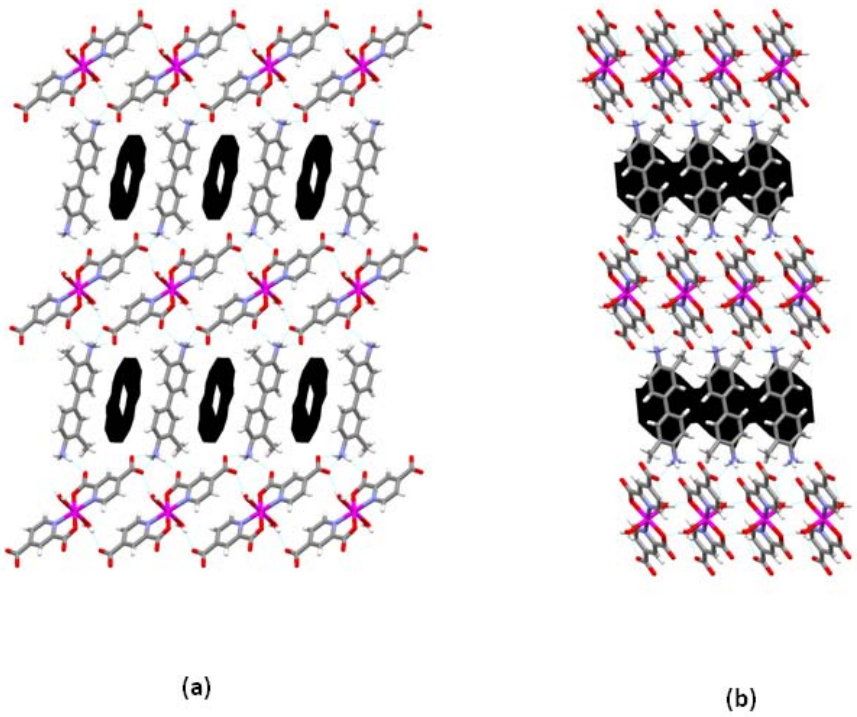

Figure 4.2 Open channels showing the voided area: (a) view down the a axis and (b) rotated 90°

4.4.1 Guests that Showed Inclusion

The first set of guest molecules that will be discussed are those which showed evidence of inclusion. Table 4.1 contains the list of guest molecules that were co-crystallized into the pillared framework. Appendix C contains the TGA and DSC data for all guest-included samples.

Table 4.1 Guest Molecules that Co-crystallized with the Pillared Framework.

Name of Guest Molecule	Structure of Guest Molecule	Molecular Weight (g/mol)	Boiling or Melting Point (° C)
acetone		**58.08**	**56**
ethyl acetate	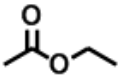	**88.10**	**75-77**
1-pentanol		**88.15**	**136-138**
1-hexanol		**102.17**	**156-157**
1-octanol		**130.23**	**196**
toluene	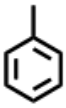	**92.14**	**110-111**
***p*-xylene**		**106.17**	**138**
***m*-xylene**	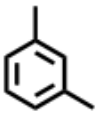	**106.17**	**138-139**

***o*-xylene**	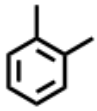	**106.17**	**143-145**
***p*-diethylbenzene**		**134.11**	**182-184**
***m*-diethylbenzene**	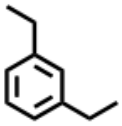	**134.11**	**182**
***o*-diethylbenzene**	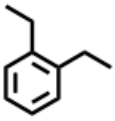	**134.11**	**183**
nitrobenzene	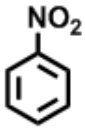	**123.11**	**210-211**
***p*-dinitrobenzene**	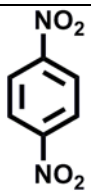	**168.11**	**183**
***p*-difluorobenzene**		**114.09**	**88-89**
***m*-difluorobenzene**	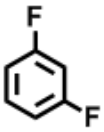	**114.09**	**82**

***o*-difluorobenzene**	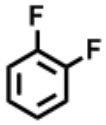	**114.09**	**92**
nitrotoluene	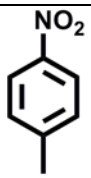	**137.14**	**238**
bromobenzene		**157.01**	**156**
anisole	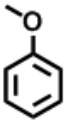	**108.14**	**154**
iodobenzene		**204.01**	**188**
4,4′-biphenol		**186.21**	**280-282(#)**

The majority of the guest molecules that were included into the pillared framework were aryl-based and contain electron-donating substituents. As for a shape preference, the pillared framework included a variety of isomers but showed some selectivity towards the para-substituted aryls. The para-substituted guest

molecules must fill the space most efficiently, which is obvious when looking at the void space, Figure 4.2b. The other two isomers (*meta* and *ortho*) have shown evidence of inclusion, but only when a small electron withdrawing or donating group is present. As long as the electron donating groups are not too large, they appear to be included into the pillared framework most efficiently.

As for mono-substituted aryls, the pillared framework shows a wide range of included guest molecules, from nitrobenzene to anisole. Here we see the inclusion of guest having large electron withdrawing groups as well as a large electron donating groups. These mono-substituted aryls that showed evidence of inclusion either contained an electron-donating group or a large (by size) electron-withdrawing group as in the case with nitrobenzene, bromobenzene and iodobenzene.

There were also a few alkyl-based guest molecules that cocrystallized with the pillared framework. All are either alkyl alcohols or small, volatile solvents. The alcohols appeared to the best suited guest for the pillar. In appears that the length of the alky-based guest is the determining factor because too small or too long molecules do not show evidence of inclusion. Furthermore, the alkyl alcohols contain a hydrogen bond donor, which can be used to anchor the guest molecule to the host framework. Specific size, shape and electronics all affect whether the guest molecule is included into our pillared framework.

4.4.2 Guests That Did Not Show Inclusion

The second set of guest molecules that will be discussed are those that showed no evidence of inclusion. Guest inclusion was determined by the combination of TGA and powder XRD analysis. Table 4.2 contains the list of guest molecules that were not included into the pillared framework.

Table 4.2 Guest Molecules that did not Co-crystallize with the Pillared Framework (# indicates melting point).

Name of Guest Molecule	Structure of Guest Molecule	Molecular Weight (g/mol)	Boiling Point (° C)
1-butanol		**74.12**	**116-118**
1,3-propanediol		**76.09**	**214**
1,4-butanediol		**90.12**	**230**
1,5-pentanediol		**104.15**	**242**
1,6-hexanediol	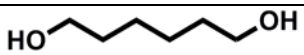	**118.17**	**250**
1,8-octanediol		**146.23**	**272**
1,10-decanediol		**174.28**	**297**
2,4-pentanedione	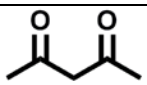	**100.12**	**140.4**
acetamide	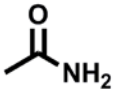	**59.07**	**221**

1,4-dioxane		**88.11**	**100-102**
pyrrolidine	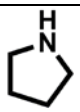	**71.12**	**87-88**
benzene		**78.11**	**80**
naphthalene	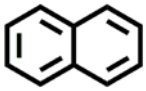	**128.17**	**218**
antracene	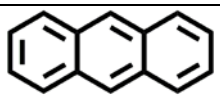	**178.23**	**340**
biphenyl		**154.12**	**255**
diphenylmethane	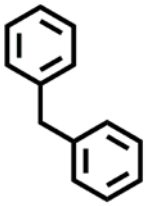	**168.23**	**264**
fluorobenzene	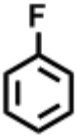	**96.10**	**85**
chlorobenzene	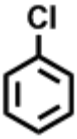	**112.56**	**132**

phenol	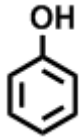	**94.11**	**182**
pyrocatechol	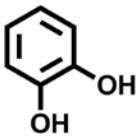	**110.11**	**245**
resorcinol	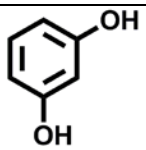	**110.11**	**178**
hydroquinone		**110.11**	**285**
2-aminophenol	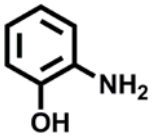	**109.13**	**170-175(#)**
3-aminophenol	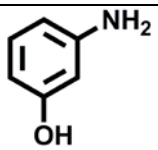	**109.13**	**164**
4-aminophenol		**109.13**	**185-189(#)**
***o*-cresol**	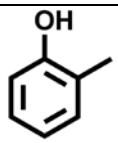	**108.14**	**191**
***m*-cresol**	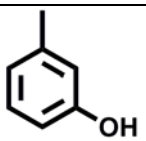	**108.14**	**203**

***p*-cresol**		**108.14**	**202**
2-cyanophenol	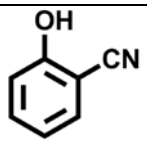	**119.12**	**149**
4-cyanophenol	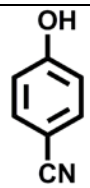	**119.12**	**110-113(#)**
2-chlorophenol	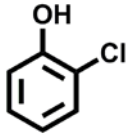	**128.56**	**175-176**
3-chlorophenol	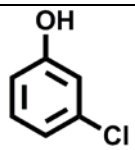	**128.56**	**214**
4-chlorophenol	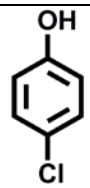	**128.56**	**220**
2-bromophenol	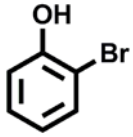	**173.01**	**195**
3-bromophenol	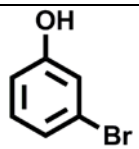	**173.01**	**236**

4-bromophenol	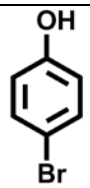	**173.01**	**2325-236**
2-phenylphenol	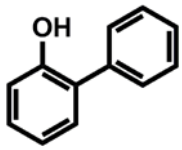	**170.21**	**282**
1-naphthol	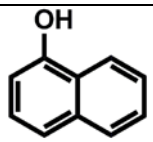	**144.17**	**278-280**
2-naphthol	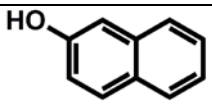	**144.17**	**285-286**
1,5-dihydroxynaphthalene	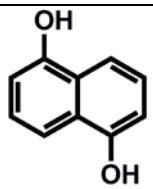	**160.17**	**259-261(#)**
1,6-dihydroxynaphthalene	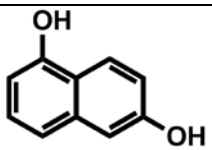	**160.17**	**130-133(#)**
1,7-dihydroxynaphthalene	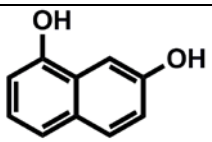	**160.17**	**180-184(#)**
2,3-dihydroxynaphthalene	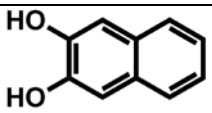	**160.17**	**161-165(#)**
2,6-dihydroxynaphthalene	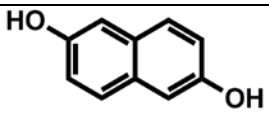	**160.17**	**223-225(#)**

2,7-dihydroxynaphthalene	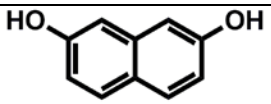	**160.17**	**185-190(#)**
***p*-dicyanobenzene**		**128.13**	**221-225(#)**
***m*-dicyanobenzene**	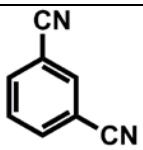	**128.13**	**163-165(#)**
***o*-dicyanobenzene**	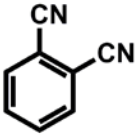	**128.13**	**137-139(#)**
4-nitro-*o*-xylene	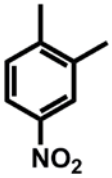	**151.16**	**143**
5-iodo-*m*-xylene	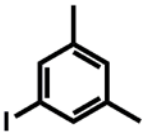	**232.06**	**92-94**
4-nitrobenzaldehyde	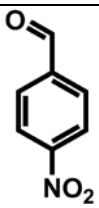	**151.12**	**103-106(#)**
4-nitrobenzoic acid	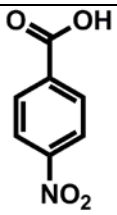	**167.12**	**237-240(#)**

nicotinic acid	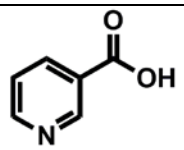	**123.11**	**236-239(#)**
nicotinamide	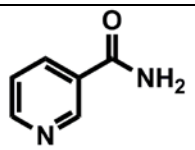	**122.12**	**128-131(#)**
isonicotinic acid	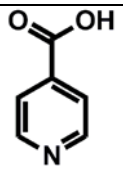	**123.11**	**300**
isonicotinamide	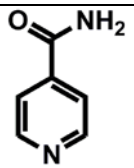	**122.12**	**155-157(#)**
2-methylnicotinic acid	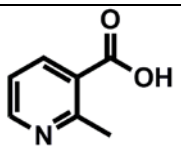	**137.14**	**228-230(#)**
2-chloronicotinic acid	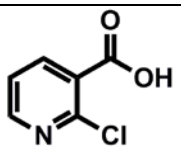	**157.55**	**176-178(#)**
6-methylnicotinic acid	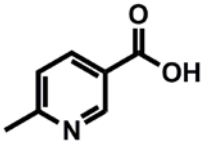	**137.14**	**210-213(#)**
6-chloronicotinic acid	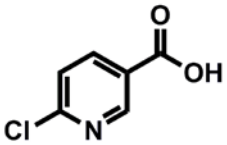	**157.55**	**190**
2-methyl-6-chloronicotinic acid	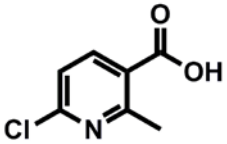	**171.59**	**220-221**

5-bromonicotinic acid	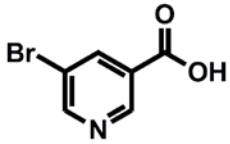	**202.01**	**178-180(#)**
2-chloronicotinamide	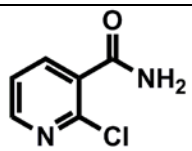	**156.57**	**164-167(#)**
6-chloronicotinamide	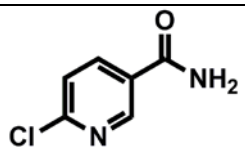	**156.57**	**210-212(#)**
***p*-xylylenediamine**	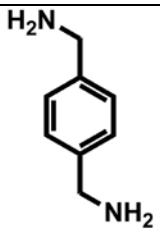	**136.19**	**230**
***m*-xylylenediamine**	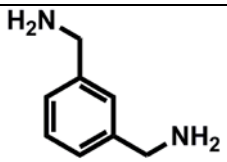	**136.19**	**265**
hexafluorobenzene	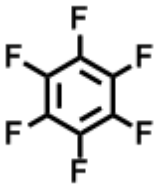	**186.05**	**80.82**
4,4′-dimethylbiphenyl		**182.26**	**295**

benzophenone	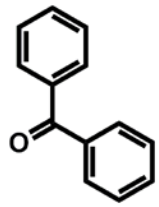	**182.22**	**305**
4-bromo-4′-methoxybiphenyl	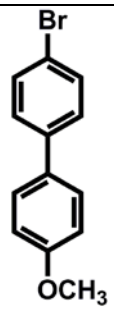	**263.13**	**143-145(#)**
4-bromo-[1,1′-biphenyl]-4-ol		**249.10**	**164-166(#)**

The TGA and PXRD data did not show any evidence that the above guest molecules were incorporated into the pillared framework. There is a wide variety of non-guest molecules in this study, ranging from small alkyl alcohols to disubstituted biphenyl molecules. Two different situations may prevent inclusion of each of these molecules. The majority of the cases involved guest molecules crystallizing out of solution before the pillared framework could be formed. The other situation had the pillared framework crystallizing with the solvent as a guest, so the solvent was preferred over the intended guest.

The alkyl-based molecules that did not include were mainly the alkyl diols and small volatile molecules. These molecules were either too small or too large to fit into the channels, and therefore they did not form the guest included pillared framework.

The aryl-based molecules that did not include ranged from extended biphenyls to simple aryls like benzene. Here we looked at various series to determine if one isomer was preferred over another but for example in the series of aminophenol, cyanophenol, and cresol there was no evidence of inclusion. It would seem that the alkyl alcohols are favored in the pillar over the phenol molecules. When looking at extended aryl-based molecules it appears that the extended molecules show no evidence of inclusion because of their size and possibly their large substituents.

Pyridine-based molecules, such as the nicotinic acids, nicotinamides, isonicotinic acid, and isonicotinamide, were also tested. These molecules typically crystallized out of solution before the co-crystallization process could occur. Apparently, the guest molecules under our current experimental procedure do not favor forming a host-guest complex. It is possible that changing the solvent system would allow for co-crystallization with these guest molecules. The following portion of the chapter will solely focus on the co-crystallizations that successfully garnered a crystal structure from single-crystal x-ray diffraction.

4.5 Procedures for Characterized Crystals

4.5.1 Synthesis of [o-tolidinium]Zn(PDCA)$_2$(H$_2$O)$_2$ · guest molecule

All of the following compounds were produced under the same synthetic conditions. Zn(HPDCA)$_2$(H$_2$O)$_2$ (0.025g, 0.06mmol) was suspended in 2mL of MeOH followed by the addition of o-tolidine (0.012g, 0.06mmol) in 2mL of MeOH. The cloudy suspension became clear upon the addition of 1mL of both DMF and H$_2$O. Finally, 1mL of the guest molecule was added and allowed to sit until crystals formed. Table 4.3 lists the various guest molecules, time for crystallization to occur, color and morphology of the isolated crystals, and % yield (grams).

Table 4.3 Crystallization Information

Guest Molecule	Length of Crystallization	Color and Morphology	% Yield
acetone	**1 week**	**Orange plates**	**48.6**
nitrobenzene	**3 days**	**Yellow plates**	**49.6**
***p*-xylene**	**3 days**	**Tan plates**	**59.6**
1-hexanol	**1 week**	**Orange plates**	**52.8**
1-pentanol	**1 week**	**Yellow-orange plates**	**54.6**
***p*-difluorobenzene**	**1 week**	**Orange plates**	**51.3**

4.6 Characterization of Crystal Structures

In all cases crystals of appropriate dimensions were mounted on Mitgen loops in random orientations. Preliminary examination and data collection were performed using a Bruker Kappa Apex II Charge Coupled Device (CCD) Detector system single crystal X-Ray diffractometer equipped with an Oxford Cryostream LT device. All data were collected using graphite monochromated MoKα radiation (λ= 0.71073 Å) from a fine focus sealed X-Ray tube. Preliminary unit cell constants were determined with a set of 36 narrow frame scans. Typical data sets consist of a combinations of ϖ and ϕ scans. Typical scan width of 0.5° was used along with exposure times between 15-30 seconds/frame. The crystal was placed at a distance of 4.0 cm from the detector.. The collected frames were integrated using an orientation matrix determined from the narrow frame scans. Apex II and SAINT software packages[18] were used for data collection and integration. Analysis of the integrated data did not show any decay. Final cell constants were determined by global refinement of reflections from the complete data set. Collected data were corrected for systematic errors using SADABS[19] based on the Laue symmetry using equivalent reflections. Structure solution and refinement were carried out using the SHELXTL-PLUS software package.[20] The structures were solved by direct methods in triclinic space groups P-1 and refined with full matrix least-squares refinement by minimizing Σ $w(F_o^2-F_c^2)^2$. All non-hydrogen atoms were refined anisotropically to convergence. Specific experimental details for individual structure are given below.

The ammonium ion and acetone were found to be disordered. The disorder was resolved with two orientations of 50% occupancy. The H atoms on the water

molecules were located and refined. All other H atoms were added in their calculated positions and refined using appropriate riding models (AFIX m3). The model was refined to convergence to the final residual values of R_1=4.1% and wR_2=10.4%.

The nitrobenzene guest molecule is disordered due to forced crystallographic symmetry. The model was refined with PART -1 to avoid the forced symmetry. All H atoms were added in the calculated position and refined using appropriate riding models (AFIX m3). The model was refined to convergence in the space group *P*-1 to the final residual values of R1=3.6% and wR2=9.6%.

In the p-xylene structure, the methyl groups of the molecule are disordered. The disorder was resolved with two orientations of 50% occupancy models. A molecule of acetone was found in the lattice of this compound. All H atoms were added in the calculated position and refined using appropriate riding models (AFIX m3). The model was refined to convergence to the final residual values of R_1=7.3% and wR_2=20.6%.

The hexanol guest molecule is disordered due to forced crystallographic symmetry. The model was refined with PART -1 to avoid the forced symmetry. The hydrogen atoms associated with the bound water molecules were located and refined. All other H atoms were added in the calculated position and refined using appropriate riding models (AFIX m3). The model was refined to convergence in the space group *P*-1 to the final residual values of R1=8.3% and wR2=22.6%.

For TGA analysis, the sample was placed on the platinum TGA pan for analysis and scanned from 40 to 550° C with a heating rate of 10° per minute. Prior to heating, the sample was held for five minutes at 40°C to allow evaporation of all excess solvent on the crystals. The temperature range that was used to calculate weight loss was derived from the differential plot generated from the software.

For DSC analysis, the powder was weighed out and sealed into a Tzero aluminum pan containing a lid and crimped for complete enclosure. The sample was help for 5 minutes at 40°C to ensure all solvent was removed from the surface of the powder and then scanned from 40 - 450° C with a heating rate of 10° C per minute.

For PXRD analysis, the powder was placed on a quartz zero background holder, prior to data collection. Data was collected in the range from $2\Theta = 2 - 30°$ at 0.02° per step and a step size of 1.5 seconds per step. The data analysis consisted of overlaying the spectra with the powder pattern from the starting material to observe any differences with the *001* peak. Additionally, the associated d-spacing was calculated for each compound.

For UV-Vis analysis, the sample was mixed with Nujol, ground in a mortar and applied to KBr plates. Scans were taken from 200nm to 800nm. A background scan consisting of Nujol was acquired prior to any sample scan. Data analysis consisted of overlaying the scans of the starting material with each subsequent pyridine scan to observe any changes in peak position.

4.7 Discussion of Crystal Structures Containing Guest Molecules

Herein, a detailed discussion of each crystal structure that contains a guest molecule is presented. A general table of the guest molecules, their molecular weight, and boiling points can be found in Table 4.1. The expected and actual weight % losses for each crystal structure can be found in Table 4.4. The crystal structures show the presence of one di-ammonium counterion per metal dianion. The host frameworks in each compound are virtually identical. The metal dianions comprise the sheets, which are held together by $N\text{-}H^{+}\cdots O^{-}$ hydrogen bonds between the cations and anions, as shown in Figure 4.3. The sheets are pillared by the linear diammonium cations, with interlayer distances of 19.63 – 19.75 Å, as measured from the Zn(II) to Zn(II) interlayer distances along the cell axes.

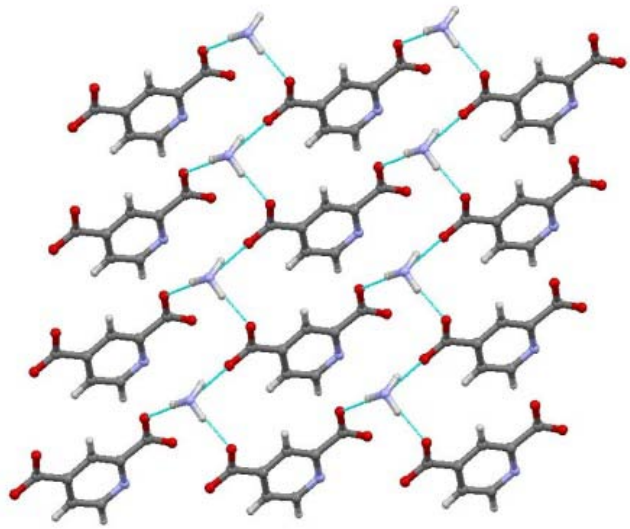

Figure 4.3 The hydrogen bonded layer (showing the ammonium – carboxylate hydrogen bonding).

The diammonium pillars are arranged orthogonal to the plane of the hydrogen-bonded sheet, resulting in a void space that accommodates a variety of guests ranging in size and shape. The aryl rings of the cations are arranged in a louvered fashion, so that the sides of each channel are walled off. Therefore, in contrast to many porous/channeled metal-organic structures, molecular transport can only take place in one direction. The distance between channel walls varies from 8.27 to 8.51Å as measured from the pillar nitrogen atoms along the cell axes. The channel width varies by up to 3% from structure to structure, demonstrating that the hydrogen bonds allow some flexibility to accommodate guest molecules.

Table 4.4 Weight losses (expected and actual) for each crystal structure.

Guest Molecules	Loss of Guest (Expected)	Loss of Water (Expected)	Loss of Guest (Actual)	Loss of Water (Actual)
acetone	**8.24%**	**5.11%**	**1.31%**	**5.86%**
nitrobenzene	**15.99%**	**4.68%**	**14.79%**	**6.16%**
***p*-xylene**	**14.12%**	**4.79%**	**16.66%**	**4.39%**
1-hexanol	**13.66%**	**4.81%**	**11.48%**	**5.09%**
1-pentanol	**12.01%**	**4.90%**	**10.11%**	**5.54%**
***p*-difluorobenzene**	**15.01%**	**4.74%**	**7.13%**	**5.11%**

4.7.1 Structure of [o-Tolidinium]Zn(PDCA)$_2$(H$_2$O)$_2$ · acetone

The pillared framework contains acetone guest molecules that insert upon crystallization from solution. The acetone molecules are orientated in a manner such that the carbonyl group is pointed toward the hydrophobic interlayer and the two methyl groups are pointed toward the hydrophilic layer, which can be seen in Figure 4.4. Basic chemical intuition would have you believe the hydrophobic methyl groups would be positioned towards the hydrophobic interlayer and the carbonyl groups towards the hydrophilic layer. The orientation of the guest molecule must indicate that the overall packing of the crystal structure will direct the position of the guest molecules and the quantity of guest molecules present. Inside the open channel reside two acetone molecules that take up a substantial amount space. These guest molecules are well behaved in the crystallographic sense which means the guest molecules are not continuously rotating within the crystal lattice, at least at low temperatures. The metal dicarboxylate portion of the framework is tilted down in the crystal structure which indicates the methyl group that is ortho to the amine is hindering the formation of a more lamellar type structure and increasing the distance between the layers to a distance of 19.71Å.

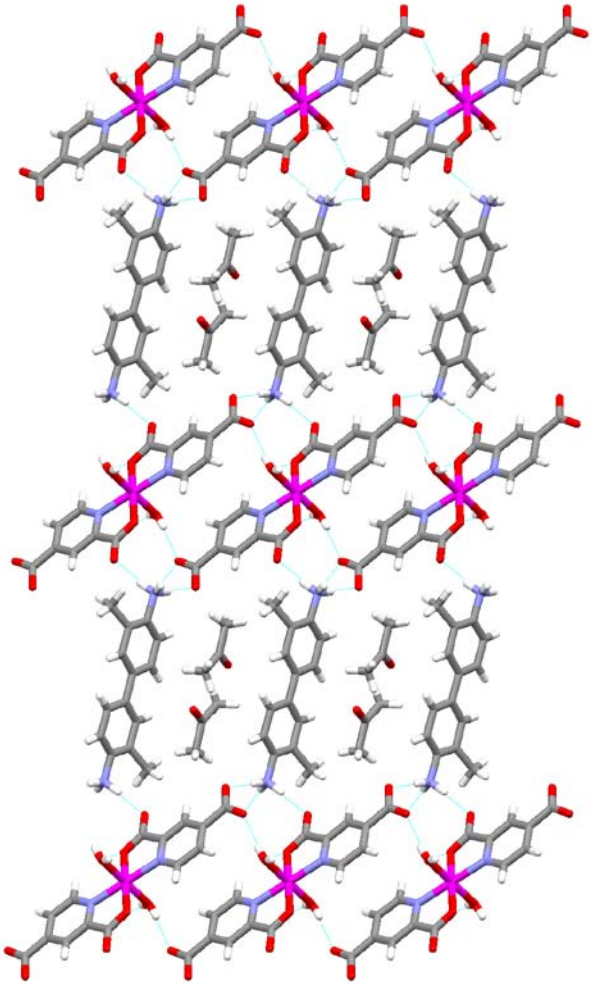

Figure 4.4 Packing diagram of the pillar containing acetone.

The TGA thermograph showed four sets of individual weight losses. The first visual weight loss of 1.31% occurred in the region of 80° - 120° C corresponding to the loss of guest molecule from the open channel. 8.24% of the weight would be lost if the acetone was present in the same proportion determined by the crystal structure. Since acetone is a small, volatile solvent this result is not surprising because loss of acetone is possible during the drying phase. The second weight loss occurring in the

region of 120° - 180° C is consistent with the loss of the two axial water ligands on the zinc metal center. The third and fourth weight losses correspond to decomposition of the pillared framework. Decomposition of the framework starts to occur after 200C.

The DSC thermograph shows three sets of endotherms which correspond to three of the four weight losses observed in the TGA. It is likely to assume that the three endotherms are associated with the loss of the axial water ligands and the decomposition of the pillared framework, which were evident in the TGA. There was no visual evidence of the guest molecule being present in this sample which would indicate that the grinding procedure releases the acetone molecule due to its volatile nature.

The powder x-ray diffraction pattern shows one major difference from the predicted pattern, a shift in the lowest two theta peak (from 4.5°to 4.85°). This peak corresponds to the *001* peak, which gives the interlayer distance. It is possible that the loss of acetone will allow the pillared framework to slip into a more stable conformation because now the interlayer distance is approximately 18.00Å, a difference of 1.5Å from the unit cell of crystal structure.

4.7.2 Structure of [o-Tolidinium] $Zn(PDCA)_2(H_2O)_2 \cdot$ nitrobenzene

The pillar framework contains a nitrobenzene as a guest molecule and exhibits the same pillared structure found in the acetone-containing framework. The

nitrobenzene guest molecule is disordered because the nitro group points toward the hydrophilic layers above and below (Figure 4.5). The hydrogen-bonded layer is the same as before, with the metal dicarboxylate portion of the framework tilted down giving a near-identical interlayer distance of 19.77Å.

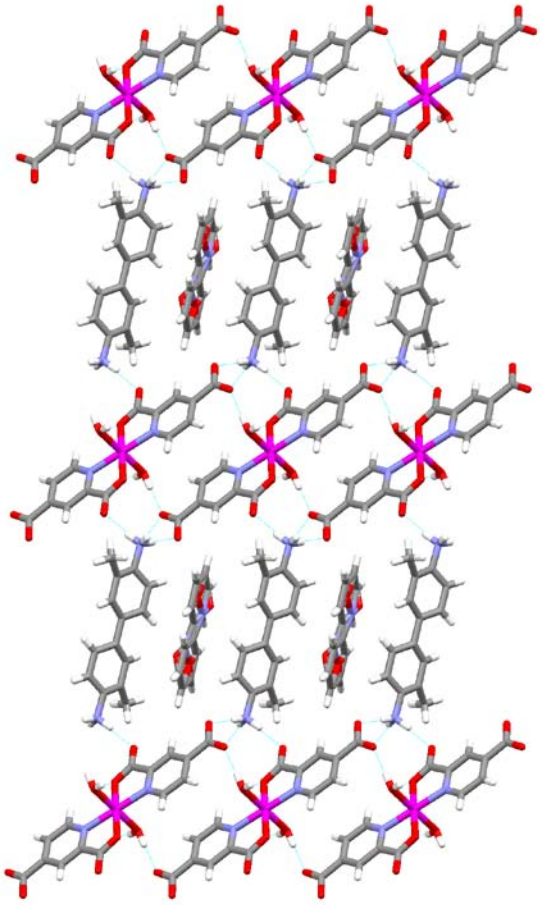

Figure 4.5 Packing diagram of the pillar containing nitrobenzene.

The TGA thermograph showed four individual weight losses. The first weight loss in the temperature region of 55° - 155° C correlates to the loss of the guest molecule, which was calculated to be a 14.79% weight loss. The theoretical weight

loss of nitrobenzene in the pillared framework is 15.99% . The second weight loss in the temperature range of 155° - 215° C correlates with the loss of the two coordinated water ligands. The second weight loss was calculated to be a loss of 6.16% which is in a good agreement with the theoretical weight percent of two coordinated water ligands. The third and fourth weight losses are associated with the decomposition of the pillared framework.

The DSC thermograph shows three individual endotherms peaks that correlate to similar regions of weight loss in the TGA thermograph. The first endotherm is a broad peak that seems to include the release of the guest molecule as well as a loss of the coordinated water ligands. It would appear that the loss of the guest molecules is a slow process because the broad endotherm begins around 95° C and ends around 215° C. The second and third endotherms are in the same temperature range as the final two weight losses that were in the TGA thermograph. These endotherms would also be associated with the decomposition of the pillared framework.

The powder x-ray diffraction pattern that contained the nitrobenzene guest matched that of the theoretical pattern that was generated from the single crystal x-ray data. One major difference between the experimental and theoretical patterns is the presence of two peaks between 4.5 – 5.0 degrees two theta in the experimental pattern. The lowest two theta peaks correlate to the theoretical 001 peak of the crystal structure and residual acetone (confirmed when the powder pattern of acetone was overlaid). The grinding process must release some of the nitrobenzene guest from the pillar framework.

4.7.3 Structure of [o-Tolidinium]Zn(PDCA)$_2$(H$_2$O)$_2$ · *p*-xylene

The pillar framework contains a p-xylene guest molecule that inserts upon crystallization and exhibits the same framework as the pillared structure that contains the acetone molecules. The p-xylene guest molecule is disordered. With the dimensions of the open channel, the structure reveals the methyl groups favor positions which are directed towards the hydrophilic layer or rotated by 90°. The open channels appear to be rectangular in shape with the longer dimension being the distance between the layers. This orientation would allow larger molecules to pack easier within the open channel as compared to two smaller acetone molecules. The packing diagram of the pillared framework with an included p-xylene molecule can be found in Figure 4.6.

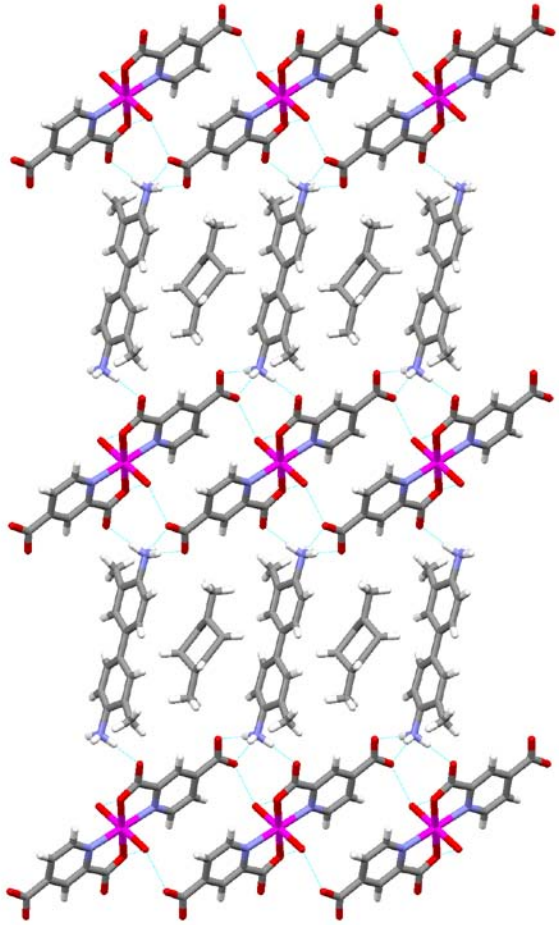

Figure 4.6 Packing diagram of the pillar containing *p*-xylene.

The TGA thermograph shows four individual weight losses. The first weight loss occurred in the temperature range of 80° - 160° C and was calculated to be 16.66%, a little more than the theoretical weight loss associated with a p-xylene guest molecule which is calculated to be 14.12%. The second weight loss occurs in the temperature range of 160° - 215° C that is associated with the loss of the two coordinated water ligands. The weight loss agreement between the loss of the water

ligands from the experimental data and the theoretical calculations are in good agreement. The third and fourth weight losses are associated with the decomposition of the pillared framework.

The DSC thermograph shows three individual endotherms that correlate to similar weight loss regions from the TGA thermograph. The first endotherm, 108° - 216° C (similar to that observed in the TGA), is a broad peak that is associated with the loss of the guest molecule as well as the loss of the coordinated water ligands. The release of the p-xylene guest molecule is a slow process, as indicated by the long temperature range that is associated with this loss. The second and third endotherm can be correlated with the decomposition of the pillared framework because the last endotherms match up with the last two weight losses from the TGA thermograph.

The powder x-ray diffraction pattern of the p-xylene included pillared framework is in good agreement with the theoretical powder pattern that was generated from the single crystal data. After grinding the sample for the powder x-ray analysis, the pattern showed that the guest molecule is not removed from the pillared framework because of the absence of the peak at 4.85 degrees two theta, which is associated with an unoccupied channel.

4.7.4 Structure of [o-Tolidinium]Zn(PDCA)$_2$(H_2O)$_2$ · 1-hexanol

This pillared framework contains 1-hexanol guest molecules that were inserted upon crystallization and exhibits the same properties as the pillared structure

that contains the acetone molecules. The hexanol molecules exhibit a positional disorder. Where the hydroxyl groups are pointed either up or down towards the hydrophilic layer, and are connected by O-H----O=C hydrogen bonds to the carboxylate. Introducing a guest molecule with hydrogen-bonding functionality might ensure insertion due to the complementary interactions that will occur. Again the metal dicarboxylate portion of the framework is tilted vertically which gives an interlayer distance of 19.63Å. The packing diagram of the pillared framework with the hexanol guest molecules can be found in Figure 4.7.

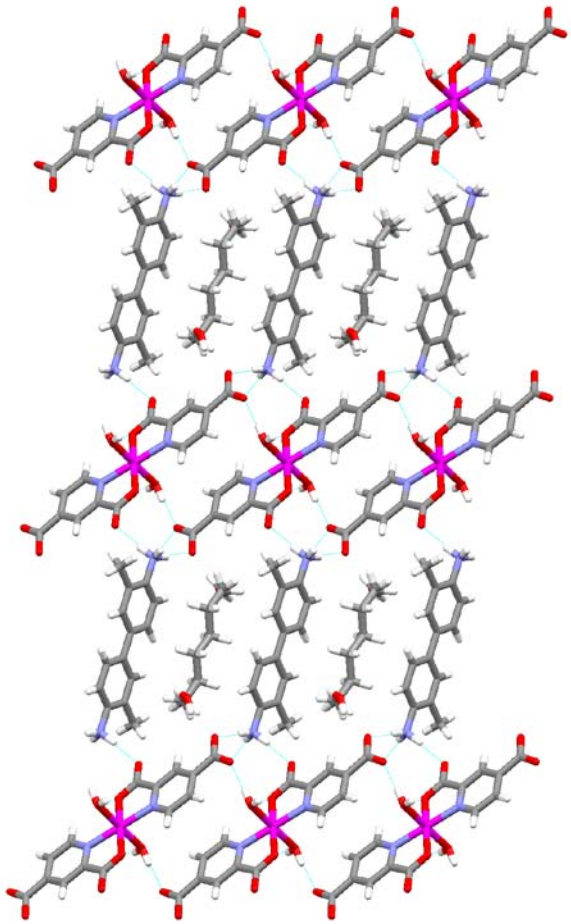

Figure 4.7 Packing diagram of the pillar containing 1-hexanol.

The TGA thermograph contains three individual weight losses. It would appear that the included hexanol guest molecules are being removed over the same temperature range as the loss of the coordinated water ligands. The first weight loss (18.50%) occurs in the temperature range of 92° - 210° C correlates to the calculated loss of the guest molecules and the two coordinated water ligands (19.52% weight loss). The second and third weight losses are associated with the decomposition of

the pillared framework, which has been reoccurring theme with the pillared frameworks.

The DSC thermograph shows three individual endotherms which are correlated to the three weight losses in the TGA thermograph. The first broad endotherm (92° - 217° C) associated with the loss of the hexanol guest molecules and two coordinated water ligands correlates to the first weight loss in the TGA thermograph. The second and third endotherm is associated with the decomposition of the pillared framework because these endotherms match up with the weight losses in the same temperature ranges in the TGA thermograph.

The powder x-ray diffraction pattern of the 1-hexanol included pillared framework powder pattern is in good agreement with the theoretical powder pattern that was generated from the single crystal data. The only difference in the powder patterns is the appearance of a peak at 4.85 degrees two theta. This extra peak correlates with the presence of empty channels because it is the same peak that is formed in the powder pattern of the acetone included (empty) framework. The grinding process of the sample must have removed a small portion of the guest molecule from this framework.

4.7.5 Structure of [o-Tolidinium]Zn(PDCA)$_2$(H_2O)$_2$ · 1-pentanol

This pillared framework contains 1-pentanol guest molecules that inserts upon crystallization and has an identical pillared structure. The pentanol guest molecules

exhibit a positional disorder, where the hydroxyl is always pointing up or down toward the hydrophilic layer. The hydroxyl group again participates in hydrogen bonding from the alcohol to the carbonyl in the metal dicarboxylate (O-H----O=C). The metal dicarboxylate portion of the pillared framework is tilted vertically giving an interlayer distance of 20.11Å. The difference in the interlayer distance of the pillared framework that contains the hexanol guest and the pentanol guest is approximately 0.48Å, which indicates that the hexanol guest molecule packs more efficiently than its shorter chain length analog. The packing diagram of the pillared framework with an included pentanol guest molecule can be found in Figure 4.8.

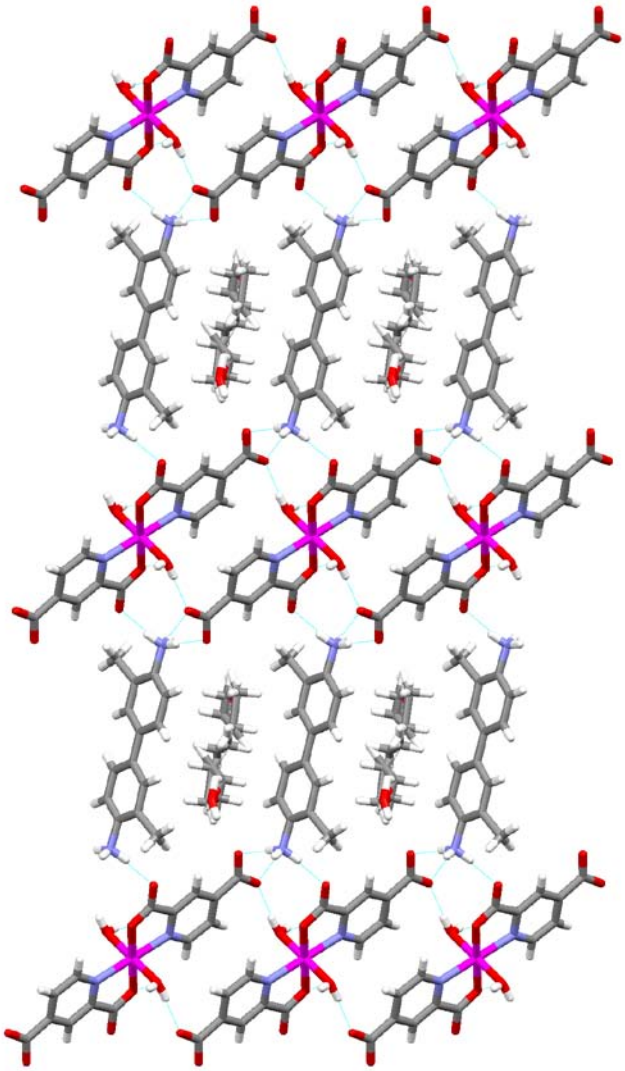

Figure 4.8 Packing diagram of the pillar containing pentanol.

The TGA thermograph reveals three distinct weight losses. The first weight loss was in the range of 62° - 205° C that showed a total weight loss of 15.70%, which can be correlates with the loss of the pentanol guest molecule and the two coordinated water ligands. The theoretical weight loss for the guest molecule and the coordinated water ligands is 16.89%. The pentanol guest molecule must be strongly

attached to the pillared framework because the weight loss associated with loss of the guest molecule occurs around the same temperature as the loss of the water molecules. The second and third weight losses are correlates with the decomposition of the pillared framework, which has been a consistent feature with the guest included pillared frameworks.

The DSC thermograph shows three individual endotherms which, correlate to the three weight losses in the TGA thermograph. The first broad endotherm (95° - 198° C) associated with the loss of the pentanol guest molecule and two coordinated water ligands correlates to the first weight loss in the TGA thermograph. The second and third endotherm is associated with the decomposition of the pillared framework because these endotherms match up with the weight losses in the same temperature ranges in the TGA thermograph.

The powder x-ray diffraction pattern of the 1-pentanol included pillared framework powder pattern is in good agreement with the theoretical powder pattern that was generated from the single crystal data. The only difference in the powder patterns is the appearance of the peak at 4.85 degrees 2Θ, indicating the presence of slightly emptied channel because it is the same peak that was found in the powder pattern of the empty, included framework. The grinding process of the sample must have removed a small portion of the guest molecule from the framework.

4.7.6 Structure of [o-Tolidinium]Zn(PDCA)$_2$(H$_2$O)$_2$ · *p*-difluorobenzene

The pillared framework contains a *p*-difluorobenzene guest molecule that was inserted upon crystallization and exhibits the same pillared structure that contains the acetone guest molecules. A structure was obtained that showed no disorder in the guest molecule and the position of the two fluoro groups were pointed toward the hydrophilic layer. The metal dicarboxylate portion of the pillared structure is again tilted vertically to yield an interlayer distance of 19.77Å. The packing diagram of the pillared framework with an included *p*-difluorobenzene guest molecule can be found in Figure 4.9.

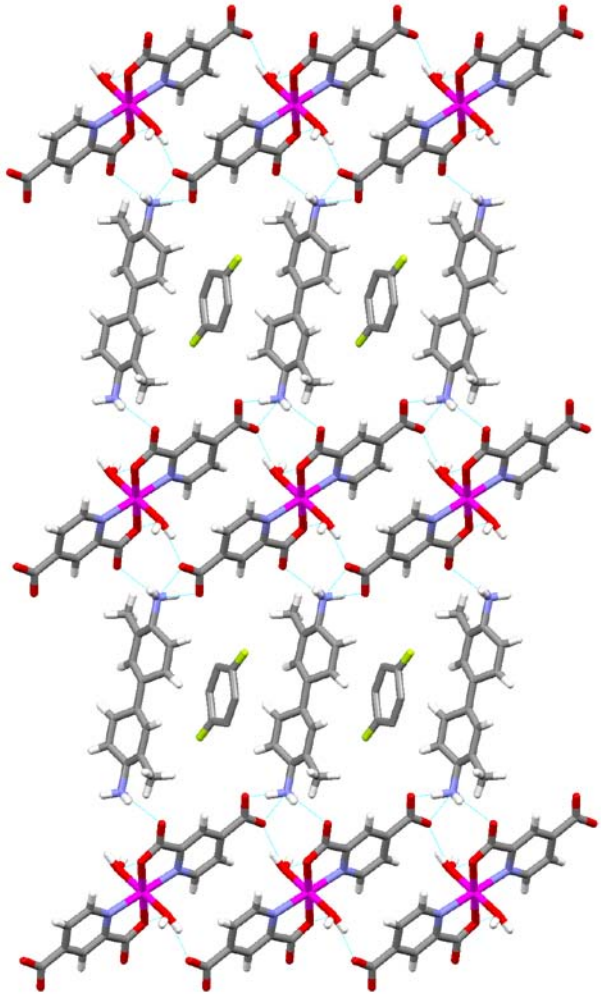

Figure 4.9 Packing diagram of the pillar containing *p*-difluorobenzene.

The TGA thermograph showed four distinct weight losses. The first weight loss occurs in the temperature range of 50° - 104° C and is only 7.13%. The theoretical weight loss for the loss of the guest molecule is 15.00%, which is a difference of 7.87% less. The difluorobenzene guest molecule is a volatile liquid, so drying the crystals, some of the guest must have been lost to the atmosphere. The second weight loss occurred in the temperature range of 104° - 170° C and correlates,

in good agreement, with the loss of the coordinated water molecules. The third and fourth weight losses are associated with the decomposition of the pillared framework.

The DSC thermograph shows three individual endotherms which are correlated to the three weight losses in the TGA thermograph. The first broad endotherm (160° - 215° C) associated with the loss of the two coordinated water ligands correlates to the first weight loss in the TGA thermograph. The release of the guest molecule must have occurred during the grinding phase because the DSC thermograph was consistent with the porous frameworks' DSC. This hypothesis seems plausible because of the relatively low boiling point of *p*-difluorobenzene. The second and third endotherm is associated with the decomposition of the pillared framework because these endotherms match up with the weight losses in the same temperature ranges in the TGA thermograph.

The powder x-ray diffraction pattern of the *p*-difluorobenzene included pillared framework powder pattern showed must major differences when compared with the theoretical powder pattern that was generated from the single crystal structure. The major difference in the powder patterns is the appearance of the peak at 4.85 degrees 2Θ (the porous pillar) and the absence of the peak at 4.5Å, which indicates that there is no guest-containing solid remaining. The grinding process of the sample must have entirely removed the guest molecule from the framework.

4.8 Stability Studies of the Hydrogen-Bonded Framework

Once it was known that the hydrogen-bonded pillared framework contains guest molecules within the channels, the next step was to determine if the framework is stable enough to allow guest removal and reinsertion. A study was conducted where acetone was removed from the crystallized framework that included acetone guest molecules. The solid was then sonicated in ethyl acetate to form a guest-filled framework. Once the ethyl acetate included solid was dried, it was analyzed by powder XRD to observe the characteristic peaks associated with the guest filled framework. The solid was then placed in a small round bottom flask, and vacuum was applied overnight with slight heat (80° C) to remove the guest molecules. This process of guest insertion and removal was repeated a total of seven times to determine if the hydrogen-bonded framework remained intact. Figure 4.10 shows the powder patterns of the solid after the sonication process and the powder pattern of the guest-free solid was not shown for clarity purposes. Figure 4.11 shows the powder pattern after the guest was removed indicating a porous solid.

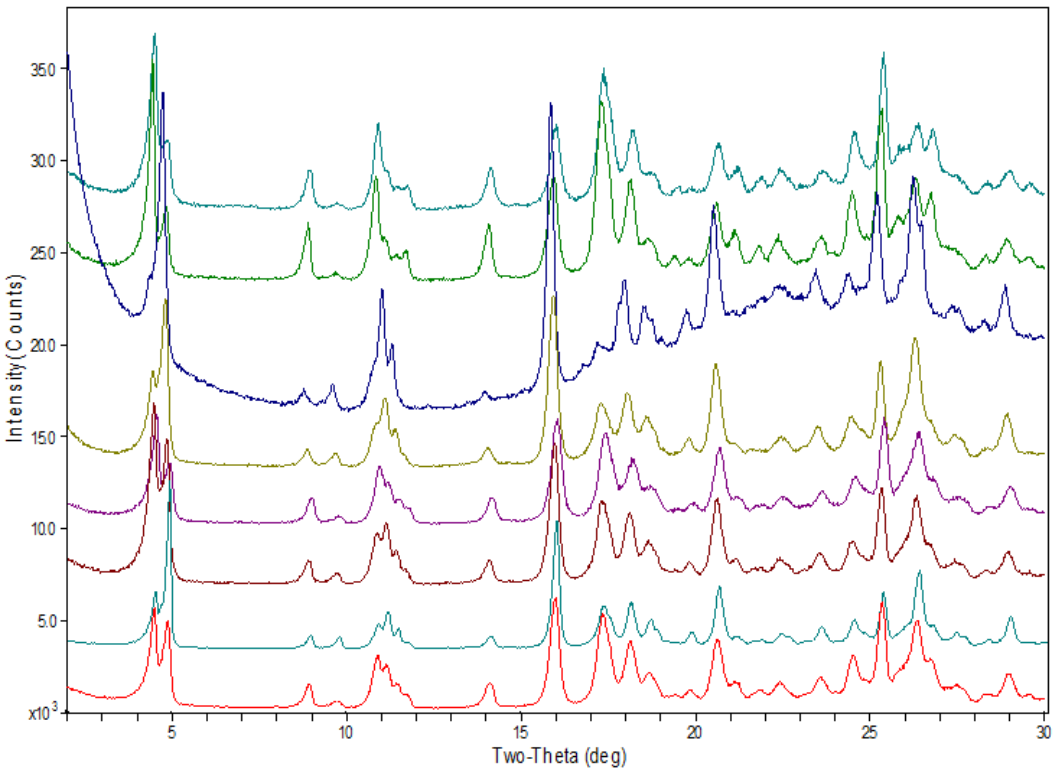

Figure 4.10 Stability of the hydrogen-bonded framework study showing the repeated inclusion of ethyl acetate (Bottom pattern is the crystallized solid and the repeated attempts to include ethyl acetate, 1-7 trials).

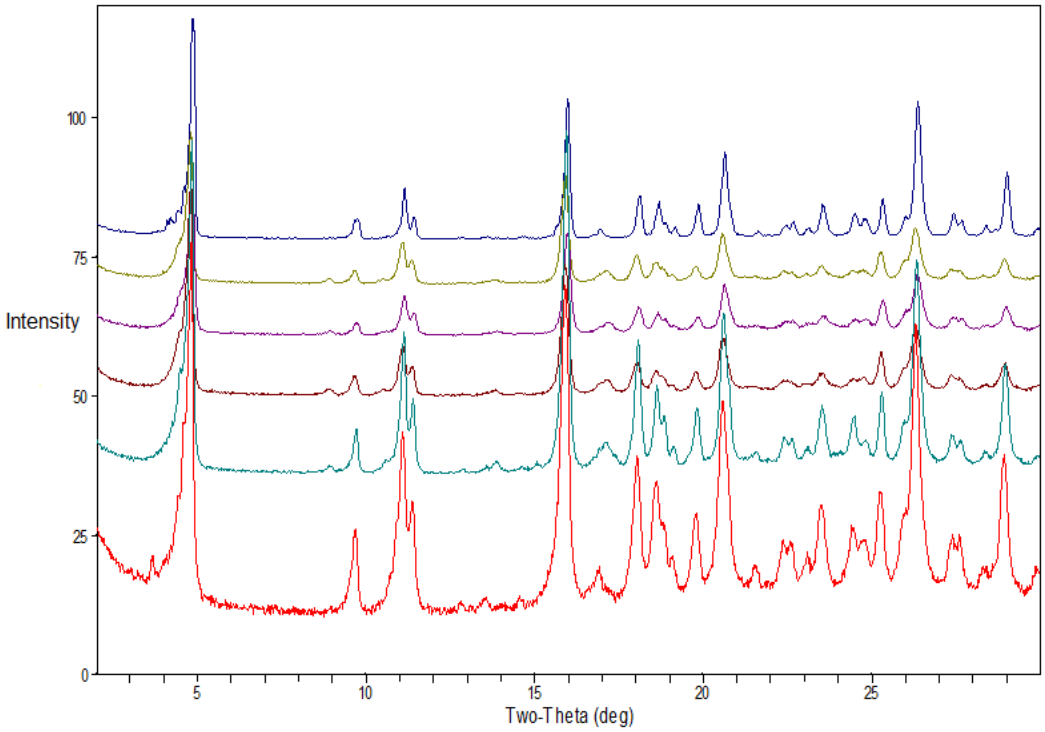

Figure 4.11 Combined PXRD patterns after the guest was removed (bottom pattern is the sonicated trial 1and above are the subsequent trials).

4.9 Conclusion

We have been successful in synthesizing a pillared hydrogen-bonded metal-organic framework. We have demonstrated the ability to insert guest molecules into the open channels. We have also shown that it is possible to insert and remove guest molecules multiple times while maintaining the integrity of the framework. (Note: This is only possible with sonication: experiments in which the solid was soaked in the guest showed little or no sign of guest inclusion.) As seen in Chapter 1.4.3, metal-organic frameworks include guest molecules but their major downside is the fact that they form an interpenetrated network, where our framework does not. Our

material did not decompose upon guest insertion but a change in the interlayer distance was noticed while varying or removing the guest molecules. This change may be due to the hydrogen bonds that make up the layer component as it “flexes” upon guest insertion to allow the guest molecule to occupy the created space. This new host framework has shown to include a wide variety of guest molecules range from aryl to alkyl. The included aryl molecules ranged from electron-donating substituents to electron-withdrawing substituents which show the pillared framework is versatile when including guest molecules. The guest did not show any signs of inclusion were either too large or too volatile, which hindered the guest inclusion upon crystallization.

4.10 References

(1) Pivovar, A. M.; Holman, K. T.; Ward, M. D. *Chem. Mater.* **2001**, *13*, 3018-3031.

(2) Horner, M. J.; Grabowski, S.; Sandstrom, K.; Holman, K. T.; Bader, M.; Ward, M. D. *ACA Transactions* **2004**, *15*, 1-10.

(3) Kim, J.; Lee, S.-O.; Yi, J.; Kim, W.-S.; Ward, M. D. *Separation and Purification Technology* **2008**, *62*, 517-522.

(4) Kondo, M.; Okubo, T.; Asami, A.; Noro, S.-i.; Yoshitomi, T.; Kitagawa, S.; Ishii, T.; Matsuzaka, H.; Seki, K. *Angew. Chem. Int. Ed.* **1999**, *38*, 140-143.

(5) Atwood, J. L.; Barbour, L. J.; Jerga, A. *Science* **2002**, *296*, 2367.

(6) Ma, S.; Sun, D.; Wang, X.-S.; Zhou, H.-C. *Angew. Chem. Int. Ed.* **2007**, *46*, 2458-2462.

(7) Gao, C.; Liu, S.; Xie, L.; Sun, C.; Cao, J.; Ren, Y.; Feng, D.; Su, Z. *CrystEngComm* **2009**, *11*, 177-182.

(8) Jacobs, P. A.; Jaeger, N. I.; Kubelkova, L.; Wichterlova, B.; Editors *Studies in Surface Science and Catalysis Vol. 69: Zeolite Chemistry and Catalysis. Proceedings of an International Symposium, Prague, Czechoslovakia, September 8-13, 1991*, 1991.

(9) Endo, K.; Koike, T.; Sawaki, T.; Hayashida, O.; Masuda, H.; Aoyama, Y. *J. Am. Chem. Soc.* **1997**, *119*, 4117-4122.

(10) Seo, J. S.; Whang, D.; Lee, H.; Jun, S. I.; Oh, J.; Jeon, Y. J.; Kim, K. *Nature* **2000**, *404*, 982-986.

(11) Melendez, R. E.; Zaworotko, M. J. *Supramolecular Chemistry* **1997**, *8*, 157-168.

(12) Biradha, K.; Dennis, D.; MacKinnon, V. A.; Sharma, C. V. K.; Zaworotko, M. J. *J. Am. Chem. Soc.* **1998**, *120*, 11894-11903.

(13) Brouwer, E. B.; Udachin, K. A.; Enright, G. D.; Ripmeester, J. A.; Ooms, K. J.; Halchuk, P. A. *Chem. Comm.* **2001**, 565-566.

(14) Kumar, V. S. S.; Nangia, A. *Chem. Comm.* **2001**, 2392-2393.

(15) Beatty, A. M.; Granger, K. E.; Simpson, A. E. *Chem.--Eur. J.* **2002**, *8*, 3254-3259.

(16) Beatty, A. M.; Schneider, C. M.; Simpson, A. E.; Zaher, J. L. *CrystEngComm* **2002**, *4*, 282-287.

(17) Beatty, A. M.; Helfrich, B. A.; Hogan, G. A.; Reed, B. A. *Cryst. Growth Des.* **2006**, *6*, 122-126.

(18) Bruker Analytical X-Ray: Madison, WI, 2008.

(19) Blessing, R. H. *Acta Cryst.* **1995**, *A51*, 33-38.

(20) Sheldrick, G. M. *Acta Cryst.* **2008**, *A64*, 112-122.

Chapter 5

Small Molecule Transport and Intercalation in Pillared HMOFs

5.1 Background

Zeolites, open-framework aluminosilicates, are useful host/guest materials because they can absorb molecules into their open framework. These frameworks have many uses in areas such as petrochemical cracking, ion exchange (water softening and purification), and the separation and extraction of gases and solvents.[1,2] They contain cavities that are irregularly shaped and therefore not suitable for stereoselective catalysis. On the other hand, we can chemically modify the pillared frameworks by exchanging components, which has been demonstrated by people such as Ward[3-7] and Wuest.[8-10] In the area of inorganic-based hydrogen bonded frameworks, there are examples of open-frameworks absorbing molecules without disrupting the hydrogen bonded network.[11-15] Here we will examine if our hydrogen bonded pillared framework, described in Chapter 4, will absorb small molecules via intercalation. Even better, with our metal center we introduce a great potential for binding at the metal center, and therefore potential uses in signaling, sensing, and catalysis. Since the potential for binding at the metal center is available we will choose to examine (1) guest molecules that can potentially bind to the metal and (2) non-coordinating guest molecules.

5.2 Purpose of Research

In particular, we must demonstrate that our hydrogen bonded framework is suitable for intercalation of the guests. It is not obvious that a hydrogen bonded framework is strong enough to support the incorporation of guest molecules. We would also like to test selectivity and to determine what kind of guest molecules we

can include. Likely benzene –based molecules will include into the pillared framework – but how big, what shape and electropositive or electronegative aryls? And will alkyls groups work? Do we need substituents capable of hydrogen bonding to anchor them to the solid?

5.3 Experimental

5.3.1 Materials

All chemicals and solvents were purchased from Sigma-Aldrich and used without further purification or modification. Solids were sonicated in a Branson 6500 model sonicator. Following sonication, samples were characterized by TGA, DSC, and powder XRD to determine if guest inclusion has occurred.

5.3.2 Experimental Procedure

Crystals were grown according to the synthetic procedure laid out in Section 4.7.1 for [o-tolidinium][$Zn(PDCA)_2(H_2O)_2$] · acetone or Zn(o-tol). Upon collection of two grams of crystalline material, the crystals were ground and placed in a round bottom flask. Vacuum was applied overnight to remove the acetone guest molecules. PXRD and TGA were used to confirm the loss of acetone guest molecule.

0.077mmol of Zn(o-tol) was placed in a 20mL scintillation vial followed by 5mL of anhydrous hexanes and 1mL of the liquid guest (X_g), or 1.0mmol of solid guest. The mixtures were allowed to sonicate overnight. The sonicated material was

filtered and washed with excess hexanes. Then the solid was finally allowed to air dry in a fume hood.

5.4 Non-Coordinating Guest Molecules

5.4.1 Aromatic-based Guest Molecules

Table 5.1 contains a list of the non-coordinating aromatic guest molecules that were used in this study, along with the results of TGA, DSC, and PXRD analysis. The guest molecules vary in size, shape, and in the nature of the substituents on the aromatic ring.

Table 5.1 Non-coordinating aromatic guest molecules, molecular weight, TGA results, and conclusion on intercalation (by PXRD).

Name of Guest Molecule	Guest Molecule	Molecular Weight (g/mol)	% Guest Occupied	Lowest 2Θ peak	Intercalation Occurred?
benzene		**78.11**	**74.58%**	**4.5°**	**Yes**
toluene	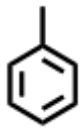	**92.14**	**100.72%**	**4.5°**	**Yes**
***p*-xylene**		**106.16**	**78.73%**	**4.5°**	**Yes**
***m*-xylene**	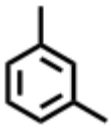	**106.16**	**14.52%**	**4.85°**	**No**

***o*-xylene**	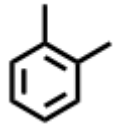	**106.18**	**13.81%**	**4.85°**	**No**
***p*-diethylbenzene**		**134.22**	**32.67%**	**4.85°**	**No**
***m*-diethylbenzene**	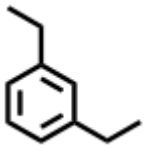	**134.22**	**16.74%**	**4.85°**	**No**
***o*-diethylbenzene**	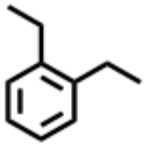	**134.22**	**11.16%**	**4.85°**	**No**
ethylbenzene	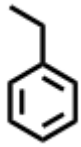	**106.16**	**43.16%**	**4.5°**	**Yes**
cumene	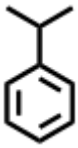	**120.19**	**6.69%**	**4.85°**	**No**
fluorobenzene		**96.10**	**9.50%**	**4.85°**	**No**
chlorobenzene	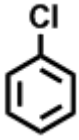	**112.56**	**9.84%**	**4.85**	**No**

bromobenzene	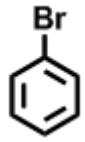	**157.01**	**96.87%**	**4.5°**	**Yes**
iodobenzene	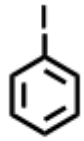	**204.01**	**40.95%**	**4.5°**	**Yes**
***p*-difluorobenzene**		**114.09**	**13.92%**	**4.85°**	**No**
***m*-difluorobenzene**	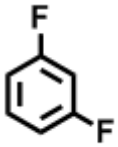	**114.09**	**14.32%**	**4.85°**	**No**
***o*-difluorobenzene**	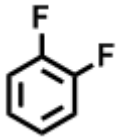	**114.09**	**13.19%**	**4.85°**	**No**
***p*-dichlorobenzene**		**147.00**	**28.42%**	**4.5°**	**Yes**
hexafluorobenzene	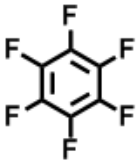	**186.05**	**7.73%**	**4.85°**	**No**
phenol	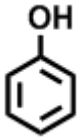	**94.11**	**88.51%**	**4.5°**	**Yes**
2-phenylethanol	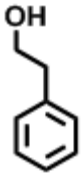	**122.16**	**80.37%**	**4.5°**	**Yes**

hydroquinone		**110.11**	**80.56%**	**4.5°**	**Yes**
nitrobenzene	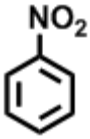	**123.11**	**68.37%**	**4.5°**	**Yes**
anisole	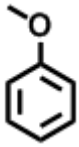	**108.14**	**79.28%**	**4.5°**	**Yes**
N,N-dimethylaniline	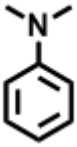	**121.18**	**27.48%**	**4.5°**	**Yes**

5.4.1.1 TGA Results

All samples that were sonicated for guest inclusion were analyzed by TGA to determine the amount of guest inclusion. In Table 5.1, a list of the guest molecules that were attempted to include in the solid pillared framework and the percent of guest loss is shown. The % Void occupied calculation can be found in Equation 5.1.

$$\% \text{ Occupied} = (\text{experimental weight loss} / \text{theoretical weight loss}) * 100\% \qquad (5.1)$$

Equation 5.1 The equation showing the % occupied calculation

5.4.1.2 DSC Results

The DSC analysis of the guest-included samples was consistent with the DSC thermographs described in Chapter 4, where three endothermic peaks, are associated with the loss of water ligands, loss of the diamine, and the decomposition of the metal complex. When the first peak (loss of water) has a “shoulder”, this indicates the loss of the included guest molecule. The reason for the increase in temperature range can be attributed to a strong interaction between the pillar and the guest. The second endotherm occurs at the same temperature as that indicated by TGA. The final endothermic peak is associated with the decomposition of the metal complex, which destroys the remaining pillared framework.

5.4.1.3 Powder X-Ray Diffraction Results

All samples were analyzed by powder XRD to determine if the guest was incorporated into the pillared framework. As can be seen from Table 5.1, the intercalation/inclusion is evident by the appearance of two peaks (4.50° and 4.85°) in the powder pattern. The peak at 4.5° indicates a guest-filled channel and the peak at 4.85° indicates a guest-free channel. A few examples from sonication of aromatic guest molecule can be found in Figure 5.1.

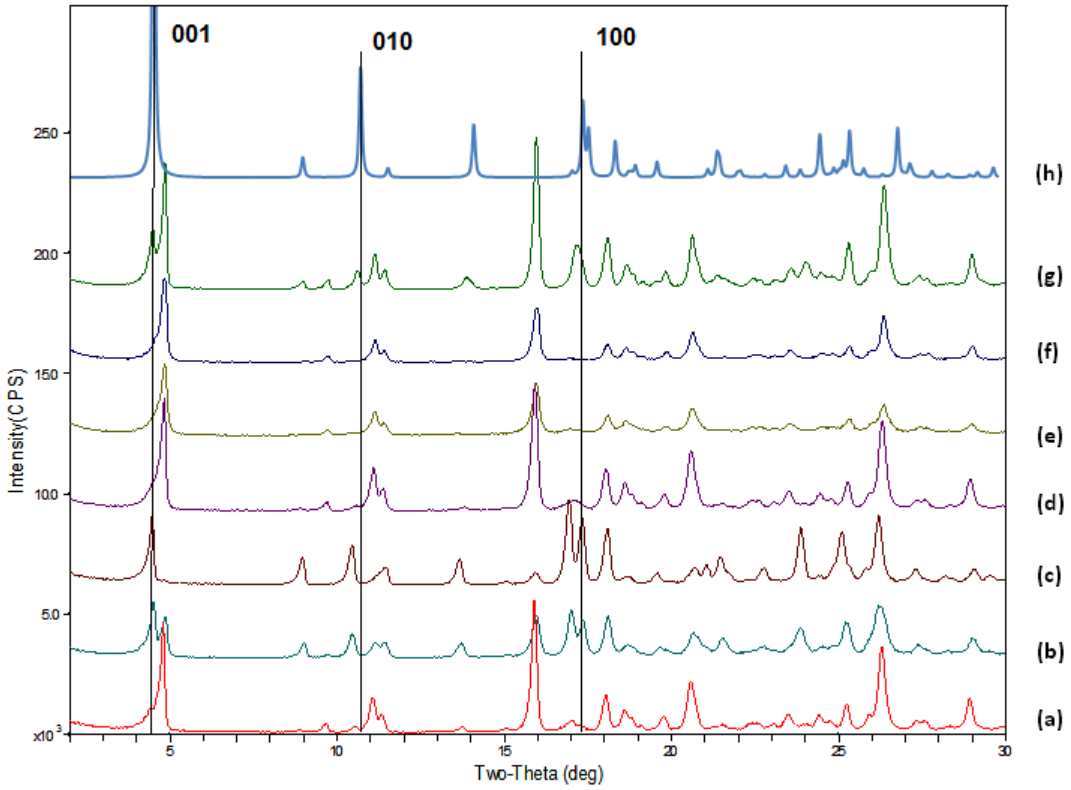

Figure 5.1 PXRD patterns from aromatic guests: (a) benzene, (b) toluene, (c) anisole, (d) cumene, (e) p-diethylbenzene, (f) *p*-difluorobenzene, (g) *p*-dichlorobenzene, and (h) theoretical pattern from single crystal XRD containing an acetone guest molecule.

5.4.2 Alkyl-based Guest Molecules

A list of the non-coordinating alkyl-based guest molecules that were used, along with data from TGA, DSC, and PXRD analysis, can be found in Table 5.2. The alkyl-based guest molecules were varied based on their size, functional group and shape. Comparison between alkanes and their corresponding alcohols, and saturated cyclic molecules and their oxygen analogues were made possible based on judicious choice of guests.

Table 5.2 Alkyl-based guest molecules, molecular weight, TGA results, and conclusion on intercalation (by PXRD).

Name of Guest Molecule	Guest Molecule	Molecular Weight (g/mol)	% Guest Occupied	Lowest 2Θ peak	Intercalation Occurred?
1-butanol		**74.12**	**N/A**	**4.85°**	**No**
1-pentanol		**88.15**	**79.5%**	**4.5°**	**Yes**
1-hexanol		**102.17**	**90.0%**	**4.5°**	**Yes**
1-heptanol		**116.20**	**N/A**	**4.85°**	**No**
1-octanol		**130.23**	**N/A**	**4.85°**	**No**
1-nonanol		**144.25**	**N/A**	**4.85°**	**No**
1-decanol		**158.28**	**N/A**	**4.85°**	**No**
pentane		**72.15**	**N/A**	**4.85°**	**No**

hexane		**86.18**	**N/A**	**4.85°**	**No**
heptane		**100.20**	**N/A**	**4.85°**	**No**
octane		**114.23**	**N/A**	**4.85°**	**No**
nonane		**128.26**	**N/A**	**4.85°**	**No**
decane		**142.28**	**N/A**	**4.85°**	**No**
ethyl acetate	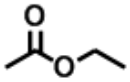	**88.11**	**75.3%**	**4.5°**	**Yes**
tetrahydrofuran		**72.11**	**25.2%**	**4.85°**	**No**
1,4-dioxane		**88.11**	**21.7%**	**4.85°**	**No**
cyclohexane		**84.16**	**6.3%**	**4.85°**	**No**

5.4.2.1 TGA Results

All samples that were sonicated for guest inclusion were analyzed by TGA to determine the amount of guest inclusion indicated by the calculated weight loss. In Table 5.2, a list of the guest molecules that were attempted to include in the solid pillared framework and the percent of guest loss is shown. The TGA exhibited extra weight loss associated with guest molecules for a few samples (pentanol, hexanol, and ethyl acetate) but the majority of the samples showed similar thermographs as the porous pillar.

5.4.2.2 DSC Results

The DSC analysis of the guest-included samples was consistent with the DSC thermographs where each thermograph contained three endothermic peaks, which are associated with the loss of water ligands, loss of the diamine, and then decomposition of the metal complex.

5.4.2.3 Powder X-Ray Diffraction Results

All samples were analyzed by powder XRD to determine if the guest was incorporated into the pillared framework. As can be seen from Table 5.2, the long chain alkane guest molecules do not show any sign of guest inclusion, and similar results were observed for the alkyl alcohols (except of pentanol and hexanol). Again, a peak at 4.5° indicates a guest-filled channel and a peak of 4.85° indicates a guest-

free channel. A few examples from the sonication of saturated guest molecule can be found in Figure 5.2.

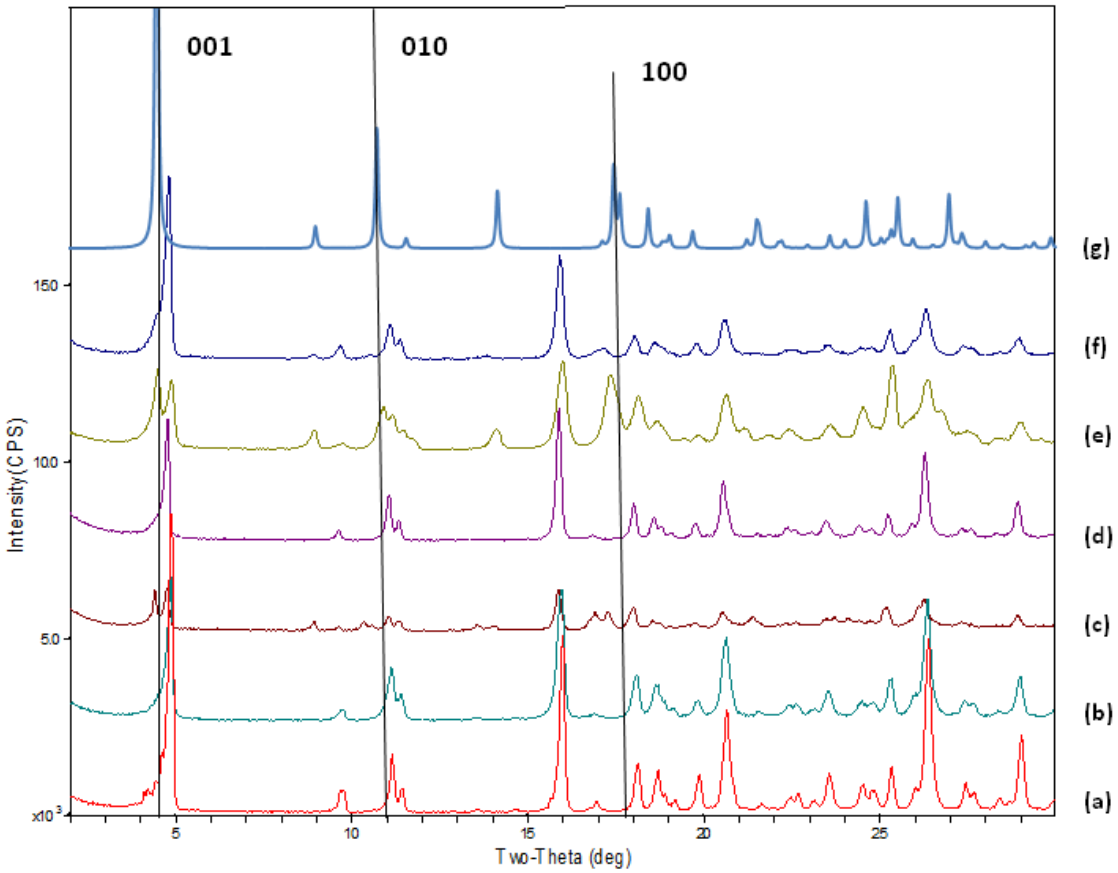

Figure 5.2 PXRD patterns from the alkyl-based guest molecules: (a) pentane, (b) decane, (c) hexanol, (d) nonanol, (e) ethyl acetate, (f) cyclohexane, and (g) theoretical powder pattern from single crystal XRD containing an acetone guest molecule.

5.4.3 Discussion of Non-Coordinating Guest Molecules

The guests found in Tables 5.1 and 5.2 were sonicated with host framework Zn(o-tol) to examine whether a new guest could replace the original and whether guest selectivity was possible. The guests ranged in nature from aryls to alkanes to alkyl alcohols. X-ray and gravimetric evidence indicated that the pillared framework

included a variety of guest molecules. The TGA evidence showed an increase in weight loss when compared to the vacant pillared framework for the following guests: benzene, toluene, ethylbenzene, bromobenzene, iodobenzene, phenol, nitrobenzene, anisole, N, N-dimethylaniline, *p*-xylene, *p*-dichlorobenzene, hydroquinone, pentanol, hexanol, and ethyl acetate. In the case of powder XRD, benzene, toluene, ethylbenzene, bromobenzene, iodobenzene, phenol, nitrobenzene, anisole, N, N-dimethylaniline, *p*-xylene, *p*-dichlorobenzene, hydroquinone, pentanol, hexanol, and ethyl acetate showed a shift (to lower 2Θ values) for the *001* peak, indicating an increase in the interlayer distance, which is consistent with guest inclusion.

Of the guest studied, benzene, toluene, ethylbenzene, bromobenzene, iodobenzene, phenol, 2-phenylethanol, hydroquinone, nitrobenzene, anisole, N, N-dimethylaniline, *p*-xylene, *p*-dichlorobenzene, hydroquinone, 1-pentanol, 1-hexanol, and ethyl acetate were all included during sonication, as shown by both TGA and PXRD. It would appear that shape directs which guest molecules can access the channels, because only 1, 4-disubstituted benzene guests were included. The nature of the substituents on the benzene ring does not appear to be the deciding factor, because there are examples of both electron donating and withdrawing groups on included guests. It is likely that the nature of the channel might prefer more electropositive guest molecules as opposed to the electronegative guest molecules. It would seem that the electron donating groups might have the upper hand since the majority of the included guests contain an electron donating group. In the case of the non-aromatic guest molecules, the ability to include guest molecules is dependent on the guest molecule to contain a hydroxyl group, which will be used to anchor the

guest to the host framework via hydrogen bonding. As seen in the experimental data, only pentanol and hexanol were included into the framework, which would indicate that the presence of the hydroxyl group as well as a specific length of the guest molecule is required for inclusion.

The guest molecules that did not show any evidence to support inclusion into the pillared framework are cumene, fluorobenzene, chlorobenzene, *m*-xylene, *o*-xylene, *p*-diethylbenzene, *m*-diethylbenzene, *o*-diethylbenzene, *p*-difluorobenzene, *m*-difluorobenzene, *o*-difluorobenzene, hexafluorobenzene, pentane, hexane, heptane, octane, nonane, decane, butanol, heptanol, octanol, nonanol, decanol, tetrahydrofuran, 1, 4-dioxane, and cyclohexane. These guest molecules did not show evidence due to their size and shape because it was shown that the *meta* and *ortho* isomers do not show any sign of guest inclusion. Two guests that were *para* isomers did not show any sign of inclusion, *p*-diethylbenzene and *p*-difluorobenzene. The *p*-diethylbenzene guest might be too large for the pillar and the *p*-difluorobenzene guest might be too electronegative to reside within the channel.

Since there was some indication that non-coordinating guest molecules would be included into the host framework, we also investigated the inclusion of coordinating (pyridine-based) guest molecules.

5.5 Coordinating Guest Molecules

A list of possible coordinating (pyridine-based) guest molecules that were used in the study can be found in Table 5.3. The same approach was taken as far the non-coordinating guest molecule (Section 5.4), where the guest molecules were

introduced to the layered solid through sonication. The pyridine-based guest molecules have substituents that vary based on size, shape and electronic properties.

Table 5.3 A list of coordinating guest molecules, molecular weight, TGA results, and conclusion on intercalation (by PXRD).

Name of Guest Molecule	Guest Molecule	Molecular Weight (g/mol)	% Guest Occupied	Lowest 2Θ peak	Intercalation Occurred?
pyridine		**79.10**	**83.13%**	**4.5°**	**Yes**
2-picoline	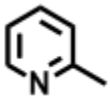	**93.13**	**18.90%**	**4.85°**	**No**
4-picoline	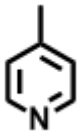	**93.13**	**16.28%**	**4.85°**	**No**
4-ethylpyridine	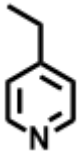	**107.15**	**65.00%**	**4.5°**	**Yes**
4-cyanopyridine	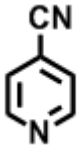	**104.11**	**62.58%**	**4.5°**	**Yes**
4,4′-bipyridine		**156.18**	**47.81%**	**4.5°**	**Yes**

4-*t*-butylpyridine	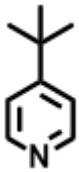	**135.21**	**34.10%**	**4.5°**	**Yes**
4-(dimethylamino) pyridine	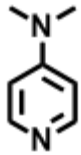	**122.17**	**29.81%**	**4.5°**	**Yes**
4-chloropyridine	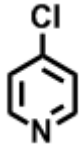	**113.54**	**54.55%**	**4.5°**	**Yes**
isonicotinic acid	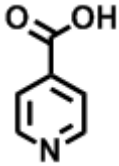	**123.11**	**55.87%**	**4.85°**	**No**
isonicotinamide	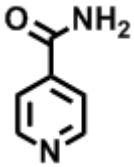	**122.12**	**31.40%**	**4.5°**	**Yes**

5.5.1 TGA Results

Similar to the samples that were sonicated with benzene-based and alkyl-based guest molecules were analyzed by TGA to determine the amount of guest inclusion. The majority of the samples showed a substantial weight loss in the 100° - 220° C range which indicates that a guest molecule resides inside the channel. The sample where pyridine was used as the guest molecule, showed the largest weight loss, which was a little less than was expected for a 1:1 host to guest ratio. There were three samples that did not show substantial weight loss: 2-picoline, 4-picoline and isonicotinamide. The results from all samples can be found in Table 5.3.

5.5.2 DSC Results

The DSC analysis of the guest-included samples was consistent within the DSC thermographs whereby there were three endothermic peaks, which are associated with the loss of water ligands, loss of the diamine, and the decomposition of the metal complex. The second endotherm occurs at the same temperature (220° - 340° C) as that indicated by TGA. The final endothermic peak is associated with the decomposition of the metal complex, which destroys the remaining pillared framework.

5.5.3 Powder X-Ray Diffraction Results

All sonicated samples were analyzed by PXRD to determine if guest inclusion is occurring via sonication. As observed previously in 5.4.1.3 and 5.4.2.3, a two peak pattern between 4.5Å to 5.0Å indicates that guest inclusion is occurring in this pillared framework. The patterns that showed these two peaks also showed a substantial weight loss in the TGA spectrum with the corresponding material. A generalized examination of the powder XRD results are found in Table 5.3. A few examples from sonication of aromatic guest molecule can be found in Figure 5.3.

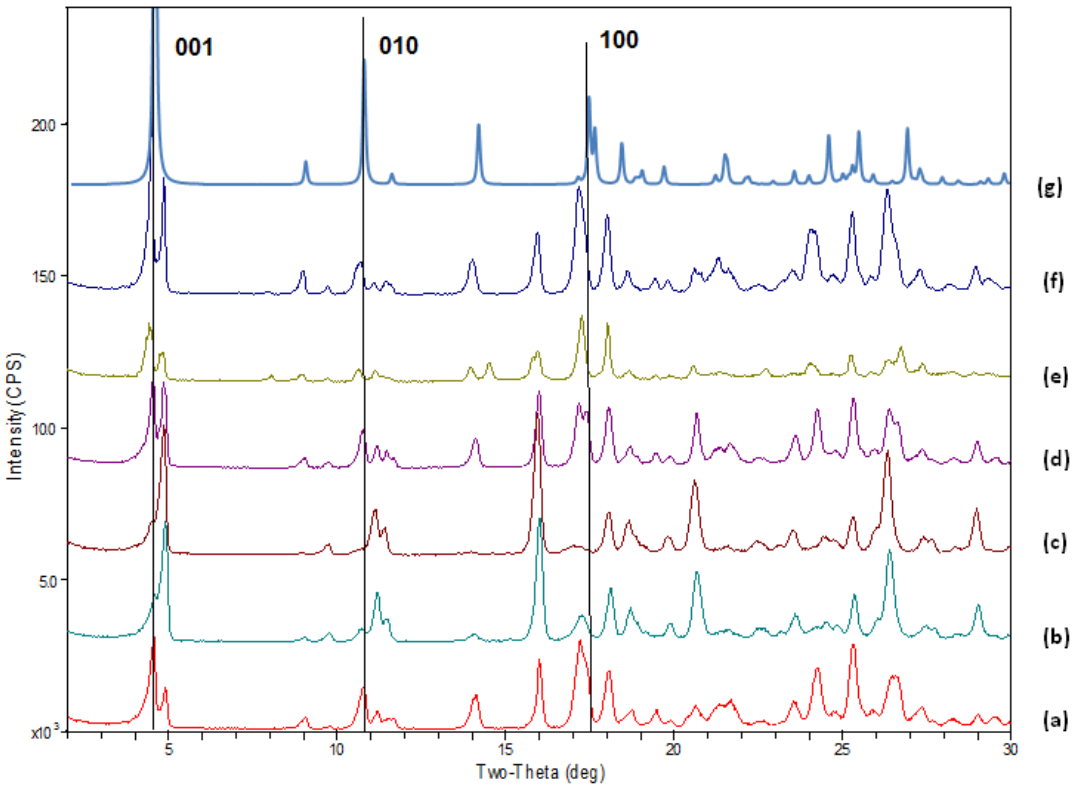

Figure 5.3 PXRD patterns from pyridine-based guest molecules: (a) pyridine, (b) 2-picoline, (c) 4-picoline, (d) 4-ethylpyridine, (e) 4-cyanopyridine, (f) 4-*t*-butylpyridine, and (g) theoretical powder pattern from single crystal XRD containing an acetone guest molecule.

5.5.4 Discussion of Coordinating Guest Molecules

In the attempt to include coordinating guest molecules, there was gravimetric, and X-ray evidence for intercalation in the majority of the guest molecules.

The guest molecules that have shown evidence of intercalation through TGA analysis are: pyridine, 4-ethylpyridine, 4-cyanopyridine, 4, 4′-bipyridine, 4-*t*-butylpyridine, 4-(dimethylamino) pyridine, 4-chloropyridine, isonicotinic acid, and isonicotinamide. Evidence for intercalation is given by a large weight loss as observed in the TGA thermograph in the temperature range of 100° - 220° C. The

guest that exhibited the highest amount of inclusion was pyridine. This means coordinating guest containing alkyl-based groups possibly work better than electron withdrawing groups. The guest molecules that have shown evidence of intercalation through PXRD analysis are: pyridine, 4-ethylpyridine, 4-cyanopyridine, 4, 4′-bipyridine, 4-*t*-butylpyridine, 4-(dimethylamino) pyridine, 4-chloropyridine, and isonicotinamide. The evidence for intercalation in these experiments was concluded by the appearance of a peak around 4.5° (from PXRD), which indicates a guest included pillared framework.

The guest molecules that did not show any sign of inclusion are 2-picoline, 4-picoline, and isonicotinic acid. The TGA data and powder XRD patterns did not show any evidence of an additional weight loss or the presence of a peak at 4.5°, which is the evidence for guest intercalation. It is surprising that 4-picoline is not included, because similar 4-substituted molecules (mentioned above) exhibited signs of guest inclusion. It is likely that 2-picoline does not include into the framework because of the steric hindrance of the methyl group in the ortho position.

5.6 Conclusions

We have determined that our host framework is indeed strong enough to withstand guest loss, and guest exchange. We examined the ability of benzene-based, long chain alkyl-based and pyridine-based guest molecules to absorb into our hydrogen bonded framework. When examining the benzene-based molecules, the host framework exhibited evidence of intercalation from thirteen out of twenty-five guests. The long chain alkyl-based molecules exhibited evidence of intercalation

from three out of seventeen samples. The group that exhibited the most consistent results was from the pyridine-based molecules because eight out of eleven samples did show evidence of intercalation. The pyridine-based molecules contain two methods for intercalation (traditional or coordinative) that allows for a greater chance for guest inclusion.

We have shown that the chemical nature of the substituent might not be extremely important because both electropositive and electronegative groups exhibit guest inclusion. The one important group is the hydroxyl because this group can anchor itself to the host material, which will lead to guest inclusion. The size and shape of the guest molecules play a determining factor if guest inclusion will occur. It was shown that disubstituted benzene molecules will only include when it's the *para* isomer indicating that shape is a major factor in whether molecules will serve as guests.

References

(1) Parnham, E. R.; Morris, R. E. *Acc. Chem. Res.* **2007**, *40*, 1005-1013.

(2) Jacobs, P. A.; Jaeger, N. I.; Kubelkova, L.; Wichterlova, B.; Editors *Studies in Surface Science and Catalysis Vol. 69: Zeolite Chemistry and Catalysis. Proceedings of an International Symposium, Prague, Czechoslovakia, September 8-13, 1991*, 1991.

(3) Ward, M. D. *Chem. Comm.* **2005**, 5838-5842.

(4) Pivovar, A. M.; Holman, K. T.; Ward, M. D. *Chem. Mater.* **2001**, *13*, 3018-3031.

(5) Plaut, D. J.; Holman, K. T.; Pivovar, A. M.; Ward, M. D. *Journal of Physical Organic Chemistry* **2000**, *13*, 858-869.

(6) Swift, J. A.; Ward, M. D. *Chem. Mater.* **2000**, *12*, 1501-1504.

(7) Holman, K. T.; Ward, M. D. *Stimul. Concepts Chem.* **2000**, *221*, 221-234.

(8) Perron, M.-E.; Monchamp, F.; Duval, H.; Boils-Boissier, D.; Wuest, J. D. *Pure Appl. Chem.* **2004**, *76*, 1345-1351.

(9) Saied, O.; Maris, T.; Wuest, J. D. *J. Am. Chem. Soc.* **2003**, *125*, 14956-14957.

(10) Brunet, P.; Simard, M.; Wuest, J. D. *J. Am. Chem. Soc.* **1997**, *119*, 2737-2738.

(11) Bradshaw, D.; Claridge, J. B.; Cussen, E. J.; Prior, T. J.; Rosseinsky, M. J. *Acc. Chem. Res.* **2005**, *38*, 273-282.

(12) Fletcher, A. J.; Cussen, E. J.; Prior, T. J.; Bradshaw, D.; Rosseinsky, M. J. *J. Am. Chem. Soc.* **2004**, *126*, 9750-9759.

(13) Fletcher, A. J.; Cussen, E. J.; Prior, T. J.; Rosseinsky, M. J.; Kepert, C. J.; Thomas, K. M. *J. Am. Chem. Soc.* **2001**, *123*, 10001-10011.

(14) Kepert, C. J.; Rosseinsky, M. J. *Chem. Commun.* **1999**, 375-376.

(15) Yaghi, O. M.; Davis, C. E.; Li, G.; Li, H. *J. Am. Chem. Soc.* **1997**, *119*, 2861-2868.

Chapter 6

Competition Studies of Mono- and Disubstituted Benzenes into a Pillared HMOFs

6.1 Background

Separation of molecules that possess similar boiling points is a difficult task, and is traditionally accomplished via fractional distillation. However, an alternative method to separate these isomers is through molecular recognition in the solid-state. This form of host/guest chemistry allows the host molecule or complex to selectively separate isomers through inclusion. There have been other groups who have observed guest selectivity via co-crystallization where the host and guest mixture are allowed to crystallize together.[1-9] The guest molecules are then separated by chromatographic methods. The previously mentioned selectivity studies used only organic molecules as the host material and the guest molecules. Since the previous studies contained only organic molecules our metal-containing pillared framework would be an excellent addition to the preceding selectivity studies. The metal-containing framework offers the potential for studies in catalysis, signaling, and magnetic/optic properties.[10-16] These host materials are in turn dependent on the shape, size, conformation, and surface charge distribution of the molecules making up the system.

6.2 Purpose and Goals of Research

The focus of this project was aimed toward looking at selectivity of the host framework and to determine the selectivity of the host framework for a guest molecule when more than one guest is in solution during the crystallization process. In order to look at selectivity, the host framework will be subjected to two guest molecules at the same time competing simultaneously for inclusion. To determine if

the host has any preference for specific guest molecules, the competition reaction will proceed by varying the concentration of each guest molecule by a mole fraction. As the concentration of guest A increases, the concentration of guest B will decrease. We will look at the inclusion process of two competing guest molecules through the method of co-crystallization. Once crystals are grown from solution, the analysis will be performed through the use of GC/MS. All guests were mono- and di-substituted aryls and varied based on the size, shape, and/or the electronegativity of the substituent.

6.3 Determination of Selectivity

One of the most important applications of host-guest chemistry is the separation of similar compounds by enclathration or inclusion. This involves the choice of a suitable host compound which (when exposed to a mixture of guests) combines selectively with a particular guest to form a crystalline inclusion compound. The inclusion compound is filtered and the guest is released by gentle heating, allowing the guest to be disposed of or recycled. The selectivity process depends on the molecular recognition between the host and the guest molecules.

If two or more guests are present within a host, then four kinds of selectivity curves can occur, as seen in Figure 6.1. The horizontal axis is the mole fraction of guest A, X_A, and the vertical axis is the amount included of guest A, Z_A. The amount of selectivity can be quantified by calculating the selectivity coefficient, Equation 6.1, which has been implemented by Ward.[9]

$$K_{A:B} = (K_{B:A})^{-1} = Z_A / Z_B \cdot X_B / X_A \;;$$

$$\text{where } (X_A + X_B = 1)$$

Equation 6.1: Where K is the selectivity coefficient, A is guest A, B is guest B, Z is the amount included of a guest, and X is the mole fraction of a guest.

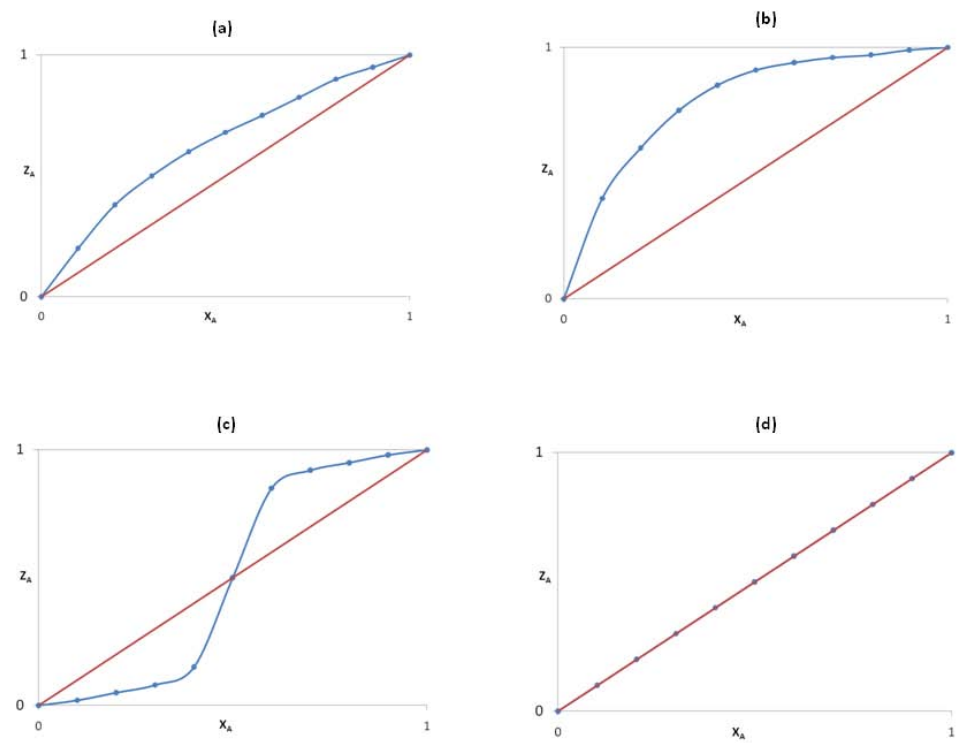

Figure 6.1 Various options in determining selectivity: (a) moderate selectivity, (b) high selectivity, (c) concentration dependent and (d) no selectivity.

6.4 Experimental

6.4.1 Materials and Instruments

All chemicals and solvents were purchased from Sigma-Aldrich and used with out further modification. The solvents used, methanol and N, N-dimethylformamide, were ACS grade and the DI water was obtained from a Millipore MilliQ Plus purifier.

GC/MS chromatographs were recorded on a Hewlett Packard GC/MS System Model 5988A. Exact masses were obtained on a JEOL MStation [JMS-700] mass spectrometer. TGA thermographs were collected on a TA Q50.

6.4.2 Experimental Procedures

Guest-containing materials were obtained in a manner previously described (Chapter 4). The molecular components used during the synthetic procedure are: the metal dicarboxylic acid (Zn(pyridine 2,4-dicarboxylic acid)$_2$(H_2O)$_2$) and an organic diamine (3,3'-dimethylbenzidine). Guest molecules were introduced according to the concentrations given in Table 6.1.

The mixtures were allowed to crystallize and after a one week period the crystals were collected and filtered. The analysis of the crystals was through GC/MS. The typical sample preparation for GC analysis included placing the sample in a 10mL Schlenk flask followed by applying a static vacuum to remove any excess guest molecules and air. The flask was then heated for ten minutes to ensure the guest molecules had an appropriate amount of time to escape the host. The head gas was extracted using an air-tight syringe and inserted into the GC. Once the corresponding peaks appeared on the chromatograph, they were integrated together to determine the percent composition of each present guest molecule. The data was then

plotted on a graph with the mole fraction of guest A vs. the percent included of guest A.

Table 6.1 General amounts of each guest molecule used in a competition reaction.

Mole Fraction (guest A)	Guest A (mmol)	Guest B (mmol)
0.0	0.0	1.2
0.1	0.12	1.08
0.2	0.24	0.96
0.3	0.36	0.84
0.4	0.48	0.72
0.5	0.60	0.60
0.6	0.72	0.48
0.7	0.84	0.36
0.8	0.96	0.24
0.9	1.08	0.12
1.0	1.2	0.0

6.4.3 Characterization

Samples were characterized by TGA and GC/MS. The TGA can confirm that guest molecule(s) are present within the host but determination of which guest molecule is impossible through TGA. Since the guest molecules that were used in the competitions were typically similar, the TGA spectrum showed a very similar plot for

each sample analyzed, but did confirm the presence of guests. The GC/MS was chosen because of its ability to separate the two guest molecules and determine the percent composition of the corresponding guest molecules, followed by integration of the two peaks to determine the GC yield of the resulting guest molecules.

6.5 Results from Competition Studies

The selectivity coefficient, K, can be used to determine which guest is selectively included along with the amount of selectivity. If the K of guest A is less than 1, then it can be concluded that guest B is more selective to inclusion in the host framework than guest A. Conversely, if K of guest A is greater than 1, then it can be concluded that guest A is more selective towards inclusion. The degree of selectivity is depends on the value of K: when K = 100 the guest is highly selective and when K = 10 the guest is moderately selective. If the selectivity factor, K, is less than 5 the guest is considered to be slightly selective and when the K is equal to 1 the host is concluded to be not selective for the guest molecules.

6.5.1 Results from the Monosubstituted Benzene Studies

All of the competition experiments will employ the use of two guest molecules for each study. The first group that will be examined is the competition studies of the mono-substituted benzene guest molecules.

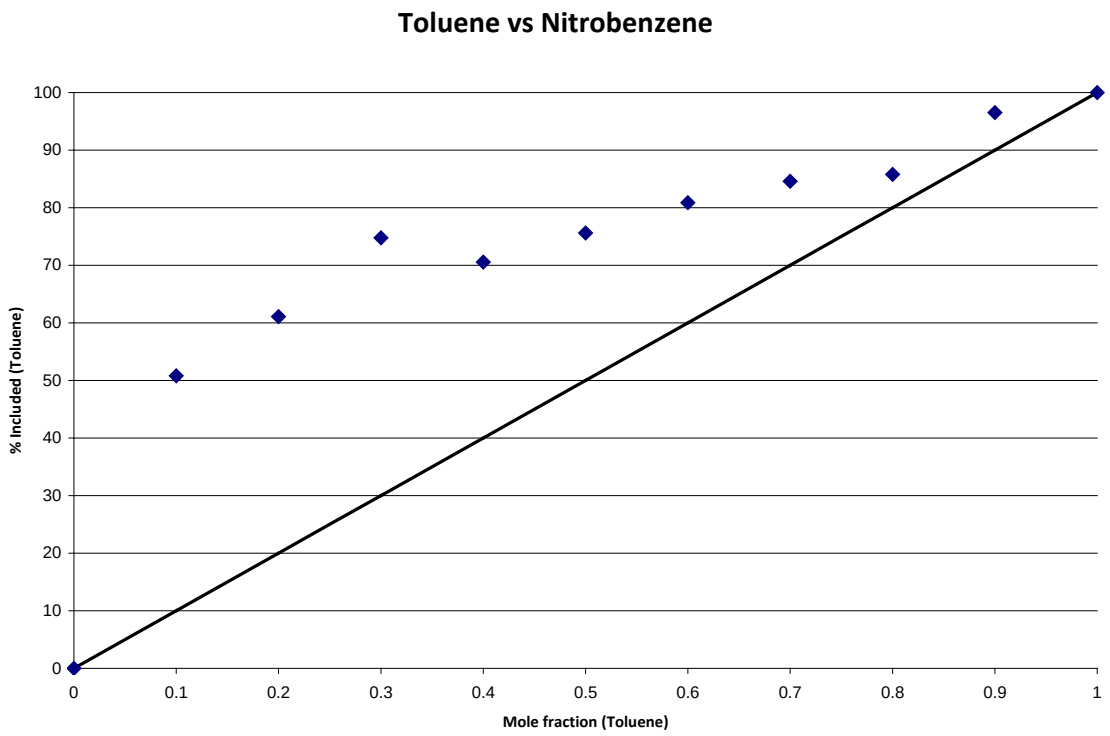

Figure 6.2 Selectivity plot of toluene vs. nitrobenzene study.

In the competition study between toluene and nitrobenzene, the host seemed to have a higher selectivity towards toluene as the guest molecule. The overall selectivity coefficient for this study is $K_{A:B} = 4.38$ which means that the host is moderately selective for toluene over nitrobenzene. The corresponding selectivity plot is given in Figure 6.2.

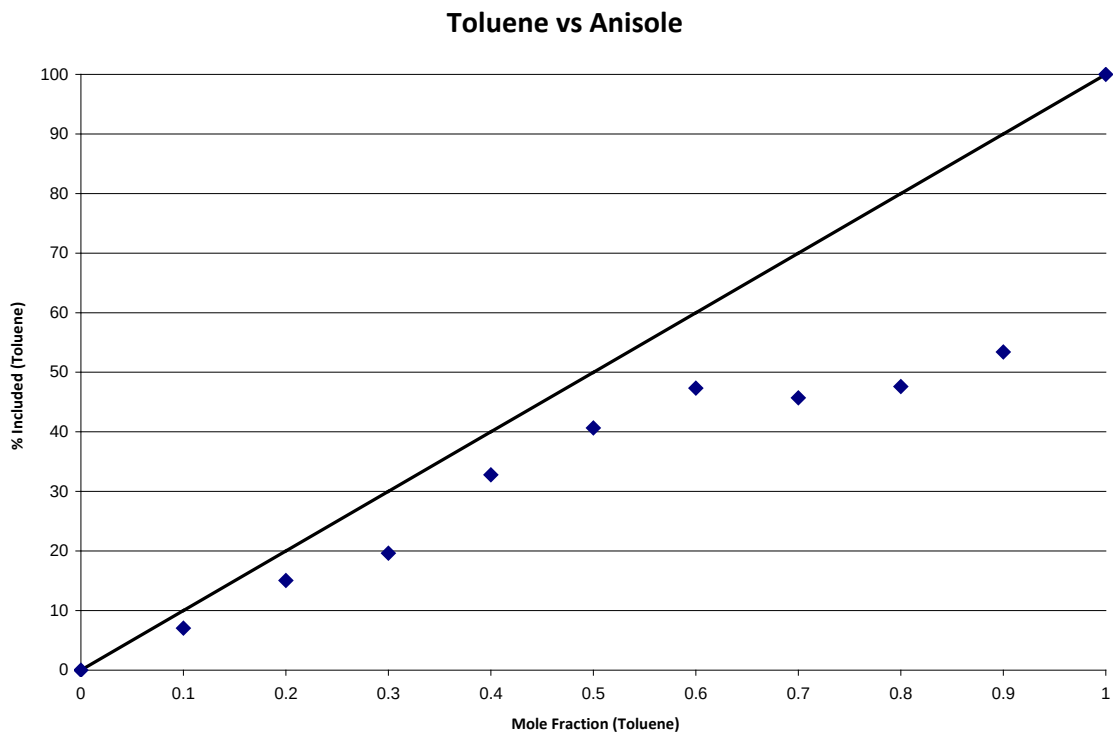

Figure 6.3 Selectivity plot of toluene vs. anisole study.

In the competition study between toluene and anisole, anisole showed to be a more favorable guest molecule. The overall selectivity coefficient for this study is $K_{A:B} = 0.53$ which indicates that there is slight selectivity for anisole. The selectivity plot was given in Figure 6.3.

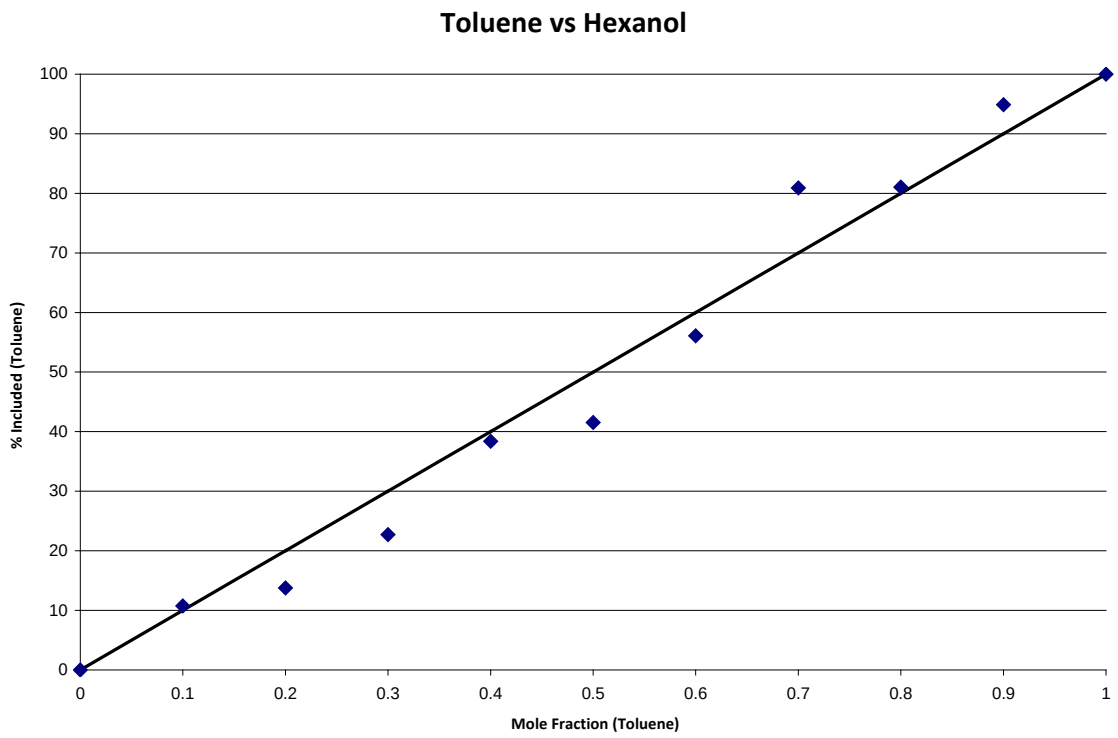

Figure 6.4 Selectivity plot of toluene vs. hexanol study.

The competition study between toluene and hexanol showed no sign of selectivity. The overall selectivity coefficient for this study is $K_{A:B} = 1.09$ which indicates no selectivity. The corresponding selectivity plot is shown in Figure 6.4.

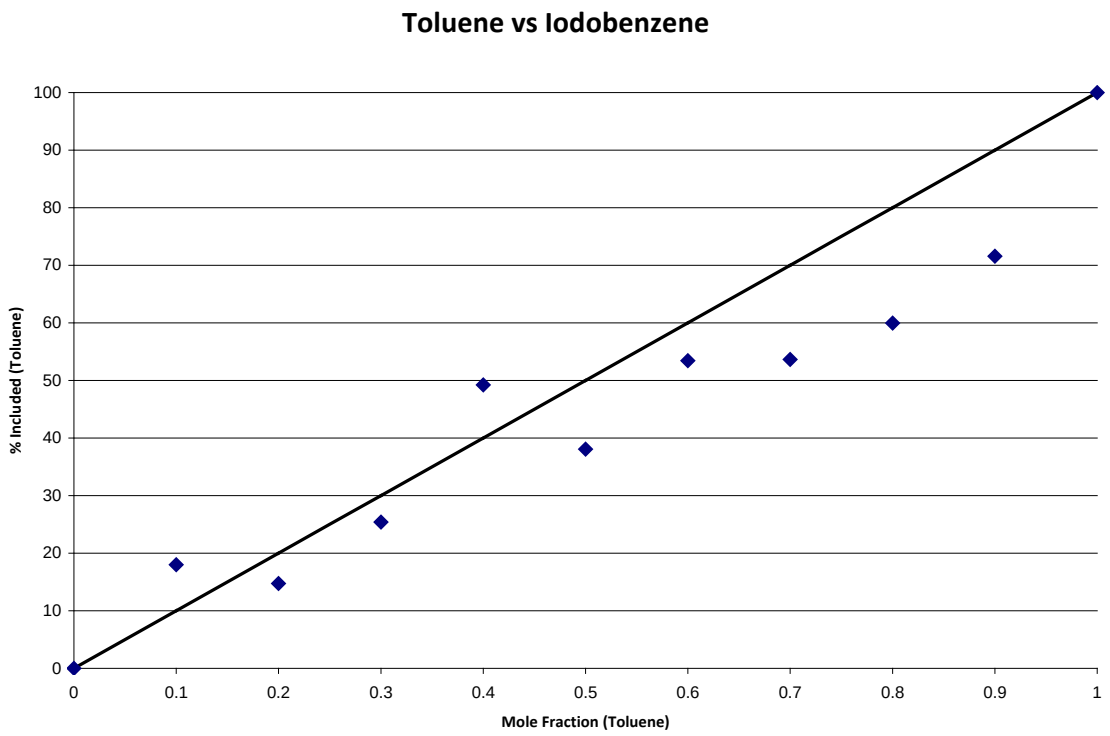

Figure 6.5 Selectivity plot from toluene vs. iodobenzene study.

The competition study between toluene and iodobenzene revealed iodobenzene was more favorable as the guest molecule. The overall selectivity coefficient for this study is $K_{A:B} = 0.82$ indicating a slightly selectivity for iodobenzene. The selectivity plot for this competition is illustrated in Figure 6.5.

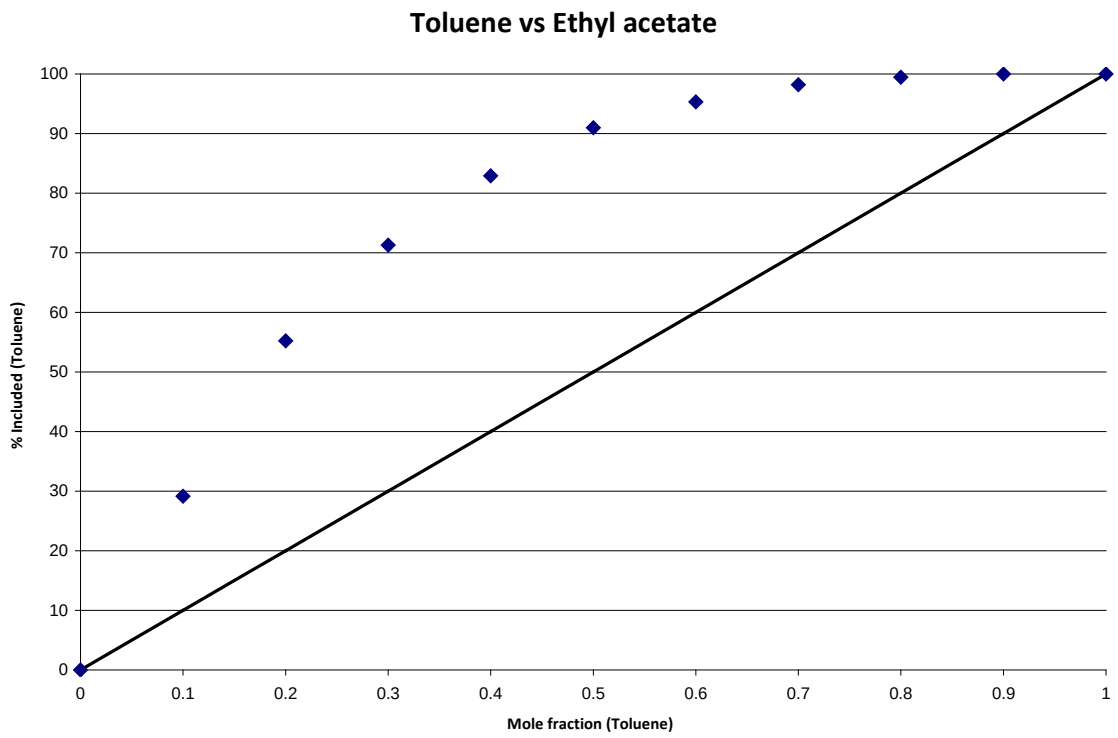

Figure 6.6 Selectivity plot from toluene vs. ethyl acetate study.

The competition study between toluene and ethyl acetate showed toluene was the more favorable guest molecule. The overall selectivity coefficient for this study is $K_{A:B} = 11.25$ which indicates moderate selectivity for toluene. The selectivity plot is given in Figure 6.6.

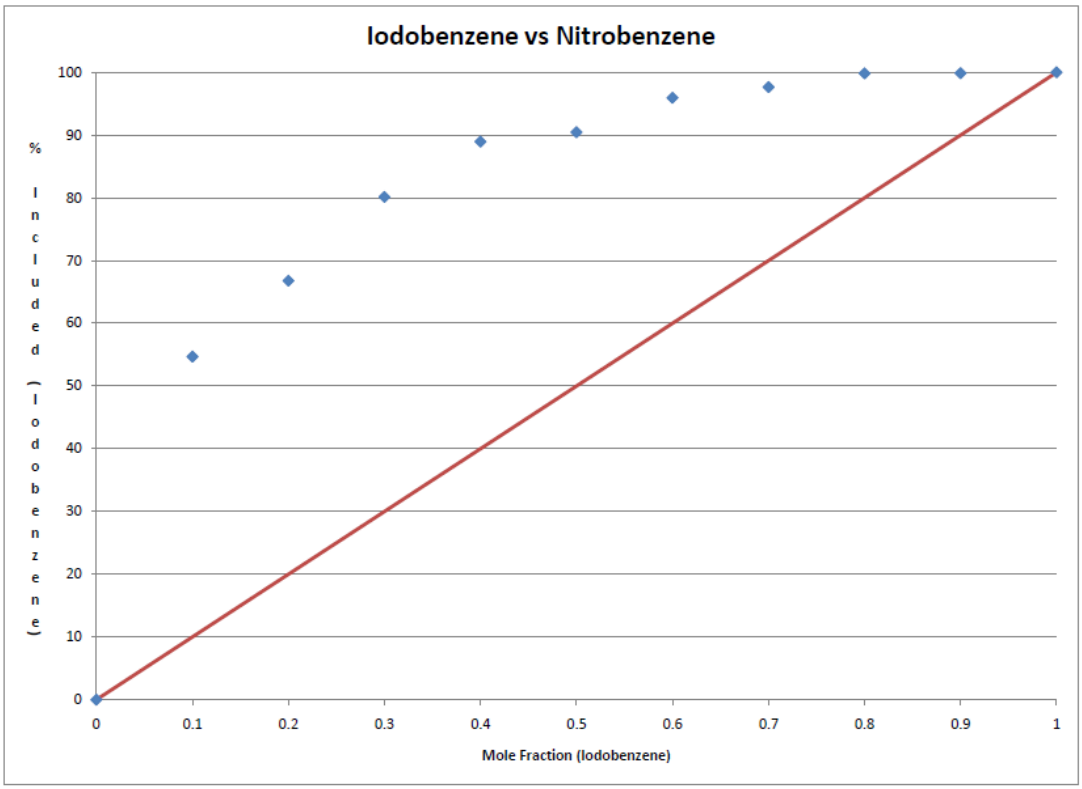

Figure 6.7 Selectivity plot of nitrobenzene vs. iodobenzene study.

In the competition reaction between iodobenzene and nitrobenzene, the host was more selective towards iodobenzene. The selectivity coefficient of this study is $K_{A:B}$ = 12.88, indicating the reaction is moderately selective for iodobenzene. The corresponding selectivity plot for this study is illustrated in Figure 6.7.

6.5.2 Results from the Disubstituted Benzene Studies

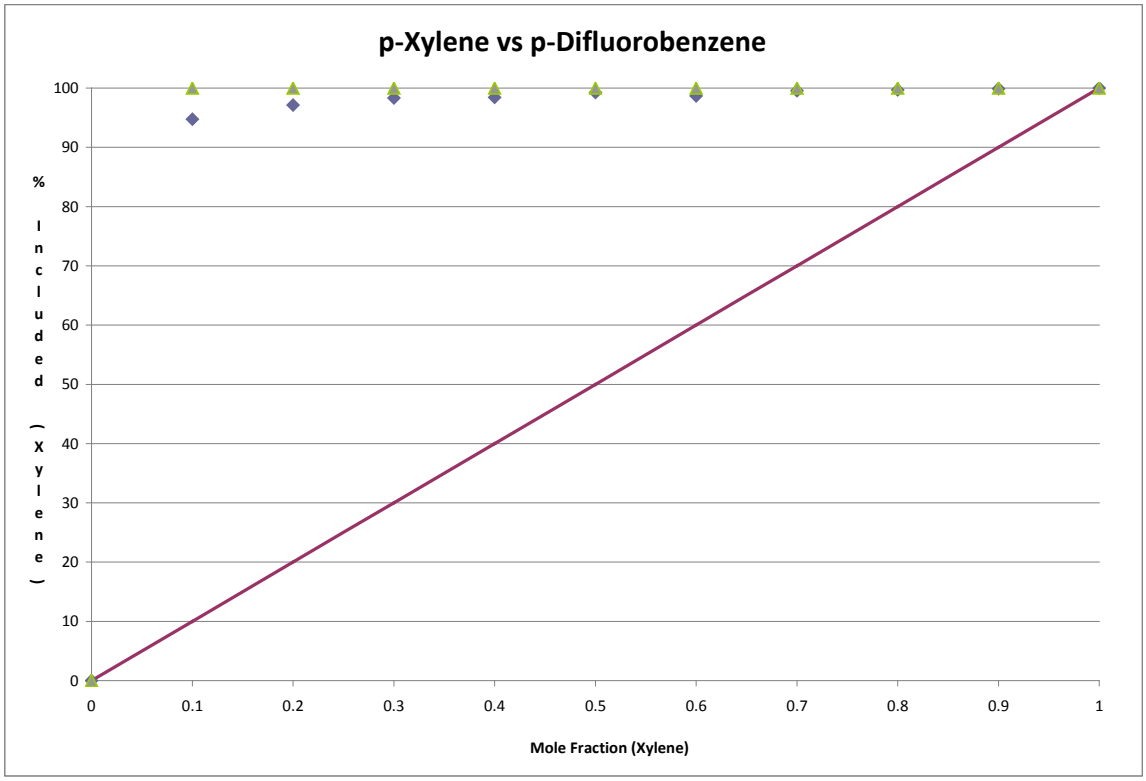

Figure 6.8 Combined selectivity plots from *p*-xylene vs. *p*-difluorobenzene study.

In the competition reaction between *p*-xylene versus *p*-difluorobenzene, the host framework was more selective towards *p*-xylene as the guest molecule. Figure 6.8 shows the two separate studies that shows very good reproducibility. The selectivity coefficient of this study is $K_{A:B}$ = 113.80, which indicates the reaction is highly selective for *p*-xylene. The selectivity coefficient for the two plots is calculated and then the average of the coefficients is reported.

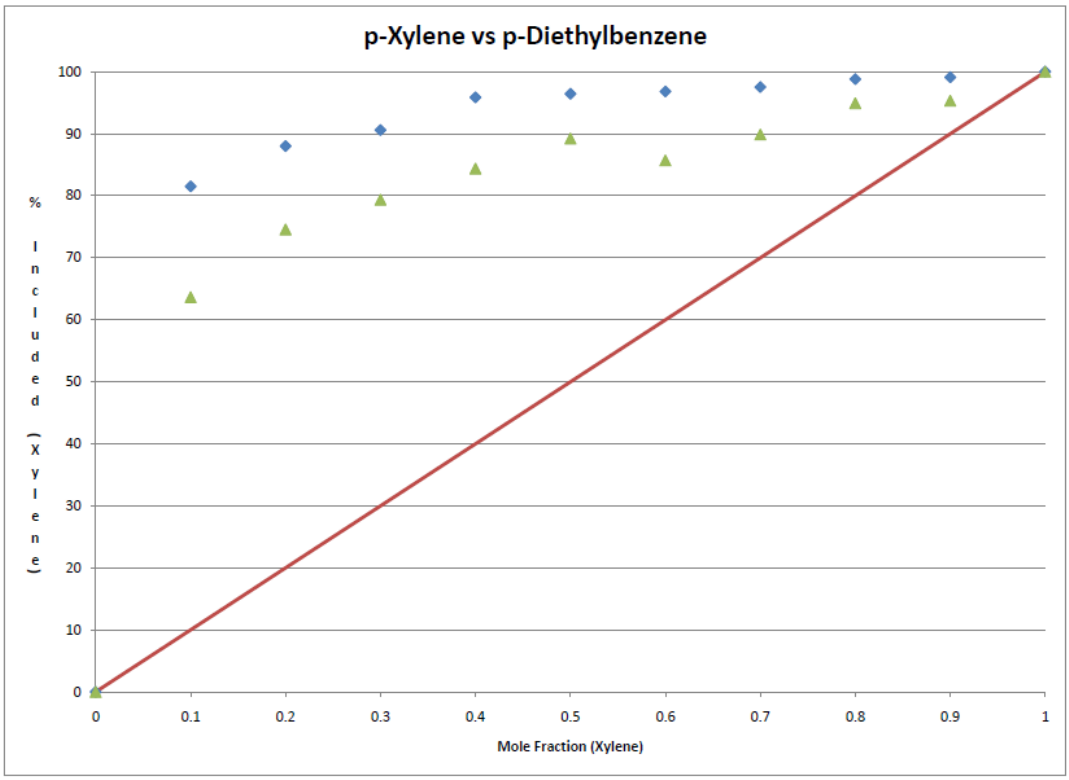

Figure 6.9 Combined selectivity plots from *p*-xylene vs. *p*-diethylbenzene study.

In the competition reaction between *p*-xylene versus *p*-diethylbenzene, the host framework was also selective towards *p*-xylene as the guest molecule. This study was performed twice and the results are given in Figure 6.9. The selectivity coefficient of this study is $K_{A:B}$ = 15.96, indicating the reaction is moderately selective for *p*-xylene.

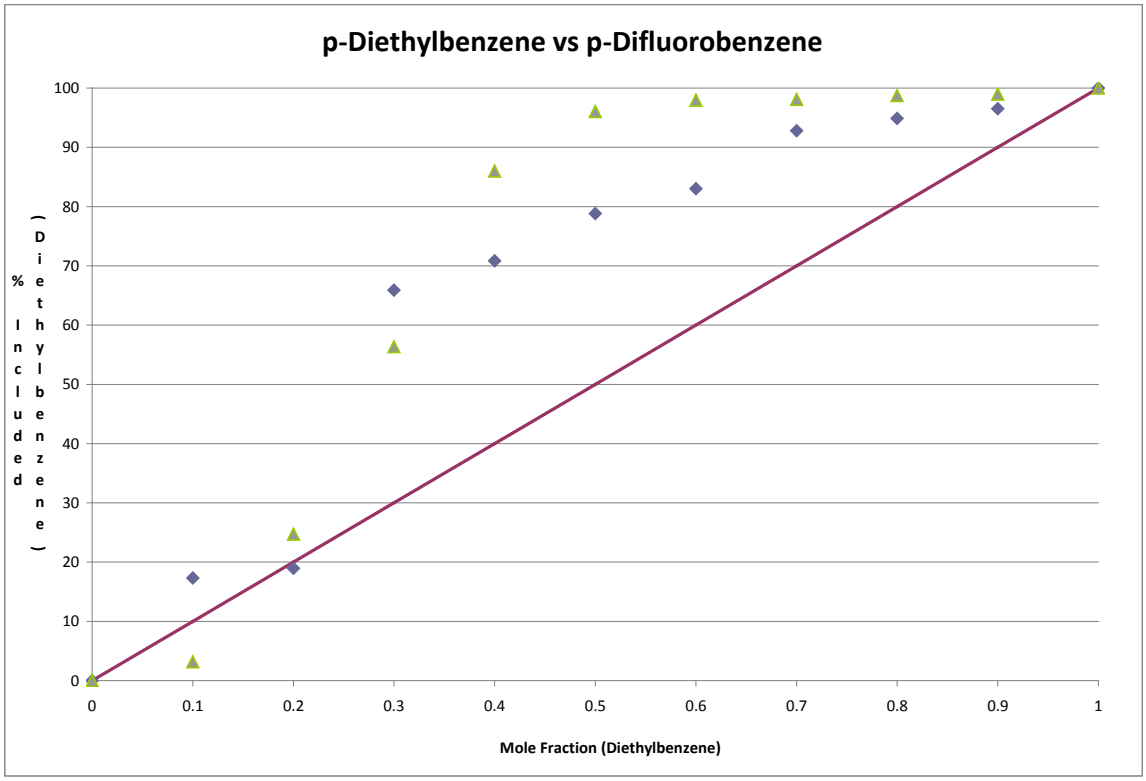

Figure 6.10 Combined selectivity plot from *p*-diethylbenzene vs. *p*-difluorobenzene study.

In the competition reaction between *p*-diethylbenzene versus *p*-difluorobenzene, the host framework was more selective towards *p*-diethylbenzene. Figure 6.10 shows two separate studies with good reproducibility. The selectivity coefficient of this study is $K_{A:B}$ = 13.58, which the selectivity of the reaction is moderately selective for *p*-diethylbenzene.

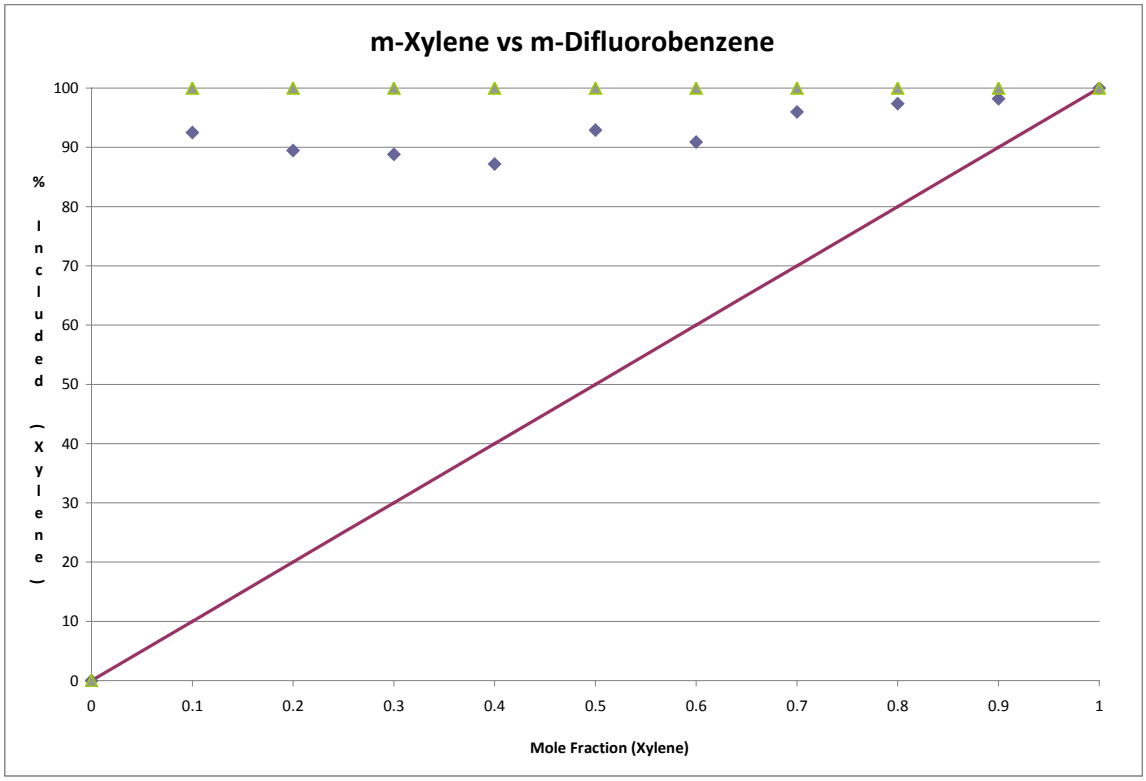

Figure 6.11 Combined selectivity plot from *m*-xylene vs. *m*-difluorobenzene study.

In the competition reaction between *m*-xylene versus *m*-difluorobenzene, the host framework was selective towards the *m*-xylene. Figure 6.11 shows the two separate studies for this competition study. The selectivity coefficient of this study is $K_{A:B}$ = 24.30, indicating the reaction is moderately selective for *m*-xylene.

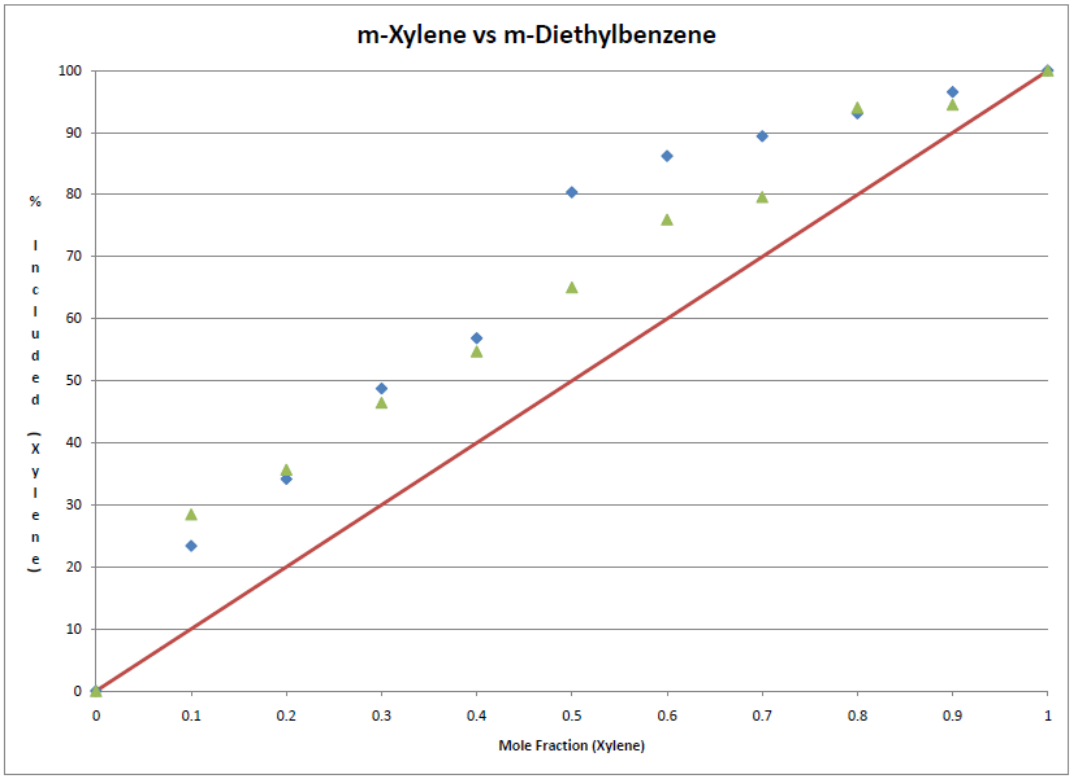

Figure 6.12 Combined selectivity plot from *m*-xylene vs. *m*-diethylbenzene study.

In the competition reaction between *m*-xylene versus *m*-diethylbenzene, the host framework was more selective towards *m*-xylene. Figure 6.12 illustrates the two separate studies for this reaction. The selectivity coefficient of this study is $K_{A:B}$ = 2.68, which indicates the reaction is slightly selective for *m*-xylene.

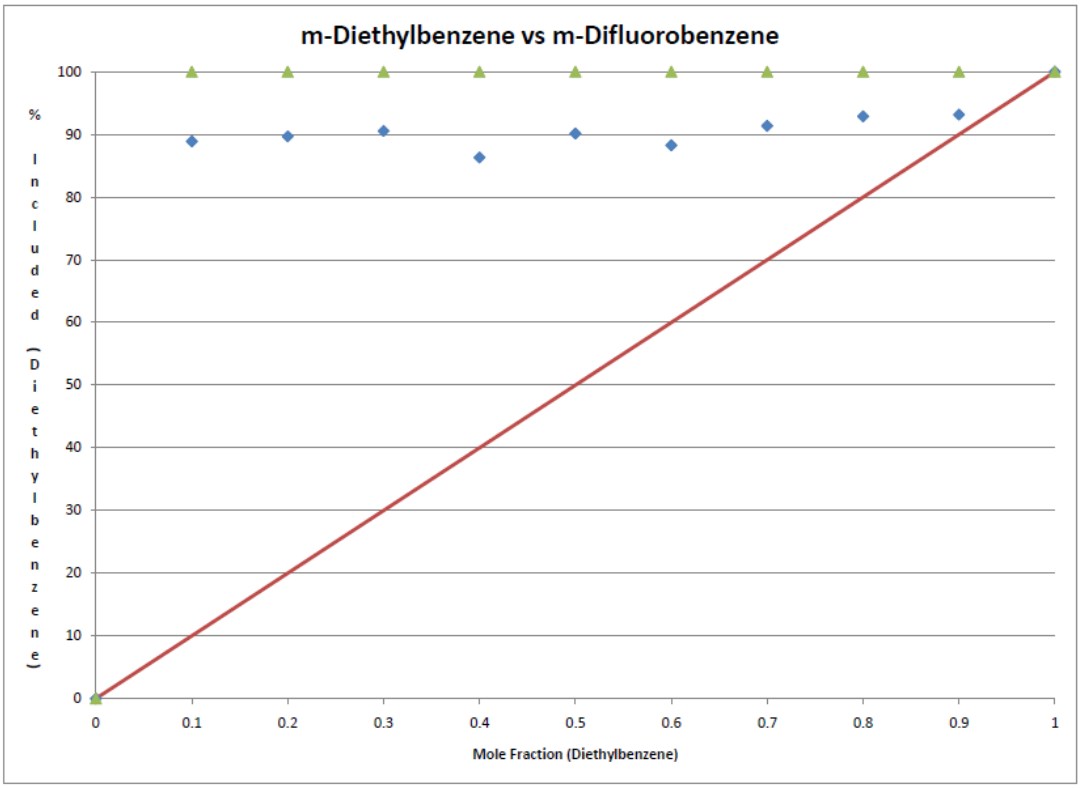

Figure 6.13 Combined selectivity plot from *m*-diethylbenzene vs. *m*-difluorobenzene study.

In the competition reaction between *m*-diethylbenzene versus *m*-difluorobenzene, the host framework was selective towards *m*-diethylbenzene as a guest molecule. Figure 6.13 shows the results for the two separate studies in this competition reaction. The selectivity coefficient of this study is $K_{A:B} = 11.37$, indicating the reaction is moderately selective for *m*-diethylbenzene.

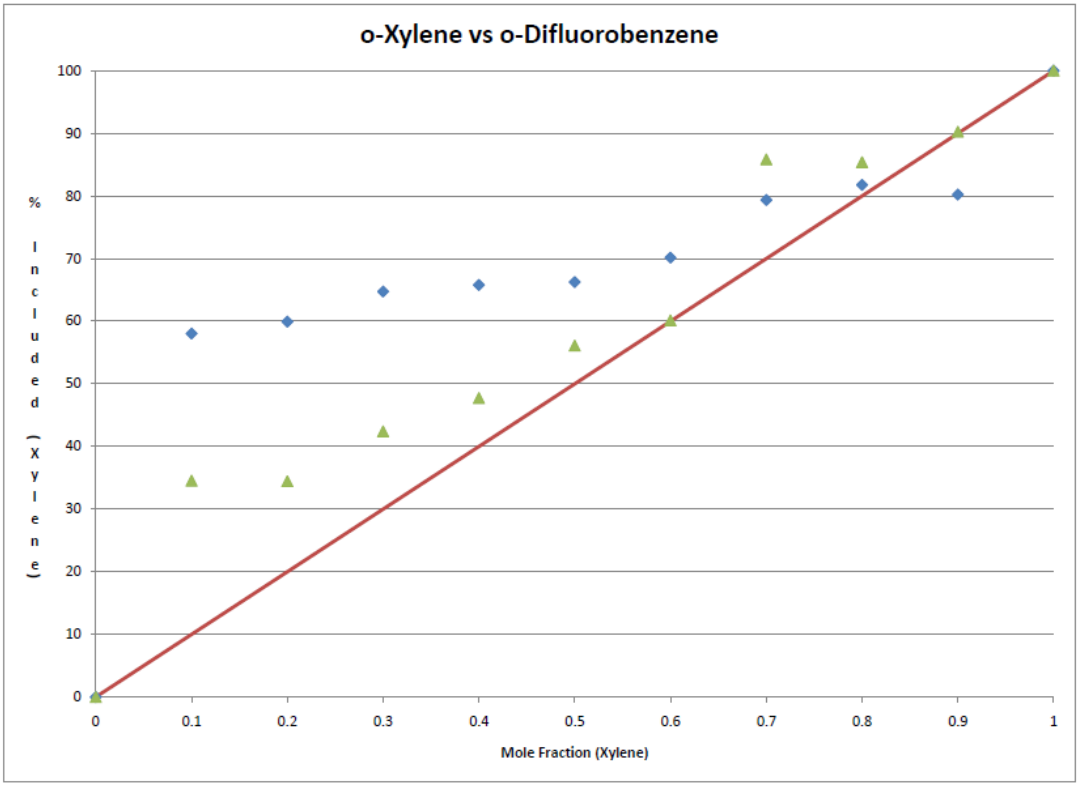

Figure 6.14 Combined selectivity plot from *o*-xylene vs. *o*-difluorobenzene study.

In the competition reaction between *o*-xylene versus *o*-difluorobenzene, the host framework was selective towards the *o*-xylene guest molecule. Figure 6.14 shows the two separate studies. The selectivity coefficient of this study is $K_{A:B}$ = 2.71, indicating the reaction is slightly selective for *o*-xylene.

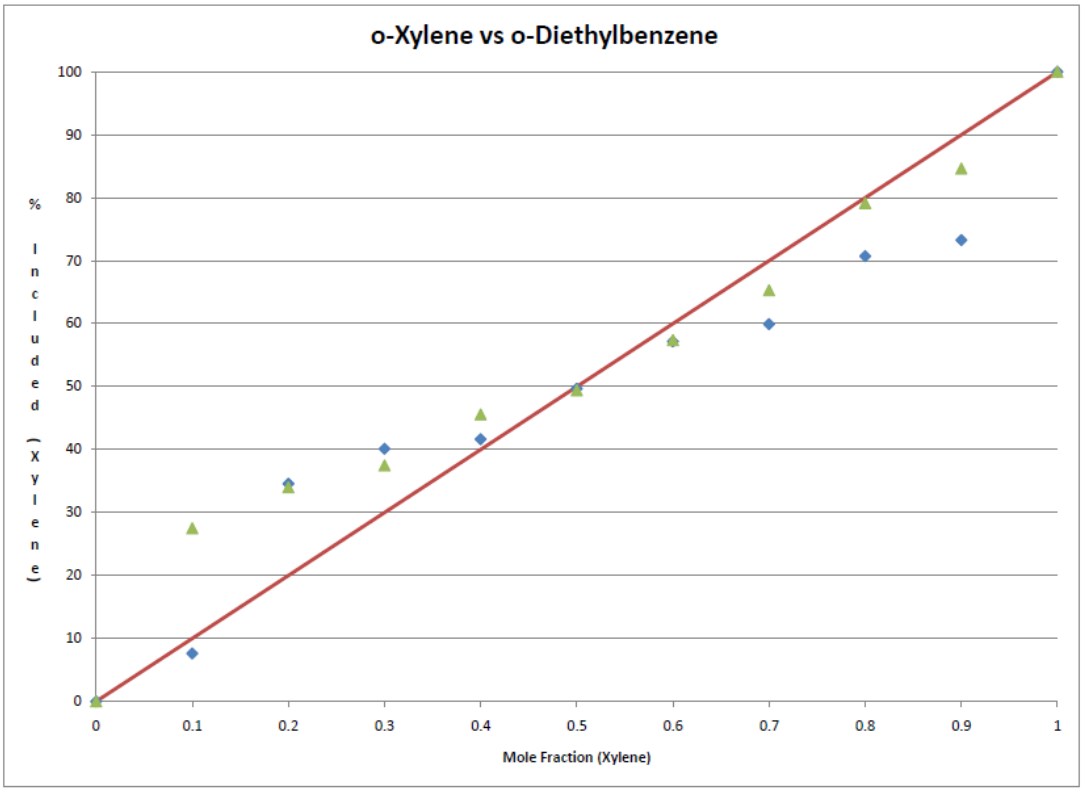

Figure 6.15 Combined selectivity plot from *o*-xylene vs. *o*-diethylbenzene study.

In the competition reaction between *o*-xylene versus *o*-diethylbenzene, no selectivity was observed. Figure 6.15 shows the two separate studies. The selectivity coefficient of this study is $K_{A:B} = 1.17$, indicating there is no real selectivity.

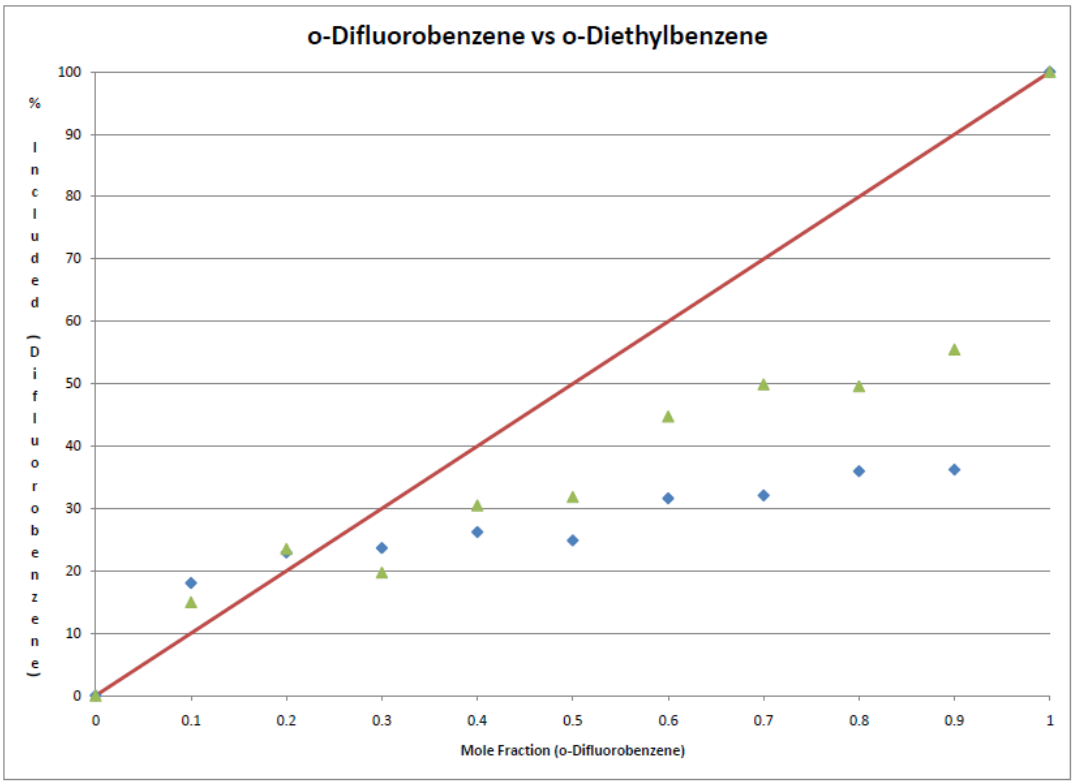

Figure 6.16 Combined selectivity plot from *o*-difluorobenzene vs. *o*-diethylbenzene study.

In the competition reaction between *o*-difluorobenzene versus *o*-diethylbenzene, the host framework was selective towards the *o*-diethylbenzene guest molecule. Figure 6.16 shows the two separate studies. The selectivity coefficient of this study is $K_{A:B} = 0.64$, indicating the reaction is slightly selective for *o*-diethylbenzene.

6.6 Discussion of Selectivity

In the selectivity studies of the monosubstituted guest molecules, the host framework has shown some sign to preferentially include one guest molecule over the other through the process of co-crystallization. One competition study from the

mono-substituted aryls did not show a sign of selectivity, whereby the host framework did not preferentially include one guest molecule over the other. When closely examining the nature of the guest molecules, it appears the size of the potential guest molecule is more a determining factor than the electronics of the guest molecule. In some examples, the electron donating group is favored but in another example the electron withdrawing group is favored. These results indicate there is no general trend forming in this selectivity study except for size dependence.

The competition study between toluene and nitrobenzene was a good example of comparing an electron donating group versus an electron withdrawing group and in this study the pillared framework favored the electron donating guest. Also the slight difference in the size of the substituents could have played a role in the inclusion process where the smaller sized guest molecule was more selective than the larger guest molecule. This pillared framework includes greater than 50% of toluene in every mole fraction point and greater than 80% from 0.6 mole fraction and higher of toluene.

The competition study between toluene and anisole was a good example of comparing two electron donating groups with varying sizes. The greater electron donating group (methoxy) shows a higher selectivity when compared to a smaller electron donating group (methyl). It appears that the size of the substituent and the electronics of the guest molecule are both factors toward selectivity. The framework includes greater than 50% of anisole is every mole fraction point, one exception being the 0.9 mole fraction of toluene.

The competition study between toluene and hexanol was a good example of comparing an electron donating aryl versus a polar alkyl, and this pillared framework showed no favoritism. The hydrogen bonding from the alcohol group or the $\pi - \pi$ interactions via the guest molecule and the framework are the two non-covalent interactions that are in question for this study. Since the data points in the inclusion graph follow the linear path that is given on the data plot, it could be inferred by observation that there was no selectivity present.

The competition study between toluene and iodobenzene was a good example of comparing an electron donating versus an electron withdrawing group and this pillared framework favored the electron withdrawing guest. Also this study was a comparison of size selectivity because the iodo group is larger than the methyl group. The size of the iodobenzene guest molecule must fill up the space of the channel more efficiently than the smaller toluene molecule which could be the main reason why there is some selectivity towards iodobenzene.

The competition study between toluene and ethyl acetate was a good example of comparing an electron donating aryl versus a volatile, polar alkyl solvent whereby the pillared framework favored the aryl guest. The toluene molecule must fill the channel more efficiently than ethyl acetate, which is not surprising after seeing the dimensions of the void area, Figure 4.2b. The aryl molecule is best suited for the pillared host over the alkyl molecule, more so the alkyl molecule does not offer any extra intermolecular interactions.

The competition study between nitrobenzene and iodobenzene was a comparison of electron withdrawing substituents. It showed that the least electron

withdrawing group was favored (iodo). It is possible that larger electron withdrawing group is not favored by the host framework. The iodobenzene molecule must fill up the channel more efficiently than nitrobenzene. The percent included of iodobenzene is greater than 50% in every mole fraction where iodobenzene was present. The pillared framework would be a good option when needing to separate nitrobenzene from iodobenzene.

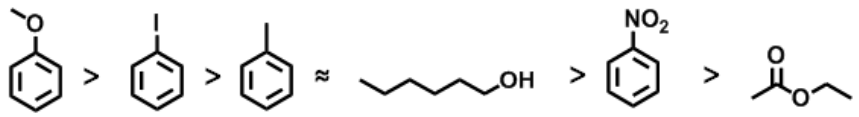

Figure 6.17 Guest ranking from competition studies.

In the selectivity studies of the disubstituted guest molecules, the host framework has shown evidence to preferentially include one guest molecule over the other through the process of co-crystallization. Here we looked at three different isomers of three molecules and compared the similar isomers to each other. In all examples xylene was favored over diethylbenzene, xylene was favored over difluorobenzene, and diethylbenzene was favored over difluorobenzene. A generalization can be drawn that xylene is more preferred than diethylbenzene, which is more preferred than difluorobenzene. In this study it is clear to see that the electron donating groups are favored over the electron withdrawing groups and that the larger ethyl groups are a worst it than the methyl groups. We learned that the smaller alkyl

group efficiently fills the channel over larger alkyl groups hence the higher selectivity for xylene over diethylbenzene in each case, *para*- , *meta*- , and *ortho*.

6.7 Conclusion

We have shown that our hydrogen bonded pillared framework can selectively include guest molecules via co-crystallization. If the substituents or the substitution pattern on the benzene ring are varied, we still observe selectivity for one guest over another. There was one instance where no selectivity was observed and that was the case of hexanol versus toluene. The mono- and disubstituted studies showed an overall selectivity towards molecules containing electron donating groups. Also, the substitution pattern of 1,4 appear to be the most favored position when examining the various isomers of each molecule. In the attempt to determine a selectivity factor, e.g. *m*- vs. *o*-xylenes was not successful because our GC separating column did not have the ability to separate such molecules. If the column of the GC could have been optimized this study would have been extremely beneficial.

References

(1) Jacobs, A.; Nassimbeni, L. R.; Nohako, K. L.; Su, H.; Taljaard, J. H. *Cryst. Growth & Des.* **2008**, *8*, 1301-1305.

(2) Roex, T. l.; Nassimbeni, L. R.; Weber, E. *New J. Chem.* **2008**, *32*, 856-863.

(3) Bourne, S. A.; Corin, K. C.; Nassimbeni, L. R. *Supramol. Chem.* **2006**, *18*, 587-592.

(4) Bourne, S. A.; Corin, K. C.; Nassimbeni, L. R.; Weber, E. *CrystEngComm* **2004**, *6*, 54-55.

(5) Nassimbeni, L. R.; Su, H. *J. Chem. Soc., Perkin Trans. 2* **2002**, 1246-1250.

(6) Nassimbeni, L. R.; Su, H. *New J. Chem.* **2002**, *26*, 989-995.

(7) Kim, J.; Yi, J.; Ward, M. D.; Kim, W.-S. *Separation and Purification Technology* **2009**, *66*, 57-64.

(8) Kim, J.; Lee, S.-O.; Yi, J.; Kim, W.-S.; Ward, M. D. *Separation and Purification Technology* **2008**, *62*, 517-522.

(9) Pivovar, A. M.; Holman, K. T.; Ward, M. D. *Chem. Mater.* **2001**, *13*, 3018-3031.

(10) Spokoyny, A. M.; Kim, D.; Sumrein, A.; Mirkin, C. A. *Chem. Soc. Rev.* **2009**, *38*, 1218-1227.

(11) Ma, L.; Carter, A.; Lin, W. *Chem. Soc. Rev.* **2009**, *38*, 1248-1256.

(12) Maji, T. K.; Kitagawa, S. *Pure Appl. Chem.* **2007**, *79*, 2155-2177.

(13) Wu, C.-D.; Hu, A.; Zhang, L.; Lin, W. *J. Am. Chem. Soc.* **2005**, *127*, 8940-8941.

(14) Shvareva, T. Y.; Skanthakumar, S.; Soderholm, L.; Clearfield, A.; Albrecht-Schmitt, T. E. *Chem. Mater.* **2007**, *19*, 132-134.

(15) Zeng, M.-H.; Feng, X.-L.; Zhang, W.-X.; Chen, X.-M. *Dalton Trans.* **2006**, 5294-5303.

(16) Kahn, O. *Acc. Chem. Res.* **2000**, *33*, 647-657.

Chapter 7

Conclusion

7.1 Concluding Remarks

The development of the field of Supramolecular chemistry has allowed for interesting and fascinating structures to be created, which exhibit intriguing properties such as: storage, signaling, catalysis, separations, and non-linear optics. We have successfully developed and synthesized two different types of hydrogen bonded metal organic frameworks (HMOFs) by varying the component that resides between our layered materials. The two HMOFs which were synthesized include a layered framework and a pillared framework. These frameworks were created by using a mono-amine and a diamine, respectively. These two HMOFs were subsequently studied for their potential properties as a storage device, signaling, and separations.

In the first study, the layered framework was created by using a mono-amine. This allowed us to control the distance and the chemical nature of the interlayer region. We created nine different layered frameworks when using nine different monoamines. We examined the phenomenon of intercalation by allowing guest molecules to enter the interlayer regions and either reside in the vacant space (non-coordinative) or replace the water ligands coordinated to the metal center (coordinative). In this study, we did not observe any signs of non-coordinative intercalation because none of the guest molecules remained between the layers upon characterization. In the second study, we observed coordinative intercalation, as supported by TGA and powder XRD evidence, and by the observation of a color change upon intercalation. The samples that showed a color change were likely to have replaced at least one

bound water molecule. The guest molecules that effected this color change were pyridine, 4-ethylpyridine, and 4-picoline. In the case using 4-picoline, there was evidence (TGA) that a third guest was present, likely residing in the interlayer region without the use of coordinative covalent bonding. There were some examples in which TGA showed evidence of intercalation, but that sample did not exhibit a color change upon guest replacement. These guest molecules were 4-chloropyridine, 4, 4'-bipyridine, 4-t-butylpyridine, and 4-(dimethylamino) pyridine. Interactions between the hydrophobic substituents working in concert are strong, and non-coordinating molecules do not become "solvated" by the organic substituents. However, coordinate-covalent bonds, because they are strong, connect to and remain inside the solid upon intercalation. Since there was no evidence of non-coordinative intercalation we decided to look into pillared frameworks in hopes that the pillared structure will allow for guest inclusion.

In the second study, the pillared hydrogen bonded framework was synthesized by using a diamine. This allows for control of the interlayer distance because it "props" up the layer, and also allows room for pores or channels. The pillared structure was synthesized by co-crystallizing the pillared components with guest molecules residing between the organic diamine. In presence of any guest, the same framework exists, as shown by single crystal and powder XRD data. Therefore, these ammonium-carboxylate hydrogen bonds are reliable for creating porous materials.

One of the first studies with the pillared framework was to test the stability of the framework upon guest loss because traditionally hydrogen bonds are not considered a strong interaction. After insertion, we removed the guest molecule and characterized the solid to ensure the framework was still intact. Then the porous framework was introduced to another guest molecule to observe if re-uptake of a guest molecule was possible. The answer is yes! Impressively, the guest was inserted and removed seven times without disrupting the hydrogen bonded framework.

The next study was to determine if the host was selective for specific types of molecules. This was examined through intercalation of guest molecules into the porous framework by varying the substituents on the guest. It was shown that the pillared framework preferred guests that contained electron donating groups but also showed evidence that guests containing electron withdrawing groups were inserted into the porous material.

In the final study, we looked into separating molecules through co-crystallization with our pillared framework. Competition reactions were setup of two competing guest molecules where the guests varied by size, shape, and chemical nature. Here we observed guest selectivity ranging from very high to no selectivity. We looked into comparing mono-substituted and disubstituted guest molecules separately and it was noticed that the guest which contained an electron donating group was often selected in preference to the other guest molecules. There was a trend that developed within similar isomers in that the 1,4-substituted molecules were more highly selective with

respect to each other than the 1,3-substituted molecules, which had a higher selectivity than the 1,2-substituted molecules. We could modify our starting material to create pockets of different size and shape to selectively include specific molecules that are in tune with the void space.

Here we are adding to the body of evidence showing that molecular, hydrogen bonded components can reliably create networks, and can be modified to allow inclusion/insertion of a variety of molecules. Thus, future work should lead to designing hosts that are sensors for specific molecules, can separate specific molecules, and/or catalyze reactions between molecules having specific substituents/sizes/shapes.

Appendix A

Crystal Structure Information and Tables

A.1 Crystal Structure Information for $Zn(HPDCA)_2(H_2O)_2 \cdot$methanol

Table 1. Crystal data and structure refinement for ab9409.

Identification code	b9409/lt/GAH0401A	
Empirical formula	$C_{16} H_{20} N_2 O_{12} Zn$	
Formula weight	497.71	
Temperature	100(2) K	
Wavelength	0.71073 Å	
Crystal system	Triclinic	
Space group	P-1	
Unit cell dimensions	a = 7.1427(5) Å	α= 93.827(3)°.
	b = 7.2275(5) Å	β= 105.334(4)°.
	c = 9.6663(6) Å	γ = 97.945(3)°.
Volume	473.83(6) $Å^3$	
Z	1	
Density (calculated)	1.744 Mg/m^3	
Absorption coefficient	1.369 mm^{-1}	
F(000)	256	
Crystal size	0.29 x 0.15 x 0.12 mm^3	
Theta range for data collection	3.00 to 38.31°.	
Index ranges	$-7 \leq h \leq 12$, $-12 \leq k \leq 12$, $-16 \leq l \leq 14$	
Reflections collected	11204	
Independent reflections	5161 [R(int) = 0.021]	
Completeness to theta = 25.00°	99.9 %	
Absorption correction	Semi-empirical from equivalents	
Max. and min. transmission	0.8585 and 0.6956	
Refinement method	Full-matrix least-squares on F^2	
Data / restraints / parameters	5161 / 3 / 155	
Goodness-of-fit on F^2	1.047	
Final R indices [I>2sigma(I)]	R1 = 0.0298, wR2 = 0.0733	
R indices (all data)	R1 = 0.0365, wR2 = 0.0762	
Largest diff. peak and hole	0.615 and -0.499 $e.Å^{-3}$	

Table 2. Atomic coordinates (x 10^4) and equivalent isotropic displacement parameters ($Å^2$x 10^3)
for ab9409. U(eq) is defined as one third of the trace of the orthogonalized U^{ij} tensor.

	x	y	z	U(eq)
Zn(1)	0	0	5000	9(1)
O(1)	1732(1)	-12(1)	3557(1)	11(1)
O(2)	4586(1)	1307(1)	3269(1)	12(1)
O(3)	-1476(1)	2108(1)	3933(1)	15(1)
O(4)	7928(1)	6282(1)	9437(1)	15(1)
O(5)	9100(1)	5849(1)	7526(1)	14(1)
N(1)	2319(1)	2117(1)	6035(1)	10(1)
C(1)	3365(1)	1097(1)	3969(1)	9(1)
C(2)	3799(1)	2258(1)	5417(1)	8(1)
C(3)	5589(1)	3399(1)	6053(1)	9(1)
C(4)	5834(1)	4445(1)	7367(1)	9(1)
C(5)	4259(1)	4376(1)	7962(1)	11(1)
C(6)	2524(1)	3185(1)	7265(1)	12(1)
C(7)	7792(1)	5604(1)	8112(1)	10(1)
O(6)	11283(1)	8173(1)	10857(1)	17(1)
C(8)	12662(2)	8918(2)	10124(1)	18(1)

Table 3. Anisotropic displacement parameters ($Å^2 x 10^3$) for ab9409. The anisotropic displacement factor exponent takes the form: $-2\pi^2[h^2 a^{*2} U^{11} + ... + 2 h k a^* b^* U^{12}]$

U^{11}	U^{22}	U^{33}	U^{23}	U^{13}	U^{12}
Zn(1)6(1)	11(1)	9(1)	-1(1)	2(1)	-2(1)
O(1)8(1)	13(1)	11(1)	-2(1)	3(1)	-3(1)
O(2)9(1)	17(1)	12(1)	-2(1)	5(1)	-2(1)
O(3)8(1)	20(1)	19(1)	8(1)	5(1)	1(1)
O(4)11(1)	20(1)	10(1)	-5(1)	2(1)	-4(1)
O(5)11(1)	17(1)	13(1)	-1(1)	5(1)	-4(1)
N(1)8(1)	12(1)	9(1)	0(1)	3(1)	0(1)
C(1)7(1)	10(1)	9(1)	0(1)	2(1)	0(1)
C(2)7(1)	9(1)	9(1)	0(1)	2(1)	0(1)
C(3)8(1)	11(1)	9(1)	-1(1)	2(1)	-1(1)
C(4)8(1)	10(1)	9(1)	0(1)	2(1)	-1(1)
C(5)10(1)	14(1)	10(1)	-2(1)	3(1)	-1(1)
C(6)9(1)	15(1)	10(1)	-2(1)	4(1)	0(1)
C(7)10(1)	10(1)	10(1)	0(1)	2(1)	-1(1)
O(6)13(1)	21(1)	12(1)	-6(1)	4(1)	-5(1)
C(8)18(1)	20(1)	16(1)	-3(1)	7(1)	-3(1)

A.2 Crystal Structure Information for Zn(o-tolidinium)$(H_2O)_2$ · acetone

Table 1. Crystal data and structure refinement for ab14708.

Identification code	b14708/lt/gah005	
Empirical formula	C_{31} H_{34} N_4 O_{11} Zn	
Formula weight	703.99	
Temperature	100(2) K	
Wavelength	0.71073 Å	
Crystal system	Triclinic	
Space group	P-1	
Unit cell dimensions	a = 5.1750(9) Å	α= 90.174(7)°.
	b = 8.3571(13) Å	β= 95.130(7)°.
	c = 19.712(4) Å	γ = 100.135(7)°.
Volume	835.7(3) $Å^3$	
Z	1	
Density (calculated)	1.399 Mg/m^3	
Absorption coefficient	0.799 mm^{-1}	
F(000)	366	
Crystal size	0.26 x 0.14 x 0.12 mm^3	
Theta range for data collection	2.70 to 23.88°.	
Index ranges	$-5 \leq h \leq 5$, $-9 \leq k \leq 9$, $-22 \leq l \leq 22$	
Reflections collected	15678	
Independent reflections	2528 [R(int) = 0.0797]	
Completeness to theta = 23.88°	97.8 %	
Absorption correction	Semi-empirical from equivalents	
Max. and min. transmission	0.9103 and 0.8193	
Refinement method	Full-matrix least-squares on F^2	
Data / restraints / parameters	2528 / 26 / 242	
Goodness-of-fit on F^2	1.042	
Final R indices [I>2sigma(I)]	R1 = 0.0733, wR2 = 0.1957	
R indices (all data)	R1 = 0.0828, wR2 = 0.2060	
Largest diff. peak and hole	1.162 and -1.177 $e.Å^{-3}$	

Table 2. Atomic coordinates (x 10^4) and equivalent isotropic displacement parameters ($Å^2$x 10^3)
for ab14708. U(eq) is defined as one third of the trace of the orthogonalized U^{ij} tensor.

	x	y	z	U(eq)
Zn(1)	0	0	0	20(1)
O(1)	-2450(6)	121(4)	768(2)	19(1)
O(2)	-3745(6)	-1090(4)	1716(2)	23(1)
O(3)	3193(7)	1507(4)	585(2)	20(1)
O(4)	-232(8)	-6042(4)	2428(2)	34(1)
O(5)	2260(7)	-7122(4)	1761(2)	31(1)
N(1)	600(7)	-2078(4)	554(2)	18(1)
C(1)	-823(9)	-2274(5)	1098(2)	17(1)
C(2)	-774(9)	-3559(6)	1533(2)	19(1)
C(3)	814(9)	-4685(5)	1422(2)	20(1)
C(4)	2281(9)	-4495(6)	859(2)	20(1)
C(5)	2117(9)	-3181(6)	441(2)	20(1)
C(6)	-2482(9)	-984(6)	1213(3)	20(1)
C(7)	960(10)	-6066(6)	1915(3)	22(1)
N(2)	-4269(9)	1447(5)	2569(2)	27(1)
C(8)	-4490(10)	1013(6)	3286(2)	24(1)
C(9)	-6574(11)	-92(8)	3445(3)	39(2)
C(10)	-6735(11)	-468(8)	4132(3)	41(2)
C(11)	-4883(10)	210(6)	4636(2)	24(1)
C(12)	-2773(15)	1298(9)	4444(3)	68(3)
C(13)	-2590(16)	1687(9)	3759(3)	67(3)
C(14)	-8300(40)	-1210(30)	2898(8)	67(8)
C(14')	-8900(40)	-480(20)	2911(10)	43(5)
O(1S)	1960(40)	13970(20)	5575(13)	185(9)
C(1S)	4430(70)	14520(30)	5862(13)	185(9)
C(2S)	4580(40)	14150(30)	6610(12)	104(5)
C(3S)	6520(40)	15390(30)	5422(11)	104(5)

Table 3. Anisotropic displacement parameters ($Å^2 x 10^3$) for ab14708. The anisotropic displacement factor exponent takes the form: $-2\pi^2[h^2 a^{*2} U^{11} + ... + 2 h k a^* b^* U^{12}]$

U^{11}	U^{22}	U^{33}	U^{23}	U^{13}	U^{12}
Zn(1)25(1)	13(1)	23(1)	14(1)	7(1)	5(1)
O(1)23(2)	13(2)	24(2)	14(1)	7(1)	4(1)
O(2)28(2)	20(2)	23(2)	10(2)	11(2)	6(2)
O(3)22(2)	14(2)	26(2)	10(2)	7(2)	8(2)
O(4)57(3)	22(2)	28(2)	21(2)	22(2)	13(2)
O(5)53(2)	19(2)	27(2)	16(2)	9(2)	19(2)
N(1)18(2)	15(2)	20(2)	7(2)	6(2)	0(2)
C(1)20(2)	9(2)	23(3)	6(2)	1(2)	4(2)
C(2)24(3)	14(2)	17(3)	8(2)	2(2)	1(2)
C(3)26(3)	9(2)	21(3)	7(2)	1(2)	-1(2)
C(4)25(3)	10(2)	25(3)	9(2)	2(2)	4(2)
C(5)21(2)	16(3)	21(3)	7(2)	6(2)	-1(2)
C(6)18(2)	17(3)	25(3)	7(2)	-1(2)	2(2)
C(7)29(3)	14(3)	23(3)	11(2)	2(2)	3(2)
N(2)46(3)	17(2)	21(2)	13(2)	6(2)	11(2)
C(8)42(3)	15(3)	17(3)	12(2)	5(2)	7(2)
C(9)36(3)	56(4)	23(3)	13(3)	2(2)	-1(3)
C(10)34(3)	60(4)	23(3)	16(3)	5(3)	-12(3)
C(11)39(3)	14(3)	20(3)	10(2)	3(2)	4(2)
C(12)82(5)	74(5)	23(3)	19(3)	-9(3)	-51(4)
C(13)101(6)	56(5)	23(3)	21(3)	7(4)	-44(4)
C(14)46(11)	110(20)	20(8)	18(11)	-1(7)	-48(12)
C(14')	54(10)	41(10)	33(9)	8(7)	4(7) 12(7)
O(1S)	144(15)	82(10)	320(20)	-69(13)	14(16) -6(9)
C(1S)144(15)	82(10)	320(20)	-69(13)	14(16)	-6(9)
C(2S)76(9)	126(13)	107(12)	-21(10)	13(8)	7(9)
C(3S)76(9)	126(13)	107(12)	-21(10)	13(8)	7(9)

A.3 Crystal Structure Information for Zn(o-tolidinium)$(H_2O)_2$ · *p*-xylene

Table 1. Crystal data and structure refinement for ab3709.

Identification code	b3709/lt/gah038	
Empirical formula	$C_{36}\ H_{38}\ N_4\ O_{10}\ Zn$	
Formula weight	752.07	
Temperature	100(2) K	
Wavelength	0.71073 Å	
Crystal system	Triclinic	
Space group	P-1	
Unit cell dimensions	a = 5.1842(5) Å	α= 89.508(6)°.
	b = 8.5087(9) Å	β= 85.077(7)°.
	c = 19.5787(19) Å	γ = 80.522(6)°.
Volume	848.69(15) $Å^3$	
Z	1	
Density (calculated)	1.472 Mg/m^3	
Absorption coefficient	0.790 mm^{-1}	
F(000)	392	
Crystal size	0.31 x 0.25 x 0.10 mm^3	
Theta range for data collection	2.43 to 35.30°.	
Index ranges	$-8 \leq h \leq 8$, $-6 \leq k \leq 13$, $-31 \leq l \leq 31$	
Reflections collected	14549	
Independent reflections	7529 [R(int) = 0.0273]	
Completeness to theta = 25.00°	99.7 %	
Absorption correction	Semi-empirical from equivalents	
Max. and min. transmission	0.9238 and 0.7942	
Refinement method	Full-matrix least-squares on F^2	
Data / restraints / parameters	7529 / 1 / 289	
Goodness-of-fit on F^2	1.031	
Final R indices [I>2sigma(I)]	R1 = 0.0407, wR2 = 0.0981	
R indices (all data)	R1 = 0.0510, wR2 = 0.1039	
Largest diff. peak and hole	0.744 and -0.480 e.$Å^{-3}$	

Table 2. Atomic coordinates (x 10^4) and equivalent isotropic displacement parameters ($Å^2$x 10^3)
for ab3709. U(eq) is defined as one third of the trace of the orthogonalized U^{ij} tensor.

	x	y	z	U(eq)
Zn(1)	10000	10000	0	11(1)
O(1)	6839(2)	11480(1)	583(1)	14(1)
O(2)	12457(2)	10109(1)	777(1)	13(1)
O(3)	13755(2)	8883(1)	1734(1)	15(1)
O(4)	10346(2)	3901(1)	2422(1)	20(1)
O(5)	7805(2)	2877(1)	1744(1)	22(1)
N(1)	9379(2)	7936(1)	563(1)	11(1)
N(2)	4336(2)	1426(1)	2537(1)	17(1)
C(1)	12490(2)	9001(1)	1221(1)	11(1)
C(2)	10824(2)	7733(1)	1105(1)	11(1)
C(3)	10809(2)	6441(1)	1543(1)	11(1)
C(4)	9217(2)	5318(1)	1420(1)	11(1)
C(5)	7731(2)	5530(1)	858(1)	12(1)
C(6)	7860(2)	6854(1)	441(1)	12(1)
C(7)	9123(2)	3915(1)	1902(1)	12(1)
C(8)	4549(3)	979(1)	3256(1)	17(1)
C(11)	4889(3)	201(2)	4633(1)	22(1)
C(12)	6724(3)	-490(2)	4133(1)	22(1)
C(13)	6598(3)	-124(2)	3438(1)	24(1)
C(15)	4794(3)	5366(2)	4297(1)	28(1)
C(18)	4558(5)	5732(4)	3551(1)	61(1)
C(9)	2163(5)	1400(3)	3728(1)	13(1)
C(10)	2310(5)	972(3)	4410(1)	13(1)
C(14)	8906(5)	-495(4)	2935(1)	19(1)
C(16)	7235(6)	4839(4)	4557(2)	27(1)
C(17)	3441(6)	6343(3)	4779(2)	23(1)
C(9')	3210(6)	1963(3)	3745(1)	15(1)
C(10')	3410(5)	1603(3)	4432(1)	15(1)

C(14')	8258(6)	-1342(4)	2879(1)	22(1)
C(16')	6315(6)	3890(3)	4527(2)	22(1)
C(17')	2633(6)	5638(4)	4766(2)	28(1)

Table 3. Anisotropic displacement parameters ($Å^2 x 10^3$) for ab3709. The anisotropic displacement factor exponent takes the form: $-2\pi^2[h^2 a^{*2}U^{11} + ... + 2 h k a^* b^* U^{12}]$

U^{11}	U^{22}	U^{33}	U^{23}	U^{13}	U^{12}
Zn(1)13(1)	11(1)	10(1)	4(1)	-3(1)	-6(1)
O(1)14(1)	15(1)	13(1)	0(1)	-2(1)	-7(1)
O(2)15(1)	14(1)	13(1)	5(1)	-4(1)	-7(1)
O(3)18(1)	16(1)	12(1)	1(1)	-6(1)	-6(1)
O(4)30(1)	17(1)	16(1)	6(1)	-11(1)	-8(1)
O(5)36(1)	17(1)	16(1)	5(1)	-8(1)	-16(1)
N(1)12(1)	11(1)	9(1)	2(1)	-2(1)	-4(1)
N(2)29(1)	14(1)	8(1)	2(1)	-5(1)	-7(1)
C(1)12(1)	12(1)	10(1)	0(1)	-1(1)	-4(1)
C(2)12(1)	11(1)	10(1)	1(1)	-2(1)	-4(1)
C(3)14(1)	12(1)	9(1)	2(1)	-3(1)	-4(1)
C(4)13(1)	10(1)	9(1)	1(1)	-1(1)	-3(1)
C(5)14(1)	12(1)	12(1)	2(1)	-3(1)	-5(1)
C(6)14(1)	13(1)	12(1)	2(1)	-5(1)	-5(1)
C(7)17(1)	11(1)	10(1)	2(1)	-2(1)	-4(1)
C(8)31(1)	12(1)	8(1)	2(1)	-5(1)	-2(1)
C(11)35(1)	17(1)	8(1)	1(1)	-2(1)	9(1)
C(12)14(1)	39(1)	11(1)	7(1)	-1(1)	4(1)
C(13)14(1)	45(1)	11(1)	7(1)	0(1)	1(1)
C(15)24(1)	28(1)	32(1)	-1(1)	-6(1)	-2(1)
C(18)45(1)	95(2)	35(1)	9(1)	-5(1)	9(1)
C(9)15(1)	14(1)	10(1)	2(1)	-3(1)	-2(1)
C(10)14(1)	16(1)	9(1)	1(1)	-1(1)	-1(1)
C(14)18(1)	23(1)	13(1)	1(1)	4(1)	-1(1)
C(16)22(1)	20(1)	41(2)	-7(1)	-3(1)	-4(1)
C(17)19(1)	15(1)	34(2)	-3(1)	-3(1)	-1(1)
C(9')24(1)	10(1)	11(1)	2(1)	-4(1)	0(1)
C(10')	22(1)	13(1)	9(1)	0(1)	-2(1) 1(1)
C(14')	18(1)	34(2)	11(1)	-3(1)	0(1) 6(1)

C(16')	20(1)	16(1)	31(1)	-6(1)	-2(1)	-4(1)
C(17')	21(1)	16(1)	49(2)	-6(1)	-13(1)	1(1)

A.4 Crystal Structure Information for Zn(o-tolidinium)$(H_2O)_2$ · nitrobenzene

Table 1. Crystal data and structure refinement for ab409.

Identification code	b409/lt/gah022	
Empirical formula	$C_{34}\ H_{33}\ N_5\ O_{12}\ Zn$	
Formula weight	769.02	
Temperature	100(2) K	
Wavelength	0.71073 Å	
Crystal system	Triclinic	
Space group	P-1	
Unit cell dimensions	a = 5.2035(2) Å	α= 90.0910(10)°.
	b = 8.3292(3) Å	β= 94.6460(10)°.
	c = 19.7543(7) Å	γ = 100.0870(10)°.
Volume	840.06(5) $Å^3$	
Z	1	
Density (calculated)	1.520 Mg/m^3	
Absorption coefficient	0.805 mm^{-1}	
F(000)	398	
Crystal size	0.28 x 0.28 x 0.15 mm^3	
Theta range for data collection	2.07 to 27.59°.	
Index ranges	$-6 \leq h \leq 6$, $-10 \leq k \leq 10$, $-25 \leq l \leq 25$	
Reflections collected	6322	
Independent reflections	3842 [R(int) = 0.0192]	
Completeness to theta = 25.00°	99.1 %	
Absorption correction	Semi-empirical from equivalents	
Max. and min. transmission	0.8902 and 0.8055	
Refinement method	Full-matrix least-squares on F^2	
Data / restraints / parameters	3842 / 108 / 293	
Goodness-of-fit on F^2	1.050	
Final R indices [I>2sigma(I)]	R1 = 0.0362, wR2 = 0.0939	
R indices (all data)	R1 = 0.0393, wR2 = 0.0962	
Largest diff. peak and hole	0.528 and -0.433 $e.Å^{-3}$	

Table 2. Atomic coordinates (x 10^4) and equivalent isotropic displacement parameters ($Å^2$x 10^3)
for ab409. U(eq) is defined as one third of the trace of the orthogonalized U^{ij} tensor.

	x	y	z	U(eq)
Zn(1)	0	0	0	14(1)
O(1)	3180(2)	1502(2)	584(1)	16(1)
O(2)	-2469(2)	117(2)	769(1)	16(1)
O(3)	-3772(3)	-1128(2)	1715(1)	19(1)
O(4)	-433(4)	-6146(2)	2399(1)	34(1)
O(5)	2168(3)	-7184(2)	1753(1)	28(1)
N(1)	590(3)	-2085(2)	554(1)	13(1)
N(2)	-4432(4)	1380(2)	2557(1)	26(1)
C(1)	-2509(3)	-1000(2)	1208(1)	14(1)
C(2)	-851(3)	-2292(2)	1092(1)	13(1)
C(3)	-844(3)	-3591(2)	1525(1)	15(1)
C(4)	748(3)	-4731(2)	1409(1)	14(1)
C(5)	2238(4)	-4518(2)	855(1)	16(1)
C(6)	2108(3)	-3185(2)	440(1)	15(1)
C(7)	826(4)	-6139(2)	1894(1)	18(1)
C(8)	-4625(5)	943(3)	3272(1)	24(1)
C(9)	-6642(5)	-163(4)	3459(1)	43(1)
C(10)	-6752(5)	-517(4)	4146(1)	45(1)
C(11)	-4914(4)	198(3)	4633(1)	24(1)
C(12)	-3402(16)	1581(8)	4430(3)	41(2)
C(13)	-3299(17)	1955(7)	3741(3)	43(2)
C(14)	-8974(11)	-575(8)	2956(3)	34(1)
C(12')	-2451(10)	1037(8)	4413(3)	27(1)
C(13')	-2311(10)	1438(7)	3739(3)	25(1)
C(14')	-8197(17)	-1537(12)	2899(3)	78(3)
C(1S)	-5030(20)	-4993(16)	4777(4)	124(6)
C(2S)	-2611(17)	-4451(18)	4527(5)	219(12)
C(3S)	-2468(18)	-4099(16)	3842(6)	214(9)

C(4S)	-4740(20)	-4288(13)	3407(4)	144(6)
C(5S)	-7159(19)	-4830(16)	3657(5)	179(8)
C(6S)	-7302(17)	-5182(17)	4342(5)	147(8)
O(1S)	-3570(40)	-5241(19)	5925(10)	251(10)
O(2S)	-7190(30)	-6100(20)	5694(5)	171(6)
N(1S)	-5540(30)	-5580(20)	5475(10)	149(6)

Table 3. Anisotropic displacement parameters ($Å^2 x 10^3$) for ab409. The anisotropic displacement factor exponent takes the form: $-2\pi^2[h^2 a^{*2} U^{11} + ... + 2 h k a^* b^* U^{12}]$

U^{11}	U^{22}	U^{33}	U^{23}	U^{13}	U^{12}	
Zn(1)14(1)	14(1)	14(1)	4(1)	3(1)	6(1)	
O(1)16(1)	18(1)	16(1)	1(1)	2(1)	8(1)	
O(2)16(1)	16(1)	18(1)	4(1)	4(1)	8(1)	
O(3)23(1)	20(1)	18(1)	2(1)	8(1)	9(1)	
O(4)56(1)	29(1)	25(1)	14(1)	22(1)	21(1)	
O(5)50(1)	24(1)	18(1)	7(1)	9(1)	23(1)	
N(1)13(1)	15(1)	12(1)	1(1)	1(1)	4(1)	
N(2)46(1)	23(1)	13(1)	4(1)	8(1)	17(1)	
C(1)14(1)	14(1)	14(1)	-2(1)	0(1)	4(1)	
C(2)13(1)	14(1)	14(1)	-1(1)	0(1)	4(1)	
C(3)16(1)	16(1)	12(1)	1(1)	3(1)	3(1)	
C(4)18(1)	13(1)	12(1)	2(1)	0(1)	3(1)	
C(5)17(1)	15(1)	16(1)	0(1)	2(1)	6(1)	
C(6)15(1)	16(1)	15(1)	1(1)	4(1)	4(1)	
C(7)28(1)	14(1)	14(1)	2(1)	2(1)	6(1)	
C(8)42(1)	22(1)	11(1)	4(1)	7(1)	11(1)	
C(9)30(1)	74(2)	16(1)	7(1)	-2(1)	-11(1)	
C(10)33(1)	73(2)	17(1)	9(1)	1(1)	-20(1)	
C(11)33(1)	24(1)	14(1)	4(1)	5(1)	0(1)	
C(12)74(5)	29(3)	10(2)	-2(2)	2(3)	-17(3)	
C(13)83(5)	22(3)	17(2)	6(2)	9(3)	-10(3)	
C(14)34(3)	48(3)	16(2)	-1(2)	-6(2)	2(2)	
C(12')	23(2)	37(3)	17(2)	3(2)	-2(2)	-3(2)
C(13')	26(2)	29(3)	17(2)	5(2)	4(2)	-2(2)
C(14')	75(5)	108(7)	25(3)	-7(4)	5(3)	-60(5)
C(1S)105(8)	86(7)	199(18)	-3(12)	119(11)	20(6)	
C(2S)161(17)	132(14)	340(30)	29(17)	53(19)	-48(13)	
C(3S)162(14)	190(16)	270(20)	41(17)	104(15)	-61(13)	
C(4S)128(10)	129(10)	160(12)	-63(9)	61(10)	-43(9)	

C(5S)152(13)	255(17)	97(9)	-83(11)	40(9)	-70(12)	
C(6S)81(8)	213(16)	130(11)	-83(11)	46(8)	-38(9)	
O(1S)	266(17)	151(12)	320(20)	-10(13)	-196(16)	104(12)
O(2S)	138(11)	305(19)	85(6)	-1(8)	48(6)	60(11)
N(1S)	106(9)	153(13)	224(16)	64(10)	77(10)	92(10)

A.5 Crystal Structure Information for Zn(o-tolidinium)$(H_2O)_2$ · hexanol

Table 1. Crystal data and structure refinement for ab16008.

Identification code	b16008/lt/gah014	
Empirical formula	$C_{34}\,H_{42}\,N_4\,O_{11}\,Zn$	
Formula weight	748.09	
Temperature	100(2) K	
Wavelength	0.71073 Å	
Crystal system	Triclinic	
Space group	P-1	
Unit cell dimensions	a = 5.2571(8) Å	α= 91.072(9)°.
	b = 8.2727(13) Å	β= 96.028(9)°.
	c = 19.632(4) Å	γ = 99.886(8)°.
Volume	835.9(2) $Å^3$	
Z	1	
Density (calculated)	1.486 Mg/m^3	
Absorption coefficient	0.803 mm^{-1}	
F(000)	392	
Crystal size	0.41 x 0.13 x 0.11 mm^3	
Theta range for data collection	3.13 to 27.86°.	
Index ranges	$-6\leq h\leq 6$, $-7\leq k\leq 10$, $-25\leq l\leq 25$	
Reflections collected	5710	
Independent reflections	3632 [R(int) = 0.053]	
Completeness to theta = 25.00°	94.3 %	
Absorption correction	Semi-empirical from equivalents	
Max. and min. transmission	0.9154 and 0.7368	
Refinement method	Full-matrix least-squares on F^2	
Data / restraints / parameters	3632 / 79 / 255	
Goodness-of-fit on F^2	1.016	
Final R indices [I>2sigma(I)]	R1 = 0.0834, wR2 = 0.2107	
R indices (all data)	R1 = 0.1002, wR2 = 0.2266	
Largest diff. peak and hole	1.707 and -1.742 $e.Å^{-3}$	

Table 2. Atomic coordinates (x 10^4) and equivalent isotropic displacement parameters ($Å^2$x 10^3)
for ab16008. U(eq) is defined as one third of the trace of the orthogonalized U^{ij} tensor.

	x	y	z	U(eq)
Zn(1)	10000	10000	0	17(1)
O(1)	7632(6)	10163(4)	778(2)	20(1)
O(2)	6368(6)	8933(4)	1715(2)	20(1)
O(3)	13256(6)	11505(4)	596(2)	19(1)
O(4)	10122(7)	4037(4)	2454(2)	28(1)
O(5)	12647(7)	2988(4)	1787(2)	28(1)
N(1)	10611(6)	7918(4)	550(2)	17(1)
N(2)	6096(7)	11541(5)	2587(2)	21(1)
C(1)	7595(7)	9023(5)	1213(2)	17(1)
C(2)	9248(7)	7735(5)	1094(2)	16(1)
C(3)	9351(8)	6481(5)	1535(2)	19(1)
C(4)	10995(8)	5350(5)	1430(2)	19(1)
C(5)	12378(8)	5542(5)	865(2)	19(1)
C(6)	12150(8)	6822(5)	440(2)	19(1)
C(7)	11254(8)	4019(5)	1933(2)	21(1)
C(8)	5805(8)	11089(5)	3295(2)	20(1)
C(9)	7714(10)	11691(6)	3815(2)	30(1)
C(10)	7404(9)	11258(6)	4481(2)	28(1)
C(11)	5180(8)	10229(5)	4641(2)	19(1)
C(12)	3321(9)	9622(6)	4094(2)	25(1)
C(13)	3599(9)	10031(6)	3423(2)	24(1)
C(14)	1549(11)	9354(9)	2839(3)	47(2)
C(1S)	3900(40)	13930(20)	6512(5)	176(18)
C(2S)	5540(30)	14767(18)	5992(4)	278(19)
C(3S)	4270(20)	14595(15)	5262(4)	184(14)
C(4S)	5801(17)	15456(12)	4745(4)	41(4)
C(5S)	4533(13)	15284(14)	4016(4)	36(3)
C(6S)	6169(14)	16120(11)	3495(3)	55(6)

O(1S)	8866(14)	15933(13)	3551(4)	80(4)

Table 3. Anisotropic displacement parameters ($Å^2 x 10^3$) for ab16008. The anisotropic displacement factor exponent takes the form: $-2\pi^2[h^2 a^{*2} U^{11} + ... + 2 h k a^* b^* U^{12}]$

U^{11}	U^{22}	U^{33}	U^{23}	U^{13}	U^{12}
Zn(1)9(1)	19(1)	26(1)	5(1)	4(1)	7(1)
O(1)12(1)	25(2)	26(2)	5(1)	6(1)	10(1)
O(2)13(1)	23(2)	26(2)	4(1)	6(1)	5(1)
O(3)13(1)	20(2)	26(2)	2(1)	2(1)	7(1)
O(4)29(2)	26(2)	31(2)	9(1)	9(1)	8(2)
O(5)38(2)	23(2)	27(2)	6(1)	4(2)	17(2)
N(1)8(2)	20(2)	25(2)	1(1)	4(1)	5(1)
N(2)21(2)	23(2)	22(2)	5(2)	3(2)	10(2)
C(1)7(2)	22(2)	23(2)	0(2)	2(2)	4(2)
C(2)6(2)	15(2)	28(2)	1(2)	-1(2)	2(2)
C(3)7(2)	20(2)	28(2)	2(2)	0(2)	1(2)
C(4)11(2)	17(2)	26(2)	0(2)	0(2)	1(2)
C(5)9(2)	19(2)	28(2)	2(2)	0(2)	5(2)
C(6)11(2)	20(2)	28(2)	2(2)	5(2)	4(2)
C(7)15(2)	16(2)	30(2)	4(2)	3(2)	1(2)
C(8)20(2)	19(2)	24(2)	2(2)	5(2)	8(2)
C(9)23(2)	34(3)	29(2)	9(2)	6(2)	-10(2)
C(10)23(2)	34(3)	21(2)	5(2)	-3(2)	-10(2)
C(11)14(2)	21(2)	23(2)	4(2)	4(2)	5(2)
C(12)13(2)	37(3)	23(2)	2(2)	4(2)	-3(2)
C(13)14(2)	34(3)	24(2)	2(2)	1(2)	2(2)
C(14)26(3)	74(5)	31(3)	8(3)	-2(2)	-18(3)
C(1S)90(20)	39(16)	420(50)	-10(20)	90(30)	19(17)
C(2S)250(30)	150(30)	430(40)	-60(30)	-50(30)	100(30)
C(3S)170(20)	85(17)	310(30)	-50(20)	-40(20)	102(16)
C(4S)38(7)	41(9)	45(7)	0(6)	28(6)	-3(6)
C(5S)16(5)	39(7)	53(7)	1(5)	10(5)	1(5)
C(6S)49(11)	87(16)	46(8)	26(8)	26(7)	44(11)

O(1S)	73(8)	79(8)	92(9)	-21(7)	31(7)	9(6)

A.6 Crystal Structure Information for Zn(o-tolidinium)$(H_2O)_2$ · pentanol

Table 1. Crystal data and structure refinement for ab1509.

Identification code	b1509/lt/gah026	
Empirical formula	$C_{33}\ H_{40}\ N_4\ O_{11}\ Zn$	
Formula weight	734.06	
Temperature	100(2) K	
Wavelength	0.71073 Å	
Crystal system	Triclinic	
Space group	P-1	
Unit cell dimensions	a = 5.2378(7) Å	α= 89.975(7)°.
	b = 8.3282(13) Å	β= 84.587(7)°.
	c = 20.114(3) Å	γ = 78.483(7)°.
Volume	855.8(2) $Å^3$	
Z	1	
Density (calculated)	1.424 Mg/m^3	
Absorption coefficient	0.783 mm^{-1}	
F(000)	384	
Crystal size	0.40 x 0.15 x 0.15 mm^3	
Theta range for data collection	2.03 to 39.44°.	
Index ranges	$-8 \leq h \leq 9$, $-12 \leq k \leq 14$, $-32 \leq l \leq 35$	
Reflections collected	17370	
Independent reflections	8717 [R(int) = 0.030]	
Completeness to theta = 25.00°	96.7 %	
Absorption correction	Semi-empirical from equivalents	
Max. and min. transmission	0.8909 and 0.7447	
Refinement method	Full-matrix least-squares on F^2	
Data / restraints / parameters	8717 / 72 / 272	
Goodness-of-fit on F^2	1.028	
Final R indices [I>2sigma(I)]	R1 = 0.0409, wR2 = 0.1049	
R indices (all data)	R1 = 0.0551, wR2 = 0.1125	
Largest diff. peak and hole	0.695 and -0.652 $e.Å^{-3}$	

Table 2. Atomic coordinates (x 10^4) and equivalent isotropic displacement parameters ($Å^2$x 10^3)
for ab1509. U(eq) is defined as one third of the trace of the orthogonalized U^{ij} tensor.

	x	y	z	U(eq)
Zn(1)	0	0	0	11(1)
O(1)	-3280(2)	1514(1)	597(1)	14(1)
O(2)	2429(2)	94(1)	768(1)	14(1)
O(3)	-2513(2)	-7134(1)	1776(1)	23(1)
O(4)	3669(2)	-1156(1)	1722(1)	16(1)
O(5)	-124(2)	-6044(1)	2462(1)	22(1)
N(1)	-568(2)	-2119(1)	549(1)	11(1)
N(2)	4043(2)	-8589(1)	2580(1)	18(1)
C(1)	2440(2)	-1031(1)	1212(1)	12(1)
C(2)	794(2)	-2316(1)	1096(1)	11(1)
C(3)	676(2)	-3603(1)	1542(1)	12(1)
C(4)	-944(2)	-4715(1)	1427(1)	12(1)
C(5)	-2336(2)	-4515(1)	858(1)	13(1)
C(6)	-2089(2)	-3204(1)	430(1)	12(1)
C(7)	-1214(2)	-6073(1)	1929(1)	15(1)
C(8)	4311(2)	-9045(1)	3285(1)	16(1)
C(9)	2331(3)	-8355(2)	3776(1)	37(1)
C(10)	2593(3)	-8739(2)	4450(1)	35(1)
C(11)	4835(2)	-9801(1)	4640(1)	14(1)
C(12)	6750(3)	-10497(2)	4127(1)	28(1)
C(13)	6520(3)	-10146(2)	3447(1)	24(1)
C(14)	8329(9)	-11272(7)	2894(2)	34(1)
C(14')	8792(8)	-10660(5)	2914(2)	24(1)
O(1S)	-7941(8)	-5588(5)	6262(2)	63(1)
C(1S)	-5323(9)	-5176(9)	6194(3)	64(2)
C(2S)	-4106(8)	-5571(5)	5484(2)	43(1)
C(3S)	-5683(7)	-4708(4)	4943(2)	38(1)
C(4S)	-4287(8)	-5011(7)	4243(2)	54(1)

C(5S)	-5861(12)	-4206(10)	3688(3)	79(2)

Table 3. Anisotropic displacement parameters ($Å^2 x 10^3$) for ab1509. The anisotropic displacement factor exponent takes the form: $-2\pi^2[h^2 a^{*2} U^{11} + ... + 2 h k a^* b^* U^{12}]$

	U^{11}	U^{22}	U^{33}	U^{23}	U^{13}	U^{12}
Zn(1)	13(1)	12(1)	10(1)	3(1)	-3(1)	-6(1)
O(1)	14(1)	16(1)	13(1)	1(1)	-2(1)	-7(1)
O(2)	15(1)	16(1)	14(1)	4(1)	-4(1)	-8(1)
O(3)	41(1)	20(1)	14(1)	4(1)	-5(1)	-18(1)
O(4)	19(1)	20(1)	13(1)	1(1)	-6(1)	-7(1)
O(5)	32(1)	21(1)	15(1)	6(1)	-10(1)	-9(1)
N(1)	12(1)	12(1)	11(1)	2(1)	-2(1)	-5(1)
N(2)	27(1)	19(1)	10(1)	3(1)	-4(1)	-9(1)
C(1)	11(1)	14(1)	11(1)	0(1)	-2(1)	-4(1)
C(2)	11(1)	12(1)	10(1)	1(1)	-2(1)	-4(1)
C(3)	14(1)	13(1)	10(1)	2(1)	-2(1)	-4(1)
C(4)	14(1)	12(1)	10(1)	2(1)	-1(1)	-4(1)
C(5)	15(1)	13(1)	12(1)	2(1)	-2(1)	-6(1)
C(6)	14(1)	13(1)	12(1)	3(1)	-4(1)	-5(1)
C(7)	20(1)	13(1)	11(1)	2(1)	-1(1)	-5(1)
C(8)	22(1)	17(1)	9(1)	2(1)	-3(1)	-7(1)
C(9)	38(1)	48(1)	13(1)	5(1)	-2(1)	22(1)
C(10)	34(1)	47(1)	11(1)	3(1)	1(1)	20(1)
C(11)	18(1)	15(1)	9(1)	1(1)	-2(1)	-3(1)
C(12)	22(1)	44(1)	11(1)	4(1)	0(1)	11(1)
C(13)	20(1)	39(1)	10(1)	2(1)	1(1)	4(1)
C(14)	29(2)	51(2)	12(1)	-4(2)	1(1)	14(2)
C(14')		24(1)	31(2)	13(1)	-1(1)	4(1) 0(1)
O(1S)		73(2)	60(2)	50(2)	-9(2)	7(2) -6(2)
C(1S)	38(2)	88(4)	63(3)	-28(3)	-6(2)	-5(3)
C(2S)	36(2)	39(2)	52(2)	-11(2)	2(2)	-8(2)
C(3S)	26(1)	26(2)	62(2)	-4(2)	3(2)	-6(1)
C(4S)	28(2)	67(3)	61(3)	8(2)	3(2)	-3(2)

C(5S)41(3)	105(6)	86(5)	40(4)	-10(3)	-4(3)

A.7 Crystal Structure Information for Zn(o-tolidinium)$(H_2O)_2$ · 1, 4-difluorobenzene

Table 1. Crystal data and structure refinement for ab909.

Identification code	b909/lt/GAH020	
Empirical formula	$C_{34}\ H_{32}\ F_2\ N_4\ O_{10}\ Zn$	
Formula weight	760.01	
Temperature	100(2) K	
Wavelength	0.71073 Å	
Crystal system	Triclinic	
Space group	P-1	
Unit cell dimensions	a = 5.1635(5) Å	α= 87.930(3)°.
	b = 8.3872(8) Å	β= 83.655(3)°.
	c = 19.771(2) Å	γ = 79.924(3)°.
Volume	837.73(14) $Å^3$	
Z	1	
Density (calculated)	1.506 Mg/m^3	
Absorption coefficient	0.809 mm^{-1}	
F(000)	392	
Crystal size	0.57 x 0.25 x 0.05 mm^3	
Theta range for data collection	2.07 to 25.44°.	
Index ranges	$-6 \leq h \leq 3$, $-10 \leq k \leq 10$, $-23 \leq l \leq 23$	
Reflections collected	5468	
Independent reflections	3046 [R(int) = 0.020]	
Completeness to theta = 25.00°	99.2 %	
Absorption correction	Semi-empirical from equivalents	
Max. and min. transmission	0.9576 and 0.6538	
Refinement method	Full-matrix least-squares on F^2	
Data / restraints / parameters	3046 / 302 / 342	
Goodness-of-fit on F^2	1.076	
Final R indices [I>2sigma(I)]	R1 = 0.0421, wR2 = 0.1151	
R indices (all data)	R1 = 0.0450, wR2 = 0.1175	
Largest diff. peak and hole	0.748 and -0.485 $e.Å^{-3}$	

Table 2. Atomic coordinates (x 10^4) and equivalent isotropic displacement parameters ($Å^2$x 10^3)
for ab909. U(eq) is defined as one third of the trace of the orthogonalized U^{ij} tensor.

	x	y	z	U(eq)
Zn(1)	0	0	0	16(1)
O(1)	2385(7)	64(4)	773(2)	17(1)
O(2)	3583(8)	-1224(5)	1727(2)	21(1)
O(3)	-3244(8)	1460(5)	579(2)	17(1)
O(4)	-2370(10)	-7264(5)	1741(2)	31(1)
O(5)	44(10)	-6270(5)	2422(2)	35(1)
N(1)	-651(8)	-2111(5)	559(2)	15(1)
C(1)	2379(10)	-1074(6)	1217(3)	16(1)
C(2)	721(10)	-2350(6)	1102(3)	15(1)
C(3)	645(10)	-3663(6)	1540(3)	16(1)
C(4)	-926(10)	-4786(6)	1418(3)	17(1)
C(5)	-2343(10)	-4544(6)	855(3)	17(1)
C(6)	-2151(10)	-3199(6)	440(3)	16(1)
C(7)	-1086(11)	-6223(7)	1901(3)	21(1)
C(8)	4411(13)	-9155(7)	3266(3)	26(1)
C(11)	4875(13)	-9829(8)	4633(3)	28(1)
N(2)	4000(40)	-8680(30)	2564(14)	26(1)
C(9)	6470(70)	-10040(30)	3461(17)	16(4)
C(10)	6730(70)	-10360(30)	4140(20)	20(5)
C(12)	3540(40)	-8412(18)	4413(7)	37(3)
C(13)	3340(40)	-8074(18)	3724(7)	39(4)
C(14)	8730(30)	-10640(20)	2926(8)	37(3)
N(2')	4310(50)	-8810(30)	2536(14)	28(1)
C(9')	6300(80)	-10570(30)	3439(19)	34(7)
C(10')	6420(70)	-10840(40)	4136(19)	31(6)
C(12')	2270(30)	-9020(20)	4430(7)	34(3)
C(13')	2060(30)	-8660(20)	3753(7)	32(3)
C(14')	7830(50)	-11670(30)	2901(9)	74(8)

F(1)	3620(70)	-4530(50)	3202(15)	307(17)
C(1S)	3410(60)	-3430(30)	3794(17)	96(15)
C(2S)	2120(50)	-4010(40)	4380(17)	100(15)
C(3S)	3290(70)	-3660(50)	5065(17)	109(15)
C(4S)	4930(80)	-5180(40)	4990(16)	143(16)
C(5S)	6320(50)	-4750(40)	4392(18)	88(12)
C(6S)	4240(50)	-4630(30)	3939(15)	121(14)
F(1')	2460(50)	-4430(30)	5117(11)	252(17)
C(7S)	4740(60)	-3730(30)	3265(11)	137(17)
C(8S)	7210(40)	-4240(30)	3541(13)	61(10)
C(9S)	6610(50)	-5740(30)	3995(13)	106(15)
C(10S)	5790(40)	-5690(20)	4407(13)	106(14)
C(11S)	3620(30)	-4281(17)	4403(11)	50(8)
C(12S)	2580(40)	-3540(30)	4001(13)	38(8)

Table 3. Anisotropic displacement parameters ($Å^2 x 10^3$) for ab909. The anisotropic displacement factor exponent takes the form: $-2\pi^2[h^2 a^{*2} U^{11} + ... + 2 h k a^* b^* U^{12}]$

U^{11}	U^{22}	U^{33}	U^{23}	U^{13}	U^{12}	
Zn(1)16(1)	17(1)	16(1)	5(1)	-5(1)	-9(1)	
O(1)18(2)	18(2)	20(2)	5(2)	-6(2)	-10(2)	
O(2)25(2)	21(2)	19(2)	2(2)	-9(2)	-9(2)	
O(3)17(2)	19(2)	18(2)	1(2)	-5(2)	-9(2)	
O(4)56(3)	24(2)	22(2)	6(2)	-13(2)	-25(2)	
O(5)57(3)	29(2)	26(2)	12(2)	-22(2)	-22(2)	
N(1)14(2)	16(2)	15(2)	1(2)	-2(2)	-5(2)	
C(1)14(2)	17(3)	16(3)	-1(2)	-2(2)	-4(2)	
C(2)13(2)	17(3)	16(3)	0(2)	-1(2)	-3(2)	
C(3)16(2)	17(3)	15(3)	0(2)	-3(2)	-3(2)	
C(4)16(2)	16(3)	17(3)	0(2)	-1(2)	-4(2)	
C(5)17(2)	17(3)	19(3)	-1(2)	-3(2)	-7(2)	
C(6)15(2)	18(3)	16(3)	0(2)	-4(2)	-6(2)	
C(7)28(3)	18(3)	17(3)	0(2)	-3(2)	-7(2)	
C(8)47(4)	21(3)	15(3)	3(2)	-10(2)	-15(3)	
C(11)42(3)	26(3)	16(3)	2(2)	-7(2)	-1(2)	
N(2)47(4)	21(3)	15(3)	3(2)	-10(2)	-15(3)	
C(9)21(7)	16(12)	14(7)	-4(9)	0(5)	-9(10)	
C(10)19(8)	16(12)	27(9)	3(9)	-4(6)	-9(8)	
C(12)65(11)	25(7)	18(7)	-5(5)	-8(7)	7(7)	
C(13)73(12)	21(7)	22(7)	7(5)	-16(7)	3(8)	
C(14)34(8)	44(9)	28(7)	-1(7)	3(6)	-1(7)	
N(2')42(3)	26(3)	16(3)	2(2)	-7(2)	-1(2)	
C(9')36(13)	35(18)	25(9)	-1(13)	-5(8)	6(13)	
C(10')	33(14)	38(18)	20(9)	4(13)	-8(8)	4(12)
C(12')	25(7)	51(10)	21(7)	-3(6)	-1(5)	4(7)
C(13')	29(7)	36(8)	27(7)	1(6)	-9(6)	4(6)
C(14')	74(14)	93(17)	32(9)	-12(10)	-13(9)	57(13)
F(1)240(30)	320(40)	360(40)	40(30)	-30(30)	-50(30)	

C(1S)120(30)	50(20)	130(30)	-20(20)	-50(30)	-40(20)	
C(2S)90(30)	50(20)	160(30)	-30(30)	-30(30)	-10(20)	
C(3S)70(30)	70(30)	210(40)	0(30)	-70(30)	-20(20)	
C(4S)140(30)	90(30)	220(40)	-50(30)	70(30)	-90(30)	
C(5S)110(30)	33(18)	130(30)	-41(19)	30(20)	-43(19)	
C(6S)120(30)	110(30)	150(30)	-20(30)	-30(30)	-30(20)	
F(1')180(30)	97(18)	500(50)	-90(30)	-140(30)	18(17)	
C(7S)150(30)	80(30)	210(40)	-40(30)	-40(30)	-80(20)	
C(8S)60(20)	46(18)	70(20)	-29(17)	-28(18)	3(16)	
C(9S)90(30)	110(30)	120(30)	-40(30)	-10(30)	0(30)	
C(10S)	100(30)	100(30)	120(30)	-70(30)	10(30)	-40(20)
C(11S)	58(18)	16(13)	80(20)	-13(14)	13(18)	-17(14)
C(12S)	38(15)	8(12)	70(20)	13(13)	-21(15)	-3(11)

Appendix B

Thermal Analysis Data for Chapter 3

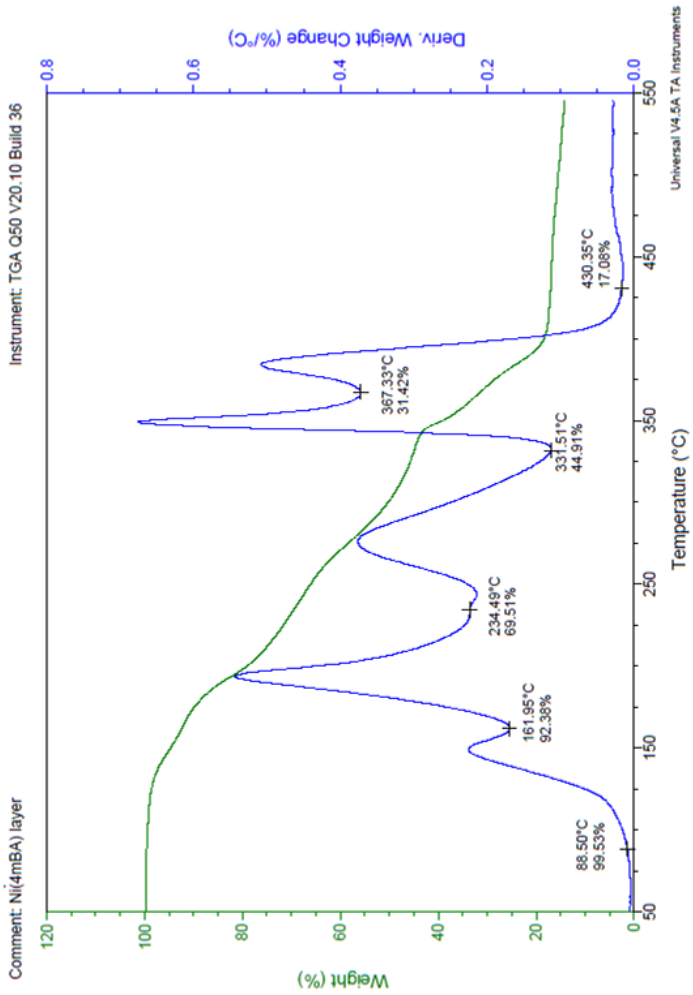

Figure B.1 TGA of the Ni(4m-BA) layered material

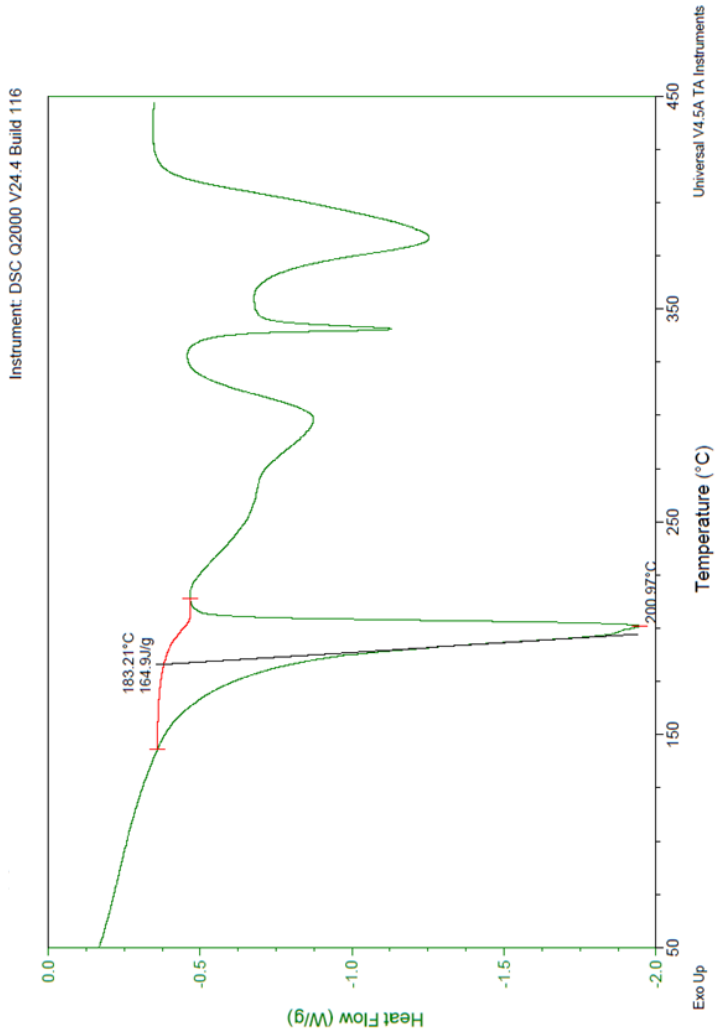

Figure B.2 DSC of the Ni(4m-BA) layered material

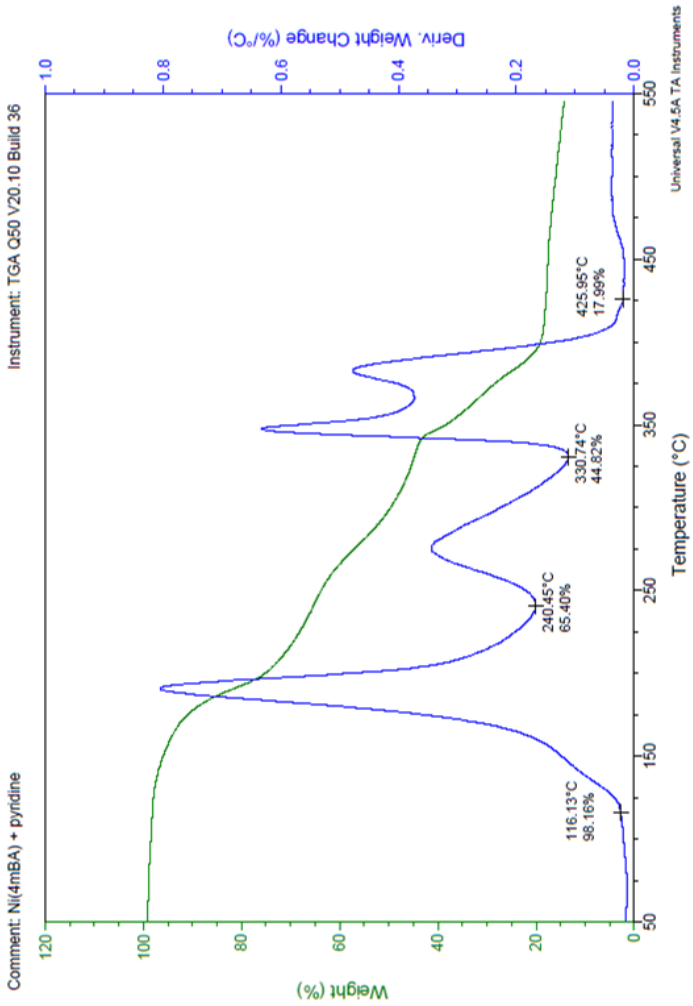

Figure B.3 TGA of the Ni(4m-BA) sonicated with pyridine

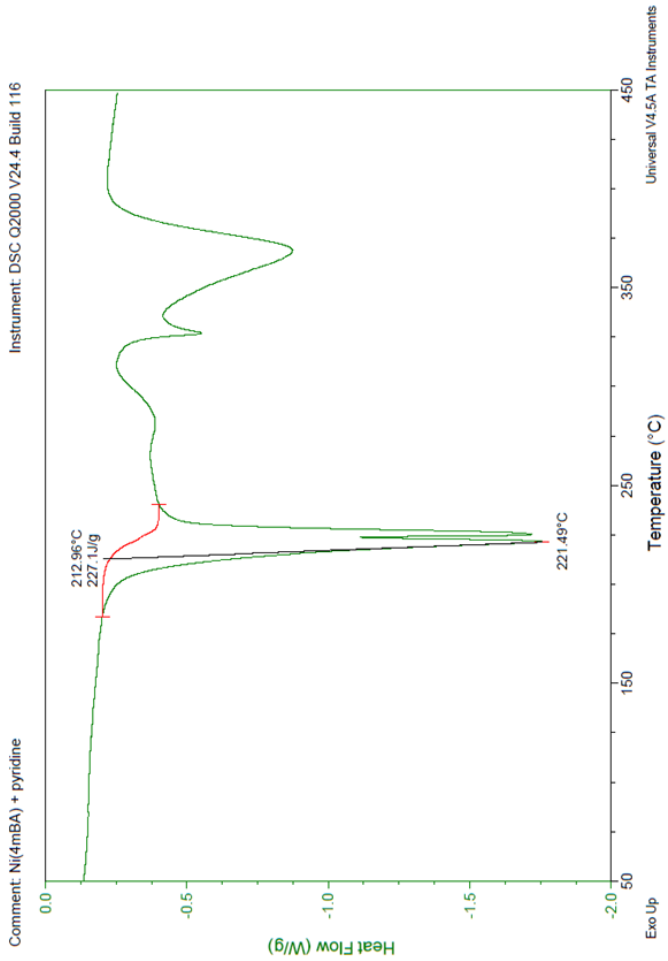

Figure B.4 DSC of the Ni(4m-BA) sonicated with pyridine

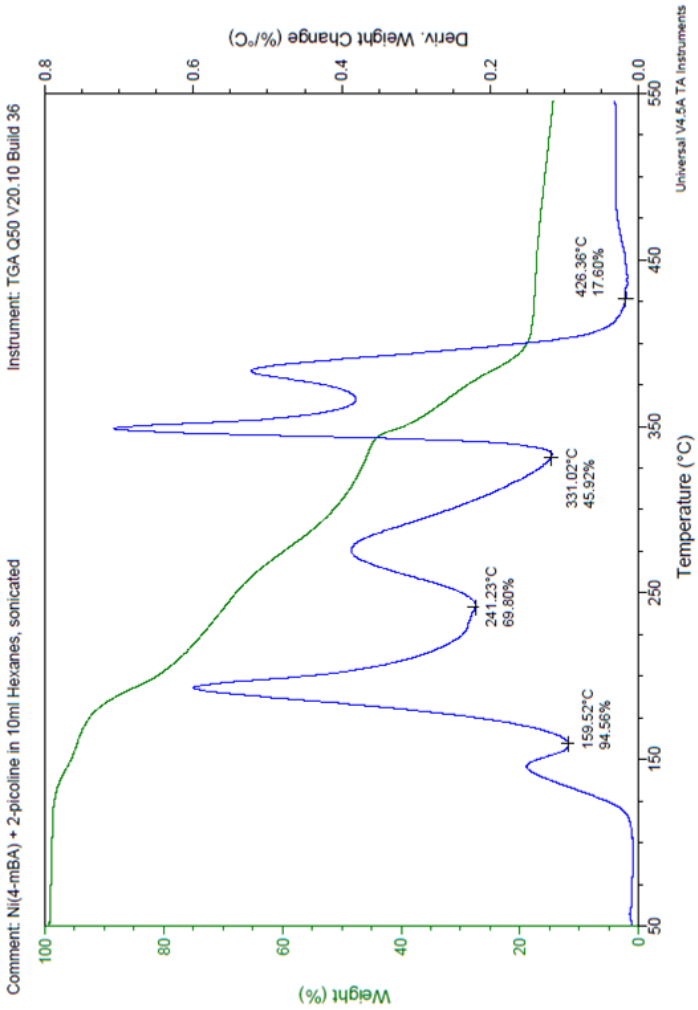

Figure B.5 TGA of the Ni(4m-BA) sonicated with 2-picoline

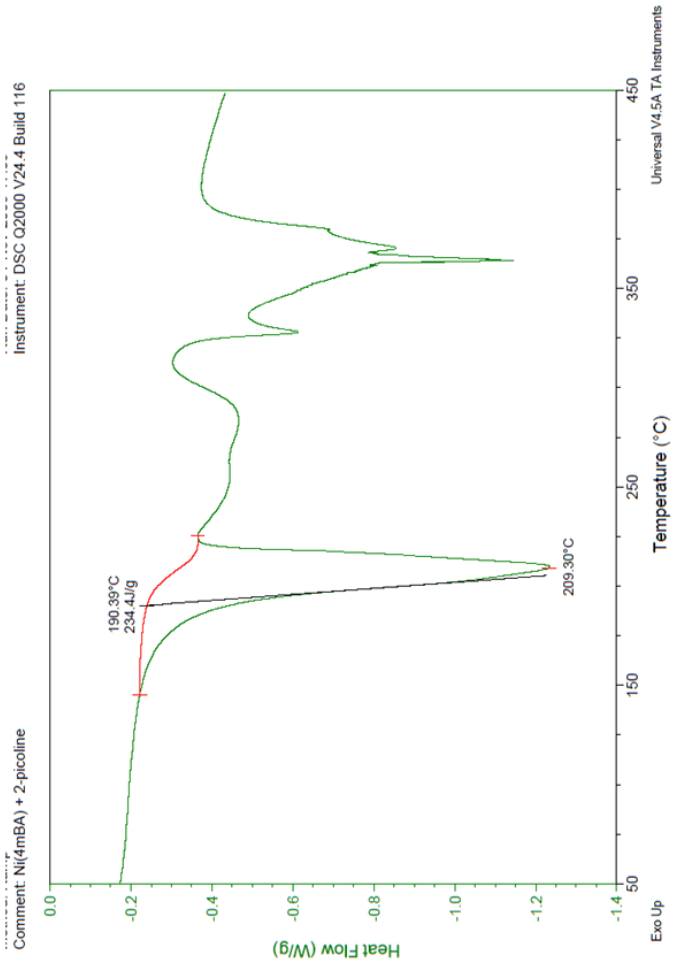

Figure B.6 DSC of the Ni(4m-BA) sonicated with 2-picoline

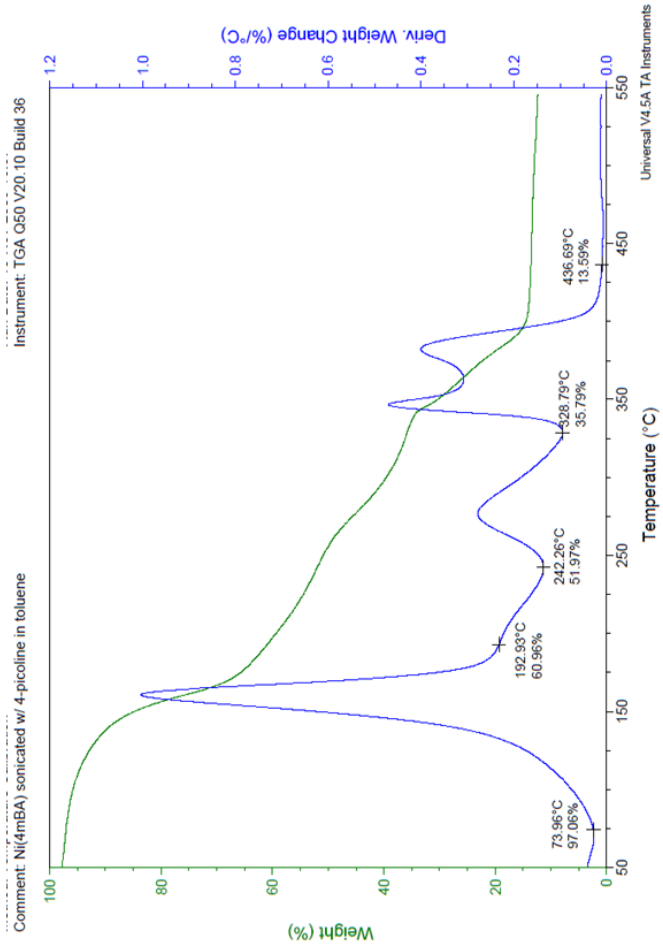

Figure B.7 TGA of the Ni(4m-BA) sonicated with 4- picoline

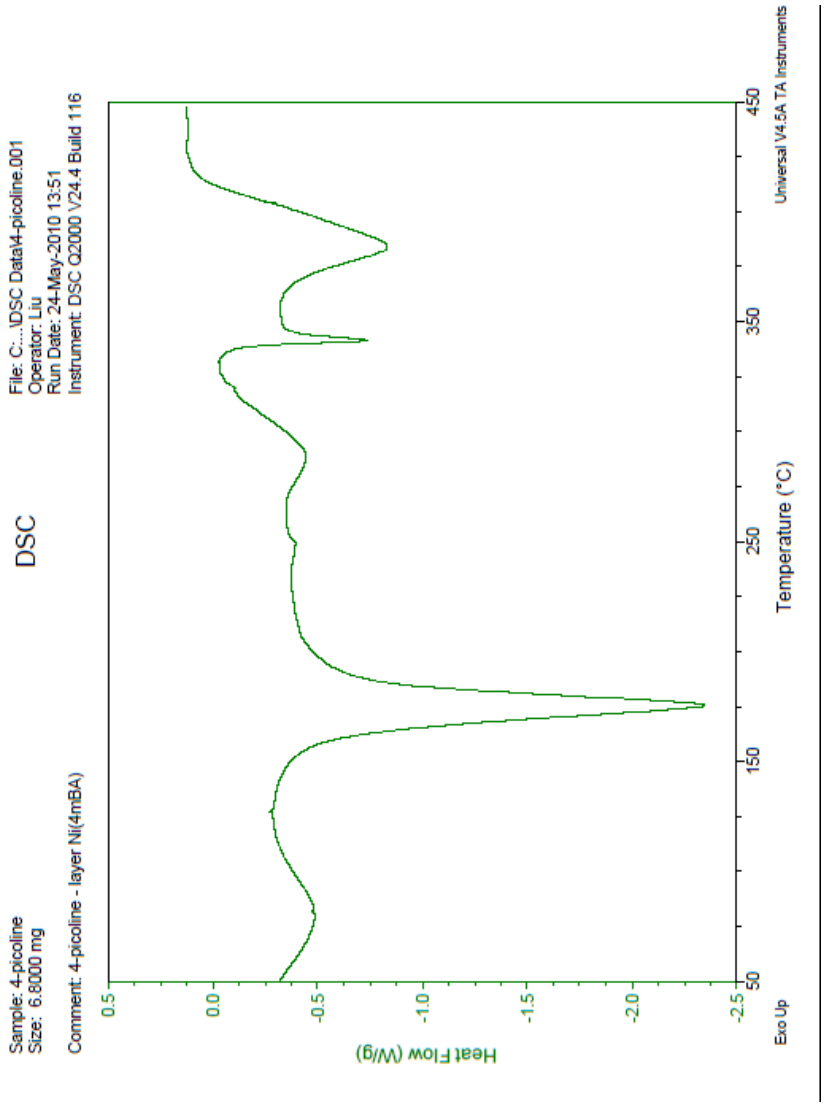

Figure B.8 DSC of the Ni(4m-BA) sonicated with 4- picoline

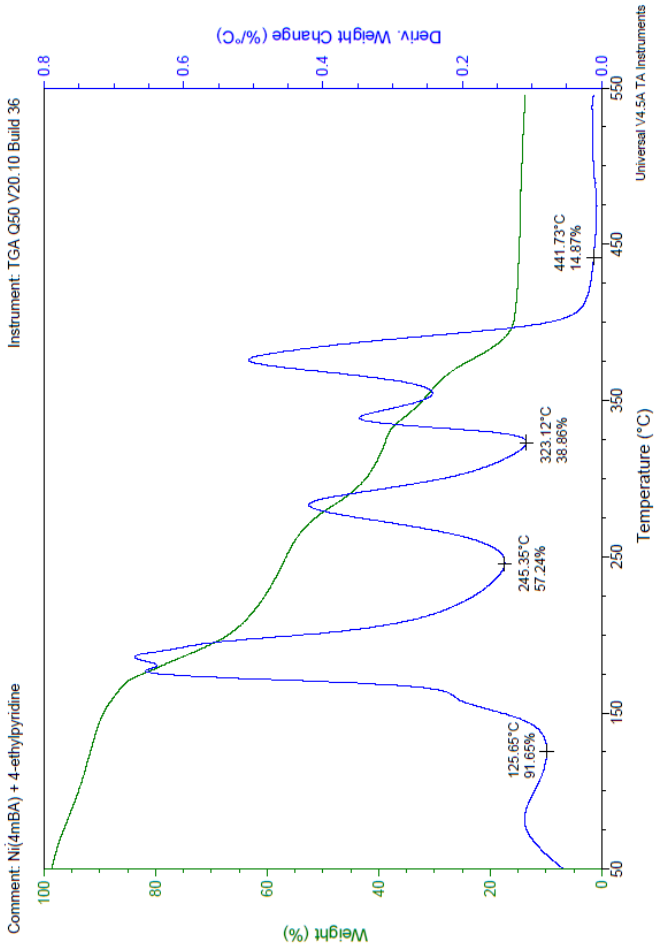

Figure B.9 TGA of the Ni(4m-BA) sonicated with 4-ethylpyridine

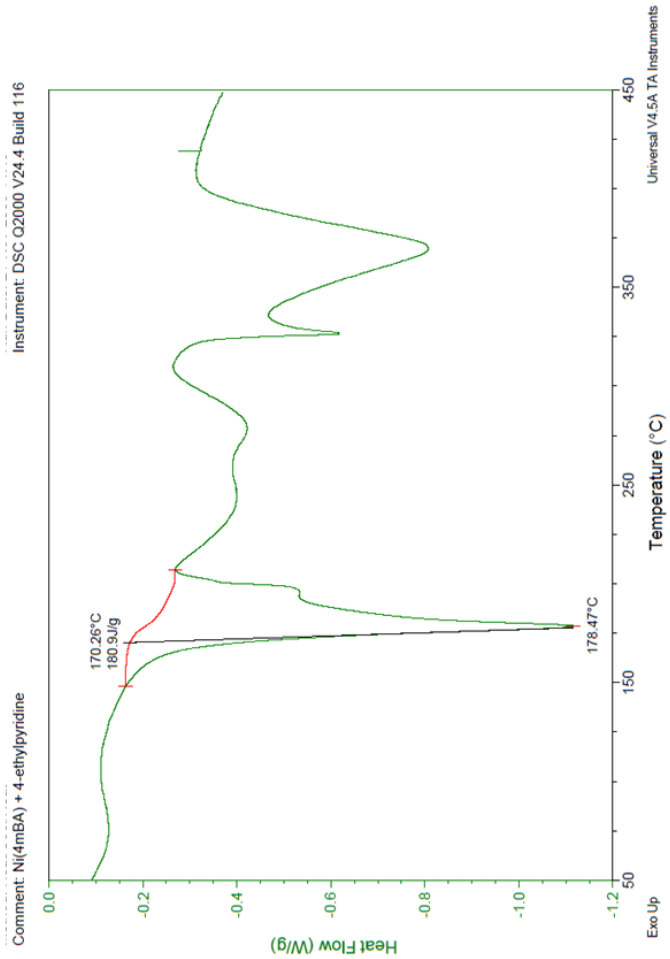

Figure B.10 DSC of the Ni(4m-BA) sonicated with 4-ethylpyridine

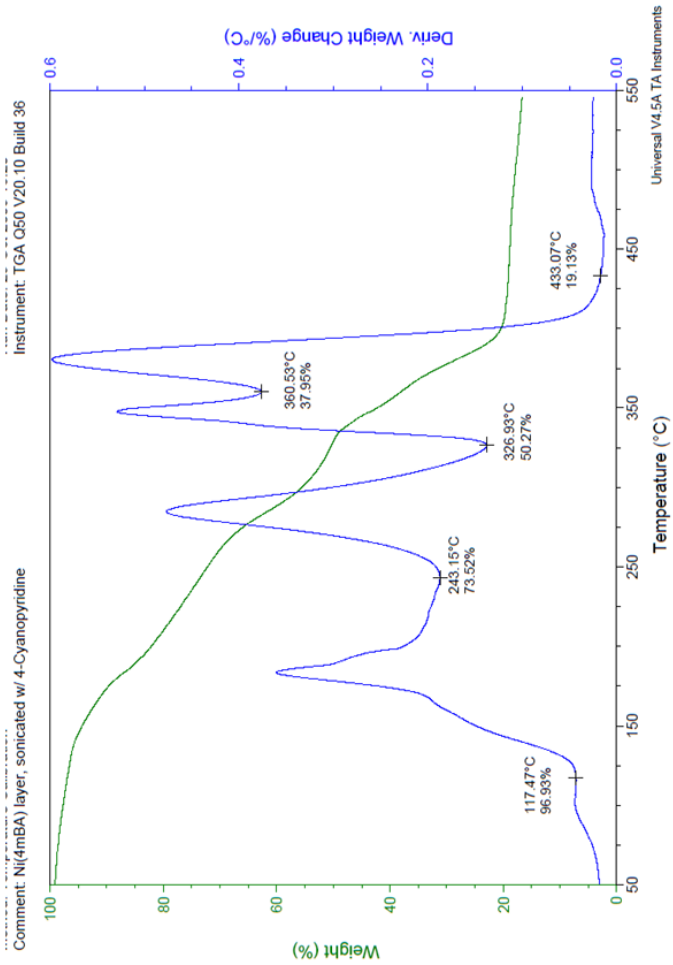

Figure B.11 TGA of the Ni(4m-BA) sonicated with 4-cyanopyridine

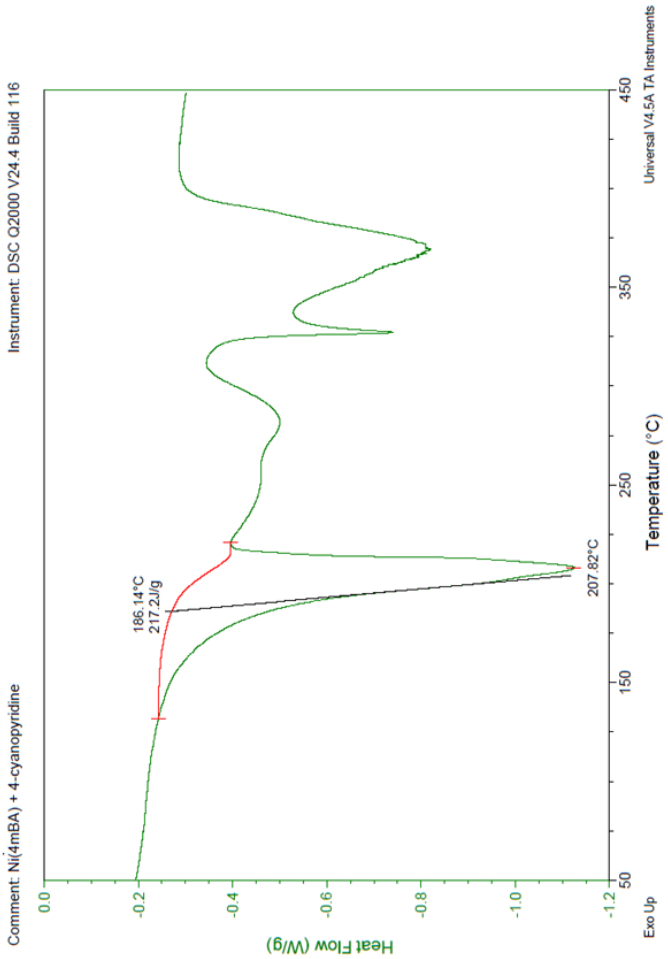

Figure B.12 DSC of the Ni(4m-BA) sonicated with 4-cyanopyridine

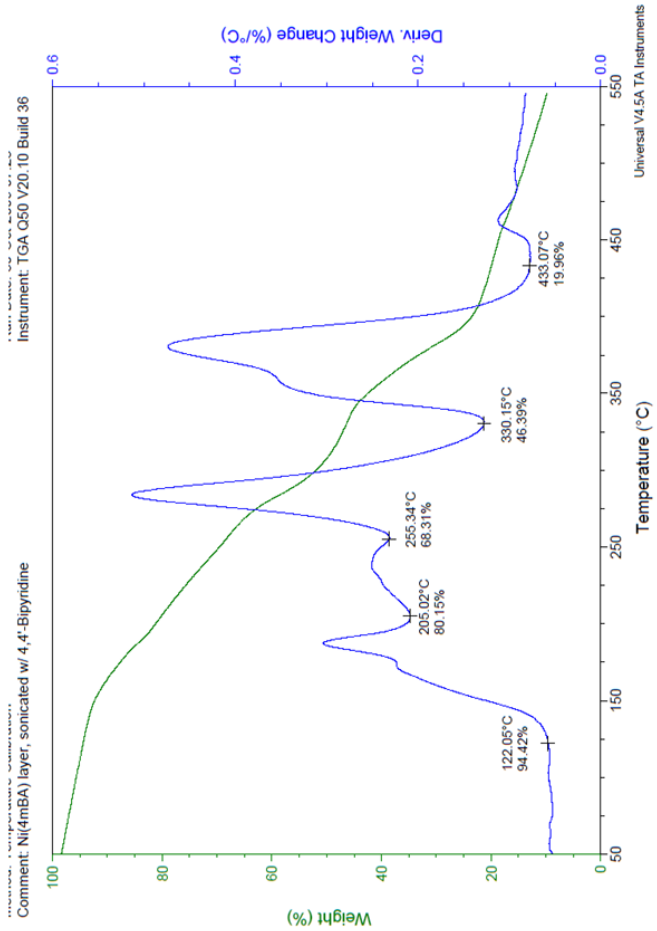

Figure B.13 TGA of the Ni(4m-BA) sonicated with 4,4'-bipyridine

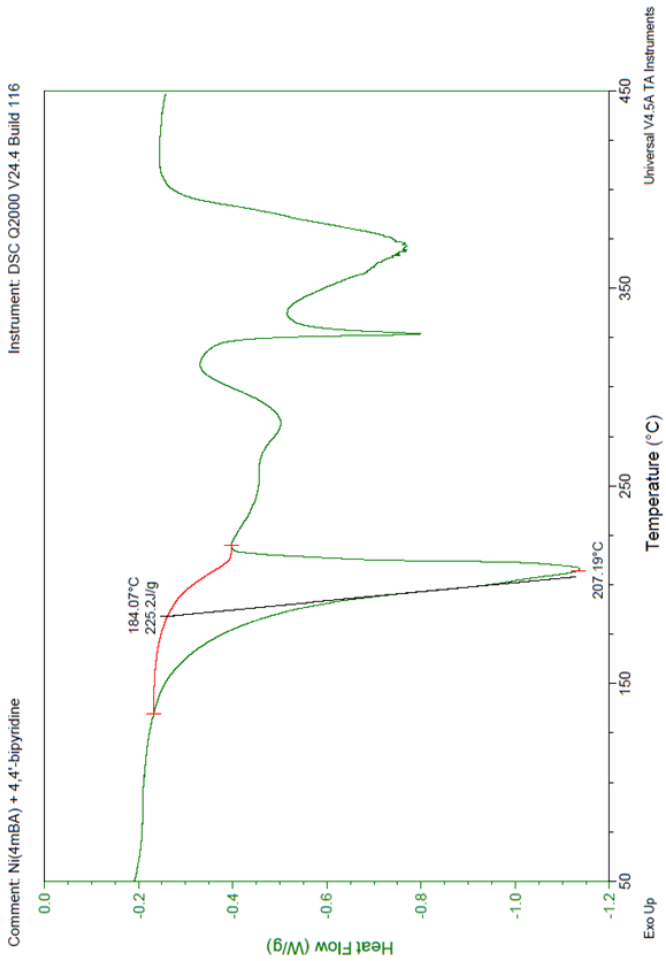

Figure B.14 DSC of the Ni(4m-BA) sonicated with 4,4'-bipyridine

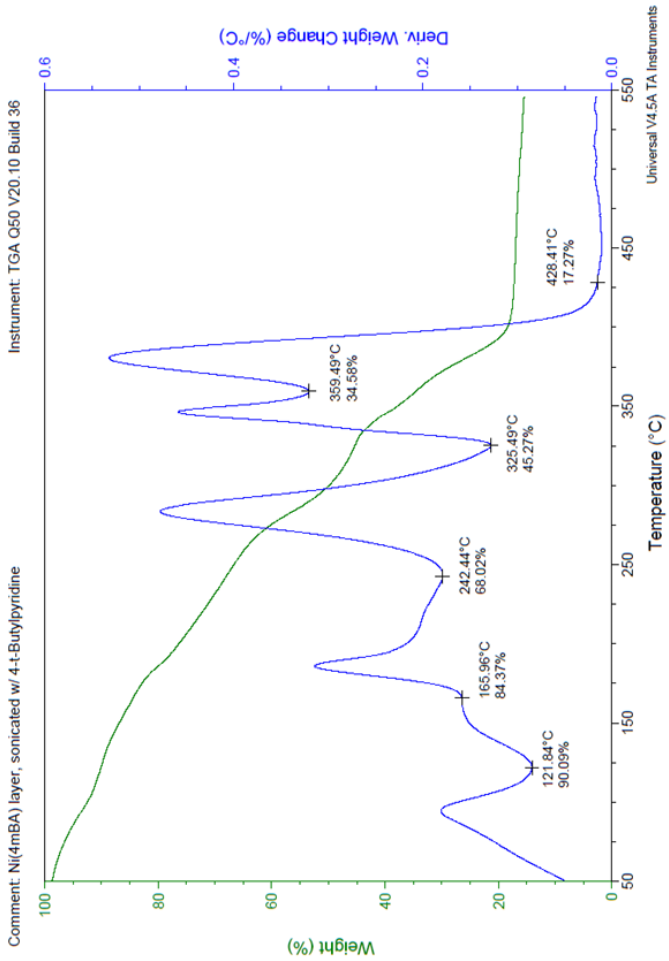

Figure B.15 TGA of the Ni(4m-BA) sonicated with 4-t-butylpyridine

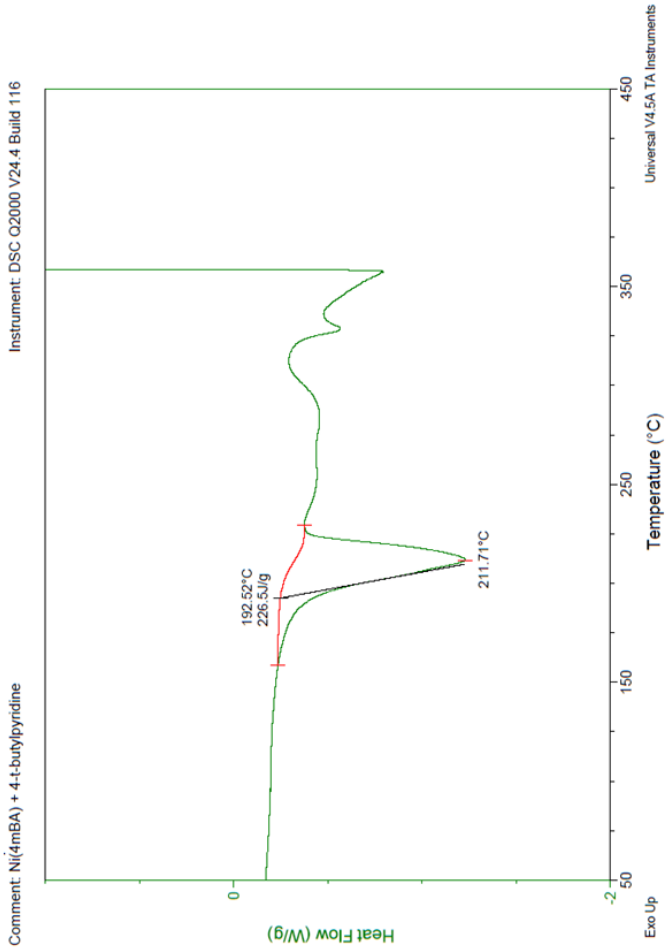

Figure B.16 DSC of the Ni(4m-BA) sonicated with 4-t-butylpyridine

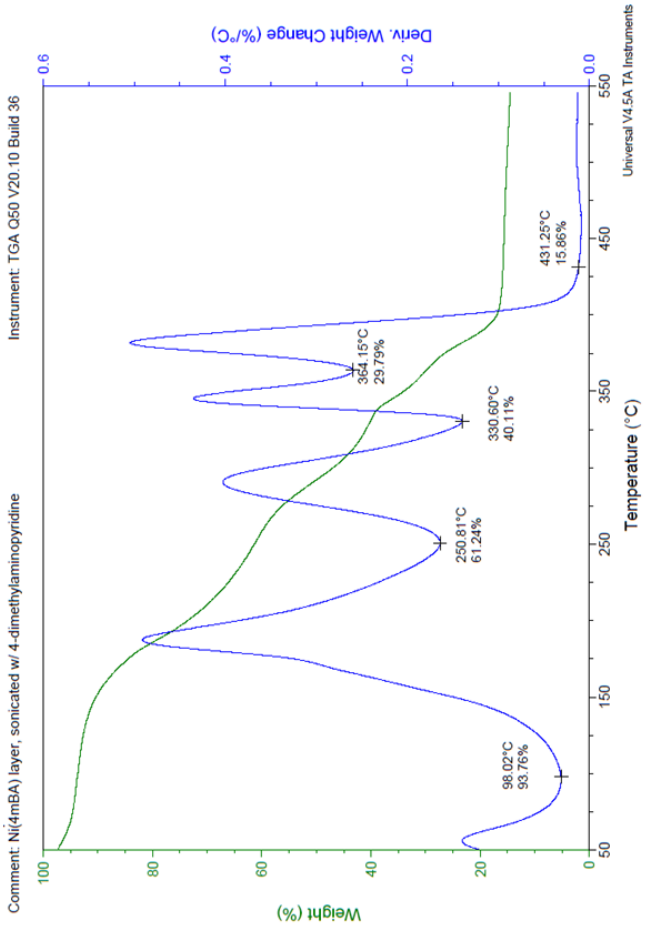

Figure B 17 TGA of the Ni(4m-BA) sonicated with 4-dimethylaminopyridine

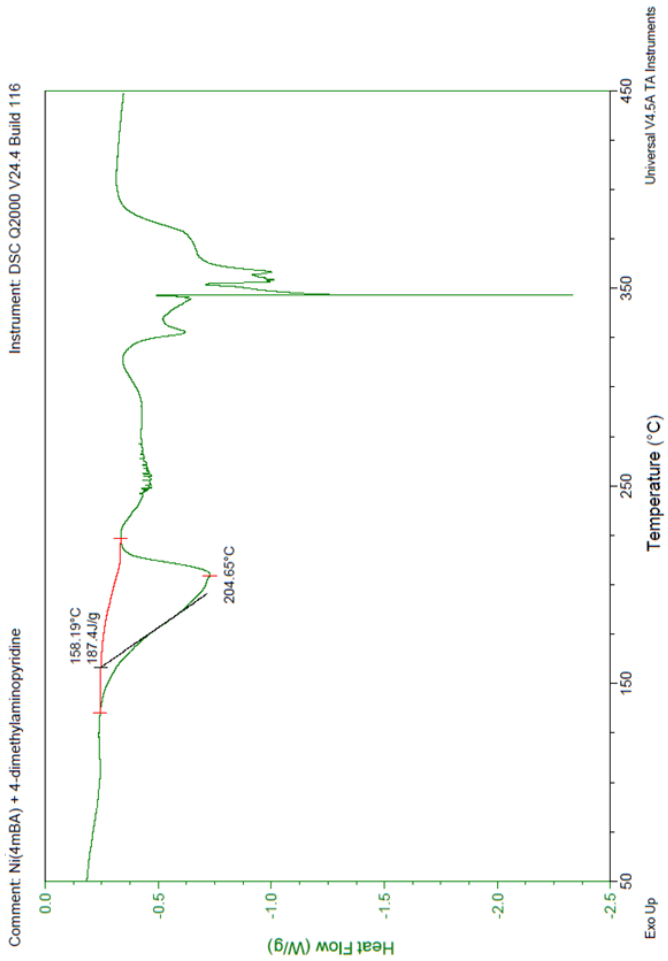

Figure B 18 DSCA of the Ni(4m-BA) sonicated with 4-dimethylaminopyridine

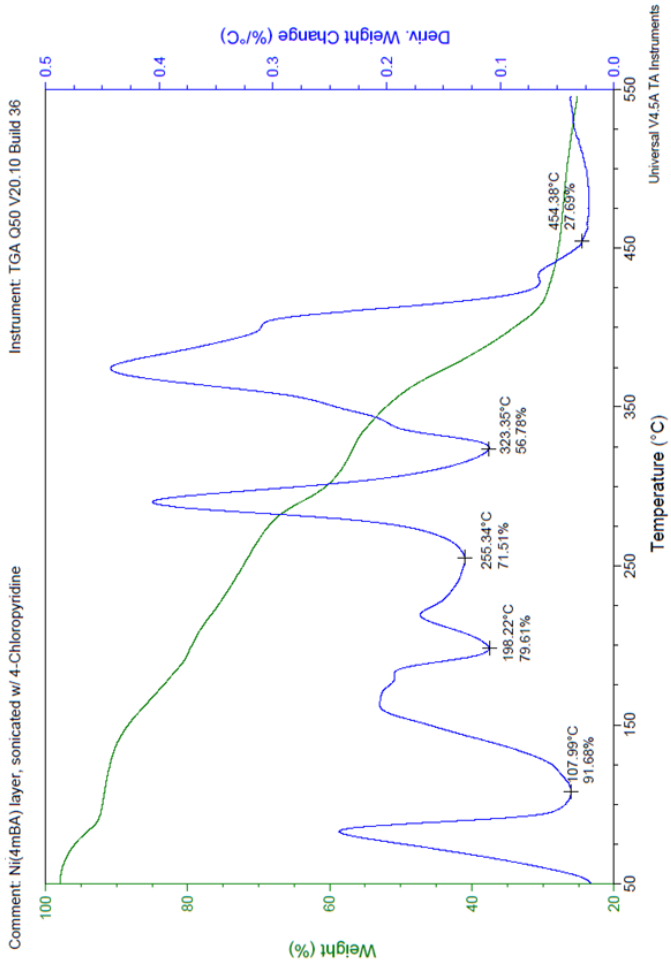

Figure B.19 TGA of the Ni(4m-BA) sonicated with 4-chloropyridine

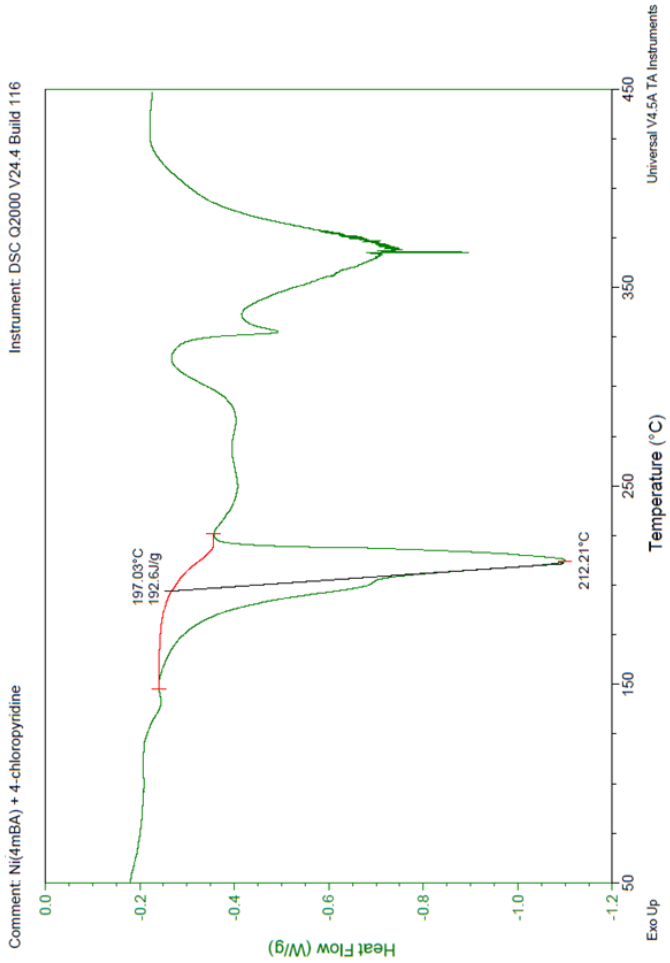

Figure B.20 DSC of the Ni(4m-BA) sonicated with 4-chloropyridine

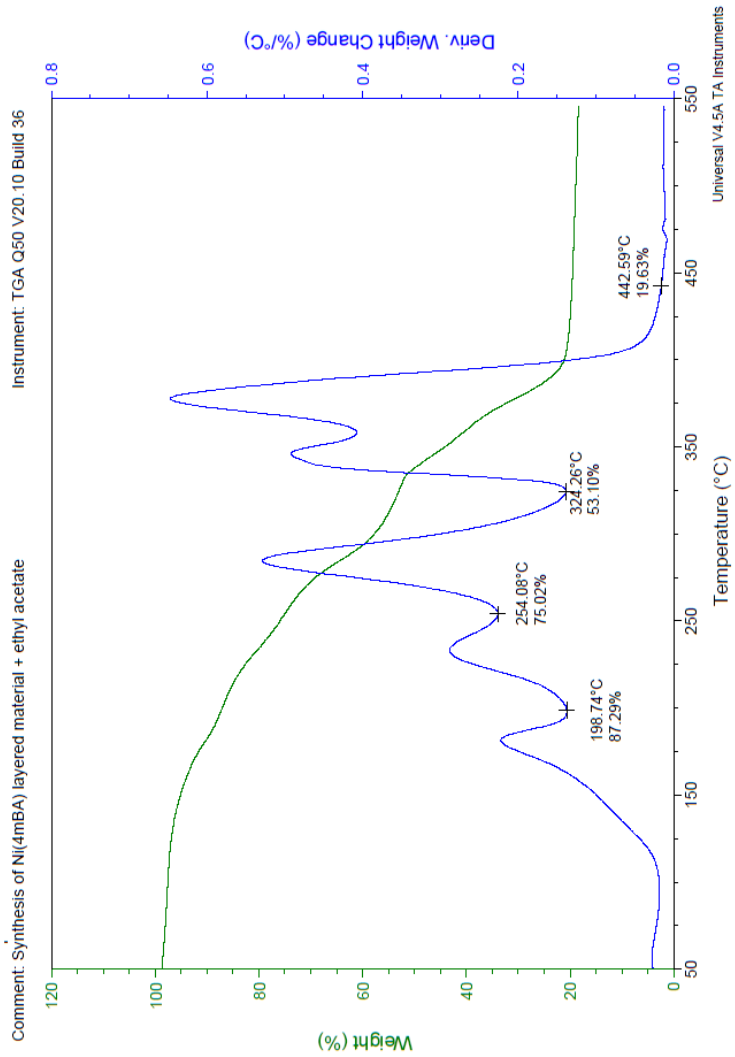

Figure B.21 TGA of the Ni(4m-BA) sonicated with ethyl acetate

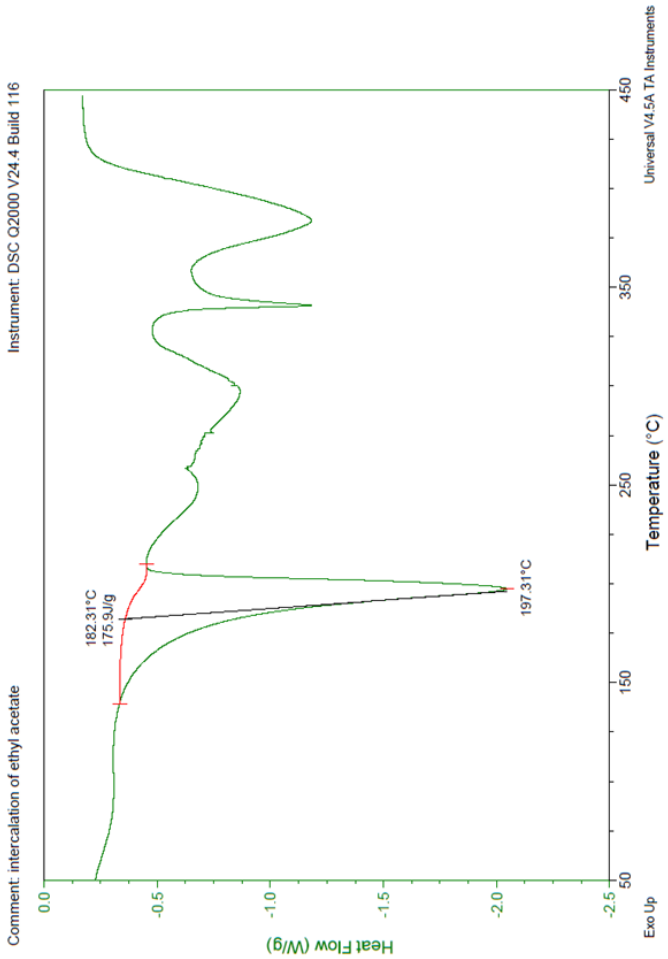

Figure B.22 DSC of the Ni(4m-BA) sonicated with ethyl acetate

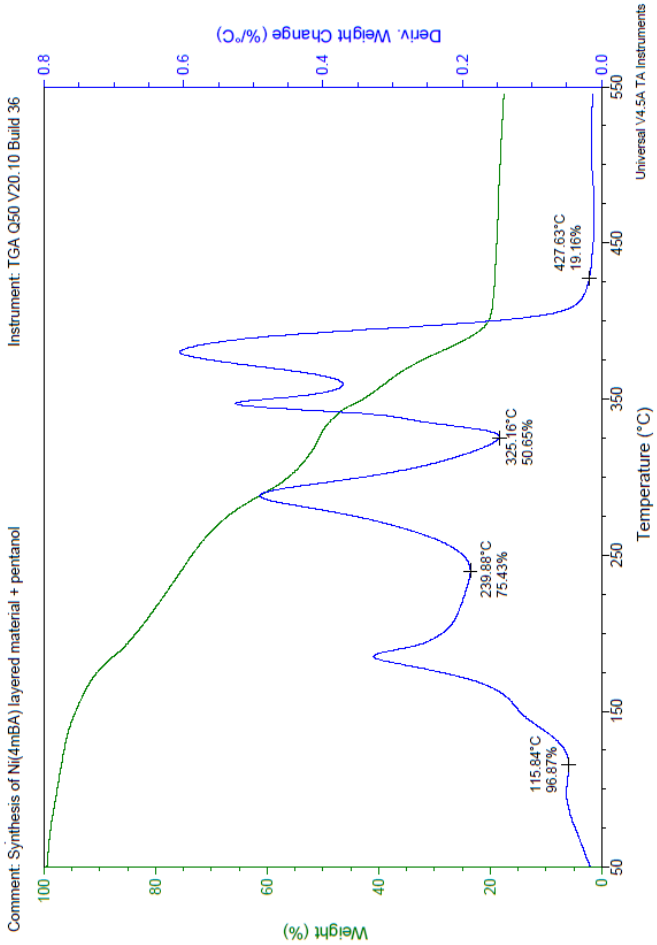

Figure B.23 TGA of the Ni(4m-BA) sonicated with pentanol

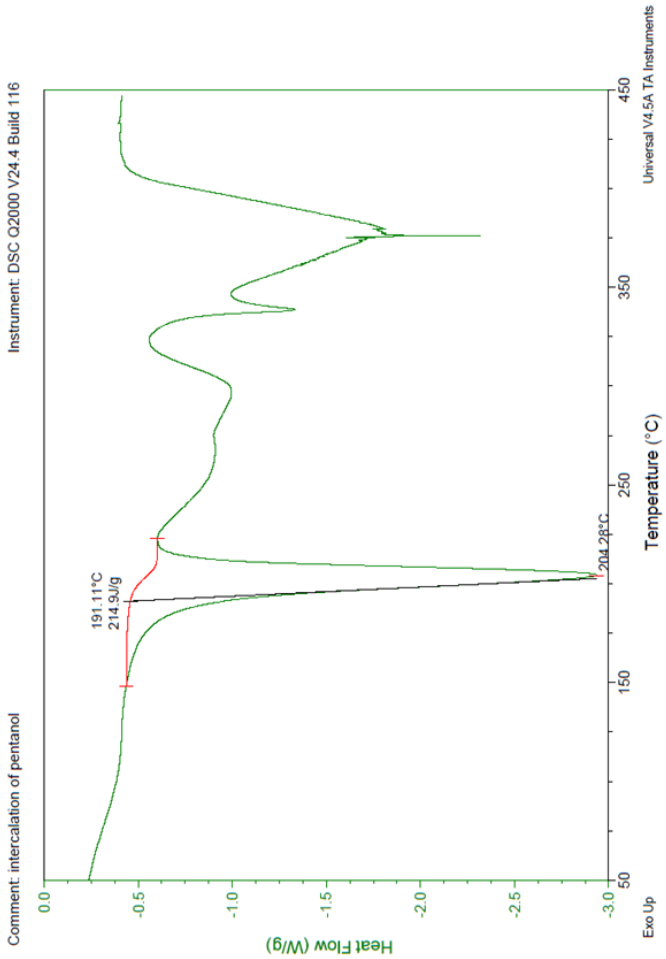

Figure B.24 DSC of the Ni(4m-BA) sonicated with pentanol

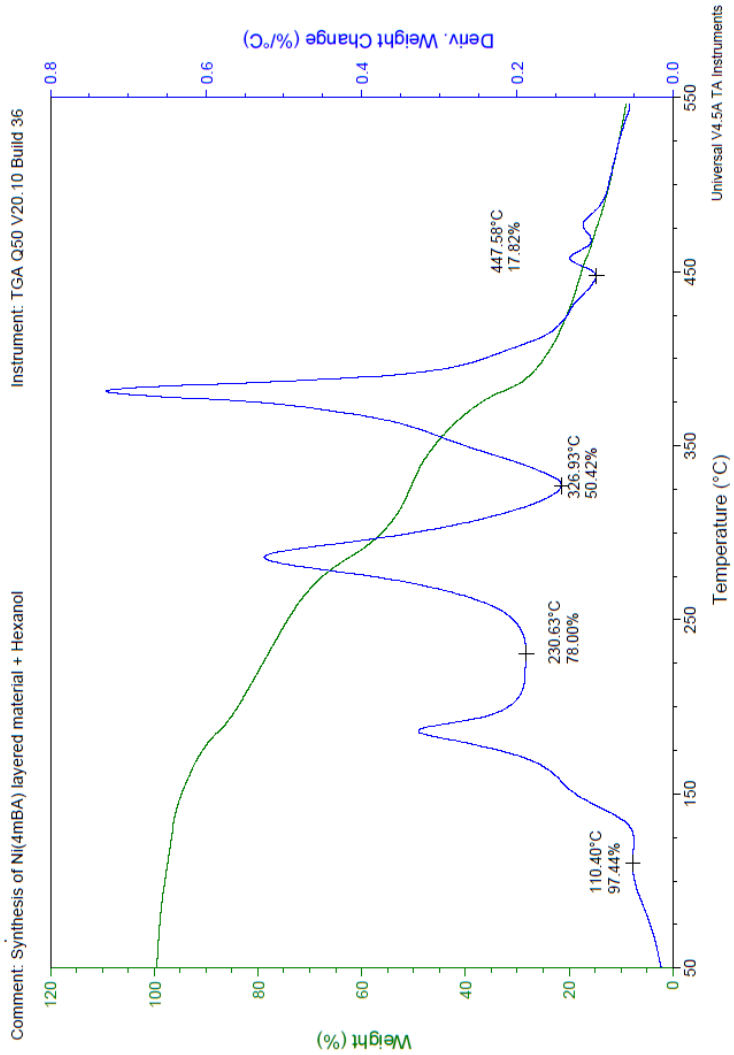

Figure B.25 TGA of the Ni(4m-BA) sonicated with hexanol

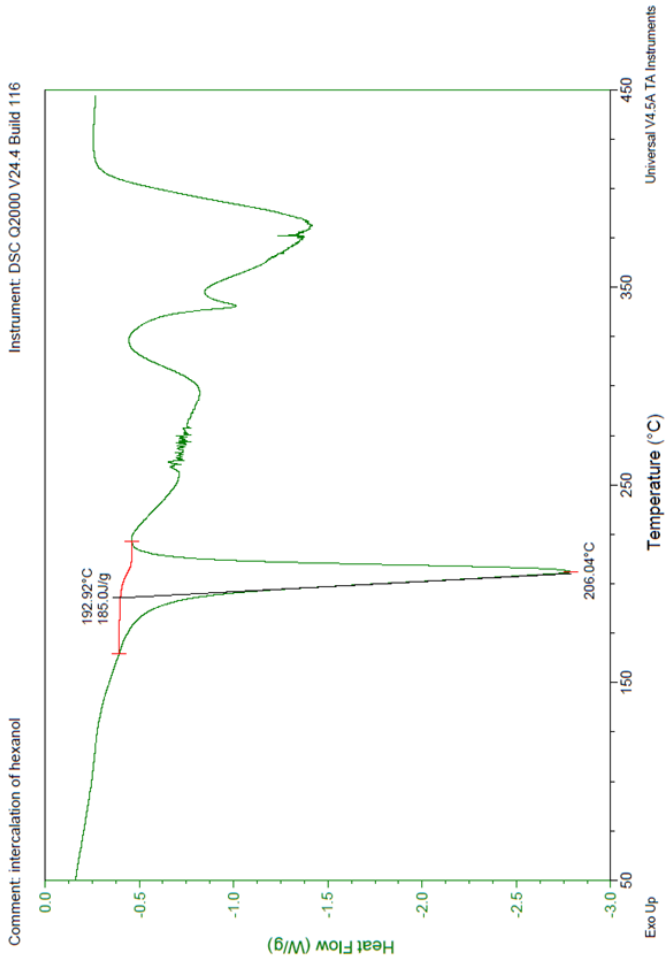

Figure B.26 DSC of the Ni(4m-BA) sonicated with hexanol

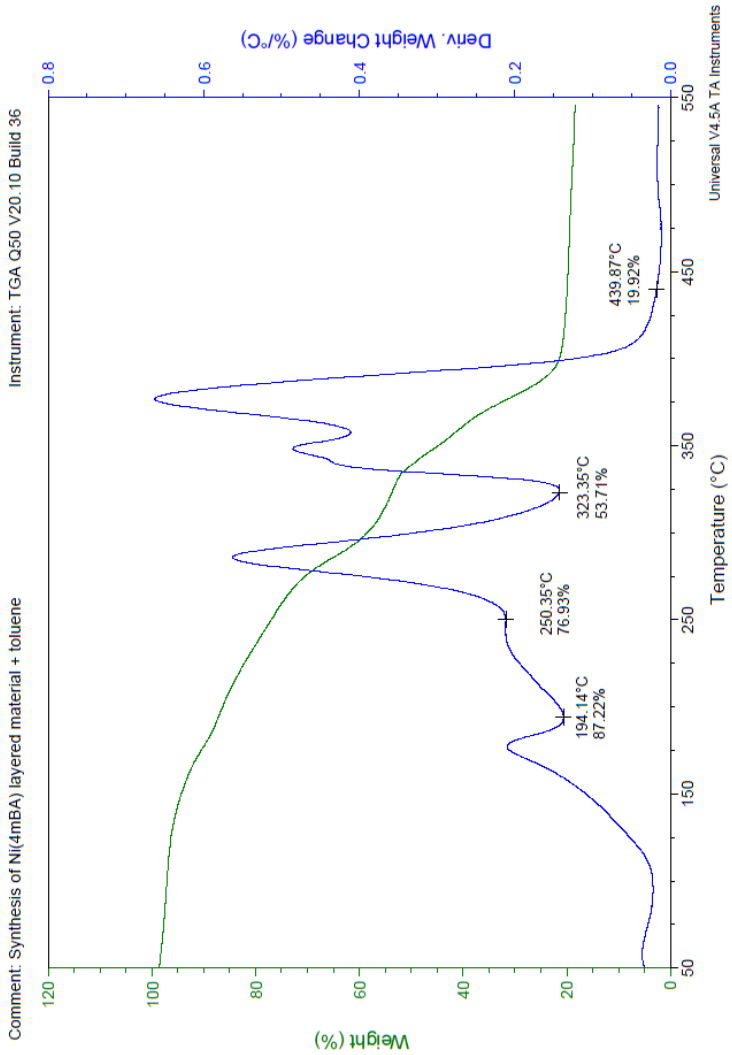

Figure B.27 TGA of the Ni(4m-BA) sonicated with toluene

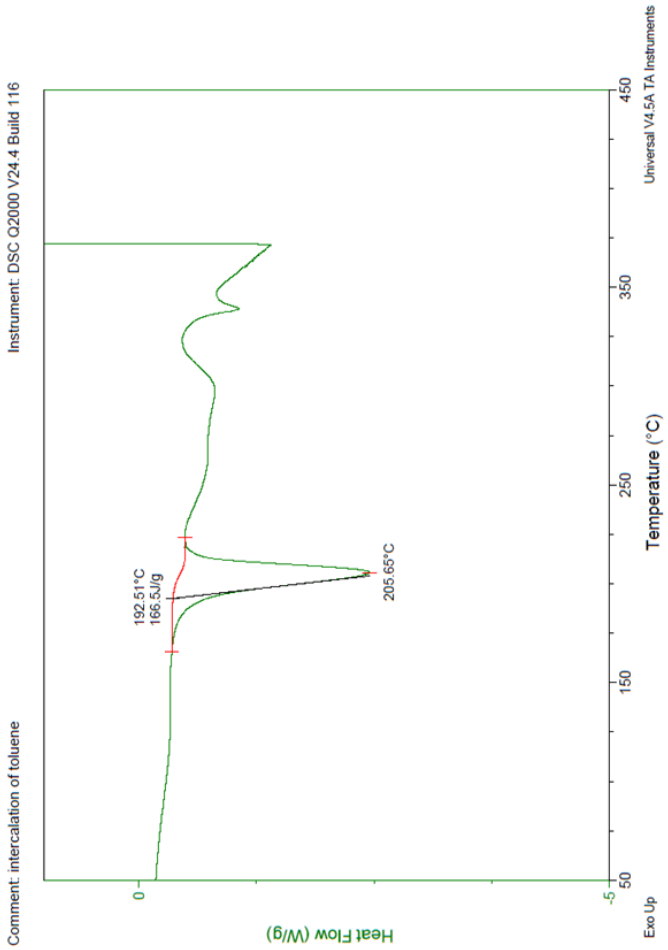

Figure B.28 DSC of the Ni(4m-BA) sonicated with toluene

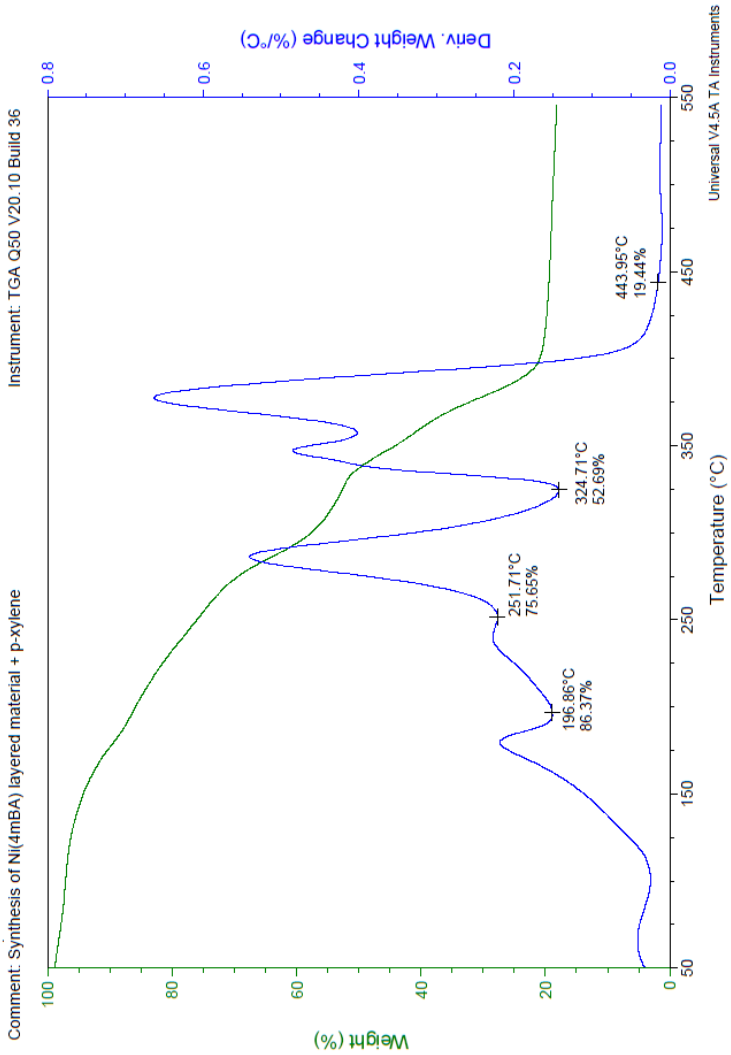

Figure B.29 TGA of the Ni(4m-BA) sonicated with p-xylene

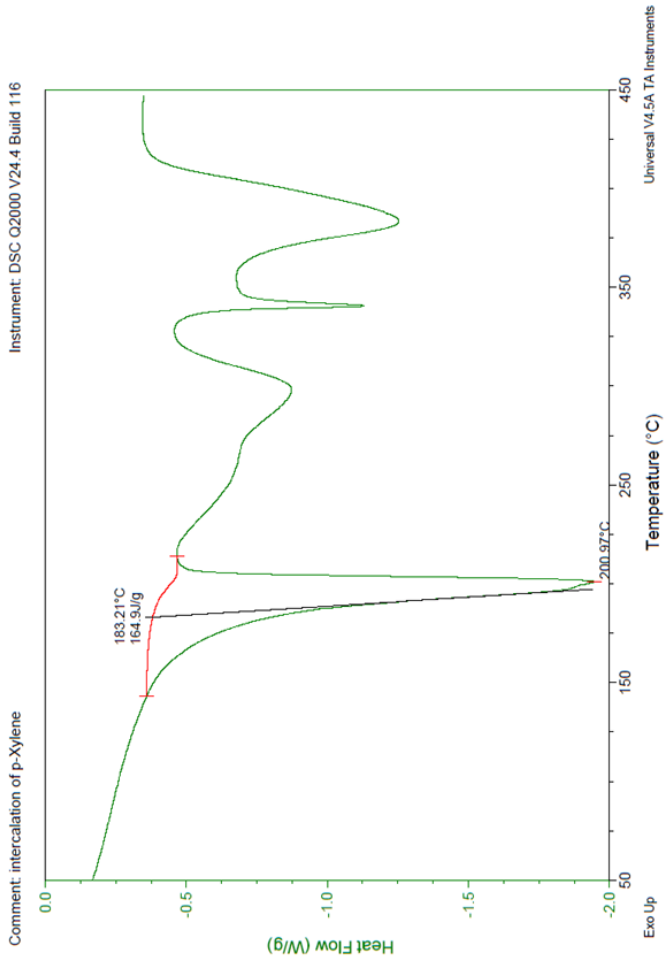

Figure B.30 DSC of the Ni(4m-BA) sonicated with p-xylene

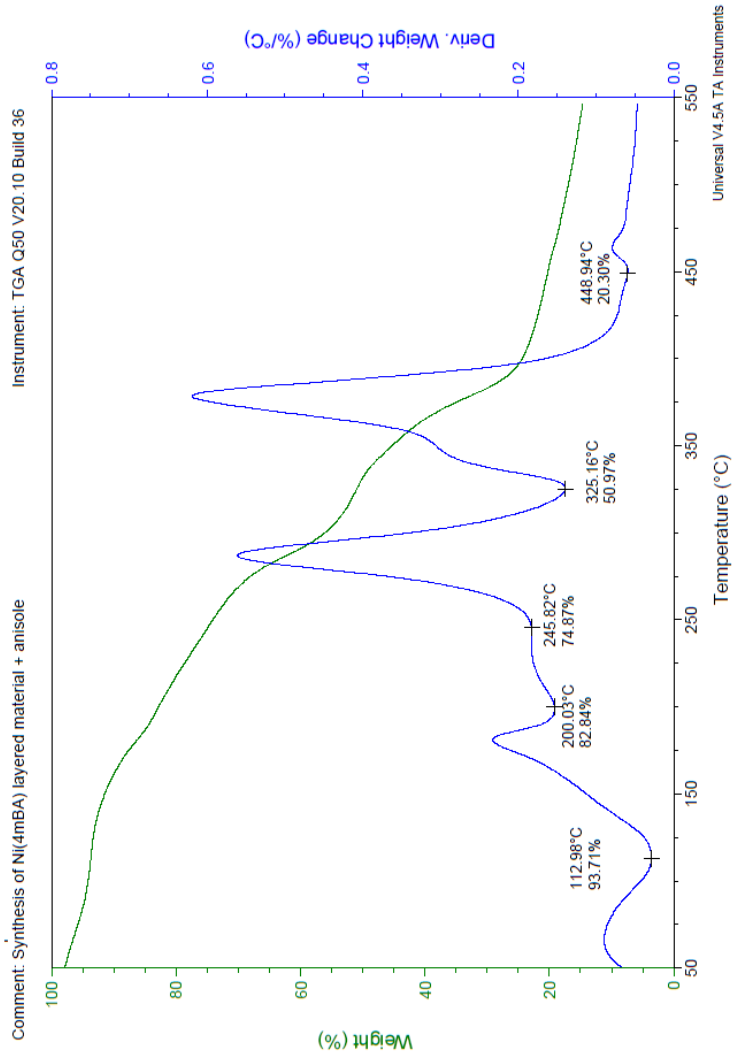

Figure B.31 TGA of the Ni(4m-BA) sonicated with anisole

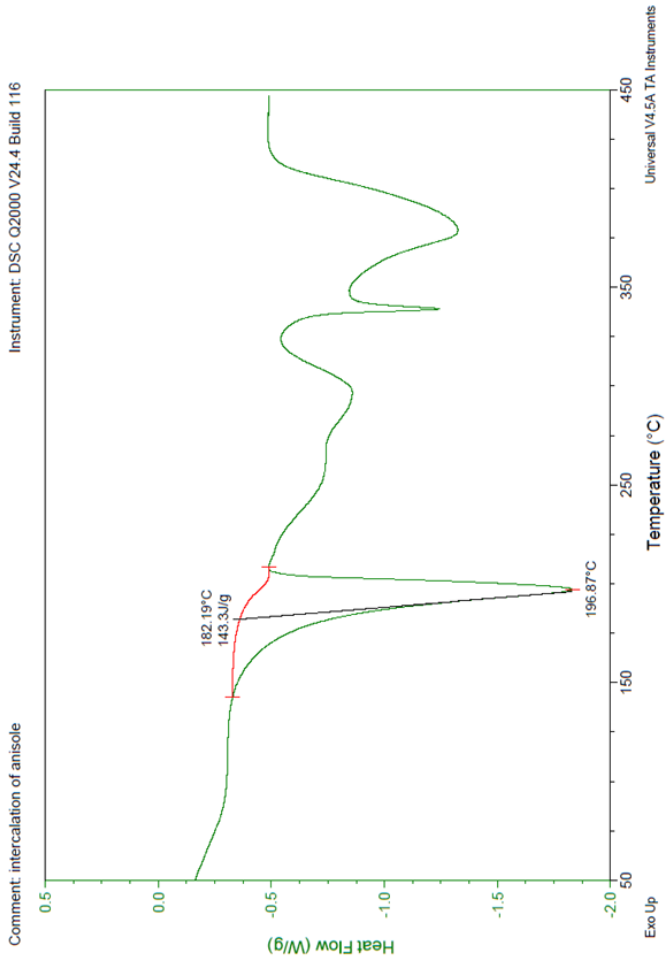

Figure B.32 DSC of the Ni(4m-BA) sonicated with anisole

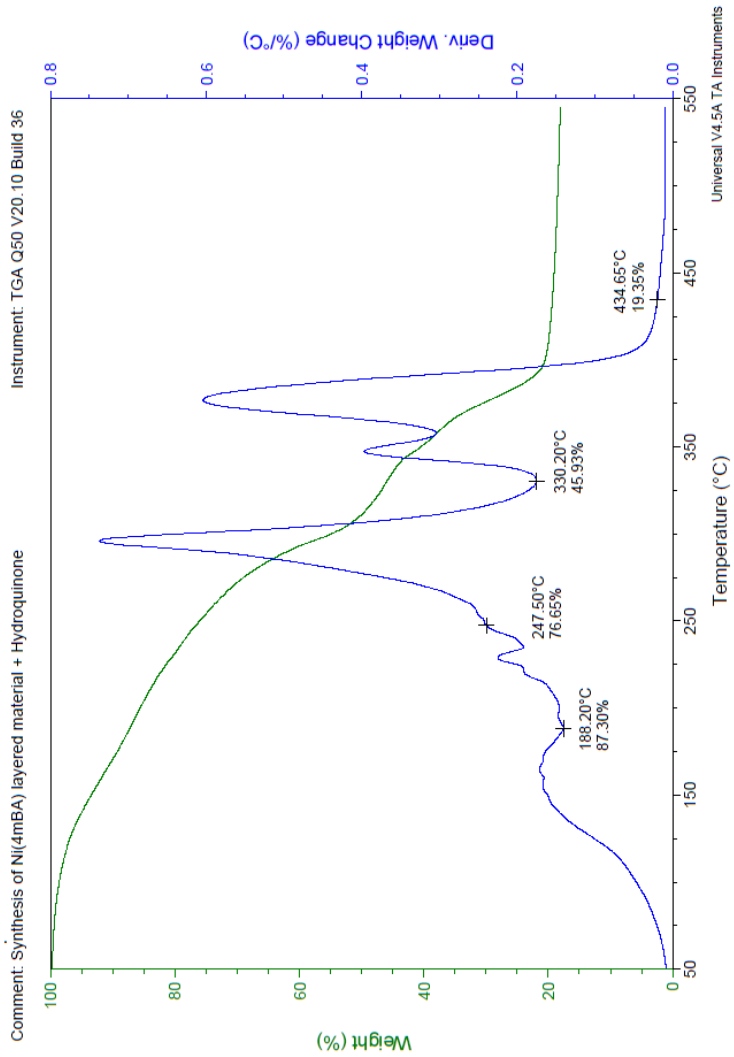

Figure B.33 TGA of the Ni(4m-BA) sonicated with hydroquinone

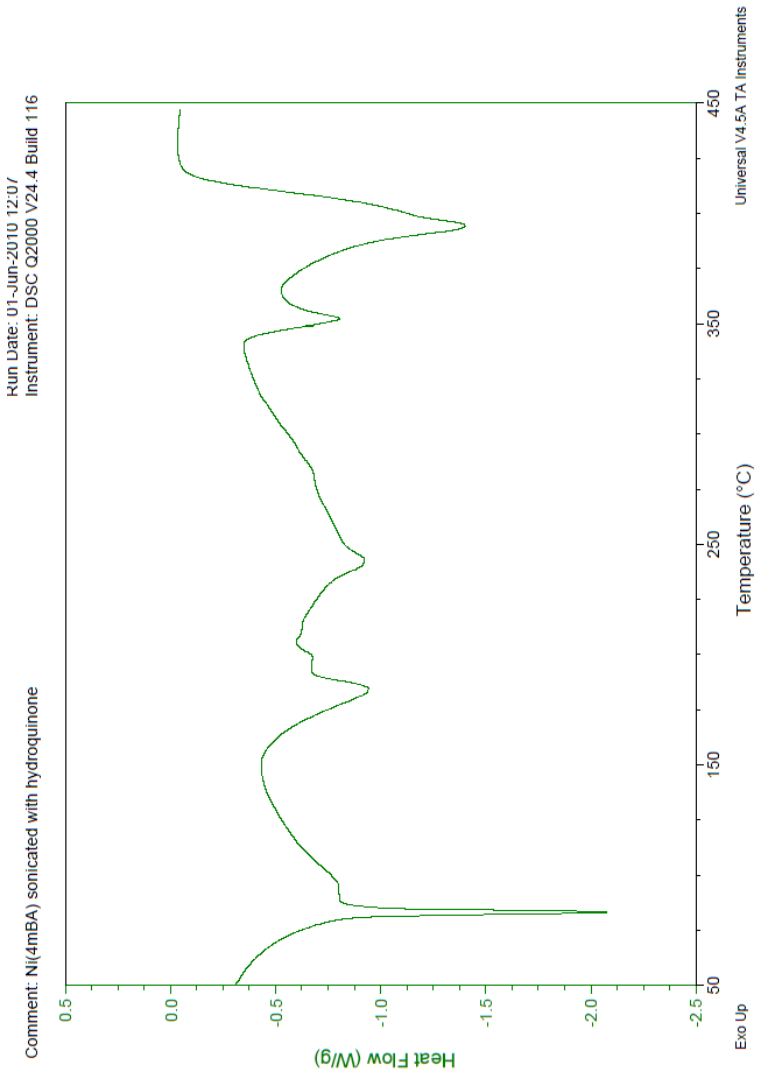

Figure B.34 DSC of the Ni(4m-BA) sonicated with hydroquinone

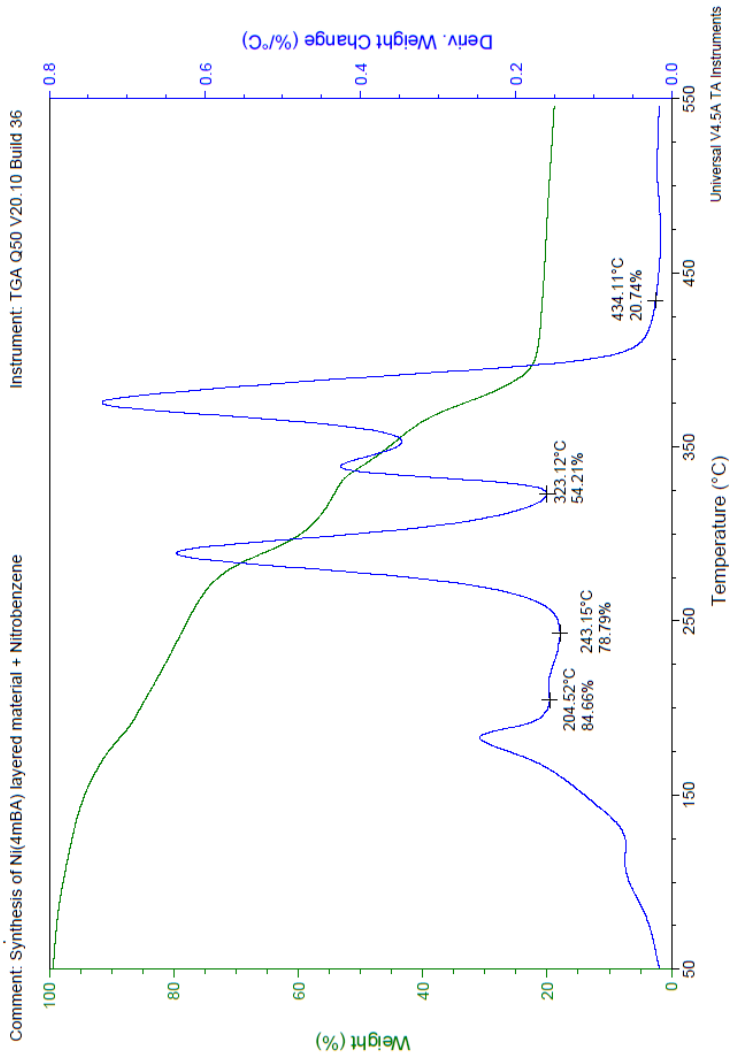

Figure B.35 TGA of the Ni(4m-BA) sonicated with nitrobenzene

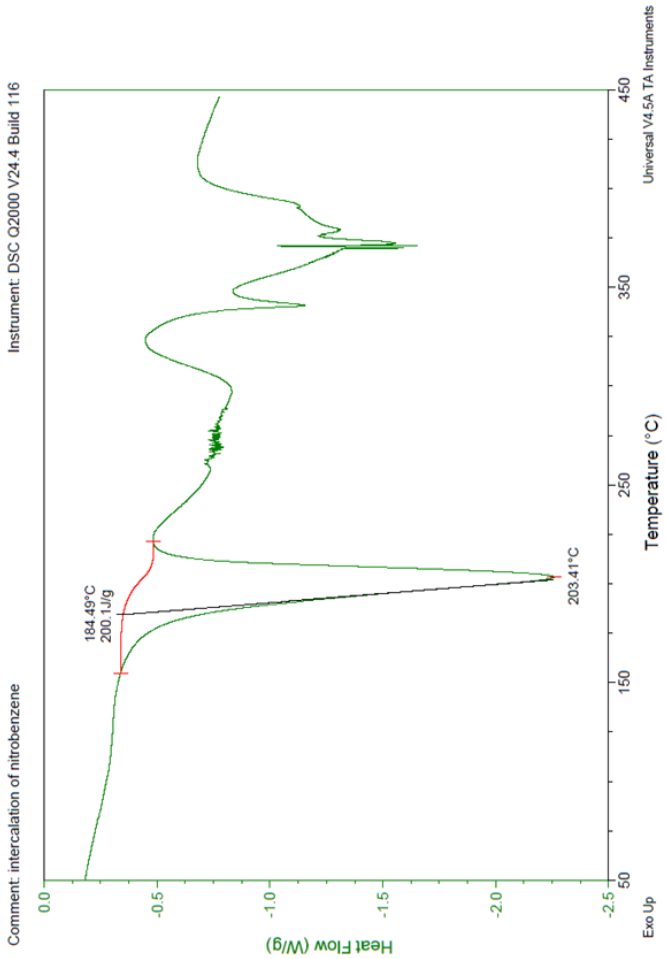

Figure B.36 DSC of the Ni(4m-BA) sonicated with nitrobenzene

Appendix C

TGA Data for Chapter 4

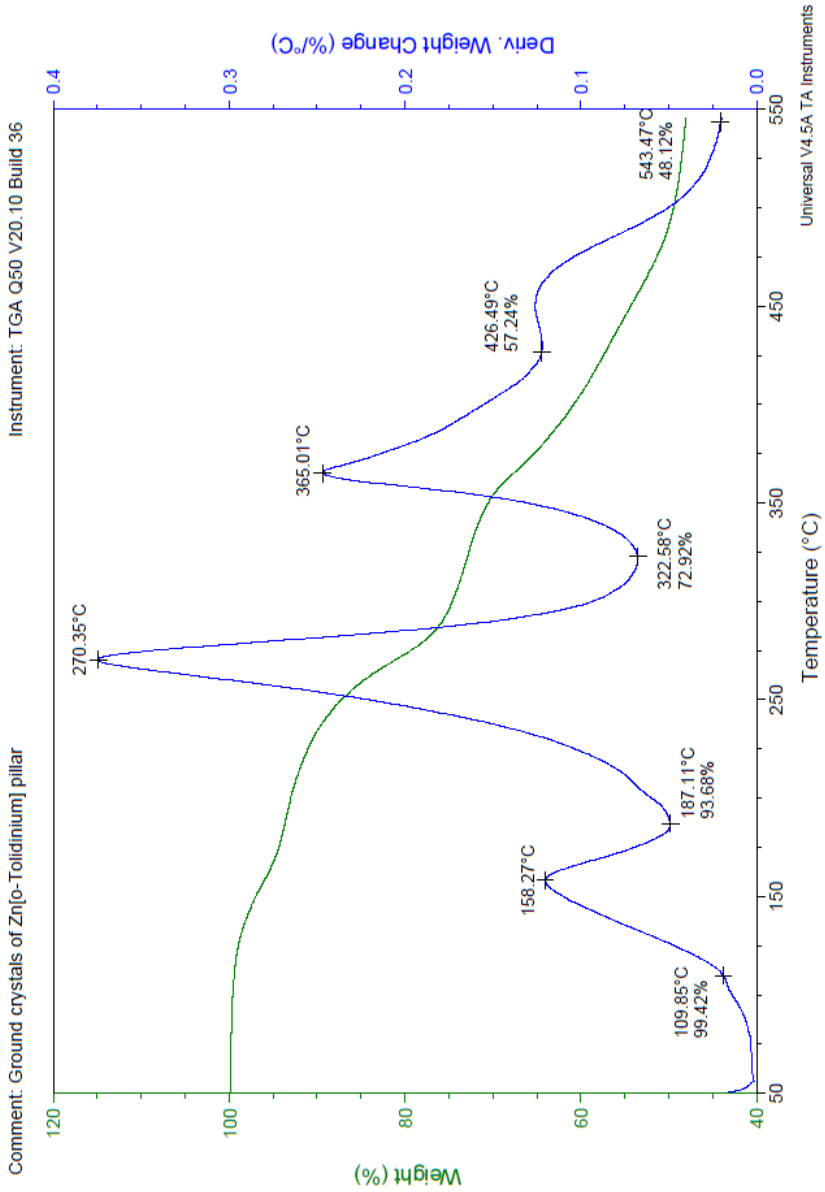

Figure C.1 TGA of the Zn(o-tolidine) pillar plus acetone

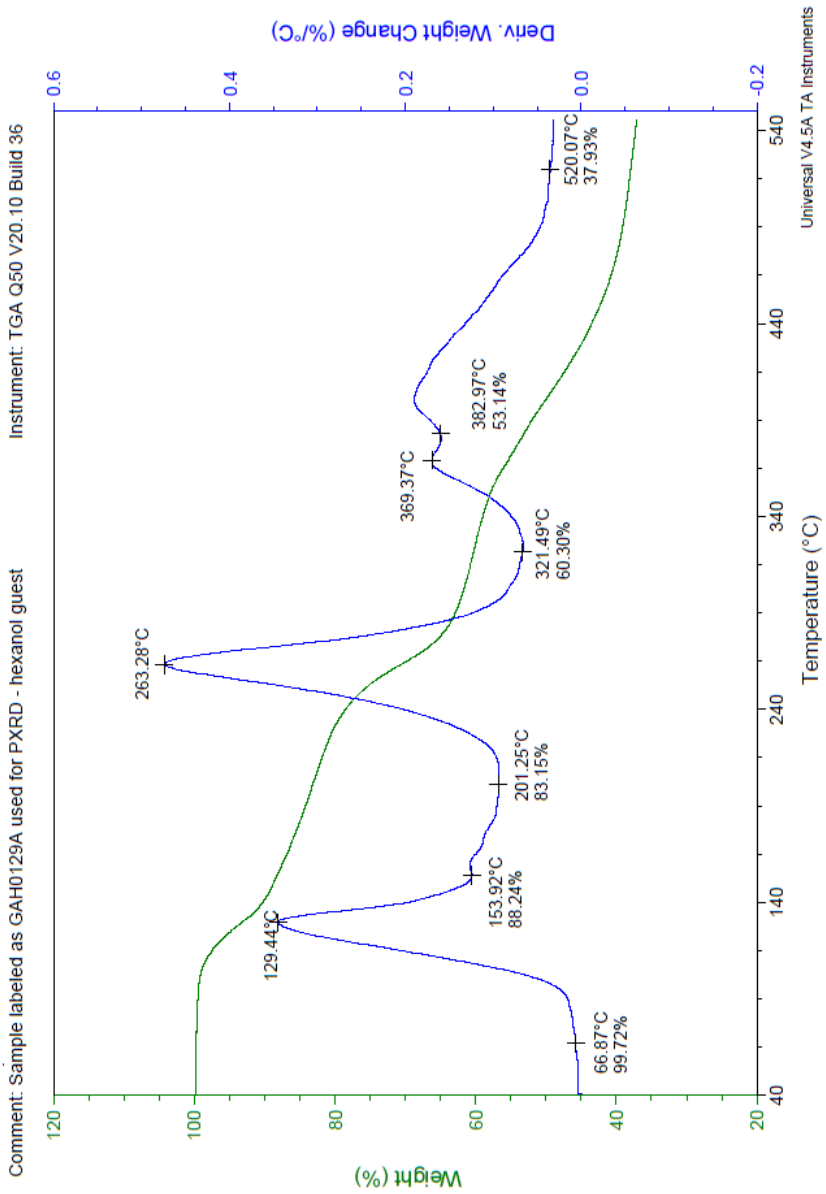

Figure C.2 TGA of the Zn(o-tolidine) pillar plus hexanol

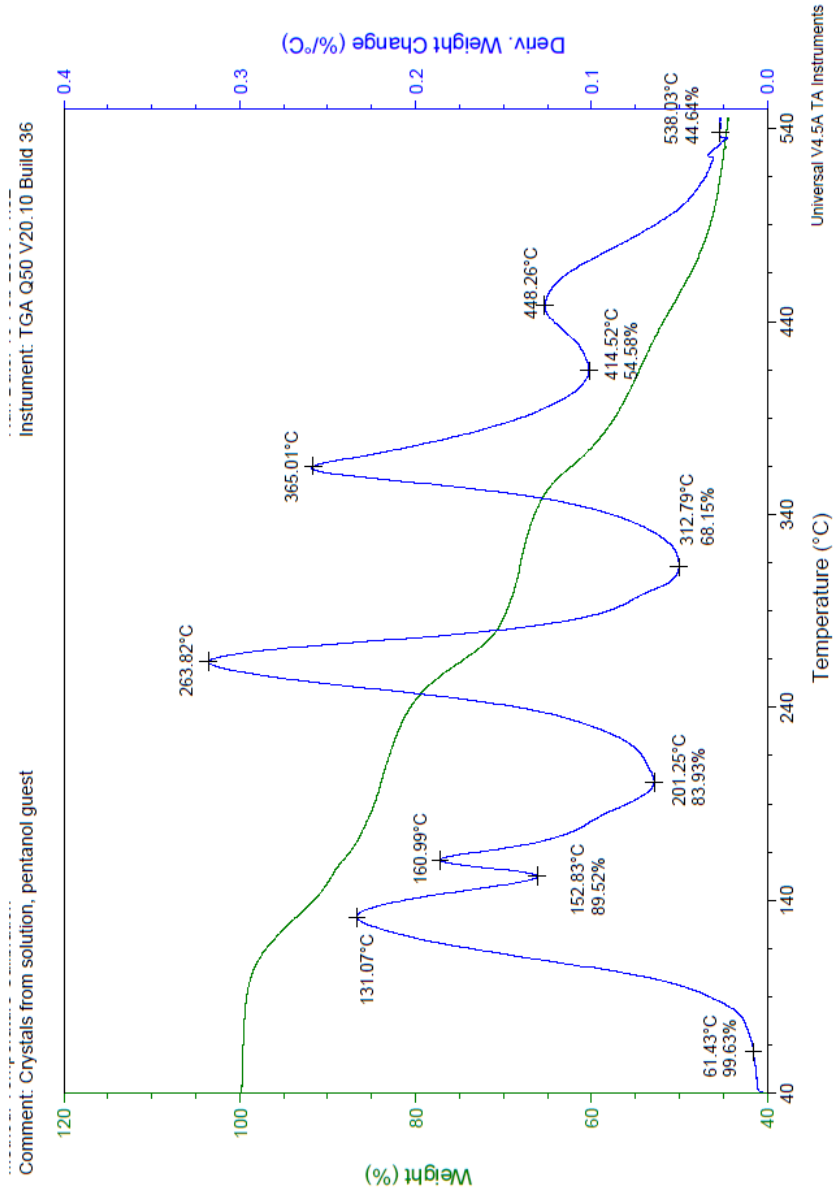

Figure C.3 TGA of the Zn(o-tolidine) pillar plus pentanol

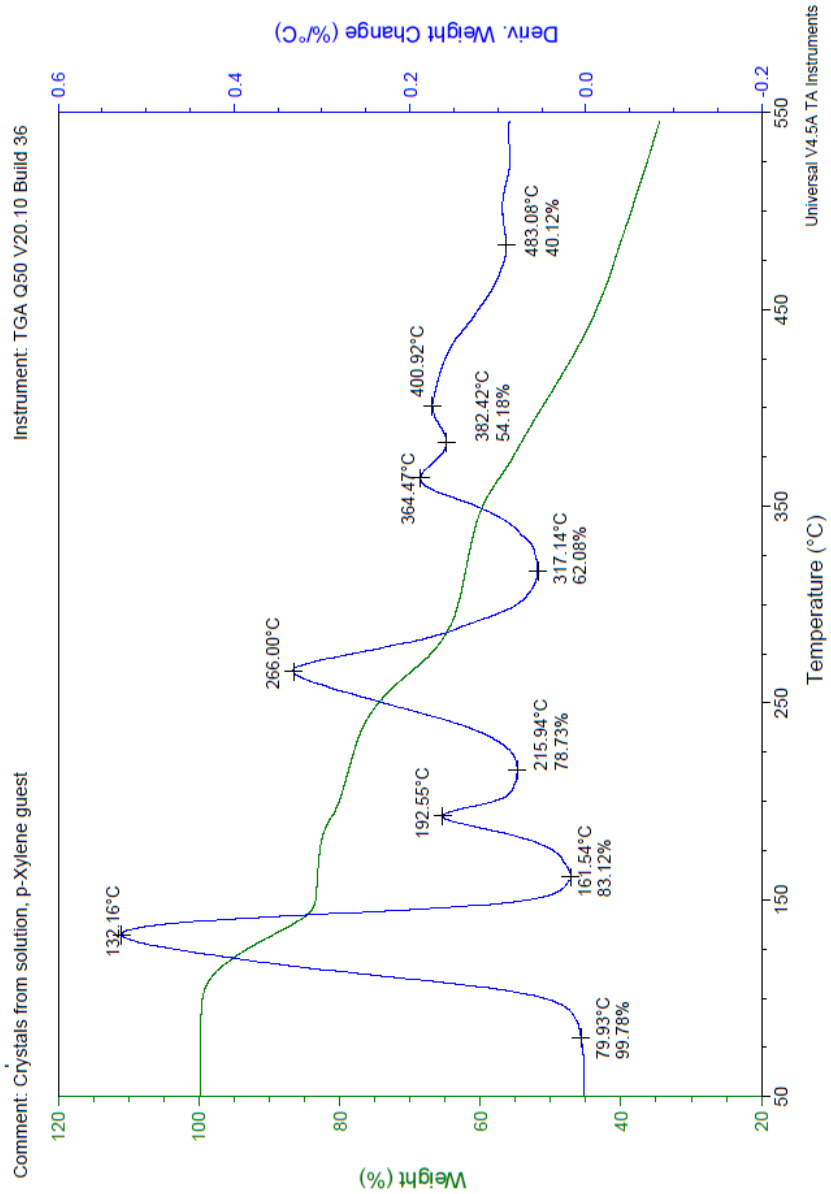

Figure C.4 TGA of the Zn(o-tolidine) pillar plus p-xylene

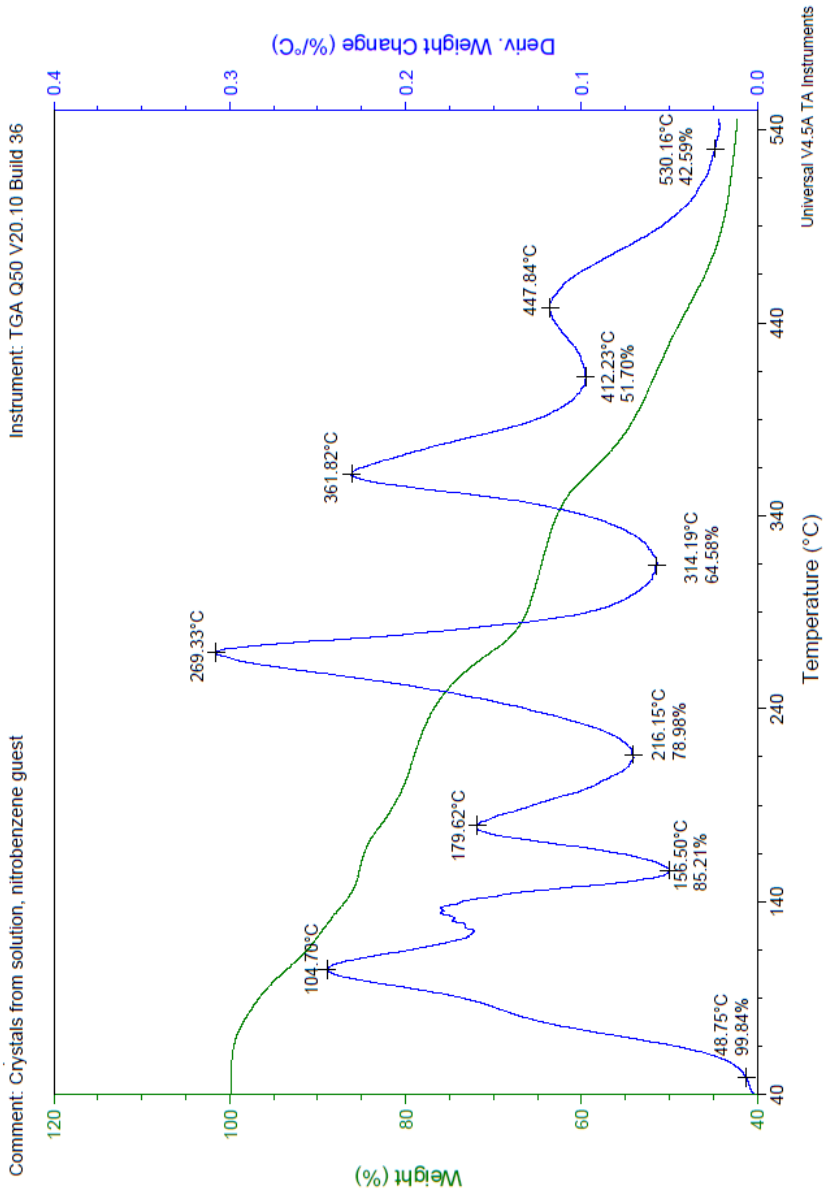

Figure C.5 TGA of the Zn(o-tolidine) pillar plus nitrobenzene

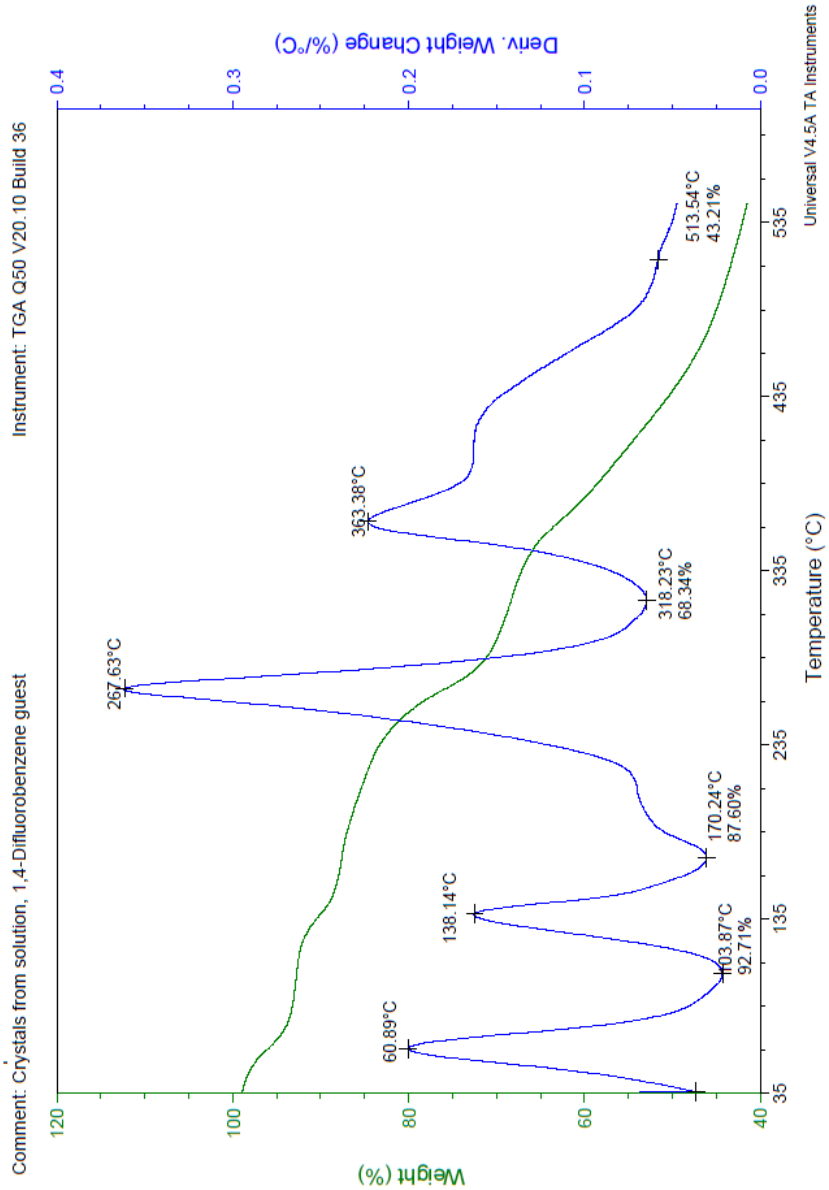

Figure C.6 TGA of the Zn(o-tolidine) pillar plus p-difluorobenzene

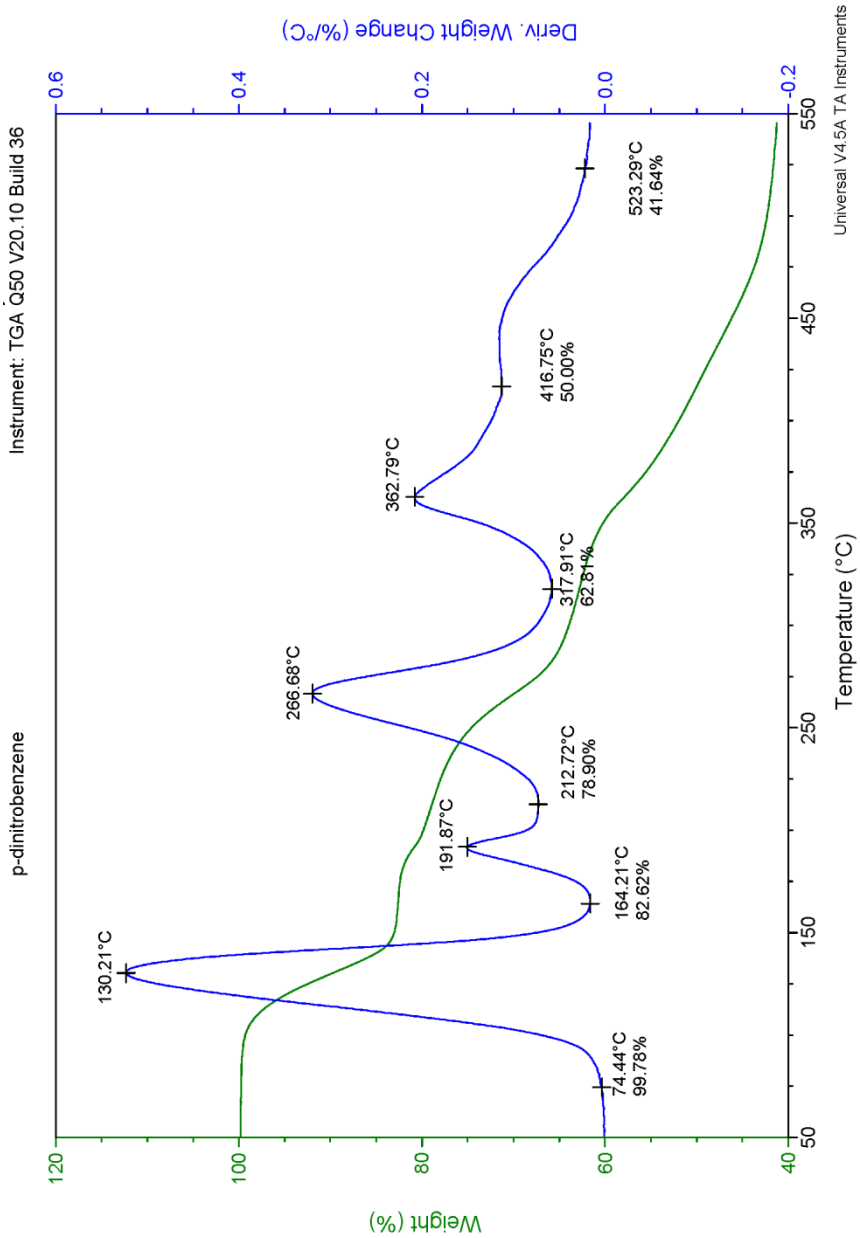

Figure C.7 TGA of the Zn(o-tolidine) pillar plus p-dinitrobenzene

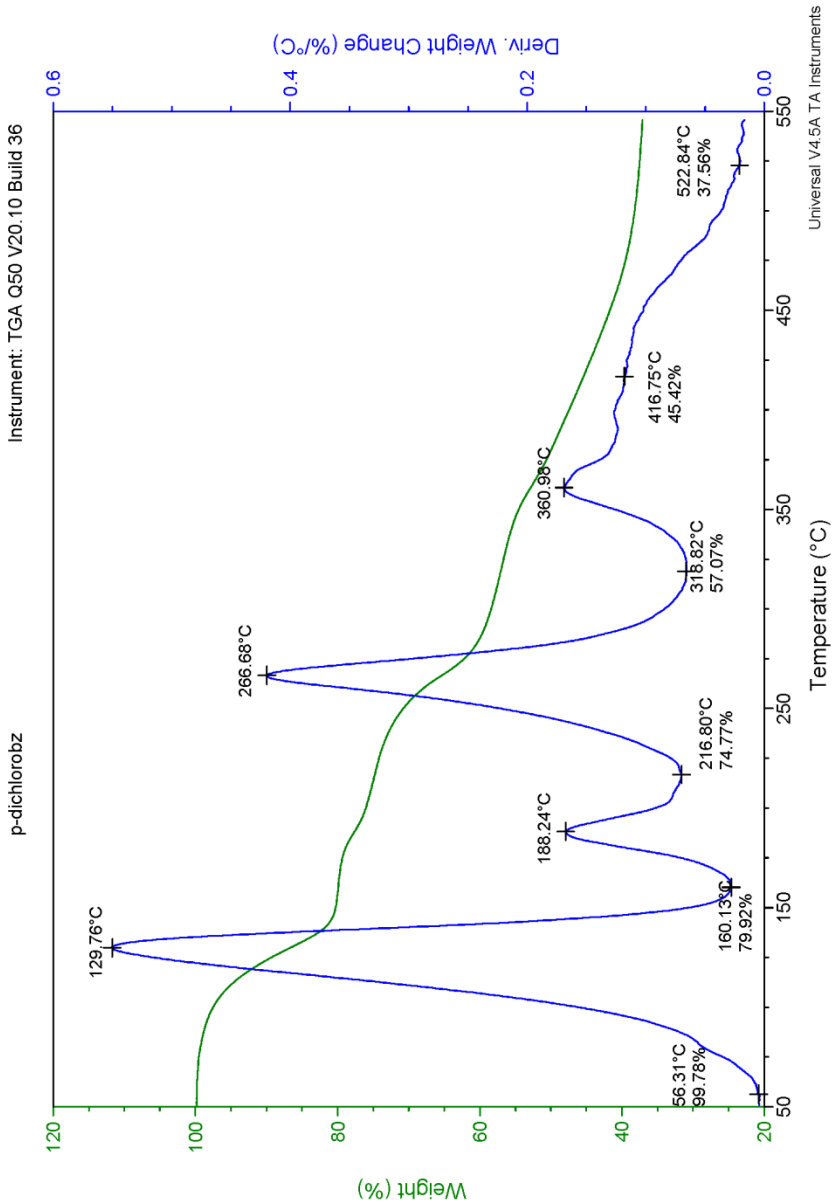

Figure C.8 TGA of the Zn(o-tolidine) pillar plus p-dichlorobenzene

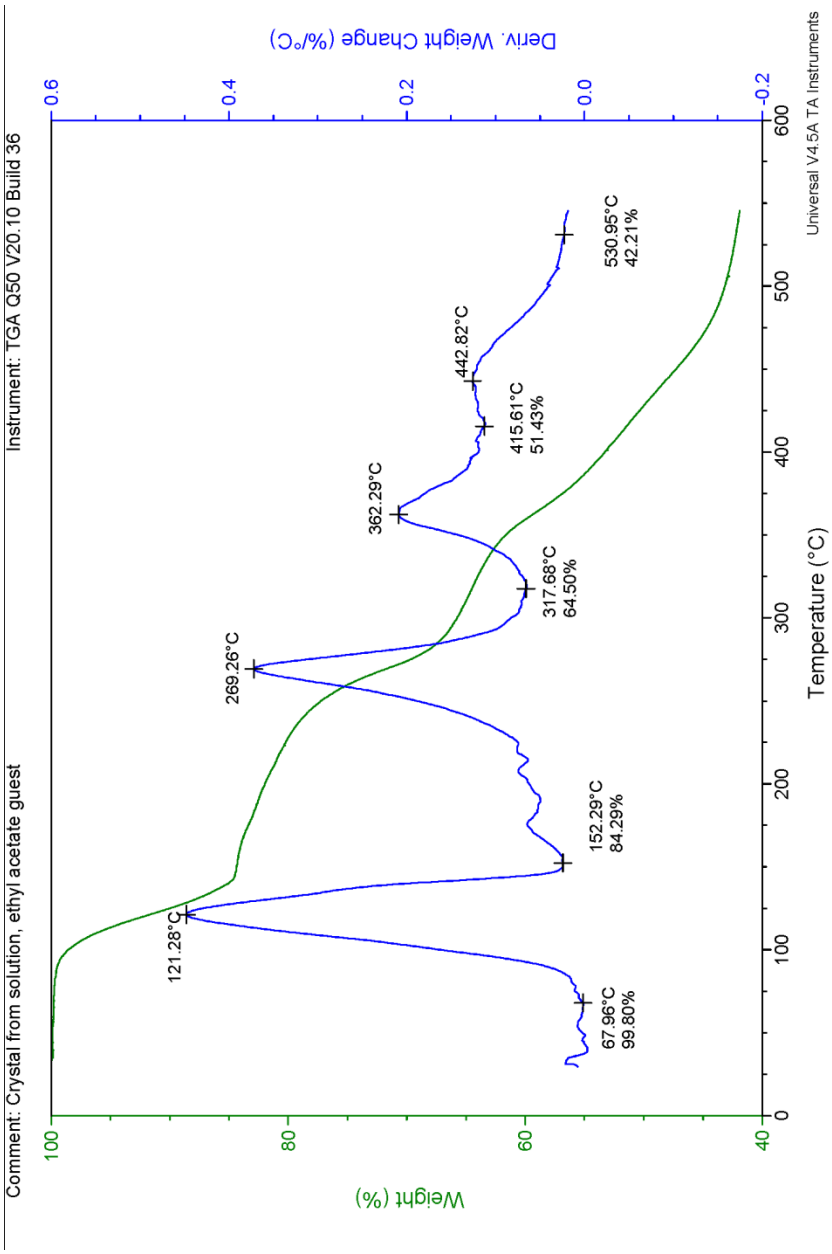

Figure C.9 TGA of the Zn(o-tolidine) pillar plus ethyl acetate

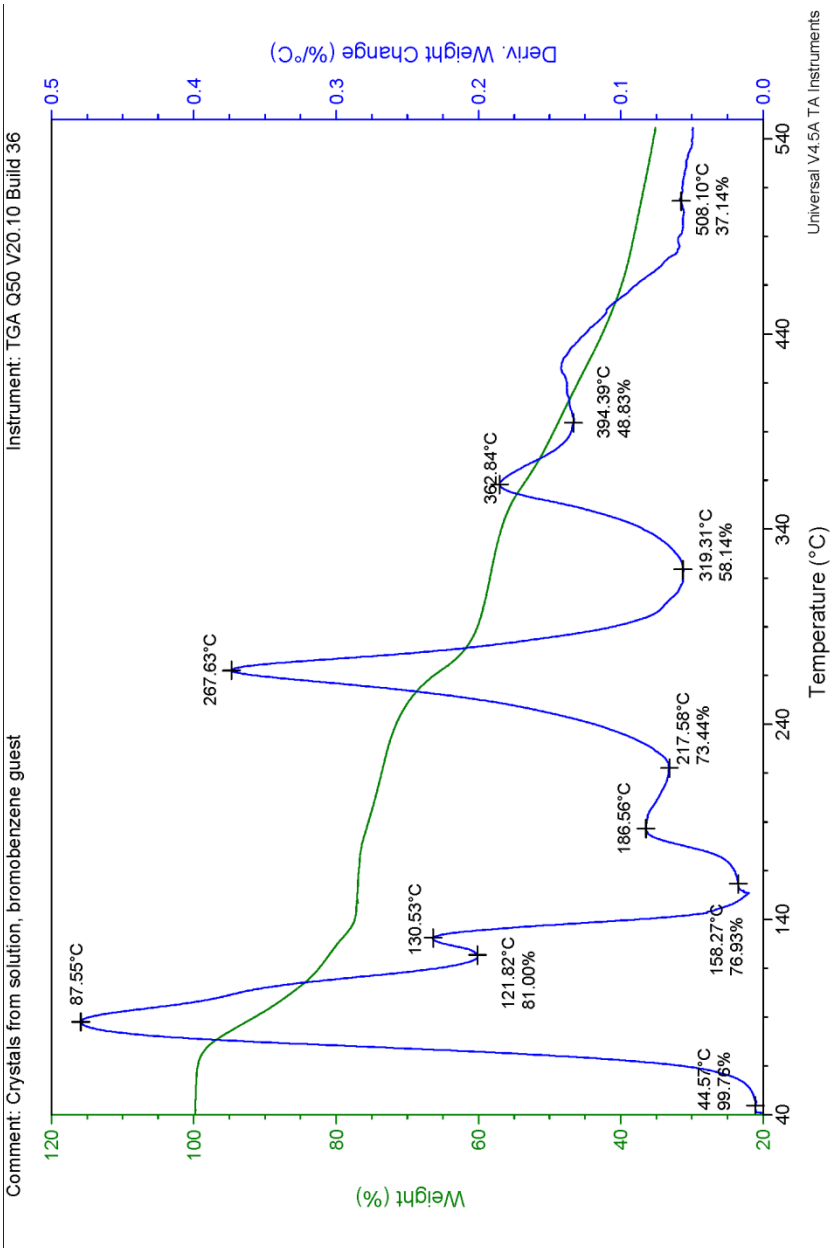

Figure C.10 TGA of the Zn(o-tolidine) pillar plus bromobenzene

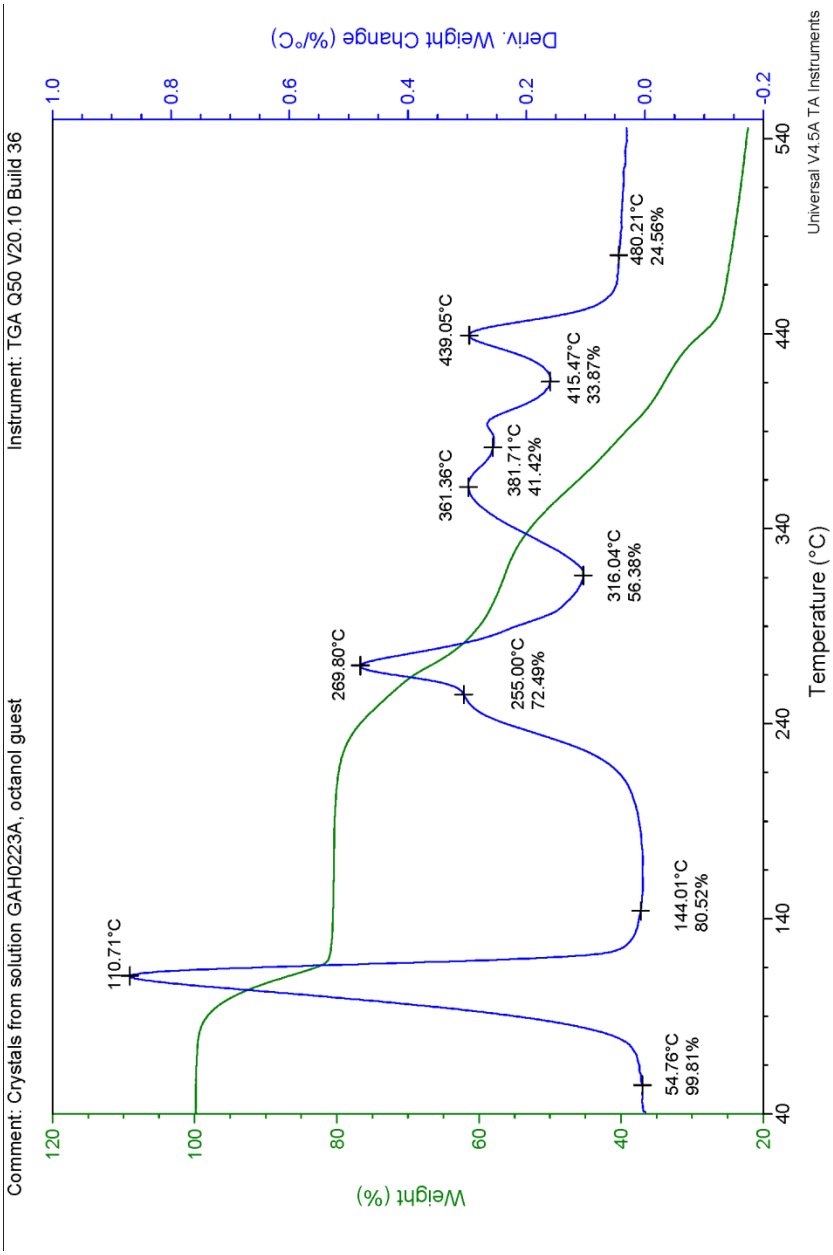

Figure C.11 TGA of the Zn(o-tolidine) pillar plus octanol

Appendix D

Thermal Analysis Data for Chapter 5

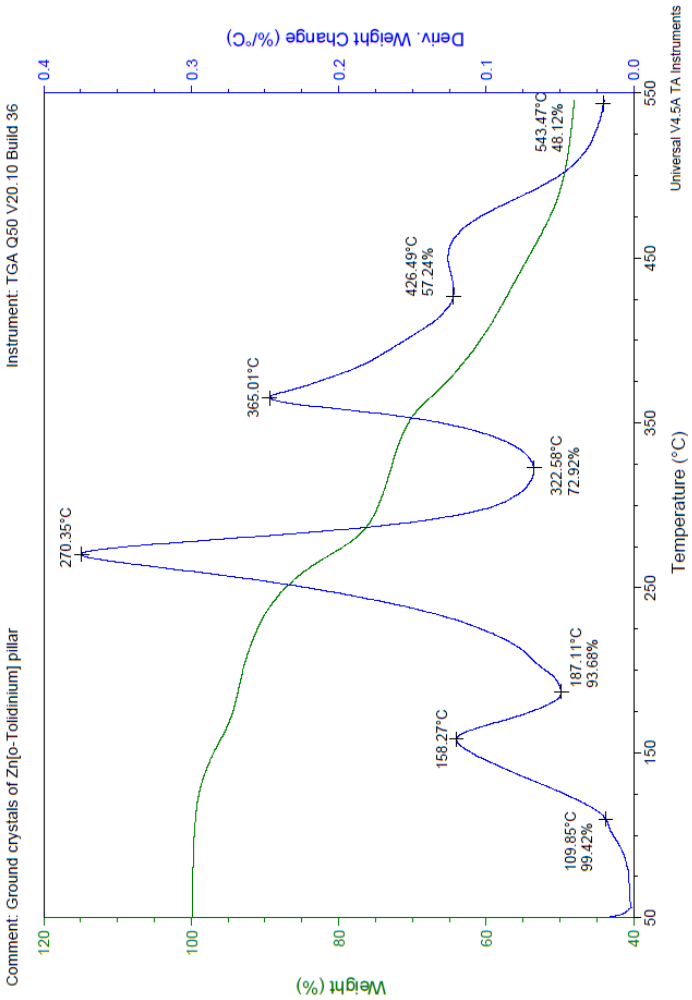

Figure D.1 TGA of porous Zn(o-tolidine) material

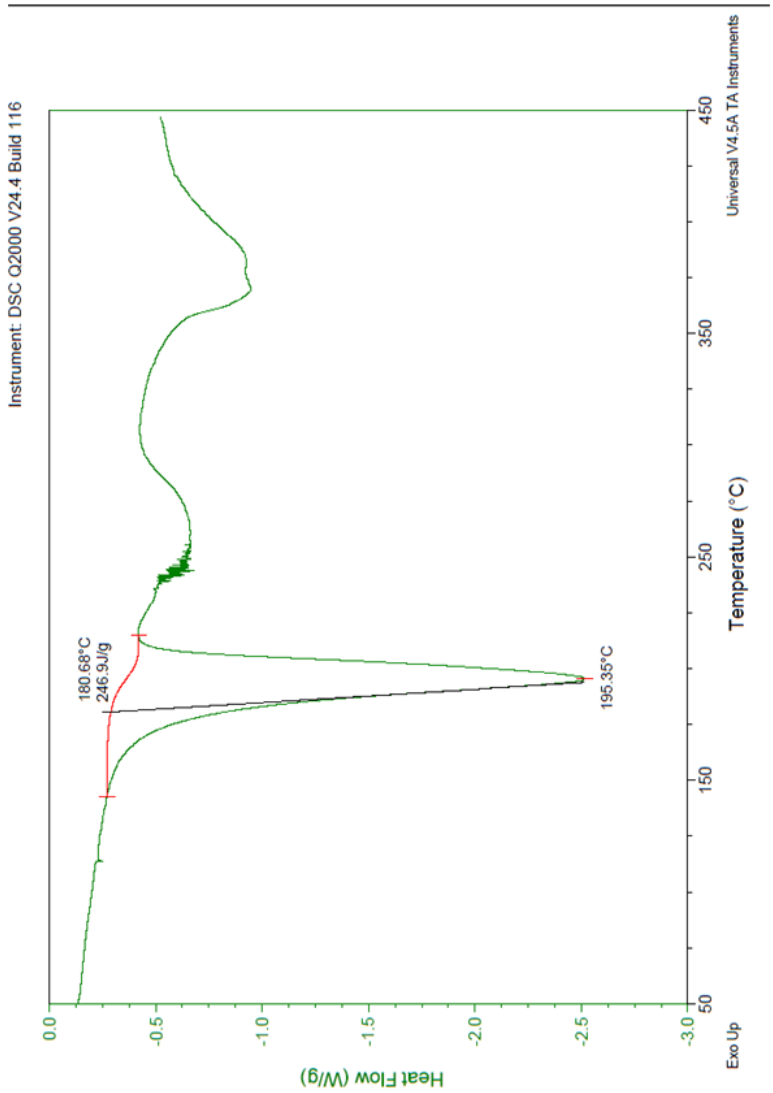

Figure D.2 DSC spectra of Zn(o-tolidine) starting material

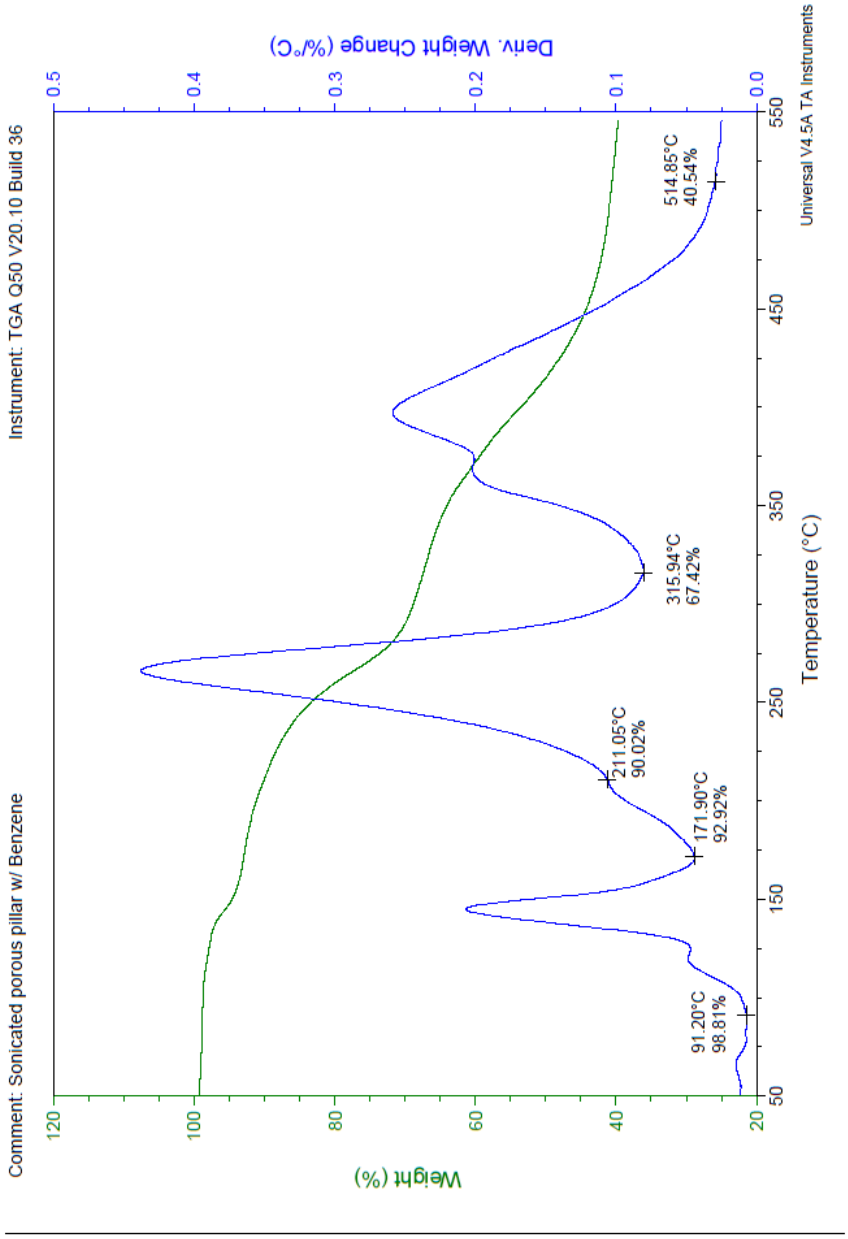

Figure D.3 TGA of porous Zn(o-tolidine) sonication with benzene

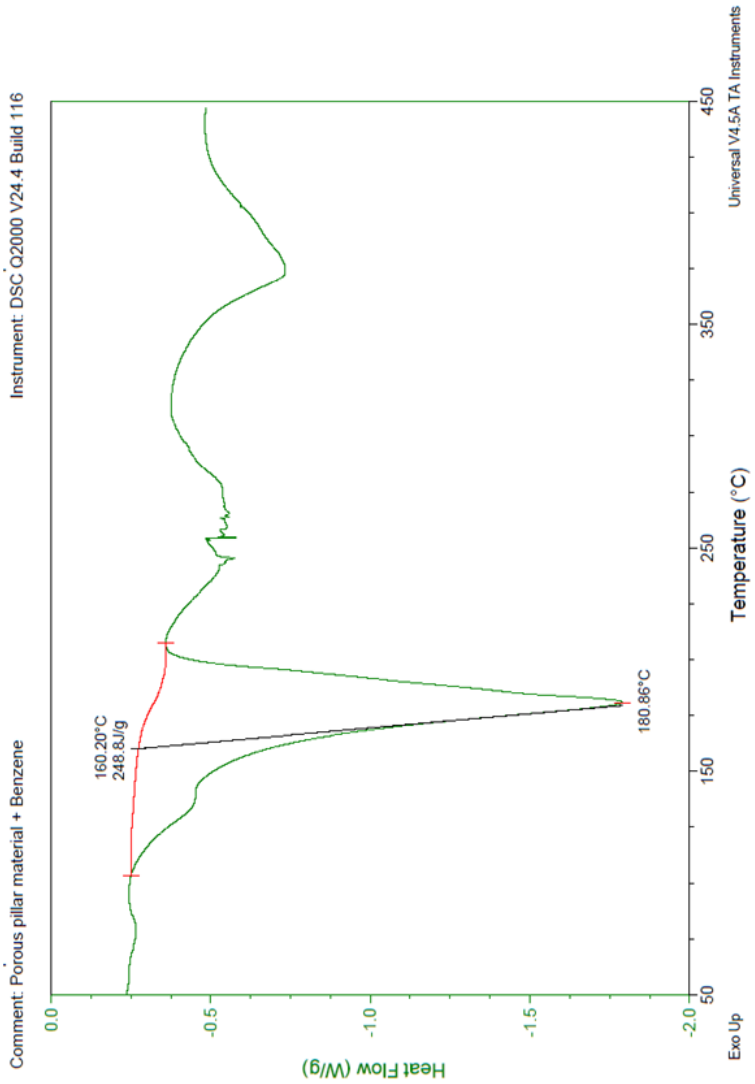

Figure D.4 DSC of porous Zn(o-tolidine) sonication with benzene

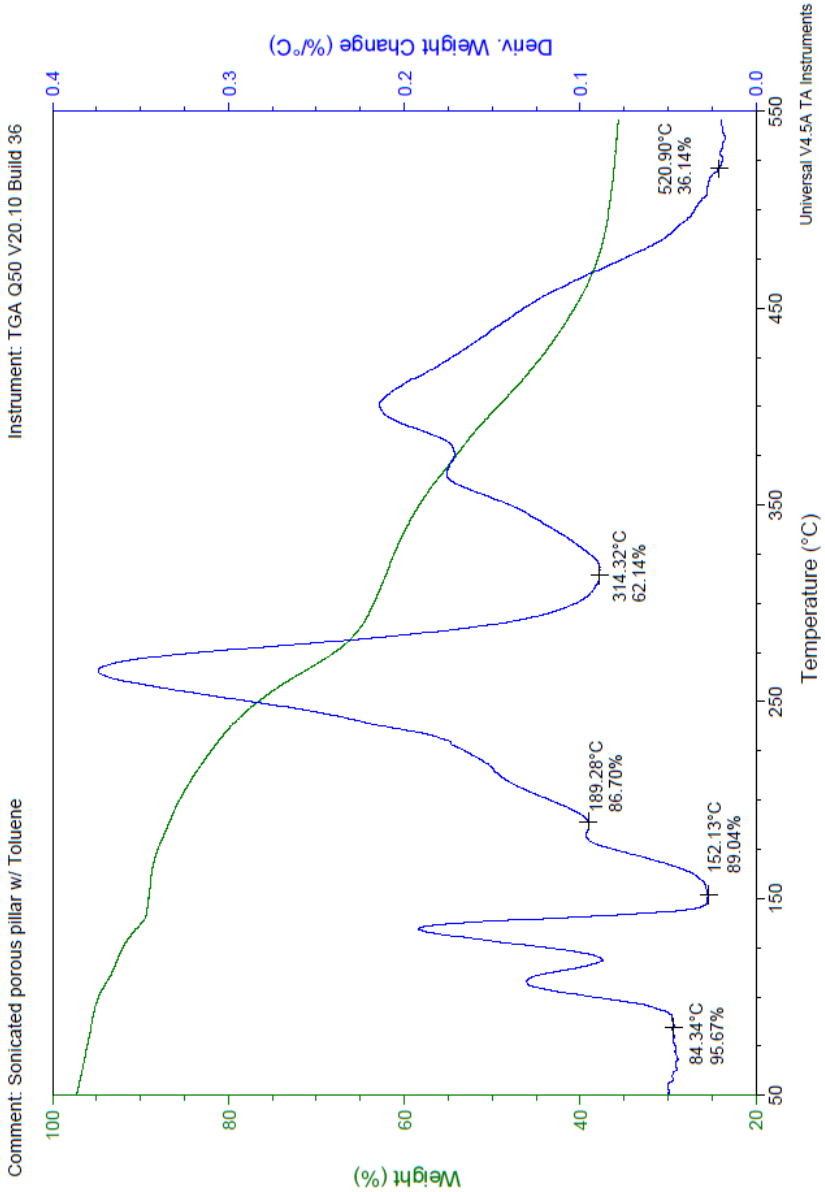

Figure D.5 TGA of the porous Zn(o-tolidine) sonicated with toluene

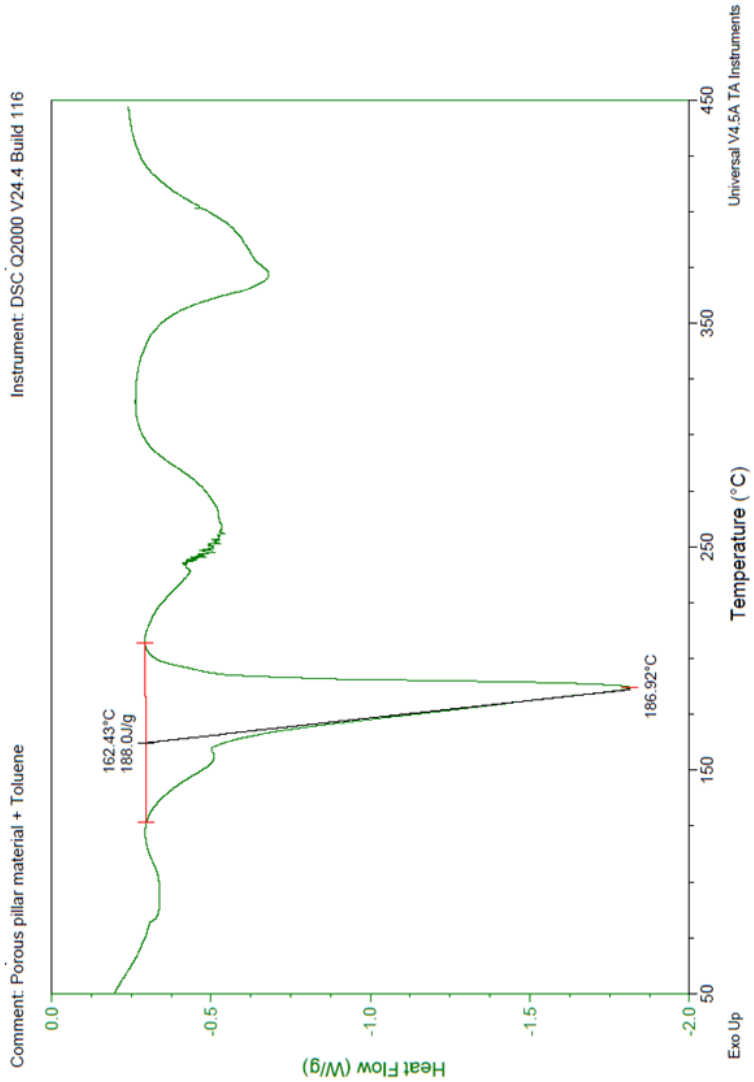

Figure D.6 DSC of the porous Zn(o-tolidine) sonicated with toluene

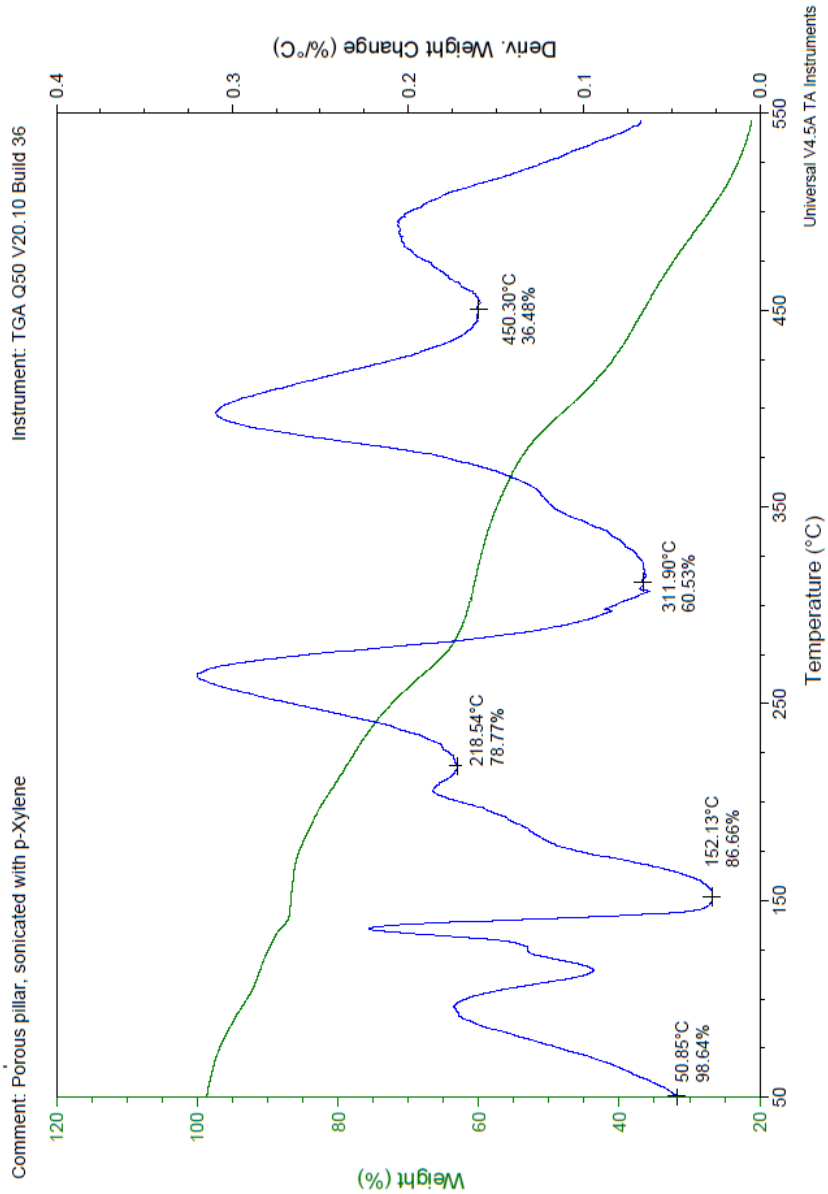

Figure D.7 TGA of the porous Zn(o-tolidine) sonicated with p-xylene

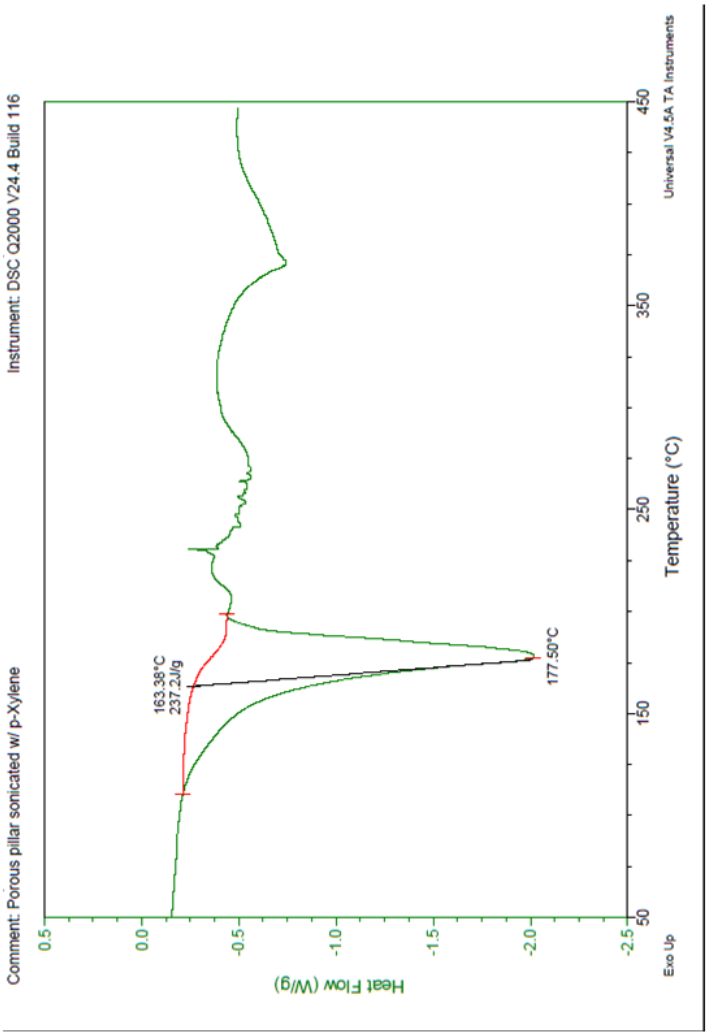

Figure D.8 DSC of the porous Zn(o-tolidine) sonicated with p-xylene

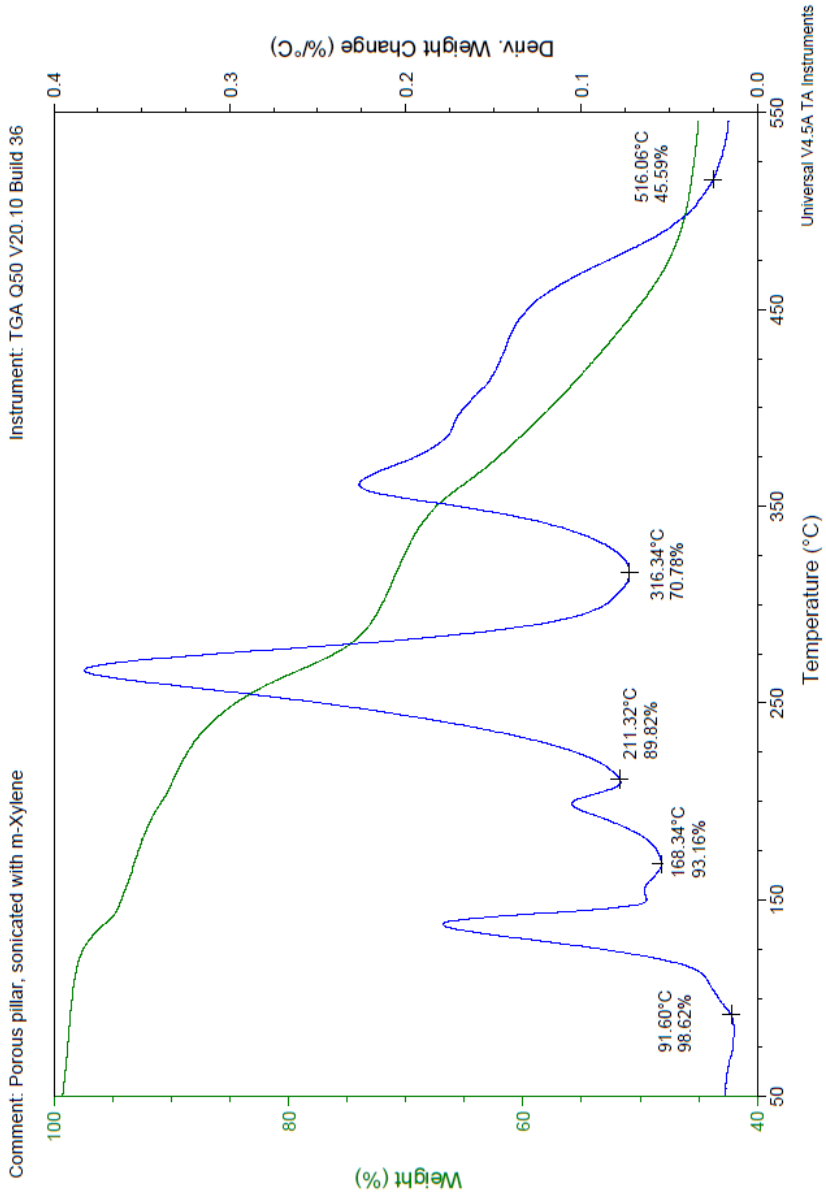

Figure D.9TGA of the porous Zn(o-tolidine) sonicated with m-xylene

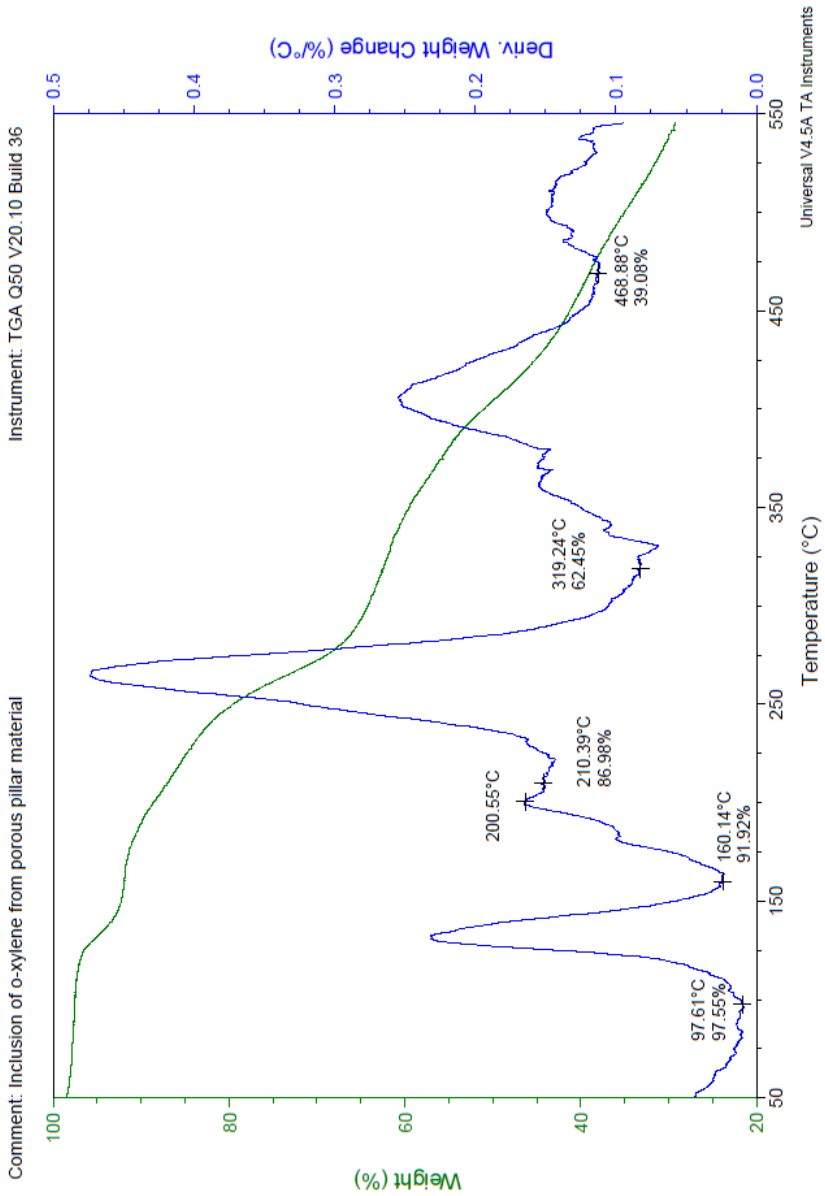

Figure D.10TGA of the porous Zn(o-tolidine) sonicated with o-xylene

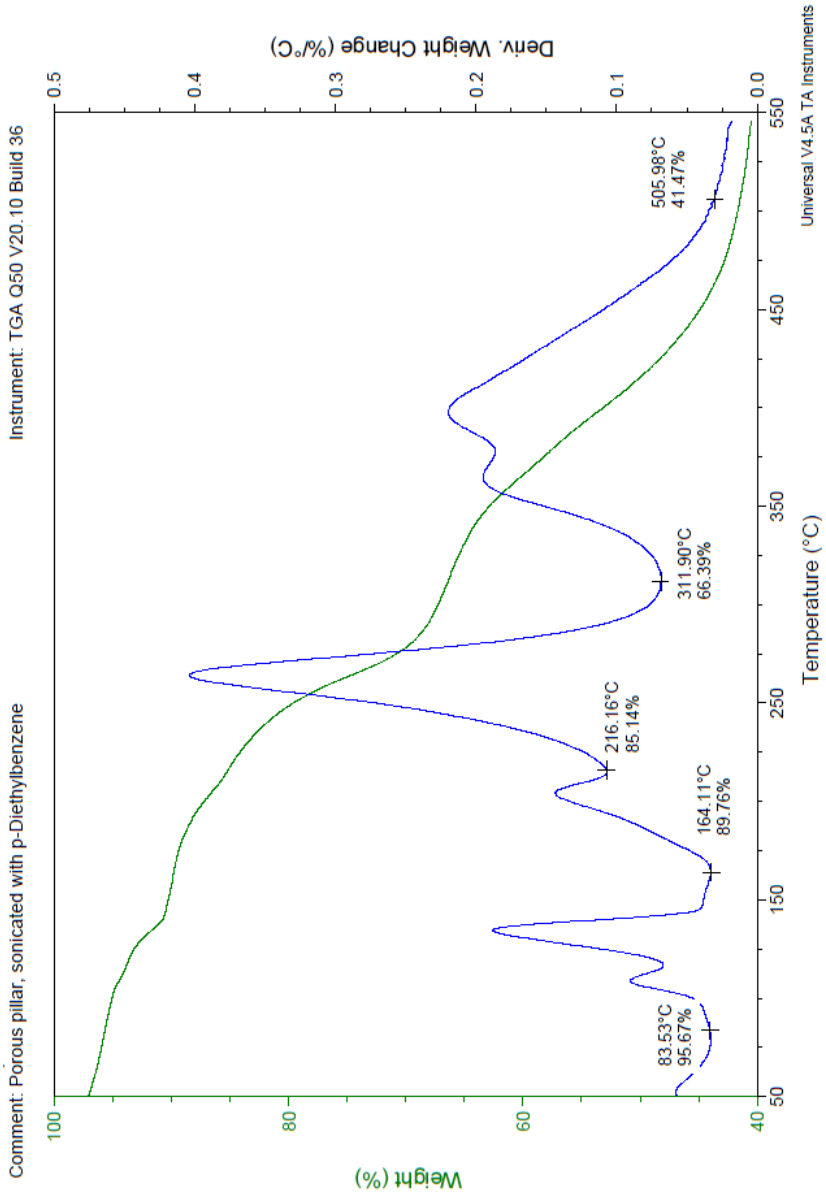

Figure D.11TGA of the porous Zn(o-tolidine) sonicated with p-diethylbenzene

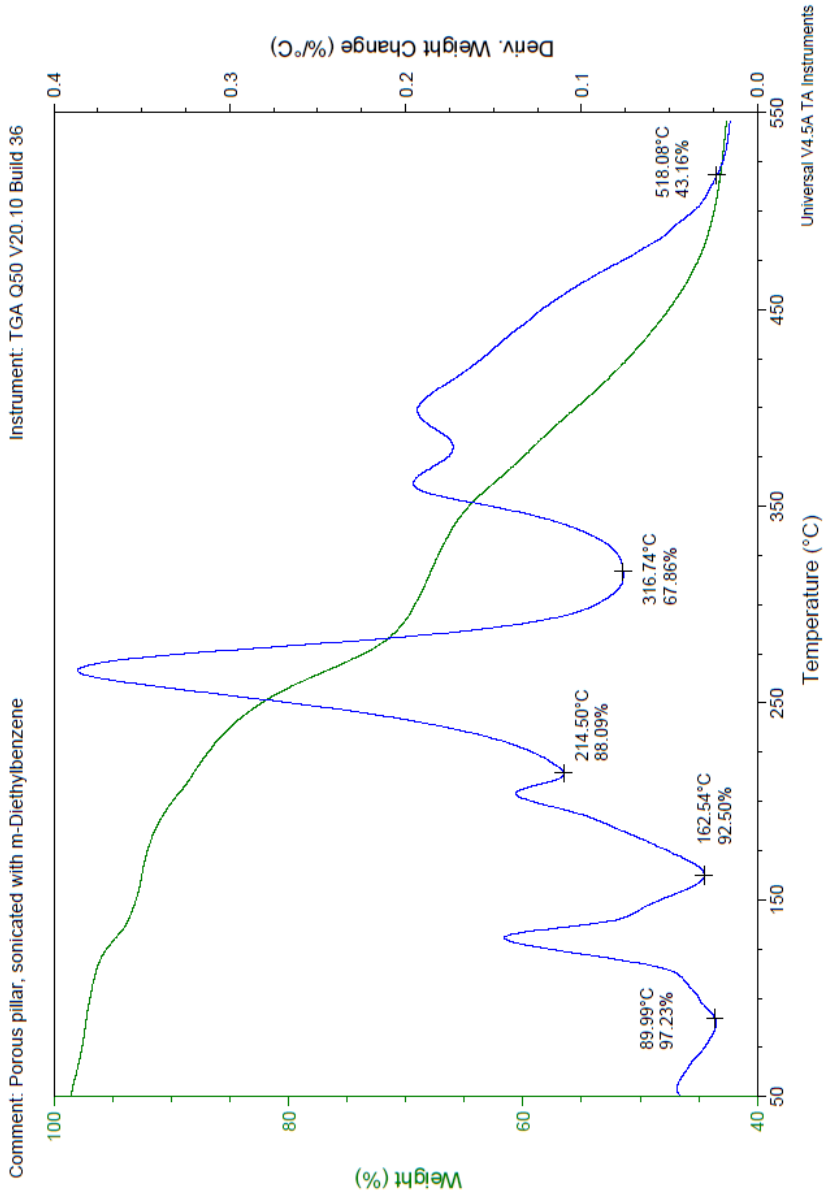

Figure D.12TGA of the porous Zn(o-tolidine) sonicated with m-diethylbenzene

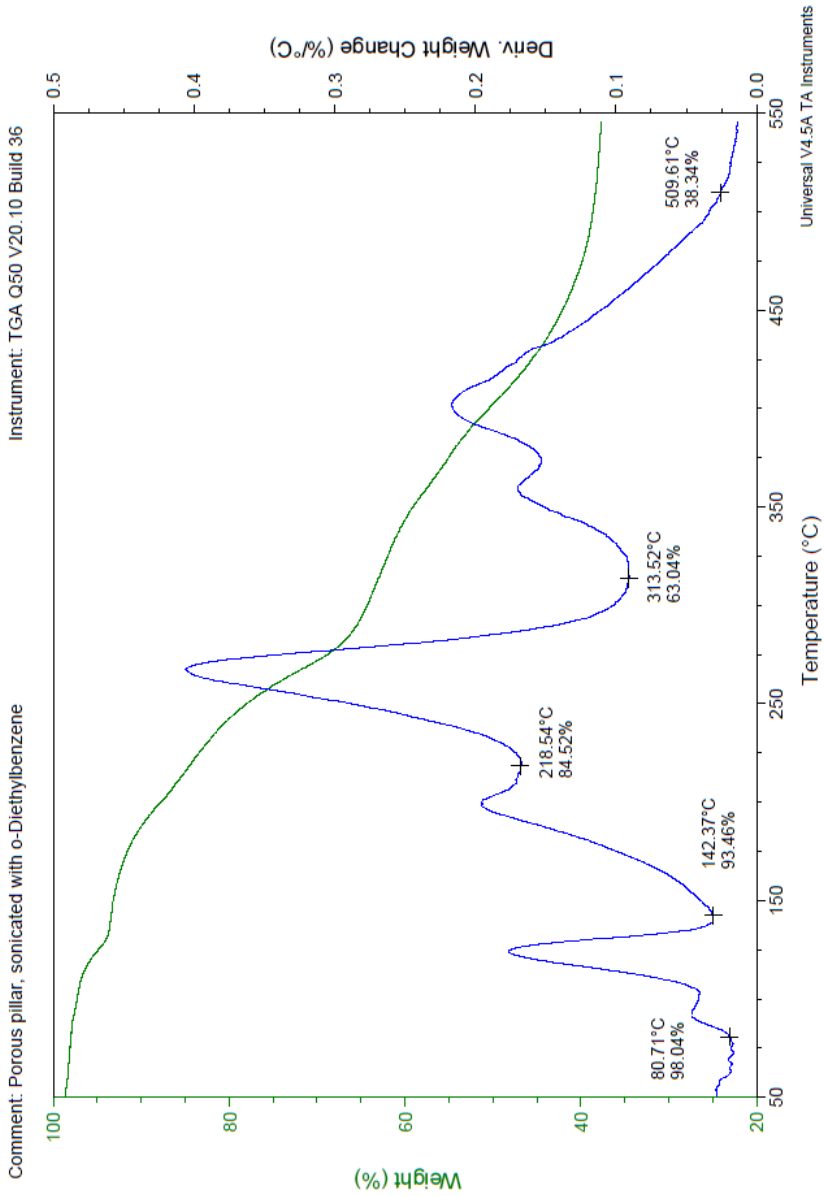

Figure D.13TGA of the porous Zn(o-tolidine) sonicated with o-diethylbenzene

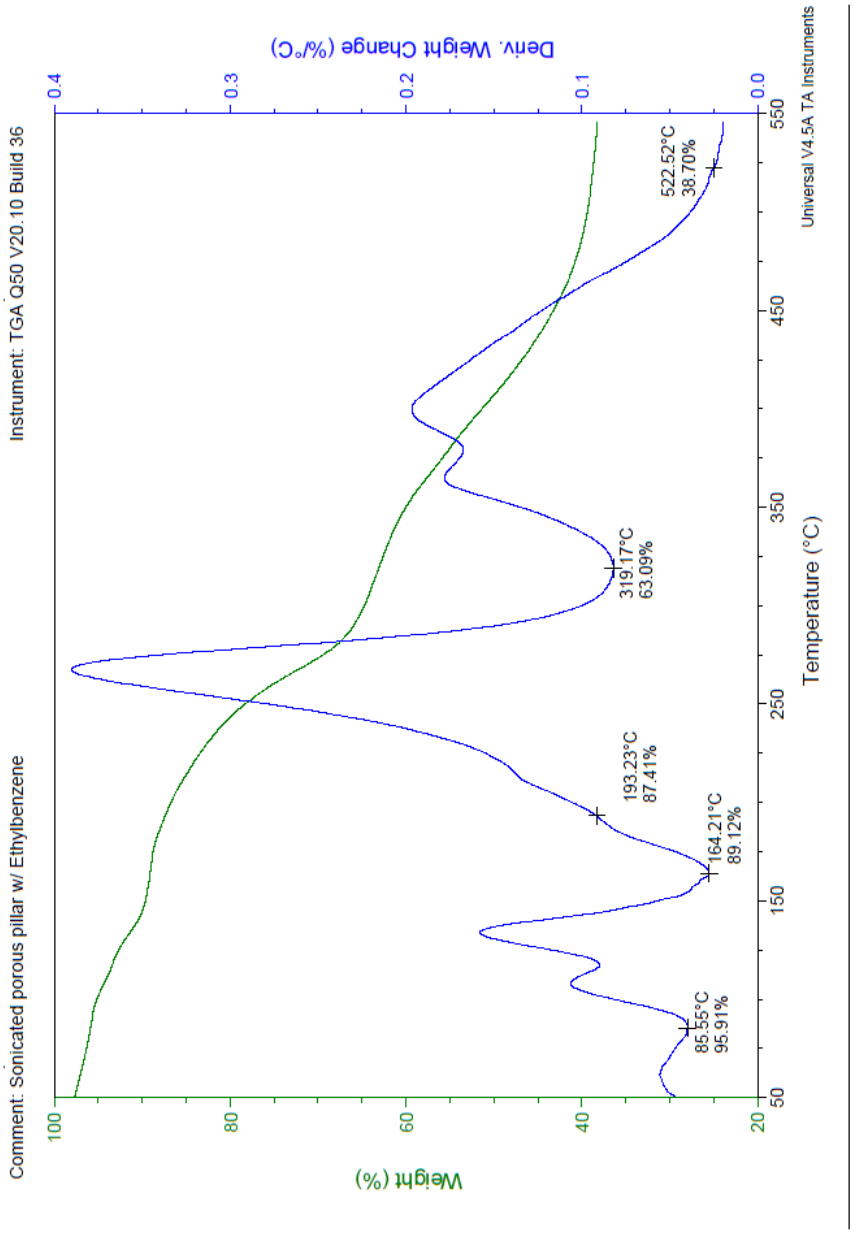

Figure D.14TGA of the porous Zn(o-tolidine) sonicated with ethylbenzene

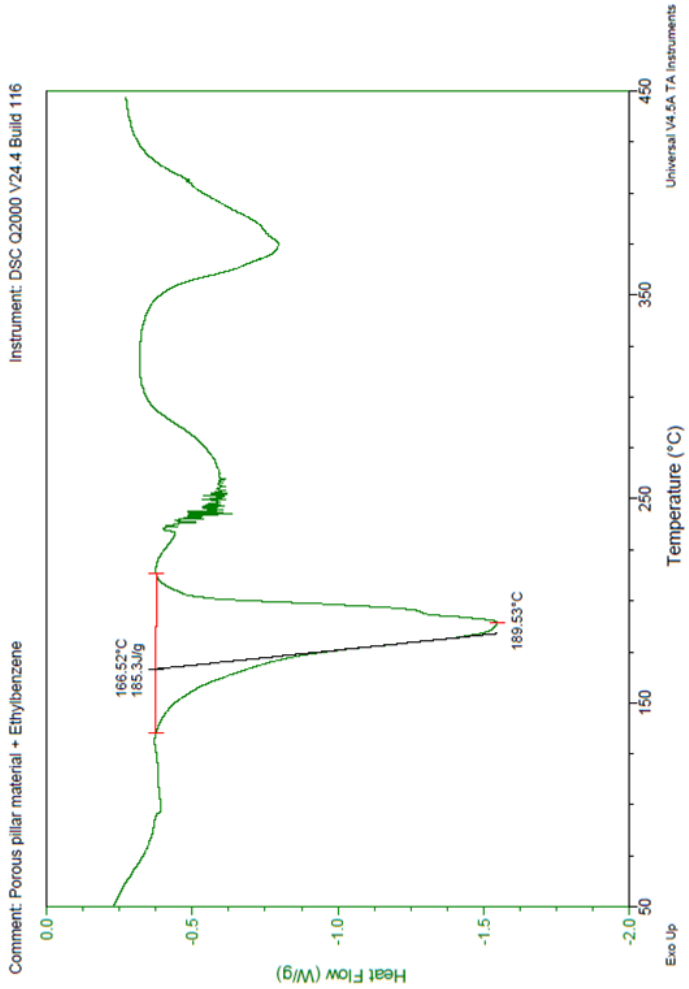

Figure D.15 DSC of the porous Zn(o-tolidine) sonicated with ethylbenzene

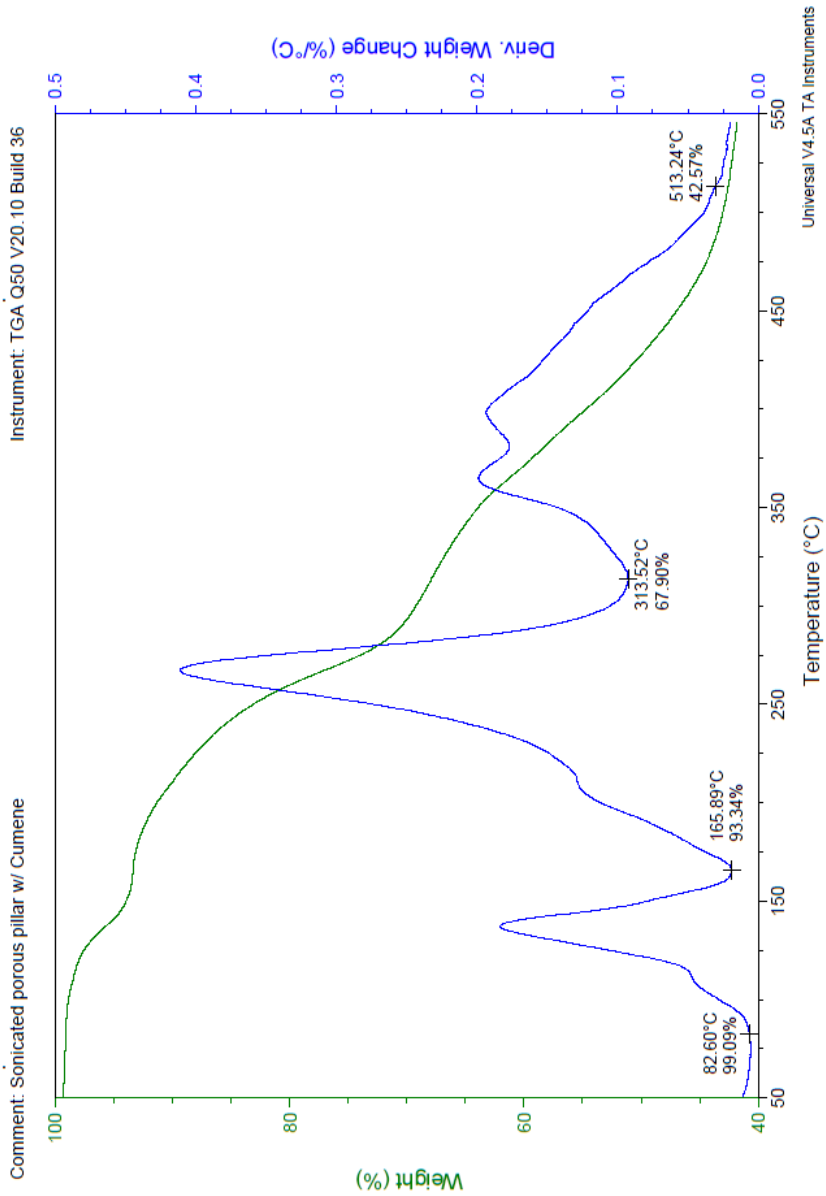

Figure D.16 TGA of the porous Zn(o-tolidine) sonicated with cumene

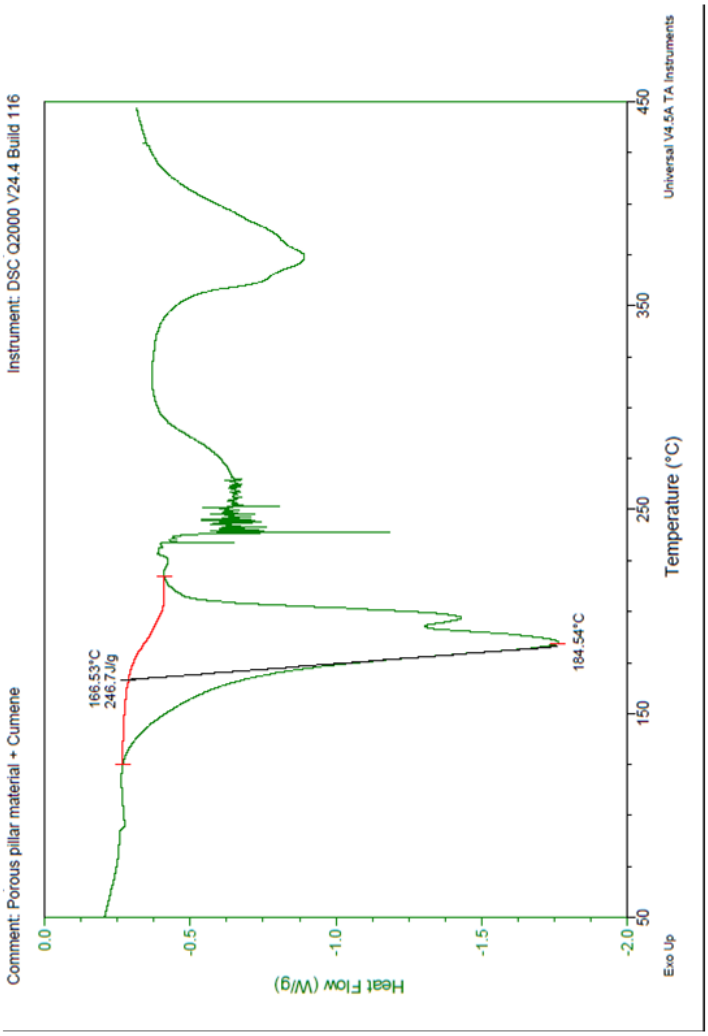

Figure D.17 DSC of the porous Zn(o-tolidine) sonicated with cumene

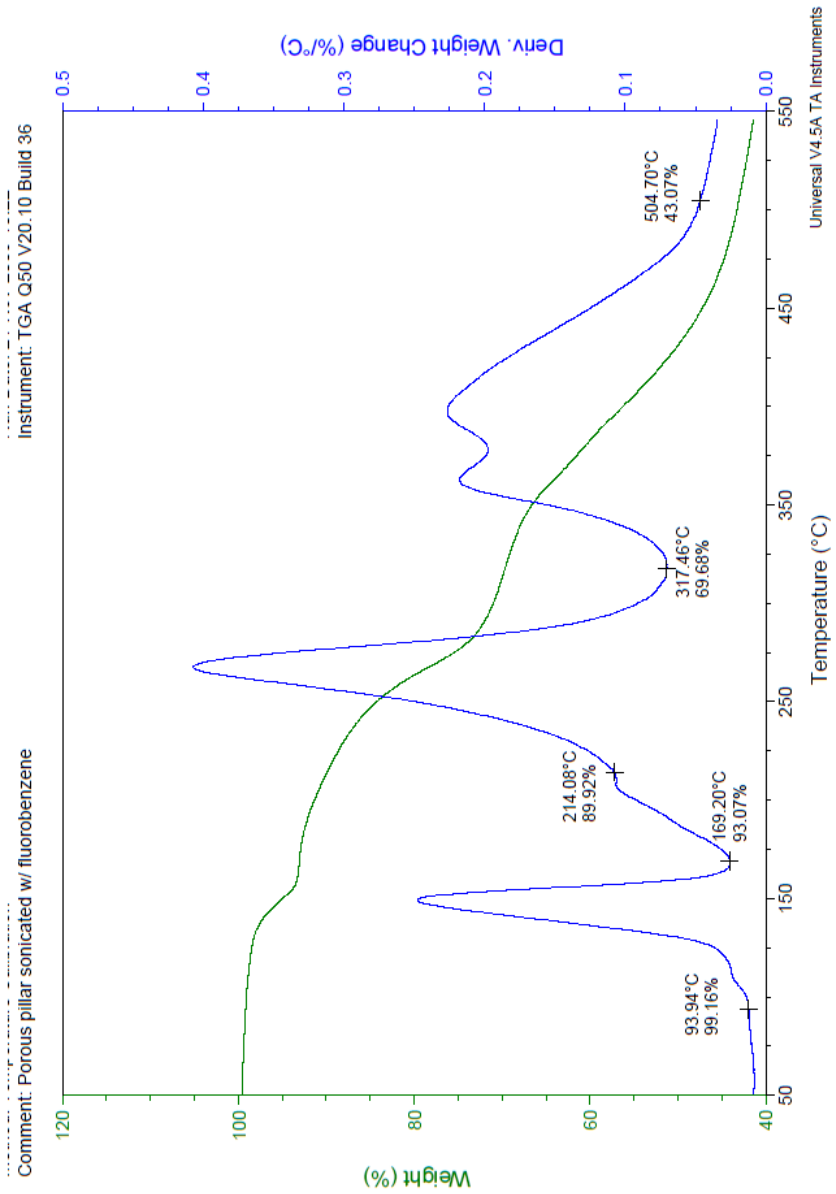

Figure D.18 TGA of the porous Zn(o-tolidine) sonicated with fluorobenzene

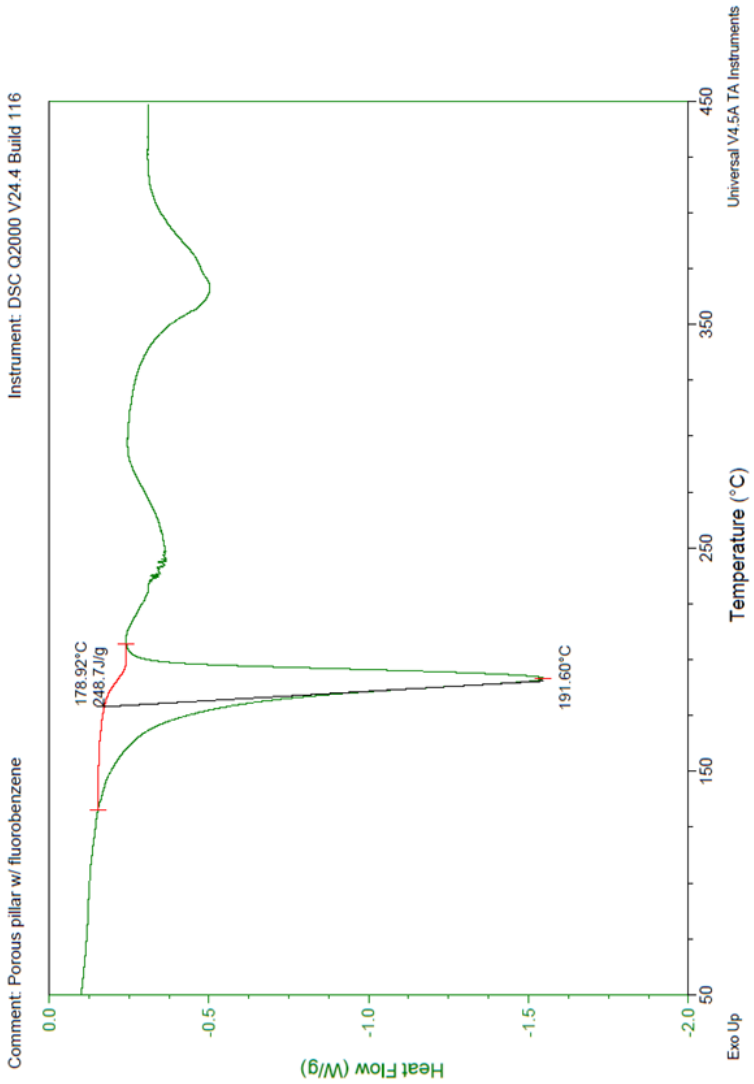

Figure D.19 DSC of the porous Zn(o-tolidine) sonicated with fluorobenzene

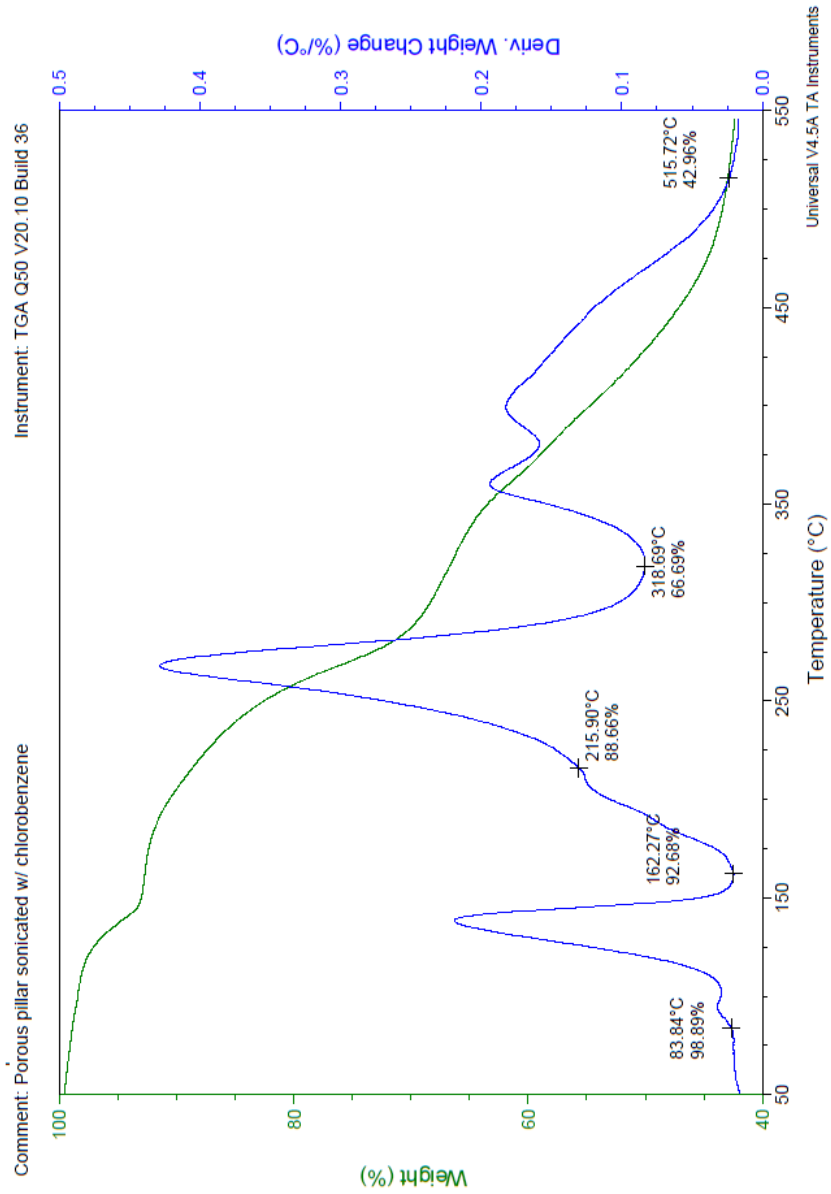

Figure D.20 TGA of the porous Zn(o-tolidine) sonicated with chlorobenzene

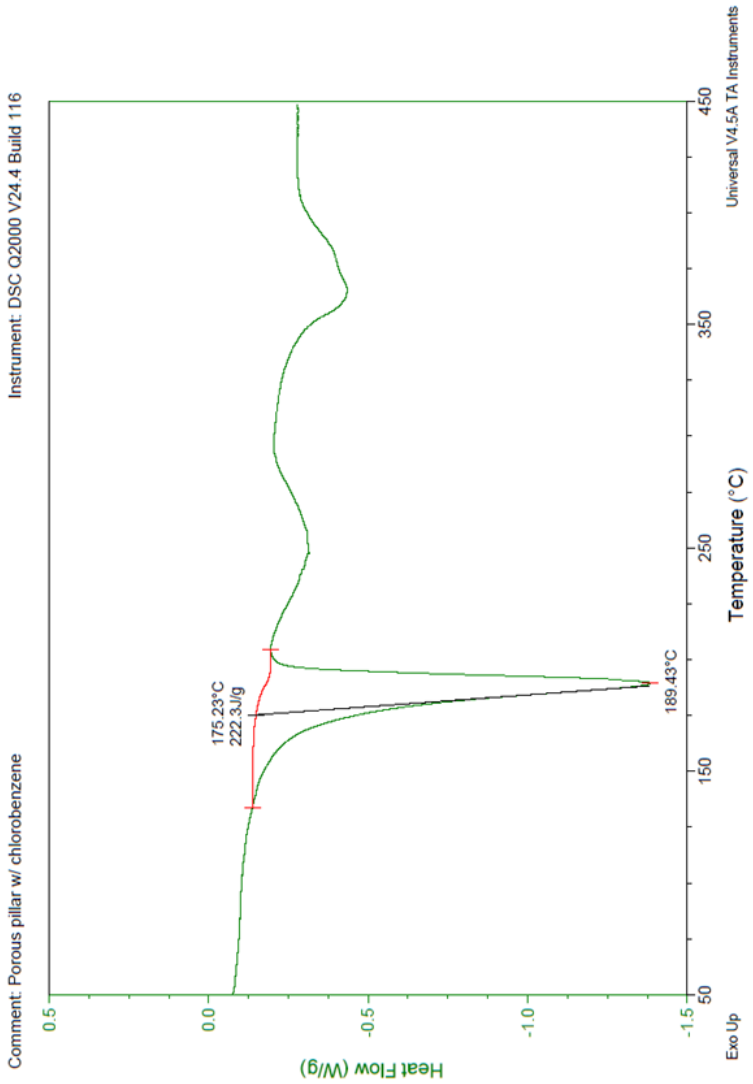

Figure D.21 DSC of the porous Zn(o-tolidine) sonicated with chlorobenzene

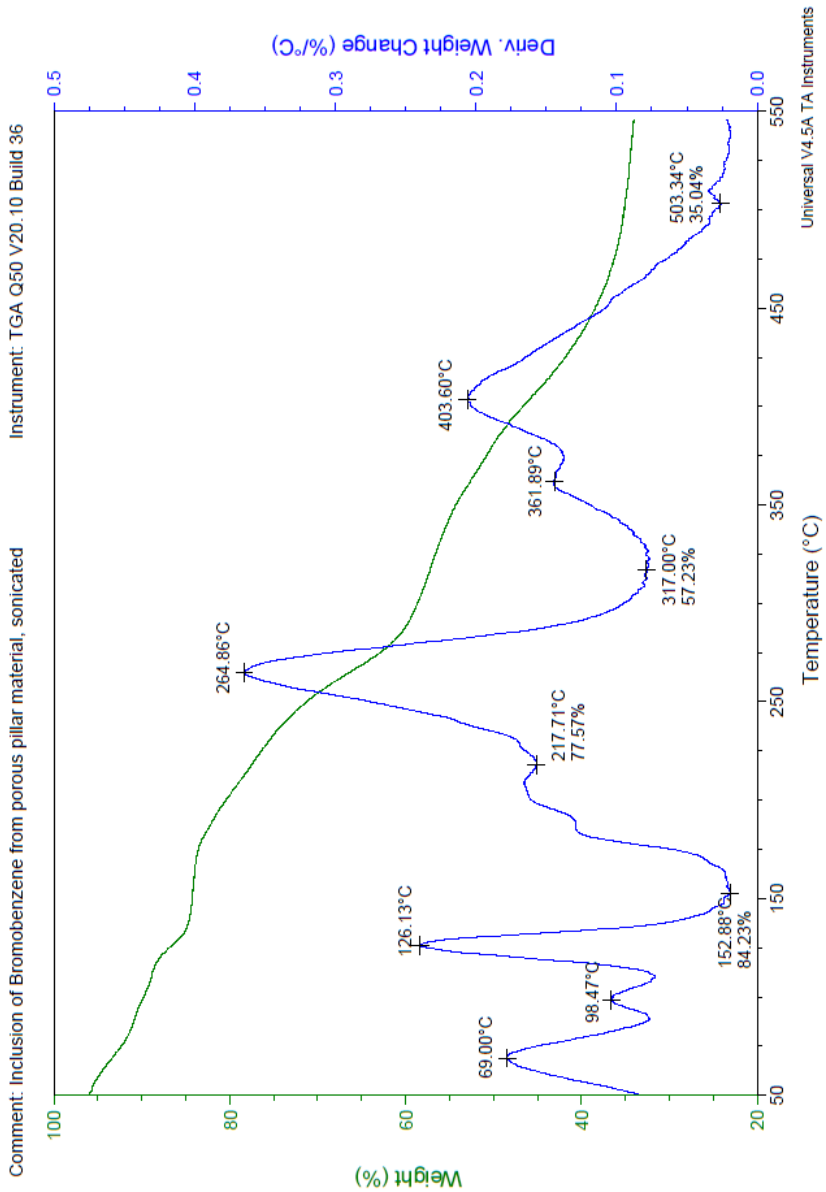

Figure D.22 TGA of the porous Zn(o-tolidine) sonicated with bromobenzene

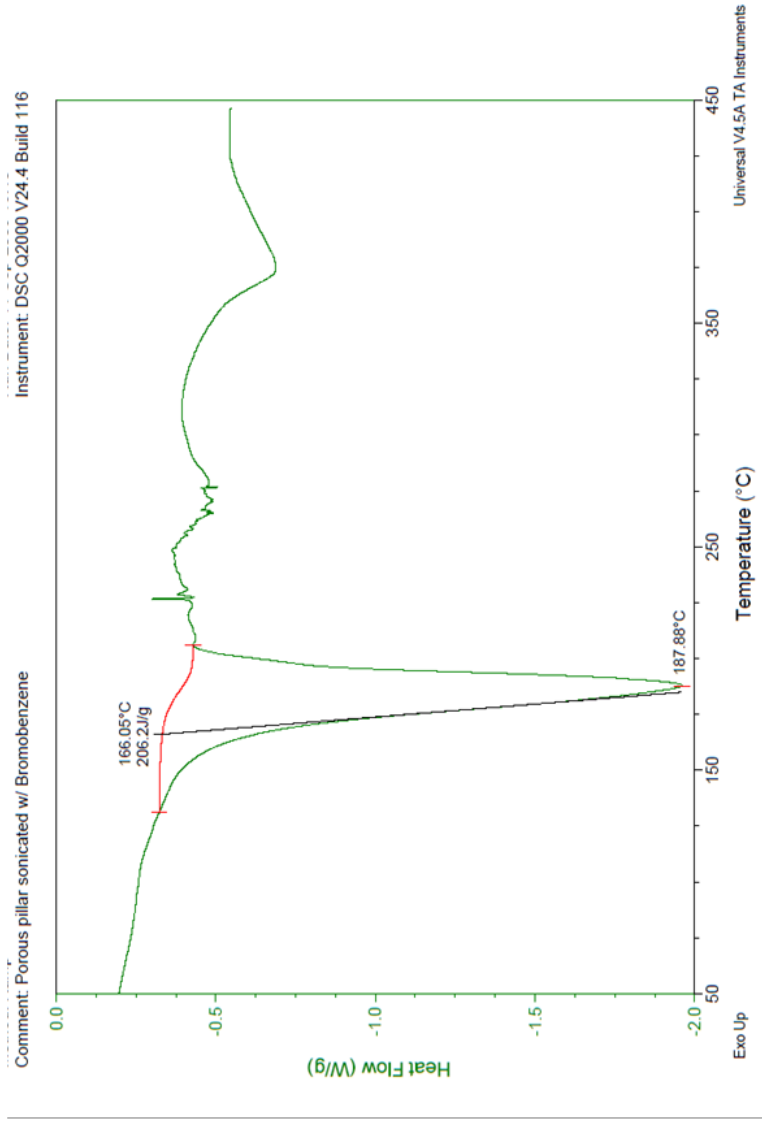

Figure D.23 DSC of the porous Zn(o-tolidine) sonicated with bromobenzene

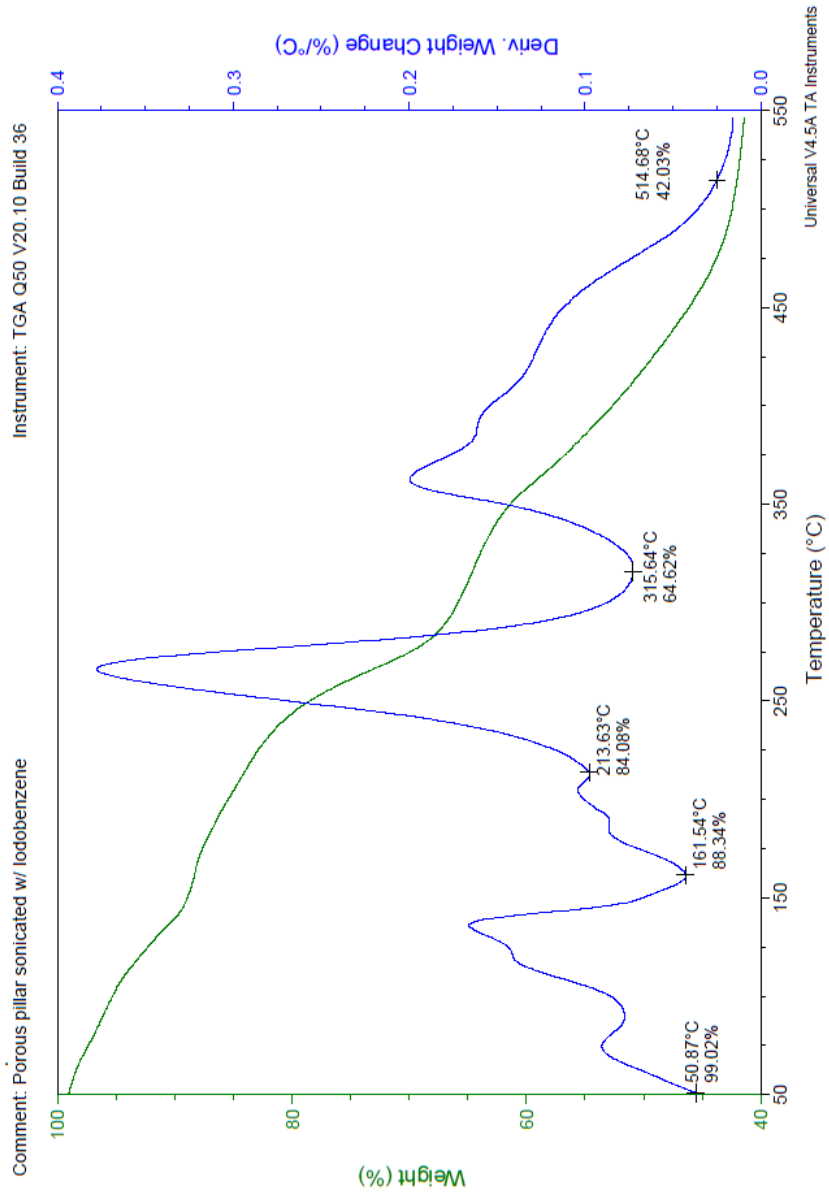

Figure D.24 TGA of the porous Zn(o-tolidine) sonicated with iodobenzene

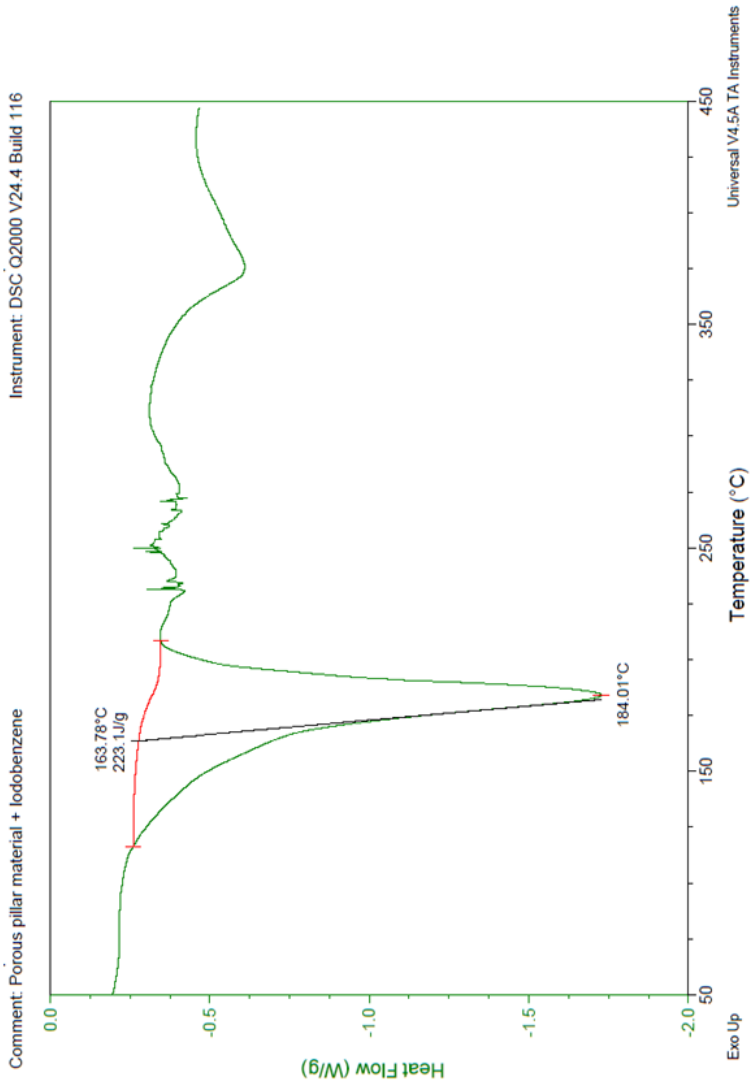

Figure D.25 DSC of the porous Zn(o-tolidine) sonicated with iodobenzene

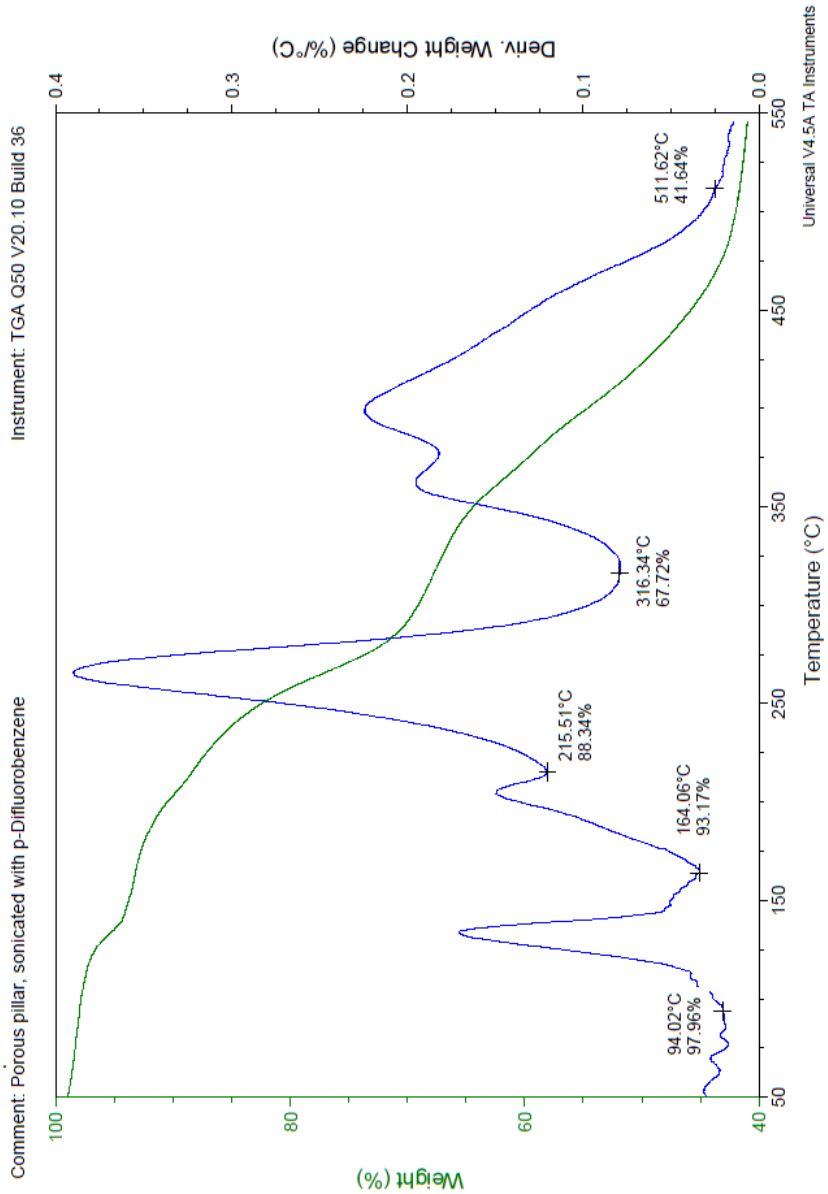

Figure D.26 TGA of the porous Zn(o-tolidine) sonicated with p-difluorobenzene

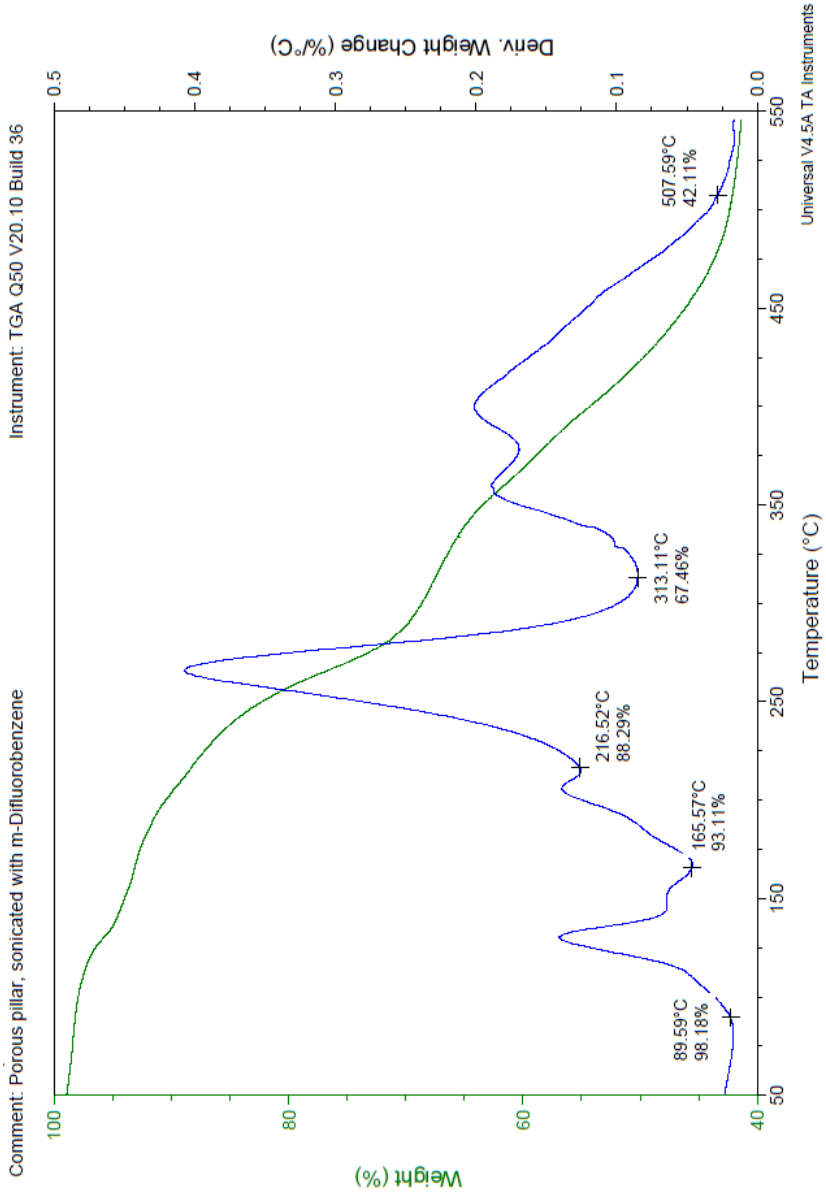

Figure D.27 TGA of the porous Zn(o-tolidine) sonicated with m-difluorobenzene

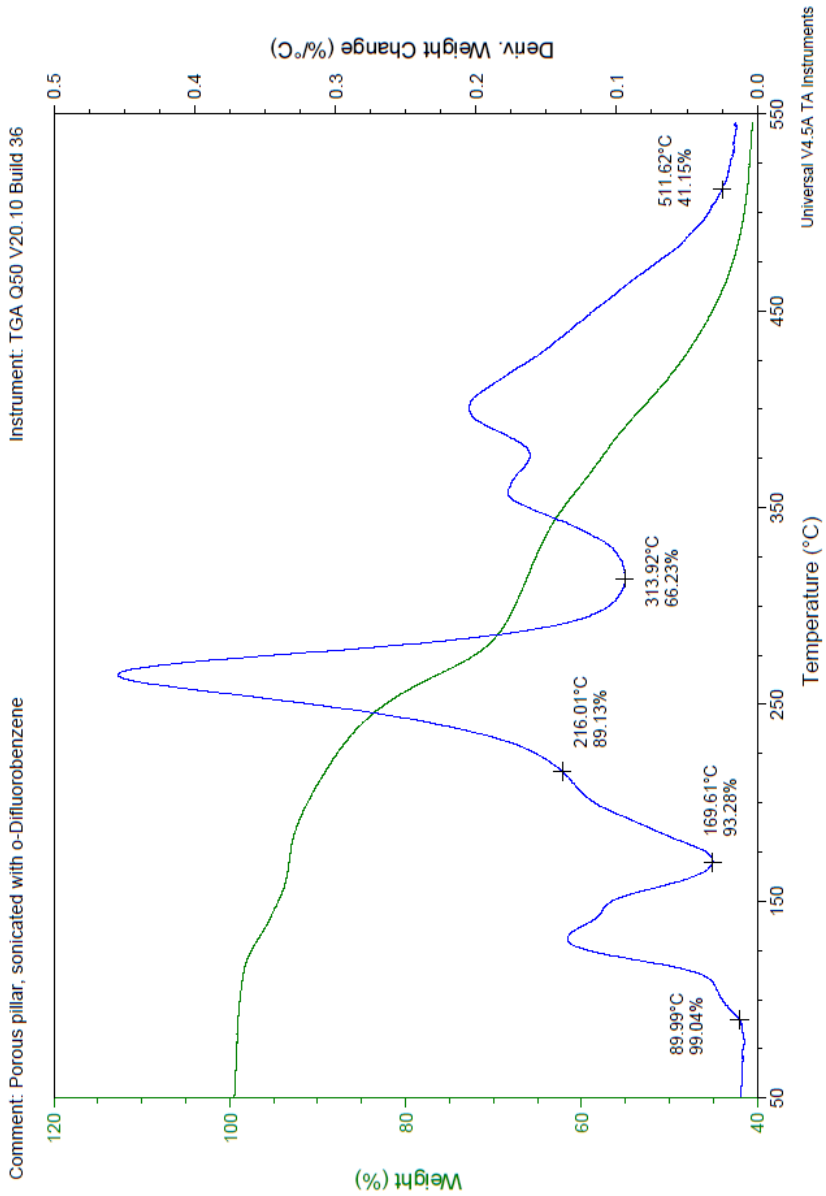

Figure D.28 TGA of the porous Zn(o-tolidine) sonicated with o-difluorobenzene

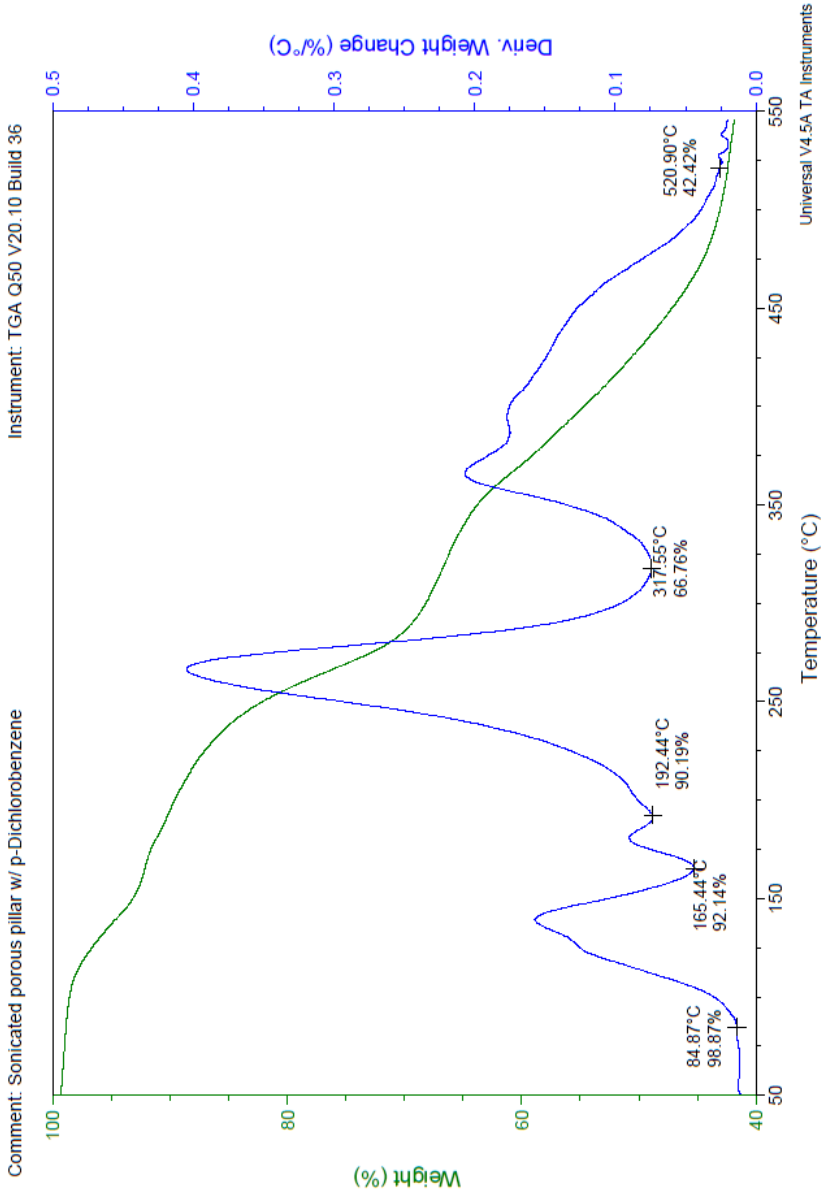

Figure D.29 TGA of the porous Zn(o-tolidine) sonicated with p-dichlorobenzene

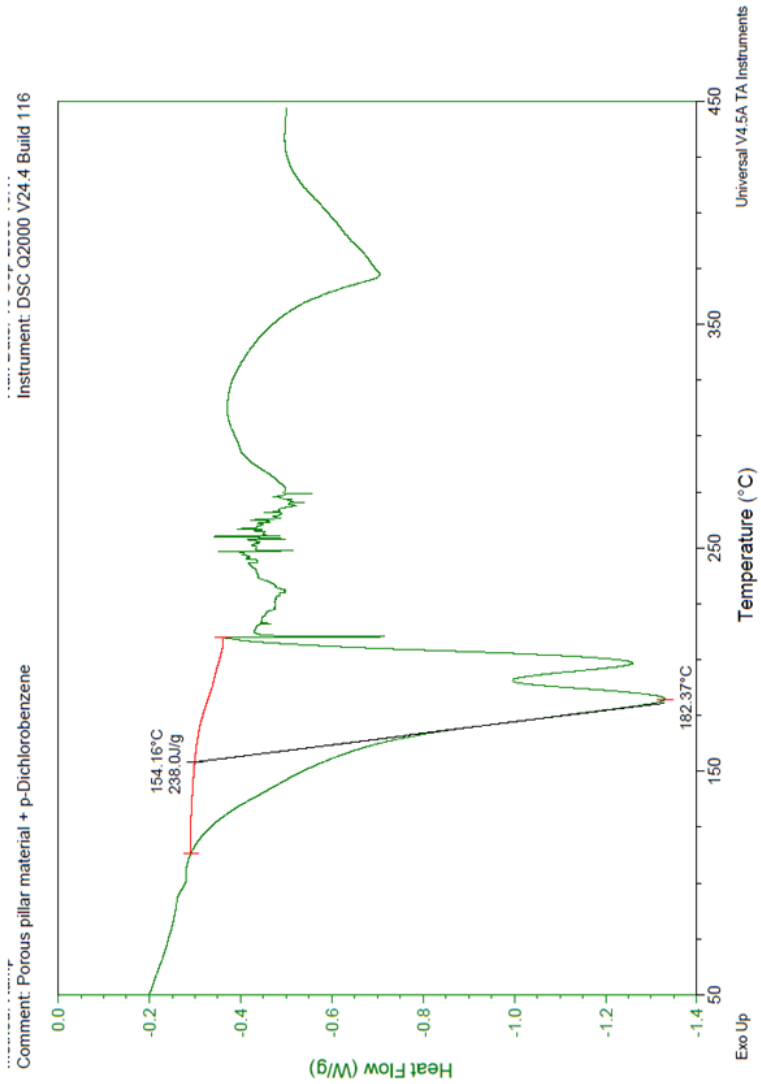

Figure D.30 DSC of the porous Zn(o-tolidine) sonicated with p-dichlorobenzene

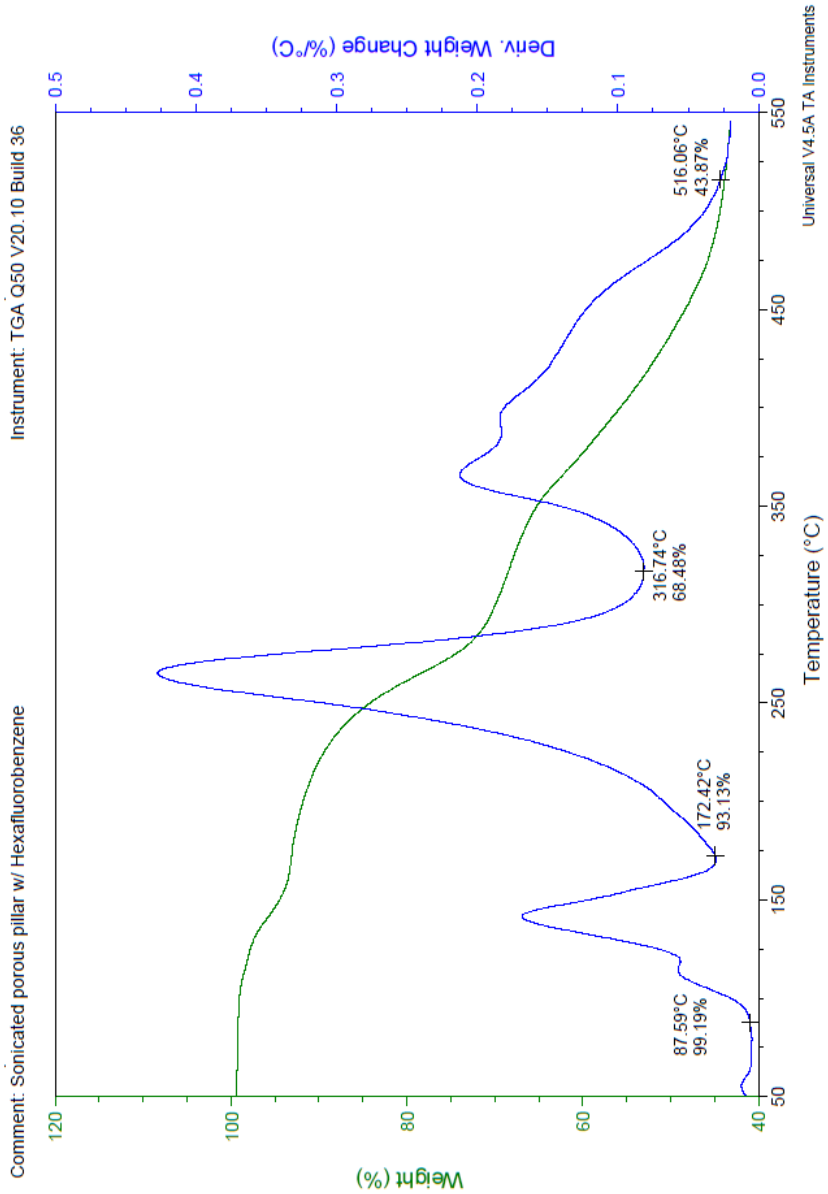

Figure D.31 TGA of the porous Zn(o-tolidine) sonicated with hexafluorobenzene

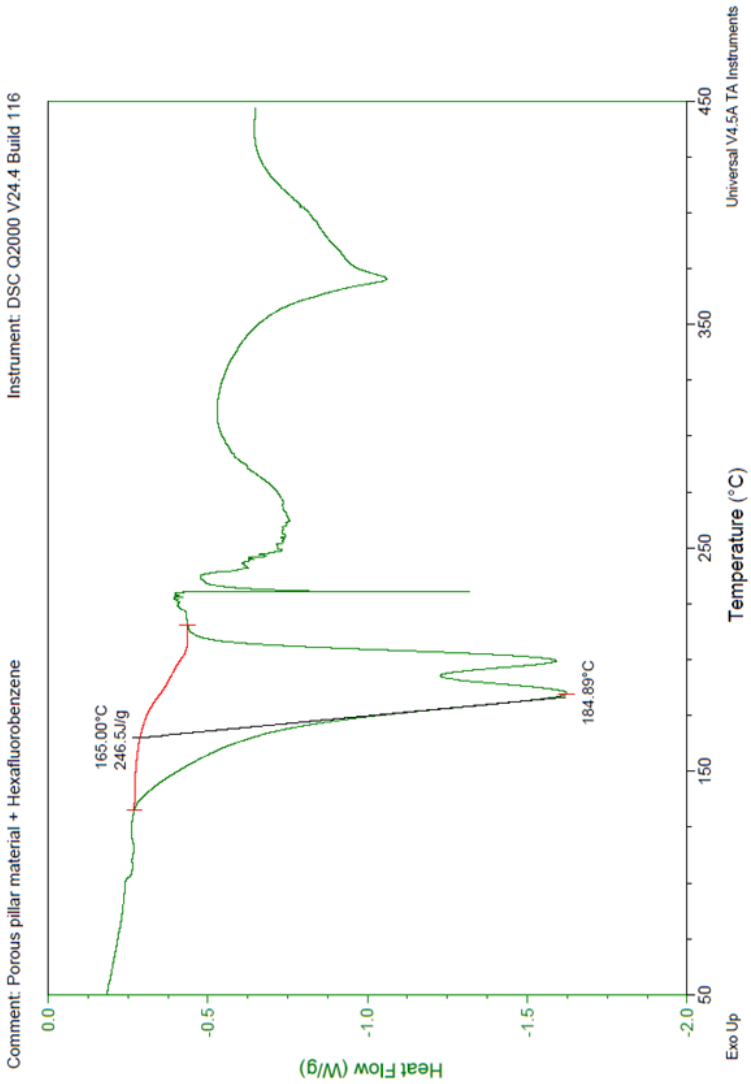

Figure D.32 DSC of the porous Zn(o-tolidine) sonicated with hexafluorobenzene

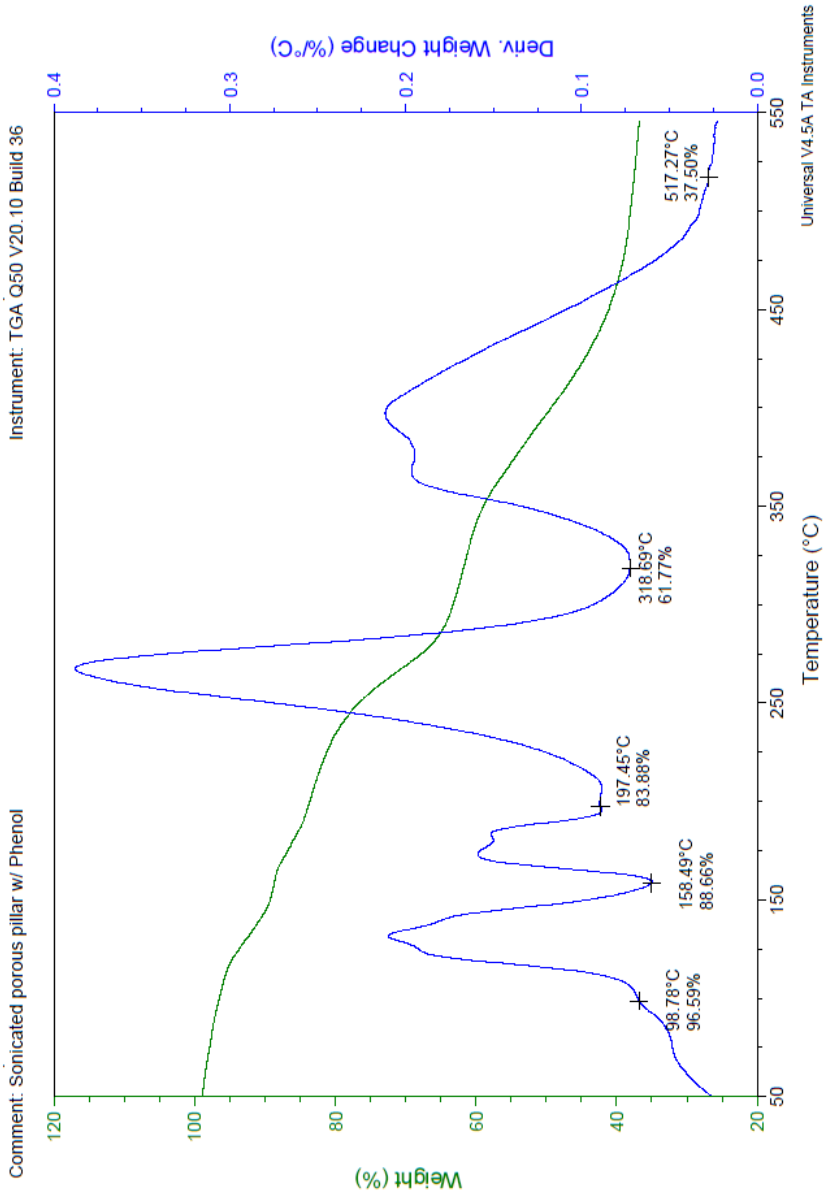

Figure D.33 TGA of the porous Zn(o-tolidine) sonicated with phenol

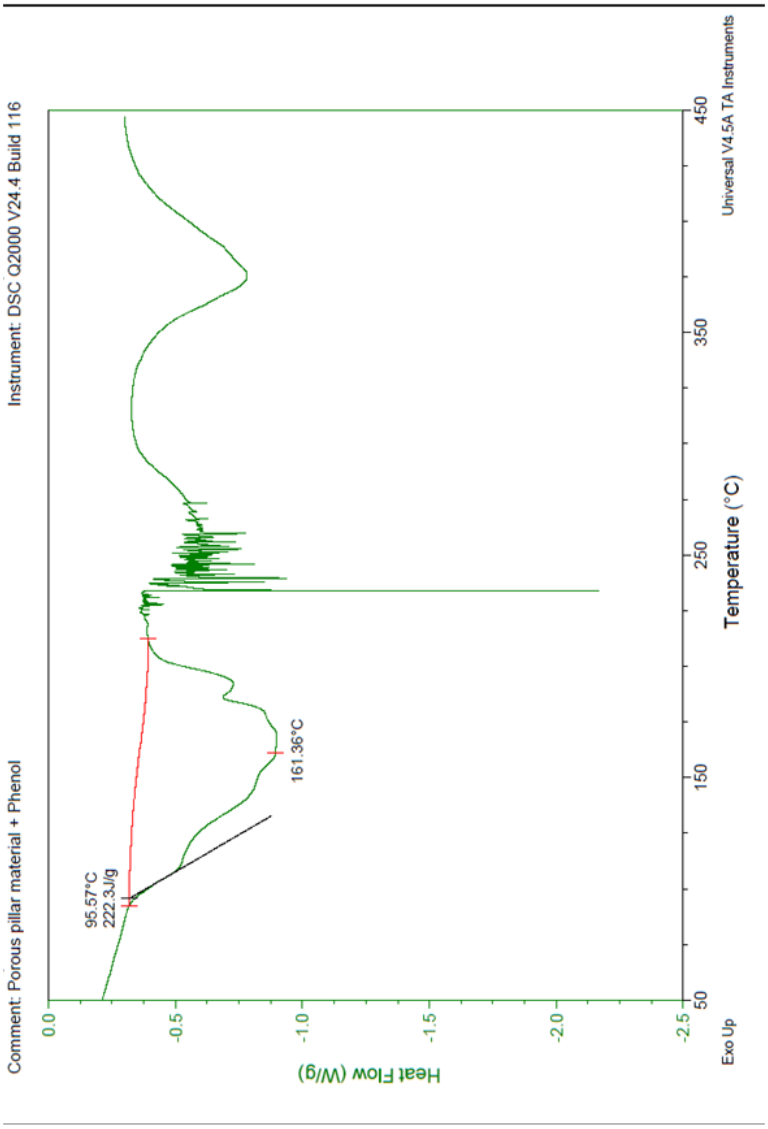

Figure D.34 DSC of the porous Zn(o-tolidine) sonicated with phenol

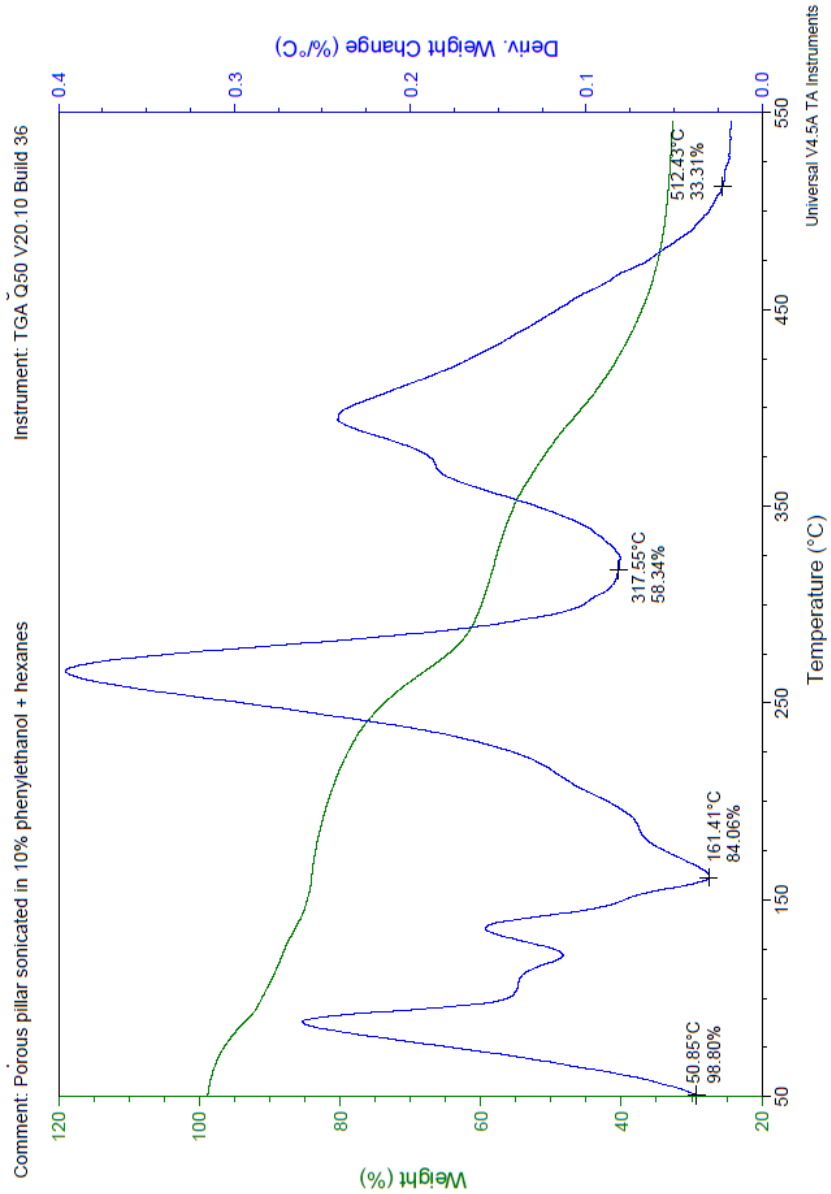

Figure D.35 TGA of the porous Zn(o-tolidine) sonicated with 2-phenylethanol

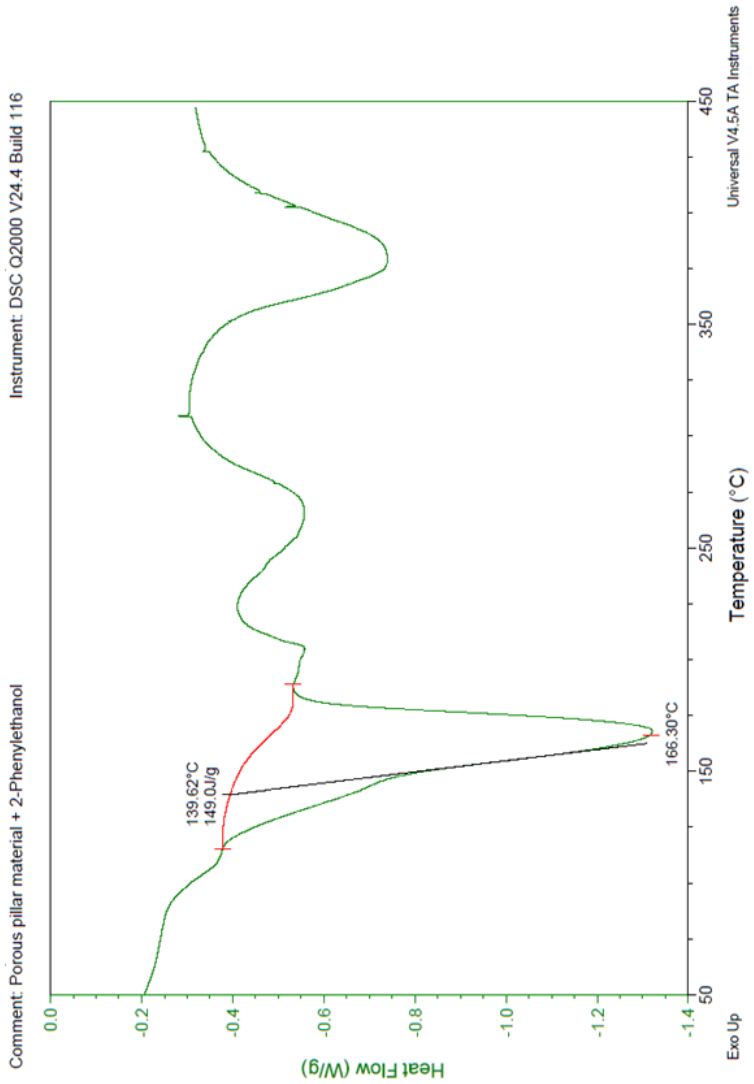

Figure D.36 DSC of the porous Zn(o-tolidine) sonicated with 2-phenylethanol

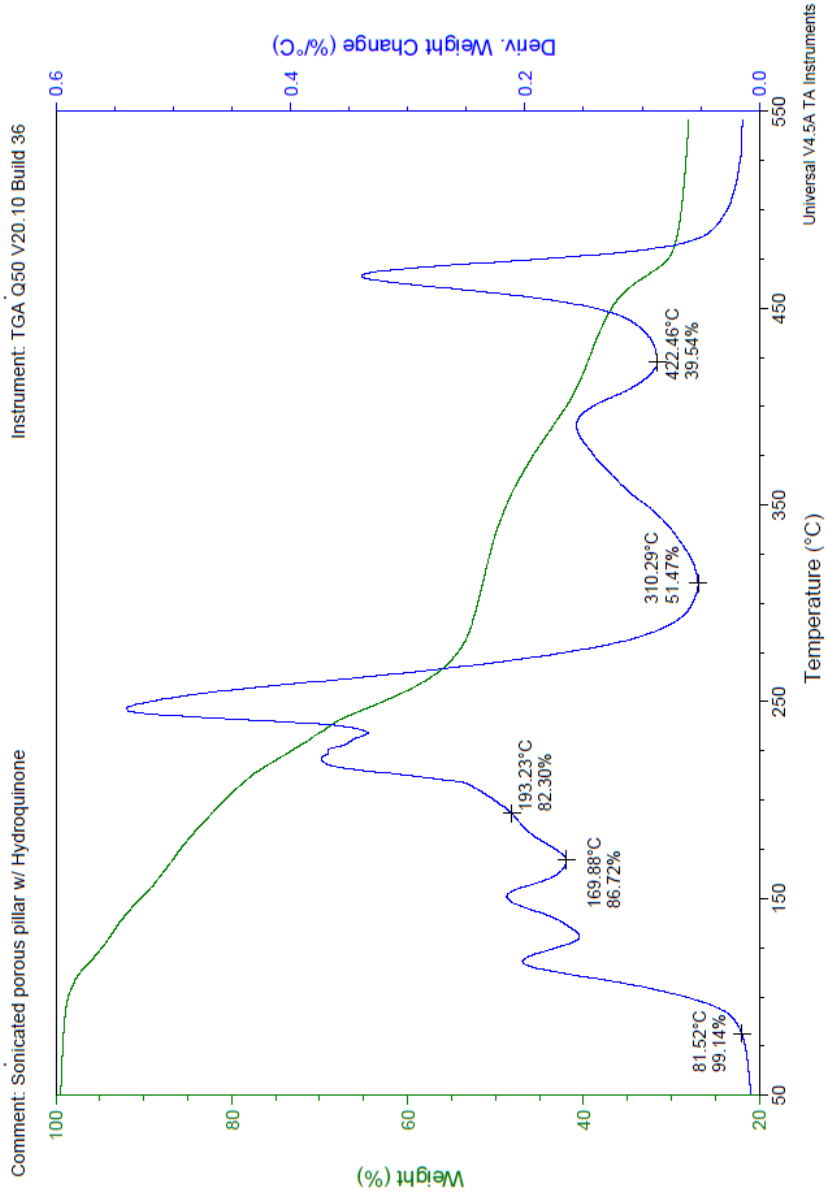

Figure D.37 TGA of the porous Zn(o-tolidine) sonicated with hydroquinone

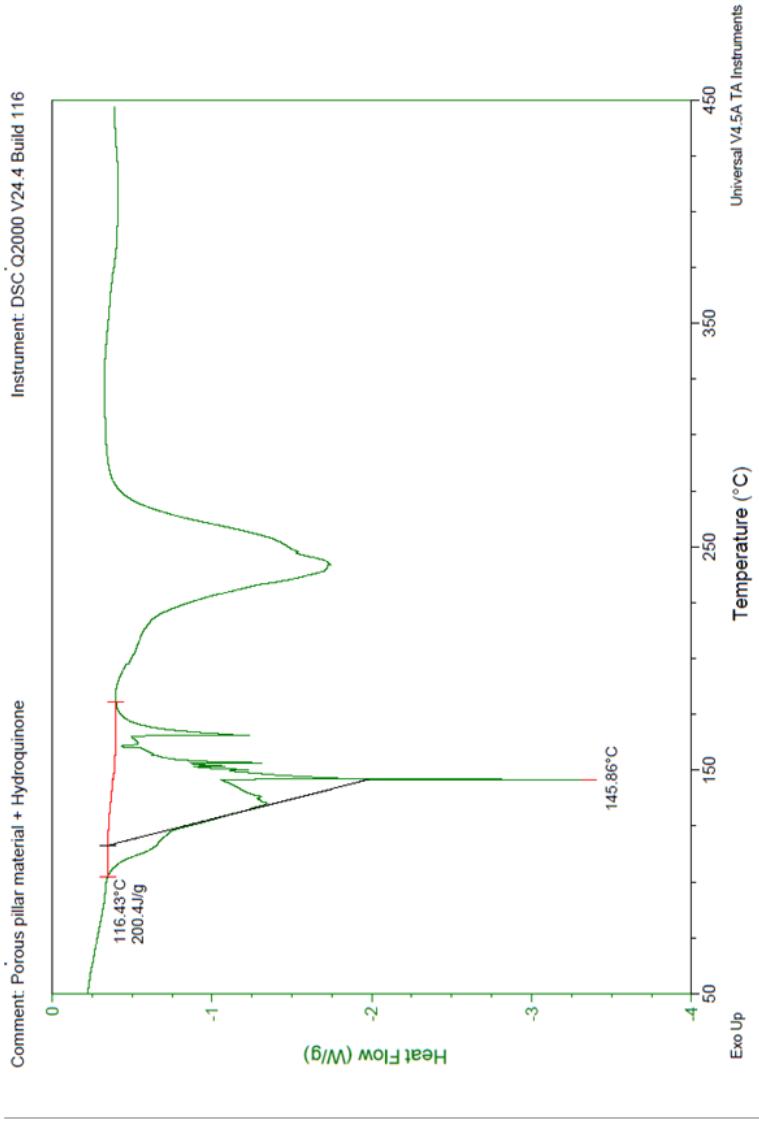

Figure D.38 DSC of the porous Zn(o-tolidine) sonicated with hydroquinone

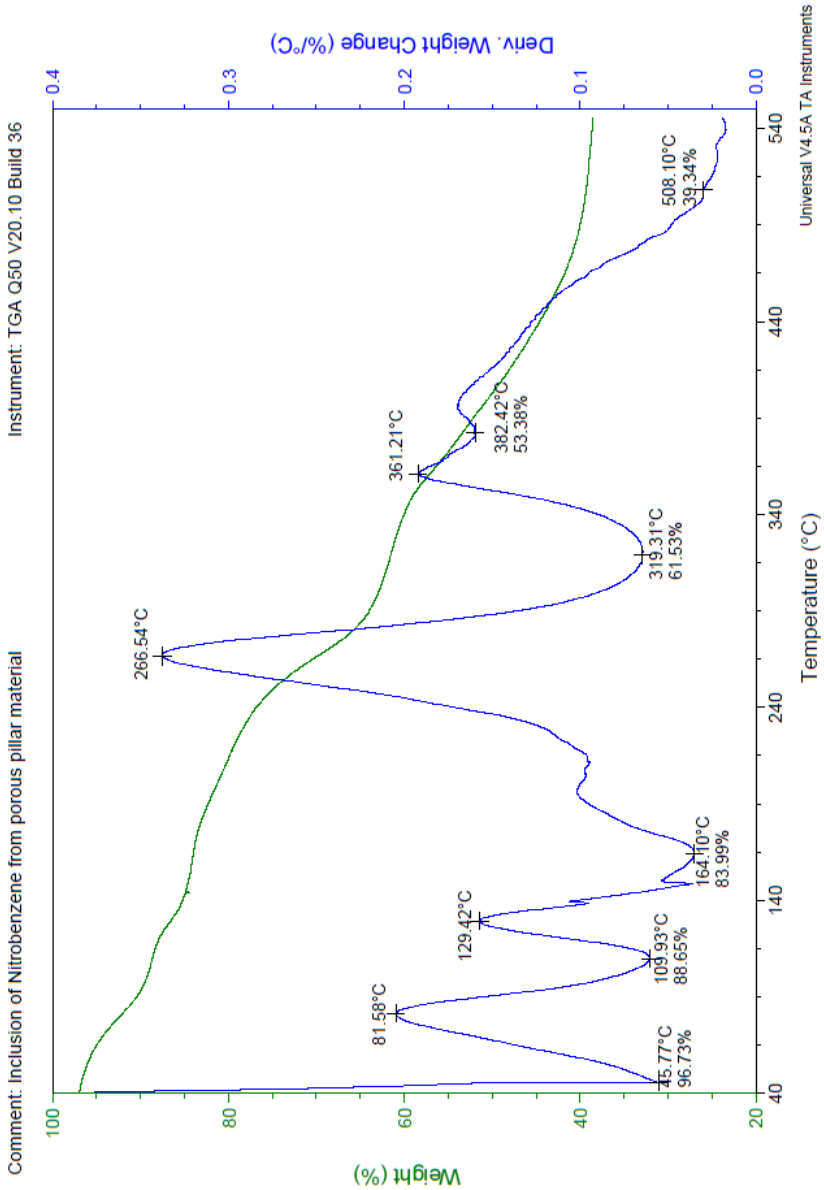

Figure D.39 TGA of the porous Zn(o-tolidine) sonicated with nitrobenzene

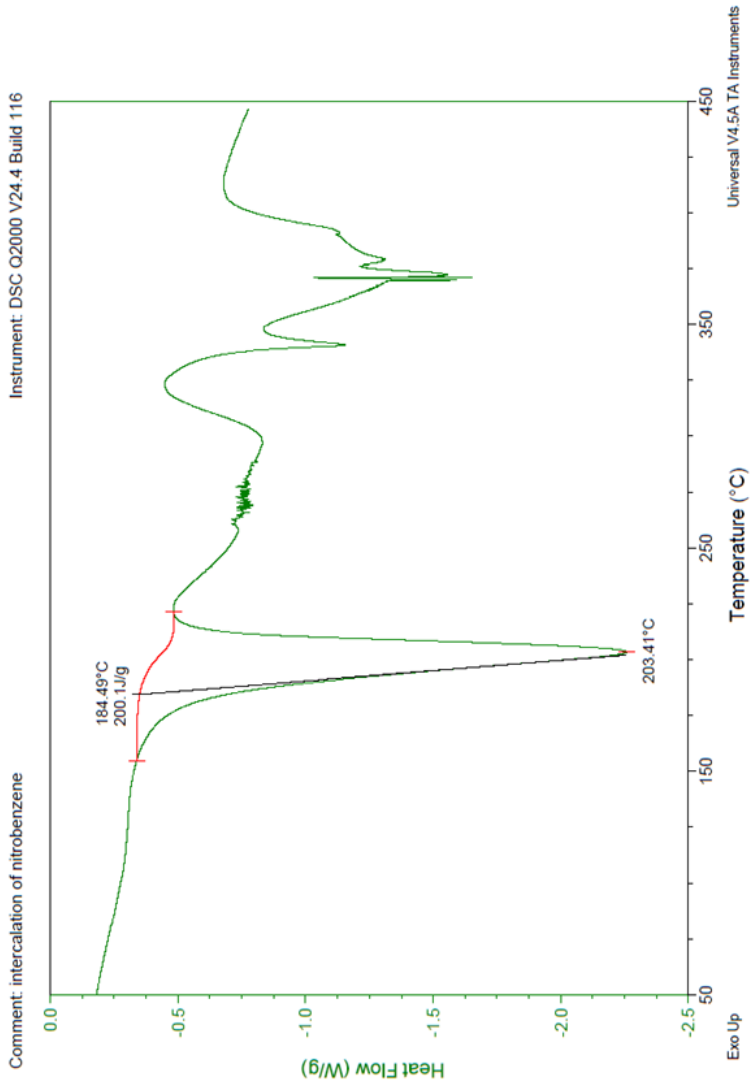

Figure D.40 DSC of the porous Zn(o-tolidine) sonicated with nitrobenzene

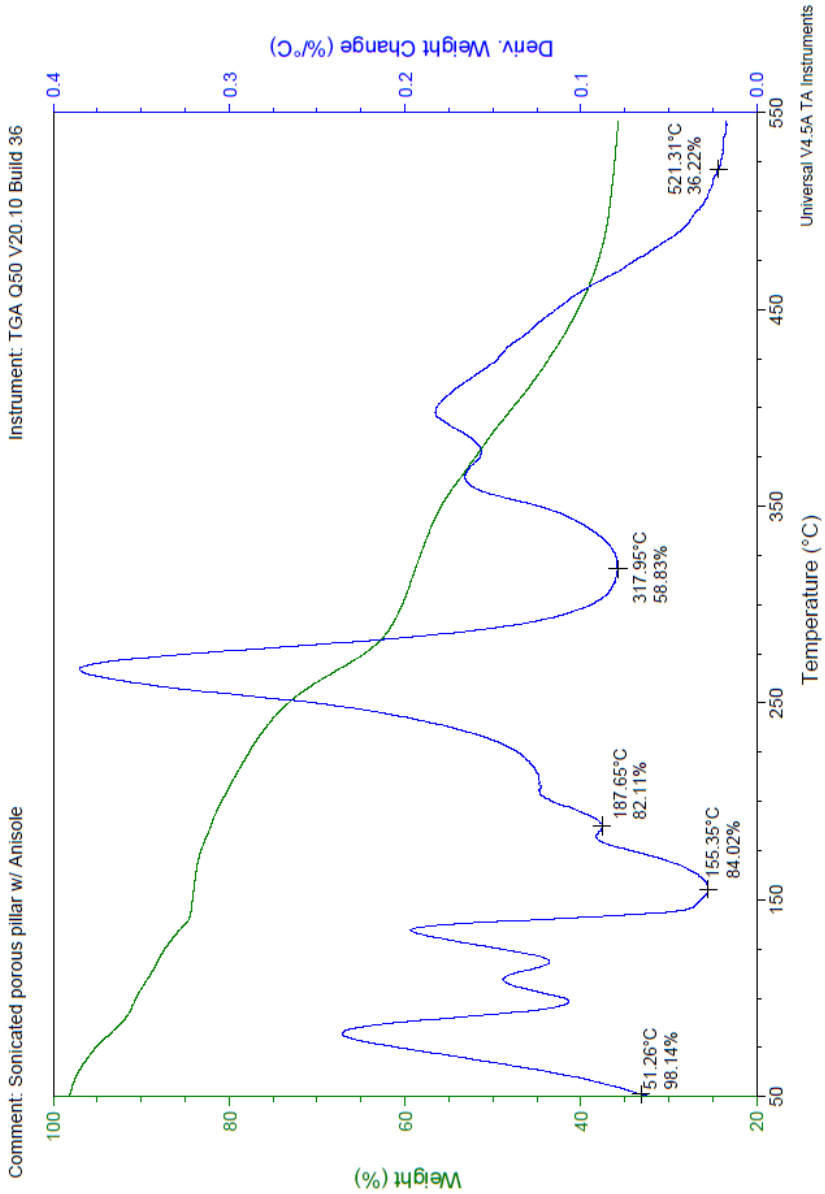

Figure D.41 TGA of the porous Zn(o-tolidine) sonicated with anisole

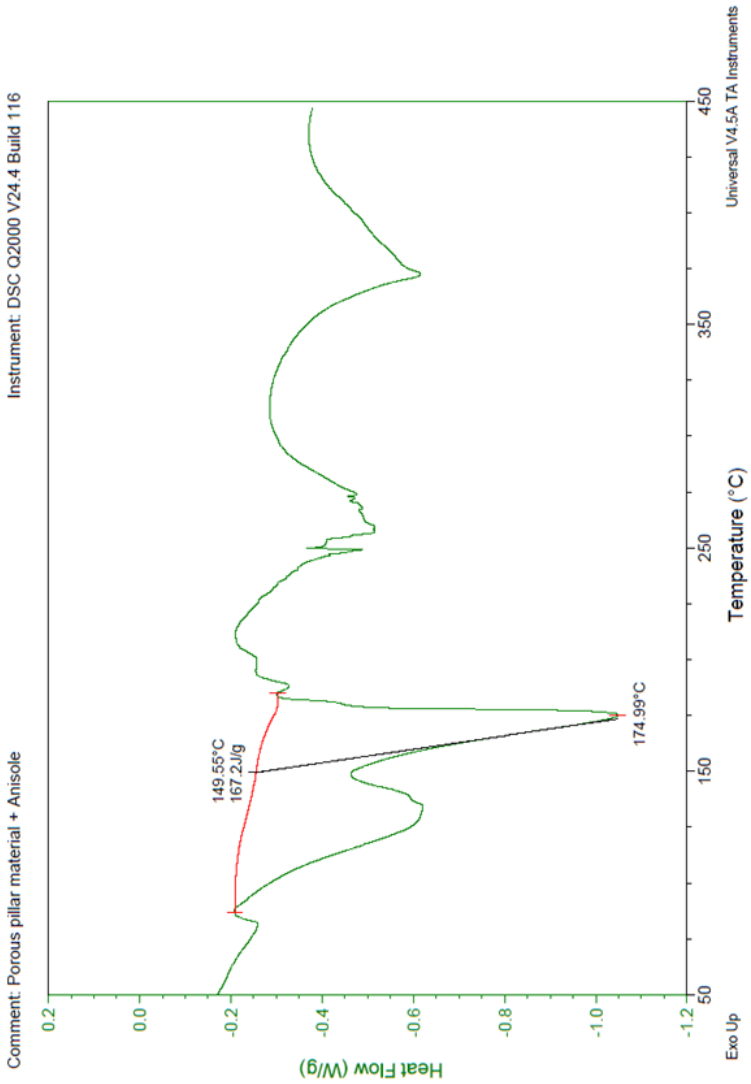

Figure D.42 DSC of the porous Zn(o-tolidine) sonicated with anisole

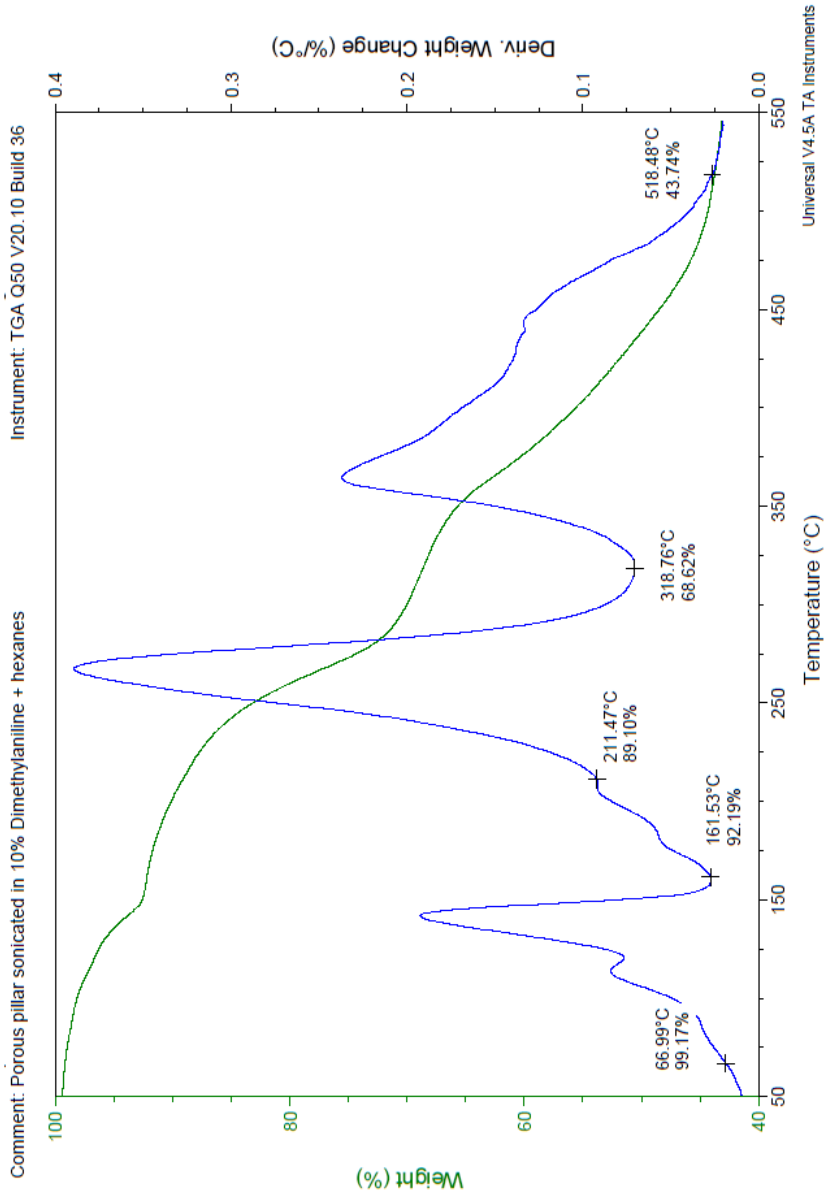

Figure D.43 TGA of the porous Zn(o-tolidine) sonicated with N,N-dimethylaniline

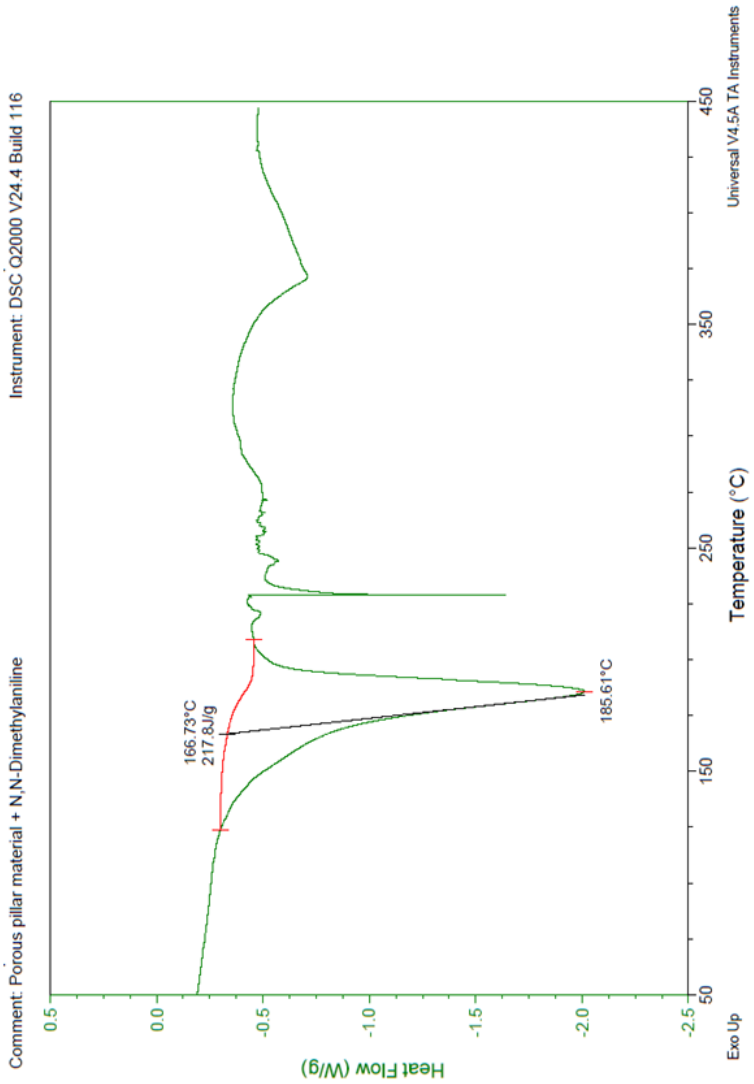

Figure D.44 DSC of the porous Zn(o-tolidine) sonicated with N,N-dimethylaniline

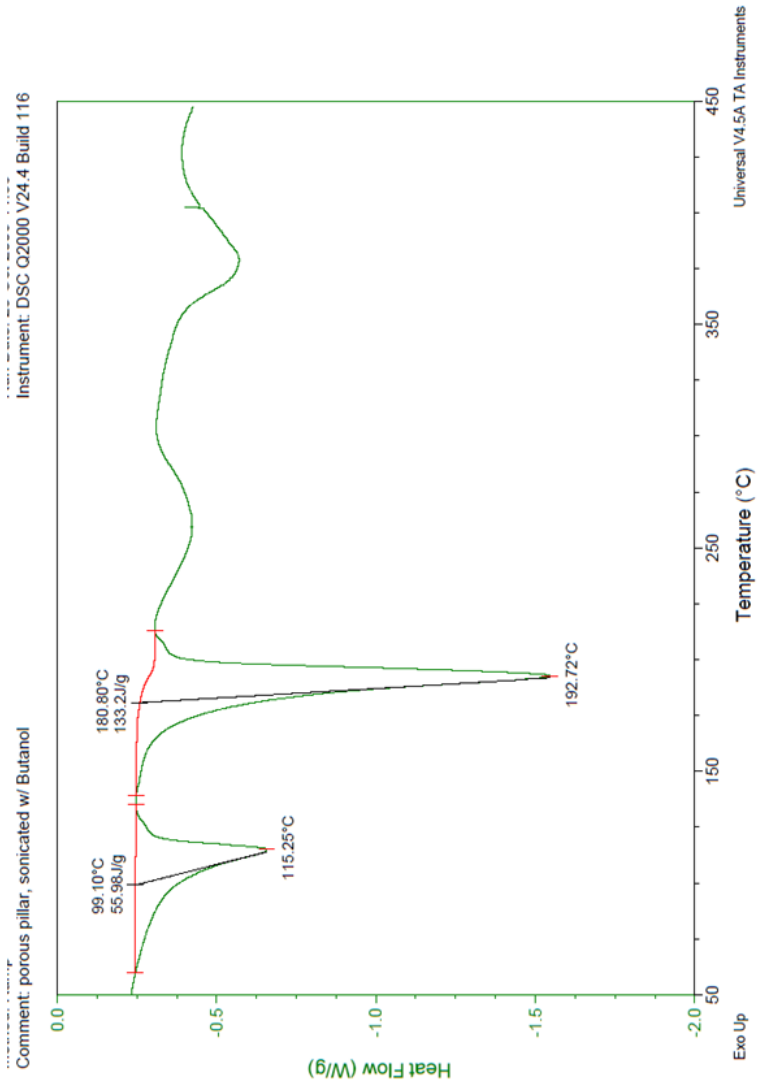

Figure D.45 DSC of the porous Zn(o-tolidine) sonicated with butanol

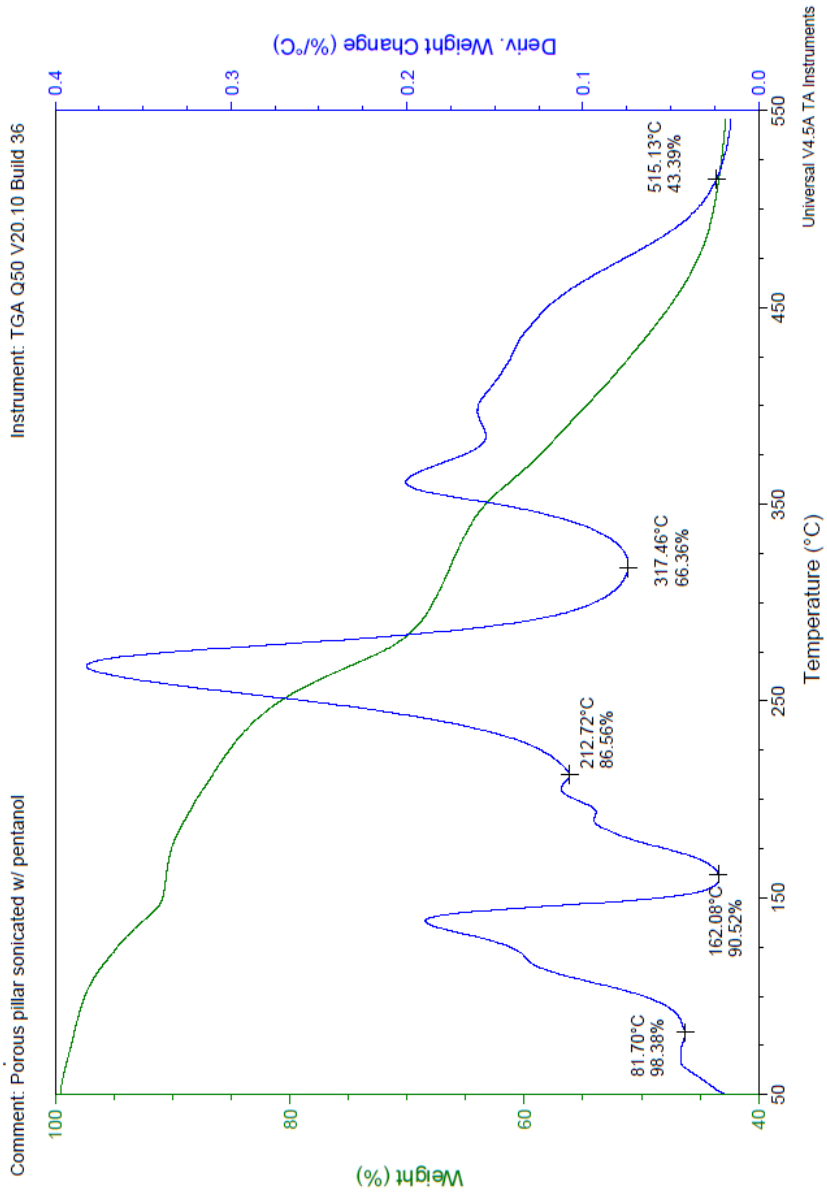

Figure D.46 TGA of the porous Zn(o-tolidine) sonicated with pentanol

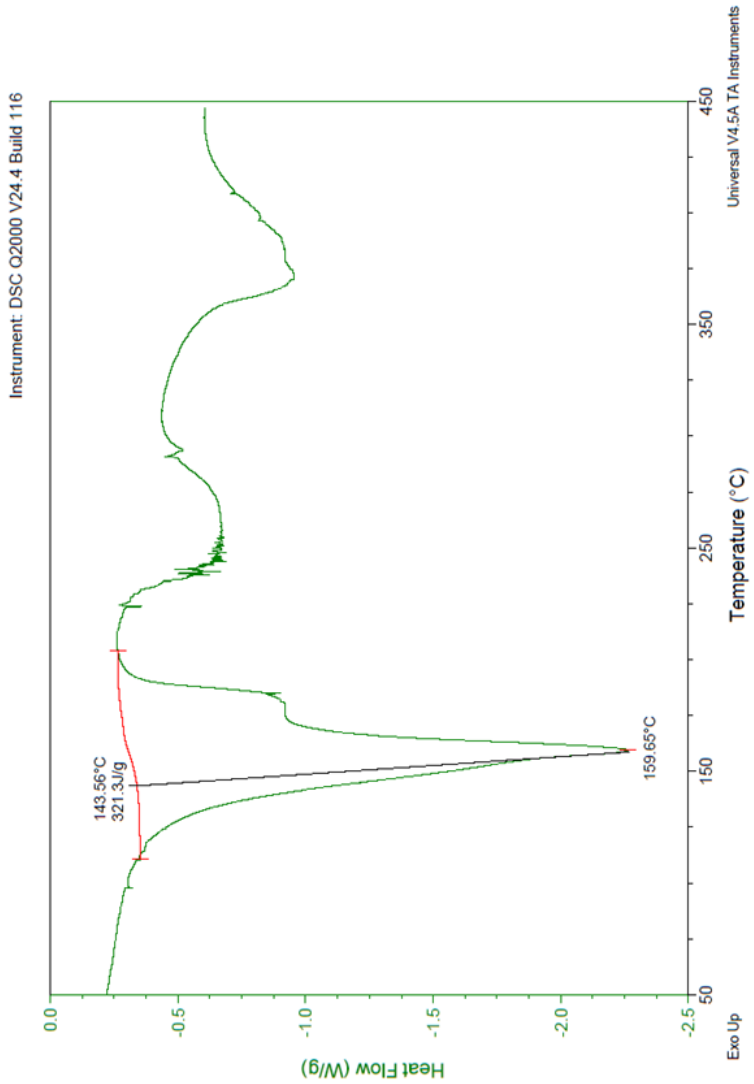

Figure D.47 DSC of the porous Zn(o-tolidine) sonicated with pentanol

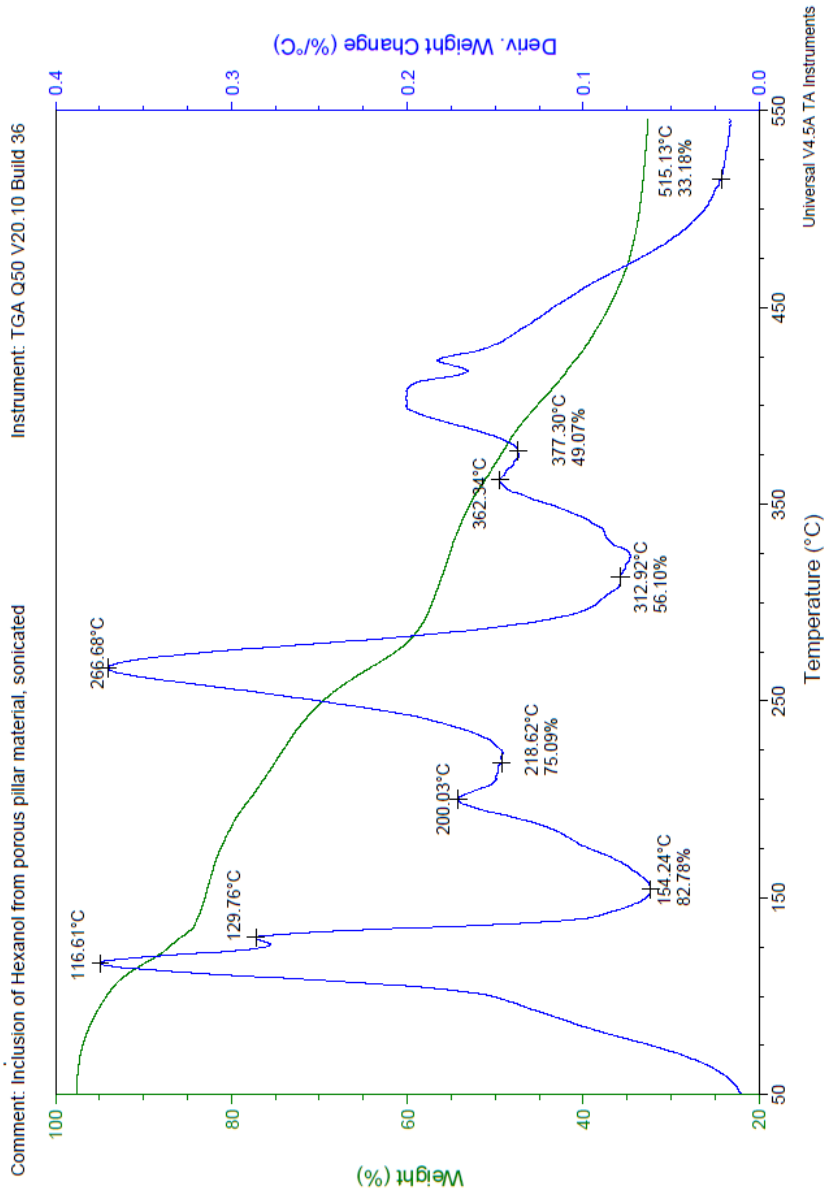

Figure D.48 TGA of the porous Zn(o-tolidine) sonicated with hexanol

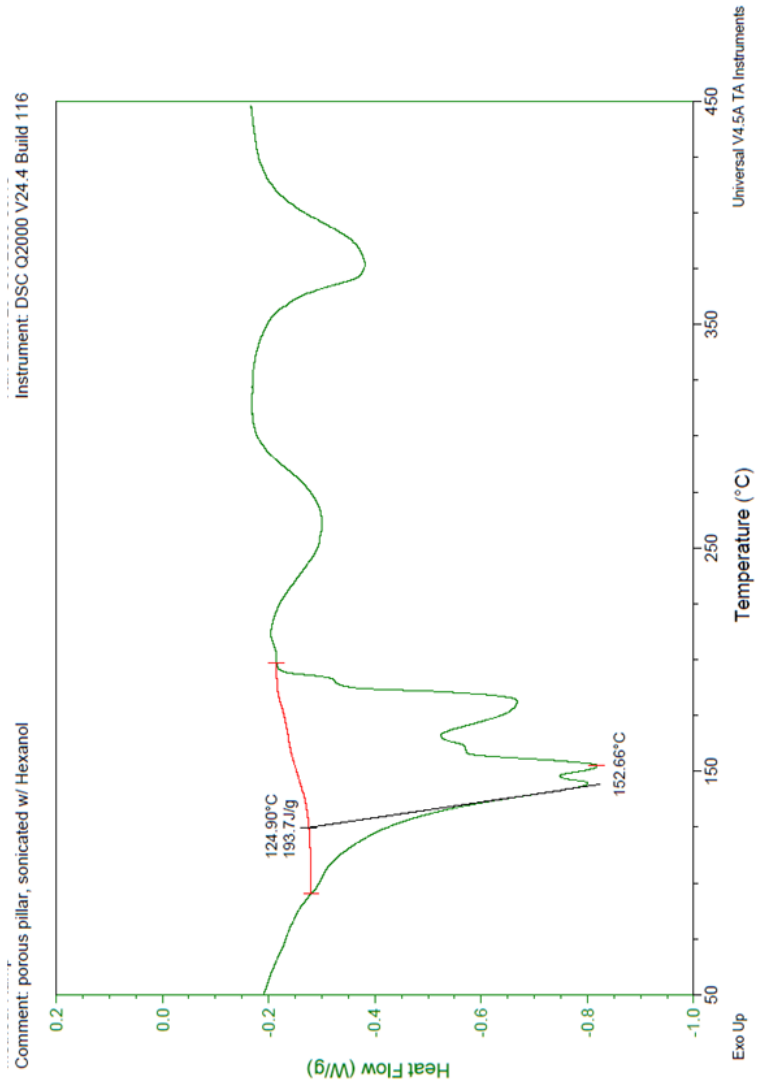

Figure D.49 DSC of the porous Zn(o-tolidine) sonicated with hexanol

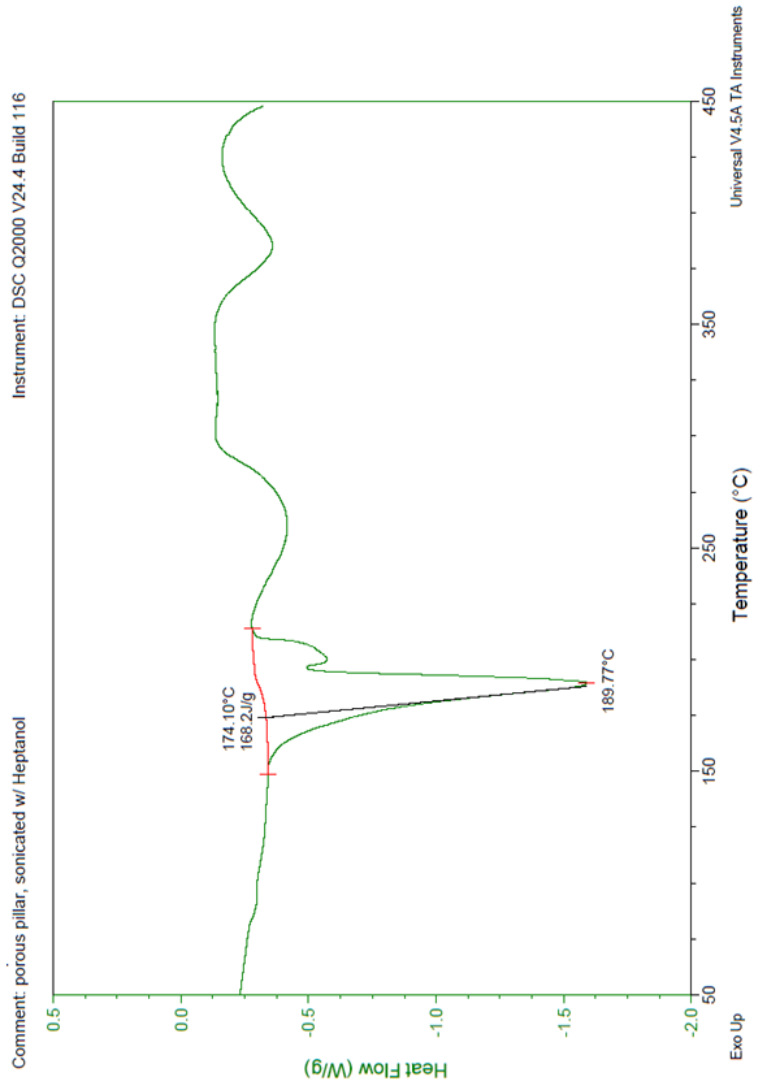

Figure D.50 DSC of the porous Zn(o-tolidine) sonicated with heptanol

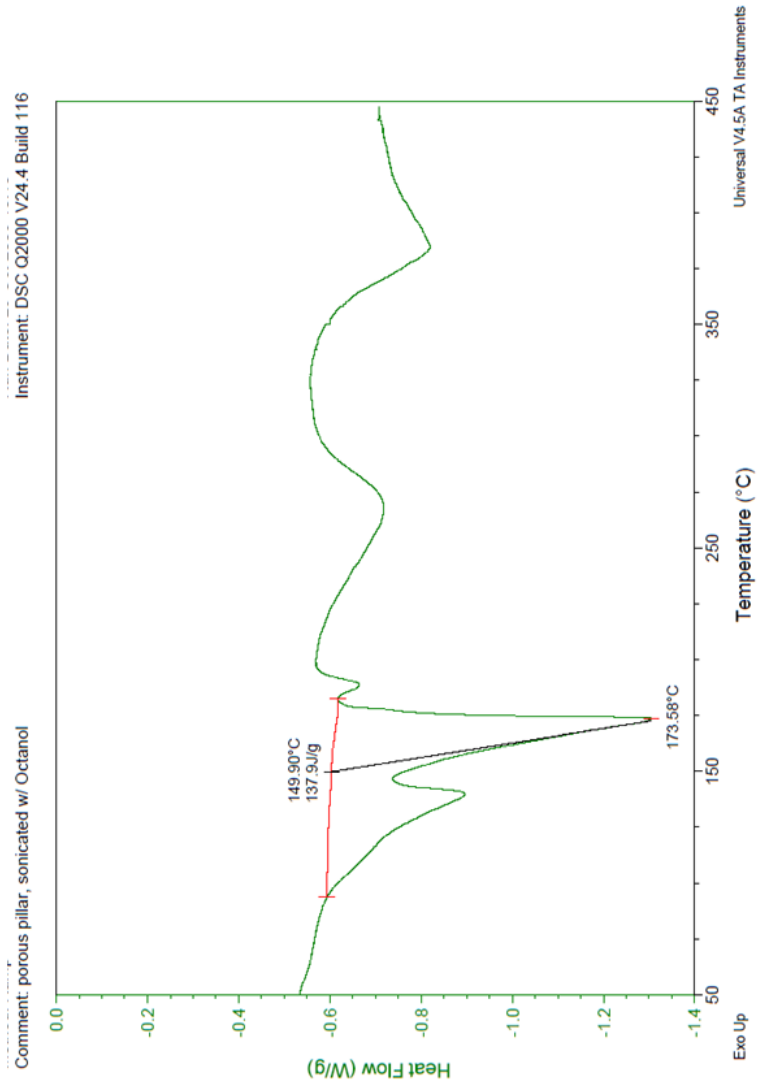

Figure D.51 DSC of the porous Zn(o-tolidine) sonicated with octanol

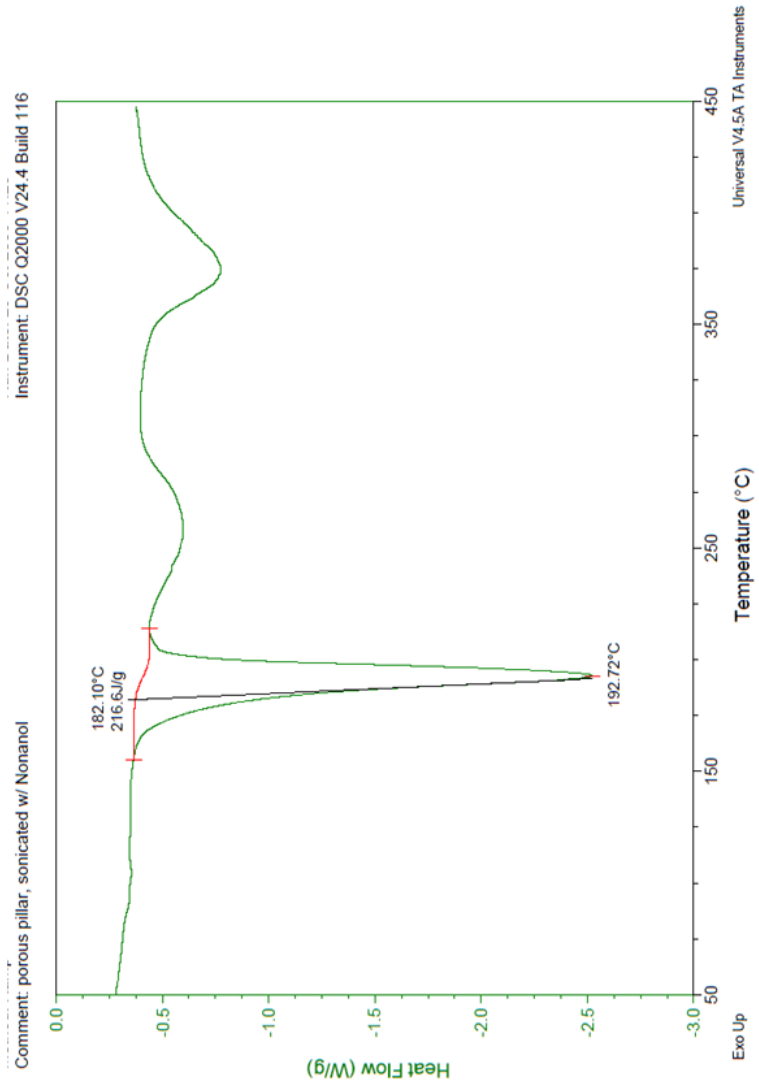

Figure D.52 DSC of the porous Zn(o-tolidine) sonicated with nonanol

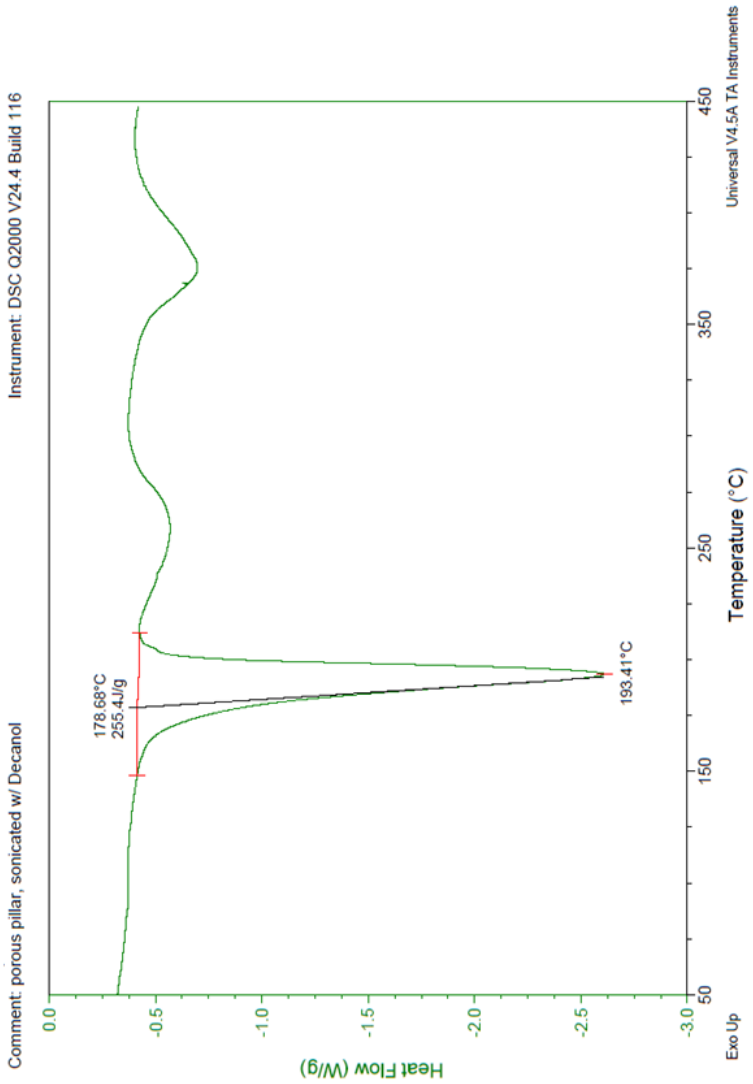

Figure D.53 DSC of the porous Zn(o-tolidine) sonicated with decanol

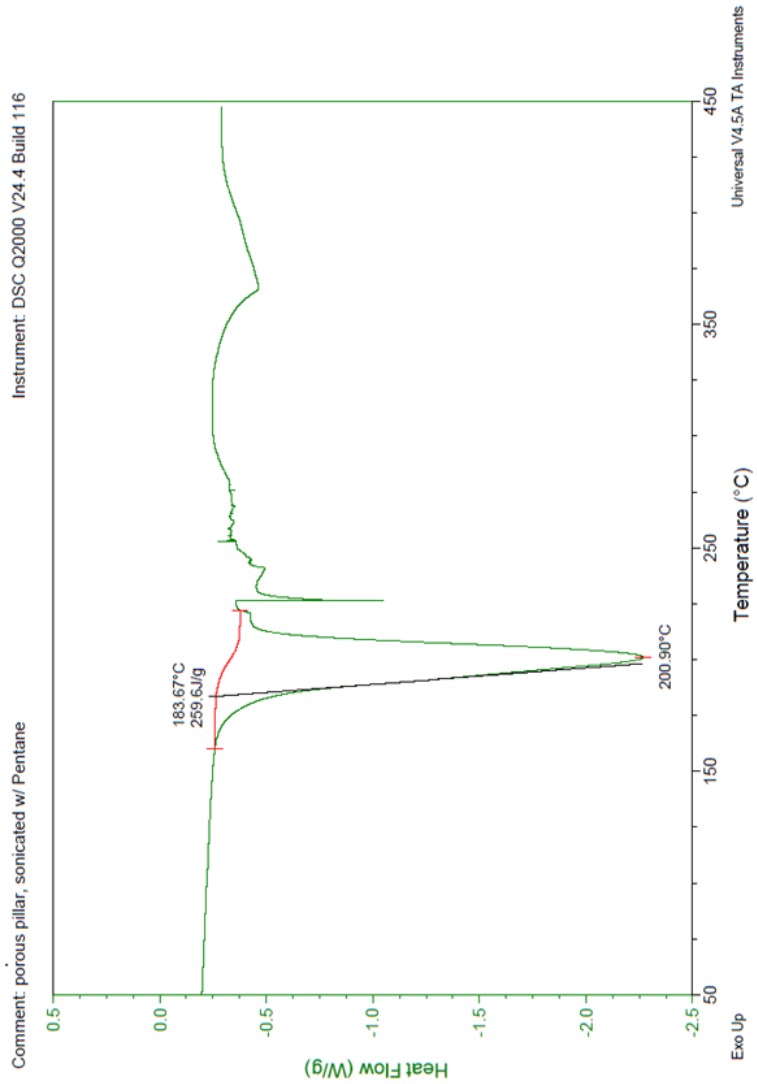

Figure D.54 DSC of the porous Zn(o-tolidine) sonicated with pentane

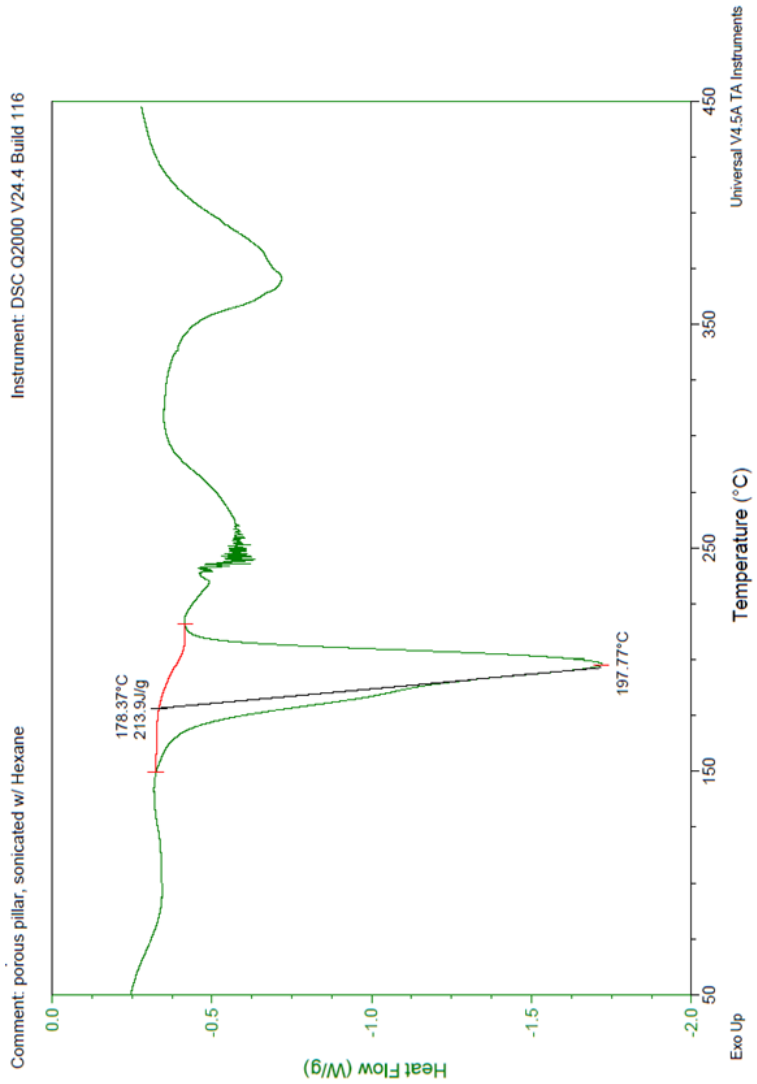

Figure D.55 DSC of the porous Zn(o-tolidine) sonicated with hexane

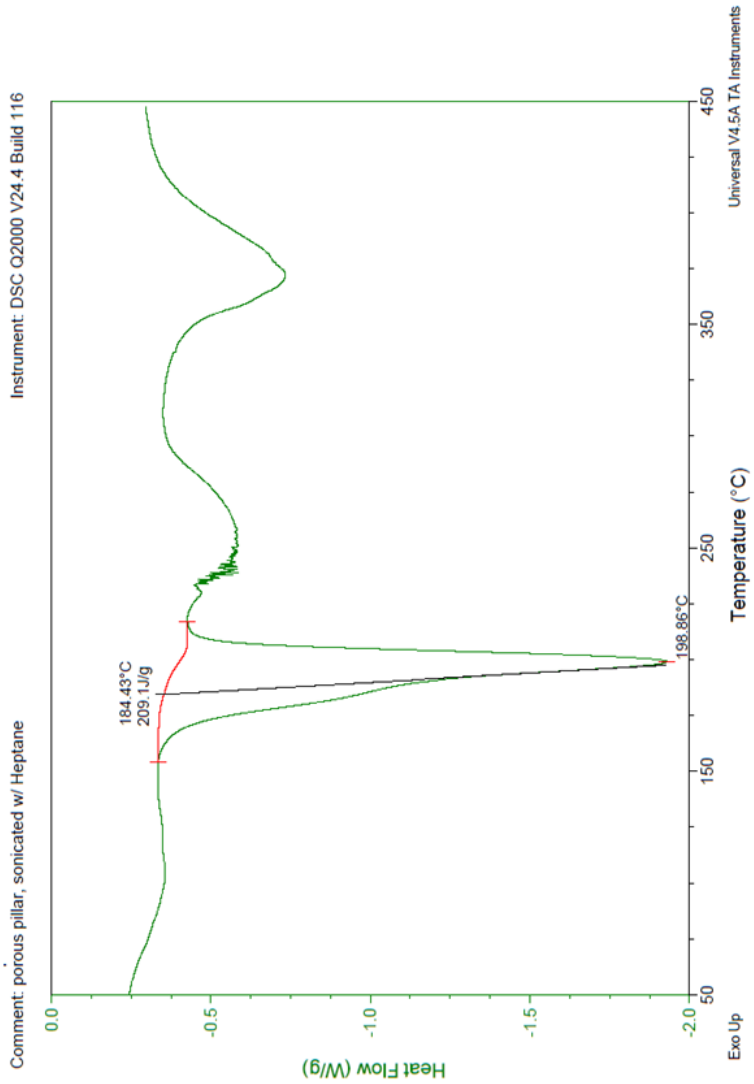

Figure D.56 DSC of the porous Zn(o-tolidine) sonicated with heptane

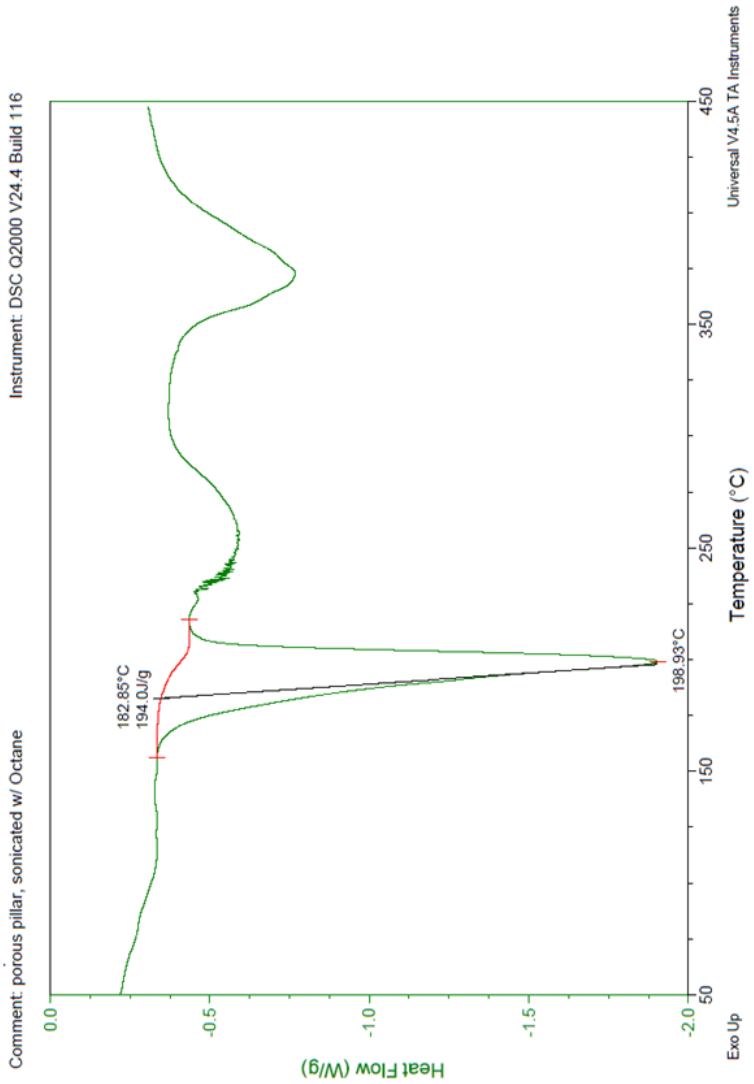

Figure D.57 DSC of the porous Zn(o-tolidine) sonicated with octane

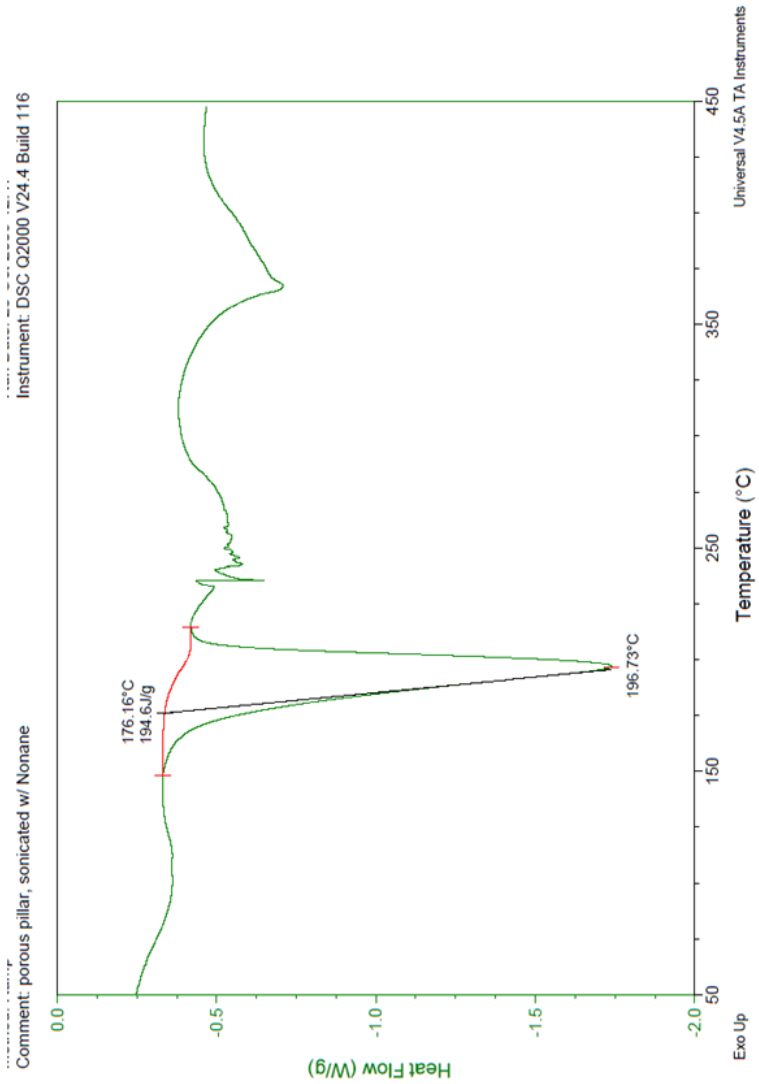

Figure D.58 DSC of the porous Zn(o-tolidine) sonicated with nonane

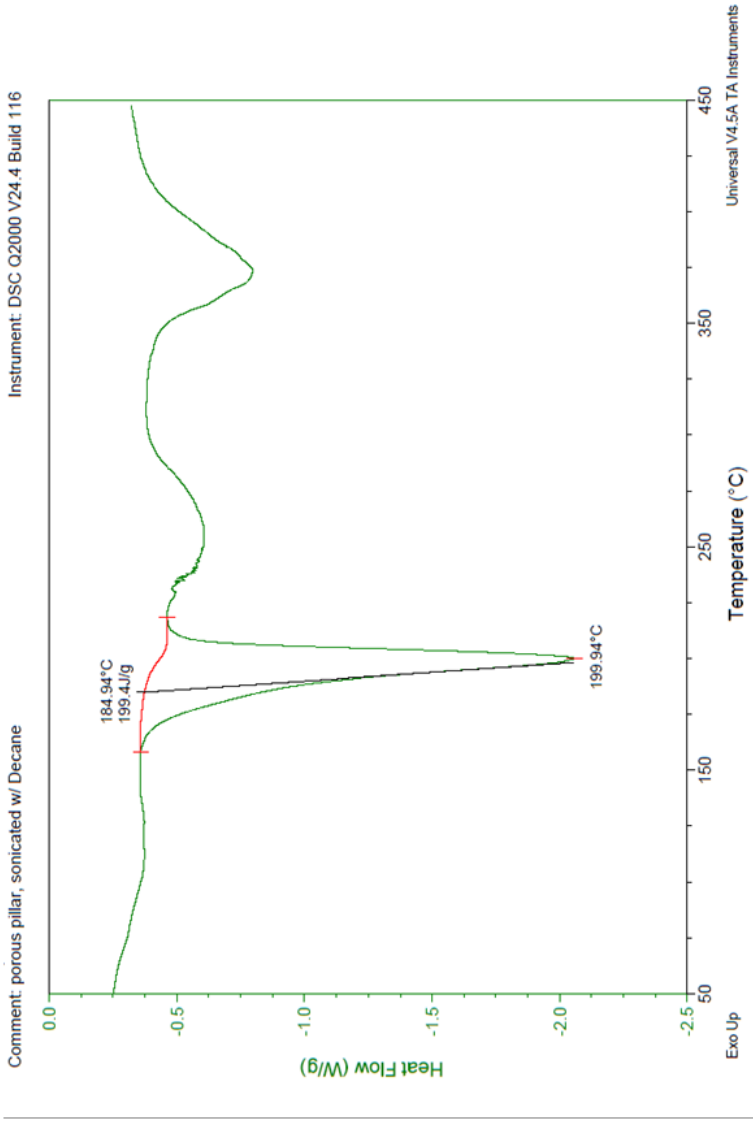

Figure D.59 DSC of the porous Zn(o-tolidine) sonicated with decane

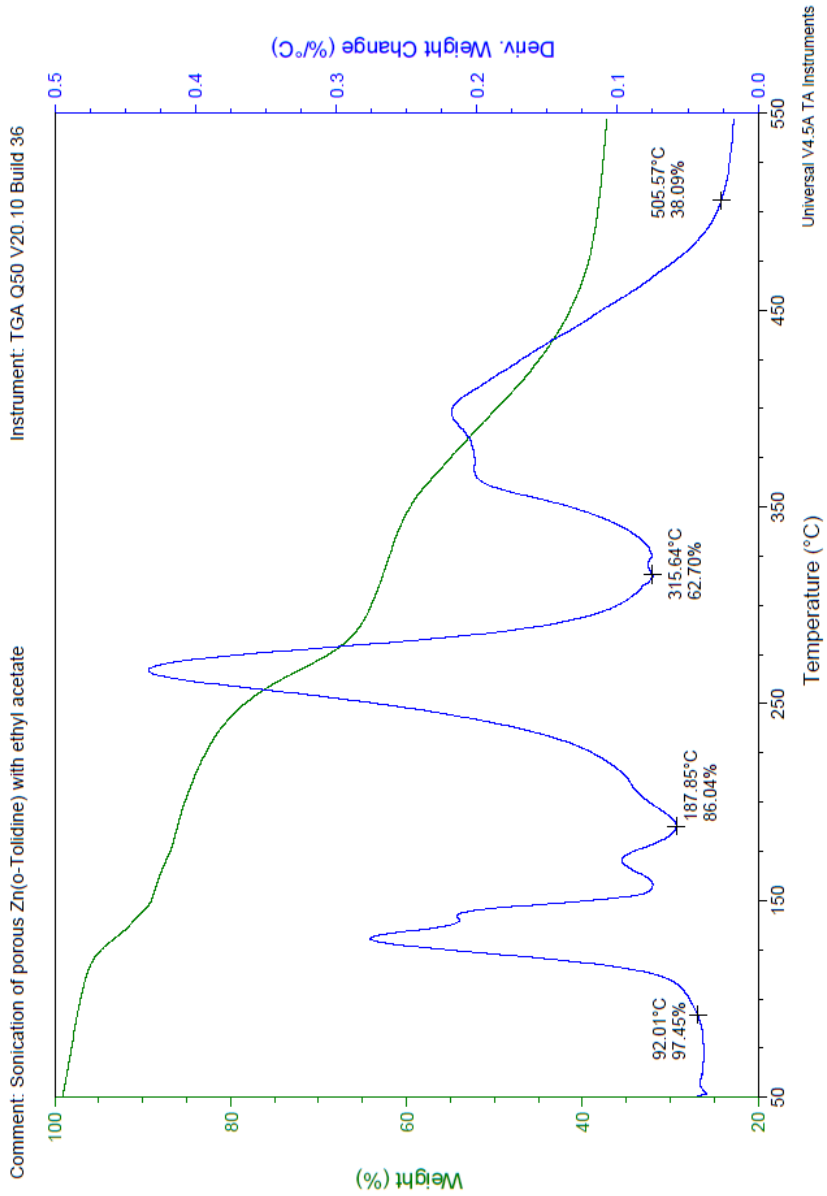

Figure D.60 TGA of the porous Zn(o-tolidine) sonicated with ethyl acetate

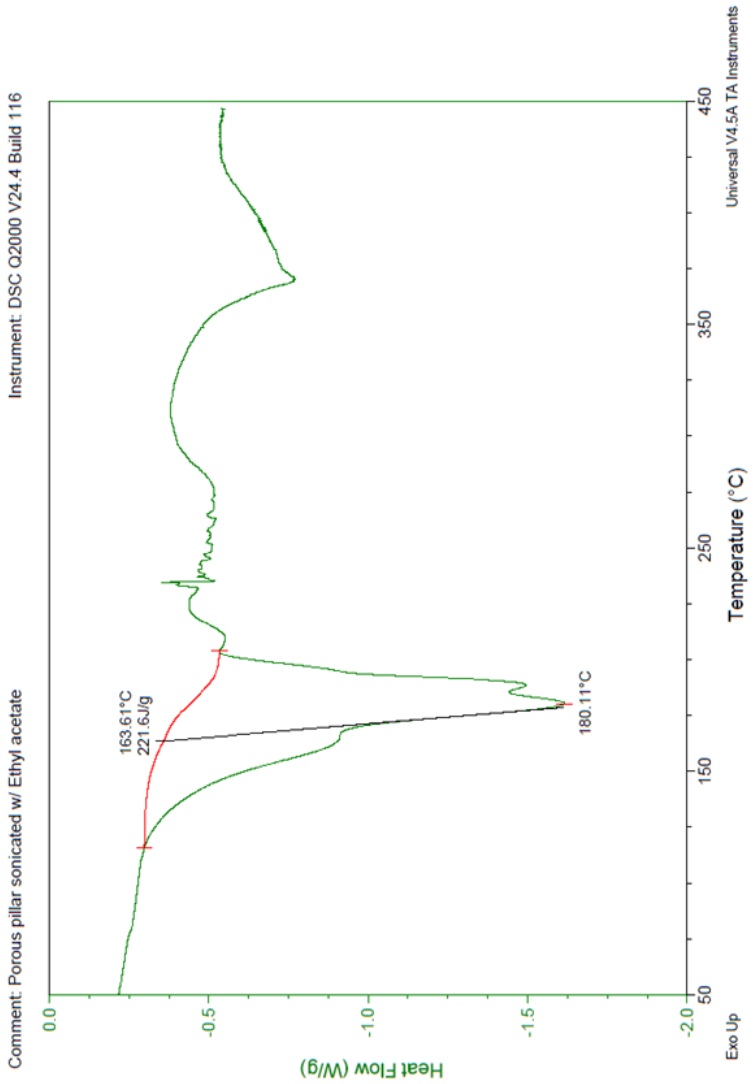

Figure D.61 DSC of the porous Zn(o-tolidine) sonicated with ethyl acetate

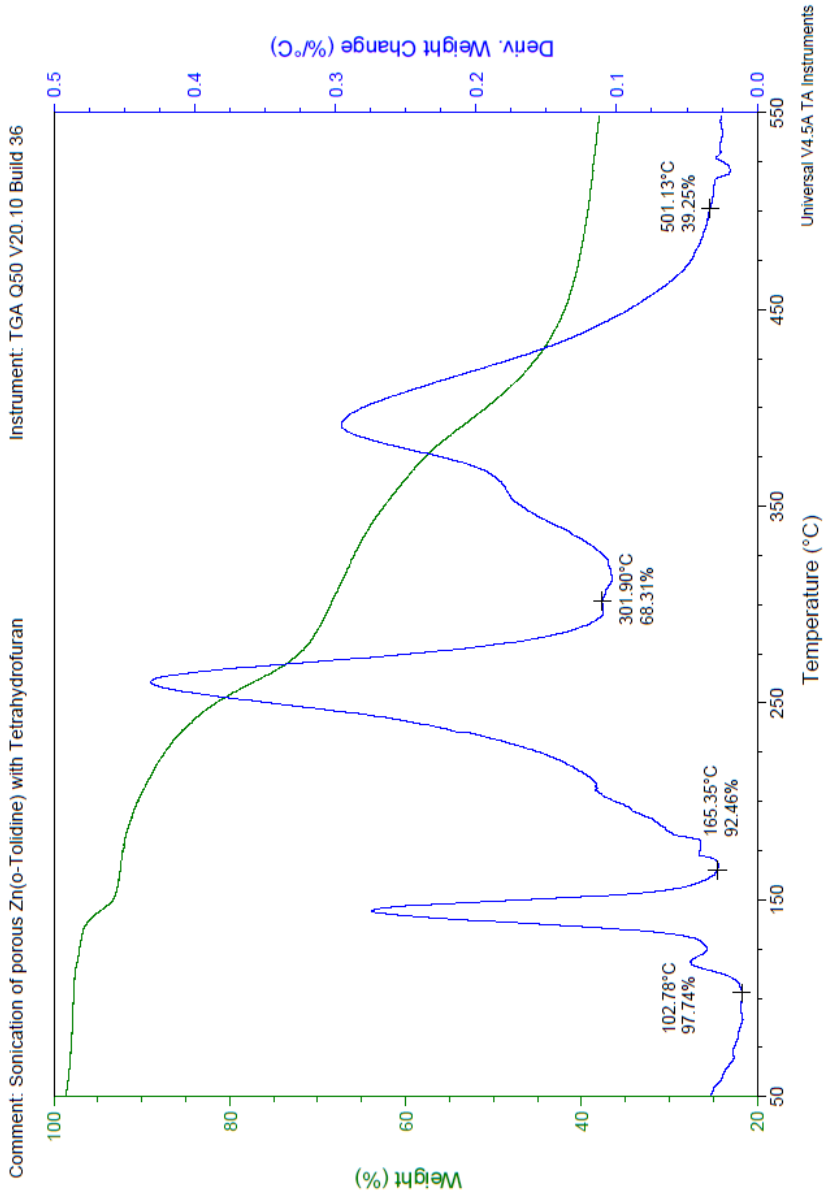

Figure D.62 TGA of the porous Zn(o-tolidine) sonicated with tetrahydrofuran

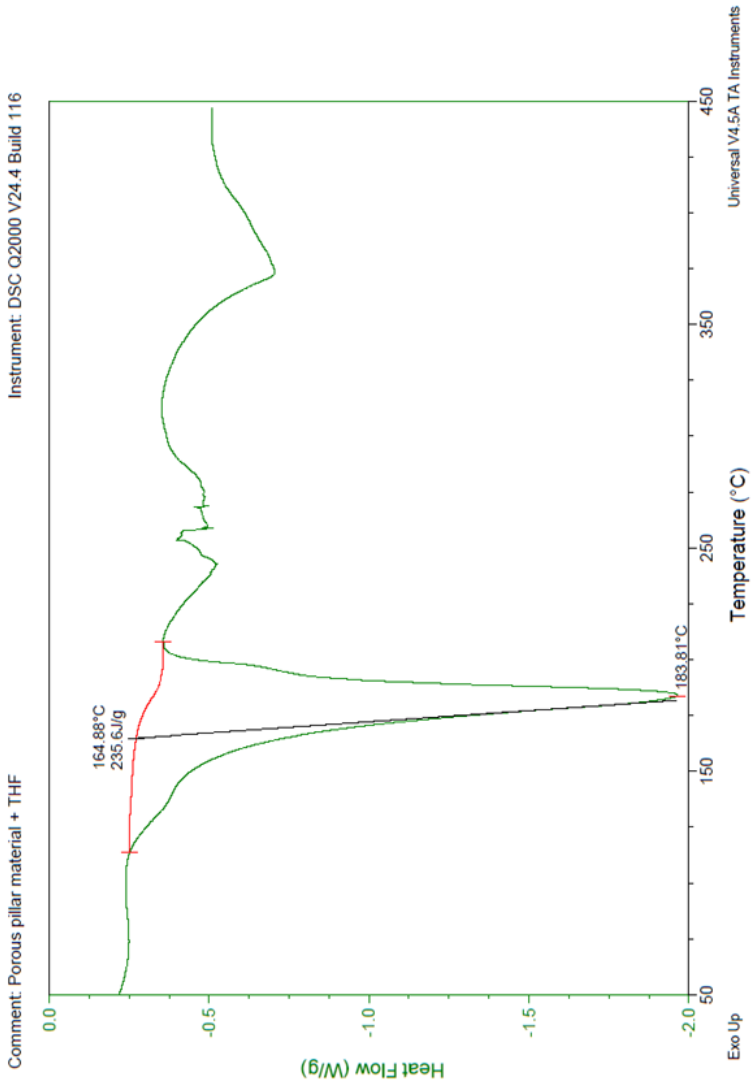

Figure D.63 DSC of the porous Zn(o-tolidine) sonicated with tetrahydrofuran

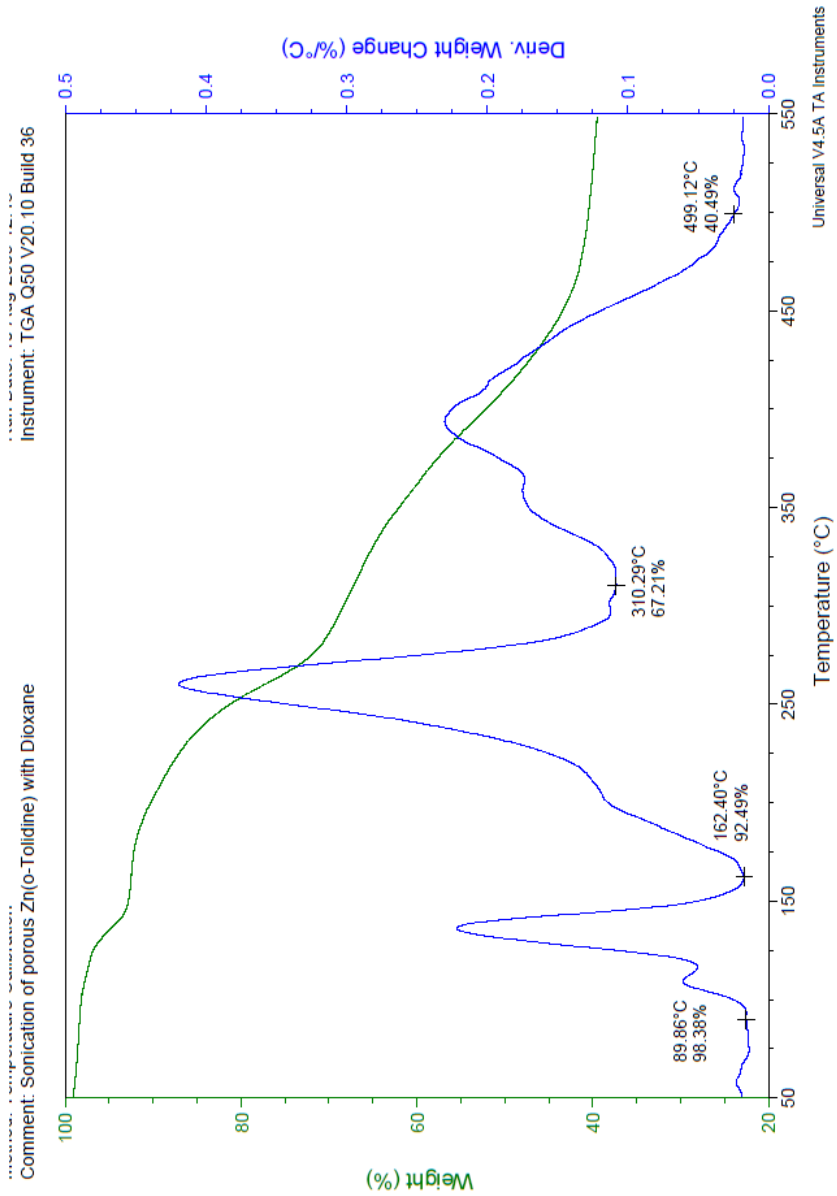

Figure D.64 TGA of the porous Zn(o-tolidine) sonicated with 1,4-dioxane

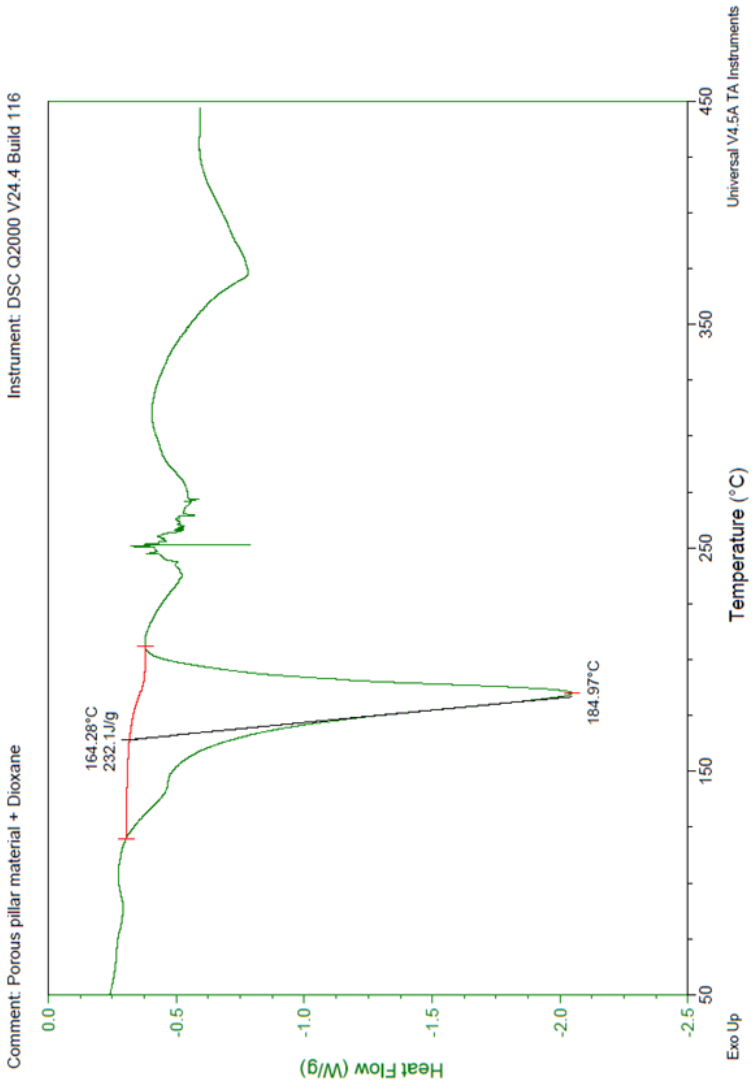

Figure D.65 DSC of the porous Zn(o-tolidine) sonicated with 1,4-dioxane

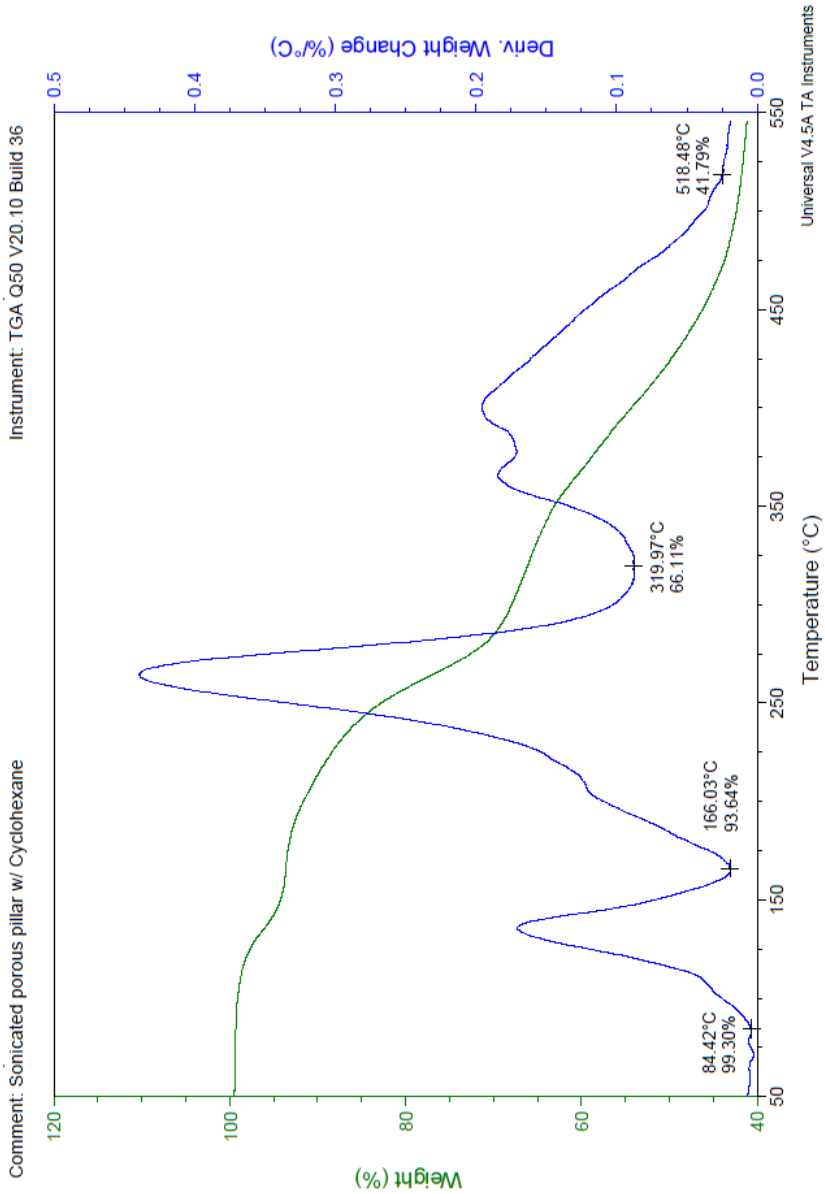

Figure D.66 TGA of the porous Zn(o-tolidine) sonicated with cyclohexane

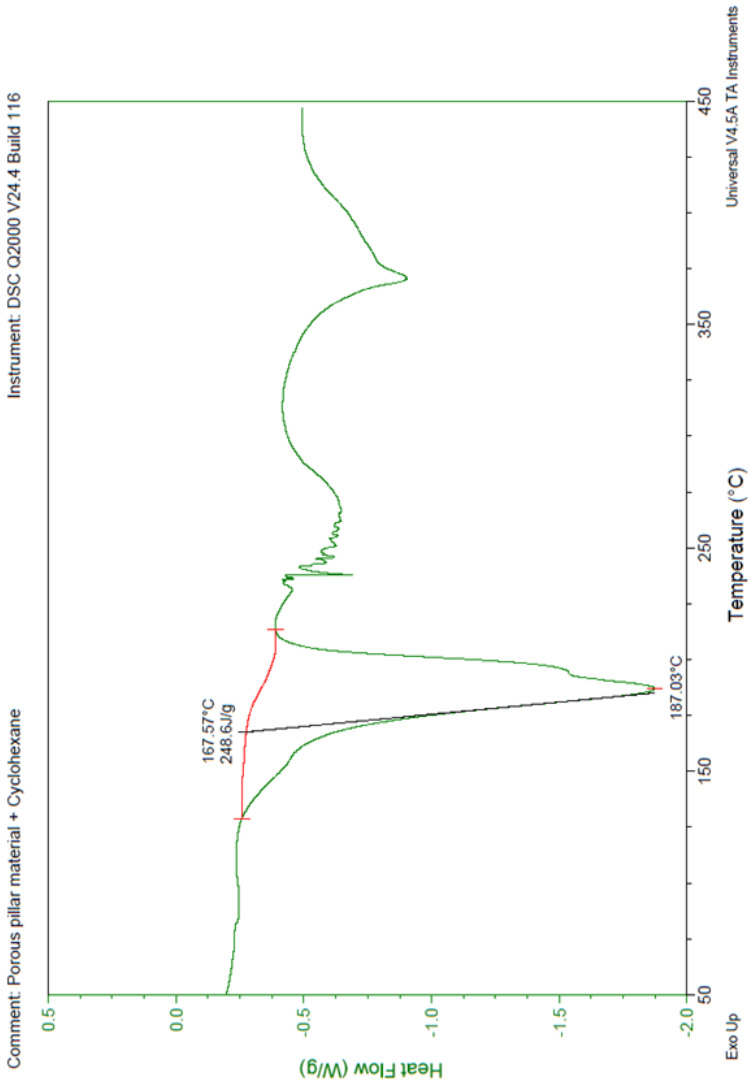

Figure D.67 DSC of the porous Zn(o-tolidine) sonicated with cyclohexane

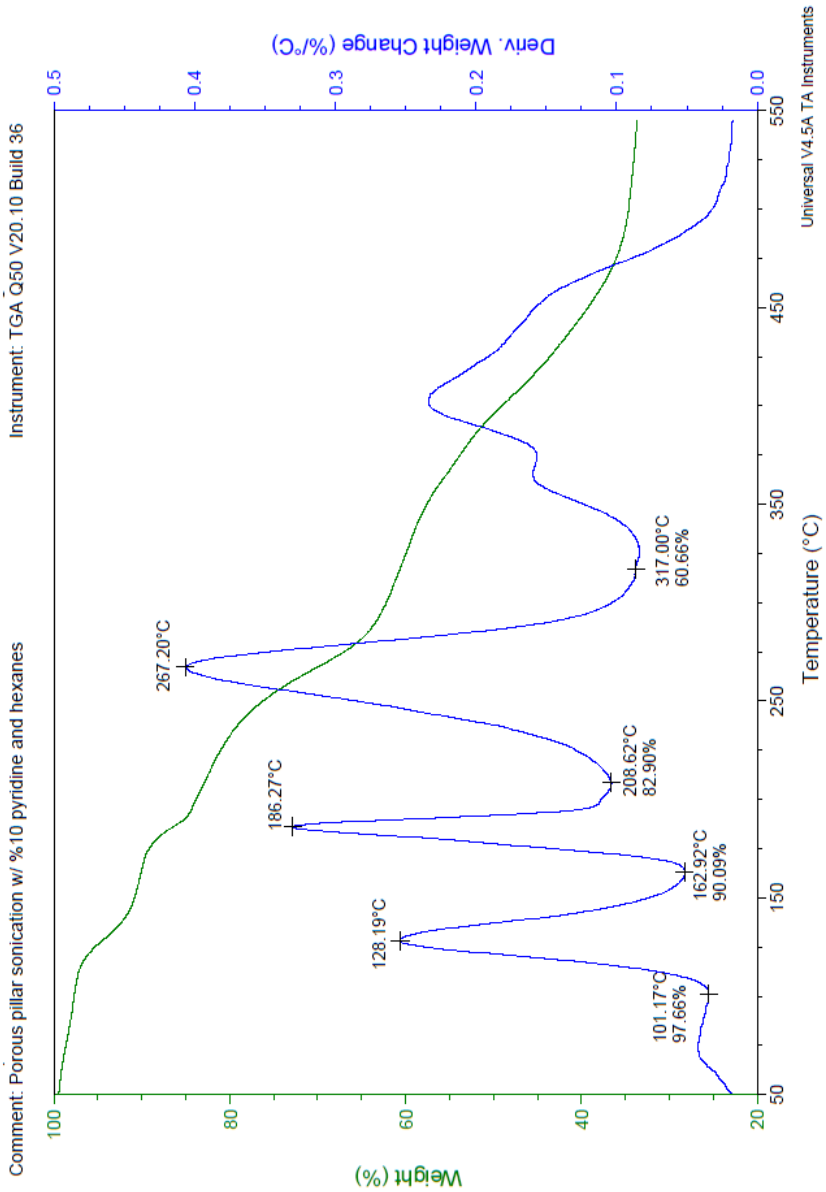

Figure D.68 TGA of the porous Zn(o-tolidine) sonicated with pyridine

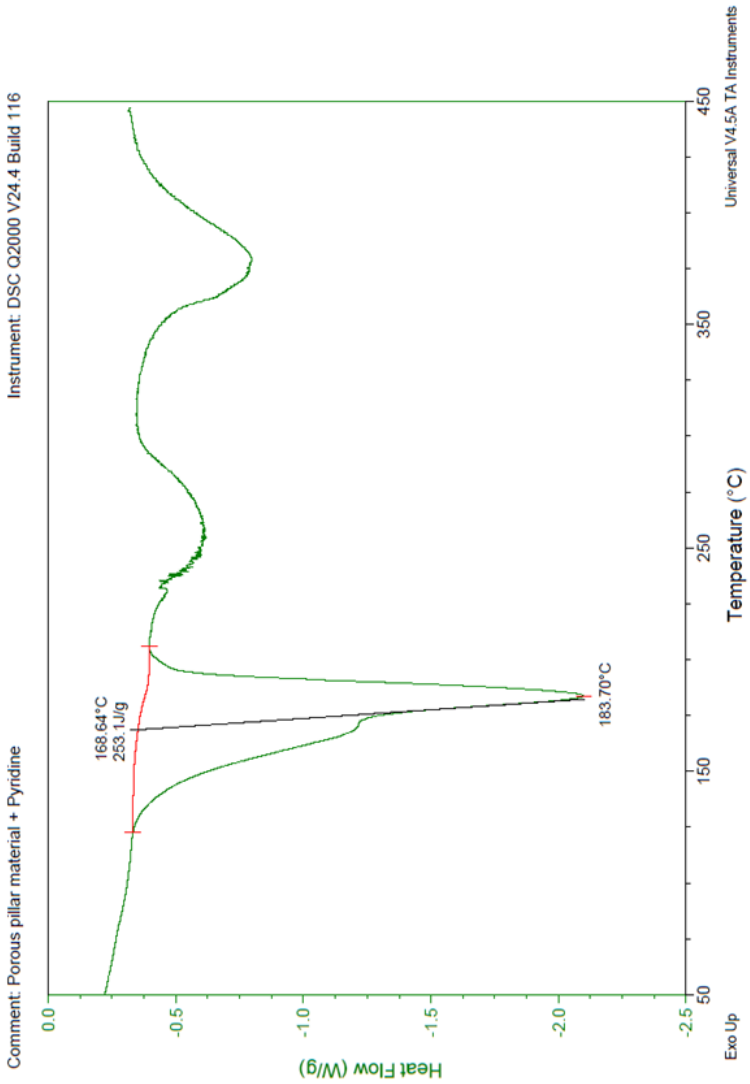

Figure D.69 DSC of the porous Zn(o-tolidine) sonicated with pyridine

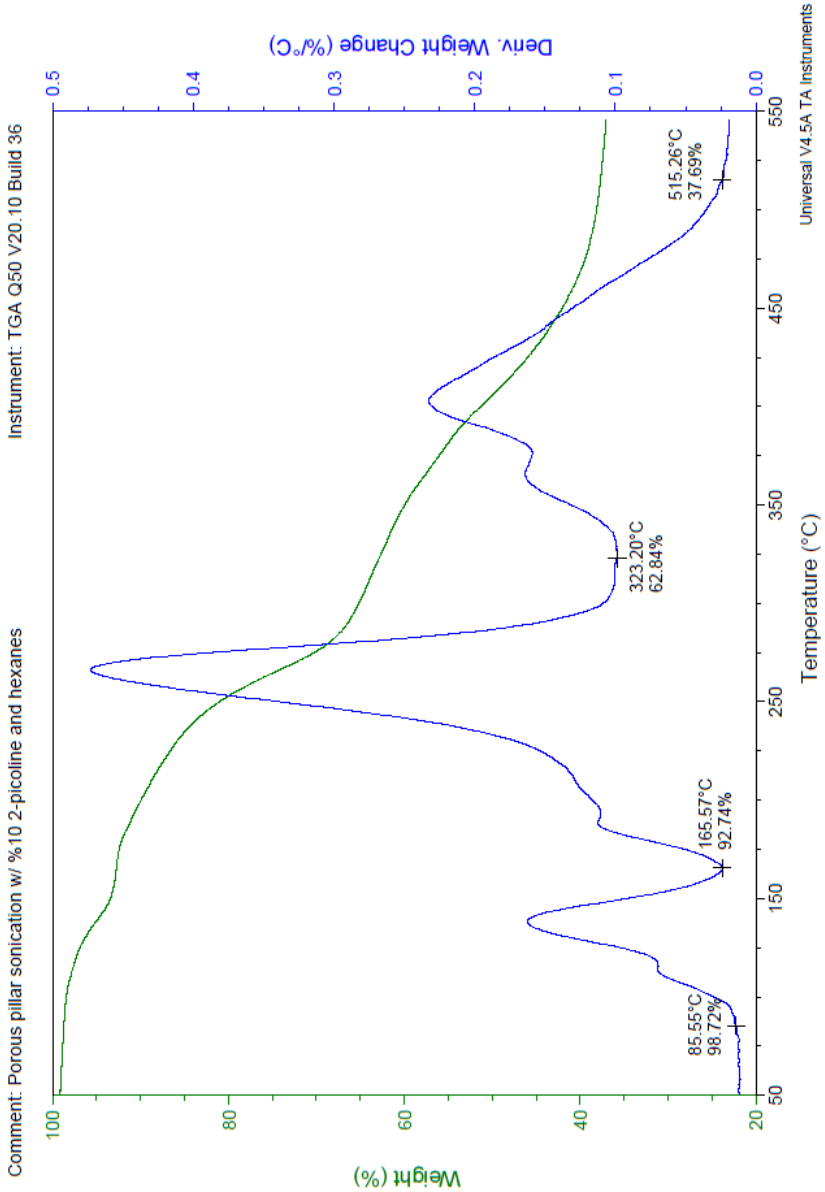

Figure D.70 TGAof the porous Zn(o-tolidine) sonicated with 2-picoline

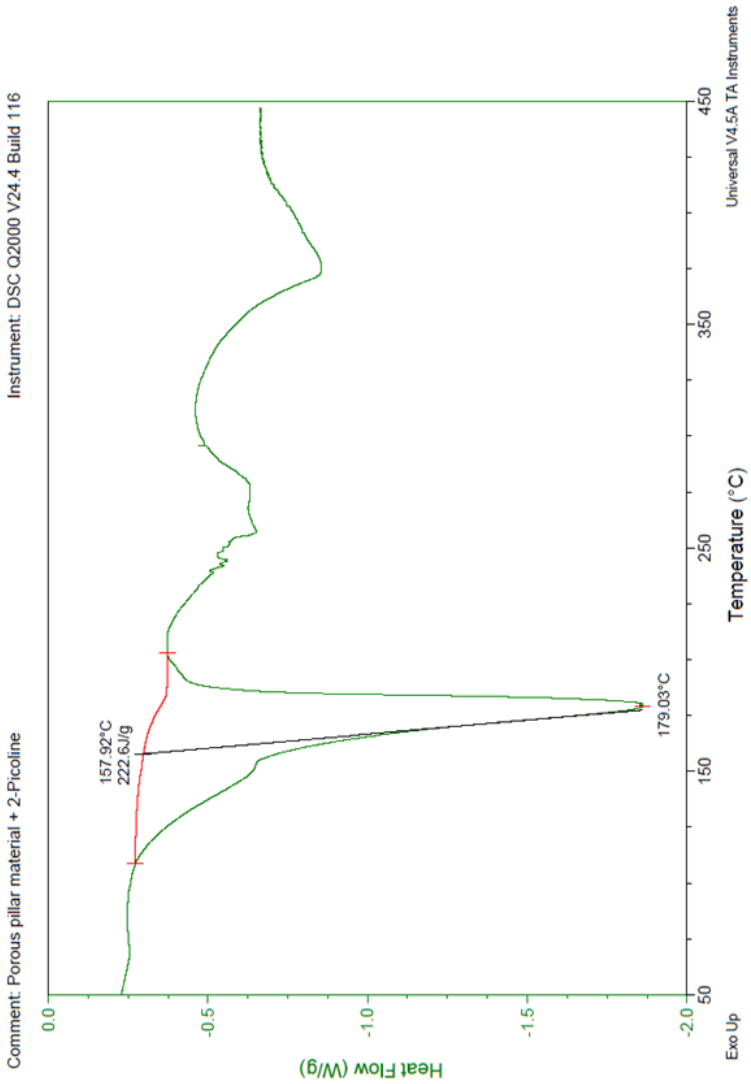

Figure D.71 DSCof the porous Zn(o-tolidine) sonicated with 2-picoline

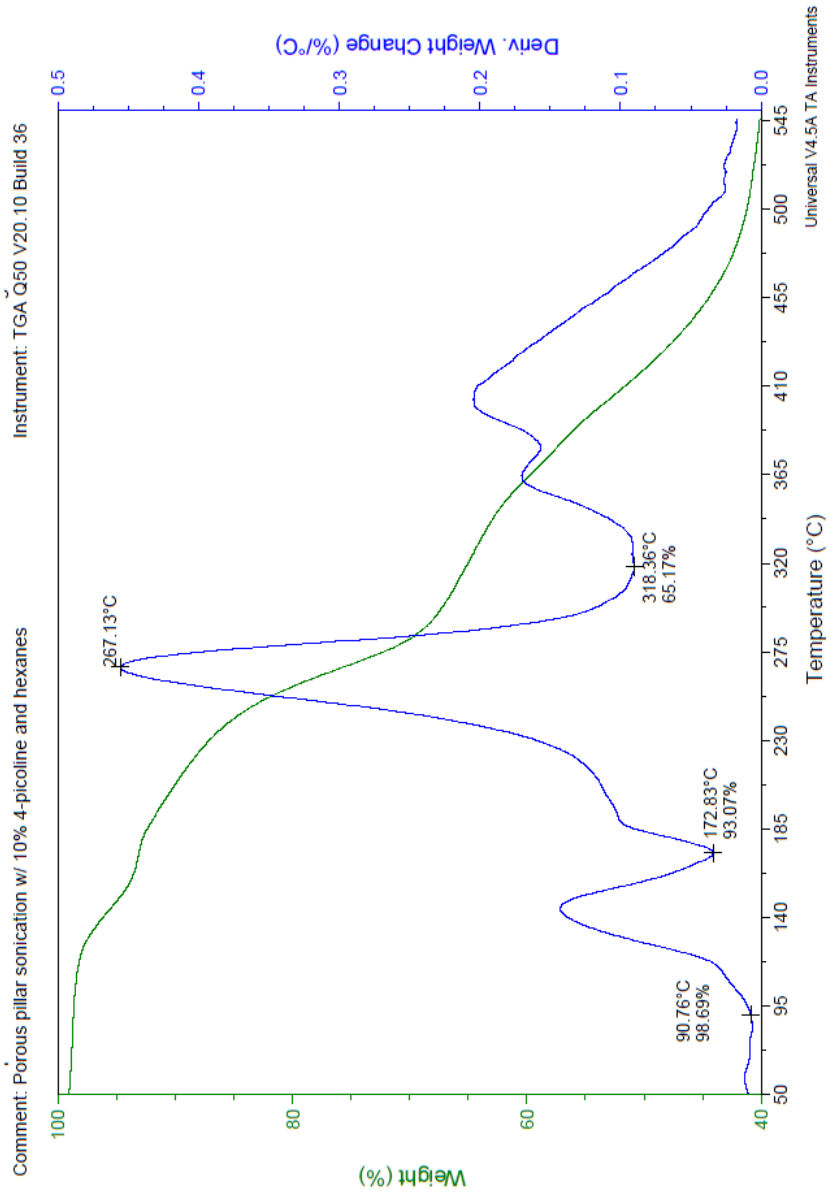

Figure D.72 TGAof the porous Zn(o-tolidine) sonicated with 4-picoline

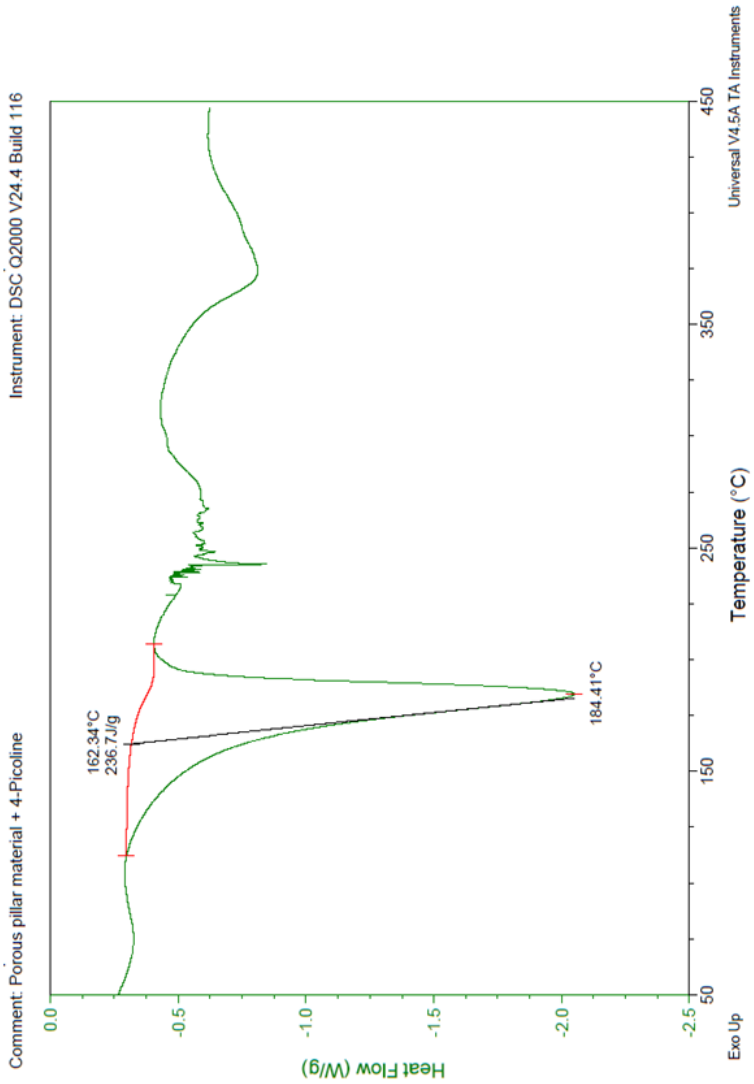

Figure D.73 DSCof the porous Zn(o-tolidine) sonicated with 4-picoline

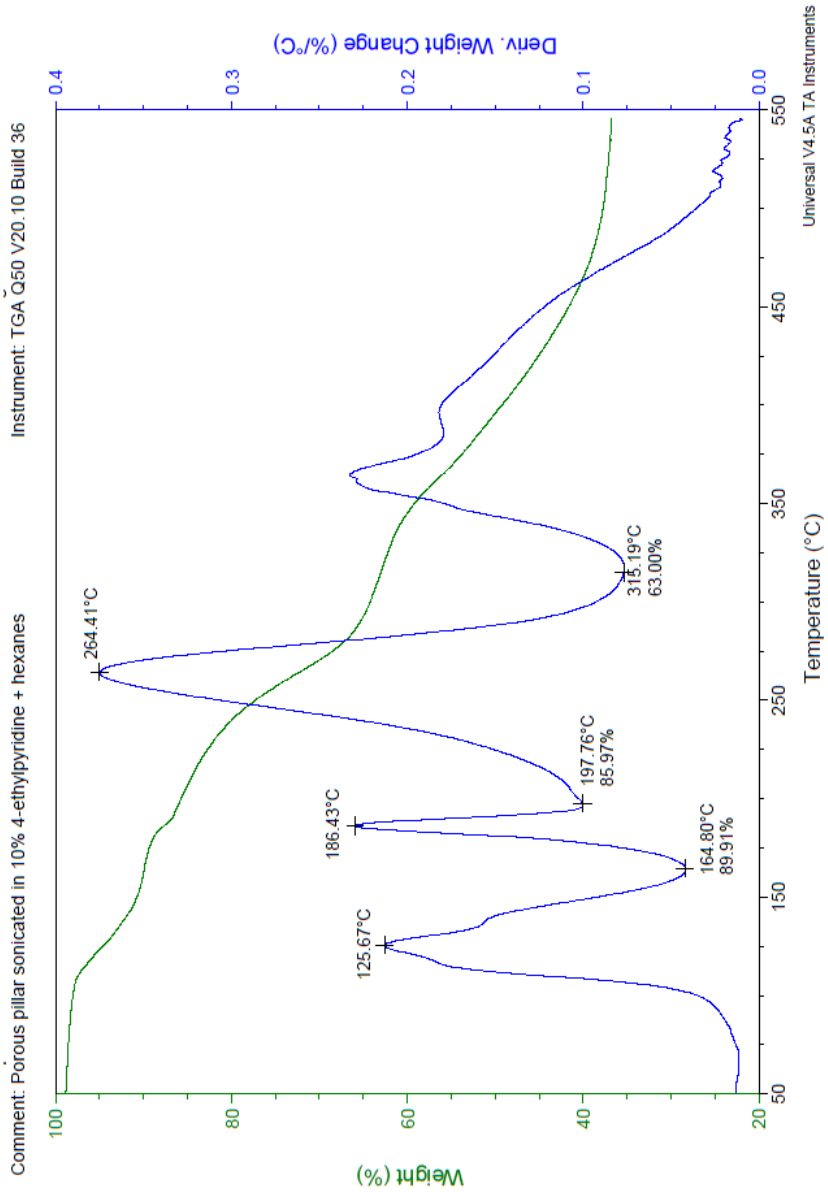

Figure D.74 TGAof the porous Zn(o-tolidine) sonicated with 4-ethylpyridine

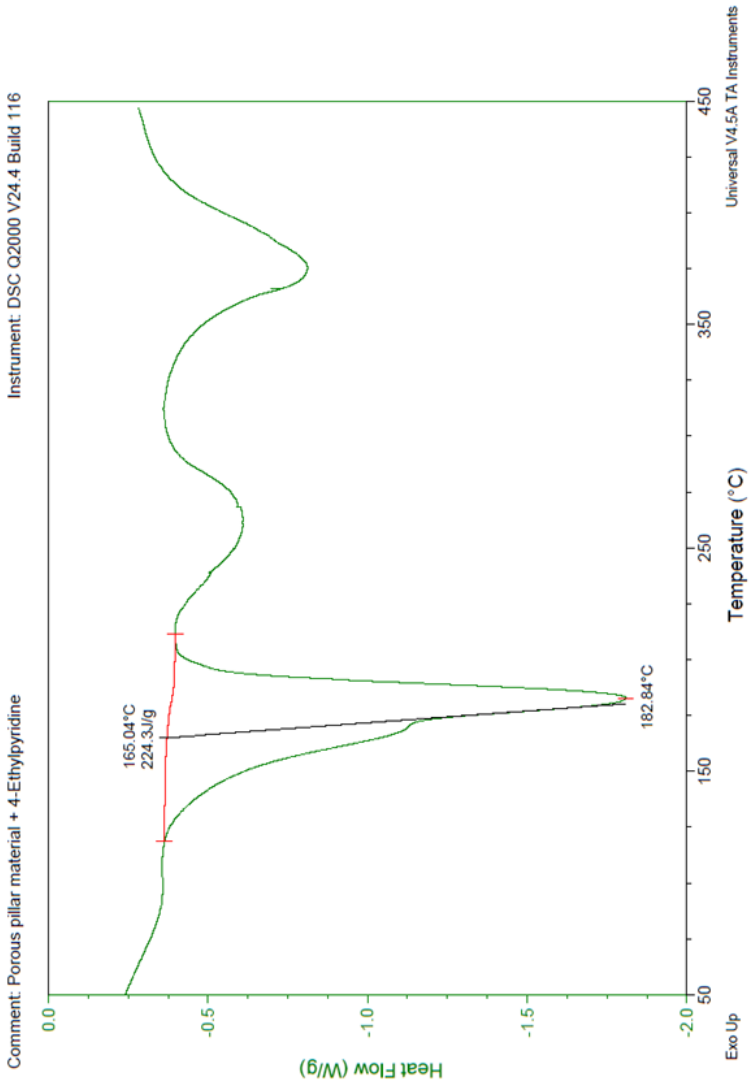

Figure D.75 DSCof the porous Zn(o-tolidine) sonicated with 4-ethylpyridine

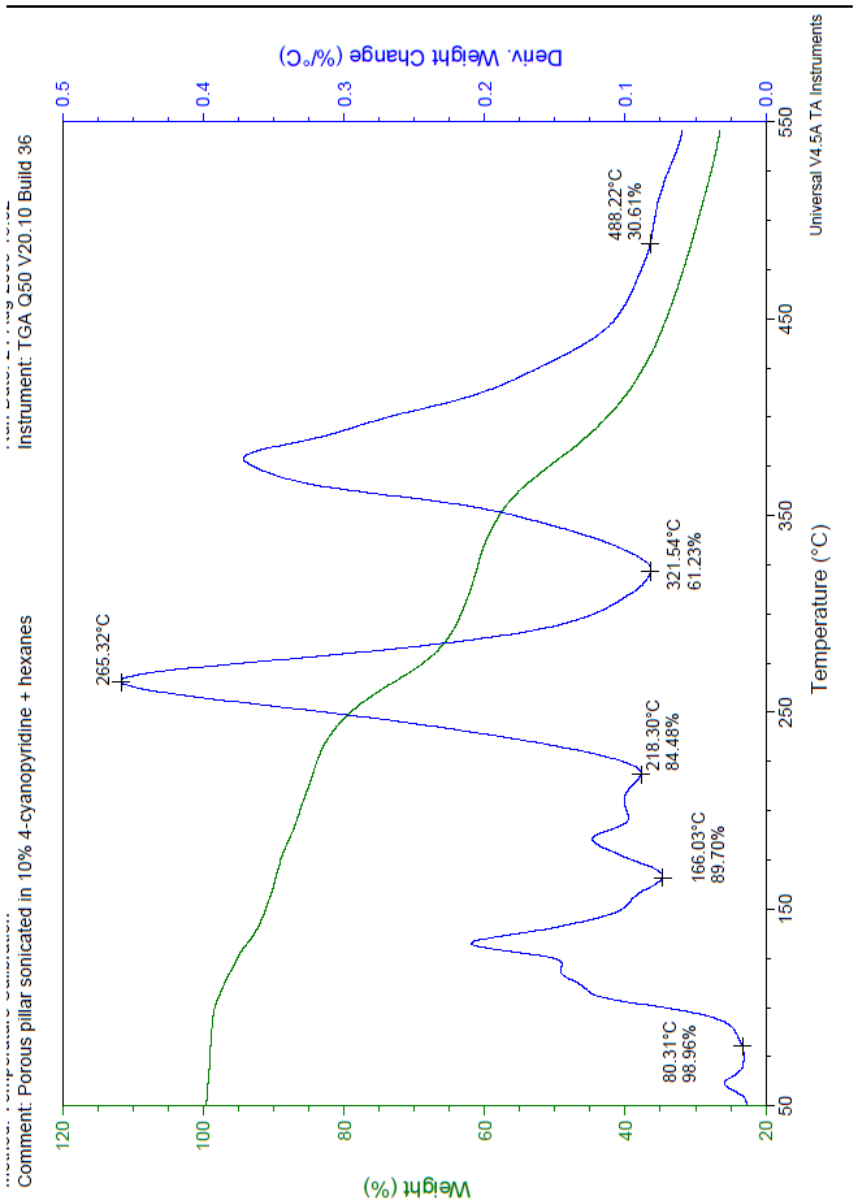

Figure D.76 TGAof the porous Zn(o-tolidine) sonicated with 4-cyanopyridine

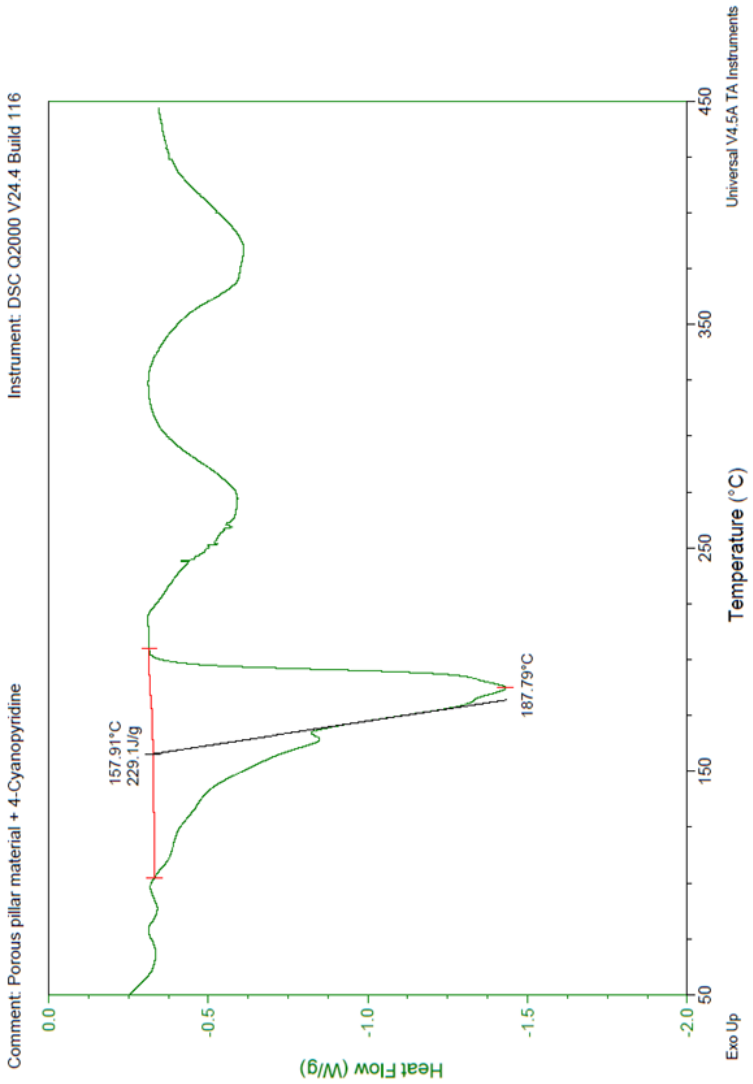

Figure D.77 DSCof the porous Zn(o-tolidine) sonicated with 4-cyanopyridine

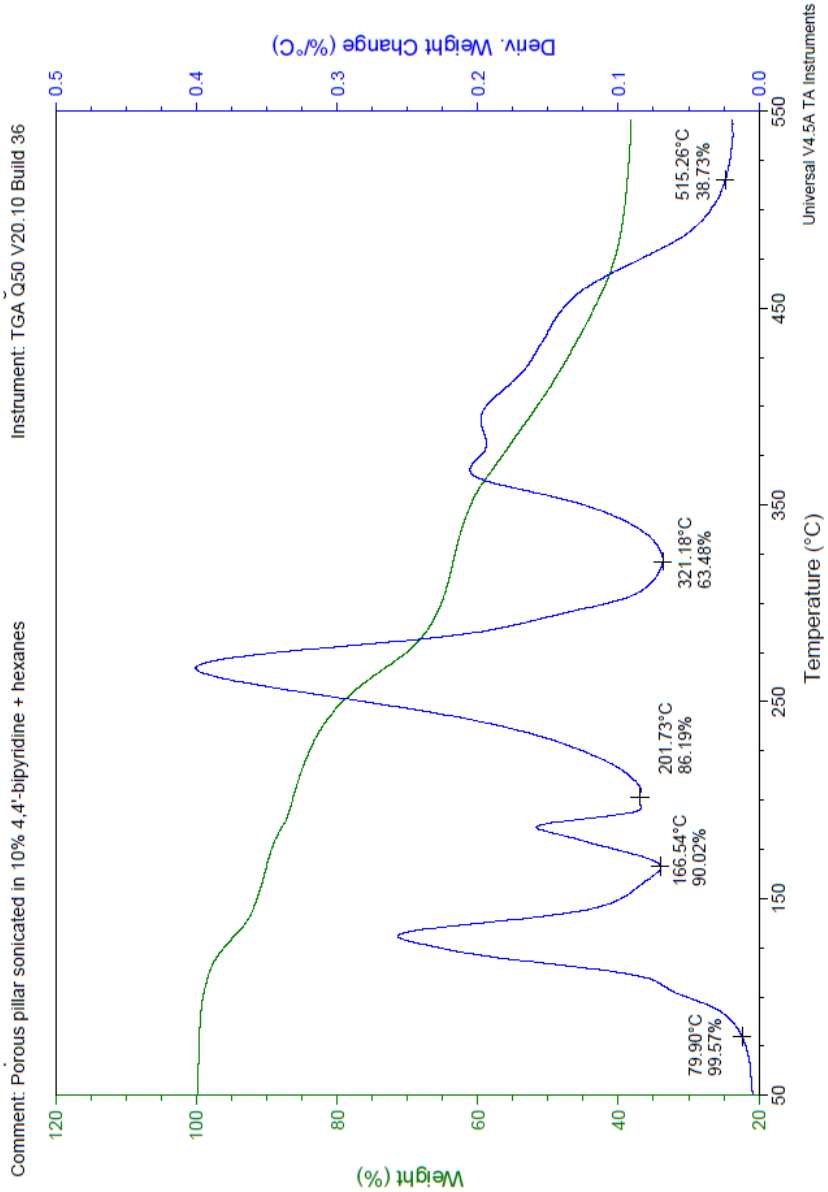

Figure D.78 TGAof the porous Zn(o-tolidine) sonicated with 4,4’-bipyridine

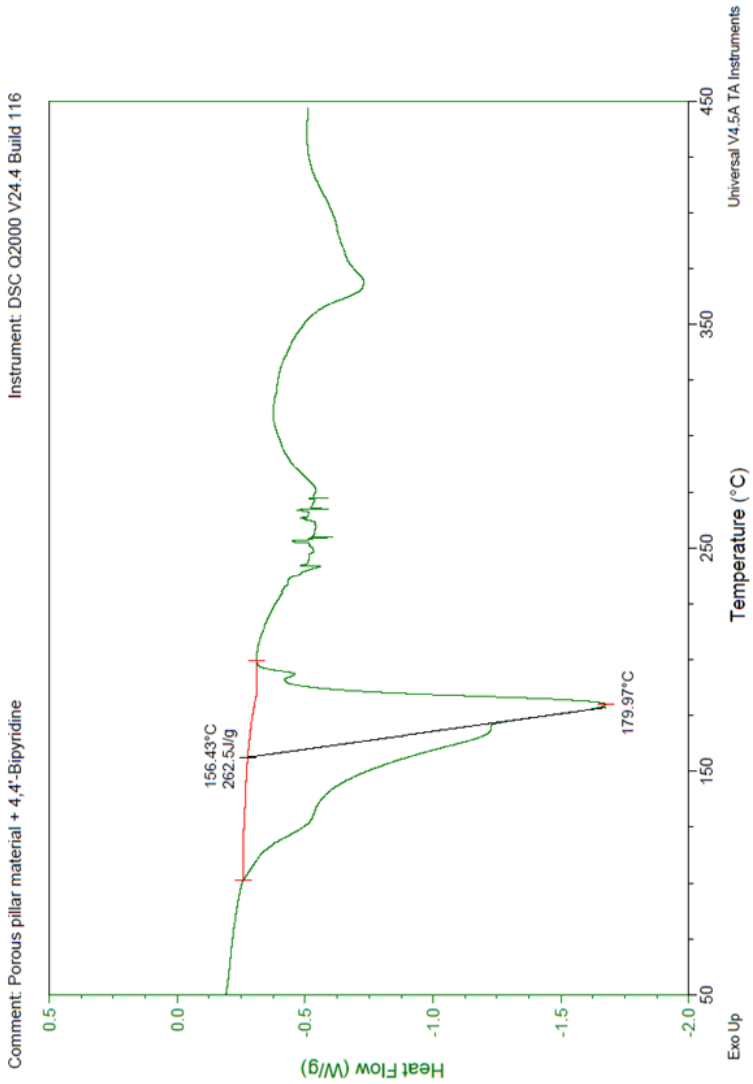

Figure D.79 DSCof the porous Zn(o-tolidine) sonicated with 4,4’-bipyridine

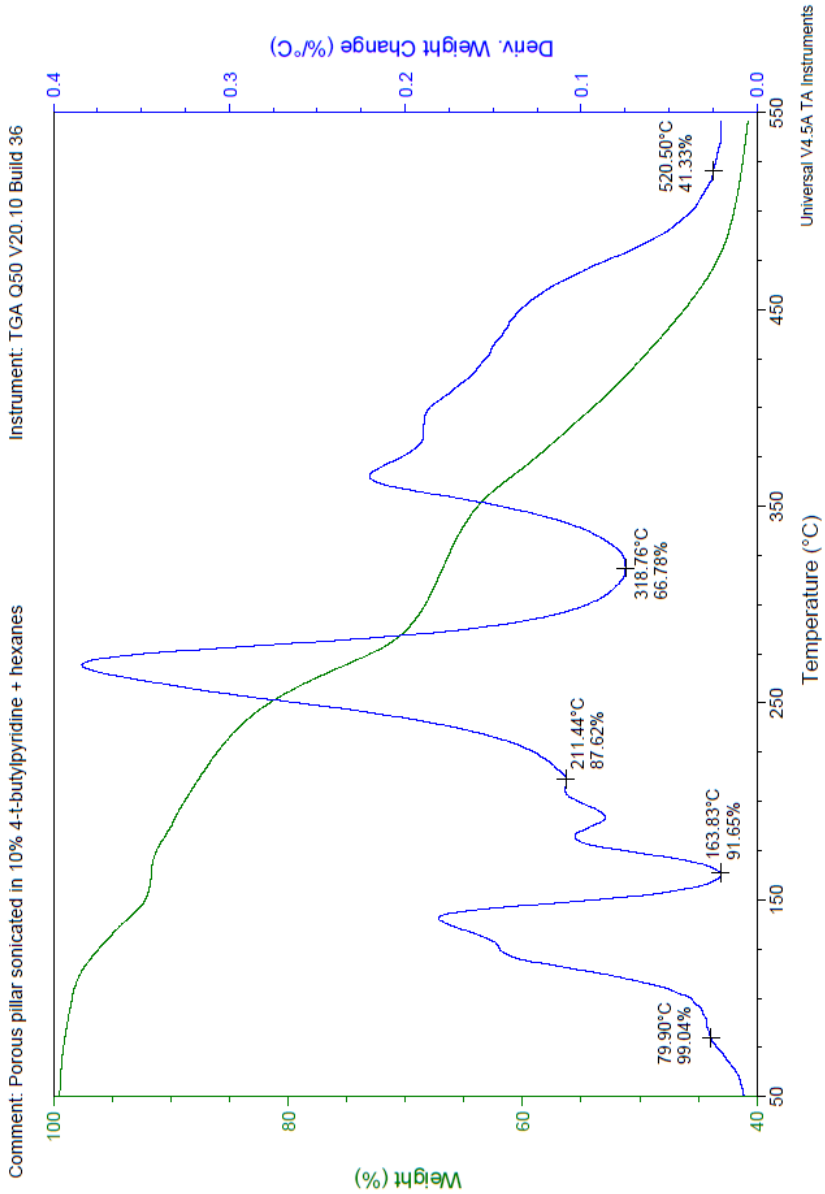

Figure D.80 TGAof the porous Zn(o-tolidine) sonicated with 4-t-butylpyridine

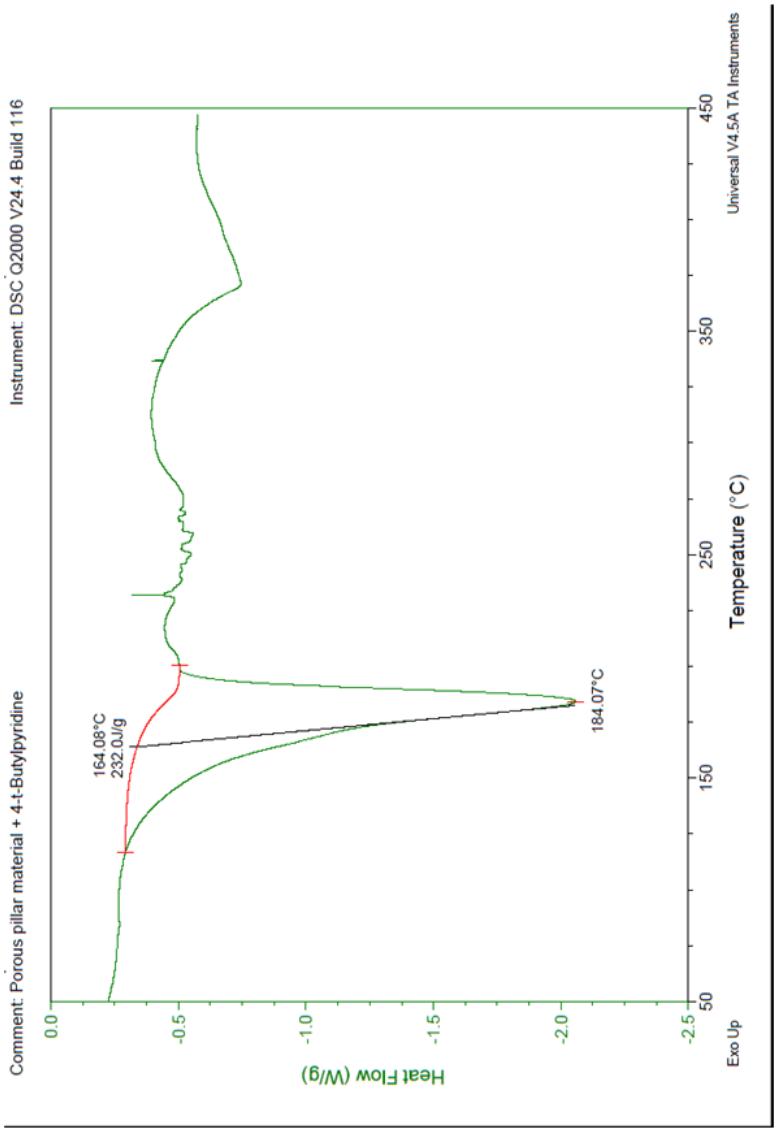

Figure D.81 DSCof the porous Zn(o-tolidine) sonicated with 4-t-butylpyridine

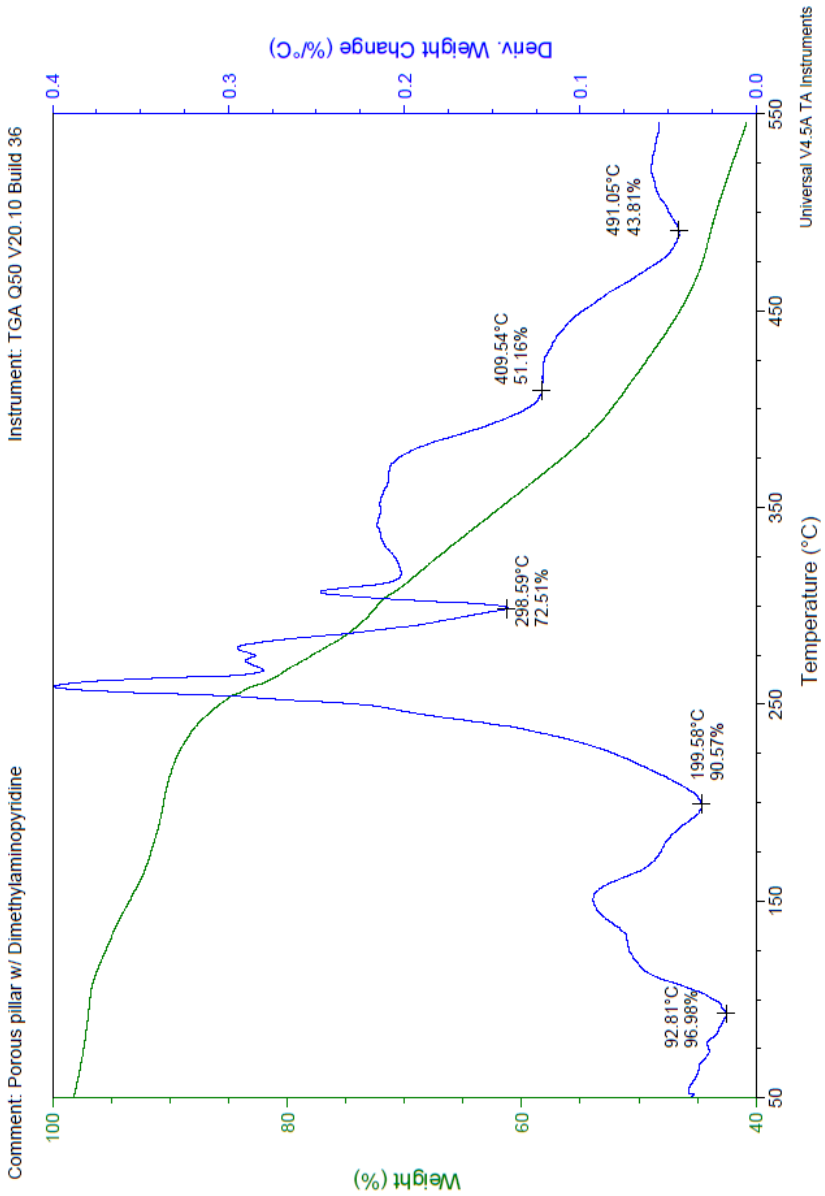

Figure D.82 TGA of the porous Zn(o-tolidine) sonicated with 4-(dimethylamino)pyridine

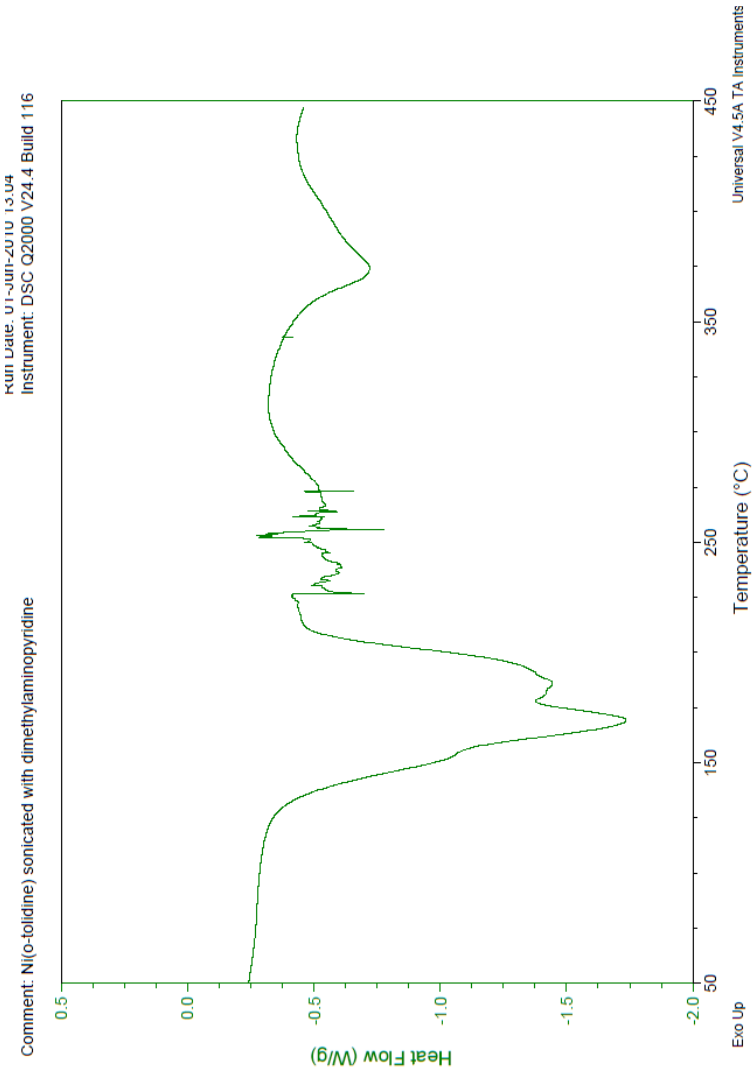

Figure D.83 DSC of the porous Zn(o-tolidine) sonicated with 4-(dimethylamino)pyridine

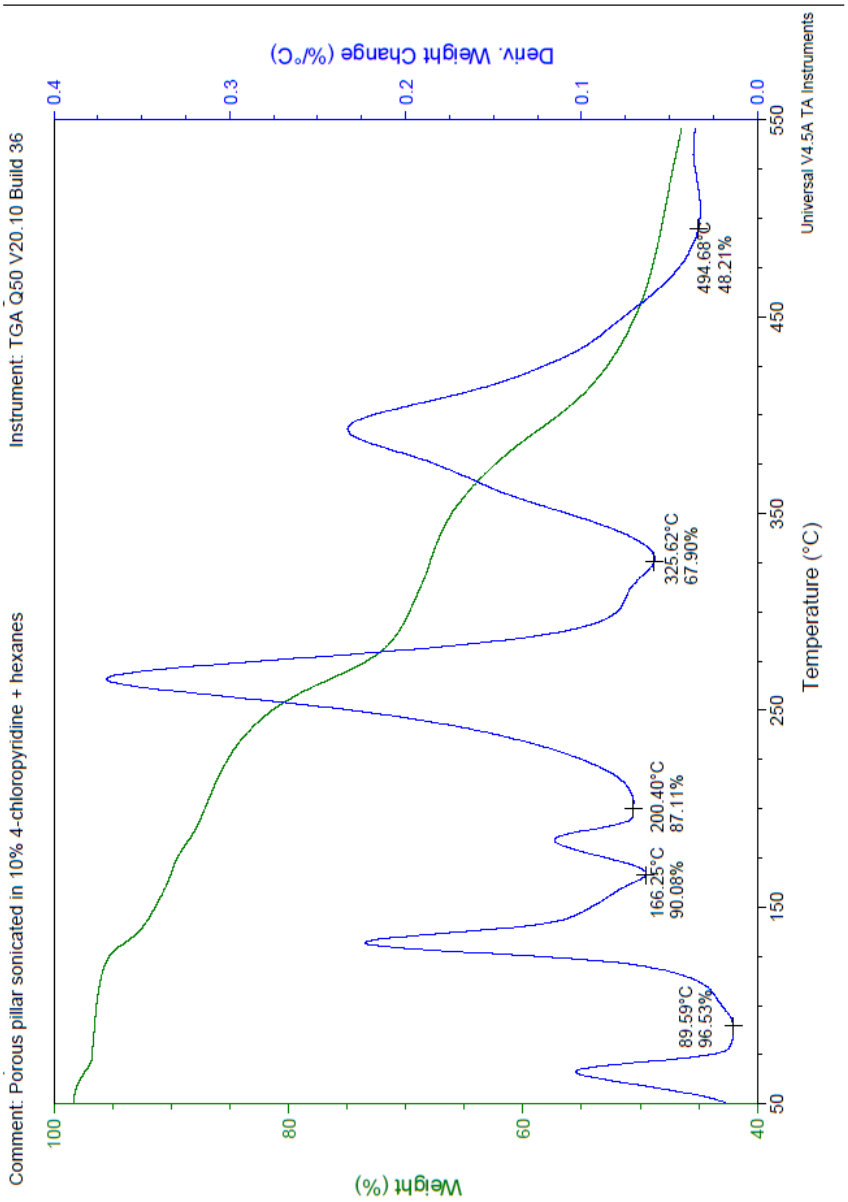

Figure D.84 TGA of the porous Zn(o-tolidine) sonicated with 4-chloropyridine

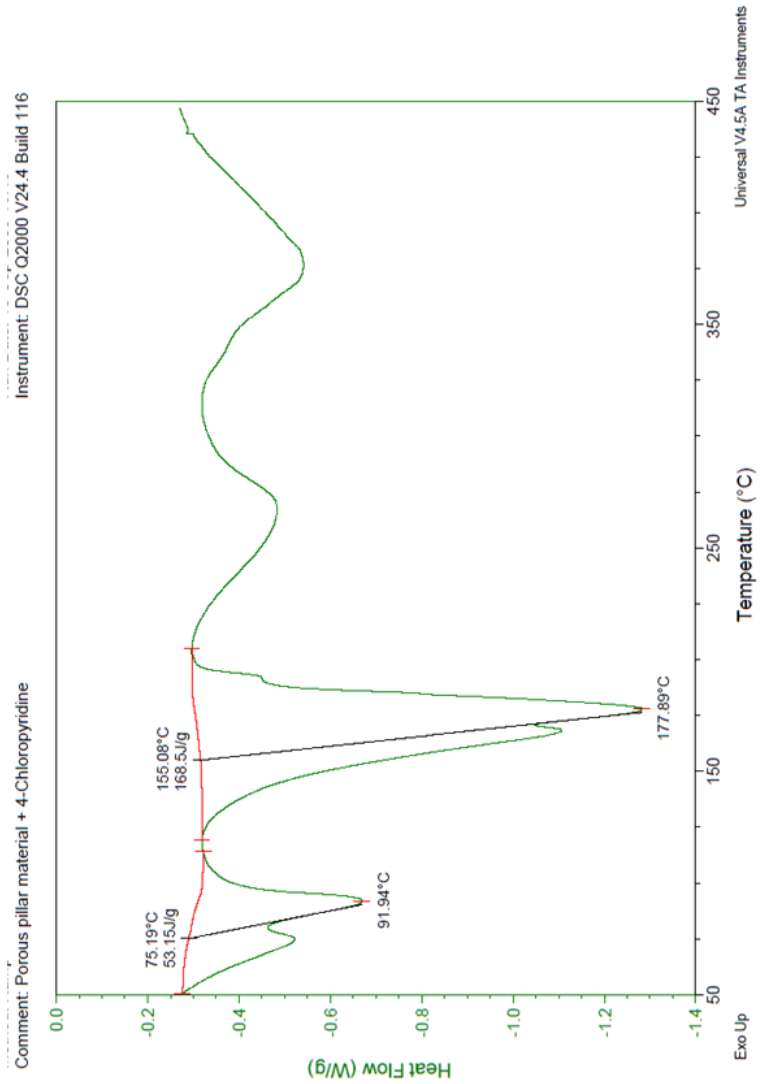

Figure D.85 DSC of the porous Zn(o-tolidine) sonicated with 4-chloropyridine

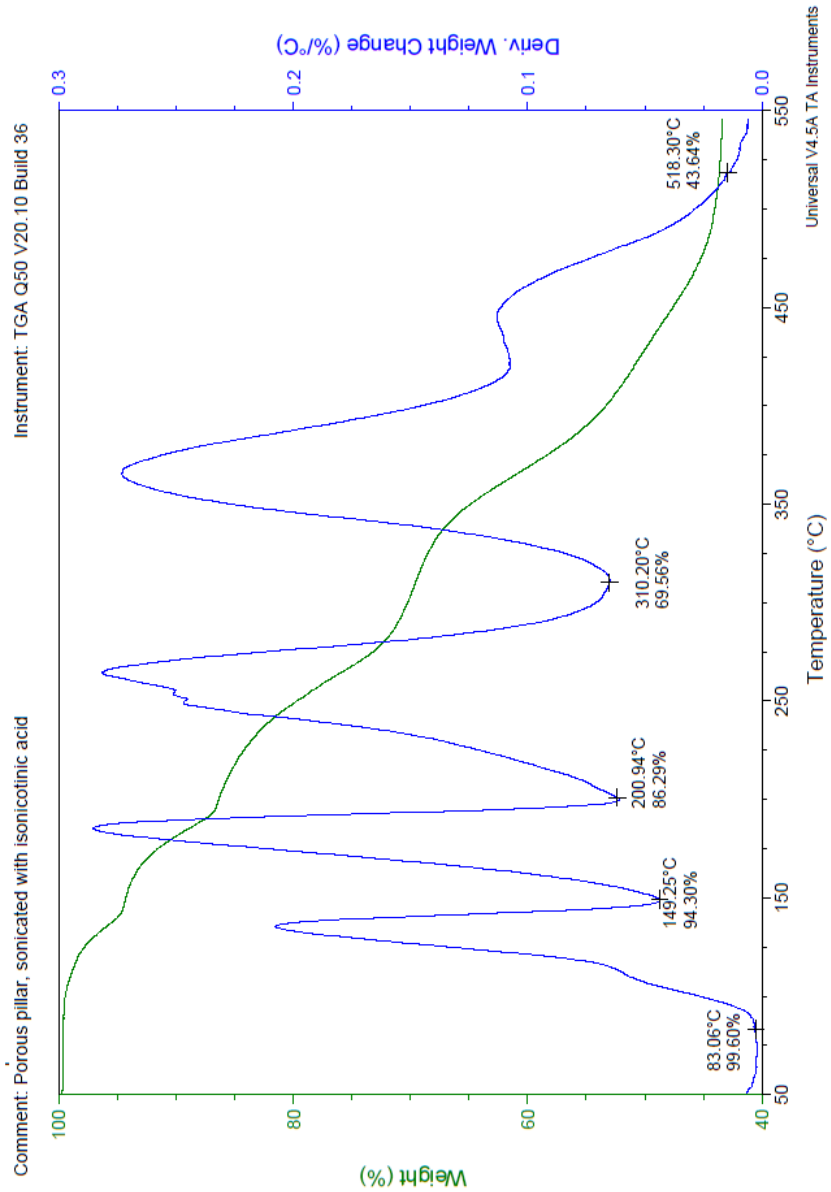

Figure D.86 TGA of the porous Zn(o-tolidine) sonicated with isonicotinic acid

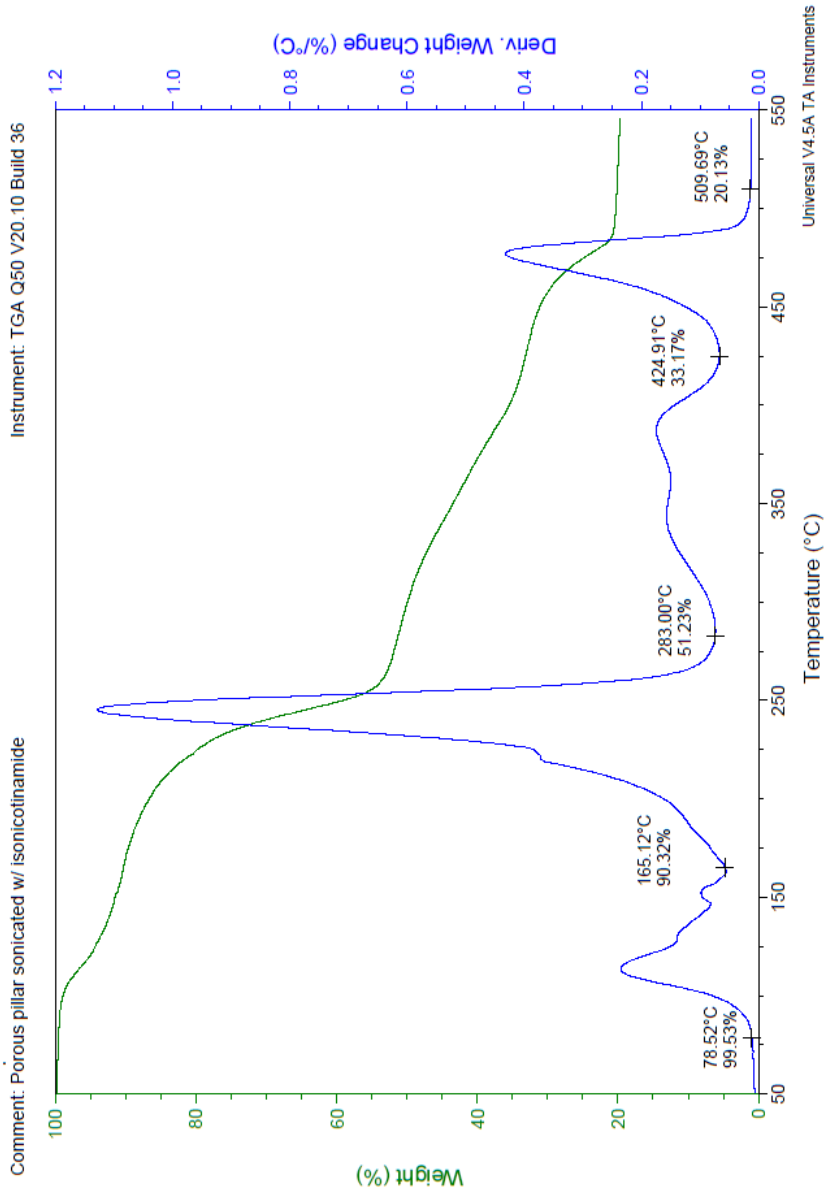

Figure D.87 TGA of the porous Zn(o-tolidine) sonicated with isonicotinamide

Appendix E

Powder X-ray Patterns and Indexing

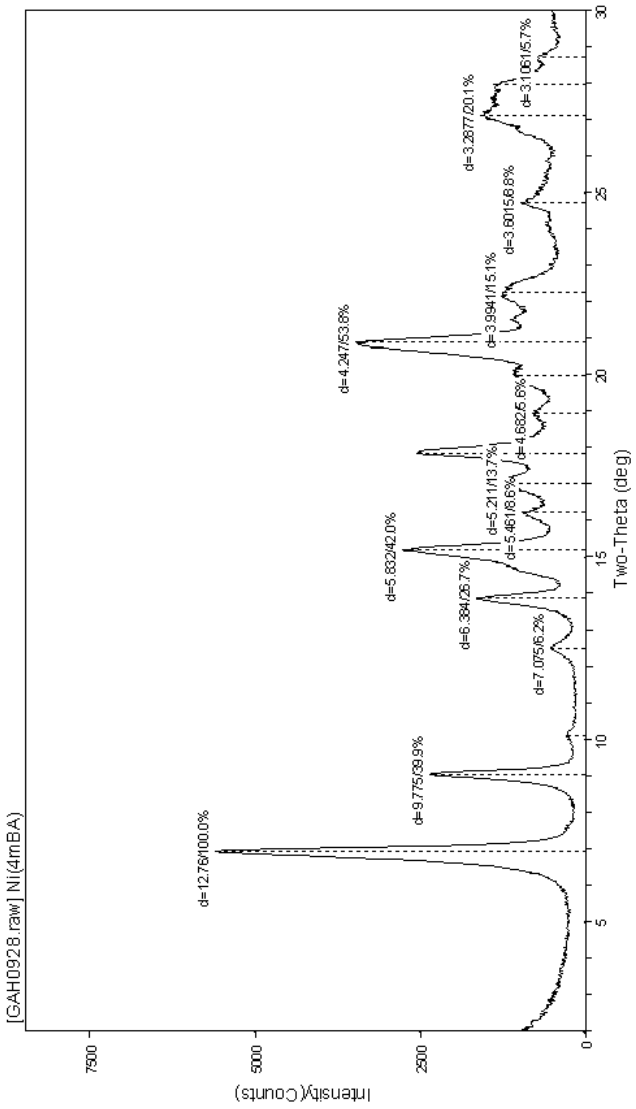

Figure E.1 Powder pattern of Ni(4mBA) starting material

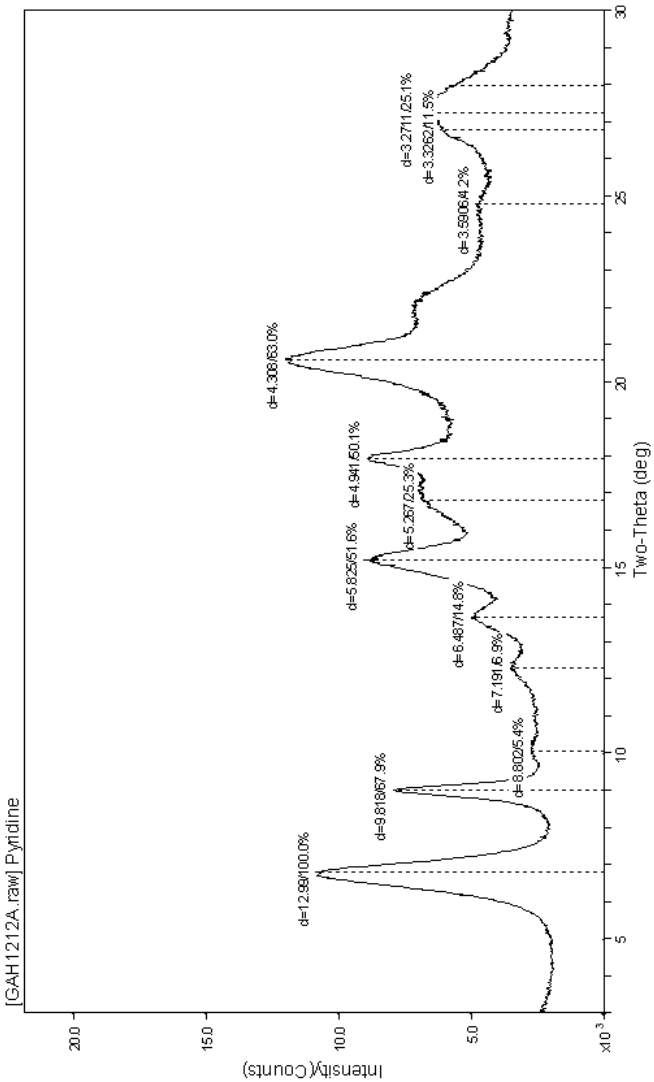

Figure E.2 Powder pattern of Ni(4mBA) sonicated with pyridine

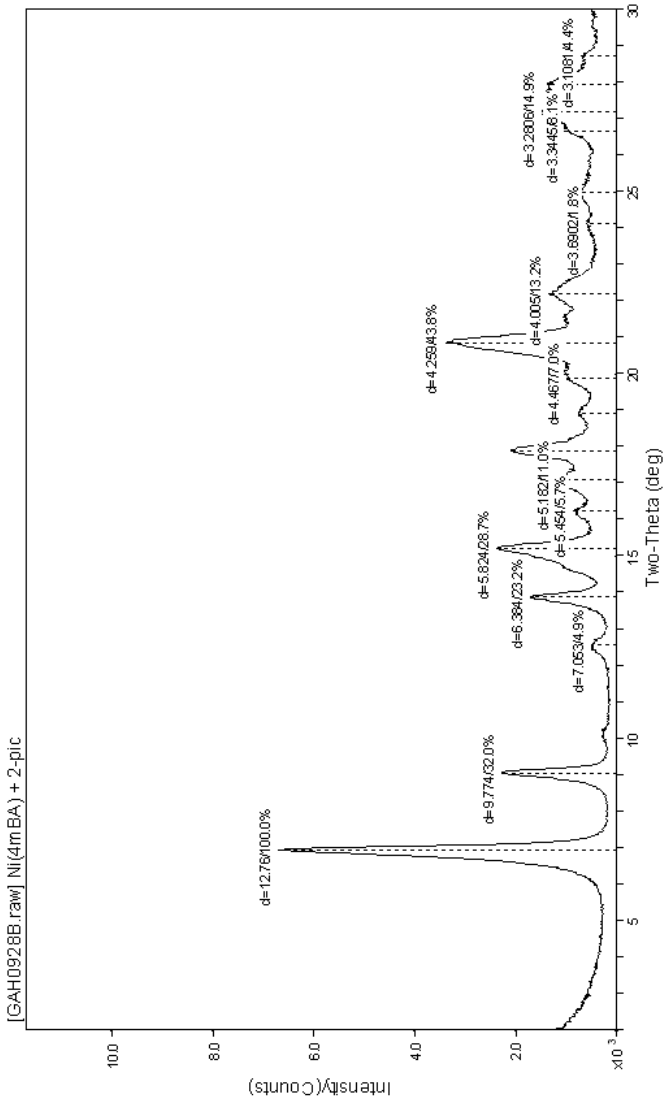

Figure E.3 Powder pattern of Ni(4mBA) sonicated with 2-picoline

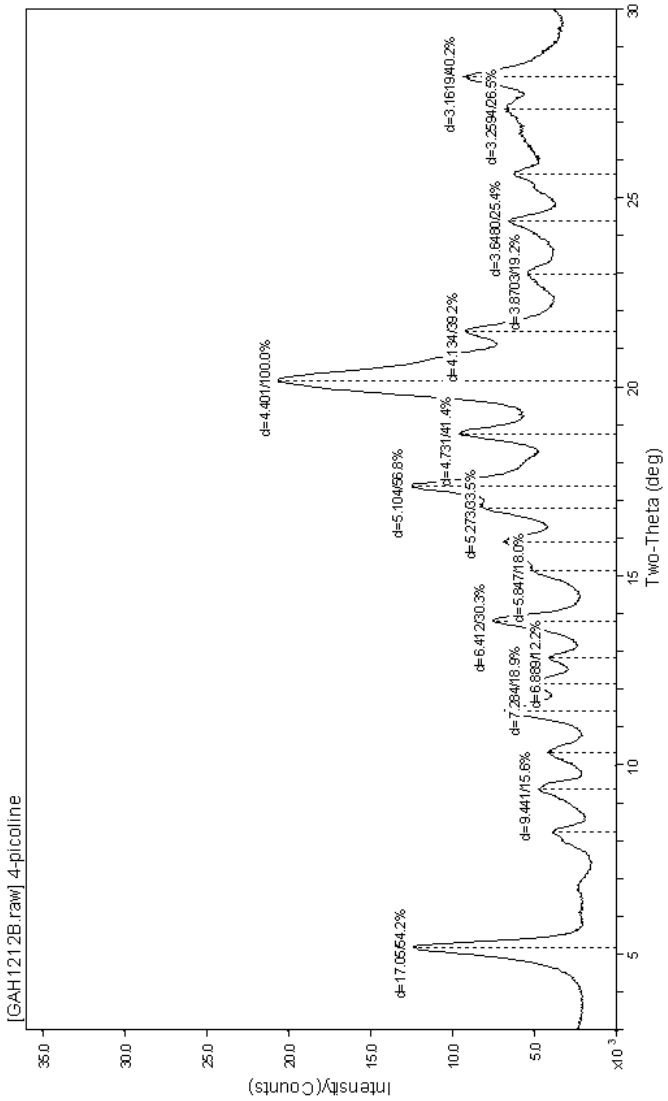

Figure E.4 Powder pattern of Ni(4mBA) sonicated with 4-picoline

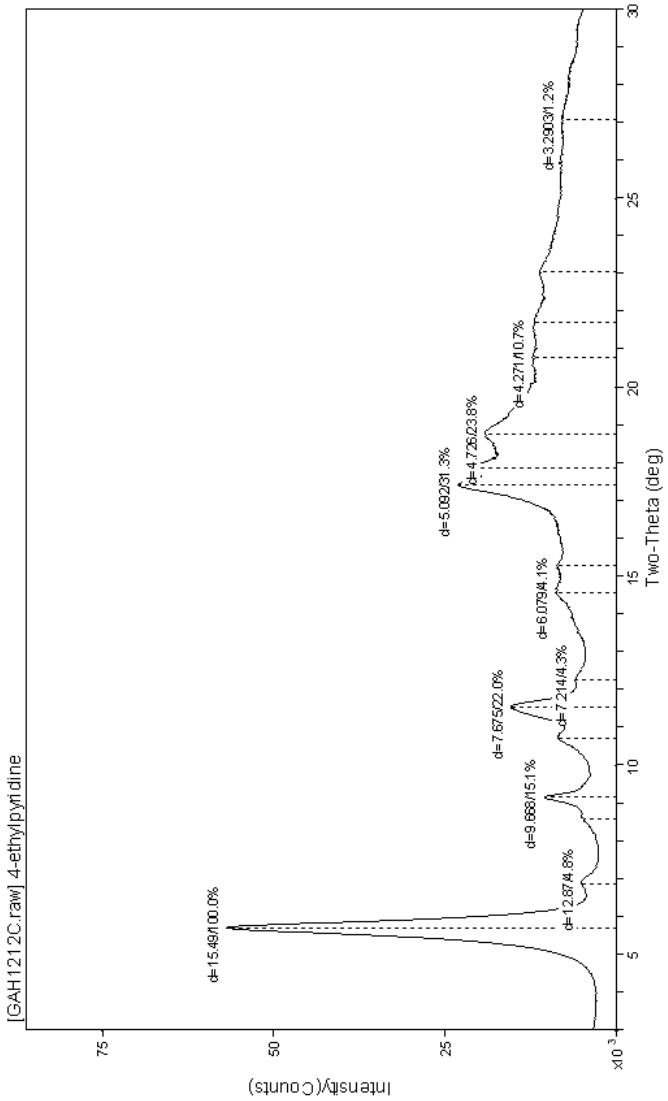

Figure E.5 Powder pattern of Ni(4mBA) sonicated with 4-ethylpyridine

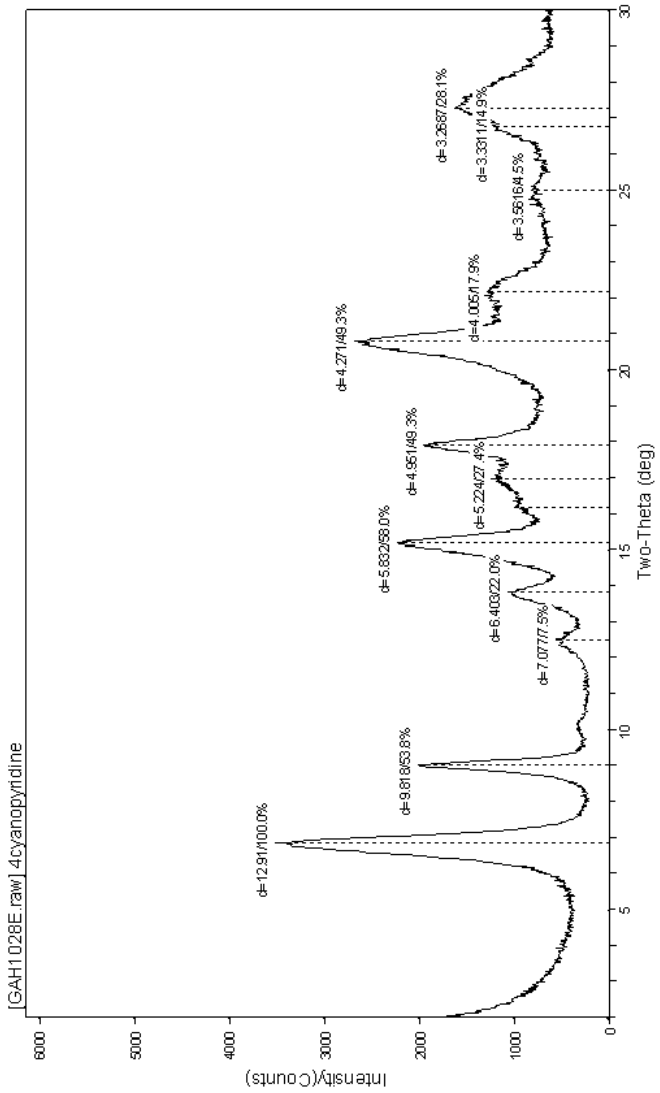

Figure E.6 Powder pattern of Ni(4mBA) sonicated with 4-cyanopyridine

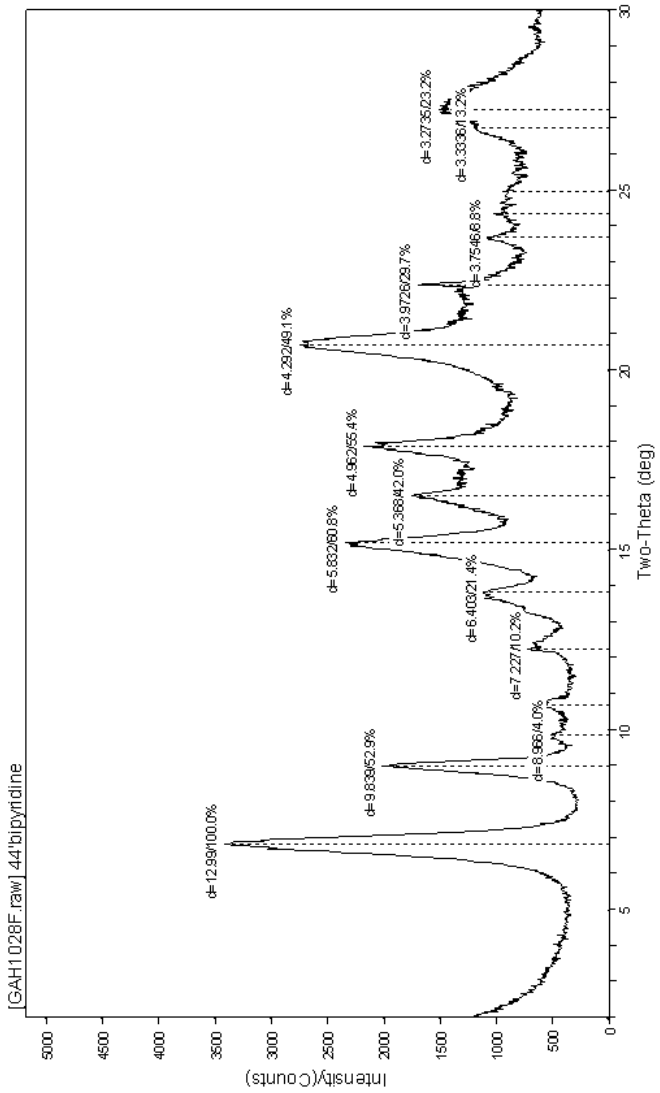

Figure E.7 Powder pattern of Ni(4mBA) sonicated with 4,4’-bipyridine

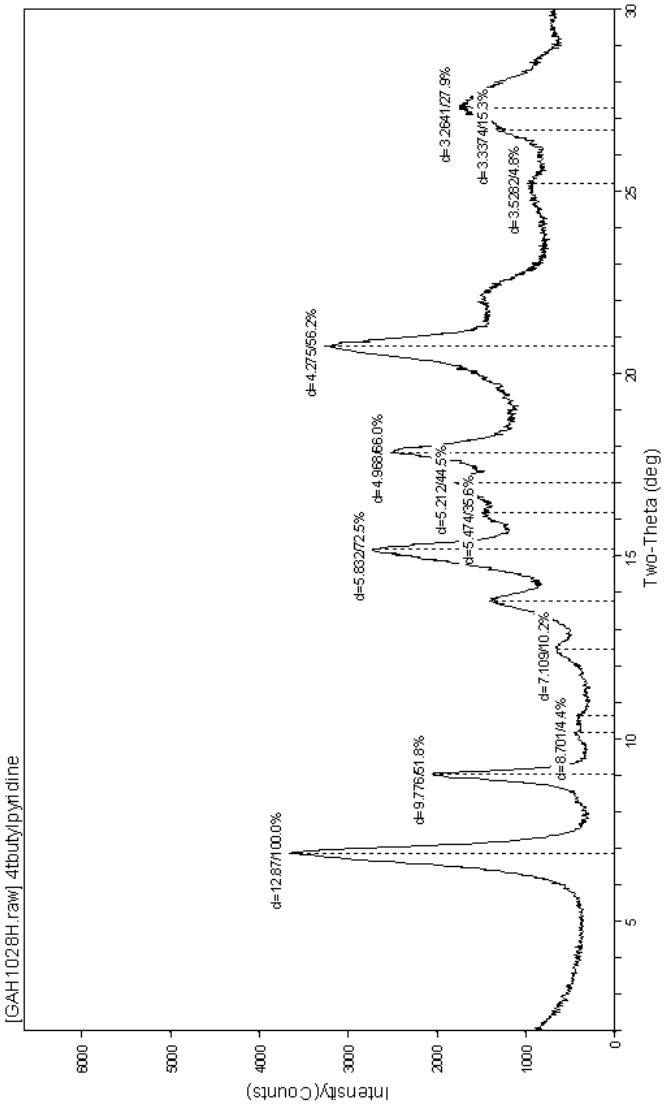

Figure E.8 Powder pattern of Ni(4mBA) sonicated with 4-t-butylpyridine

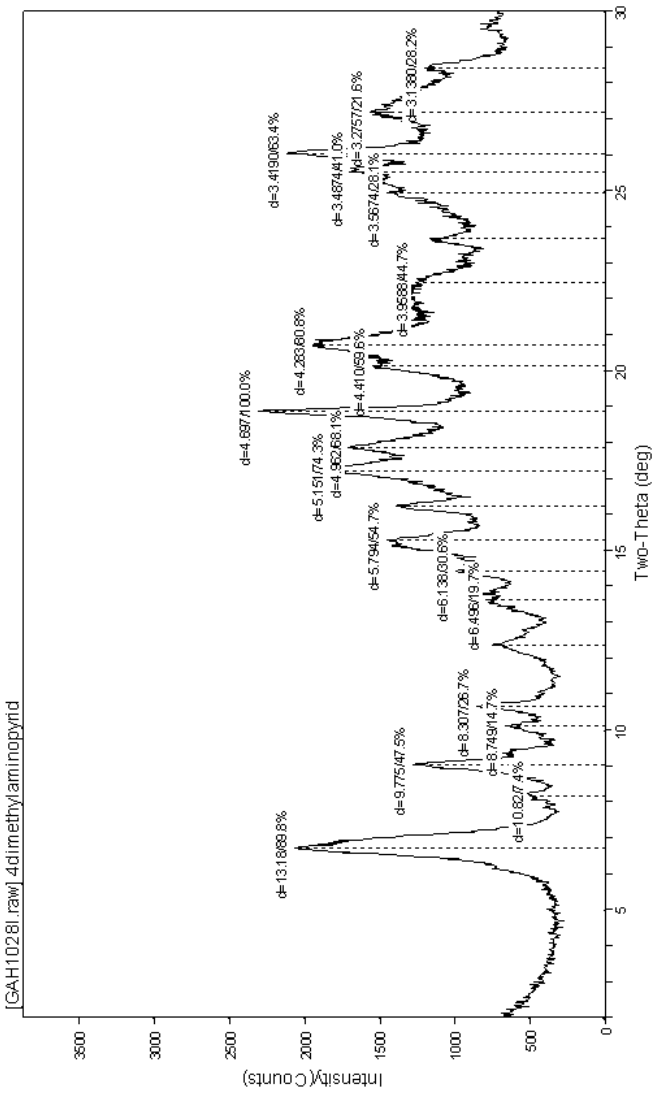

Figure E.9 Powder pattern of Ni(4mBA) sonicated with 4-(dimethylamino)pyridine

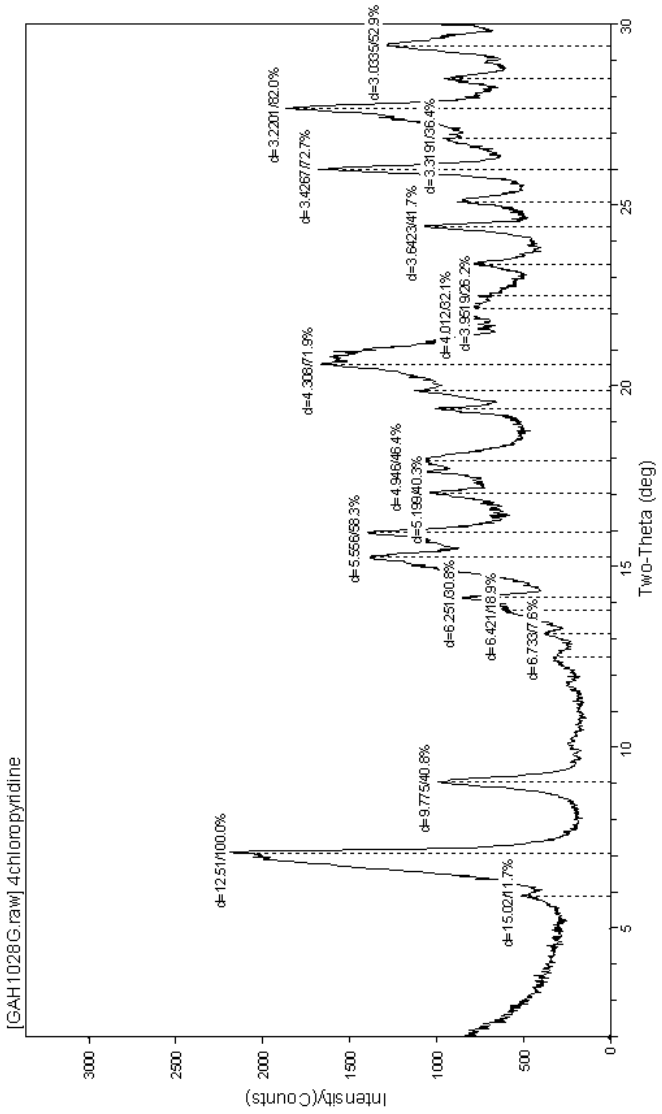

Figure E.10 Powder pattern of Ni(4mBA) sonicated with 4-chloropyridine

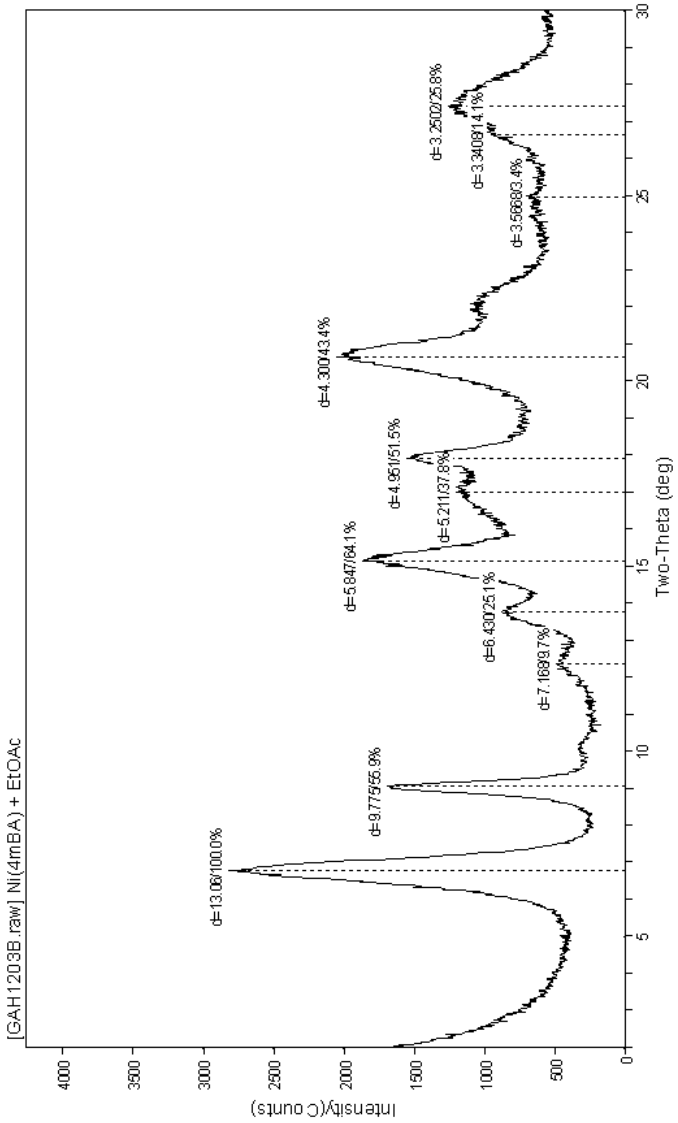

Figure E.11 Powder pattern of Ni(4mBA) sonicated with ethyl acetate

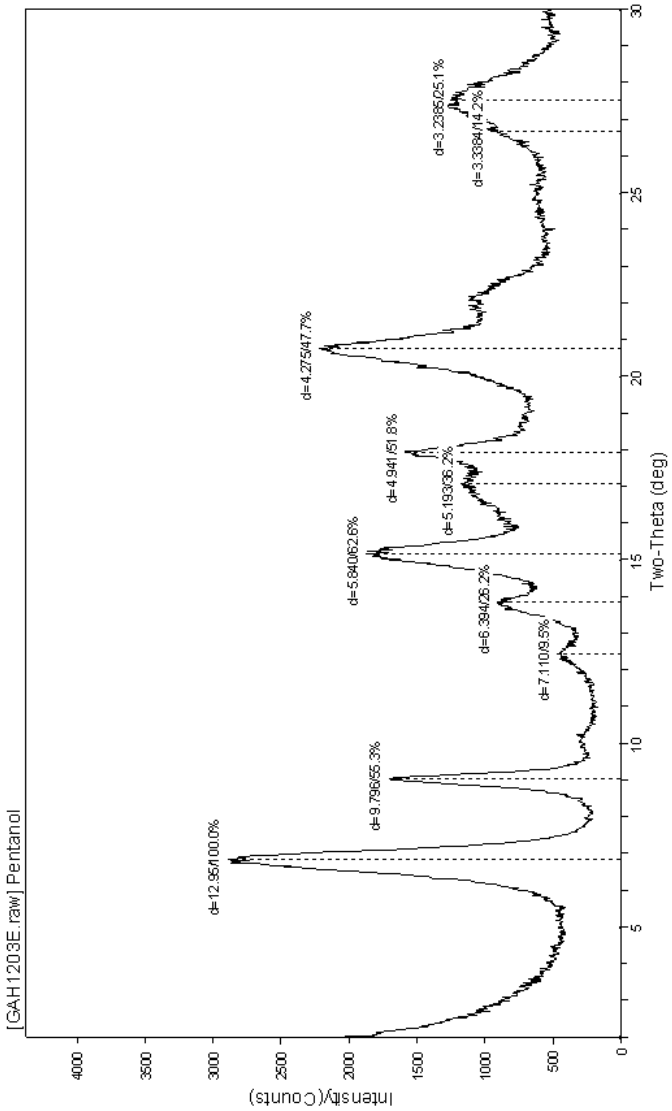

Figure E.12 Powder pattern of Ni(4mBA) sonicated with pentanol

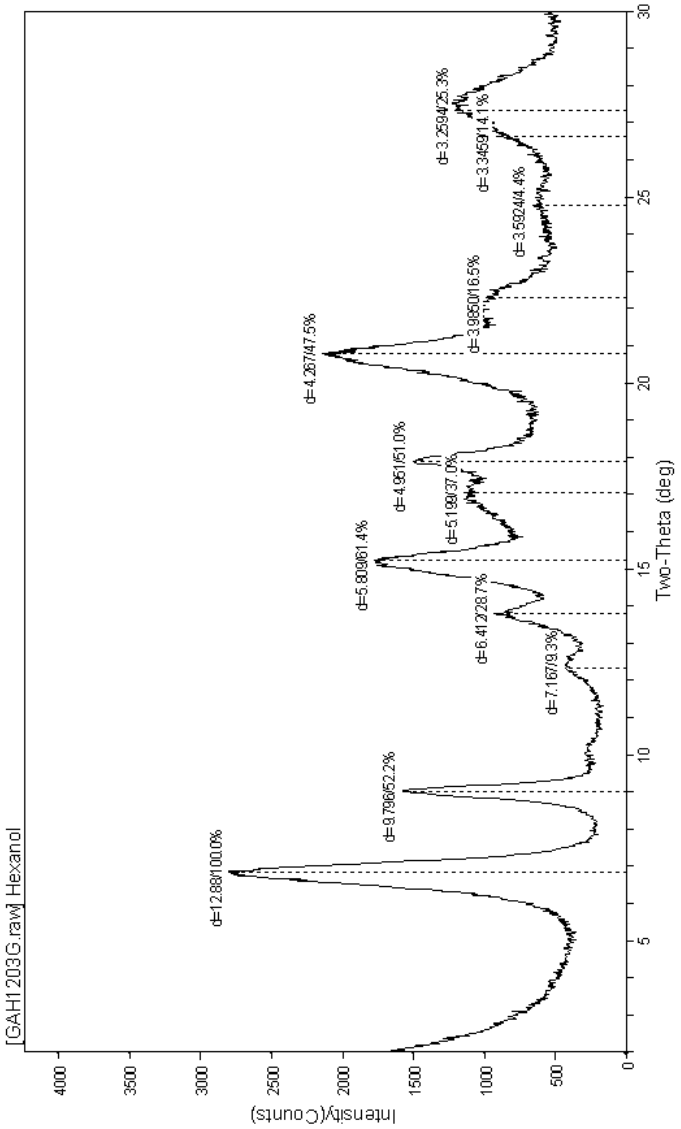

Figure E.13 Powder pattern of Ni(4mBA) sonicated with hexanol

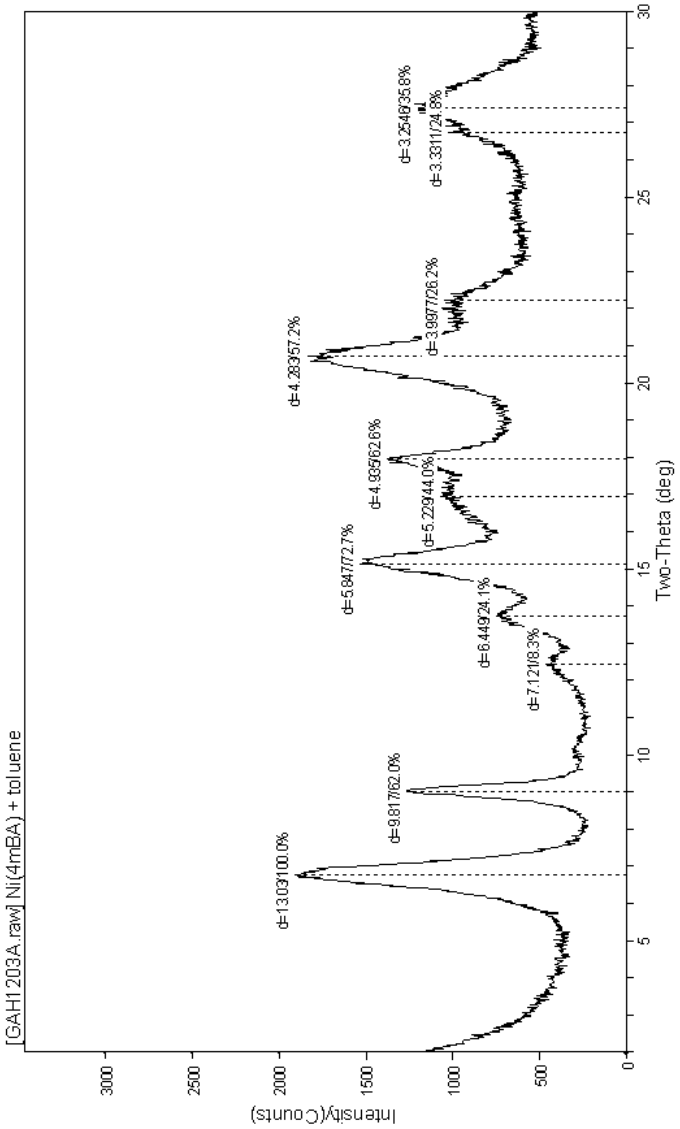

Figure E.14 Powder pattern of Ni(4mBA) sonicated with toluene

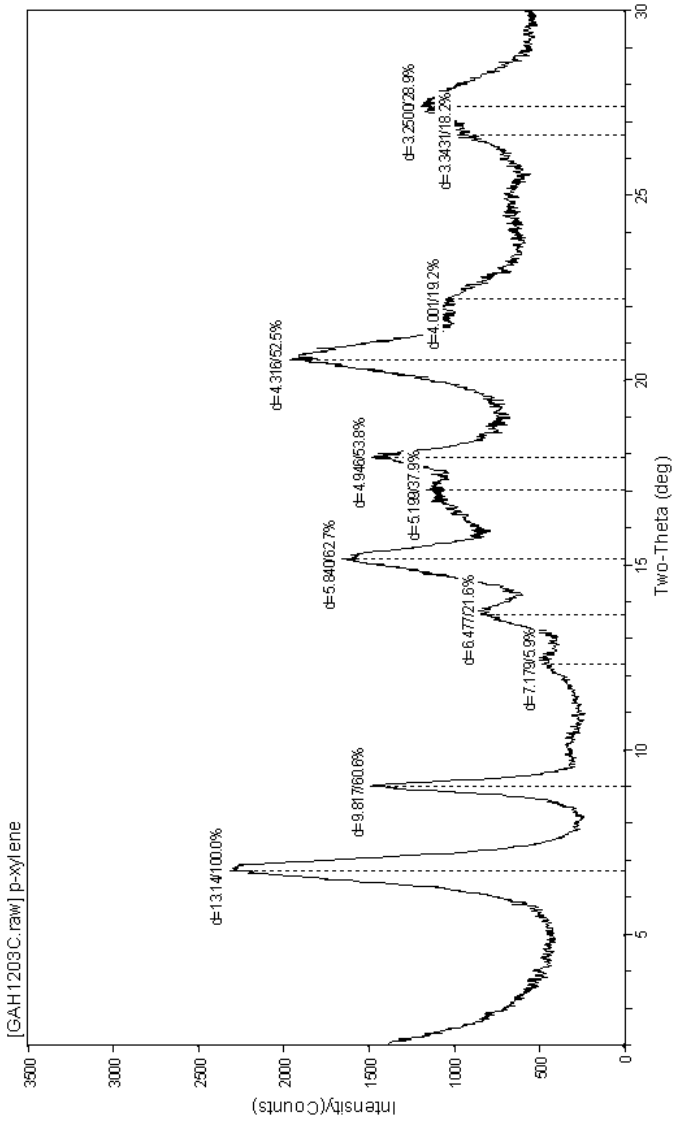

Figure E.15 Powder pattern of Ni(4mBA) sonicated with p-xylene

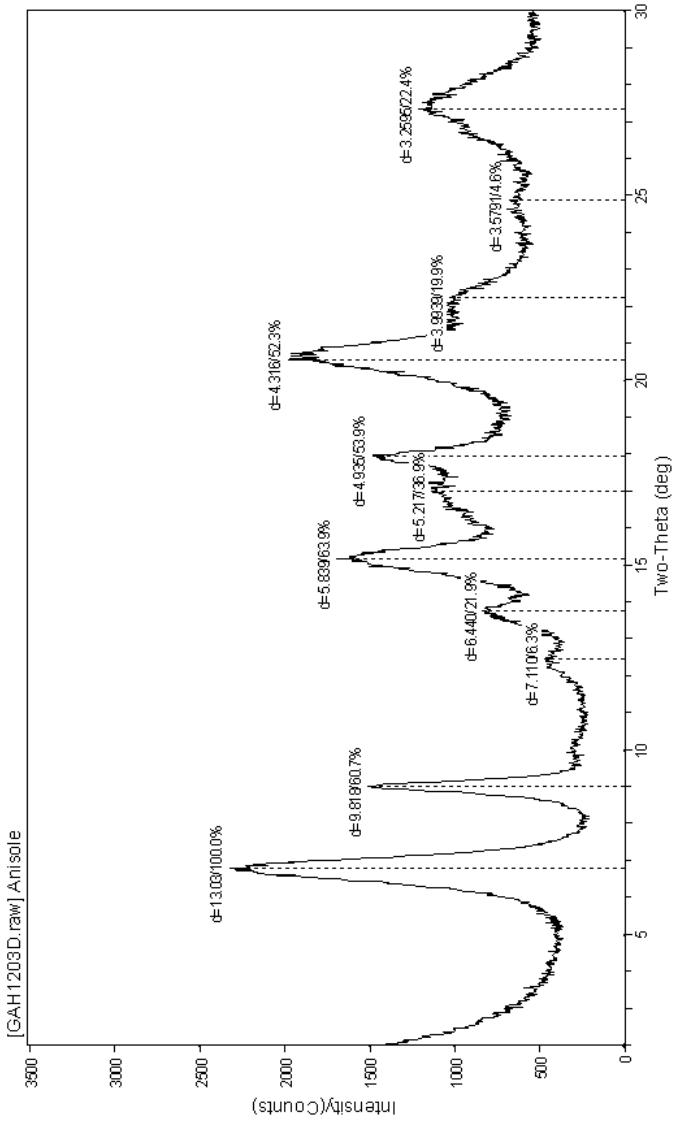

Figure E.16 Powder pattern of Ni(4mBA) sonicated with anisole

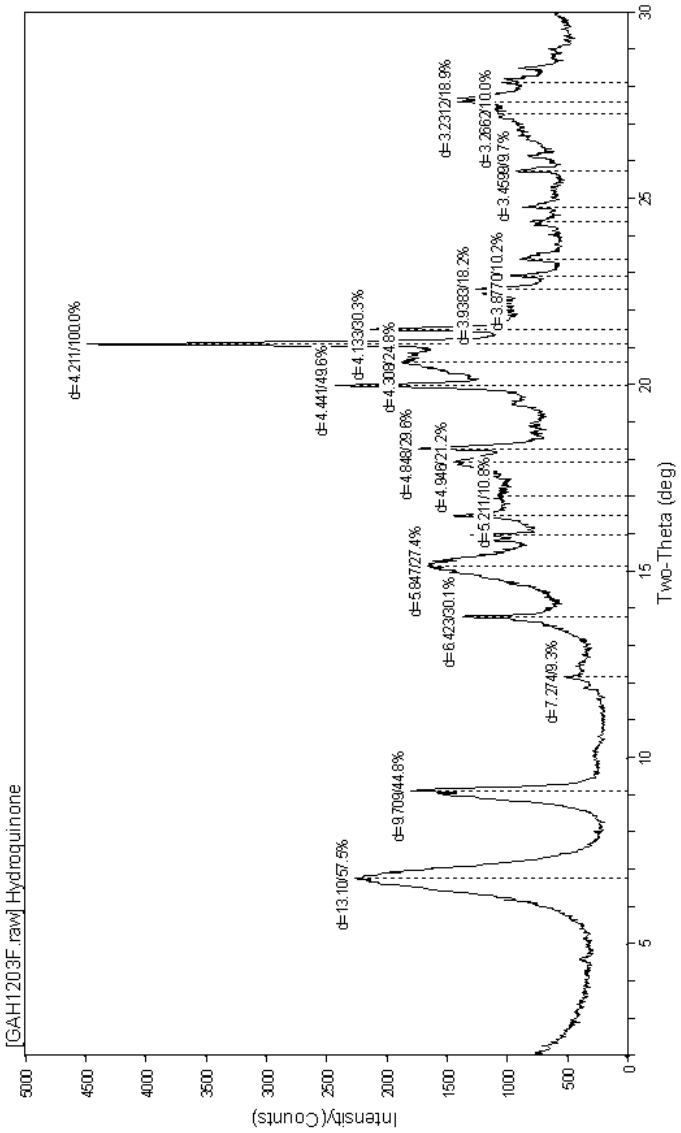

Figure E.17 Powder pattern of Ni(4mBA) sonicated with hydroquinone

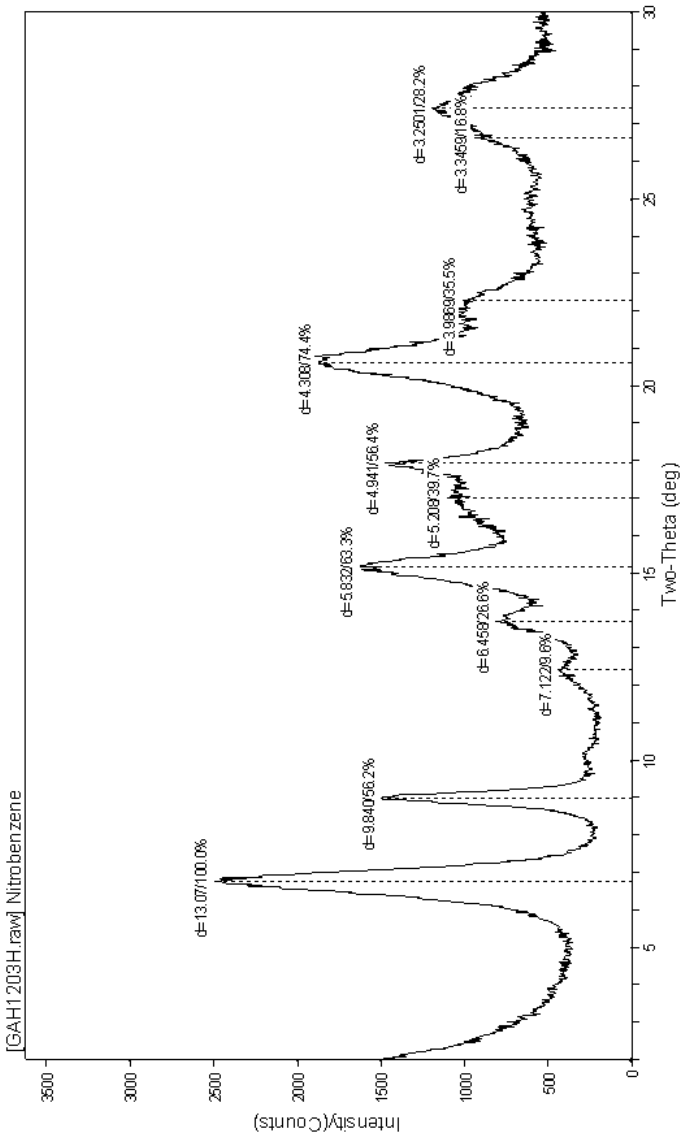

Figure E.18 Powder pattern of Ni(4mBA) sonicated with nitrobenzene

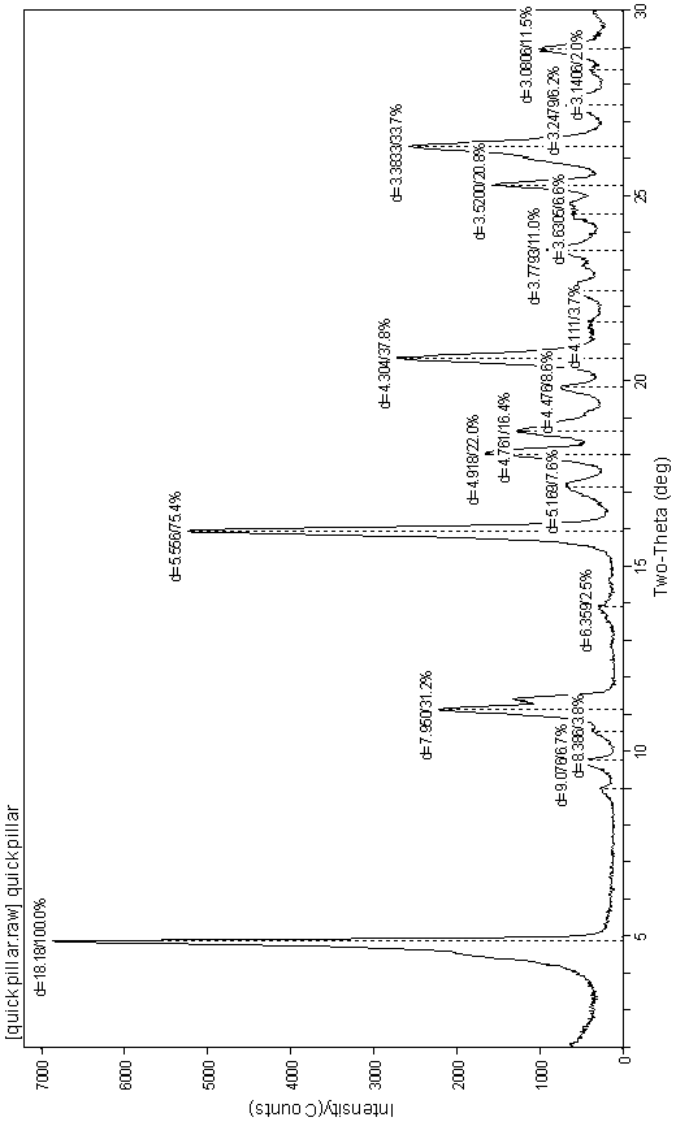

Figure E.19 Powder pattern of Zn(o-tolidine) pillar starting material

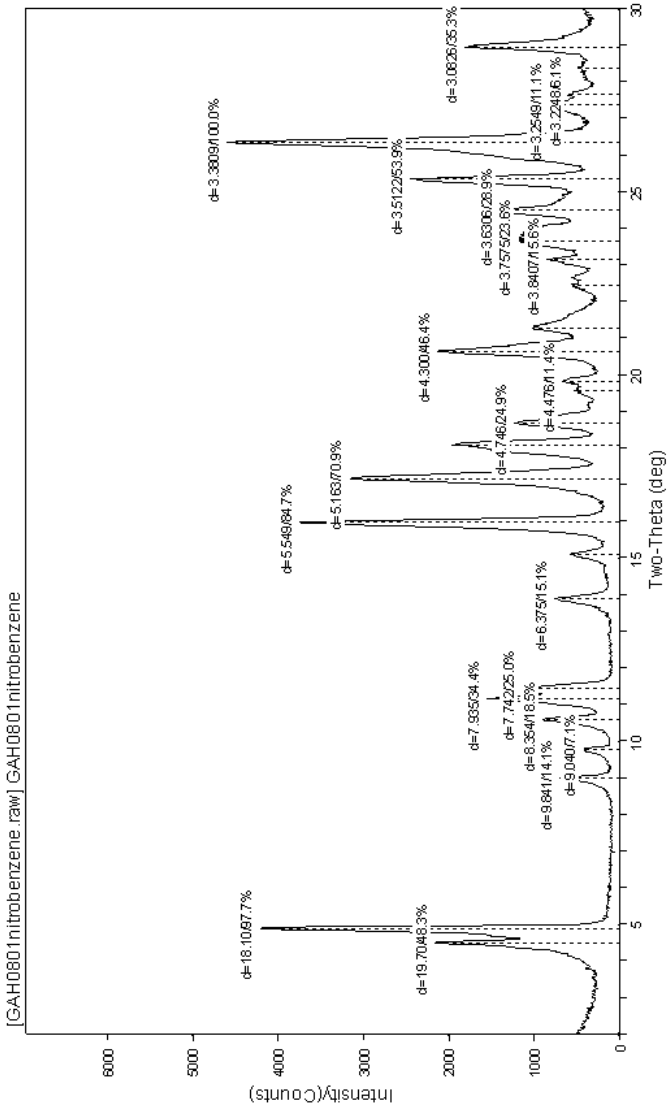

Figure E.20 Powder pattern of Zn(o-tolidine) crystallized with nitrobenzene

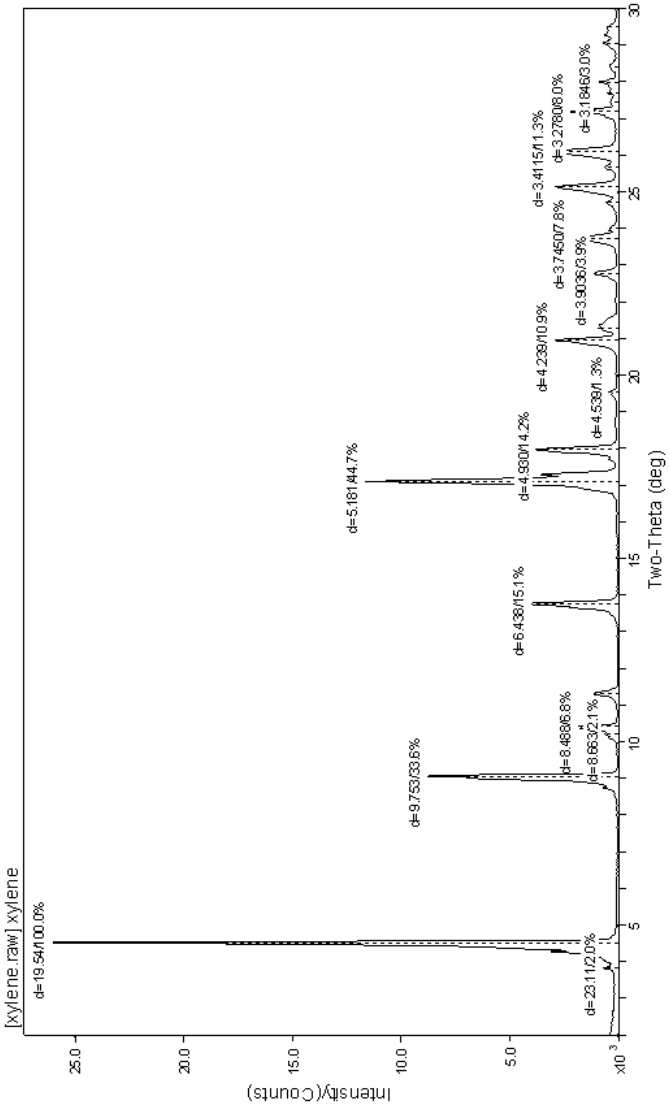

Figure E.21 Powder pattern of Zn(o-tolidine) crystallized with p-xylene

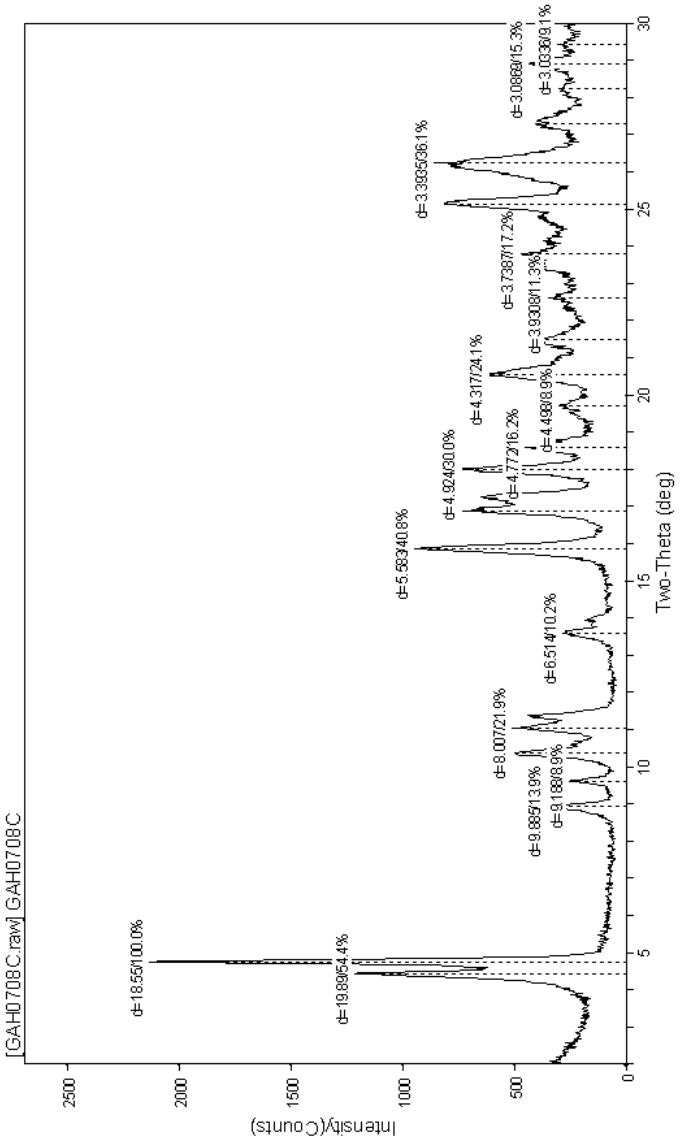

Figure E.22 Powder pattern of Zn(o-tolidine) crystallized with pentanol

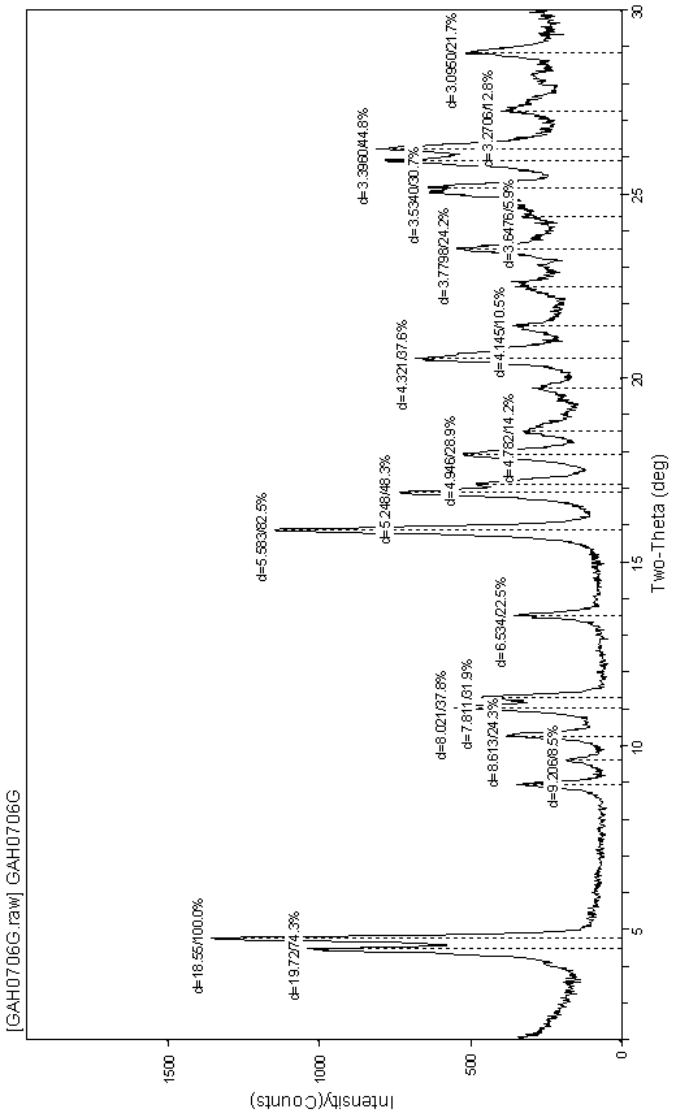

Figure E.23 Powder pattern of Zn(o-tolidine) crystallized with hexanol

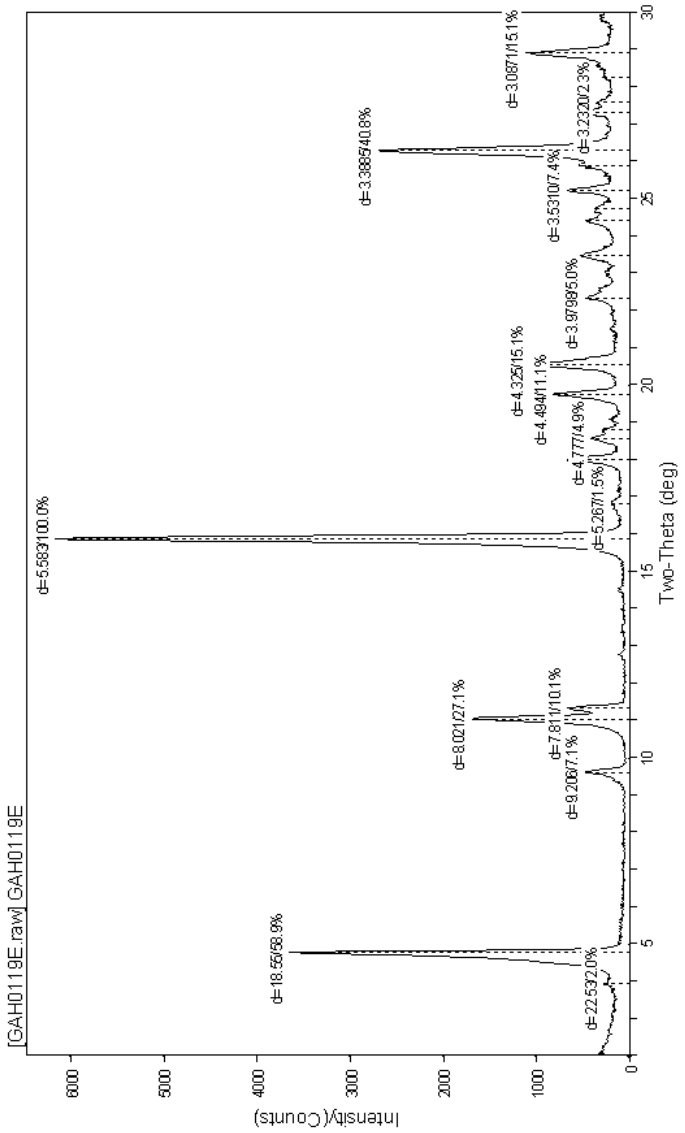

Figure E.24 Powder pattern of Zn(o-tolidine) crystallized with 1,4-difluorobenzene

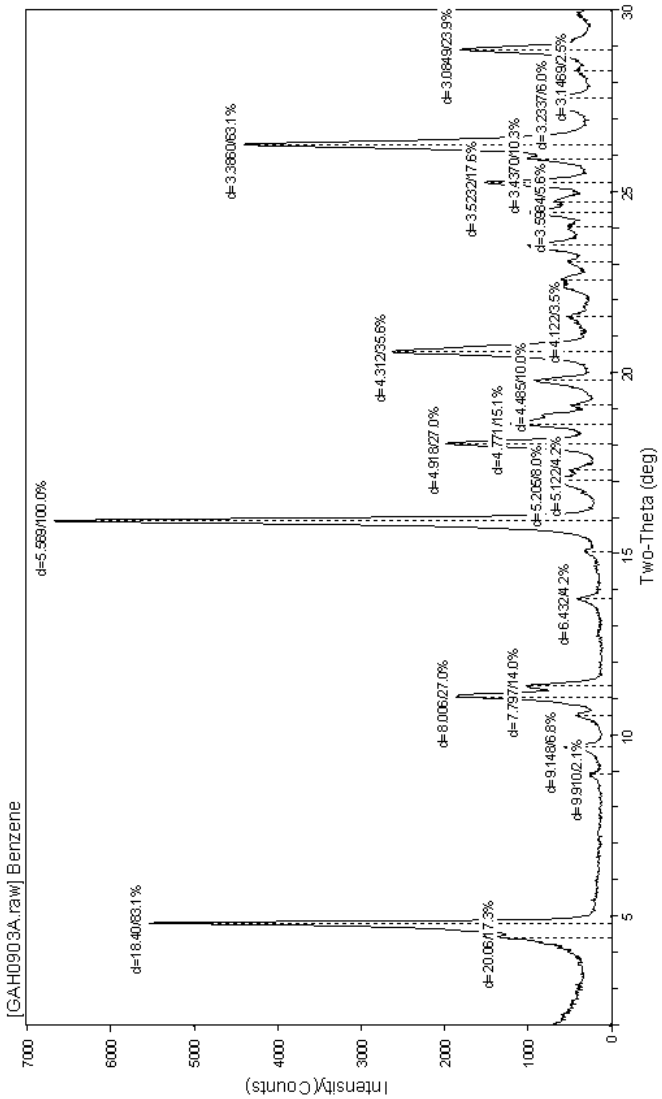

Figure E.25 Powder pattern of porous Zn(o-tolidine) sonicated with benzene

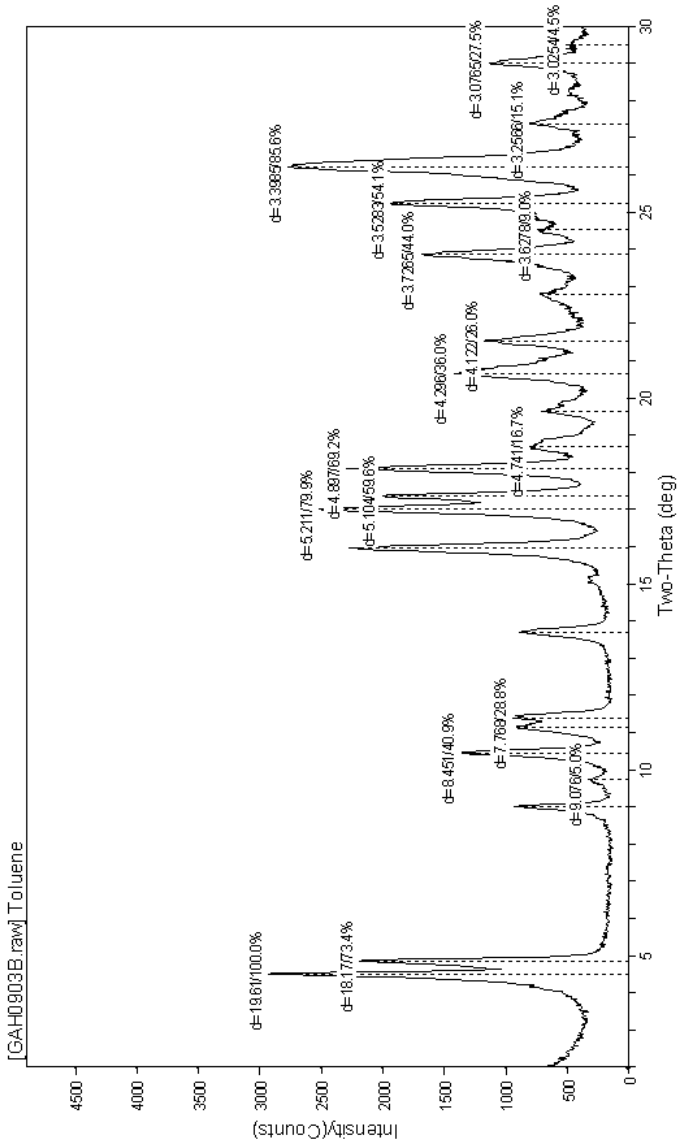

Figure E.26 Powder pattern of porous Zn(o-tolidine) sonicated with toluene

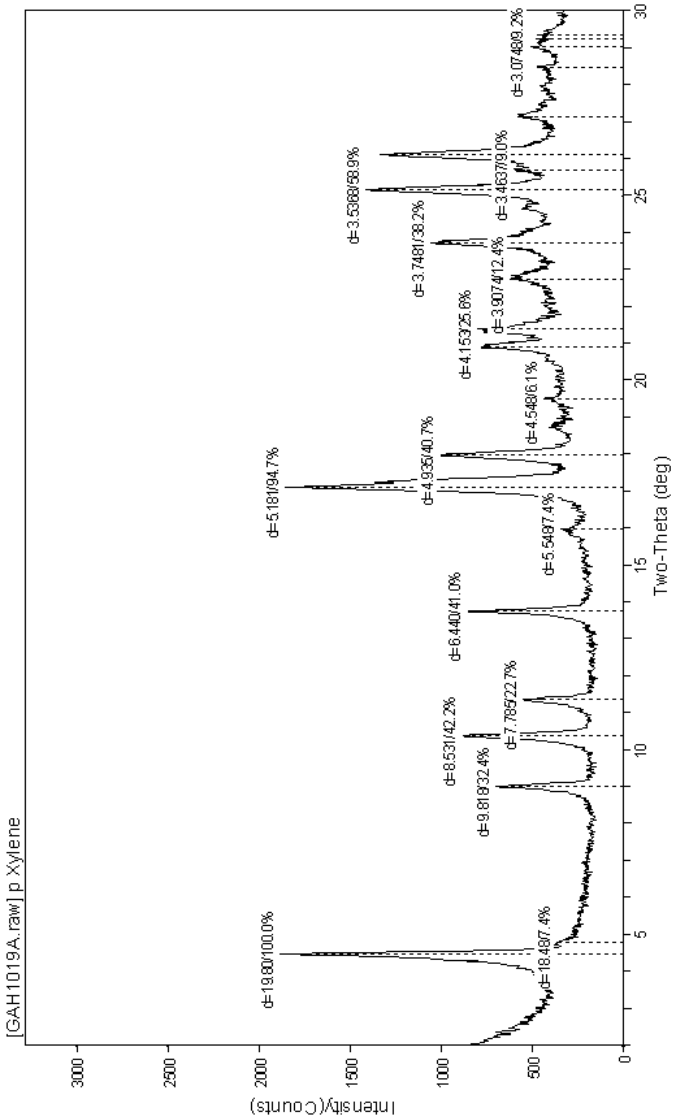

Figure E.27 Powder pattern of porous Zn(o-tolidine) sonicated with p-xylene

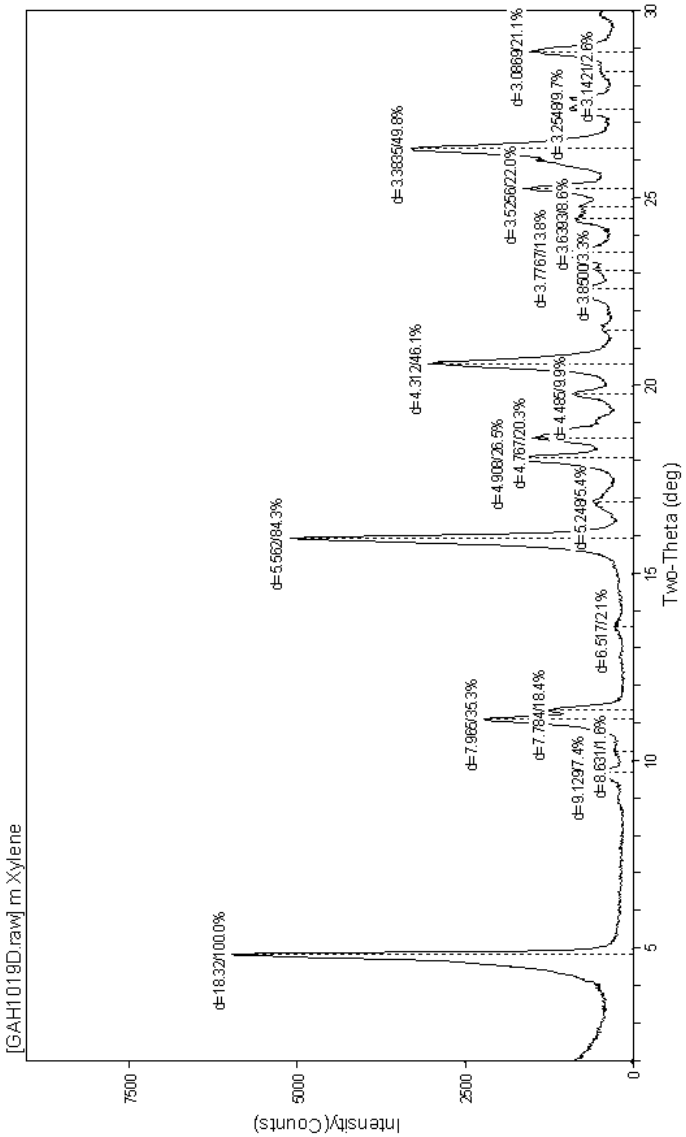

Figure E.28 Powder pattern of porous Zn(o-tolidine) sonicated with m-xylene

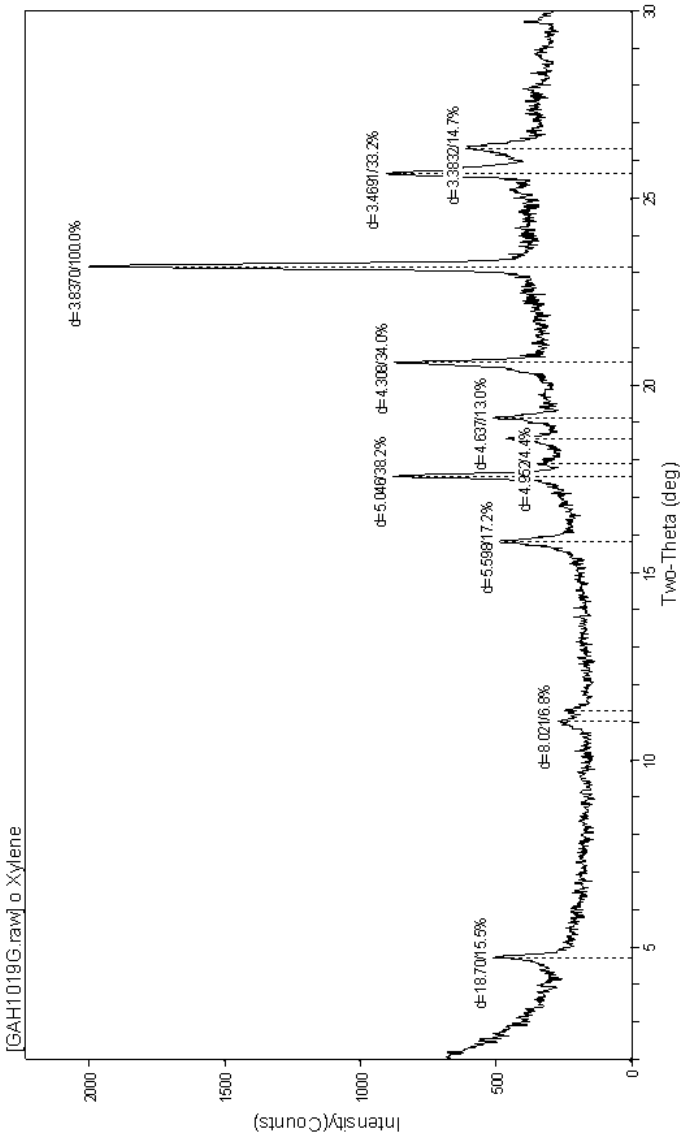

Figure E.29 Powder pattern of porous Zn(o-tolidine) sonicated with o-xylene

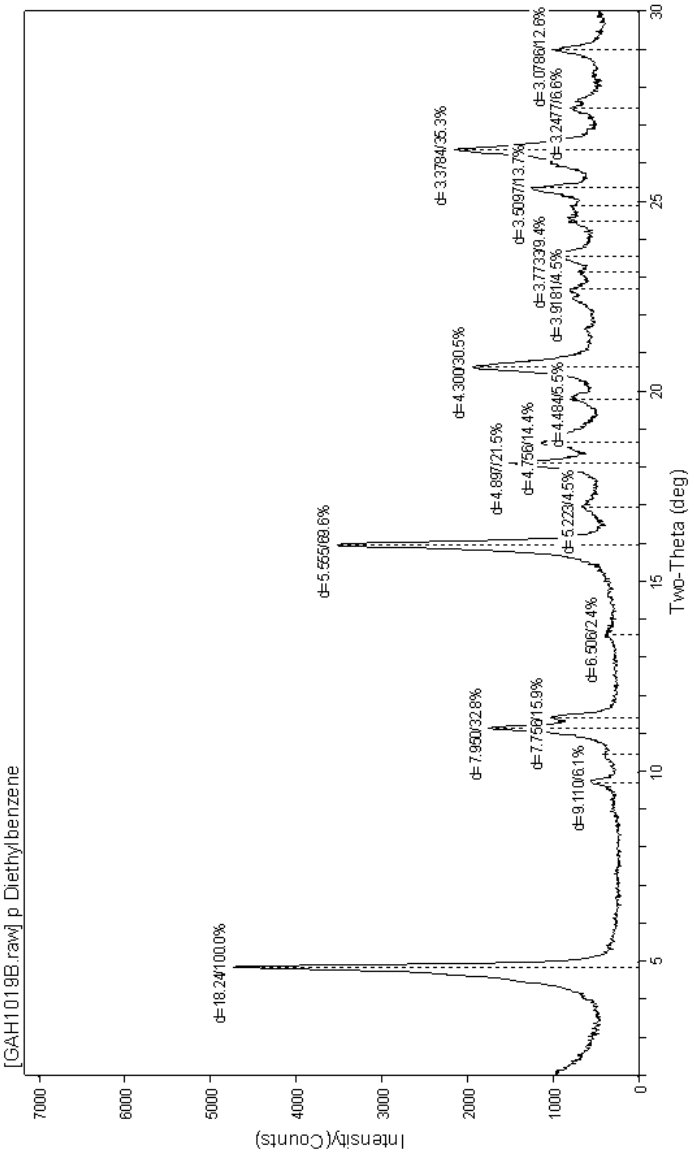

Figure E.30 Powder pattern of porous Zn(o-tolidine) sonicated with p-diethylbenzene

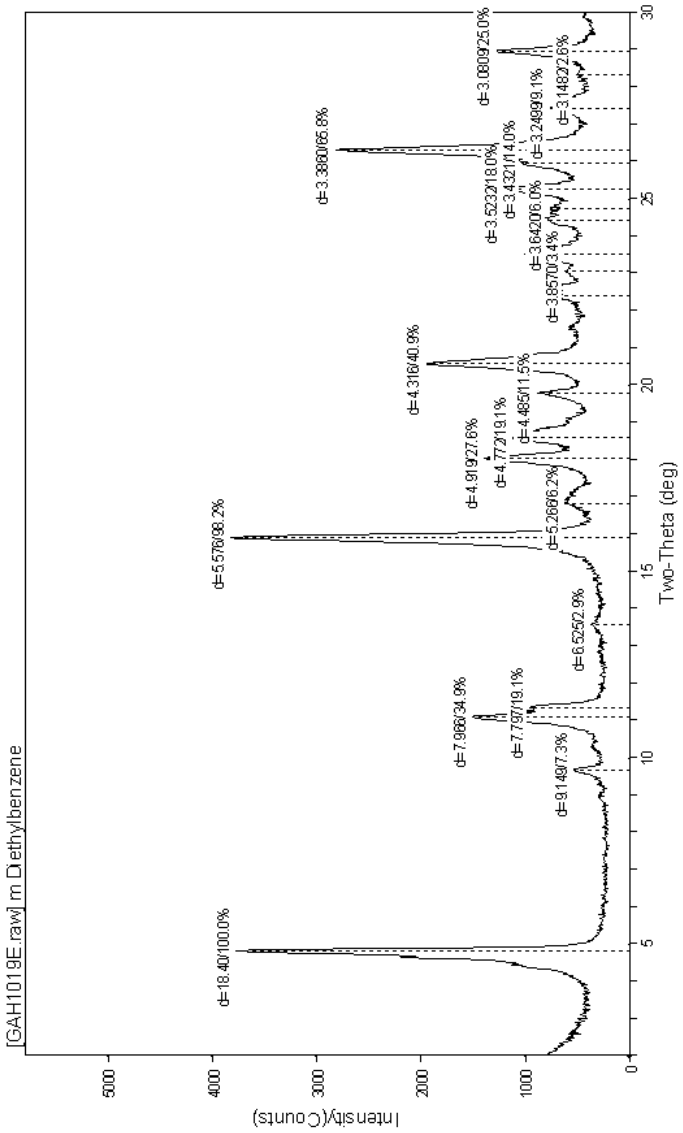

Figure E.31 Powder pattern of porous Zn(o-tolidine) sonicated with m-diethylbenzene

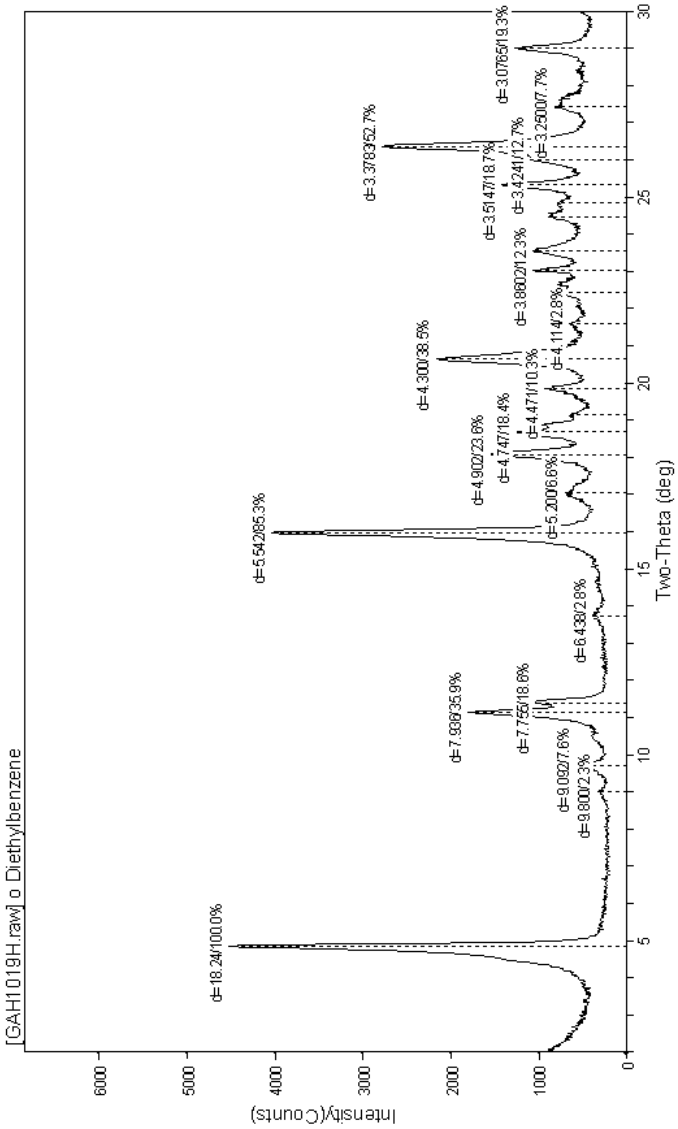

Figure E.32 Powder pattern of porous Zn(o-tolidine) sonicated with o-diethylbenzene

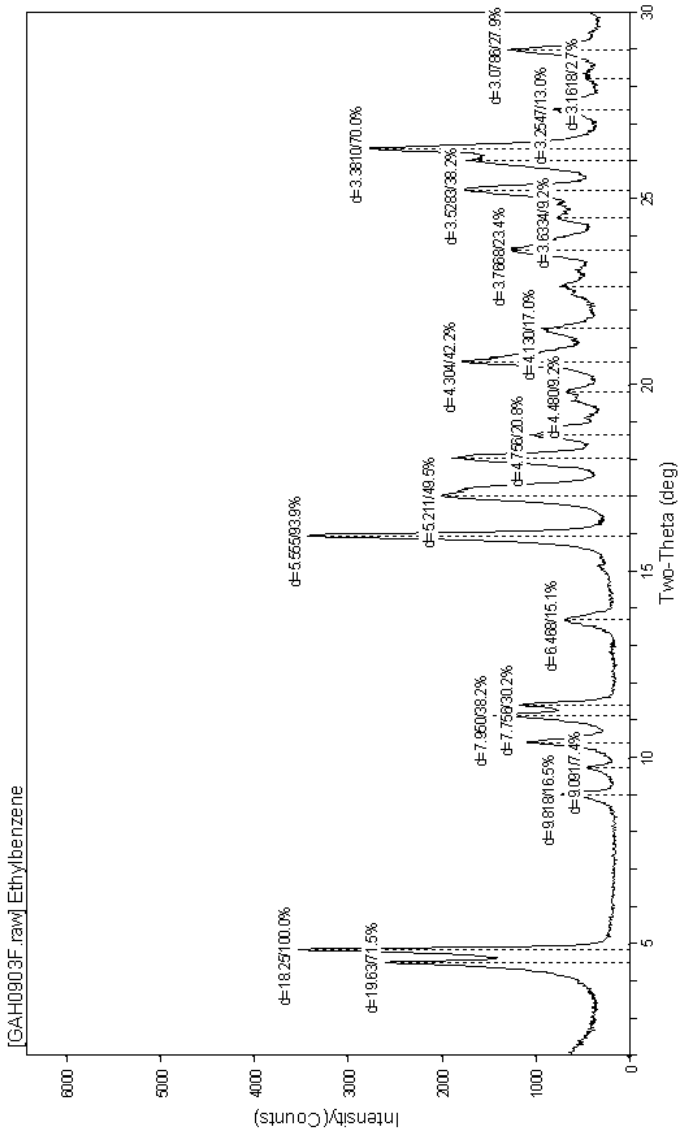

Figure E.33 Powder pattern of porous Zn(o-tolidine) sonicated with ethylbenzene

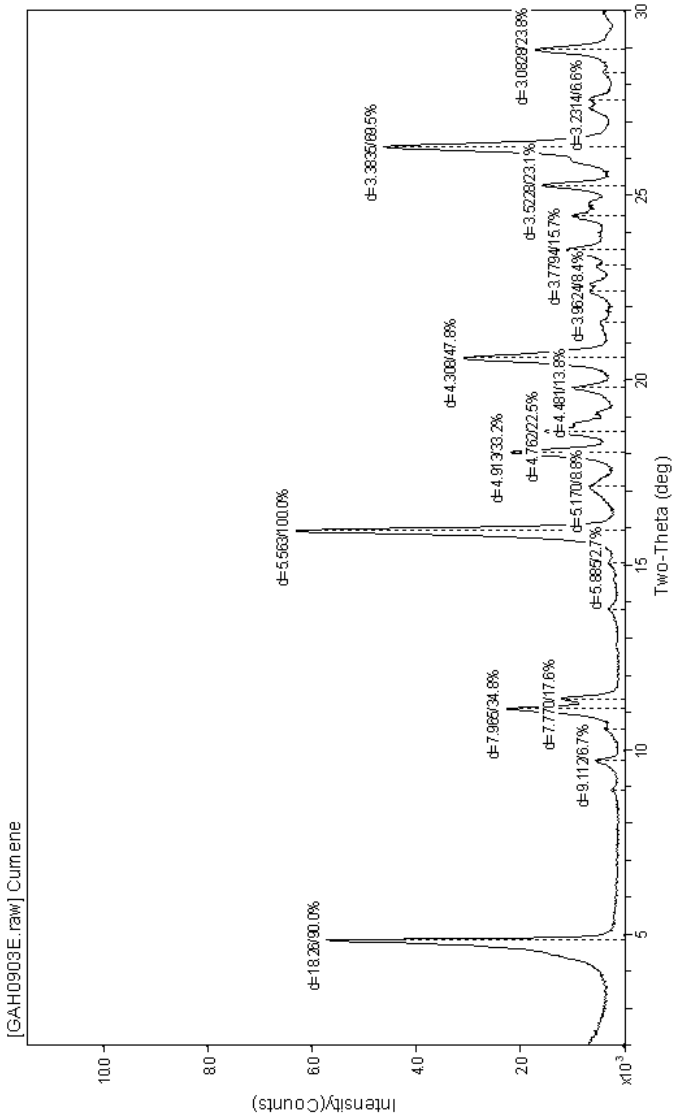

Figure E.34 Powder pattern of porous Zn(o-tolidine) sonicated with cumene

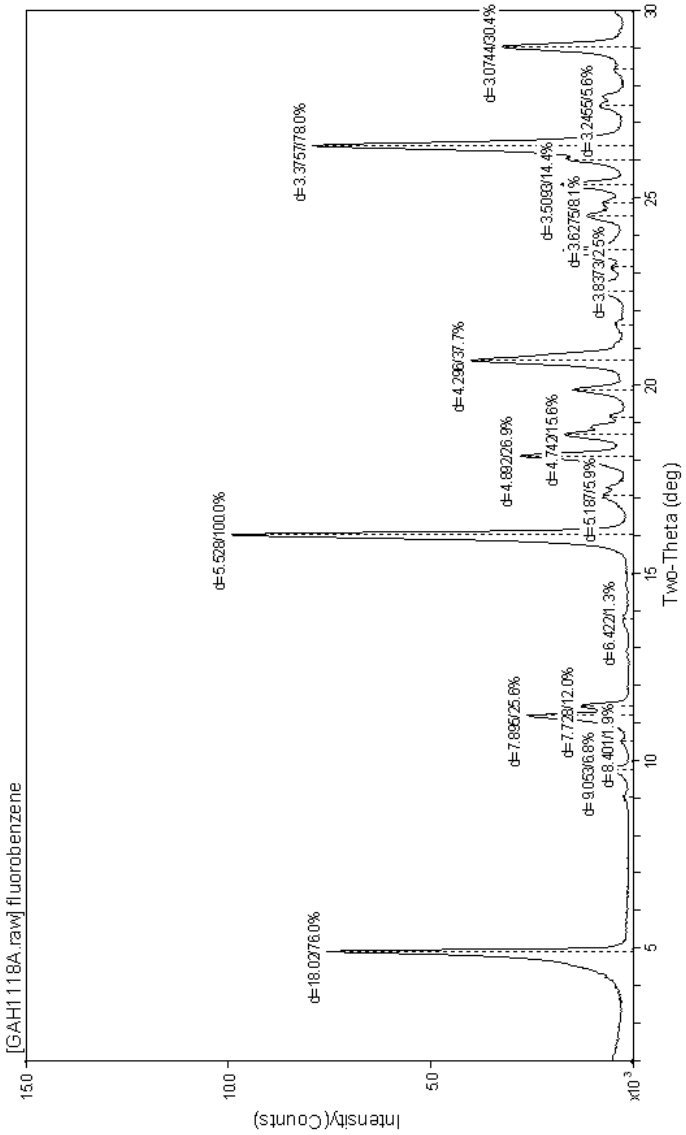

Figure E.35 Powder pattern of porous Zn(o-tolidine) sonicated with fluorobenzene

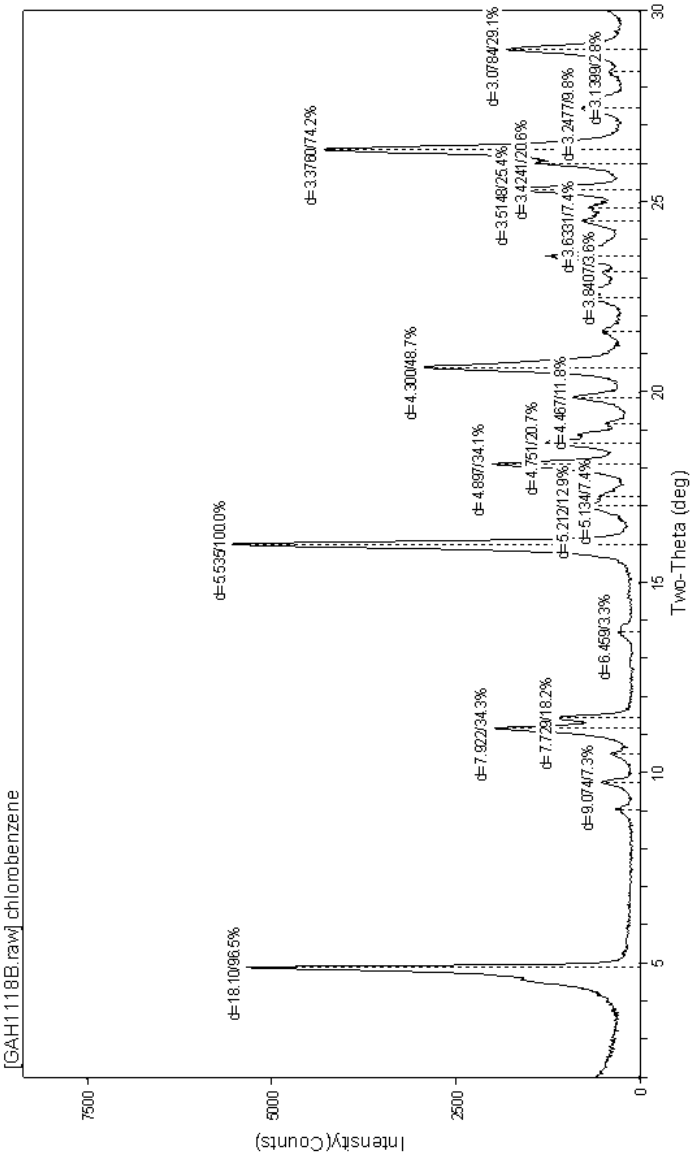

Figure E.36 Powder pattern of porous Zn(o-tolidine) sonicated with chlorobenzene

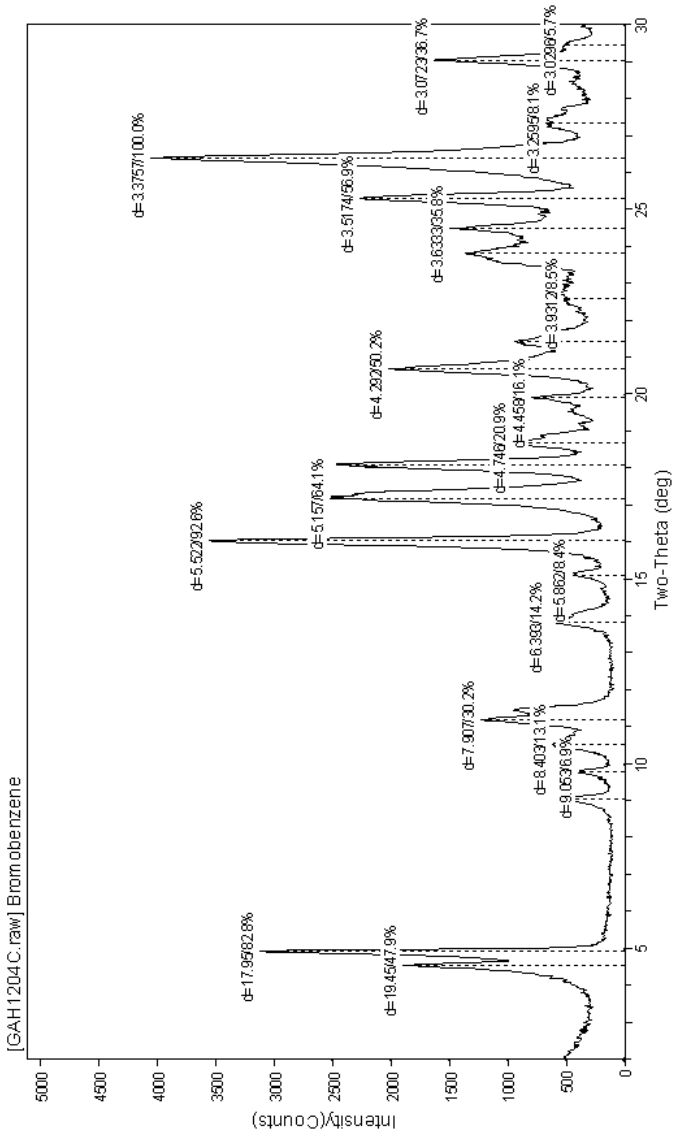

Figure E.37 Powder pattern of porous Zn(o-tolidine) sonicated with bromobenzene

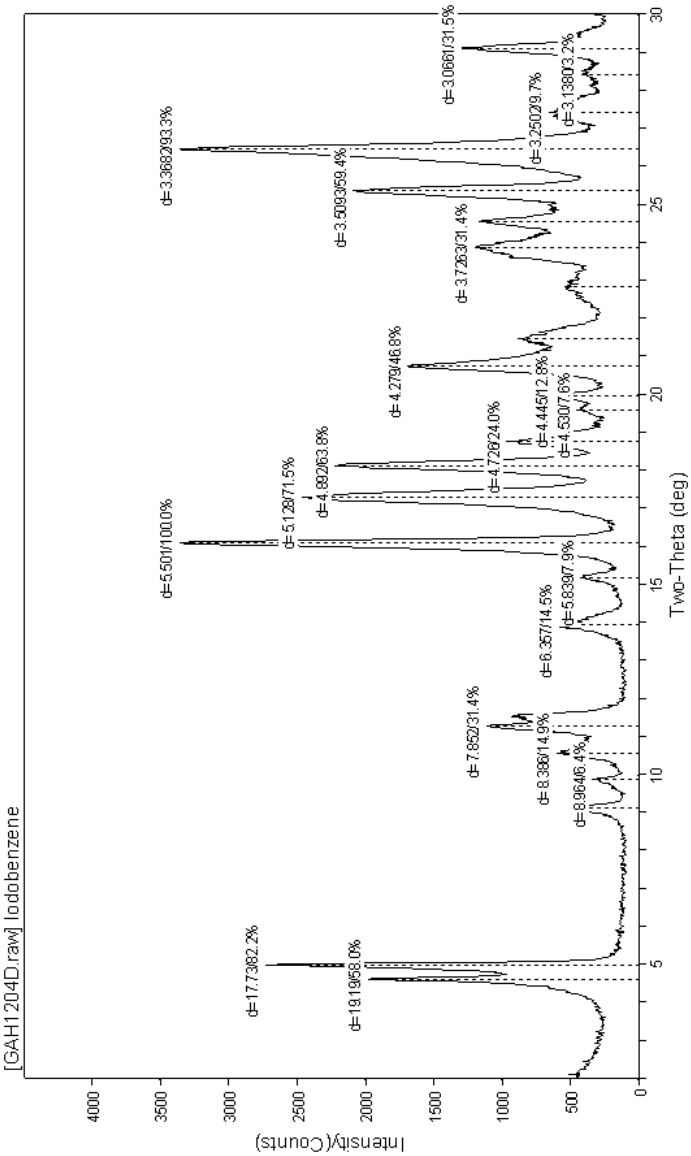

Figure E.38 Powder pattern of porous Zn(o-tolidine) sonicated with iodobenzene

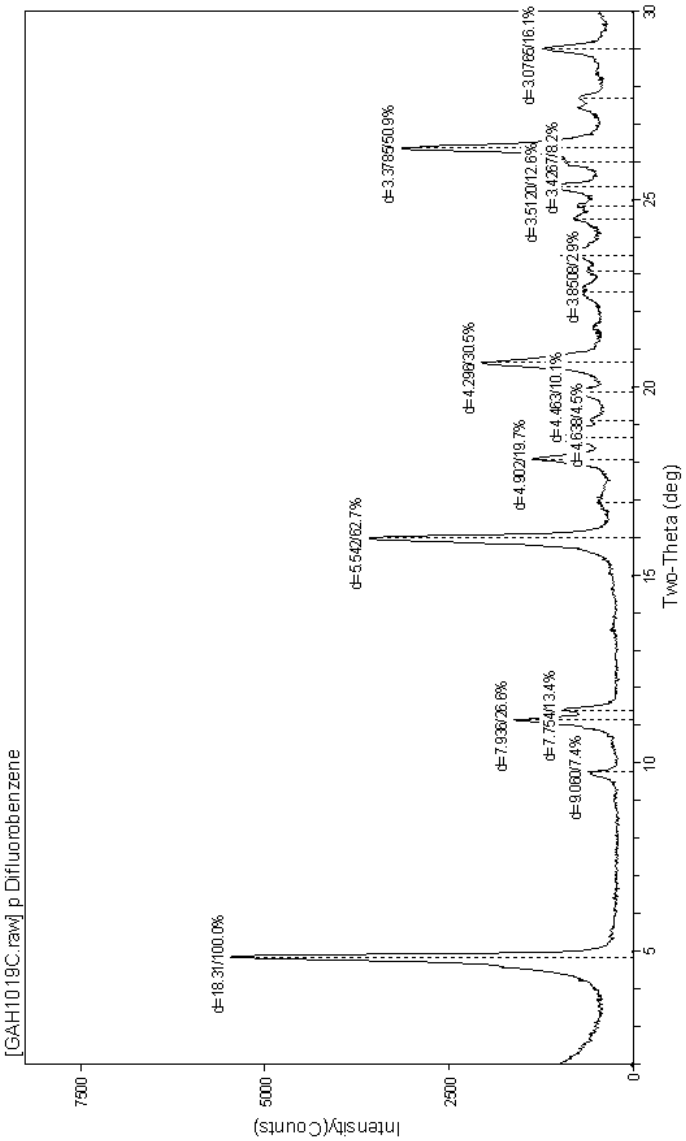

Figure E.39 Powder pattern of porous Zn(o-tolidine) sonicated with p-difluorbenzene

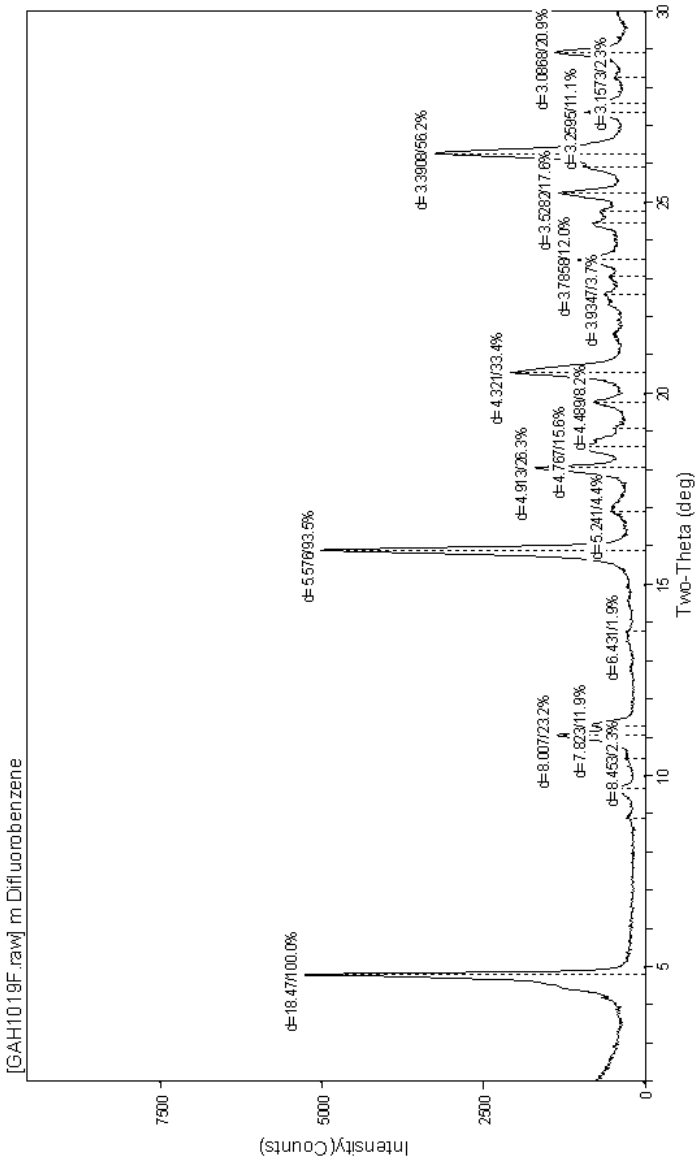

Figure E.40 Powder pattern of porous Zn(o-tolidine) sonicated with m-difluorobenzene

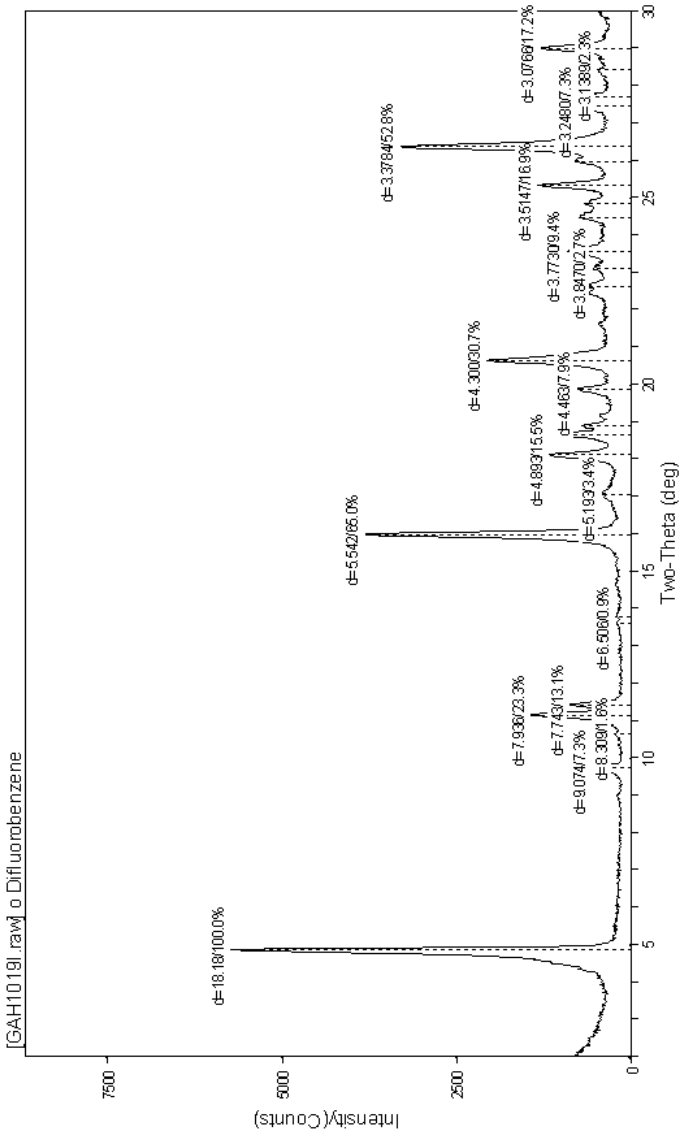

Figure E.41 Powder pattern of porous Zn(o-tolidine) sonicated with o-difluorobenzene

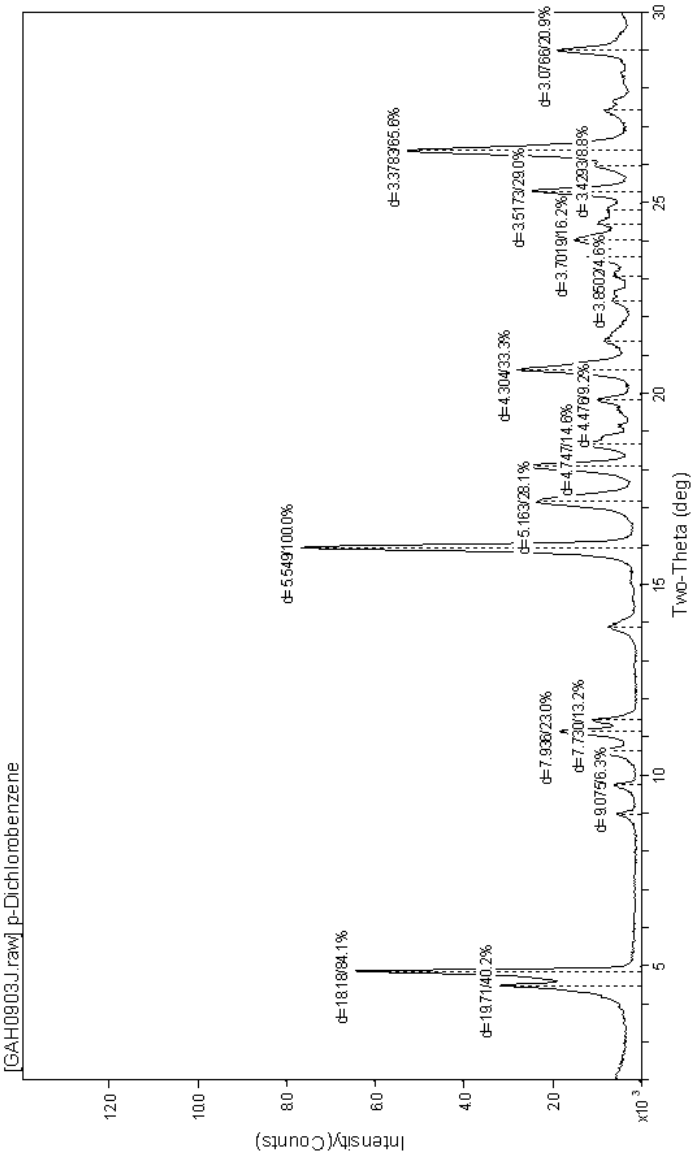

Figure E.42 Powder pattern of porous Zn(o-tolidine) sonicated with p-dichlorobenzene

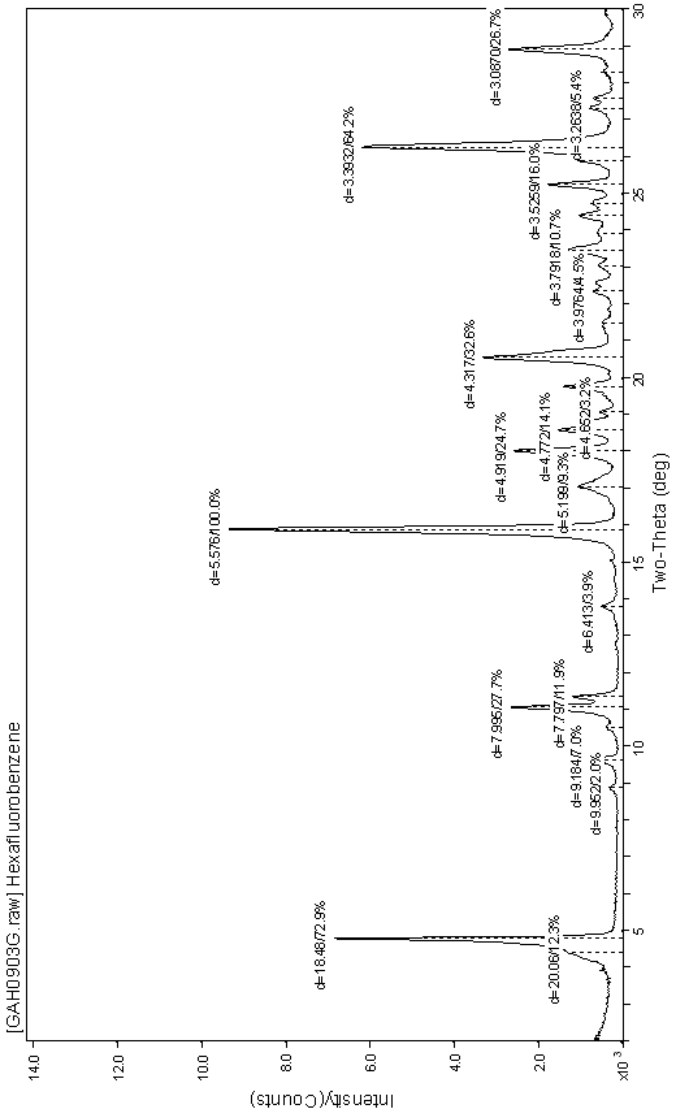

Figure E.43 Powder pattern of porous Zn(o-tolidine) sonicated with hexafluorobenzene

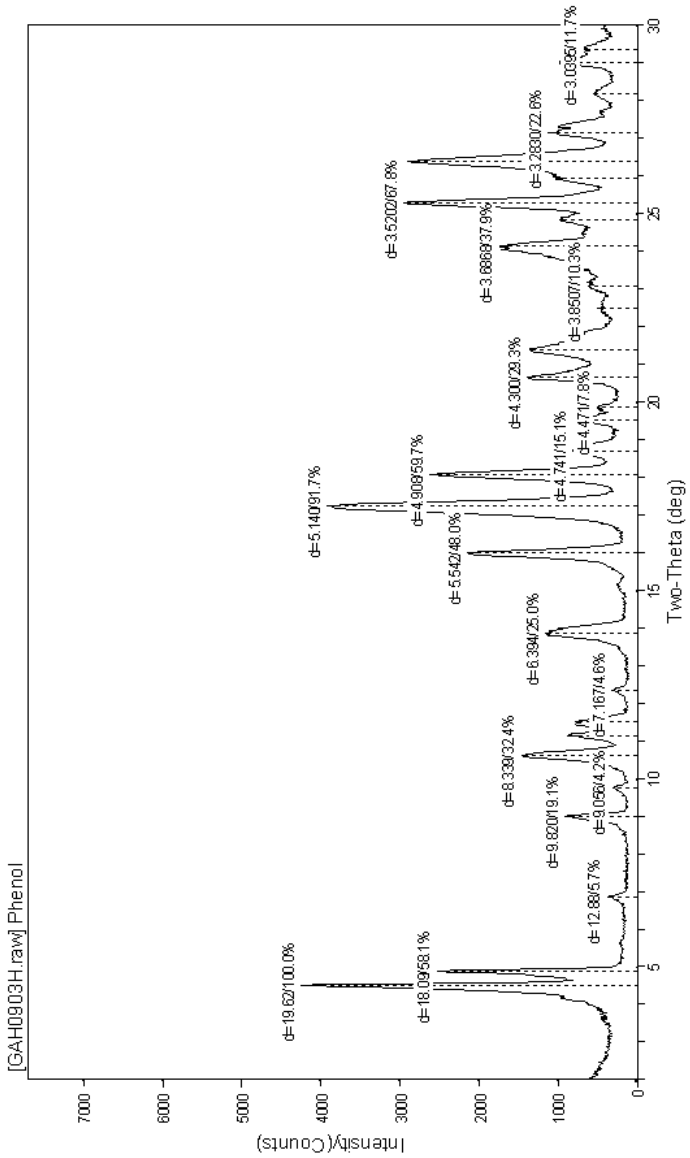

Figure E.44 Powder pattern of porous Zn(o-tolidine) sonicated with phenol

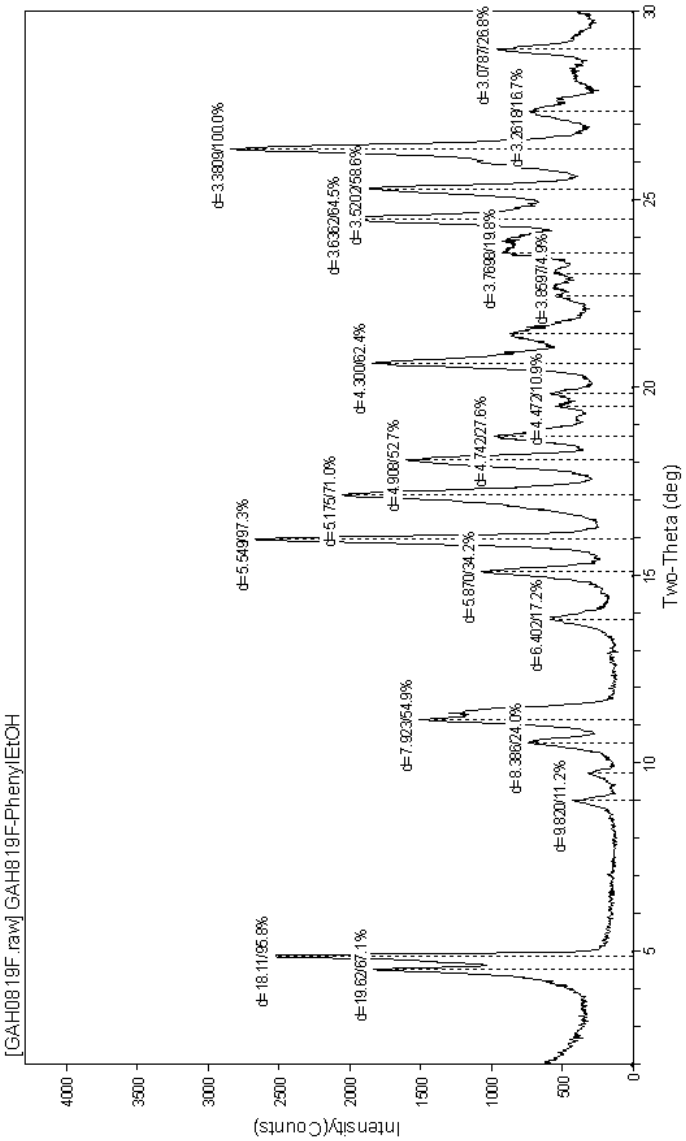

Figure E.45 Powder pattern of porous Zn(o-tolidine) sonicated with 2-phenylethanol

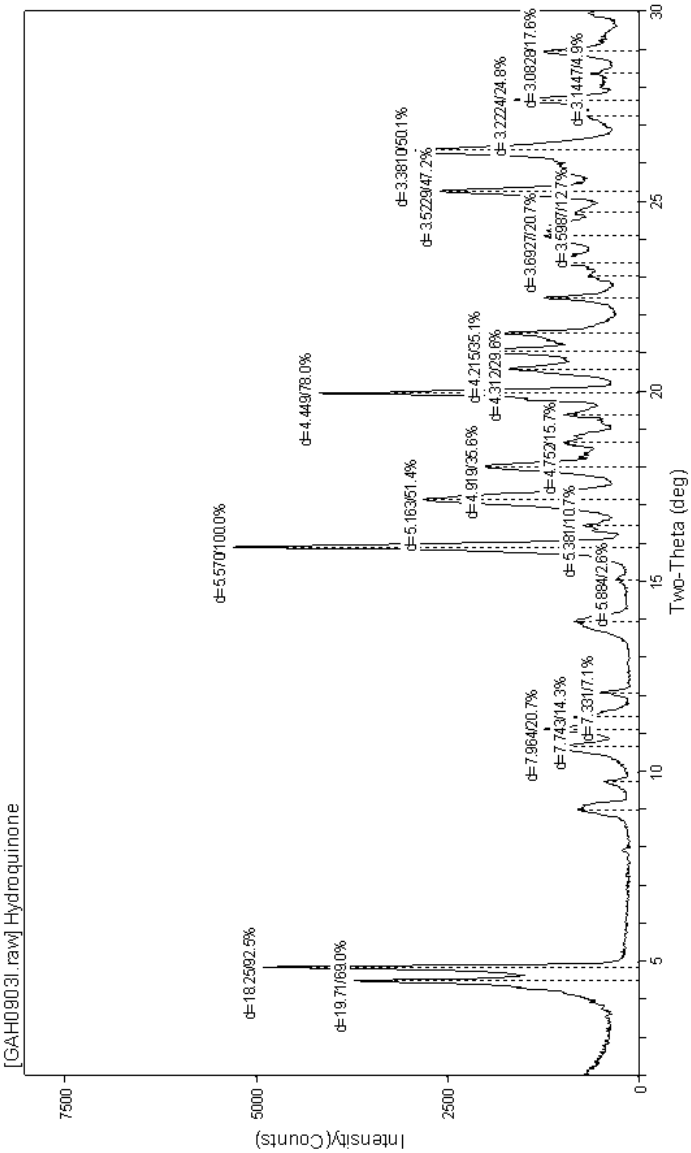

Figure E.46 Powder pattern of porous Zn(o-tolidine) sonicated with hydroquinone

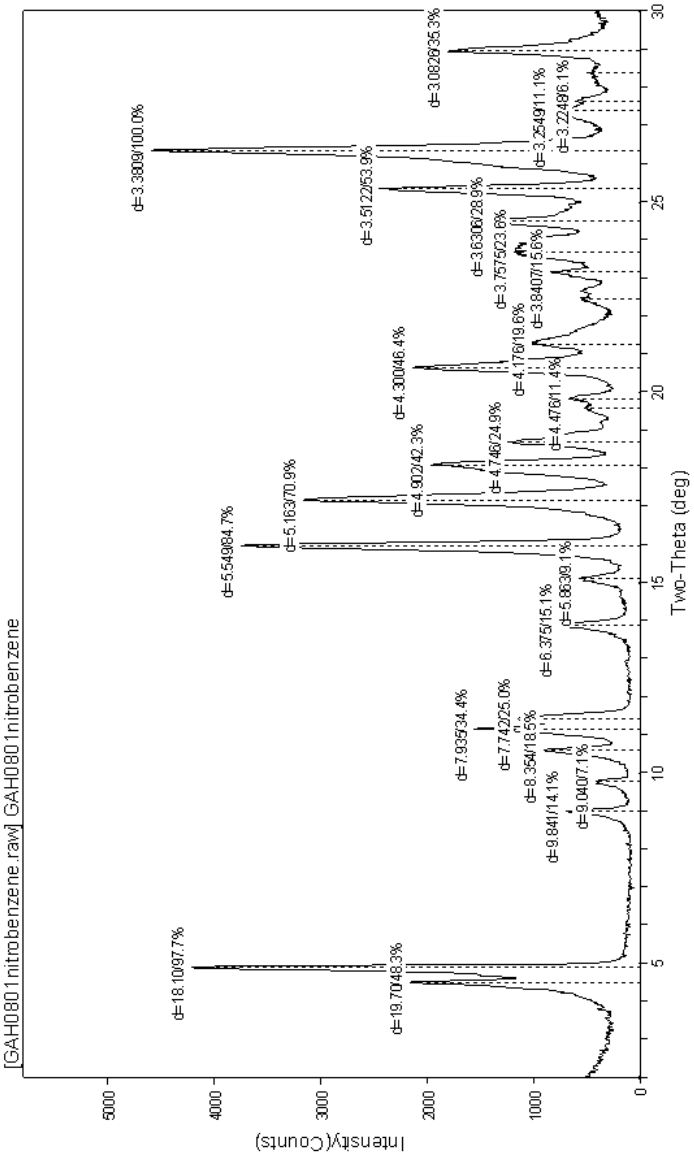

Figure E.47 Powder pattern of porous Zn(o-tolidine) sonicated with nitrobenzene

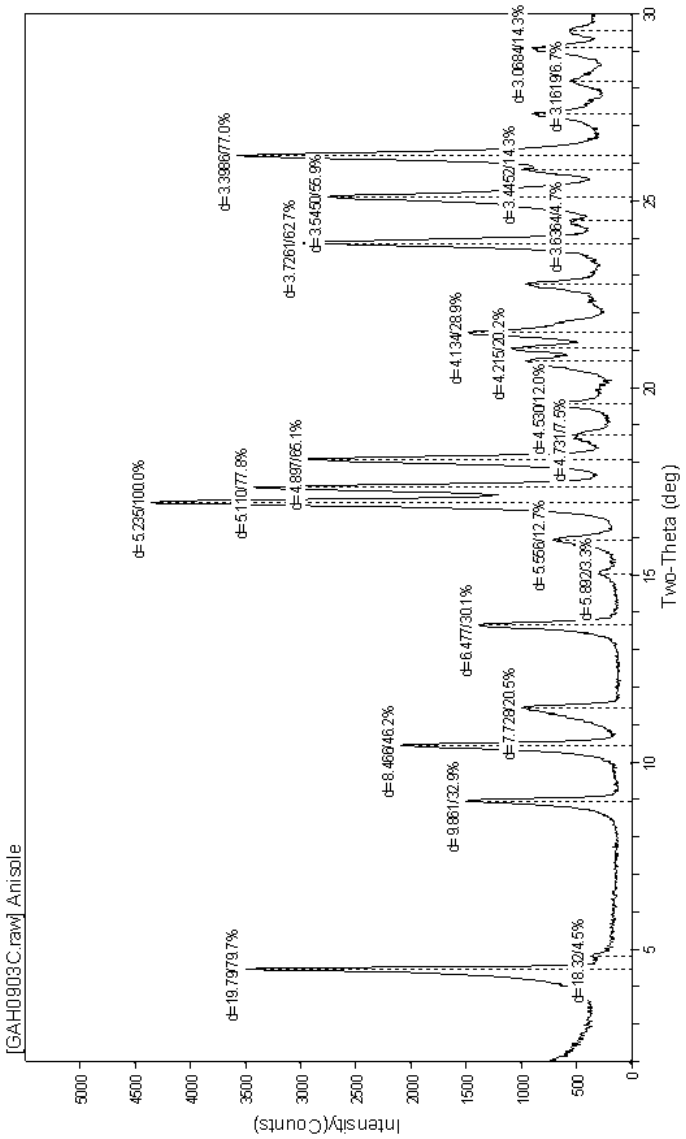

Figure E.48 Powder pattern of porous Zn(o-tolidine) sonicated with anisole

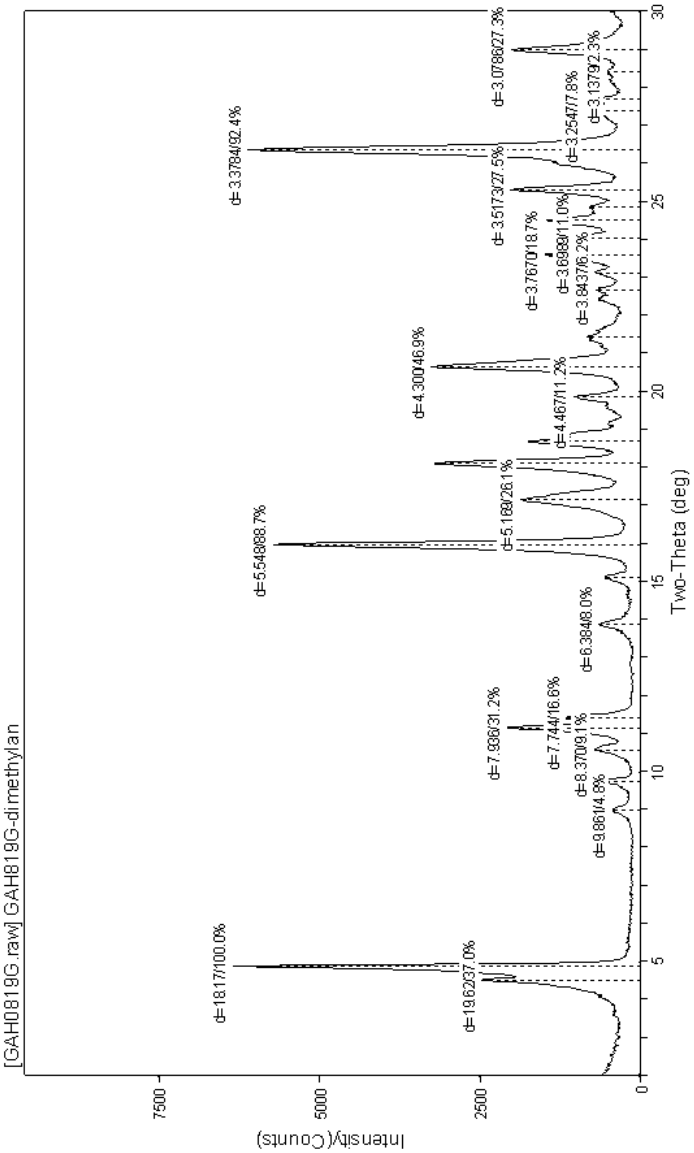

Figure E.49 Powder pattern of porous Zn(o-tolidine) sonicated with N,N-dimethylaniline

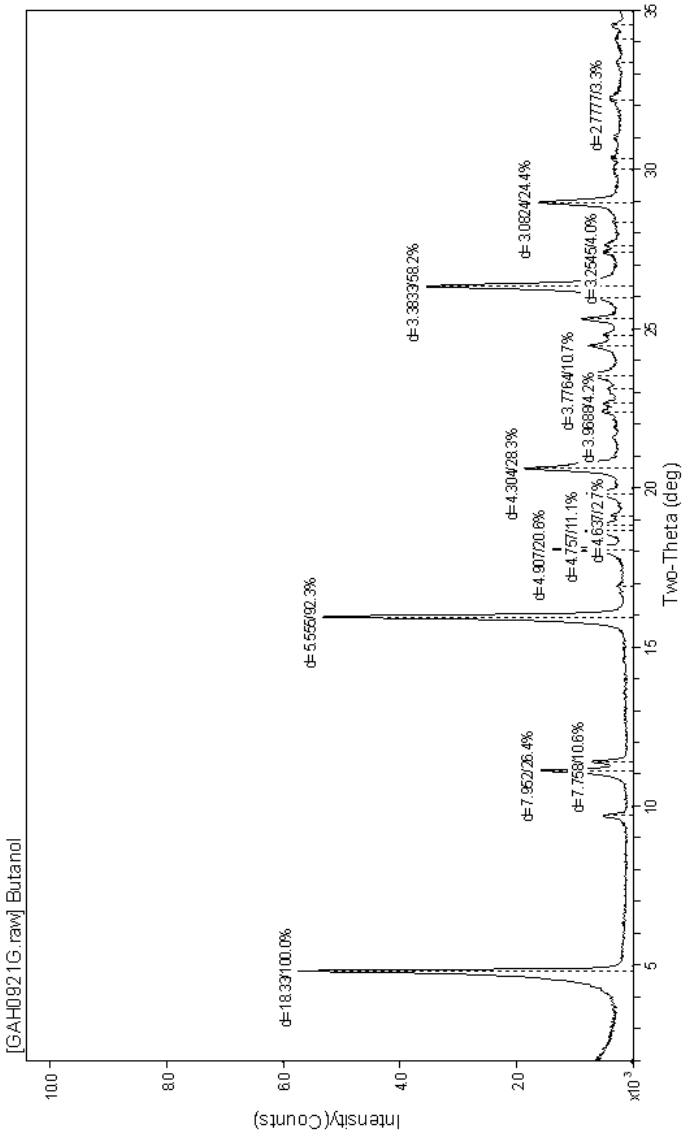

Figure E.50 Powder pattern of porous Zn(o-tolidine) sonicated with butanol

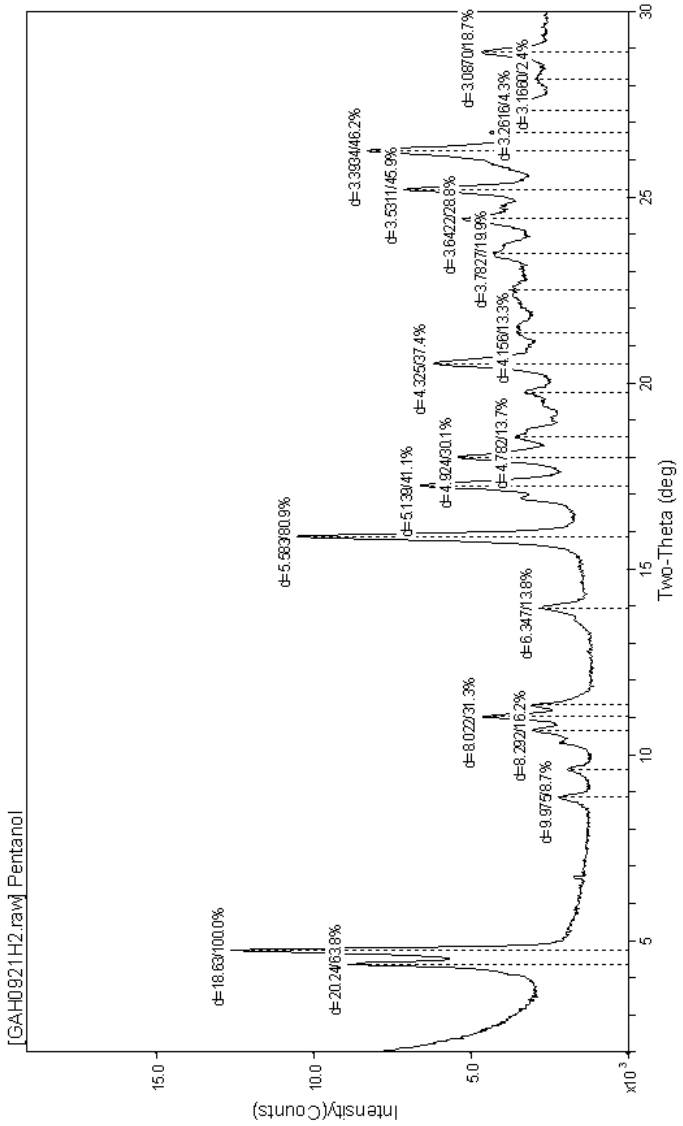

Figure E.51 Powder pattern of porous Zn(o-tolidine) sonicated with pentanol

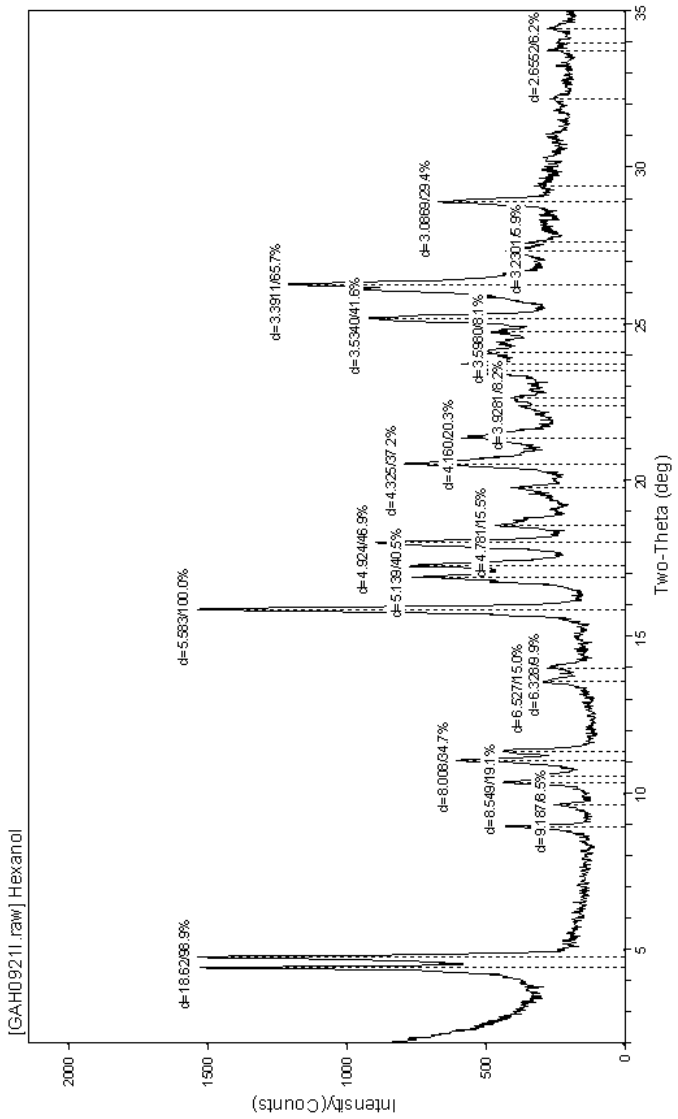

Figure E.52 Powder pattern of porous Zn(o-tolidine) sonicated with hexanol

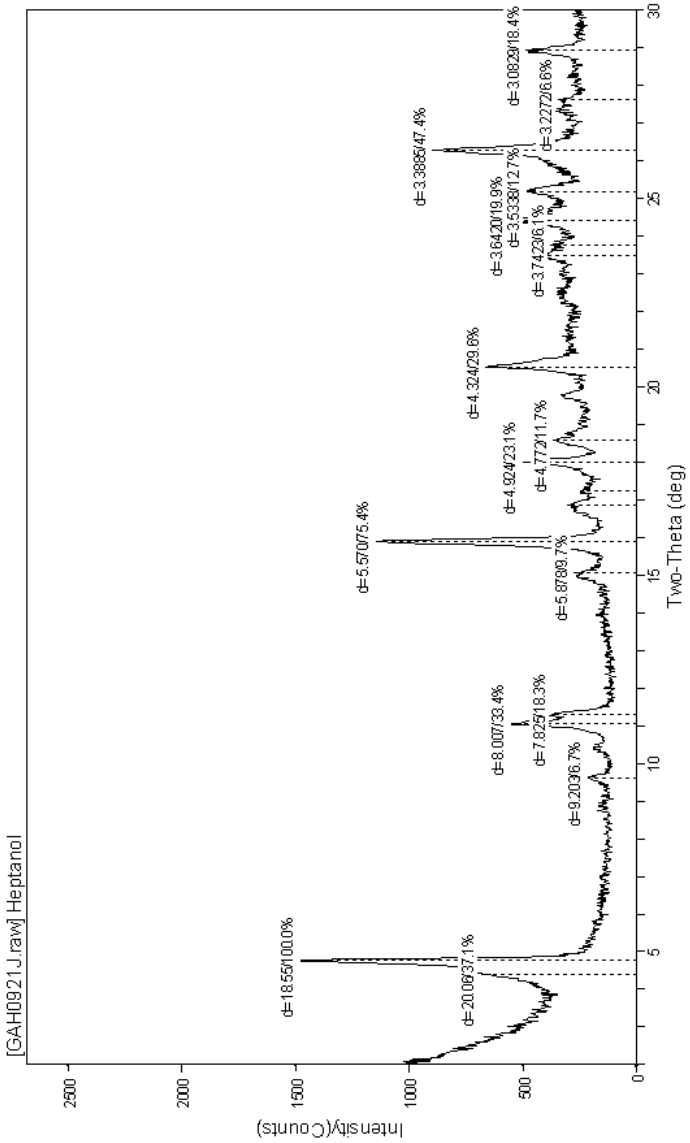

Figure E.53 Powder pattern of porous Zn(o-tolidine) sonicated with heptanol

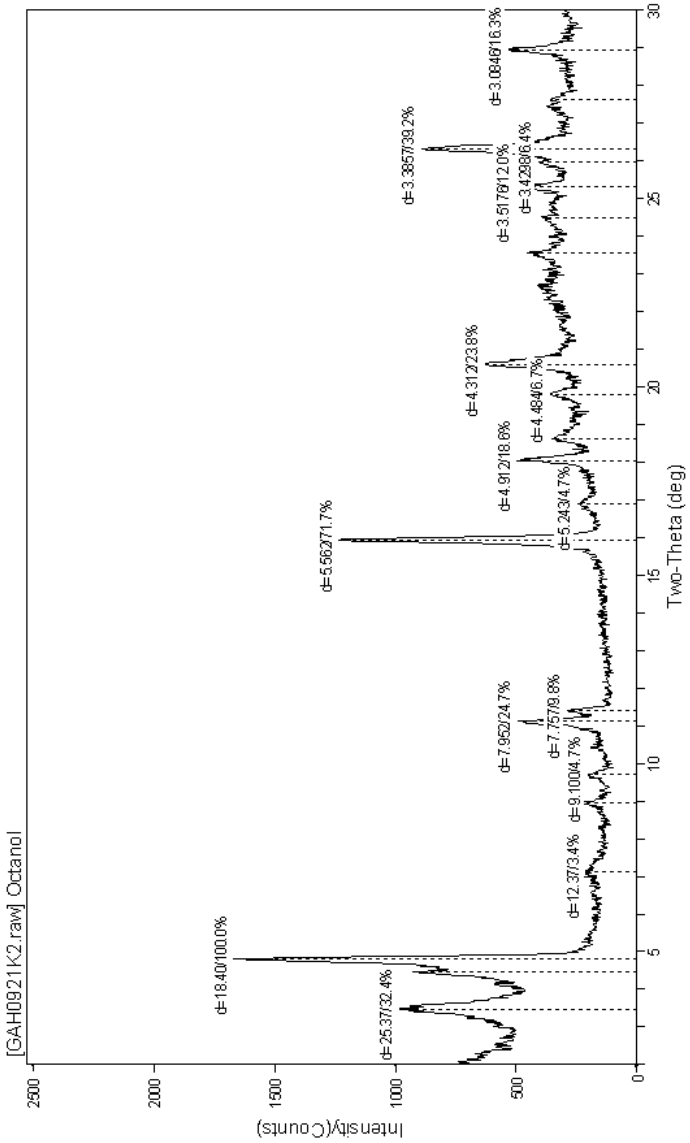

Figure E.54 Powder pattern of porous Zn(o-tolidine) sonicated with octanol

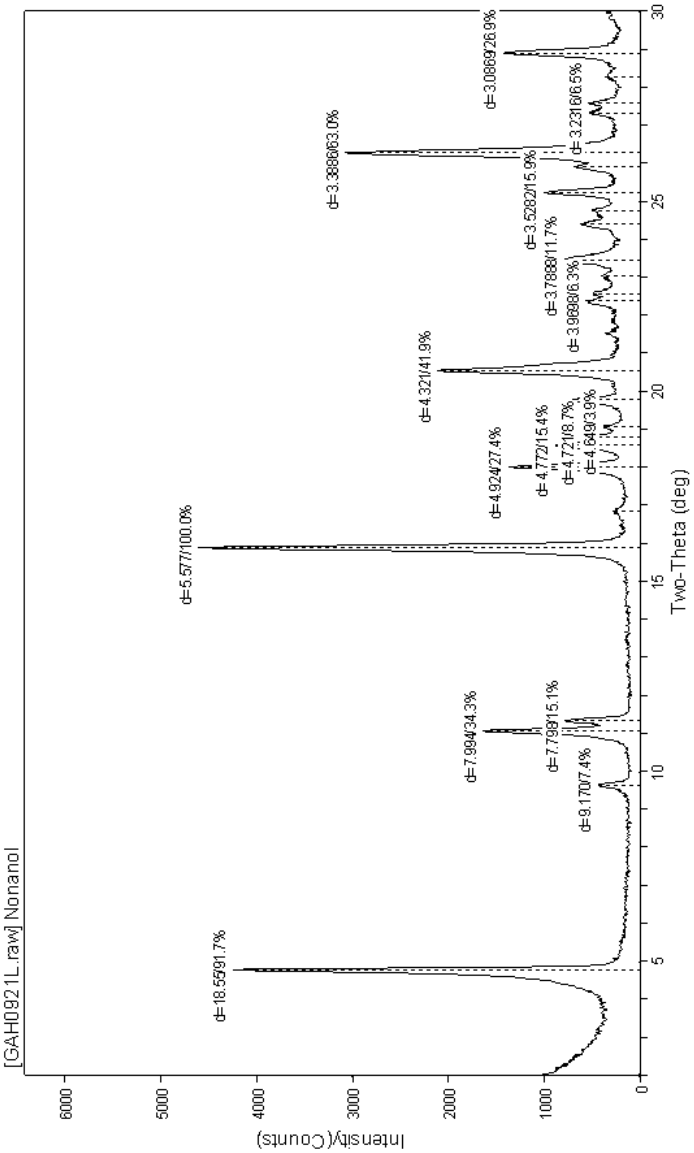

Figure E.55 Powder pattern of porous Zn(o-tolidine) sonicated with nonanol

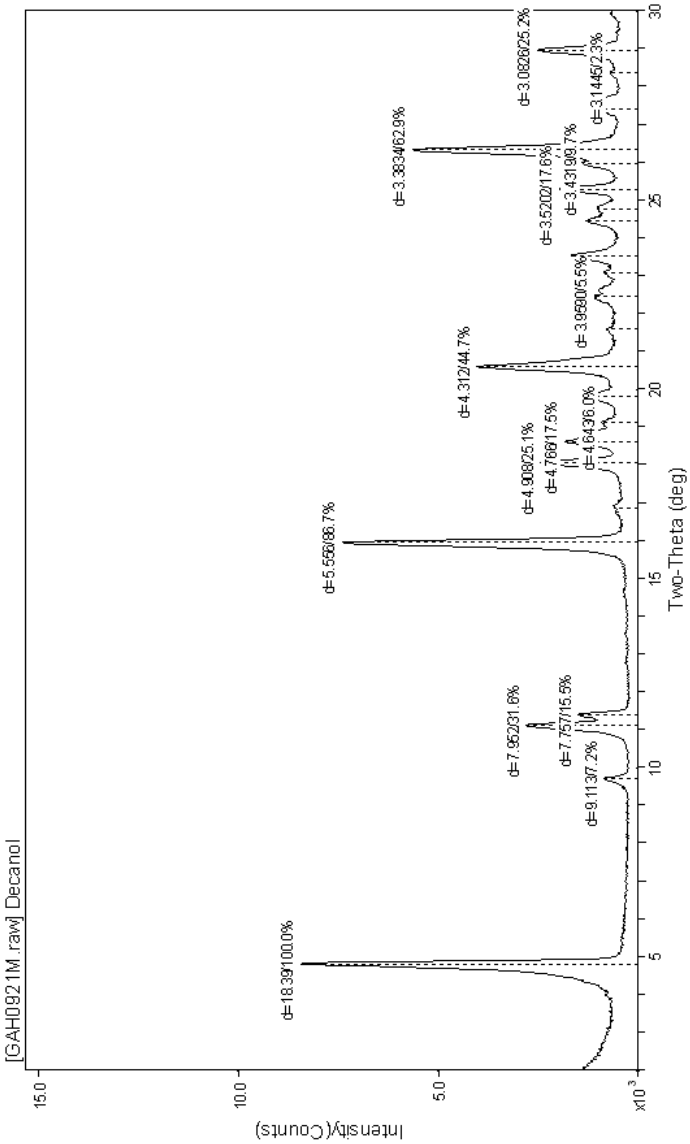

Figure E.56 Powder pattern of porous Zn(o-tolidine) sonicated with decanol

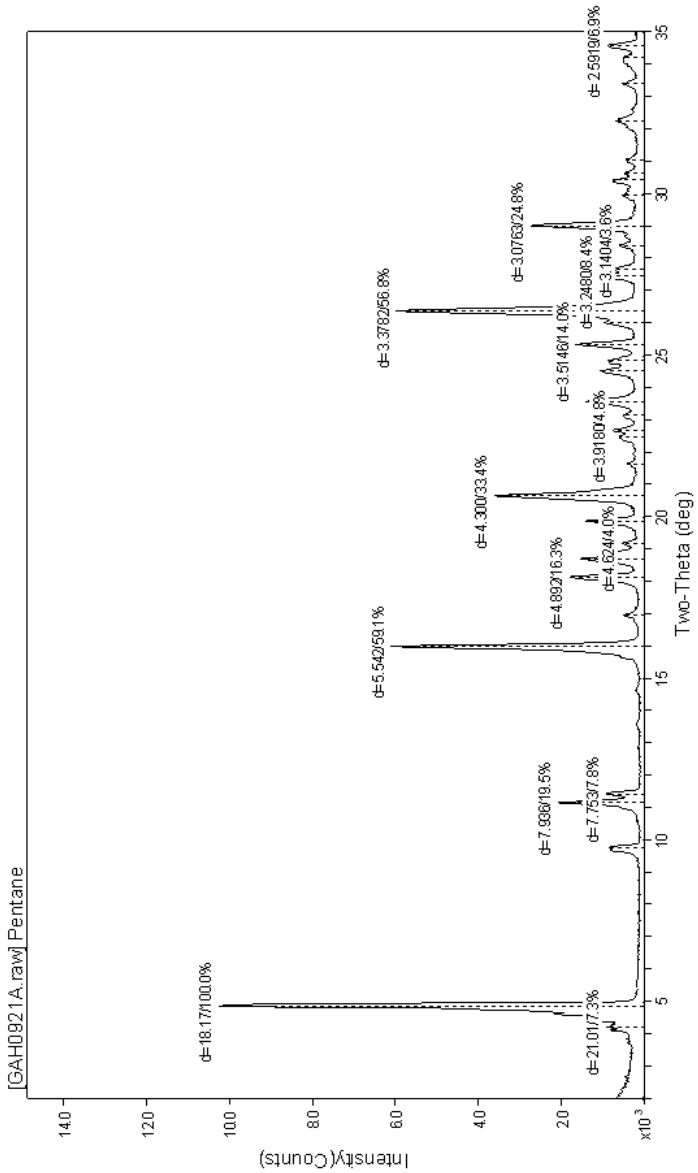

Figure E.57 Powder pattern of porous Zn(o-tolidine) sonicated with pentane

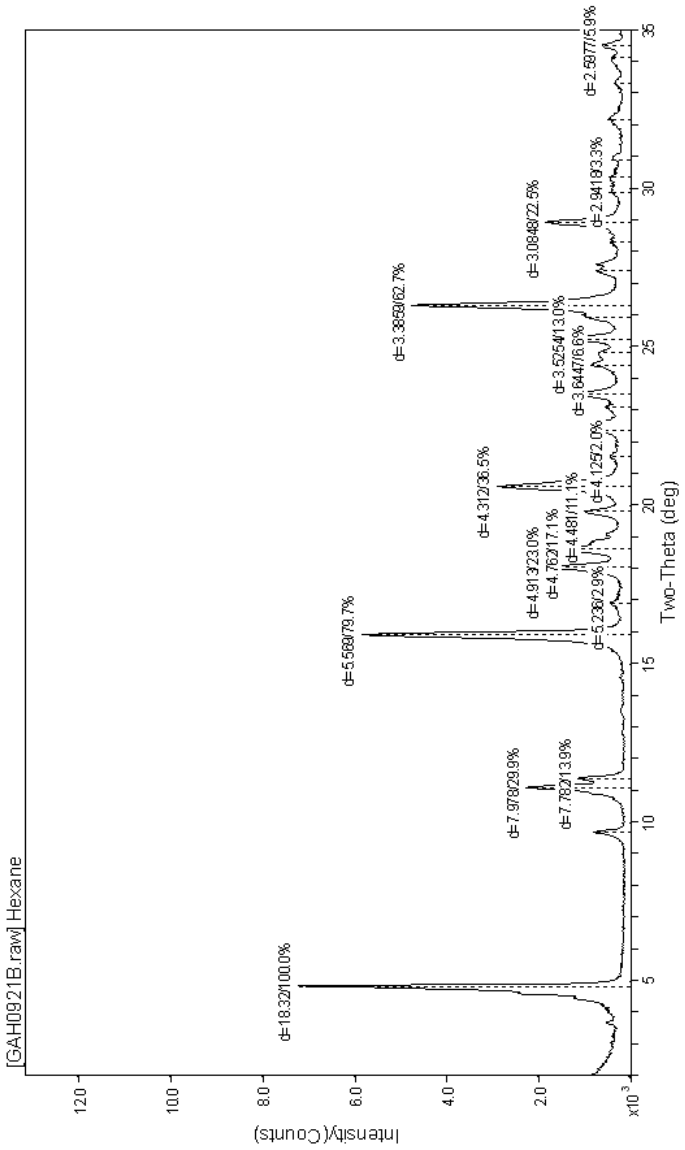

Figure E.58 Powder pattern of porous Zn(o-tolidine) sonicated with hexane

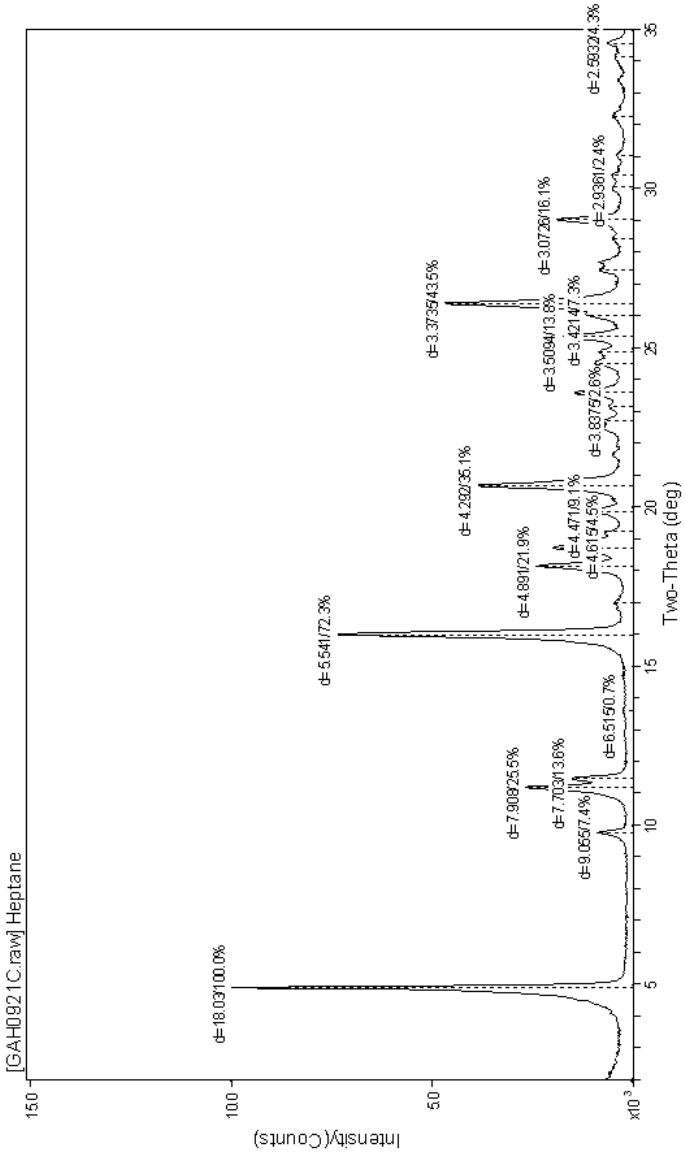

Figure E.59 Powder pattern of porous Zn(o-tolidine) sonicated with heptane

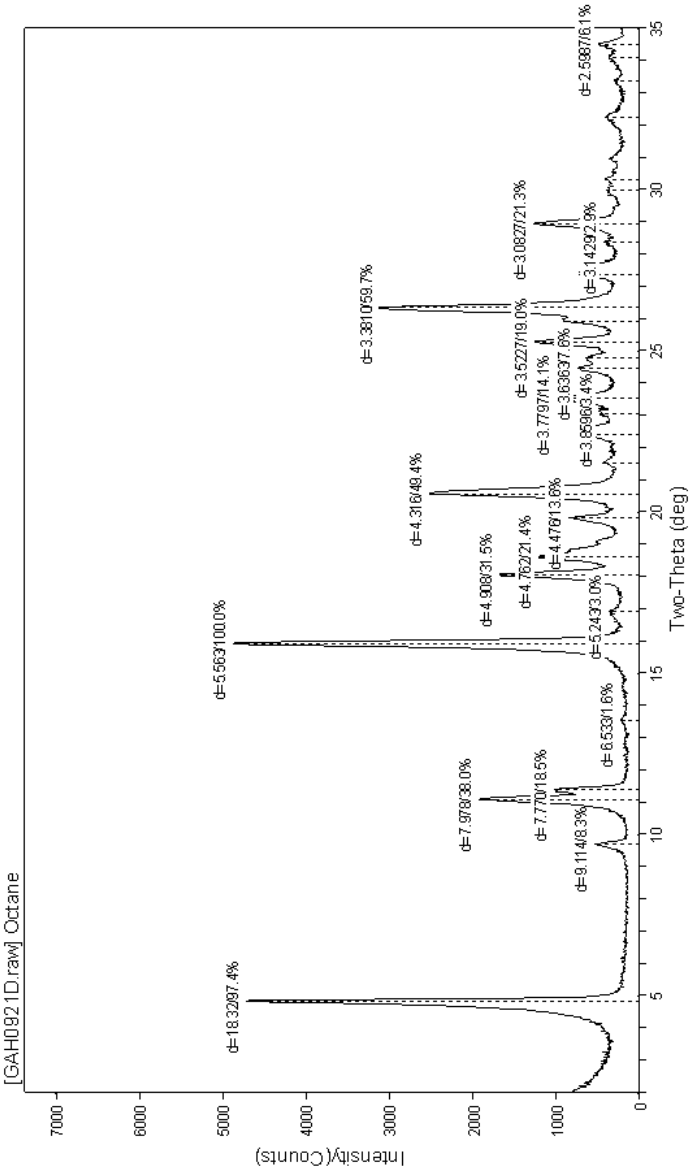

FigureE.60 Powder pattern of porous Zn(o-tolidine) sonicated with octane

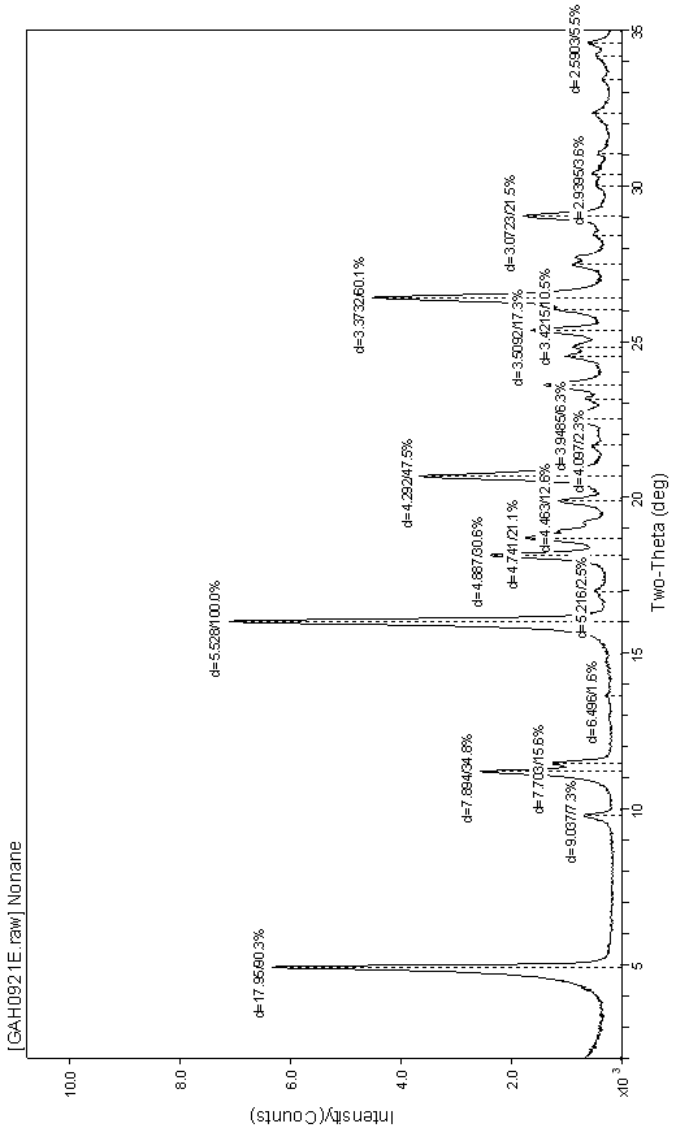

Figure E.61 Powder pattern of porous Zn(o-tolidine) sonicated with nonane

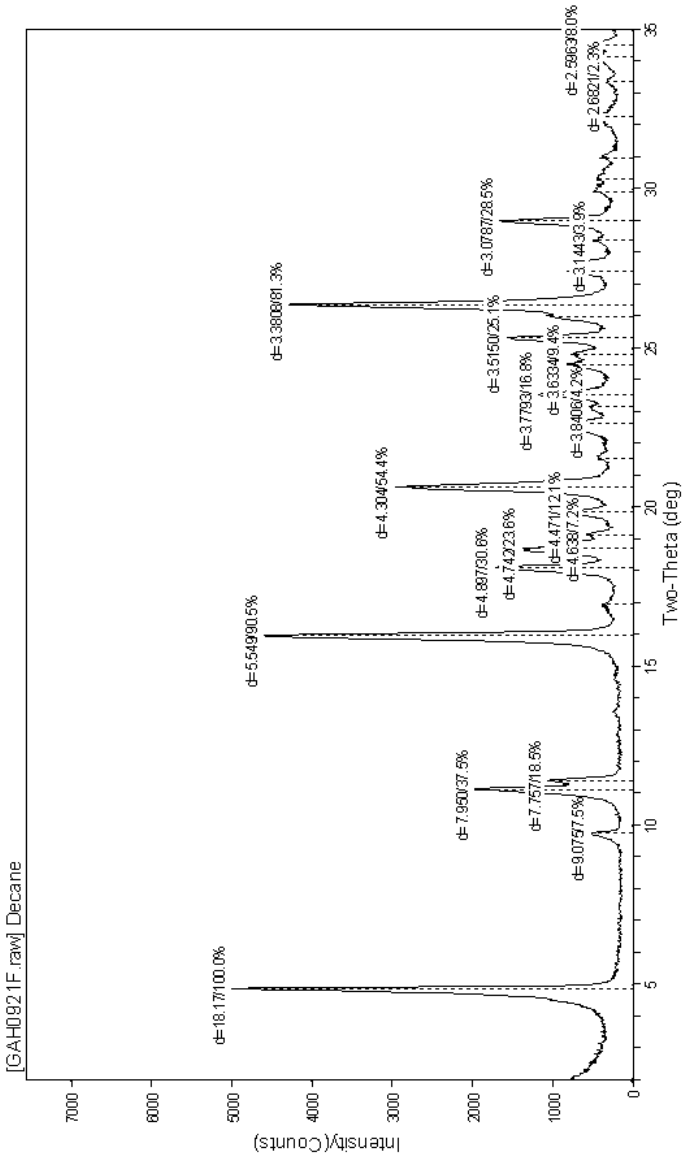

Figure E.62 Powder pattern of porous Zn(o-tolidine) sonicated with decane

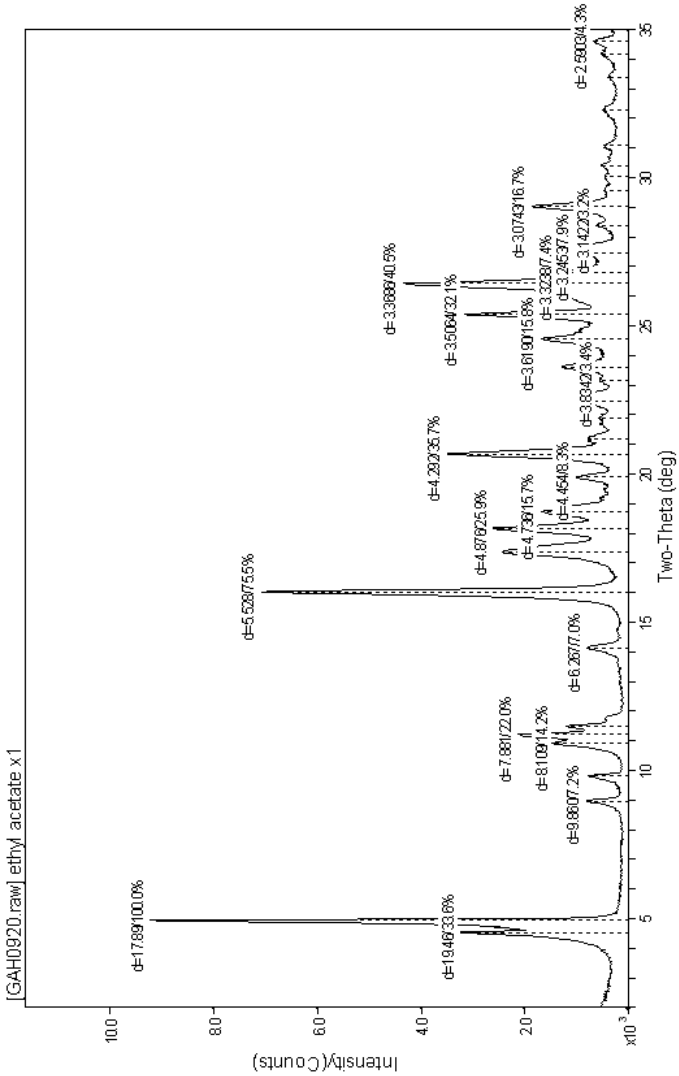

Figure E.63 Powder pattern of porous Zn(o-tolidine) sonicated with ethyl acetate

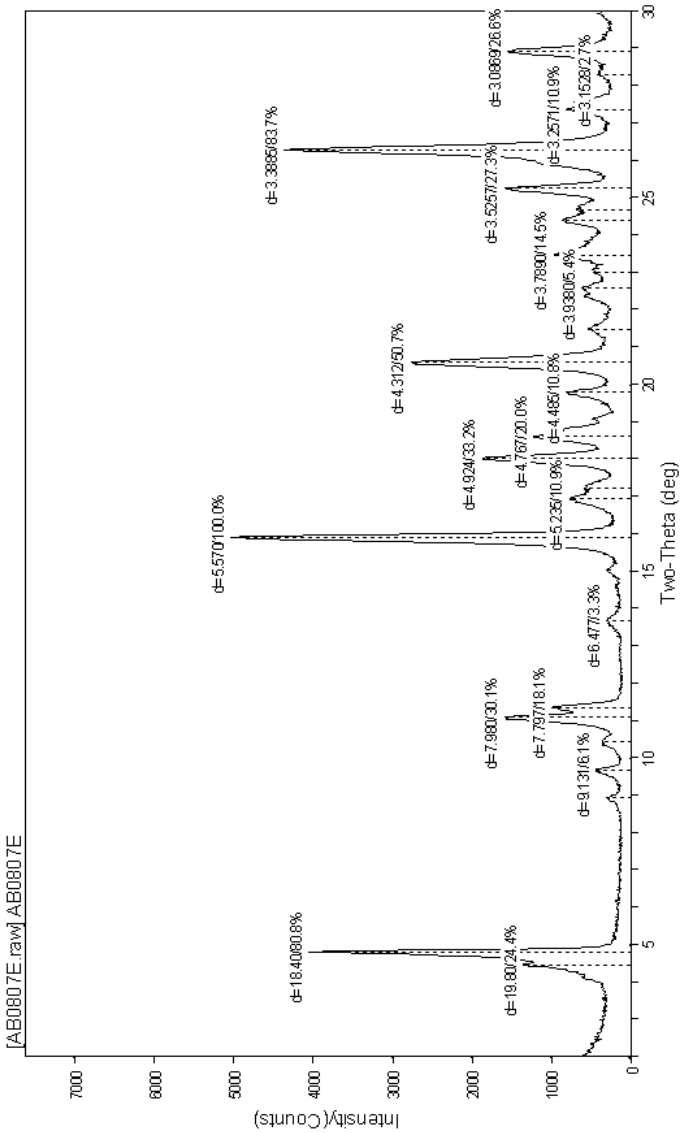

Figure E.64 Powder pattern of porous Zn(o-tolidine) sonicated with tetrahydrofuran

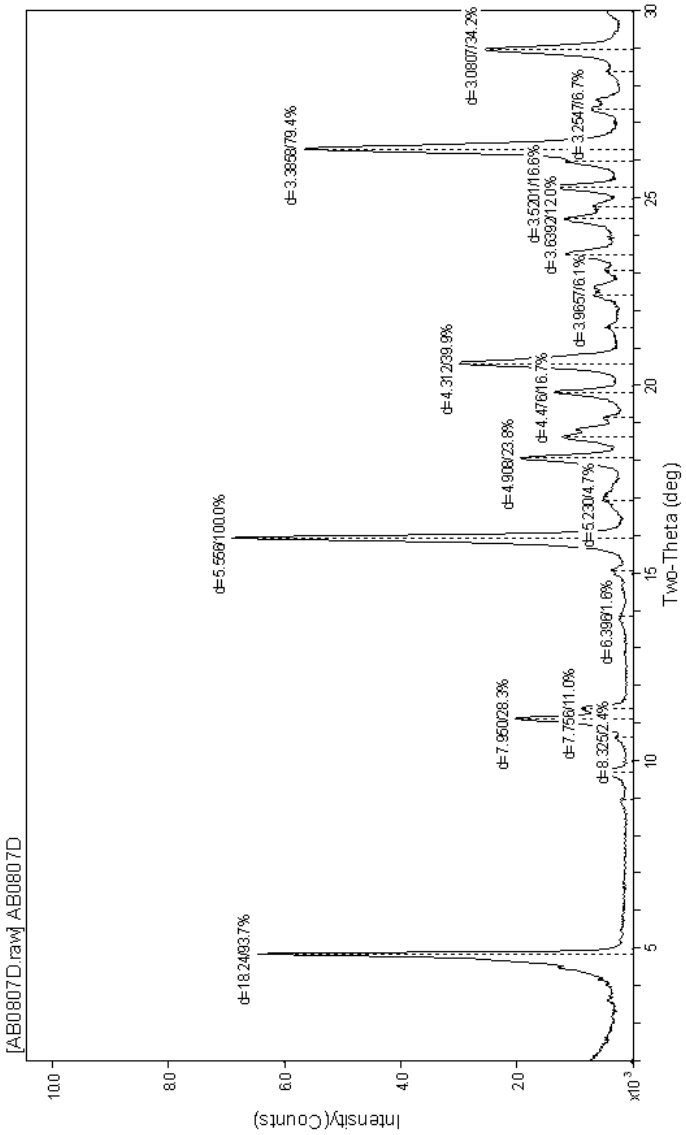

Figure E.65 Powder pattern of porous Zn(o-tolidine) sonicated with 1,4-dioxane

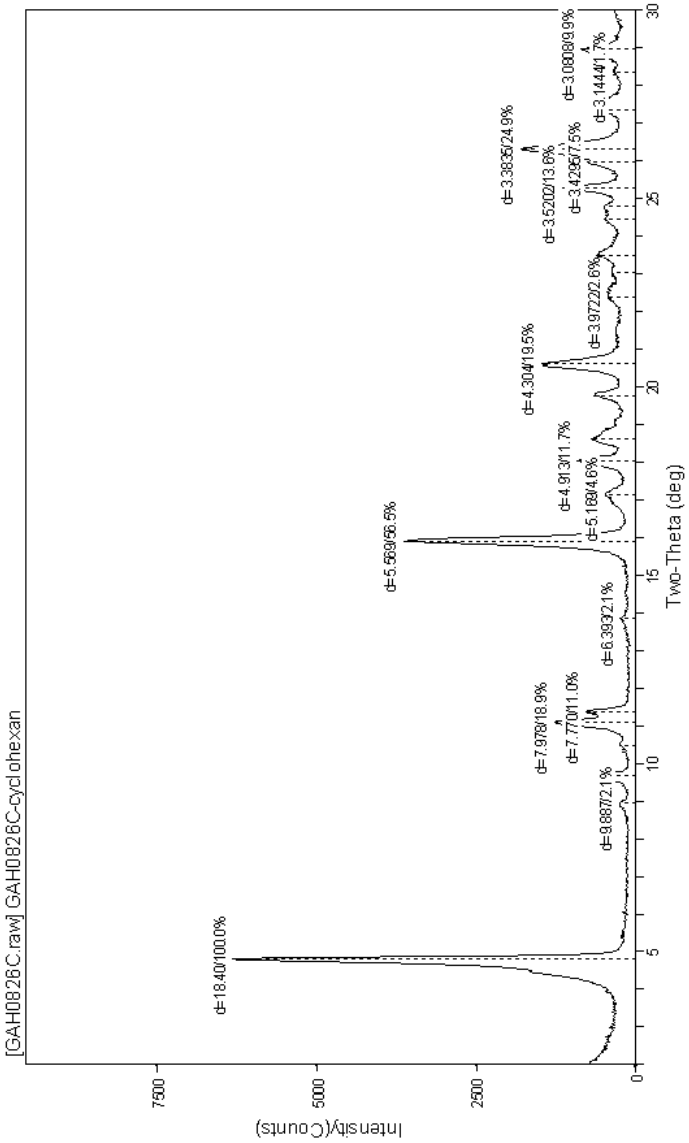

Figure E.66 Powder pattern of porous Zn(o-tolidine) sonicated with cyclohexane

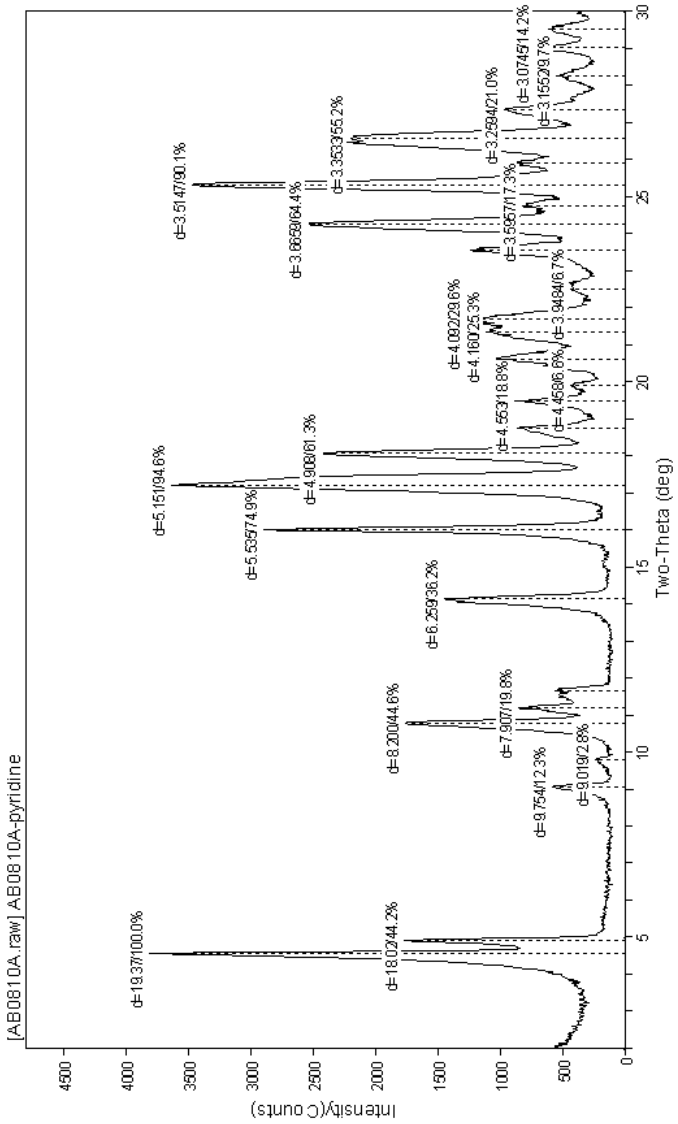

Figure E.67 Powder pattern of porous Zn(o-tolidine) sonicated with pyridine

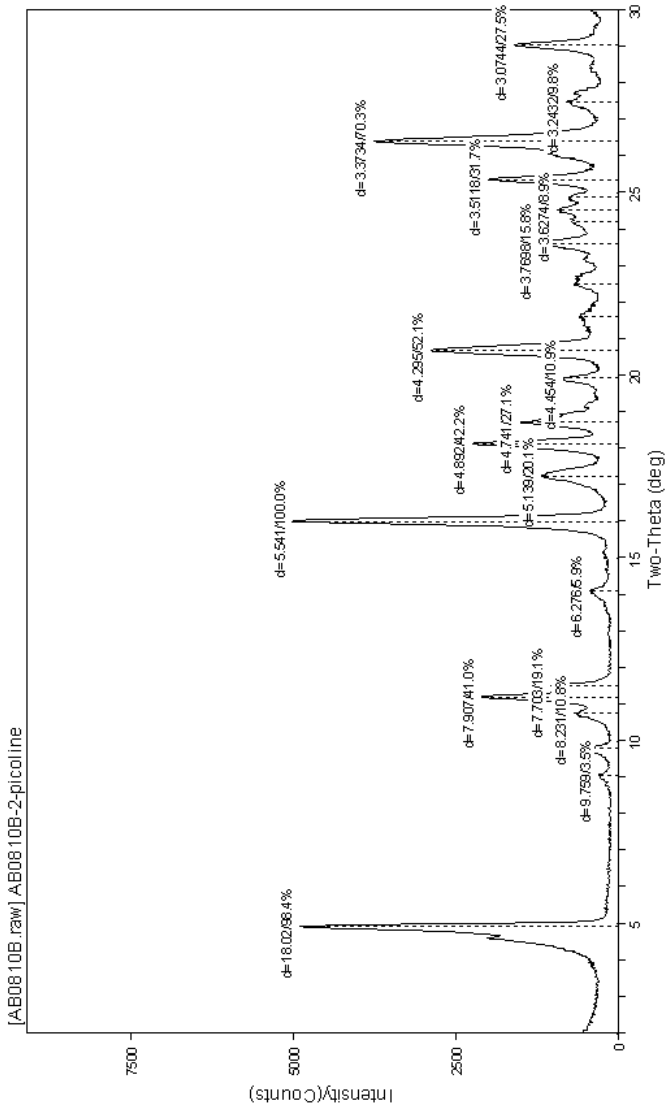

Figure E.68 Powder pattern of porous Zn(o-tolidine) sonicated with 2-picoline

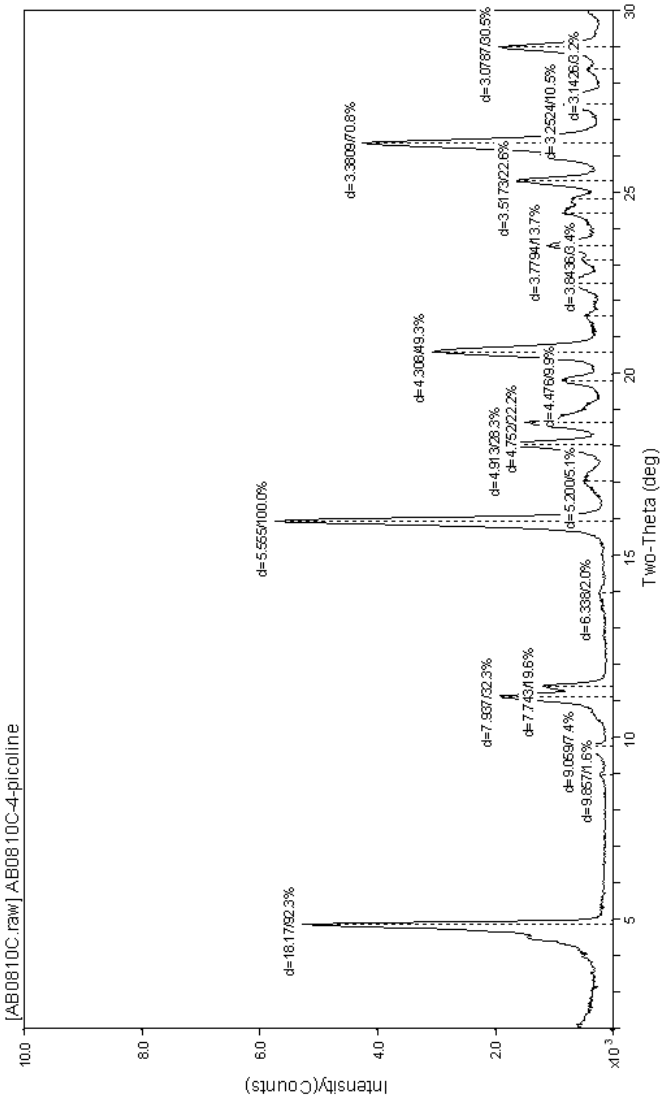

Figure E.69 Powder pattern of porous Zn(o-tolidine) sonicated with 4-picoline

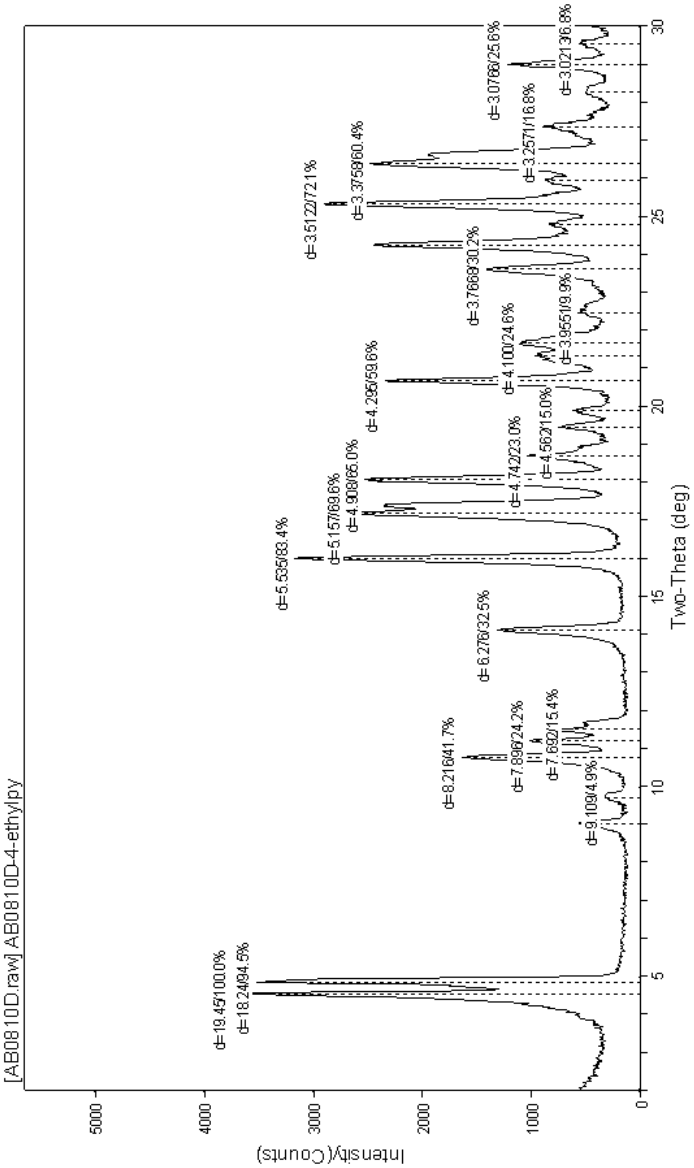

Figure E.70 Powder pattern of porous Zn(o-tolidine) sonicated with 4-ethylpyridine

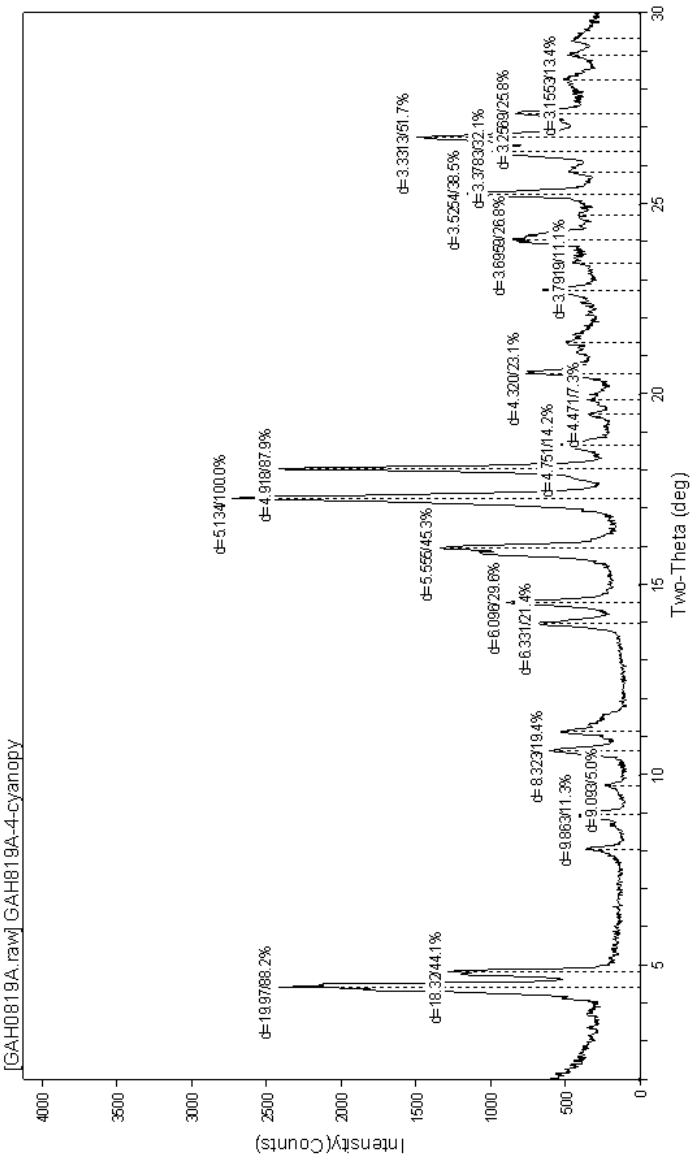

Figure E.71 Powder pattern of porous Zn(o-tolidine) sonicated with 4-cyanopyridine

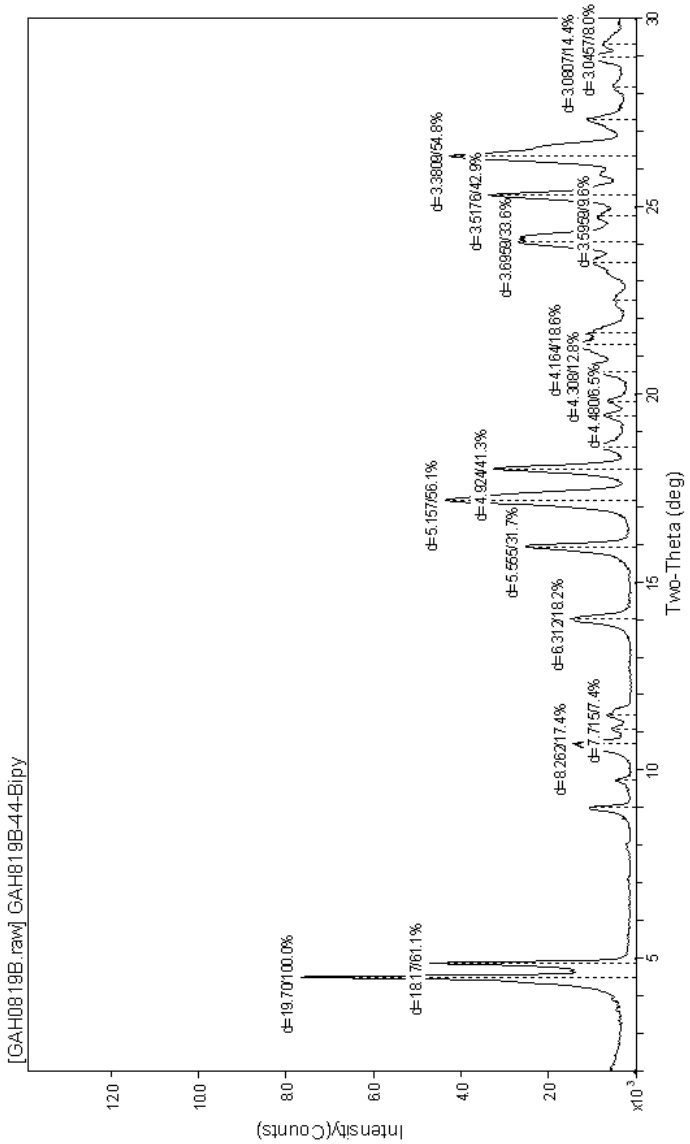

Figure E.72 Powder pattern of porous Zn(o-tolidine) sonicated with 4,4’-bipyridine

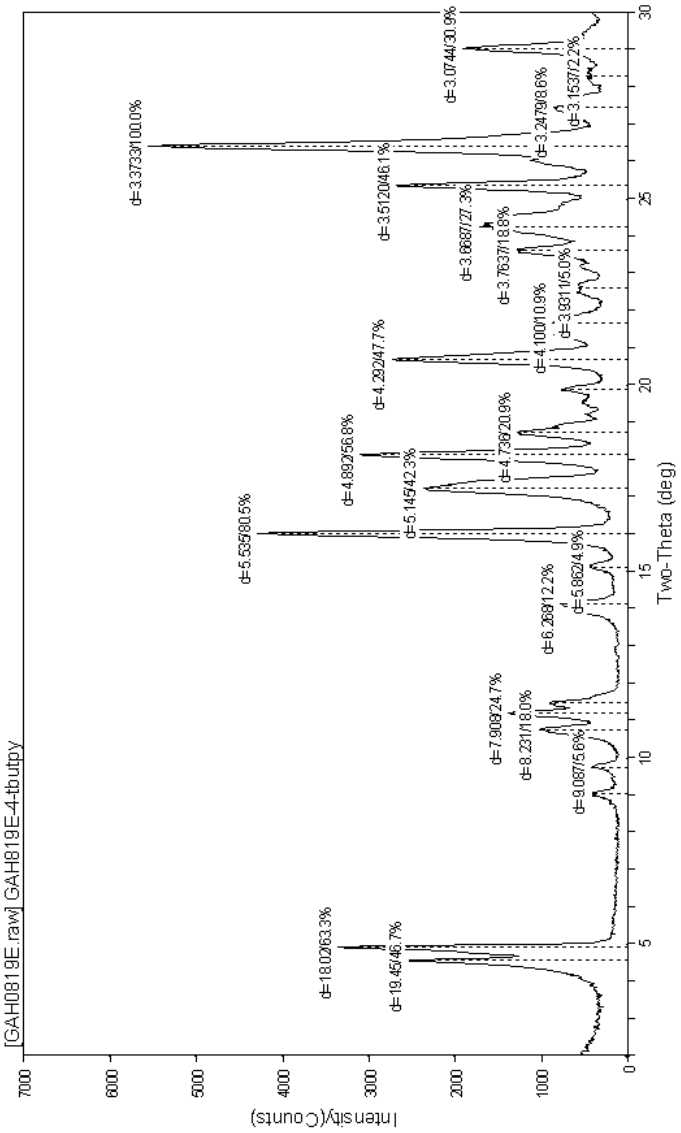

Figure E.73 Powder pattern of porous Zn(o-tolidine) sonicated with 4-t-butylpyridine

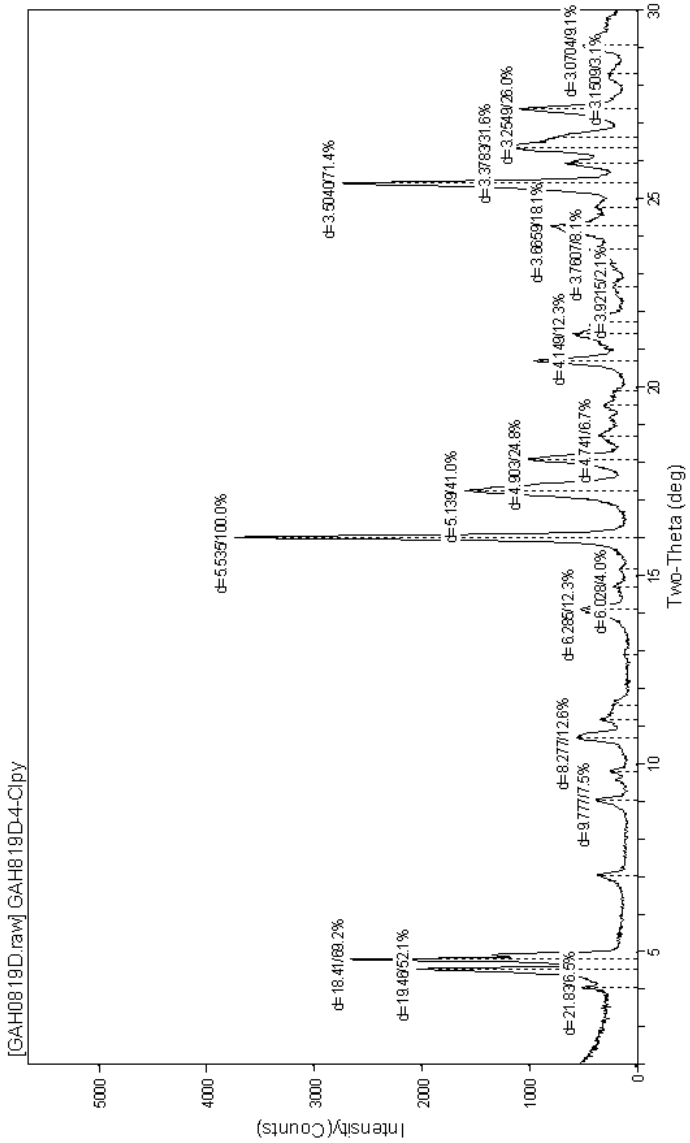

Figure E.74 Powder pattern of porous Zn(o-tolidine) sonicated with 4-chloropyridine

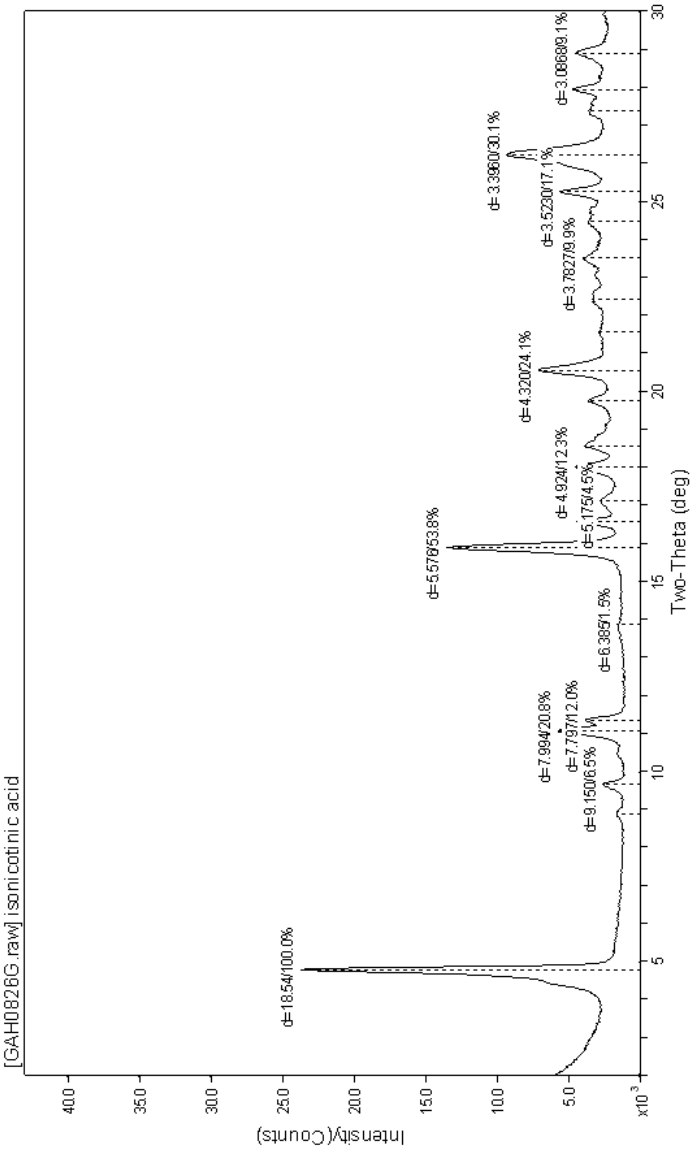

Figure E.75 Powder pattern of porous Zn(o-tolidine) sonicated with isonicotinic acid

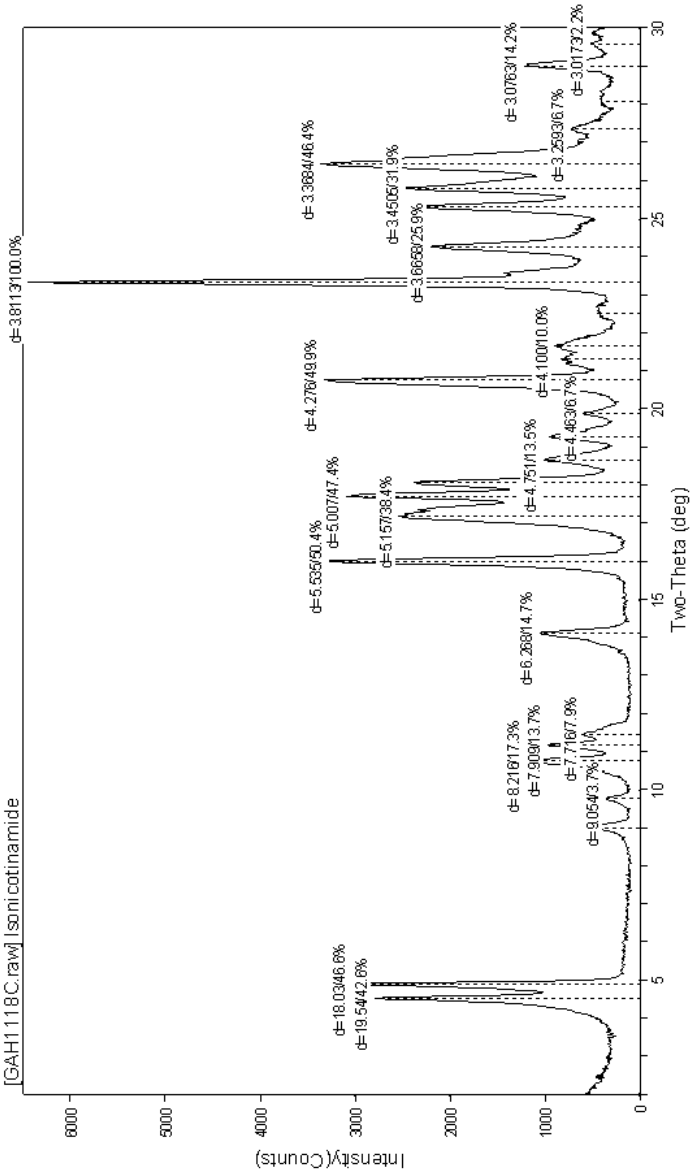

Figure E.76 Powder pattern of porous Zn(o-tolidine) sonicated with isonicotinamide